ENHANCED SEISMIC PERFORMANCE OF SPECIAL TRUSS MOMENT FRAMES AND STAGGERED TRUSS FRAMING SYSTEM FOR SEISMICALLY ACTIVE AREAS

by

SANPUTT SIMASATHIEN

Presented to the Faculty of the Graduate School of

The University of Texas at Arlington in Partial Fulfillment

of the Requirements

for the Degree of

DOCTOR OF PHILOSOPHY

THE UNIVERSITY OF TEXAS AT ARLINGTON

MAY 2016

Acknowledgements

The author would like to express his sincere gratitude to his supervising advisor, Dr. Shih-Ho Chao, for his valuable guidance, support, mentorship, and patience, as well as for giving the author the opportunity to work on such interesting and innovative research. Special gratitude is also due to the committee members Dr. Ali Abolmaali, Dr. Anand Puppala, Dr. Nur Yazdani, and Dr. Taichiro Okazaki.

The authors would like to thank Professor Carol K. Shield, Paul Bergson, Rachel Gaulke, Michael Boldischar, Samantha Thomas, Christopher Bruhn, Lauren Snyder and the staff at the University of Minnesota's Multi-Axial Subassemblage Testing (MAST) Laboratory, a member of the George E. Brown Jr. Network for Earthquake Engineering Simulation (NEES), for their assistance. Contribution and collaboration from fellow UT Arlington doctoral student, Chatchai Jiansinlapadamrong, is also greatly appreciated. Special thanks are also due to Guillermo Palacios, Dr. Poorya Hajyalikhani, Dr. Jae-Sung Cho, Kaka Venkateshbab, and all members of the research group for their help, support, and friendship.

The author would like to acknowledge the sponsorship of the U.S. National Science Foundation (NSF), who provided support under award number CMMI-0936563, and the American Institute of Steel Construction (AISC).

Finally, all of this would not have been possible without the unconditional love and limitless support of the author's family to whom the author is eternally grateful.

April 22, 2016

Abstract

ENHANCED SEISMIC PERFORMANCE OF SPECIAL TRUSS MOMENT FRAMES AND STAGGERED TRUSS FRAMING SYSTEM FOR SEISMICALLY ACTIVE ARES

Sanputt Simasathien, PhD

The University of Texas at Arlington, 2016

Supervising Professor: Shih-Ho Chao

Due to their ability to achieve large column-free floor spaces, special truss moment frames (STMFs) and staggered truss frames (STFs) are unique valuable options for structural engineers. However, although STMFs and STFs offer a wide range of structural, architectural, and economical benefits, limited research data is available on the seismic performance of these systems.

STMF system is a relatively new type of steel framing system for use in high seismic areas. STMFs dissipate earthquake energy through ductile special segments located near the mid-span of the truss girders, while the other members outside the special segment, including truss members, columns, and girder-to-column connections, are designed to remain elastic. When an STMF is subjected to seismic forces, the induced shear force in the middle of the truss girder is resisted primarily by the chord members in the special segment. One of the major advantages of using the STMF system is that the truss girders can be economically used over longer spans, and greater overall structural stiffness can be achieved by using deeper girders. In addition, the open-webs can easily accommodate mechanical and electrical ductwork. As a consequence, this system offers a wide range of structural, architectural, and economical benefits due

to their ability to achieve a large column-free floor. Due to the lack of continuing research to reflect the current practice in design and detailing on STMFs, the seismic performance research data of the system is limited. Substantial improvement in design methodology and confidence could be gained for STMFs by further research.

STF system was developed to achieve a more efficient structural framing system to resist wind loads and at the same time provide versatility of floor layout with large open areas. The result was an efficient steel framing system for mid- to high-rise buildings with low floor-to-floor heights and large column-free spaces that was simple to fabricate and erect. Because of the design flexibility, construction efficiency, and overall cost efficiencies, STF system has become a popular system in regions of low seismicity. Although STF system was originally developed for low seismic regions, the high lateral stiffness and light weight structural frames make this system attractive for use in high seismic regions. However, strong ground motions anticipated in regions of high seismicity significantly change the response of the STF system and necessitate system elements that are adequate in low-seismicity regions. Limited studies have been conducted on the behavior of STF system under strong earthquake ground motions. A key to the lateral-load resisting mechanism of STF system is the active participation of the floor diaphragms (typically consists of prestressed hollow-core planks) to transfer the inertial forces cumulating in a staggered manner across the height of the structure. The increasingly large diaphragm shear force in the lower stories brings concerns regarding the cyclic behavior of diaphragm-to-truss connections, local stress demand in the diaphragms under in-plane force and out-of-plane displacement. The stability of the system needs to be investigated if the trusses are designed to take inelastic action since the trusses serve as both the gravity and lateral-load resisting systems.

Table of Contents

List of Illustrations

List of Tables

Chapter 1

Organization of Dissertation

This dissertation is comprised of two different research projects and thus organized into two major parts. Chapter 1 will discuss the organization of the report.

Part 1 will be covered in Chapter 2 through Chapter 6, and will discuss the cyclic loading performance of special truss moment frames (STMFs). Chapter 2 will present a literature review on the development of the STMF system and the STMF seismic design criteria. The development of the design equations from AISC Seismic Provisions for Structural Steel Buildings including the current design practice will also be discussed. Research objectives of Part 1 will be presented at the end of Chapter 2. Chapter 3 will discuss the experimental testing program including component specimen testing and the full-scale STMF subassemblage test specimens, test setup and procedures, instrumentations, and data acquisition for the experimental test program. Chapter 4 will address the full-scale STMF subassemblage experimental testing covering test observations and the response of the specimens. Chapter 5 will discuss the experimental test results including the proposed special detailing, the expected vertical shear strength of STMFs, requirement for the stability bracing of trusses, predictive formula and strain gauge data, and the suggesting design approach. Finally, the summary, conclusion, and design recommendation of the STMF research project will be summarized in Chapter 6.

Part 2 will be covered in Chapter 7 through Chapter 11, describing a proposed modified structural layout for staggered truss frames (STFs). An overview of STF system along with its benefits will be presented in Chapter 7. Chapter 8 will discuss the research objectives of the Part 2 including limitations of STF system in seismic regions. Chapter 9 will present prototype STF structures with modified structural layouts, the design process and procedures for the prototype structures along with the pushover and non-linear time

history analysis models used in this research. Analysis results such as lateral force transfer pattern and discussions on the pushover and non-linear time history analyses and seismic behavior of structural floor diaphragm in STFs will be presented in Chapter 10. Lastly, the summary, conclusions, and recommendation for future study of the STF research project will be summarized in Chapter 11.

Chapter 2

Part I : Introduction

2.1 Overview

Special truss moment frame (STMF) system is a type of steel moment-frame system recognized in the 2010 Seismic Provisions for Structural Steel Building by the American Institute of Steel Construction (AISC), AISC 341-10, (AISC, 2010a) for use in seismically active areas. STMFs dissipate earthquake energy through inelastic action of members located near the mid-span of the frames called “special segment.” Currently, there are two configurations of STMFs recognized by AISC as shown in Figure 2-1.

The first configuration is STMFs with a single Vierendeel panel in the special segment. The second one is STMFs with X-diagonal web members separated by vertical members. The first STMF configuration develops ductility through plastic hinge formation at the ends of the chord members in the special segment. For STMFs in the second configuration, yielding and buckling of the X-diagonal members also contribute to the ductility of the trusses. The basic design concept of the STMF system is to dissipate the earthquake energy in a ductile manner through the special segment in the middle of the truss as a structural fuse, while the other truss members outside the special segment including the truss-to-column connections stay in the elastic range.

STMF system provides higher lateral stiffness with relatively less weight compared to other moment-frame systems with solid beams (SEAOC Seismology Committee, 2008). Another advantage of using STMF system over other moment-frame systems is that trusses can be economically designed with longer spans and other nonstructural components such as mechanical and electrical ductwork can pass through the web openings. As a consequence, STMF system has gain popularity in seismically

active areas since building seismic specifications and codes adopt the STMF design criteria in 1997 (Dusicka, Itani, and Sahai, 2002).

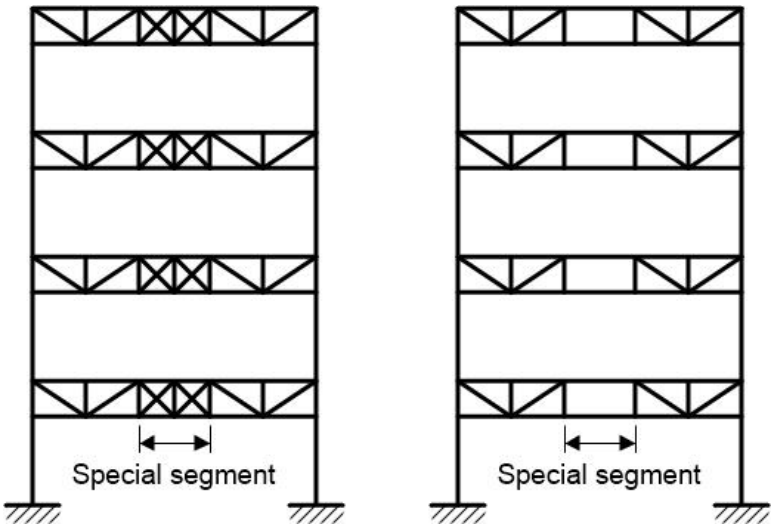

Figure 2-1 Configurations of special segment

2.2 Literature Review

2.2.1 Early Development of STMF

The development of the concept and design procedure of ductile truss girders, later called STMF, began in the late 1980s (Goel et al., 1998). After the 1985 Mexico City earthquake, Hanson and Martin (1987) found out that the conventional truss moment frames performed poorly. STMF with X-brace diagonal member configuration was developed as an enhanced seismic-resistant truss moment frames to increase the lateral strength and stiffness (Itani and Goel, 1991). Experimental and analytical investigations were carried out to study the seismic behavior and performance of an open-web truss moment frame designed as an ordinary moment resisting frame (OMRF) according to the 1988 Uniform Building Code (UBC) (ICBO, 1988). Test results from three full-scale half-span truss-column subassemblages showed that the conventional open-web truss moment framing system performed poorly under cyclic loading due to buckling and early

fracture of truss web members (Goel and Itani, 1994a). A modified truss configuration with X-brace diagonal web members was proposed to increase the ductility and to provide more stable hysteretic behavior of the trusses (Goel and Itani, 1994b). The concept was adapted from the eccentric braced frame (EBF) system where lateral seismic forces are mainly resisted by both tension and compression members in order to prevent sudden loss of lateral strength and stiffness caused by buckling of compression braces. The location of the X-panels special segment was strategically placed near midspan of the trusses where axial forces in chord members are minimum. Additional vertical web members were added to resist the unbalanced force on the chord members when yielding and buckling of web members occur. A design concept of “strong column-weak beam” where plastic hinges form in the chord members at the ends of the middle segment after the X-diagonal members buckle and yield was proposed. Figure 2-2 shows typical hysteretic loops of the conventional open-web truss specimens and STMF from the previous study, respectively.

In 1994, Basha and Goel studied another STMF configuration with Vierendeel configuration in the special segment of the truss (Basha and Goel, 1994) where inelastic activity was restricted solely to the chord members of the special segment. The Vierendeel configuration was proposed due to its advantage over the X-diagonal configuration from more open space in the special segment which can be utilized for ductwork and piping. Basha and Goel (1995) also reported about 7% in steel weight reduction comparing to the X-diagonal configuration. Experimental test results showed more stable hysteretic response without pinching or degradation up to 3% drift level as shown in Figure 2-3.

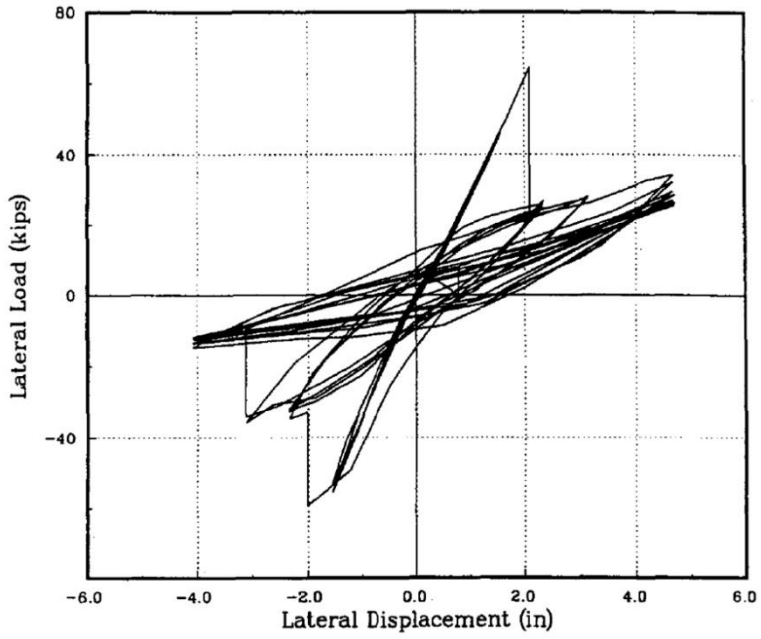

(a)

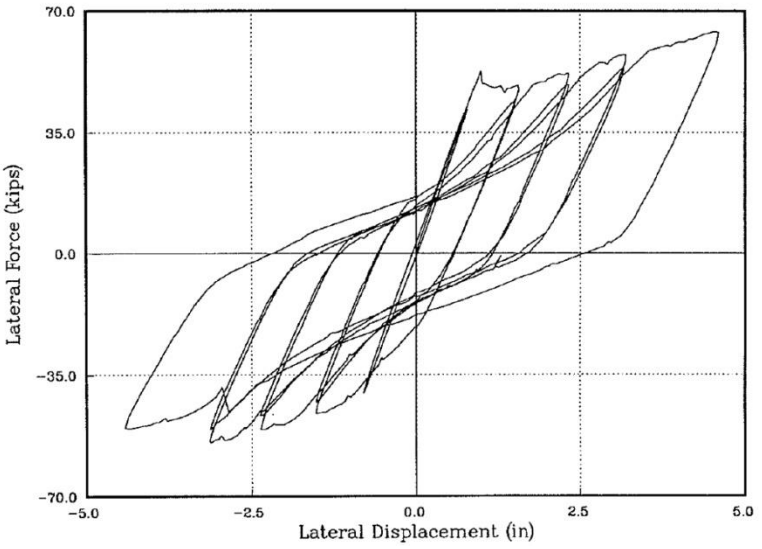

(b)

Figure 2-2 Typical hysteretic loops of testes specimens (Goal and Itani, 1994a; 1994b):

(a) conventional open-web trusses; (b) STMF subassemblage 1

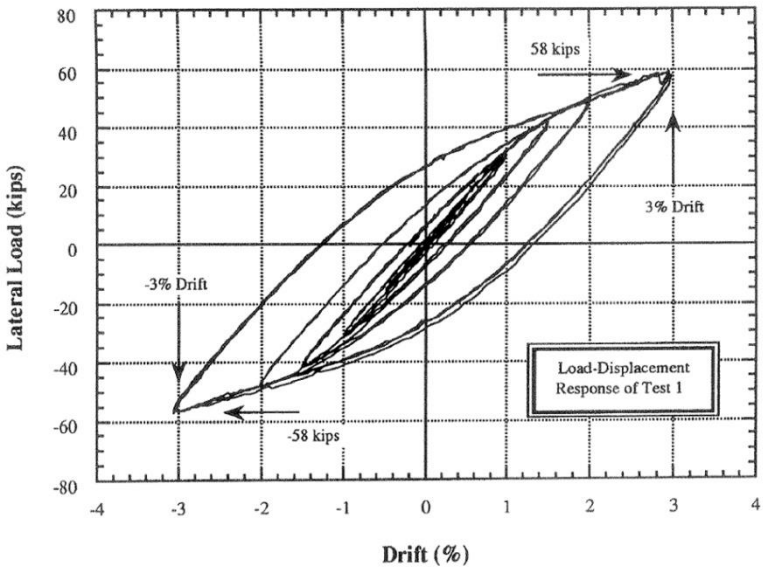

Figure 2-3 Experimental hysteretic loops (Basha and Goel, 1994)

2.2.2 STMF Seismic Design Criteria

Experimental and analytical investigation research work on STMF in the late 1980s through the 1990s (Itani and Goel, 1991; Goel and Itani, 1994b; Basha and Goel, 1994) led to the development of the STMF seismic design criteria and was adopted by building seismic specifications and codes in the late 1990s (AISC, 1997; ICBO, 1997). The design criteria was based on the concept of ductile truss girder with limit state (plastic) design approach. Under seismic latera forces, after the X-diagonal members of the middle special segment panels (when used) buckle and yield, plastic hinges form at the ends of the chord members at the ends of the special segments (with plastic hinges also forming at the base of the columns if they are fixed) as shown in Figure 2-4. This is the preferred yield mechanism of the system.

In order to achieve the preferred yield mechanism, the required shear strength of the special segments shall be calculated based on the load combinations in the applicable building code with the seismic lateral forces necessary to develop the

expected vertical shear strength, V_{ne}, of the special segment at mid-length. After designing the members of the special segments, truss members outside of the special segments including truss-to-column connections and columns are required to remain in elastic range and are designed for forces generated by the fully yielded and strain-hardened chord members in the special segment including applicable gravity loads. Goel et al. (1998) presented design concept and step-by step design procedures for both X-diagonal and Vierendeel configurations of STMFs.

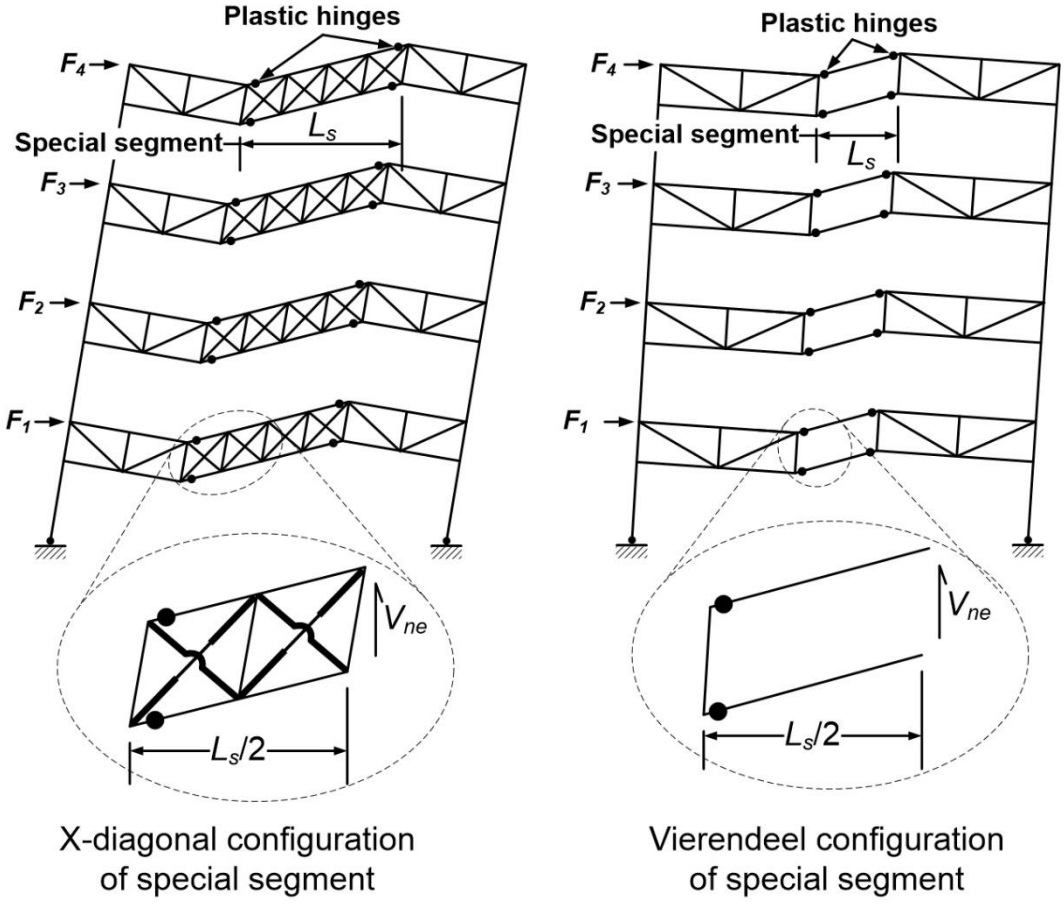

Figure 2-4 Preferred yield mechanism in STMFs

2.2.3 Expected Vertical Shear Strength of Special Segment

In order to ensure elastic behavior of the members outside of special segments, a reasonable estimate of the shear force that can be developed in the special segment is needed. Basha and Goel (1996) proposed an expression for "maximum amplified vertical shear force, V_{ss}," in the special segment as follows:

$$V_{ss} = 3.4\left(\frac{M_s}{L_s}\right) + 0.11EI\left(\frac{L - L_s}{L_s^3}\right) + \left(1.25P_{st} + 0.3P_{sc}\right)\sin\alpha \qquad [2\text{-}1]$$

where

EI = flexural stiffness of the chord members

L = span length of the truss

L_s = 0.9 times the length of special segment

M_s = flexural strength of a chord member of the special segment

P_{st} = axial tension strength of diagonal members

P_{sc} = axial compression strength of diagonal members

α = angle of diagonal members with the horizontal members

Eq. 2-1 takes an account of an overstrength factor attributed to strain hardening of material and the actual yield strength of steel which could be greater than the nominal (specified) yield strength. The overstrength factor also depends on the maximum vertical translation and rotational deformation in chords of the special segment. AISC adopted Eq. 1-1 with a slight modification and renamed V_{ss} as the "expected vertical nominal shear strength, V_{ne}," as shown in Eq. 2-2 (AISC, 1997).

$$V_{ne} = \frac{3.75 R_y M_{nc}}{L_s} + 0.075 EI \left(\frac{L - L_s}{L_s^3} \right) + R_y \left(P_{nt} + 0.3 P_{nc} \right) \sin \alpha \qquad [2\text{-}2]$$

where

$E =$ modulus of elasticity of a chord member of the special segment

$I =$ moment of inertia of a chord member of the special segment

$L_s =$ length of the special segment

$M_{nc} =$ nominal flexural strength of a chord member of the special segment

$P_{nt} =$ nominal tensile strength of a diagonal member of the special segment

$P_{nc} =$ nominal compressive strength of a diagonal member of the special segment

$R_y =$ ratio of the expected yield stress to the specified minimum yield stress

Eq. 2-2 was derived based on an assumption that the post-yield strength of the chord members in the special segment is 15% of the yield strength and that the maximum shear strength of the special segment is developed when the story drift ratio is at 3%. The V_{ne} equation remained practically unchanged though the subsequent two AISC Seismic Provisions (AISC, 2002; 2005).

2.2.4 A Modified Equation for Expected Vertical Shear Strength of Special Segment

Higher capacity demands for STMFs in high seismic areas call for much heavier members. Analytical studies by Chao and Goel (2008a) using experimental component test results conducted on double-channel specimens (Parra-Montesinos et al., 2006) led to a new design equation for the V_{ne} equation (Eq. 2-3) in the 2010 AISC Seismic Provisions (AISC, 2010a).

$$V_{ne} = \frac{3.60 R_y M_{nc}}{L_s} + 0.036 EI \left(\frac{L}{L_s^3} \right) + R_y \left(P_{nt} + 0.3 P_{nc} \right) \sin \alpha \qquad [2\text{-}3]$$

While the equation was found to be conservative (Olmez and Topkaya, 2011), it was derived strictly based on analytical studies. In addition, previous tests on STMF subassemblages with light angle sections did not adequately reflect the current practice in which large openings are demanded by architectural requirements, thereby leading to the use of multiple Vierendeel special segments, separated by intermediate vertical members. Furthermore, Eq. 2-3 still does not include the contribution of intermediate vertical members and experimental studies on STMF subassemblage made of double-channel built up members had not been carried out.

Chao and Goel (2008) proposed a V_{ne} equation which includes the contribution of intermediate vertical members as shown in Eq. 2-4. However, AISC 341-10 did not adopt the proposed equation due to the lack of experimental test results. Despite the fact, STMFs with multiple Vierendeel panels have already been utilized in practice, e.g. the Mineta San Jose International Airport in San Jose, California (Palmer, 2010; Wendt, 2011).

$$V_{ne} = \frac{3.60 R_y M_{nc}}{L_s} + 0.036 EI_c \frac{L}{L_s^3} + \frac{m}{2} \left(\frac{3.60 R_y M_{nv}}{L_s} + 0.036 EI_v \frac{L}{L_s^3} \right) \qquad [2\text{-}4]$$

An accurate estimation of the V_{ne} equation is critical to an STMF's seismic performance and economy. Underestimating the shear strength of a special segment would lead to undesirable yield mechanism due to undesirable failure of members outside the special segment. On the other hand, over-conservative estimation of V_{ne} would require costly fabrication and heavy reinforcement for the truss members, columns, and connections.

2.3 STMFs in Current Practice

An example of STMF that has been used in current practice is shown in Figure 2-5. The chord members are made of light double-angle sections with heavy double-angle sections for the intermediate vertical members in the special segment. While Eq. 2-4 was derived using the test results from heavier double-channel built-up members (2C12×20.7 and 2C12×25), there has not been an experimental test performed on STMF subassemblages with heavy intermediate vertical members. It should be noted that previous STMF tests with X-diagonals and vertical members in the special segment (Itani and Goel, 1991) were done on light double-angle sections with considerably small moment and rotational capacity; therefore, the performance of STMF subassemblages was not affected by light intermediate double-angles even they were not considered in the design.

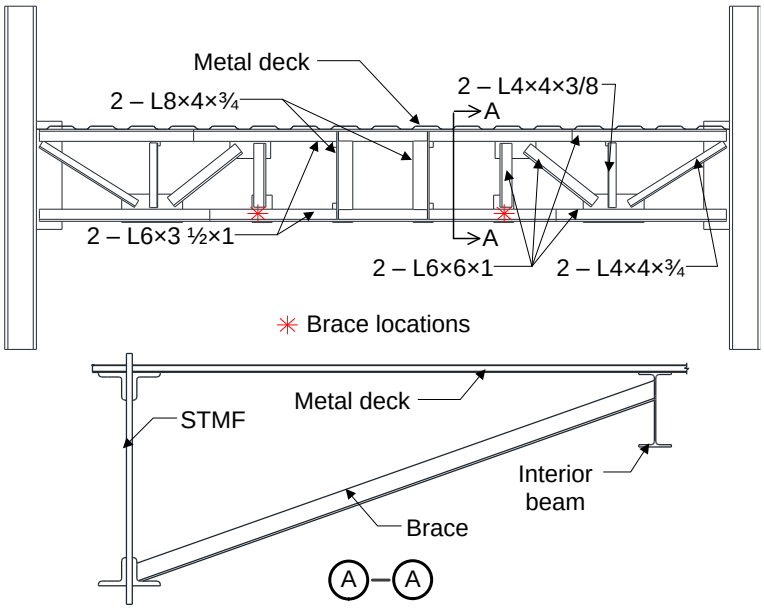

Figure 2-5 Multiple Vierendeel panel STMF

The safety issues that raise concerns about current practices are:

1. The increase in V_{ne} due to the addition of intermediate vertical members is not well understood. In addition, if the intermediate vertical members in the special segment are stronger than the chord members, it could lead to an early failure of the chord members.

   Prior analytical study suggested that 70% of the energy be dissipated by the chord members and the remainder by intermediate vertical members, unless further research could show that yielding of intermediate vertical members is not detrimental to the overall performance of an STMF (Chao and Goel, 2008a).

2. The location of stability bracing at bottom chords of the truss.

   Each flange of the chord members are required to be laterally braced at the end of the special segment to control the lateral-torsional buckling (LTB) per AISC 341-10. For the top chord, trusses are typically braced through metal deck welded to the chord member. Diagonal brace elements are typically welded to the bottom chords and the adjacent interior beams as shown in Figure 2-5. Note that AISC's Seismic Provisions does not allow welding in the plastic hinging region (i.e., the "Protected Zones"). Welding the bracing elements at the end of the special segment can potentially restrain the plastic flow when the plastic hinges occur at the chord members, thereby inhibiting the rotational capacity of the chord members and the drift capacity of STMFs.

3. Heavy welds used for attaching stiffeners or vertical members at the end of special segment (Figure 2-6).

   In practice, unlike built-up members such as double-angle where sections are welded to gusset plates at the connection, when I-shaped sections are used for the truss members, flanges of the vertical members would be welded directly to flanges of the chord members. Continuity plates are also used to transfer force between the vertical

member and the chord member. This practice introduces considerable restraint on the flanges of the chord members at the ends of the special segments (i.e., the plastic hinging regions). Consequently, large inelastic deformation capability of the chord members could be compromised. In addition, it could also lead to undesirable early fractures and, hence, reduced rotational capacity of the chord members. Note that in Figure 2-6 the chord members are tapered so the moment capacity of the chords in the special segment is smaller than that of the chords outside of the special segment.

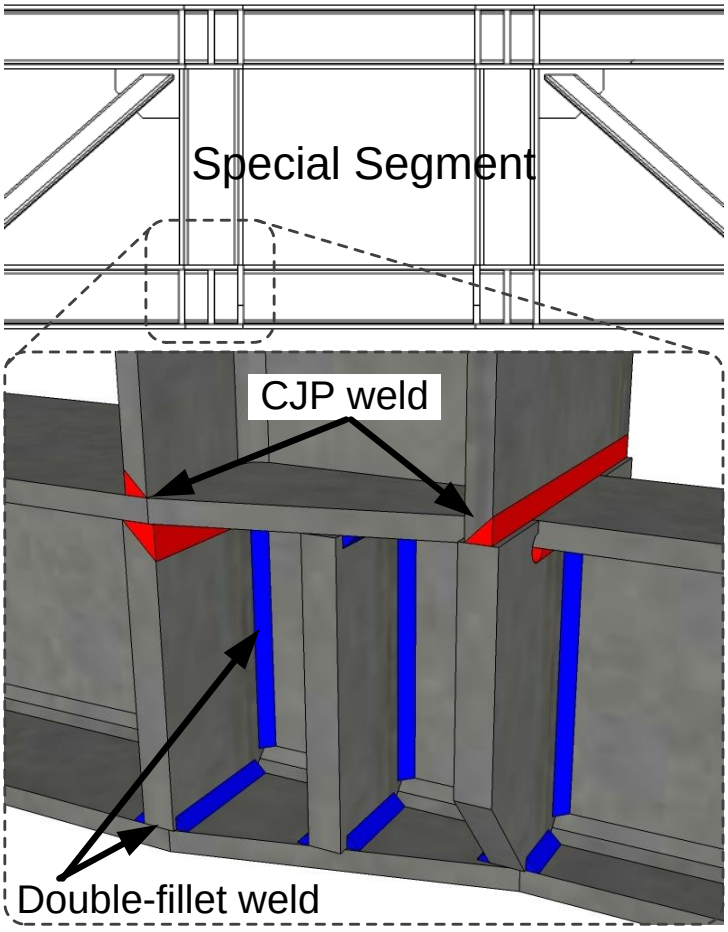

Figure 2-6 Connection detail of vertical members at the ends of special segment

2.4 Research Objectives and Scope of Study

The objective of this research is to verify the behavior of STMFs designed and constructed according to recommendations from the latest American Institute of Steel Construction (AISC) Seismic Provisions as well as to investigate the innovative detailing used in designing the truss members. Test results of a National Science Foundation (NSF) Network for Earthquake Engineering Simulation (NEES) project on two of the full-scale STMF subassemblage specimens with double-channel section as chord members and one specimen with double-hollow structural sections (HSS) as chord members, with innovative connection details, were used to verify the current V_{ne} equation as specified in the 2010 AISC Seismic Provisions for Structural Steel buildings and make suggestions for a more refined equation. At the same time, an equation which includes the contribution of intermediate vertical members will also be proposed.

The key investigations of this research are:

1. Verifying the V_{ne} equation according to latest Seismic Provisions for Structural Steel Buildings (AISC 341-10).

   Previous tests on STMF subassemblages were done with light double-angle sections. Moreover, in STMFs with multiple Vierendeel panels, the increase in V_{ne} due to the addition of intermediate vertical members has not been experimentally investigated. Heavy channel sections were used in this investigation to evaluate performances of STMFs with single and multiple Vierendeel panels as well as the contribution of intermediate vertical members.
2. Investigating seismic performance of STMFs with single and multiple Vierendeel panels.

STMFs with multiple Vierendeel panels (Figure 2-5) have been used in practice even though they lack experimental research data to verify their practicality. While the vertical intermediate members increase the redundancy of the seismic energy dissipation mechanism and allow flexibility in mechanical and architectural layouts when compared to STMFs with X-diagonals (Chao and Goel, 2008a), their presence can also significantly increase the force demand in the members outside of the special segments.

3. Verifying the proposed detailing configuration and boundary condition of plastic hinge region of the double-channel chord members in the special segment.

   Both top and bottom chord members are required to be laterally braced at the end of the special segment to control LTB per AISC 341-10. In this research, an innovative and practical detailing configuration for double-channel flexural members was developed and test results showed that LTB could be eliminated, which led to a more stable and ductile hysteretic behavior of the double-channel members. With the proposed detailing configuration the need for lateral bracing could be eliminated. STMF subassemblage tests were conducted to verify the viability of this new detailing.

4. Verifying whether double-channel built-up chord members with the proposed detailing could accommodate large rotational demand.

   As opposed to moment frames in which the plastic rotational demand in beams is close to the story drift ratio, the demand of chord members in special segments of STMF's special segment is significantly higher than the story drift ratio. For example, for a typical STMF with the ratio of truss girder span to the length of special segment equaled to 3.75, the rotational demand of the chord members is as high as 6% at a 2% story drift ratio (Simasathien et al., 2014). Previous research on double-channel

flexural members showed that once the onset of LTB was delayed, the hysteretic behavior of the member became significantly more stable and ductile (Parra-Montesinos et al., 2006). In this research, an innovative and practical detailing configuration that could prevent LTB without the need for lateral brace near plastic hinging region for double-channel flexural member was developed and implemented in the full-scale STMF subassemblages.

5. Investigating the behavior of an STMF with double-HSS built-up chord and web members and to determine if the double-HSS built-up chord members can accommodate the large rotational demands in STMFs.

   HSS are highly efficient structural sections used in resisting compression, torsion, and bending. Their high torsional rigidity generally eliminates LTB, thereby eliminating the need for lateral bracing in beam-type members. Consequently, the plastic rotational capacity and strength degradation rate are primarily governed by flange local buckling (FLB) and web local buckling (WLB). Fadden and McCormick (2012) investigated the cyclic responses of single-HSS beam-column connections. The failure mode was largely controlled by the effect of local buckling. They concluded that larger width-to-thickness ratios of the flanges (*b*/*t*) led to a more significant decrease in the moment capacity as well as rotational capacity due to the importance of the flange in resisting cyclic bending. They suggested that *b*/*t* ratios below 25 and *h*/*t* ratios below 40 are necessary to maintain 90% of the maximum moment strength at beam rotations of 0.04 radian.

6. Investigating the current requirements for the stability bracing of trusses.

   According to AISC 341-10, the required strength of the lateral brace, P_u, shall be $0.06R_yF_yA_f$, where A_f is the gross area of the flange (either top or bottom flange)

of the special segment chord member. This requirement was based partly on what was used during the development of the first specifications for STMF in which specimens were constructed using light double-angle sections as chord members in the original testing program (AISC, 2010a). With heavy double-channel sections, this requirement could be underestimated. However, the requirement might be over-conservative for STMFs with double-HSS as chord members since HSS do not suffer from LTB.

7. Investigating the possibility of relaxing splicing locations of the chord members.

   AISC 341-10 states that “splicing of chord members shall not be permitted within the special segment, nor within one-half the panel length from the ends of the special segment.” This requirement presents a post-earthquake limitation to rehabilitation of STMFs that suffer damages from seismic activity.

8. Investigating the possibility of increasing the length-to-depth (aspect) ratio of the Vierendeel panel in the special segment.

   AISC 314-10 Provisions state that the length-to-depth ratio of the special segment in an STMF shall neither exceed 1.5 nor be less than 0.67. The lower bound was suggested to limit the rotational demand of the chord member because rotational demands of the chord members in the special segment of STMF are much larger than that of flexural members in typical moment frame systems. For STMFs of the same overall length and depth, the special segments with larger aspect ratios will reduce rotational demand of the chord members in a special segment. For the specimens in this research, the aspect ratio of 2.5 were chosen for all specimens to purposely violate this requirement.

9. Investigating the possibility of relaxing the spacing of stitching for build-up chord members.

According to AISC 341-10, “spacing of stitching for built-up chord members in the special segment shall not exceed $0.04Er_y / F_y$, where r_y is the radius of gyration of individual components about their weak axis.” If the spacing of the stitching could be relaxed, in other words, reducing the number of stitches, fabrication cost and time could be reduced.

As previously mentioned, for STMFs of the same overall length and depth, the special segments with larger aspect ratios will reduce rotational demand of the chord members in a special segment. On the other hand, a large length-to-depth ratio of the special segment can lead to the reeducation of overall lateral stiffness of an STMF. The relationship between the story drift ratio and plastic hinge rotation of the chord members, as shown in Figure 2-7, can be approximately estimated by Eq. 2-5 (Goel and Chao, 2008a).

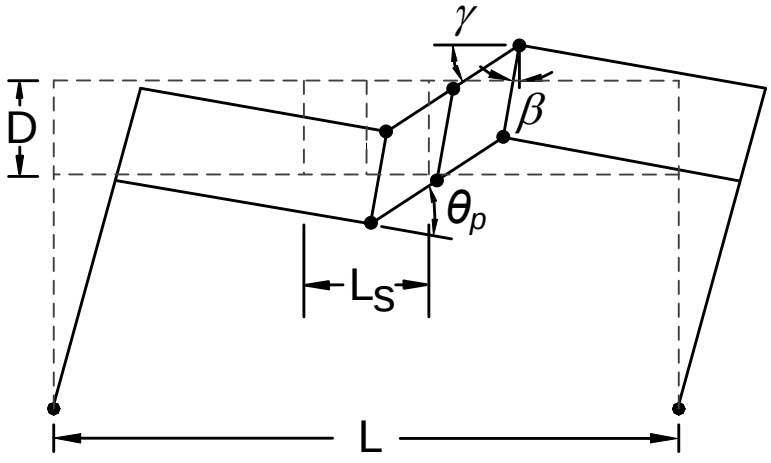

Figure 2-7 Deformed shape of an STMF

$$\theta_p = \gamma + \beta \approx \frac{L}{L_S} \times (story\ drift) - 0.015(rad.) \quad [2\text{-}5]$$

For a typical STMF with the ratio of truss girder span to the length of the special segment of 3.75, the relationship between the story drift and the plastic rotation of the special segment chord members is shown in Table 2-1. It can be seen that the plastic rotational demand of the chord member in the special segment is as high as 6% and 10% at 2% and 3% story drift ratios, respectively. These are beyond the typical rotational capacity of flexural members used in special moment frames.

Table 2-1 Relation Between Plastic Rotation of Chord Members and Story Drift Ratio of a Typical STMF

Story Drift Ratio (%)	Plastic Rotation of Chord Members (rad)
0.50	0.00
0.75	0.01
1.00	0.02
1.25	0.03
1.50	0.04
1.75	0.05
2.00	0.06
2.25	0.07
2.50	0.08
2.75	0.09
3.00	0.10

For the specimens in this research, an aspect ratio of 2.5 were chosen for the subassemblage specimens to purposely violate AISC requirements. Preliminary nonlinear pushover analysis indicates that, with this aspect ratio, an STMF can maintain high lateral stiffness while the rotational demand of the chord reduces to the level that a ductile member is able to sustain.

Chapter 3

Part I : Experimental Program

3.1 Overview

The experimental program consisted of two parts. The first part, component tests, involved cantilevered double-channel built-up members under reversed cyclic bending. The purpose of the component test was to investigate behaviors of the members under different connection details representing the chord members at the end of special segments and the intermediate vertical members in the special segment and also to establish a refined plastic hinge model for the nonlinear analysis of the full-scale STMF subassemblages in the second part.

Using test results from the component tests, three full-scale STMF subassemblages were designed to resemble the overall dimensions of a prototype building previously studied (Goal and Chao, 2008). The specimens were analyzed using nonlinear pushover analysis based on the expected vertical shear force demands that would be imposed on the chord members in the special segment. The analysis results were then used to determine an equivalent lateral force for the design of the first and second specimens. The design of elements outside of the special segments, including truss members, columns, and connections, was based on the capacity design approach such that those elements would remain elastic when V_{ne} was reached in the middle of the truss girder.

3.2 Component Tests

3.2.1 Component Test Specimens Representing Chord Members in the Special Segment of a Prototype STMF with Single Vierendeel Panel

Component specimen C-2C12-1 and C-2C12-2 represent half of the chord member in a special segment of a prototype STMF. The overall specimen dimensions

and the details at the plastic hinge region including the welds for the first set of component test specimens are shown in Figure 3-1. Each specimen consisted of a 1 in.-thick gusset plate and a double-channel built-up member made of 2C12×20.7 section. The end of the gusset plate was welded to a W14×193 reaction frame column. The proposed innovative detailing composed of an extended “weld-free” region between the gusset plate and the member allowing the member to freely slide against the gusset plate while providing a self-stabilizing lateral support at the plastic hinge region. Two pair of web stiffeners, one on each side, were also welded to the webs, the top and bottom flanges of the specimens. This detailing provided a direct LTB support without violating the AISC’s protected zone requirements. An additional 2C12×20.7 section was also welded to the gusset plate perpendicular to the specimen to simulate the vertical members at the end of special segments. The loading point represented the mid-length of the chord members in the special segment of the STMF subassemblage in the full-scale STMF subassemblage experimental program (discussed later). The first specimen (C-2C12-1) represented the truss chord members at the end of the special segment where the end of vertical members are welded up against the flanges of chord members (similar to the current practice shown in Figure 2-5 and 2-6), while the second specimen (C-2C12-2) simulated the condition where vertical members are not welded up against the chord members.

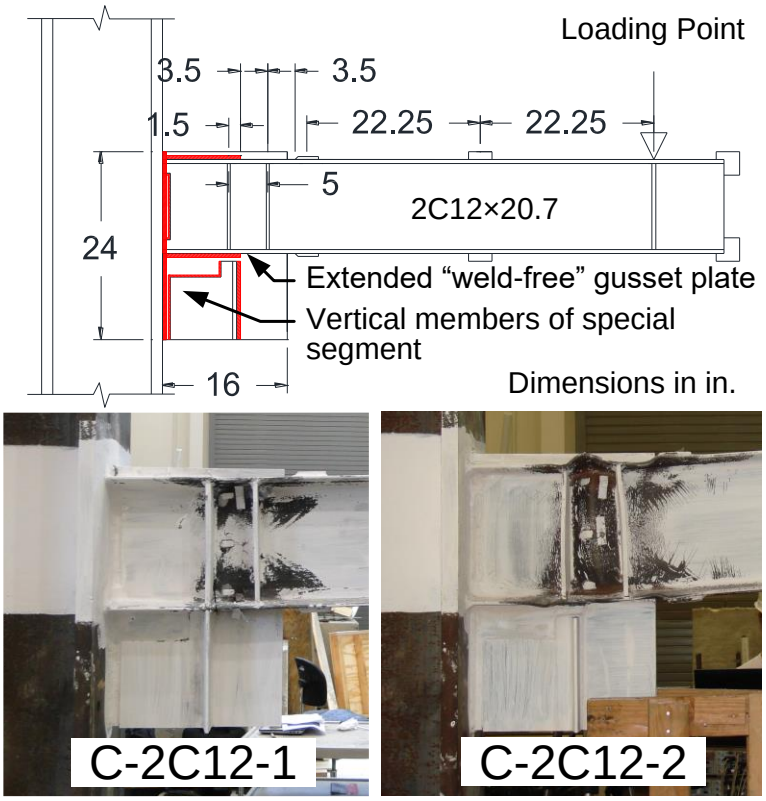

Figure 3-1 2C12×20.7 component specimens

The displacement history planned for the component test specimens similar to Figure 3-2 was developed based on a preliminary nonlinear pushover analysis of an STMF subassemblage similar to the one in the full-scale testing program (discussed later). It consisted of six cycles at 0.0078, 0.0105, and 0.018 radian member rotation, four cycles at 0.0265 radian member rotation, and two cycles at 0.0435, 0.0605, 0.0731, and 0.0911 radian member rotation. These member rotations corresponded to story drift ratios according to the AISC’s loading protocol for beam-to-column moment connections (AISC, 2010a) except an additional intermediate story drift ratio of 2.38% was added to increase stringency. The relationship between the member rotations and the story drift ratios was obtained by performing a nonlinear pushover analysis of the full-scale STMF

subassembly specimens and assuming that inflection points occur at mid-height of columns above and below the STMF. This prototype subassemblage had the same dimensions as subassemblage used in full-scale tests but with slightly different member sizes. The moment versus member rotation response of the 2C12×20.7 component specimens are shown in Figure 3-3 along with the calculated plastic moment capacity, M_p, based on nominal section properties. As shown in Figure 3-3, both specimens exhibited higher capacities than the calculated plastic moment capacity. While specimen C-2C12-1 had a higher capacity, the rotational capacity (equivalent to approximately 0.043 radian member rotation) was substantially smaller than that of specimen C-2C12-2 which exhibited a stable response and significantly larger energy dissipation capacity up to failure at member rotation approximately 0.09 radian. This was due to the restraint of inelastic strains of the flanges by the perpendicular element representing the vertical members in a truss girder.

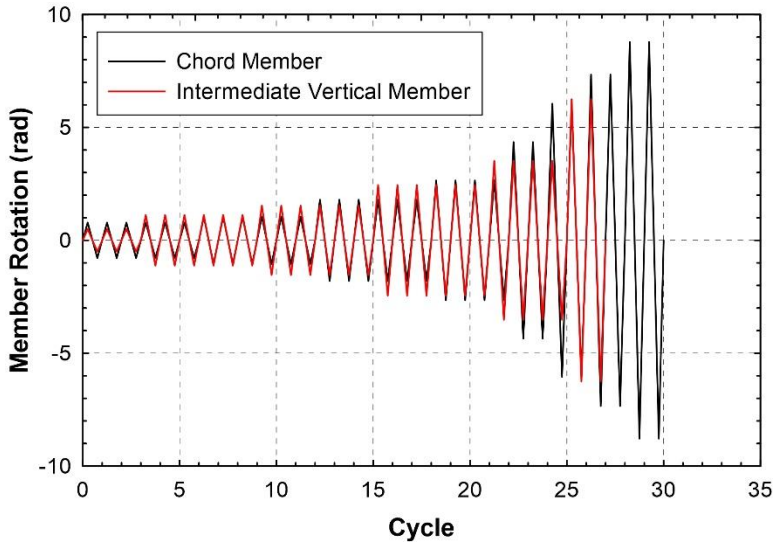

Figure 3-2 Displacement history of component specimens

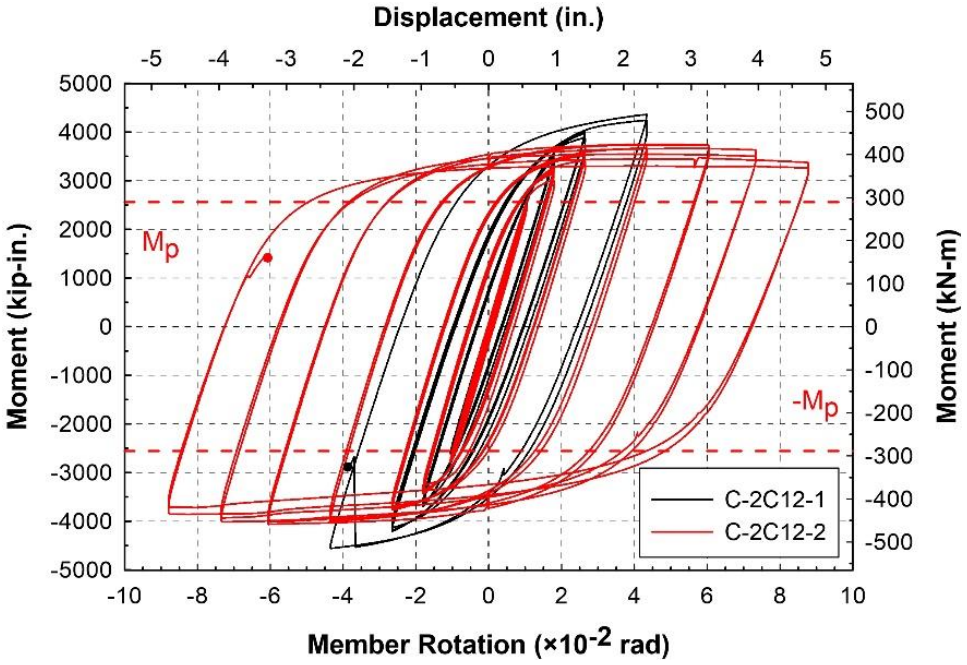

Figure 3-3 Moment vs. member rotation response of 2C12×20.7 component specimens

3.2.2 Component Test Specimens Representing Intermediate Vertical Members in the Special Segment of a Prototype STMF with Multiple Vierendeel Panels

The second set of component test specimens was made of 2C6×13 sections representing the intermediate vertical members inside the special segment of the full-scale STMF subassemblage as shown in Figure 3-4. The displacement history for this set of specimens consisted of three cycles at 0.005 radian member rotation, six cycles at 0.0112, 0.0154, and 0.0245 radian member rotation, four cycles at 0.0352 radian member rotation, and two cycles at 0.0625, and 0.1059 radian member rotation. When compared to loading protocol of specimens representing the chord member in STMF subassemblage, it can be seen that the rotational demand of the intermediate members was much greater than that of the chord members at the same story drift ratio.

The main investigation for this set of specimens was concerned with whether the web stiffeners in the plastic hinge region of the intermediate vertical members could enhance rotational capacity of 2C6×13 section. According to the test results on 2C12×20.7 section, web stiffeners potentially helped reduce web buckling and flange buckling amplitudes. Since *h*/*t* ratio of 2C6×13 was only 11.0, compared to 36.3 of 2C12×20.7, web stiffeners might not have the same benefit on behavior of the deeper channels. As shown in Figure 3-5, the moment versus drift ratio response of the specimen with the stiffeners (C-2C6-1) was not stable once the peak moment was reached at approximately 6 radian member rotation. Specimen without stiffeners (C-2C6-2) exhibited a superior response compared to the previous specimen. The responses of the specimen C-2C6-2 were stable up to the end of positive 10.6 radian member rotation cycles. Note that the unsymmetrical response was due to the limited tensile capacity of the actuator. As can be seen in Figure 3-4, the presence of stiffeners and welds restrict the spreading of inelastic deformation which was mainly contained between the web stiffeners. Without stiffeners, inelastic deformation spread over approximately one member depth from the end of the welds in the web of the member and about twice as much on the flanges.

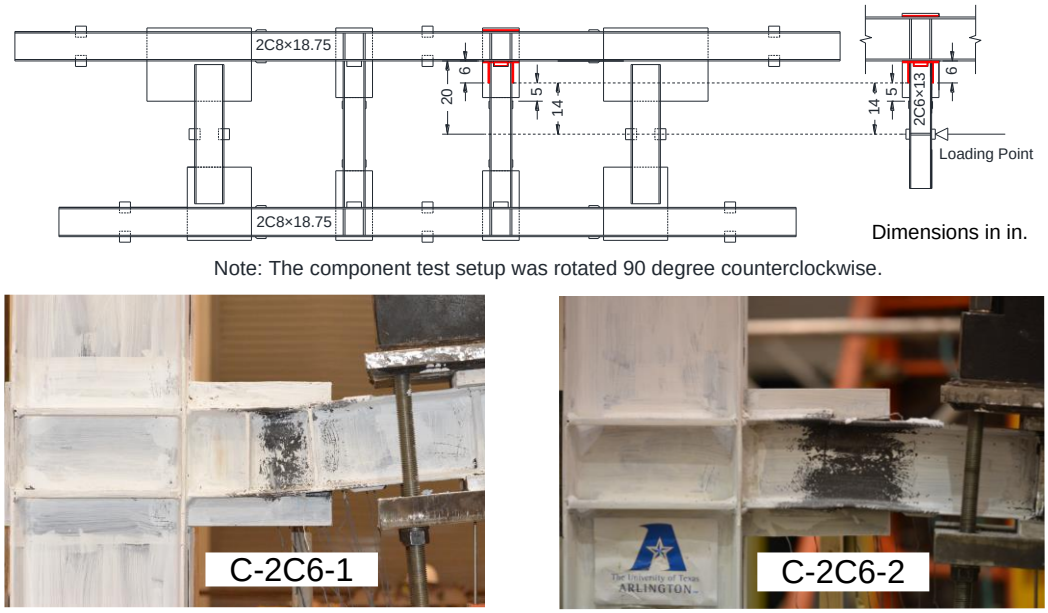

Figure 3-4 2C6×13 component specimens

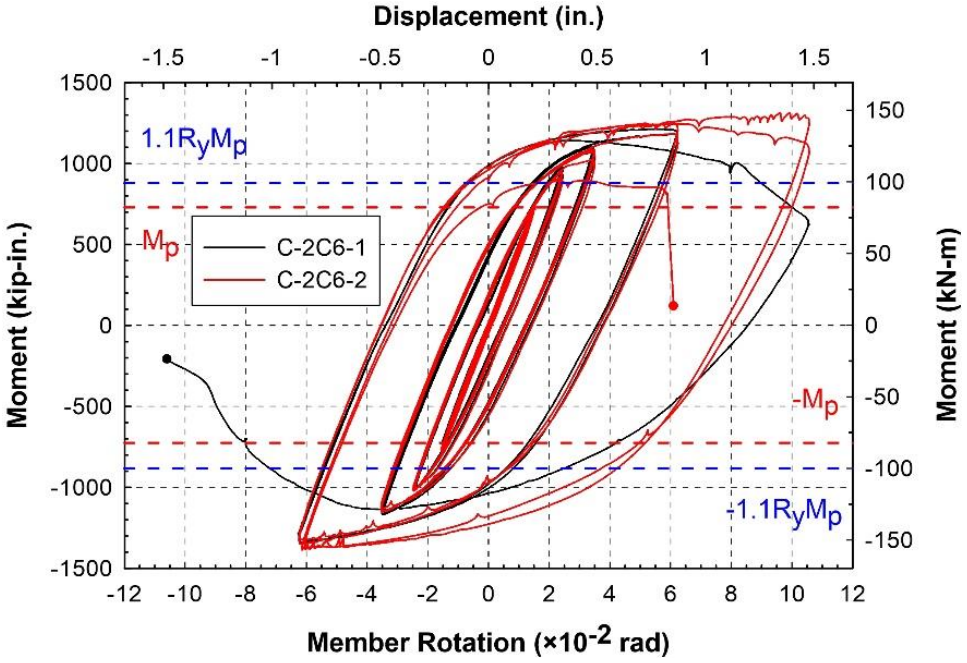

Figure 3-5 Moment vs. member rotation response of 2C6×13 component specimens

3.2.3 Component Test Specimens Representing Chord Members in the Special Segment of the full-scale STMF subassemblage with Single Vierendeel Panel

3.2.3.1 Component Specimen with 2C8×18.75

Component test specimen C-2C8 was made of 2C8×18.75 section. This specimen represented the chord members of the full-scale STMF subassemblage in the second part of the experimental program as shown in Figure 3-8. The loading history of this specimen is similar to that of 2C12×20.7 specimens. It consists of six cycles at 0.0069, 0.092, and 0.0153 radian member rotation, four cycles at 0.0217 radian member rotation, and two cycles at 0.0361, 0.0538, 0.0714, and 0.0911 radian member rotation. Since 2C8×18.75 section has a smaller *h*/*t* ratio of 13.5, which is close to that of 2C6×13, and the test results of 2C6×13 sections showed that stiffeners were not beneficial, the web stiffeners were not used in this specimen. It can be seen, in Figure 3-9, that this specimen exhibited a stable response up to the peak member rotation of 9.1 radian and did not showed strength degradation until failure. Yielding of the specimen spread over approximately 2.5 times the member depth along the flanges indicating an exceptional energy dissipation capacity.

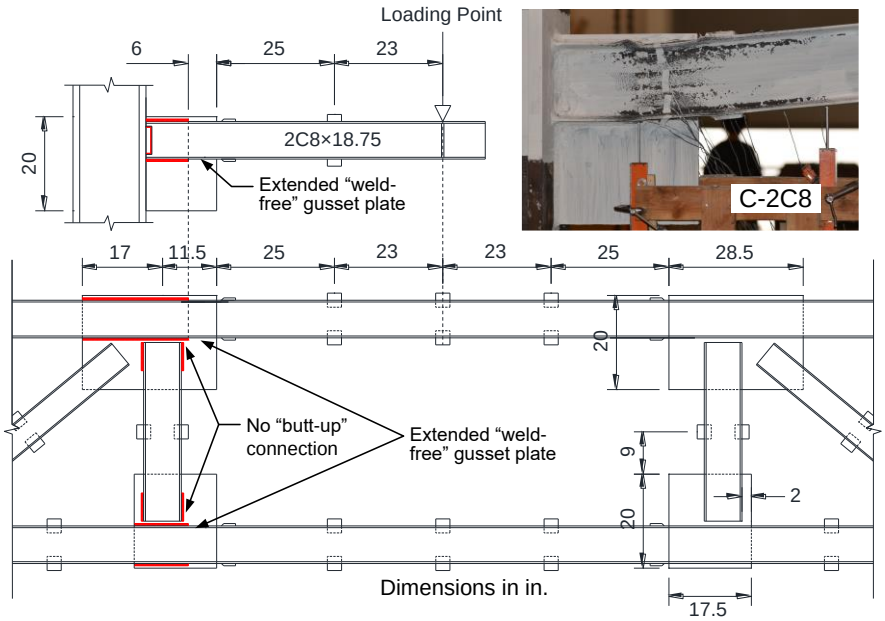

Figure 3-6 2C8×18.75 component specimen

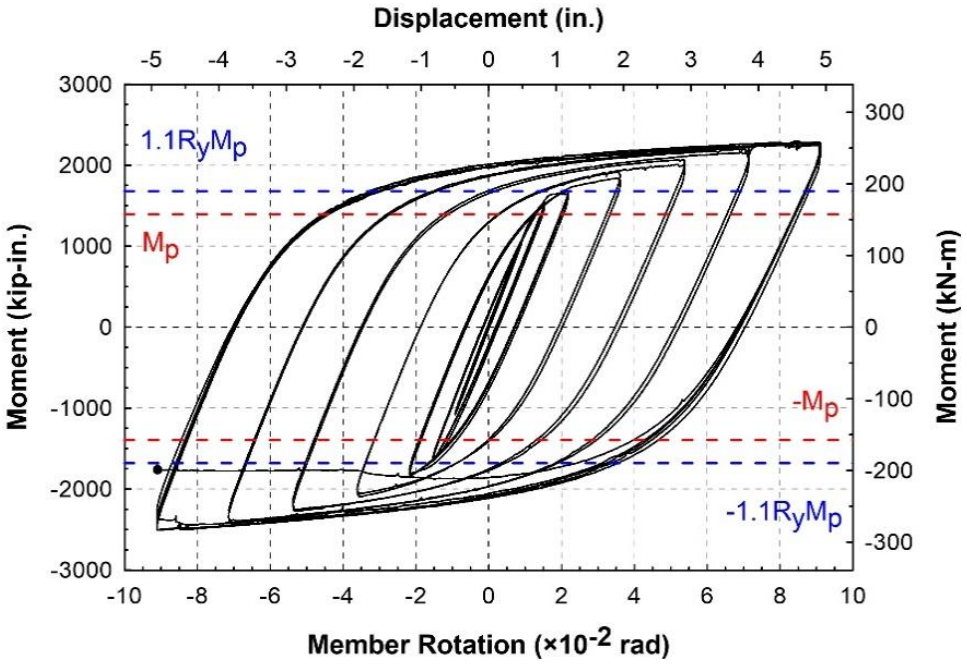

Figure 3-7 Moment vs. member rotation response of 2C8×18.75 component specimen

3.2.3.2 Component Specimen with 2HSS8×4×1/2

A component specimen made of 2HSS8×4×1/2 (C-2HSS8) representing the chord members of the full-scale STMF subassemblage in the second part of the experimental program, as shown in Figure 3-8, was tested to investigate the behavior of the double-HSS build-up member under cyclic flexural load. Its overall dimensions were similar to specimen C-2C8. The displacement history for this specimen consisted of six cycles at 0.0079, 0.0105, and 0.018 radian member rotation, four cycles at 0.0265 radian member rotation, and two cycles at 0.0435, 0.0605, 0.0731, and 0.0911 radian member rotation.

Figure 3-9 shows hysteresis response of the double-HSS component along with the nominal plastic moment capacity, M_p. It can be seen that the member exhibited a stable response without strength degradation up to member rotation of 0.06 radian. Afterward, strength maintained a slow degradation rate until the first cycle of 0.09 radian member rotation. As shown in Figure 3-10, the local buckling in the double-HSS section was much less severe than that observed in the single-HSS section (Fadden and McCormick, 2012) that had similar strength as the double-HSS used in this research. This result proved that the double-HSS is capable of sustaining high rotational demand required by special segments in STMFs. The strength of the member drastically dropped due to fracture propagation in the following cycles and the test was terminated when the strength was approximately 40% of the peak strength (Figure 3-9). The member did not exhibit lateral torsional buckling (Figure 3-10) as previously observed in the double-channel built-up members for STMF in a previous study (Parra-Montesinos et. al, 2006).

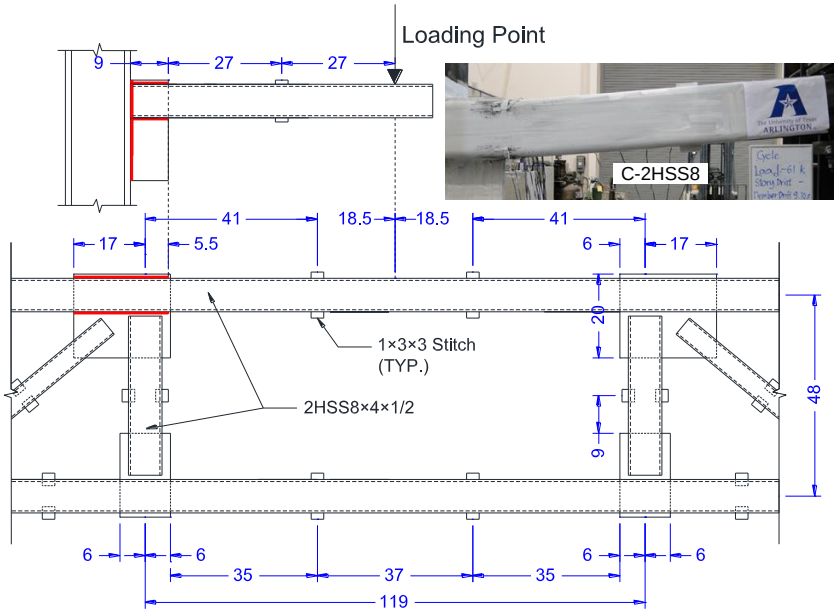

Figure 3-8 2HSS8×4×1/2 component specimen

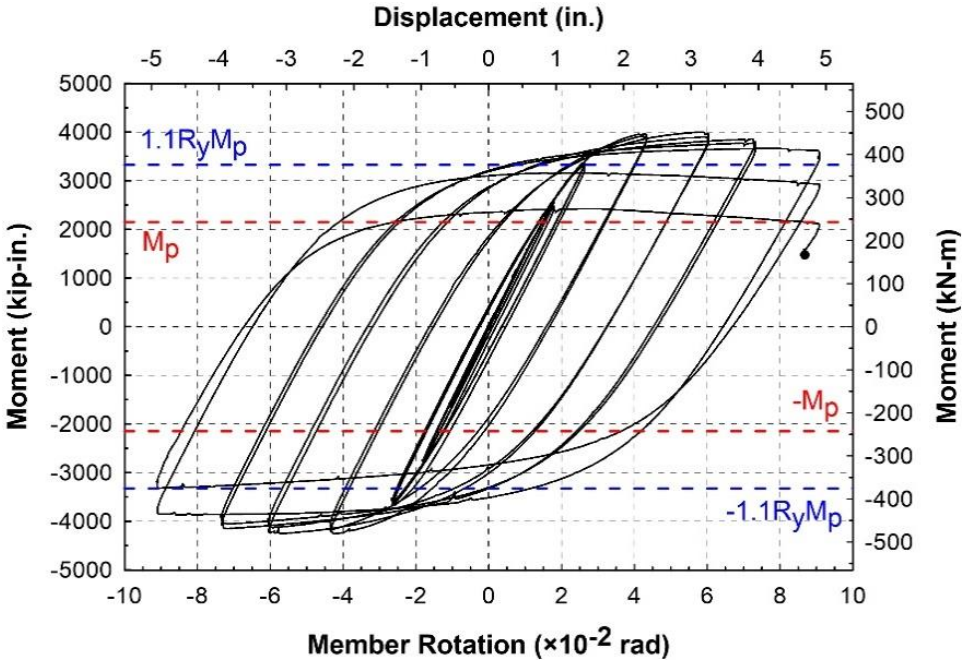

Figure 3-9 Moment vs. member rotation response of 2HSS8×4×1/2 component specimen

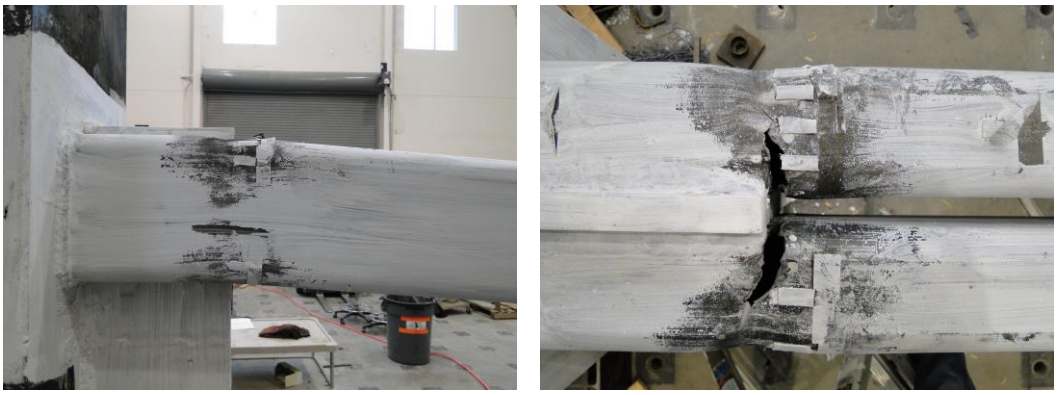

Figure 3-10 Specimen C-2HSS8 at end of test

3.3 Component Test Findings

3.3.1 Double-channel built-up members

The component test results suggested that double-channel built-up members could sustain large moment and rotational capacities by employing the new proposed details and boundary condition at the end of the special segment where a vertical web member met a chord member. Followings were the main reasons for such improvement:

1. The extended gusset plate with “weld-free” zone at the end of the special segment provided self-stabilizing lateral support which resulted in elimination of LTB at plastic hinging region of chord member.
2. For a joint at the end of the special segment, flanges of the vertical member were not welded to the flange of the chord member. This boundary condition would allow large inelastic deformation of the plastic hinge to freely spread, thus avoiding premature failure due to fracture.

3.3.2 Double-HSS built-up members

Double-HSS have the advantages of minimizing lateral torsional buckling and maximizing compactness in the flanges as compared to single HSS with the same flexural capacity. Component test results indicated that using double-HSS truss members

is a viable alternative for STMFs in high seismic regions. The benefits of using double-HSS are as follows:

1. Effective delay of FLB and an enhanced rotational ductility is accomplished by reducing the width-to-thickness ratio (*b*/*t*) without increasing the wall thickness of the members. A double-HSS flexural member can have similar moment capacity with an equivalent single-HSS beam, while having approximately half of the flange *b*/*t* ratio.
2. The stringent compactness ratio ($0.55\sqrt{E/F_y}$) requirement for walls of HSS in the AISC Seismic Provisions (2010a) limits the single-HSS members that could be practically used for chord members of STMFs to satisfy both compactness and strength requirements. Using the proposed double-HSS members (2HSS8×4×11/2; *b*/*t* = 5.6 and *h*/*t* = 14.2) increases the number of sections that can be selected for STMFs. Note that the *b*/*t* and *h*/*t* ratio is 13.9 for rectangular HSS with specified minimum yield stress of 46 ksi (ASTM A500/A500M Gr. B).
3. Double-HSS members provide stronger sections for STMFs in high seismic regions as compared to double-angle sections.
4. Double-HSS members utilize simple gusset plate connections with direct welding between the gusset plate and the double-HSS without the inconvenience of making the necessary slots at both ends of a member in order to obtain welded gusset plate connections for single-HSS truss members.

3.4 Full-scale STMF Subassemblage Tests

3.4.1 STMF with Single Vierendeel Panel Special Segment (STMF-2C8-1)

The chord members of STMF-2C8-1 were double-channel built-up members made of 2C8×18.75 section. The overall length (center-to-center of the columns) was 31 ft, 9 in. The length of the special segment was 9 ft, 11 in. long and the depth of the truss

was 4 ft. Length of the weld-free extended part of the gusset plate was 0.75 times the depth of the chord member and there was a 1-in. gap between the ends of the vertical members at the end of the special segment and the flanges of the chord members. Figure 3-11 shows the overall dimensions of the first subassemblage specimen along with the proposed details at the end of the vertical and chord members in the special segment as follows:

1. The stitch spacing on the chord members inside the special segments is greater than the AISC 341-10 requirement (13.9 in. for C8×18.75).
2. Extended gusset plates with “weld-free” zone at the end of the special segment providing self-stabilizing lateral support at plastic hinge regions of chord members.
3. Connections at the end of vertical members near the special segment were not butted up against the chord members. This arrangement allows large inelastic deformations to freely spread thus increasing the rotational capacity of the chord members.

It should be noted that the members outside of the special segment in this specimen were designed considering the higher maximum expected vertical shear strength of the special segment induced by the addition of intermediate vertical members in the second subassemblage specimen. This was done so the members outside of the special segment could be reused for the subsequent test.

3.4.2 STMF with Multiple Vierendeel Panels Special Segment (STMF-2C8-2)

After subassemblage specimen STMF-2C8-1 was tested, the damaged section (contained within the special segment) was cut out and the special segment of specimen STMF-2C8-2 (partial subassemblage), which had three Vierendeel panels made of 2C8×18.75 chord members along with two intermediate vertical members made of the 2C6×13 section, was spliced to the remaining undamaged (remain elastic during the test)

part of subassemblage STMF-2C8-1 (Figure 3-12). Unlike in current practice where the intermediate vertical members were heavier than the chord members (Figure 2-5), the nominal moment capacity of 2C6×13 section was 52% of that of 2C8×18.75 section The dimensions of the special segment are shown in Figure 3-13. Special details used in subassemblage STMF-2C8-1 were also implemented in STMF-2C8-2 along with additional special details at the end of the intermediate vertical members similar to that of component test specimen C-2C6-2. The additional special features for this specimen were as follows:

1. Multiple Vierendeel panels in the special segment.
2. Intermediate vertical members were butted up against the chord members with web cut out in order to increase the welding area between these members and the chord members to the gusset plate. It is worth to mention that the moment and rotational demand of the chord member at these locations were smaller than at the ends of the special segment where plastic hinges would form. As a result, welding the flanges of the intermediate vertical members to the flanges of the chord members would not lead to premature fracture of the chord members.
3. Web stiffeners acting as continuity plates on the chord members were used to transfer load at the end of intermediate vertical members to the chord members in the special segment.

3.4.3 STMF with Single Vierendeel Panel Special Segment and Double-HSS as Chord Members (STMF-2C8-2)

The last STMF subassemblage specimen in the experimental program was constructed with double-HSS built-up sections (2HSS8×4×1/2) as chord members. The vertical members at the ends of special segment were the same sections as the chord members as suggested by Basha and Goel (1994). The vertical and diagonal members

outside of the special segment were also double-HSS built-up sections (2HSS5×5×3/8). The overall dimensions were the same as the previous two specimens. Figure 3-14 shows the overall dimensions of the subassemblage specimen. The proposed details at the end of vertical and chord member in the special segment (also shown in Figure 3-14) were as follows:

1. Extended gusset plates with “weld-free” zone at the end of the special segment were not utilized since HSS do not suffer from LTB.
2. Connections of vertical members at the end of the special segment were not butted up against the chord members in order to allow large inelastic deformations to freely spread. This was done to prevent any restraint at the plastic hinge region which reduces the rotational capacity of the chord members.
3. Flare-bevel groove welds were used between truss members and gusset plates throughout the truss.

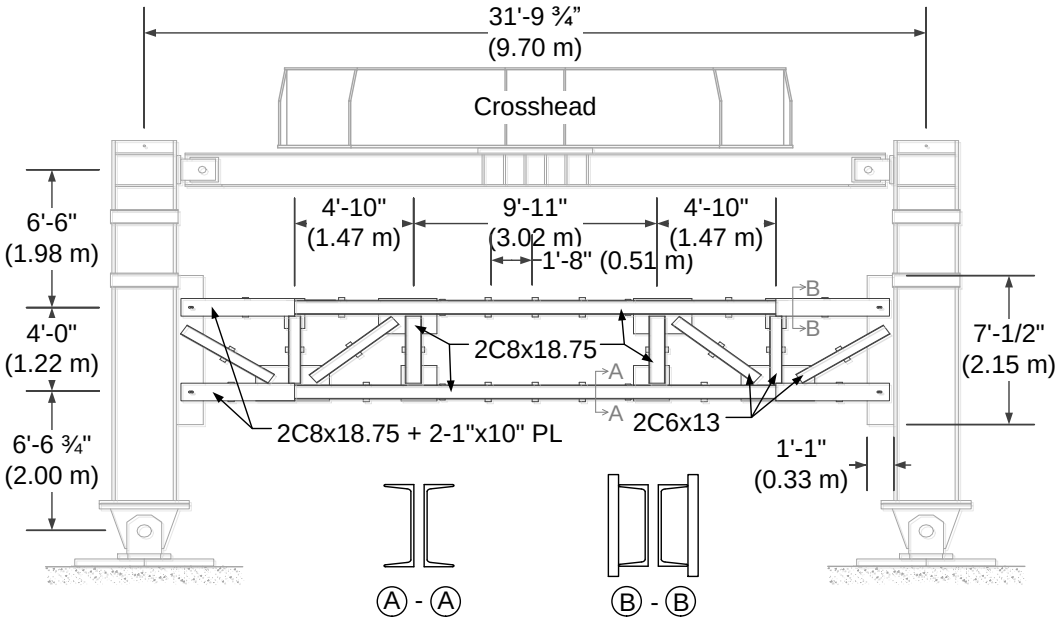

(a)

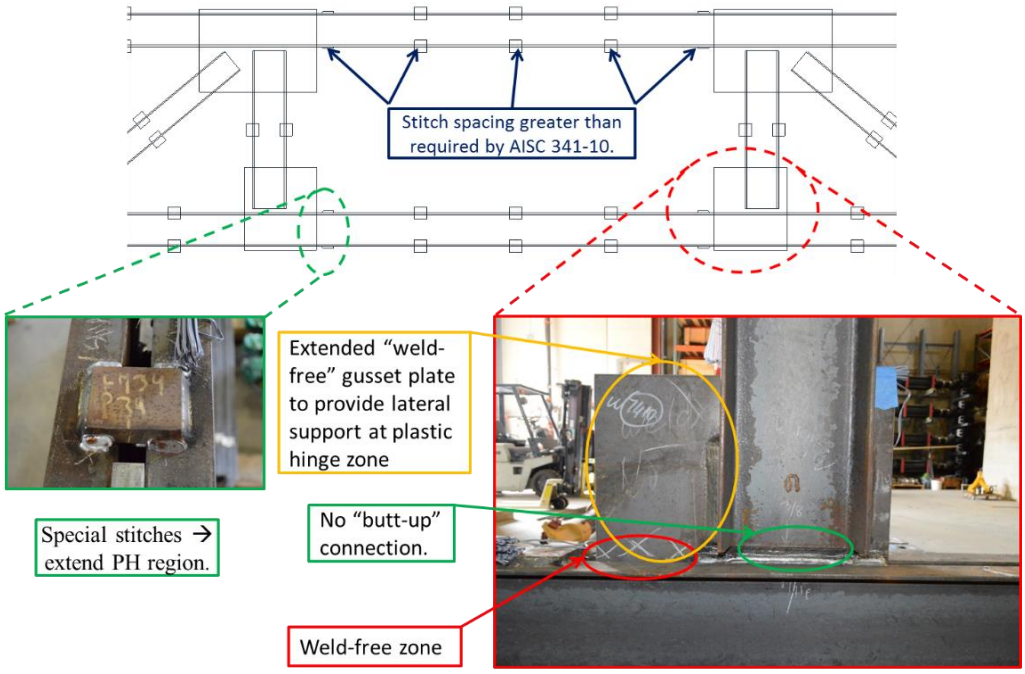

(b)

Figure 3-11 Subassemblage specimen STMF-2C8-1: (a) overall dimensions; (b) proposed details

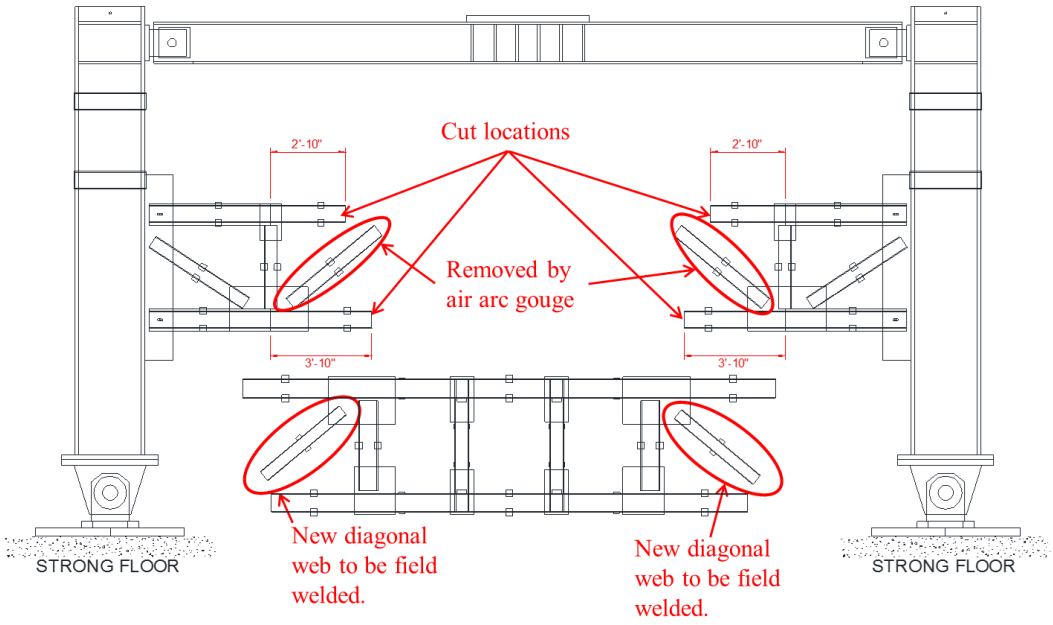

Figure 3-12 Splicing of specimen STMF-2C8-2

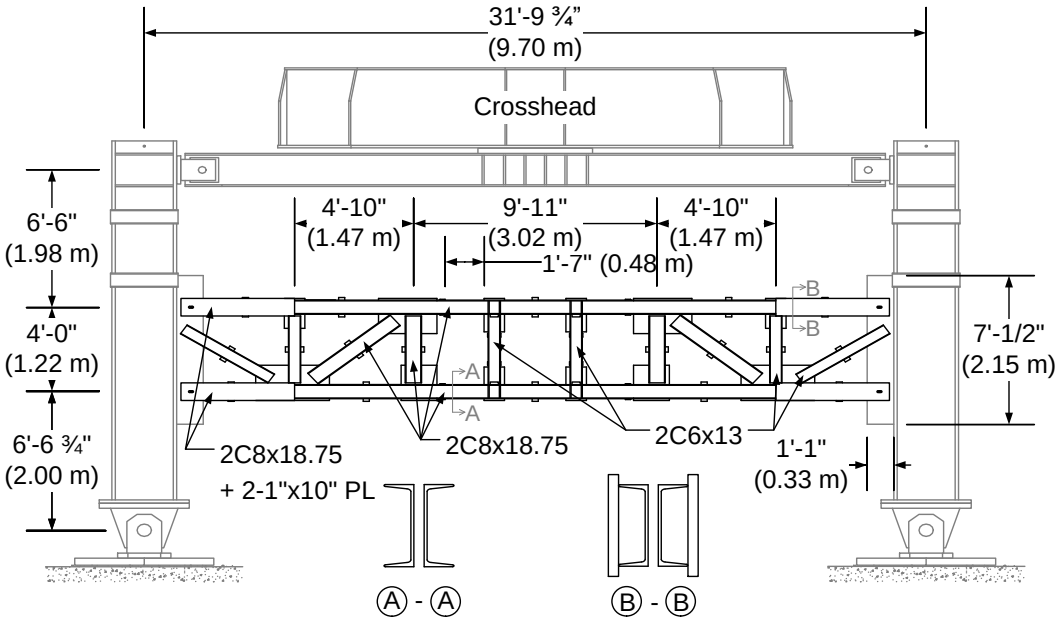

(a)

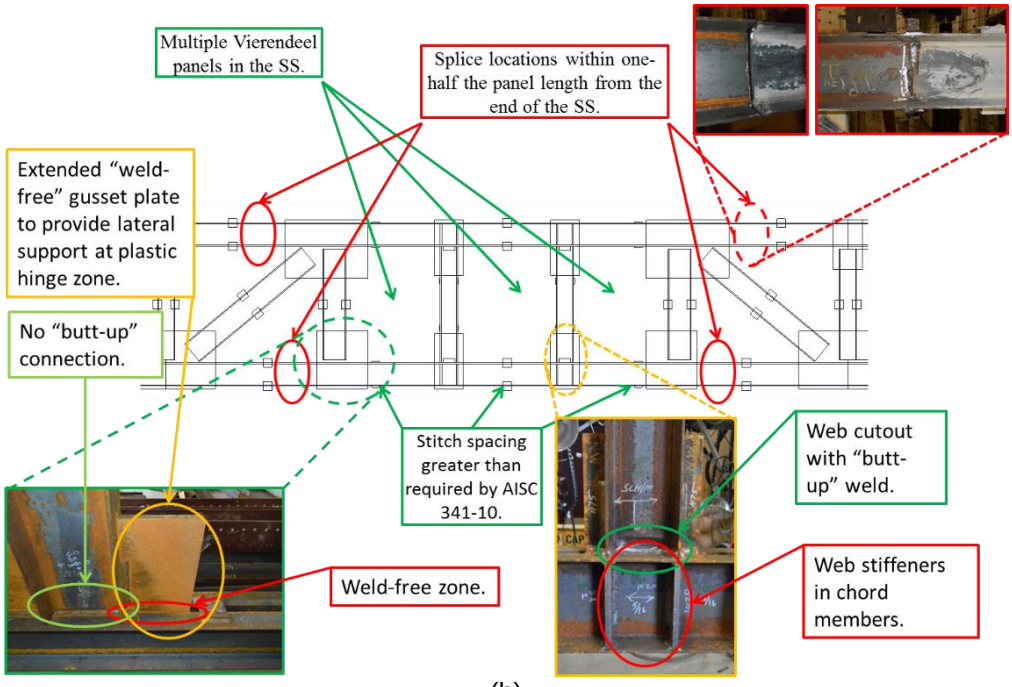

(b)

Figure 3-13 Subassemblage specimen STMF-2C8-2: (a) overall dimensions; (b) proposed details

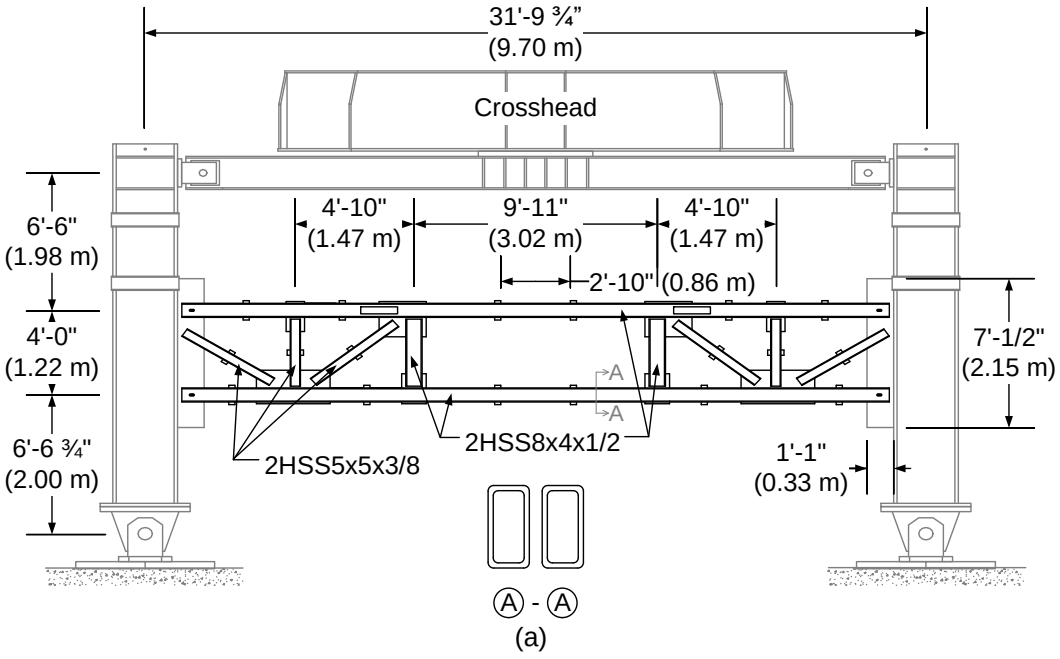

(a)

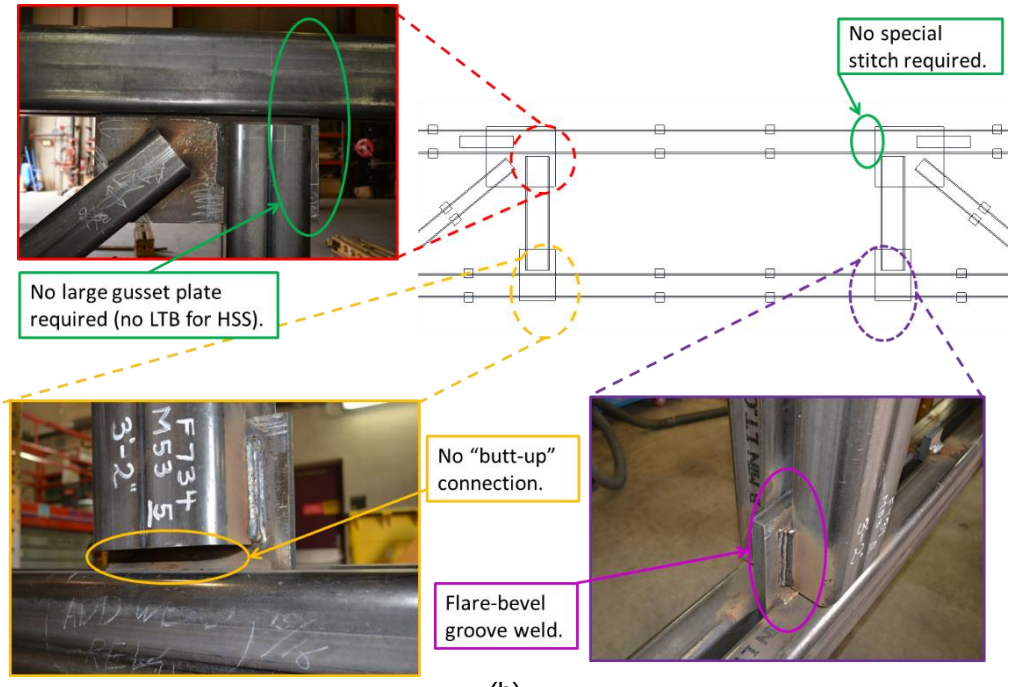

(b)

Figure 3-14 Subassemblage specimen STMF-2HSS8: (a) overall dimensions; (b) proposed details

3.5 Subassemblage Test Setup and Procedures

The overview of the test setup at the University of Minnesota's Multi-Axial Subassemblage Testing (MAST) Laboratory, a member of the George E. Brown Jr. Network for Earthquake Engineering Simulation (NEES), is shown in Figure 3-15. Stability bracing of the truss was provided, as required by AISC 341-10, through the truss lateral support system. However, it was located slightly outside of the special segment rather than at the end of the special segment as required by AISC 341-10 so that it would not obstruct the movement of the specimen when local buckling initiated at the plastic hinges at large story drift ratios. Stability bracing of the truss-to-column connection was provided as per AISC 341-10 around both columns. Pin connections were used at the top and the bottom of the columns to simulate the inflection points of columns in multi-story STMF structures.

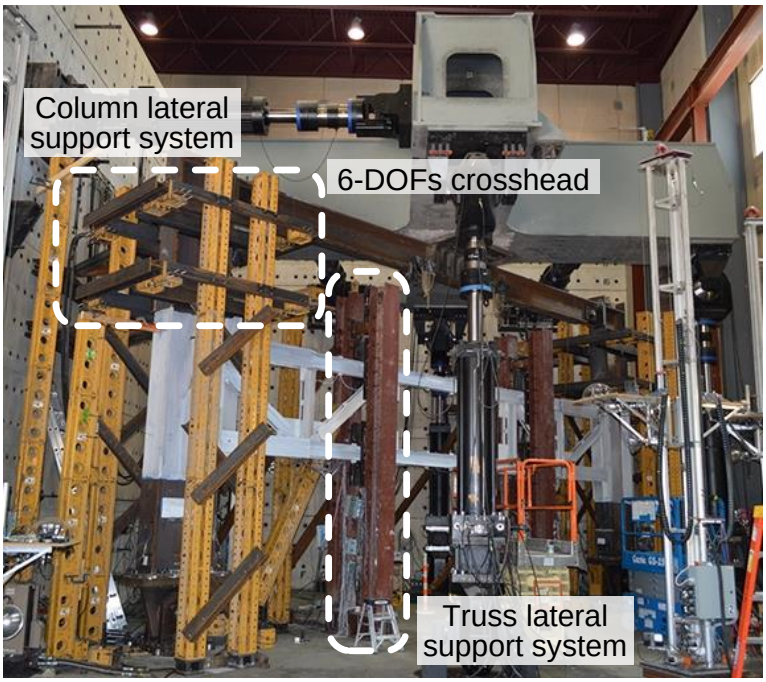

Figure 3-15 Subassemblage specimen test setup

MAST global coordinate system was rotated by 45 degrees about the +Z axis to an X'-Y'-Z' system to align with the orientation of the STMF specimen, as shown in Figure 3-16. Specimens were oriented in this way due to the overall length of the test setup was too large for the original global coordinate. Figure 3-17 shows the three dimensional view of the specimen and MAST crosshead, as well as the relative directions of the strong floor and reaction walls. The "Longitudinal", "Lateral", and "Vertical" directions are aligned with X', Y', and Z'-directions, respectively.

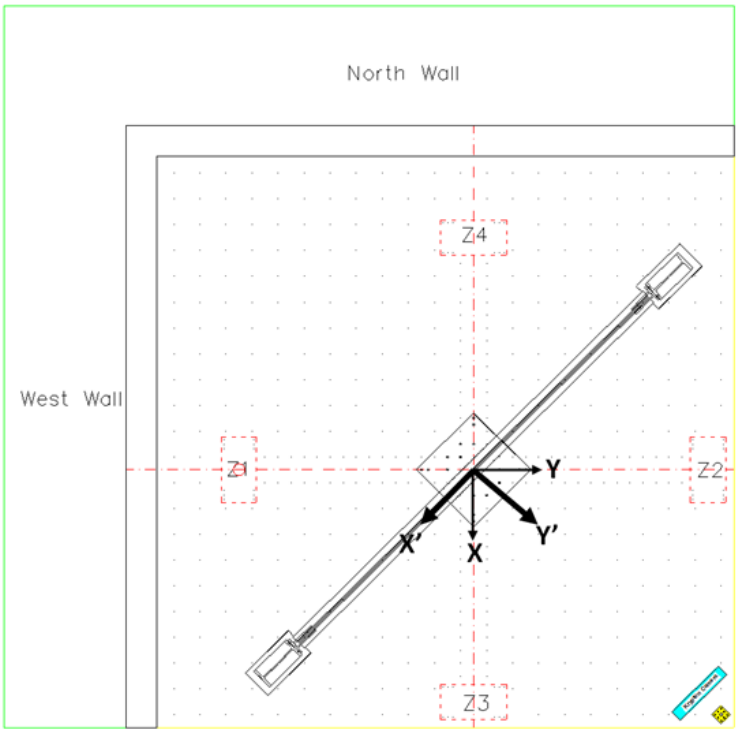

Figure 3-16 Orientation of the subassemblage specimens

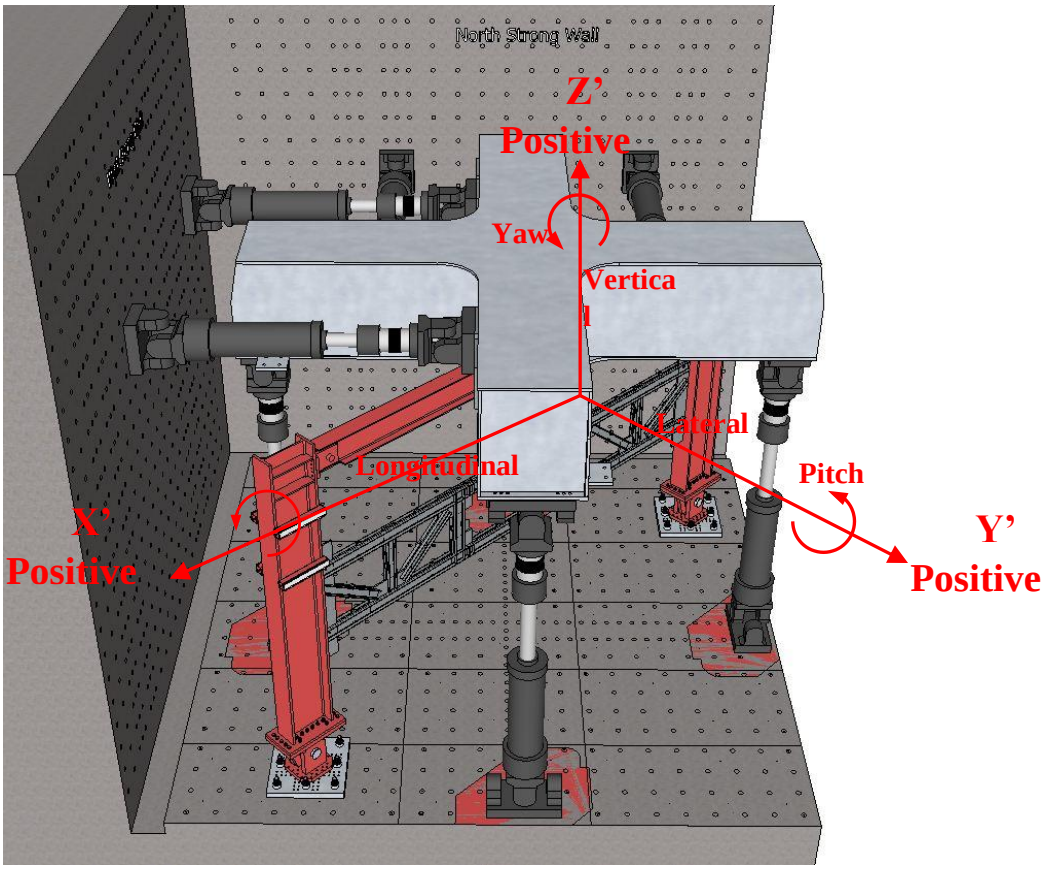

Figure 3-17 Overview of the test setup with the rotated MAST control coordinate system

3.5.1 Displacement History and Loading Procedures

The specimens were cyclically loaded according to a loading protocol similar to the AISC 341-10 loading sequence for beam-to-column connections of moment frames by means of lateral force applied by the crosshead through a load transfer beam. Graphical representation of the displacement and story drift ratio history is shown in Figure 3-18. Prior to applying the prescribed displacement history, a small displacement of 0.2 in. was applied in both directions to verify that all instruments were working properly.

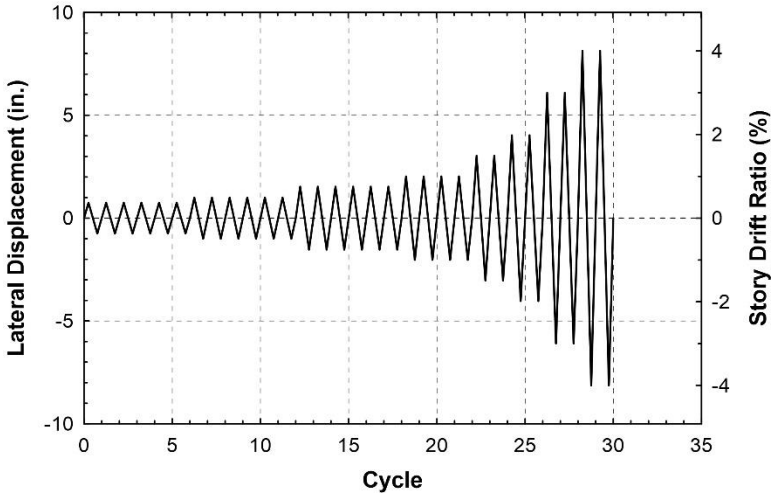

Figure 3-18 Displacement history

The constraints on various degrees of freedom (DOFs) are summarized in Table 3-1. In X'-direction, displacement was applied according to the protocol specified in Figure 3-18. Displacement in the Y'-direction was restrained to zero to maintain out-of-plane stability of the specimen. Rotation about the X' and Z'-axes of the specimen was maintained at zero by displacement-control. The overturning moment about the Y'-axis was slaved to the force applied in the X'-direction to minimize moment in the load transfer beam. The eccentricity from the load (bottom of the crosshead to the mid-height of the load transfer beam) was calculated by summing up the nominal thickness of the 3-in.-thick plate and half of the beam depth (9.35 in. for W18×106), which was 12.35 in. However the measured depth of the beam was 18-7/8 in. and the thickness of the load transfer plate was 3-1/16 in., which led to an eccentricity of 12.5 in.

The peak lateral displacement values used to control the crosshead movement in Figure 3-18 were derived based on the assumption that the load transfer beam, columns, and truss members outside of the Special Segments were rigid. Due to the geometry of the test setup, the rotations of the test setup columns were slightly different than the

rotation of the truss specimen measured at the center of the top chord at story drift levels larger than 3%. The crosshead lateral displacements shown in Figure 3-18 corresponded to the drift at the center of the special segment top chord member at specified drift levels. Figure 3-19 shows an example of how the peak lateral displacements were obtained using CAD drawings at story drift ratio of 3% and beyond.

Table 3-1 Control Mode of the 6-DOFs Crosshead

DOF	Control Mode	Note
Translation X'; $(\Delta_{X'})_{crosshead}$	Displacement	Specified history
Translation Y'	Displacement	$\Delta_{Y'} = 0$
Translation Z'	Force (kips)	$F_{Z'} = 0$
Rotation X'	Displacement	$\theta_{X'} = 0$
Rotation Y'	Force (kip-in.)	$M_{Y'}$ slaved to X'-Force, $F_{X'}$ (kips) $M_{Y'} = -F_{X'} \times (9.4375'' + 3.0625'') = -12.5 \times F_{X'}$
Rotation Z'	Displacement	$\theta_{Z'} = 0$

Additional information regarding the loading protocol for individual subassemblage specimen can be found in Appendix D.

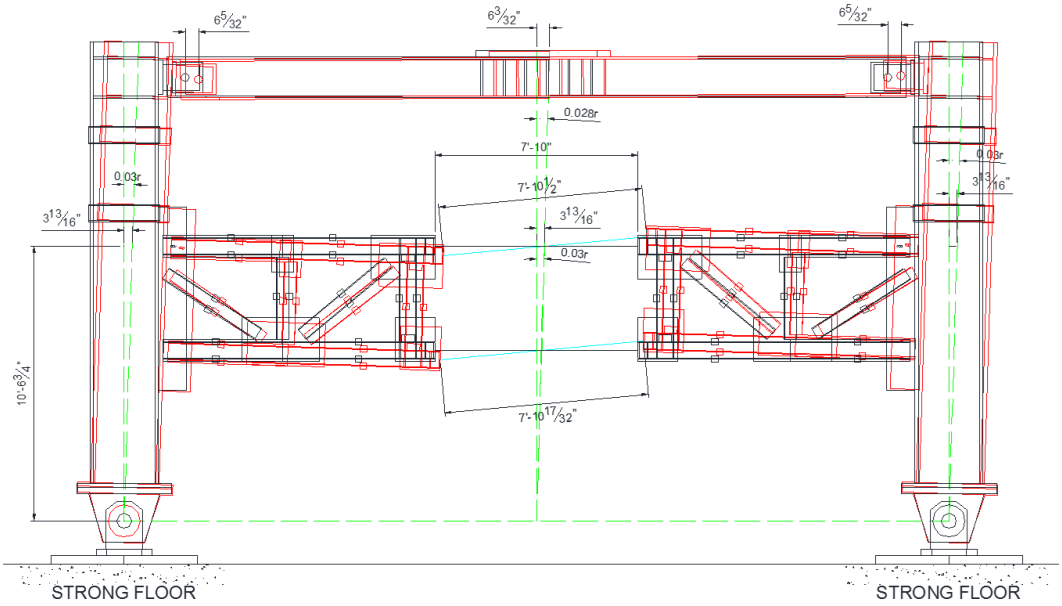

Figure 3-19 Deflected shape of STMF subassemblage specimen at 3% story drift ratio

3.6 Instrumentations and Data Acquisition

In order to achieve the objectives as described in previous section, key response variables were measured by the instruments as follows:

[a] Forces and displacements in all 6 DOFs introduced by the MAST crosshead.

[b] Reactions at the column supports.

[c] Small translation of pin base with respect to strongfloor plate.

[d] Small translation of strongfloor plate with respect to strong floor.

[e] Axial force, shear force, and yielding of truss elements in the special segment.

[f] Axial force and shear force in truss elements outside of the special segment.

[g] Shear force in truss-to-column gusset plates.

[h] Forces in the truss lateral support system.

[i] Forces in the column lateral support system.

[j] Axial force and strain level in load transfer beam.

[k] Axial force and moment distribution in the columns.

[l] Force in the column's stiffener plates.

[m] Panel zone deformation in the columns.

[n] Lateral displacement at various heights: top clevis, top chord, and bottom chord elevations.

[o] Vertical displacement at the end of special segment at the bottom chord elevation.

[p] Rotation of the special segment.

[q] Out-of-plane displacement of the special segment.

Key response parameters are summarized in Table 3-2. Strain gages, string potentiometers, LVDTs, tilt meters and the Krypton camera system were used to measure the response variables listed above. Measurements from these sensors during the loading sequence were collected at a rate of 1 Hz. Table 3-3 lists the total number of instruments used for each specimen.

Table 3-4 and Table 3-5 list further details of the instrument with the category as defined in Table 3-2. Instrumentation drawings can be found in Appendix E.

Table 3-2 Key Response Parameters

Response Parameters	Response Variables	Instruments Used to Measure the Variables
Story drift	[a], [n]	MAST HCC, string pots
Axial force, shear force, and moment of truss elements in the special segment	[e]	Strain gauges
Onset yielding of truss elements in the special segment	[e]	Strain gauges
Vertical displacement of the special segment	[o]	String potentiometers
Shear rotation in the special segment	[p]	String pots, tiltmeters, and Krypton system
Out of plane displacement of truss elements in the special segment	[q]	Krypton system

Table 3-3 Instrument Channel Requirement

Channel Type	Number Required
Voltage	
LVDT (± 0.5 in.)	12
String pot (± 20 in.)	6
String pot (± 15 in.)	2
String pot (± 10 in.)	2
String pot (± 5 in.)	2
Tilt meter	6
Load cell	2
Total voltage channels	32
Strain gauge	
Uniaxial	183
Rosette (No. of gauges)	48 (16)
LVDT (± 3.94 in.)	2
Total strain gauge channels	233

Table 3-4 Instrumentation Schedule Label Abbreviation List

Label	Instrument	Response variables	Drawing (Appendix B)
-	Whitewash	-	-
	Krypton LEDs	[p], [q]	IN-05
	Actuators	[a]	-
	2 DOF load cell	[b], [e]	-
SS-C-1 and SS-C-2	Single strain gauge	[l]	IN-02
SS-C-1-1 through SS-C-1-4 and SS-C-2-1 through SS-C-2-4	Single strain gauge	[m], [k]	IN-02
SS-LBT-1, SS-LTB-1-1 through SS-LTB-1-4, SS-LTB-2-1 through SS-LTB-2-4	Single strain gauge	[j]	IN-02
SS-BR(x)-(x)	Single strain gauge	[h]	IN-02
SS-TB1 through SS-TB12	Single strain gauge	[h], [i]	IN-08 to 09
MS-M1-1-(x) and MS-M1-2-(x)	Multiple strain gauge	[f]	IN-02
MS-M2-(x)	Multiple strain gauge	[f]	IN-02
MS-M3-1-(x) through MS-M3-4-(x)	Multiple strain gauge	[e]	IN-02
MS-M4-1-(x) and MS-M4-2-(x)	Multiple strain gauge	[e]	IN-02
MS-M5-1-(x) and MS-M5-2-(x)	Multiple strain gauge	[f]	IN-02
MS-M6-1-(x) through MS-M6-4-(x)	Multiple strain gauge	[f]	IN-02
MS-M7(x)-(x) and MS-M8-(x)-(x)	Multiple strain gauge	[f]	IN-02
MS-M9-1-(x) and MS-M9-2-(x)	Multiple strain gauge	[f]	IN-02
MS-M10-1-(x) and MS-M10-2-(x)	Multiple strain gauge	[e]	IN-02
RS-1 through RS-3	Rosette strain gauge	[m], [g], [e]	IN-02
TM-1 through TM-6	Tiltmeter	[p]	IN-04
SPC-1 and SPC-5	String pot	[n]	IN-03a
SPC-2 and SPC-6	String pot	[n]	IN-03a
SPC-3 and SPC-7	String pot	[n]	IN-03a
SPC-4 and SPC-8	String pot	[n]	IN-03a
SPT1 through SPT4	String pot	[o], [p]	IN-03a
UTA-SW and UTA-NE	Additional LVDT	[n]	IN-03b
L-SW-W, L-SW-S, L-NE-W, L-NE-S	LVDT	[c]	IN-07
L-SW-SW(x), L-SW-SE(x), L-NE-SW(x), and L-NE-SE(x)	LVDT	[d]	IN-07

Table 3-5 Instrumentation Schedule Label Abbreviation List

Label abbreviation	Meaning
SS	Single strain gauge
CS	Column stiffener
C	Column
M	Truss member
LTB	Load transfer beam
BR	Bracing rods
TB	Tube bracing
MS	Multiple strain gauge
RS	Rosette strain gauge
TM	Tilt meter
SPC	Column string sot
SPT	Truss string pot
L-(corner)-(side)(number)	Meaning
SE	Single strain gauge
SW	Column stiffener
NE	Column
W	Truss member
S	Load transfer beam
(x)	Bracing rods
UTA-(corner)	Tube bracing

Chapter 4

Part I : Experimental Test Results

4.1 Overview

Figure 4-1 through Figure 4-8 show the subassemblage specimens during the tests at different drift ratios. The behavior of all specimens was stable and ductile. Plastic hinges were formed at the expected locations (the ends of the chord members and the intermediate vertical members) without any yielding in the members outside the special segment. The lateral forces recorded at crosshead versus drift responses of the specimens are shown in Figure 4-9 through Figure 4-11.

Table 4-1 summarizes the calculated values of V_{ne} according to AISC 341 and the proposed equation from Chao and Goal (2008a) (Eq. 2-4) and the equivalent shear force computed from the measured reactions from test results using equilibrium conditions.

Table 4-1 Calculated V_{ne} and Equivalent Vertical Shear Force from Test Results

Specimen	Calculated V_{ne} (kips)			Equivalent Vertical Shear Force from Test Results (kips)	
	AISC 341-05 (Eq. 2-2)	AISC 341-10 (Eq. 2-3)	Chao & Goel (Eq. 2-4)	Positive Drift	Negative Drift
STMF-2C8-1	78	67	67	79	81
STMF-2C8-2	N/A	N/A	99	145	144
STMF-2HSS8	144	126	126	145	137

(a) (b)

(c) (d)

(e) (f)

Figure 4-1 STMF subassemblage during test at 0.375% inter story drift: (a) STMF-2C8-1 at positive drift; (b) STMF-2C8-1 at negative drift; (c) STMF-2C8-2 at positive drift; (d) STMF-2C8-2 at negative drift; (e) STMF-2HSS8 at positive drift; (f) STMF-2HSS8 at negative drift

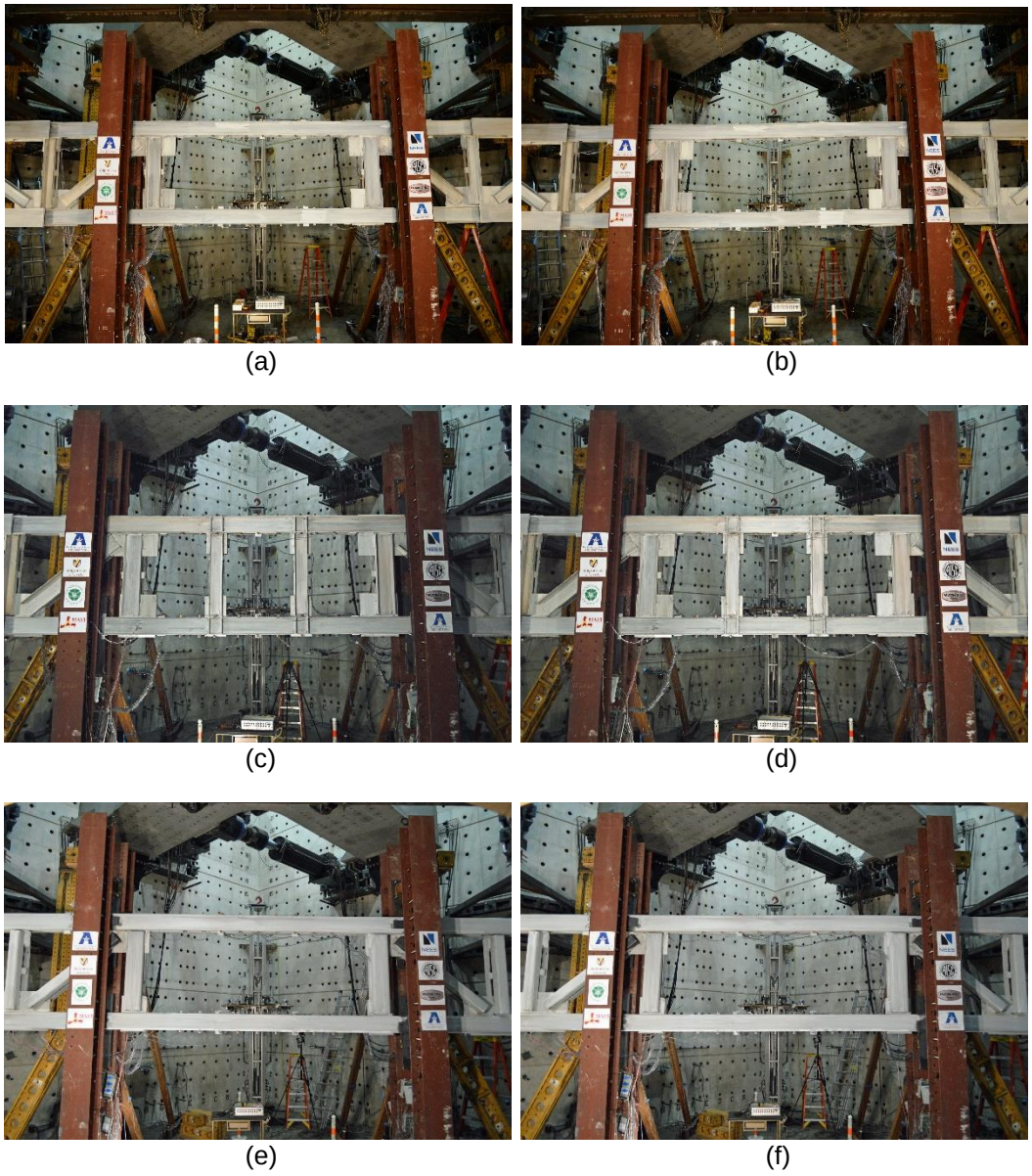

Figure 4-2 STMF subassemblage during test at 0.5% inter story drift: (a) STMF-2C8-1 at positive drift; (b) STMF-2C8-1 at negative drift; (c) STMF-2C8-2 at positive drift; (d) STMF-2C8-2 at negative drift; (e) STMF-2HSS8 at positive drift; (f) STMF-2HSS8 at negative drift

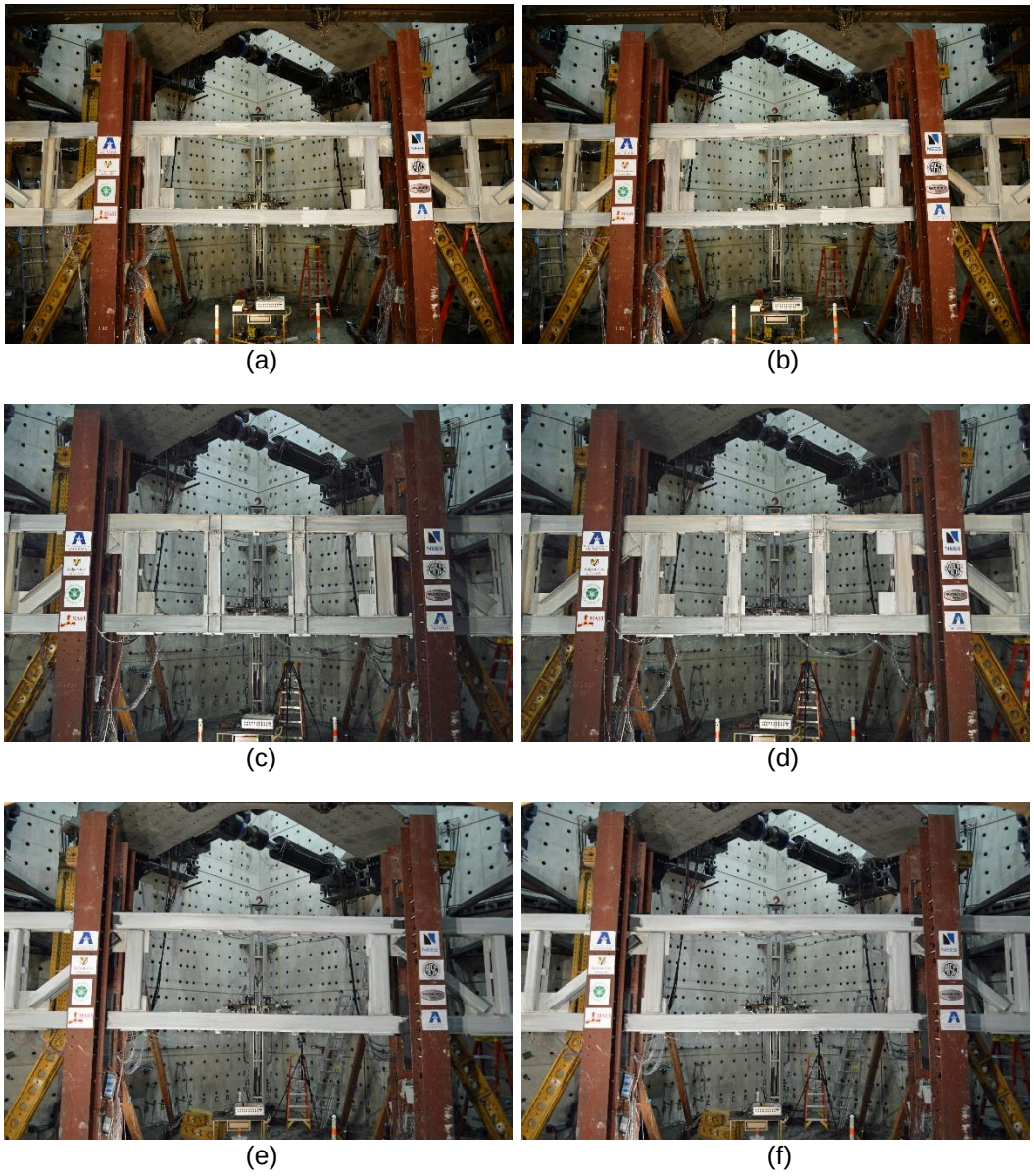

Figure 4-3 STMF subassemblage during test at 0.75% inter story drift: (a) STMF-2C8-1 at positive drift; (b) STMF-2C8-1 at negative drift; (c) STMF-2C8-2 at positive drift; (d) STMF-2C8-2 at negative drift; (e) STMF-2HSS8 at positive drift; (f) STMF-2HSS8 at negative drift

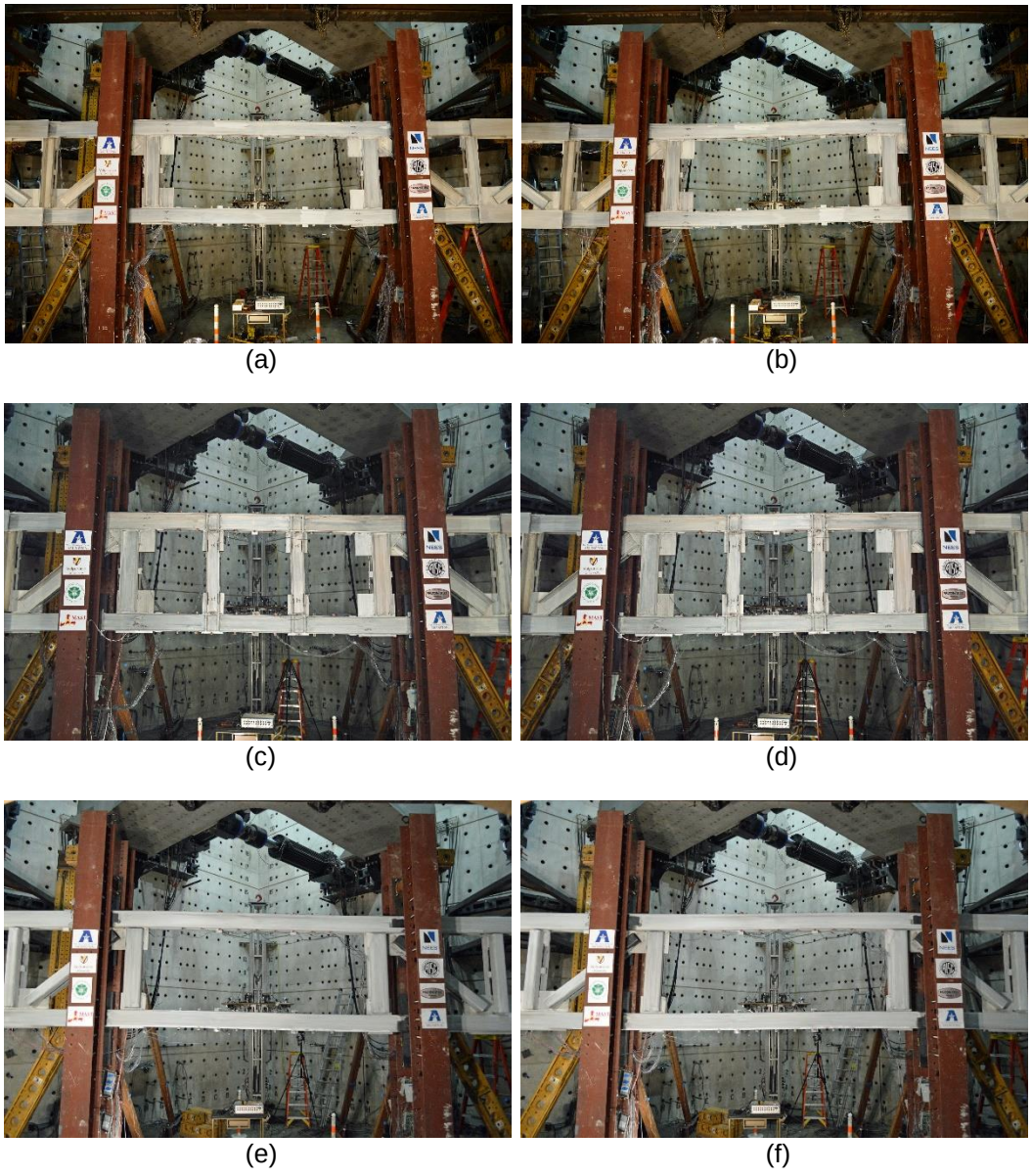

(a) (b) (c) (d) (e) (f)

Figure 4-4 STMF subassemblage during test at 1% inter story drift: (a) STMF-2C8-1 at positive drift; (b) STMF-2C8-1 at negative drift; (c) STMF-2C8-2 at positive drift; (d) STMF-2C8-2 at negative drift; (e) STMF-2HSS8 at positive drift; (f) STMF-2HSS8 at negative drift

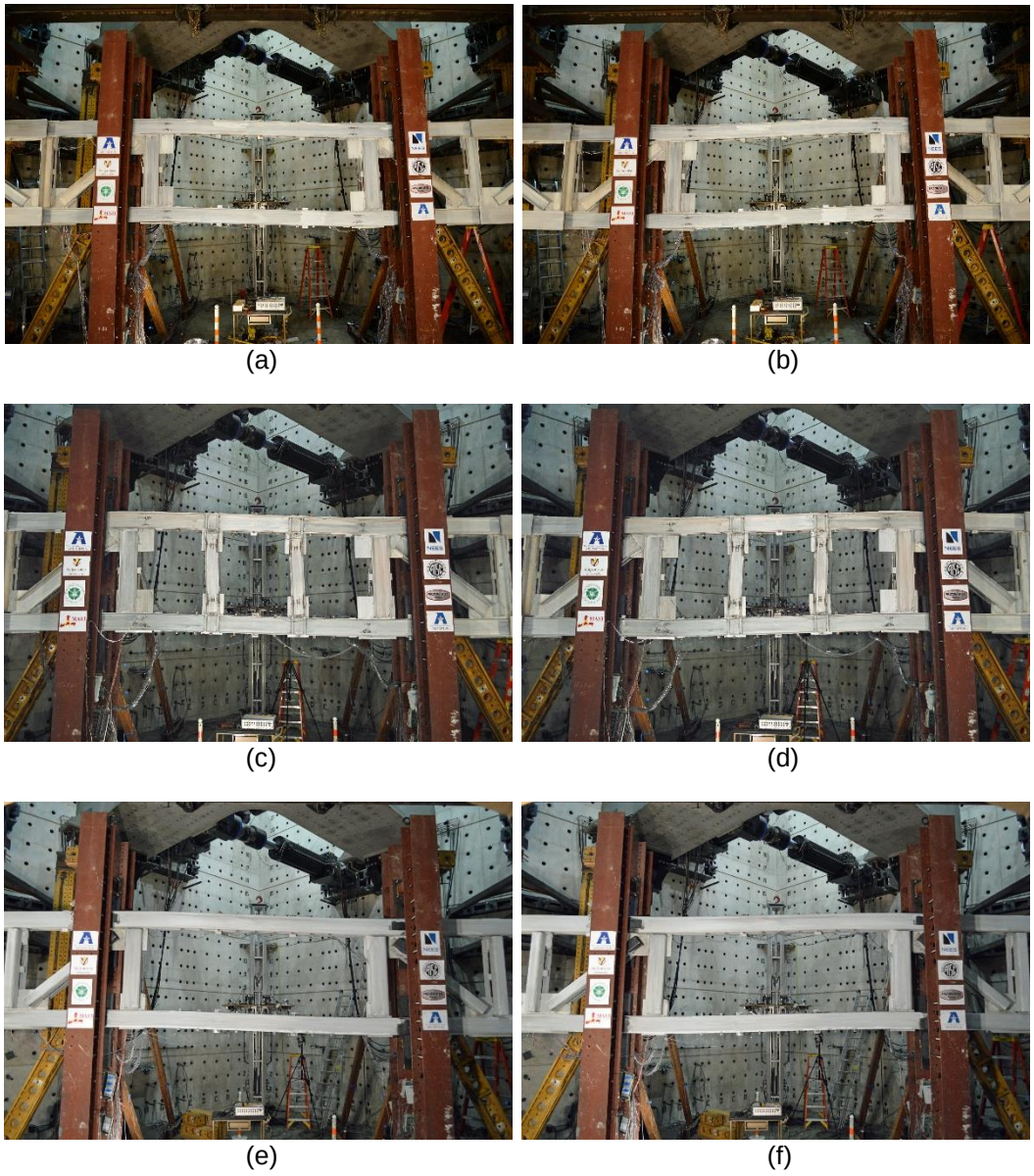

(a) (b) (c) (d) (e) (f)

Figure 4-5 STMF subassemblage during test at 1.5% inter story drift: (a) STMF-2C8-1 at positive drift; (b) STMF-2C8-1 at negative drift; (c) STMF-2C8-2 at positive drift; (d) STMF-2C8-2 at negative drift; (e) STMF-2HSS8 at positive drift; (f) STMF-2HSS8 at negative drift

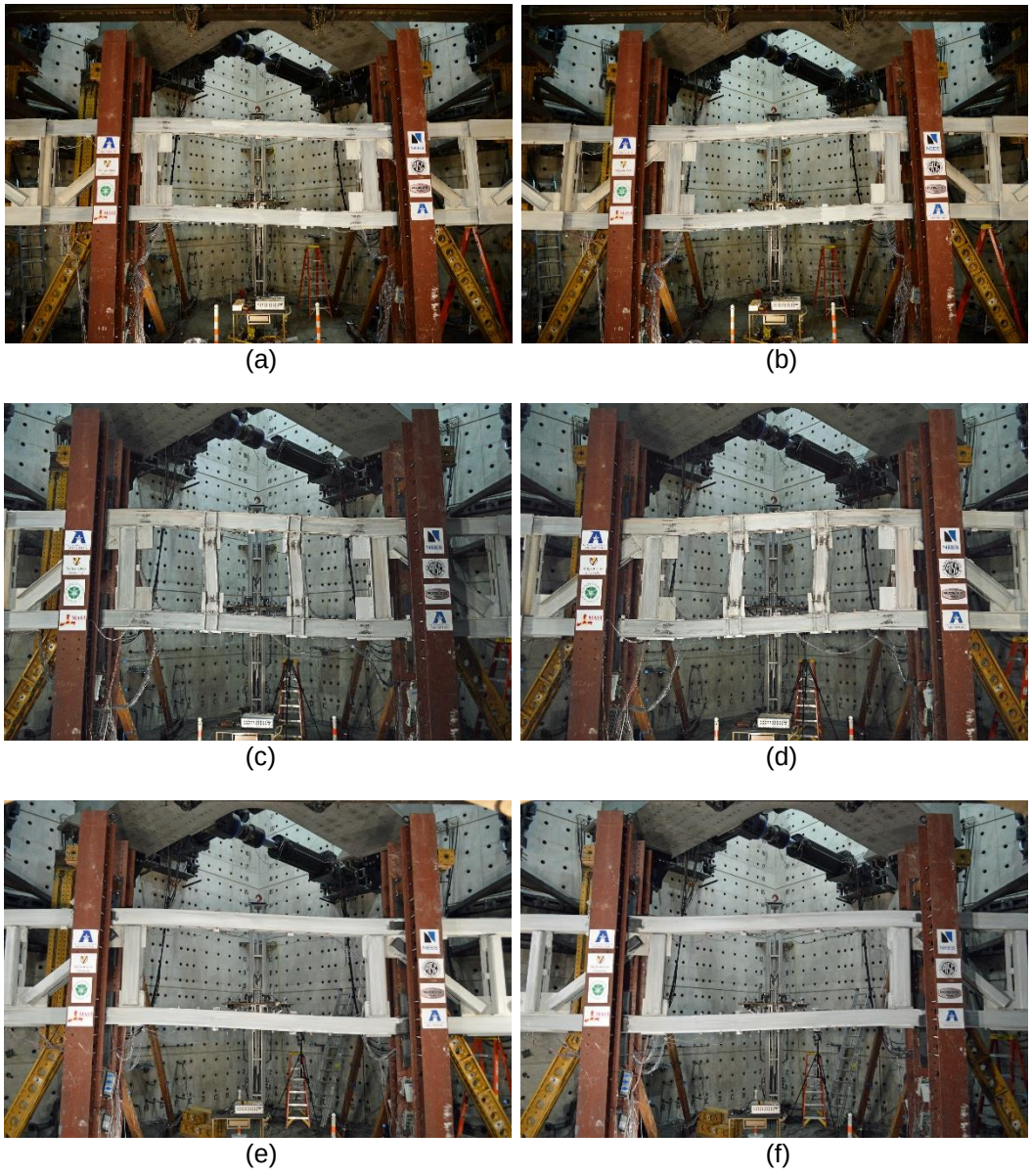

(a) (b) (c) (d) (e) (f)

Figure 4-6 STMF subassemblage during test at 2% inter story drift: (a) STMF-2C8-1 at positive drift; (b) STMF-2C8-1 at negative drift; (c) STMF-2C8-2 at positive drift; (d) STMF-2C8-2 at negative drift; (e) STMF-2HSS8 at positive drift; (f) STMF-2HSS8 at negative drift

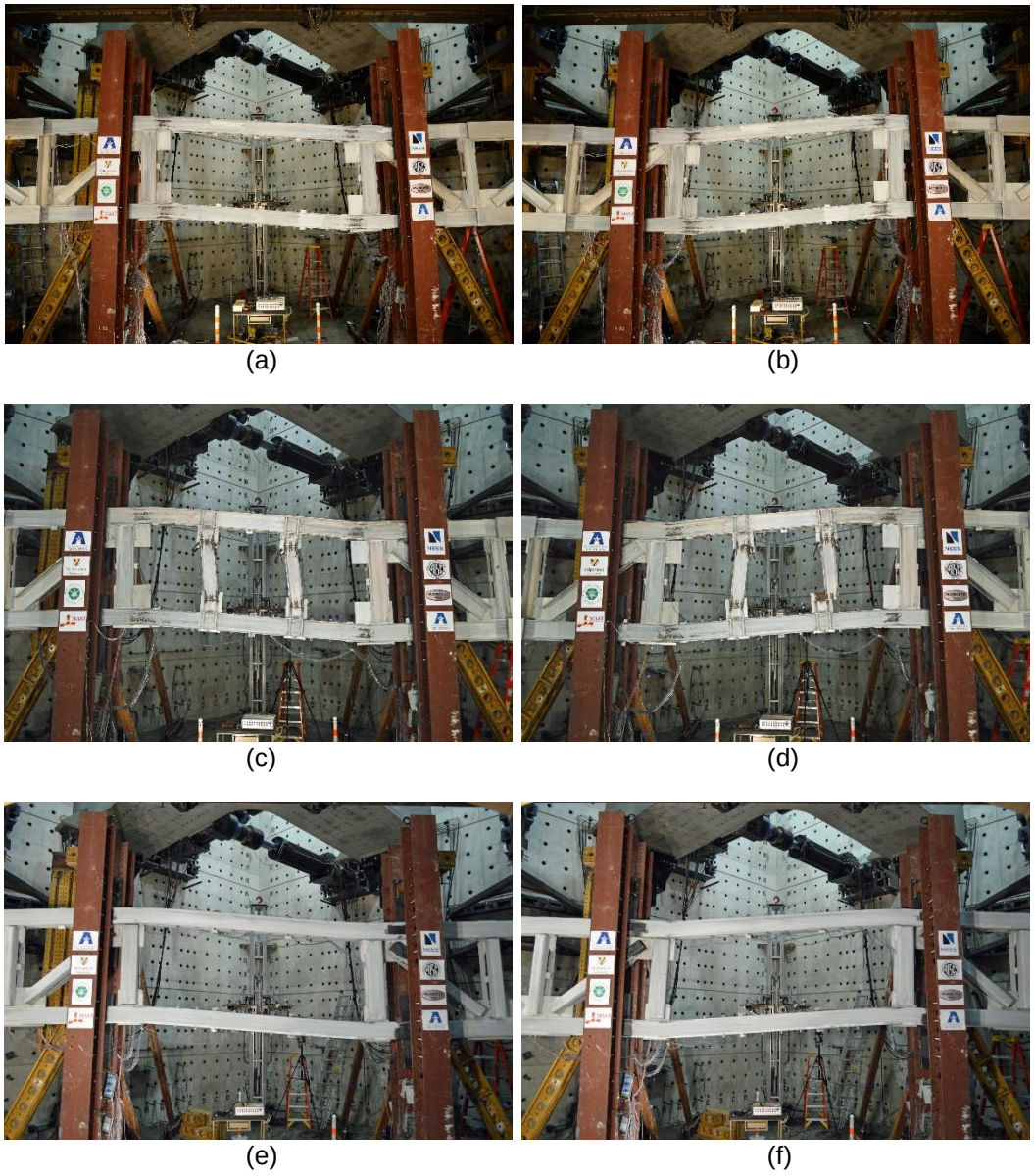

Figure 4-7 STMF subassemblage during test at 3% inter story drift: (a) STMF-2C8-1 at positive drift; (b) STMF-2C8-1 at negative drift; (c) STMF-2C8-2 at positive drift; (d) STMF-2C8-2 at negative drift; (e) STMF-2HSS8 at positive drift; (f) STMF-2HSS8 at negative drift

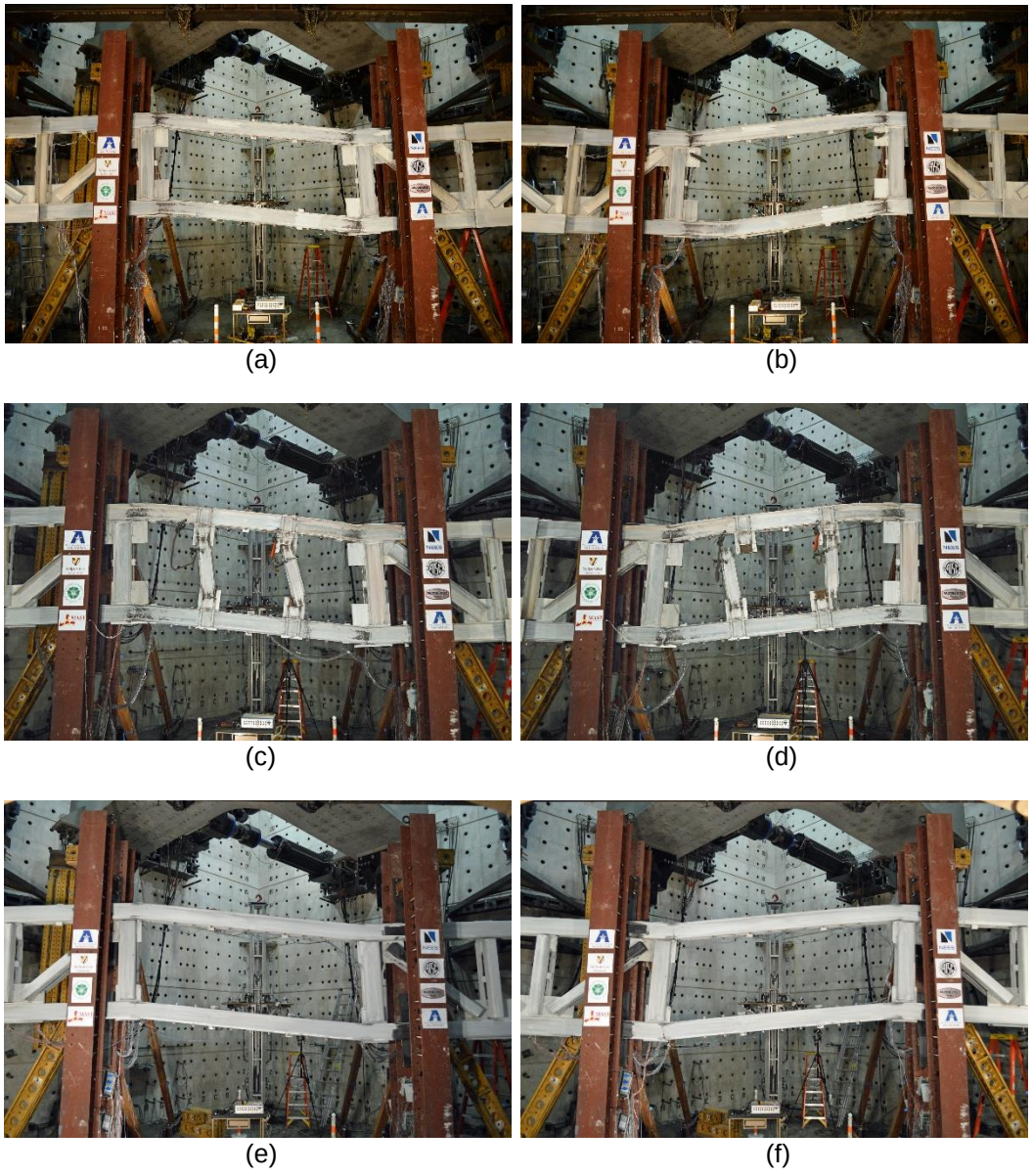

Figure 4-8 STMF subassemblage during test at 4% inter story drift: (a) STMF-2C8-1 at positive drift; (b) STMF-2C8-1 at negative drift; (c) STMF-2C8-2 at positive drift; (d) STMF-2C8-2 at negative drift; (e) STMF-2HSS8 at positive drift; (f) STMF-2HSS8 at negative drift

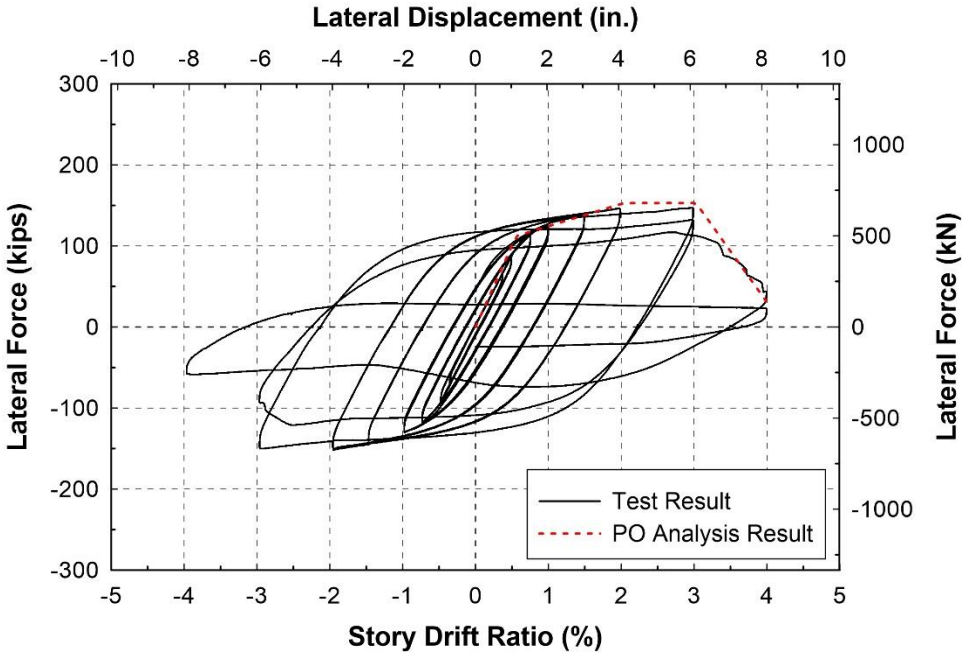

Figure 4-9 Lateral force versus drift response of STMF-2C8-1

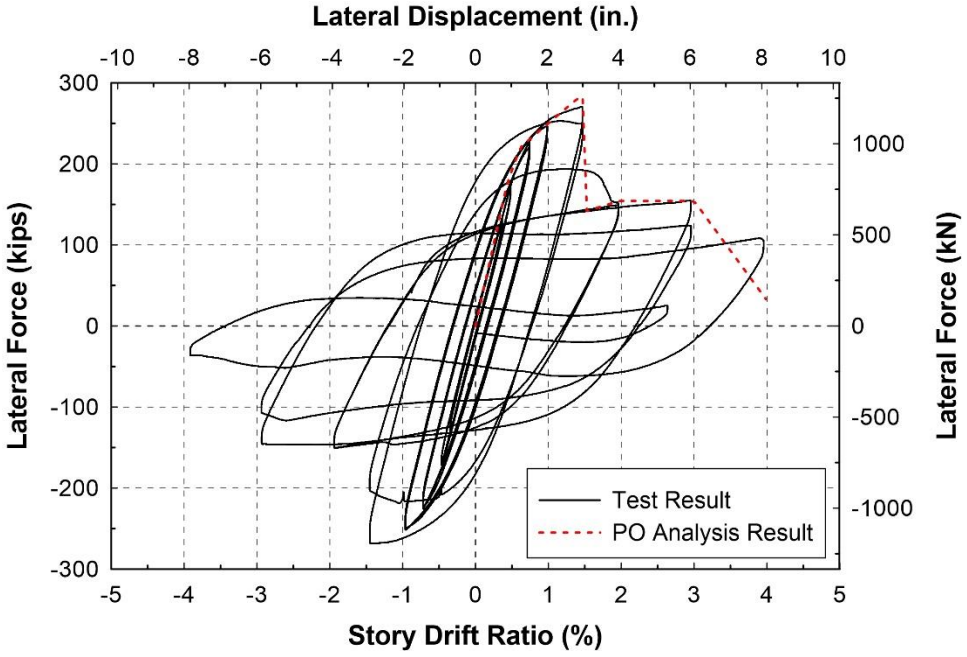

Figure 4-10 Lateral force versus drift response of STMF-2C8-2

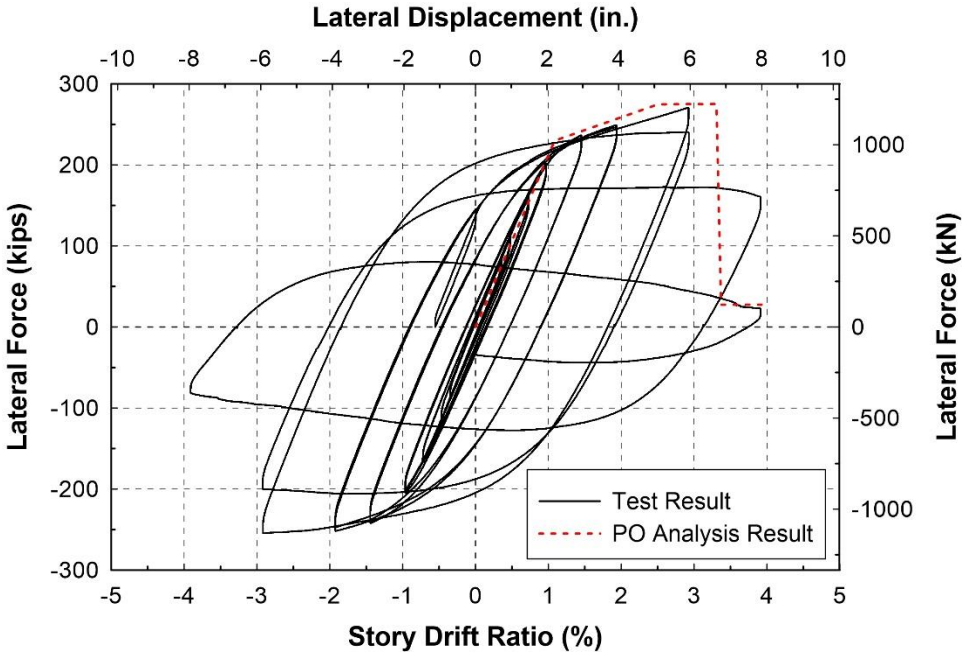

Figure 4-11 Lateral force versus drift response of STMF-2HSS8

4.2 Experimental Observations

4.2.1 STMF-2C8-1 Observations

STMF-2C8-1 exhibited stable and ductile behavior up to the first cycle of the 3% story drift ratio. Strength of STMF-2C8-1 kept increasing up to 3% story drift ratio. At 1% story drift ratio, fractures initiated at the end of the welds connecting the chord members to the gusset plates at the ends of the special segment. Fracture then propagated into the flanges of the chord members starting at 1.5% story drift ratio as shown in Figure 4-12. Nevertheless, this did not lead to degradation of the lateral strength. By the second cycle of the 3% story drift ratio, fractures at the plastic hinges in the chord members propagated into approximately half the depth of the web as seen in Figure 4-13. As a result, the strength of STMF-2C8-1 started to degrade significantly and the chord

members (the portion beyond the “weld-free” regions) in the special segment started to twist.

Figure 4-12 Fracture at 1.5% story drift ratio in STMF-2C8-1

Figure 4-13 Fracture at 3% story drift ratio in STMF-2C8-1

At the second cycle of the 4% story drift, majority of the chord members in the special segment were torn at plastic hinges and the capacity of STMF-2C8-1 drastically dropped to approximately 17% of the peak strength and the experiment was terminated.

For STMF-2C8-1, It can be seen in Figure 4-14 that the peaks equivalent vertical shear forces were close to the expected vertical shear strength, V_{ne} , predicted by AISC 341-05 (Eq. 2-2), but higher than that by that of AISC 341-10 (Eq. 2-3) by nearly 20%. However, according to strain gauge readings, there was no yielding in the members outside of the special segment. The maximum strain found in all members outside of the special segment was $0.68\varepsilon_y$, where ε_y ,or yield strain, was approximately 2000 micro-strain. This means that the predicted V_{ne} value from the AISC 341-10 is still conservative. It is also worth to mention that the peak equivalent vertical shear forces obtained from test results were calculate based on the lateral forces at the crosshead, which included the frictions from the lateral support system. Therefore, the calculated equivalent shear is on the conservative side (for designing members outside of the special segment). However, it could mean that the section sizes for the member outside of the special segment could be over-design. While this is a conservative design approach, it might not be an economical one.

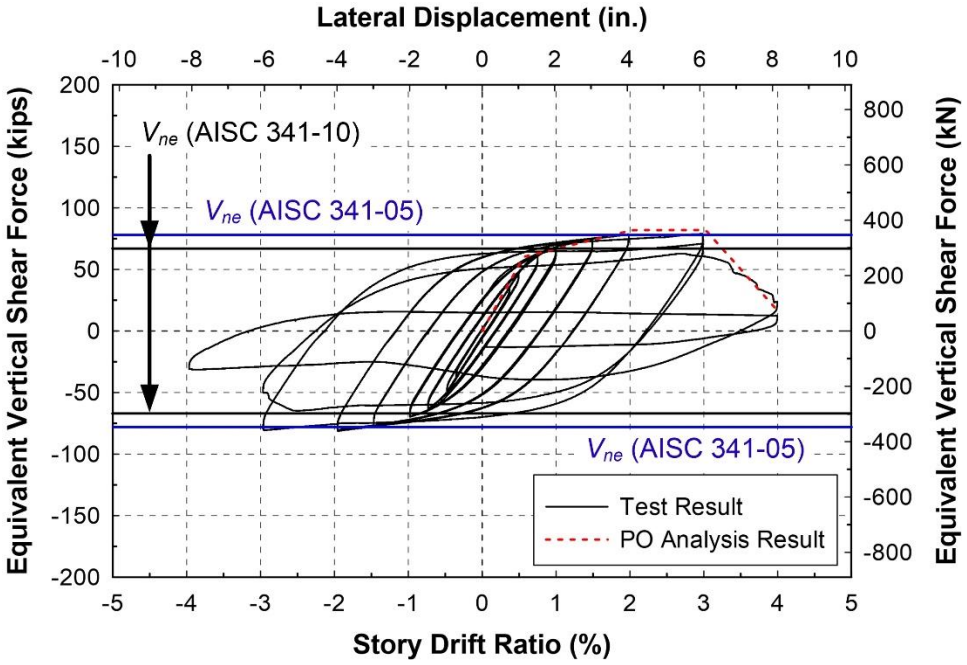

Figure 4-14 Equivalent shear force of STMF-2C8-1

4.2.2 STMF-2C8-2 Observations

STMF-2C8-2 exhibited significantly higher elastic stiffness and ultimate strength than STMF-2C8-1 (approximately 90% and 80%, respectively) due to the additional contribution from intermediate vertical members. Figure 4-15 indicates that STMF-2C8-2 started to yield at 0.75% story drift ratio. During the second cycle of the 1.5% story drift ratio, its strength started to drop slightly due to fractures around the plastic hinge regions of intermediate vertical members. By 2% story drift ratio, the strength of STMF-2C8-2 drastically dropped due to complete failure of the intermediate vertical members and the hysteretic response began to resemble that of STMF-2C8-1 until the end of the test at the first cycle of 4% story drift ratio. It can be seen from Figure 4-15 that the peak equivalent vertical shear force of STMF-2C8-2 was larger than the value obtained from Eq. 2-4 (Chao and Goel, 2008a) by approximately 46%. The members outside of the special

segment, however, did not experience any yielding. The maximum strain in members outside of the special segment was $0.71\varepsilon_y$.

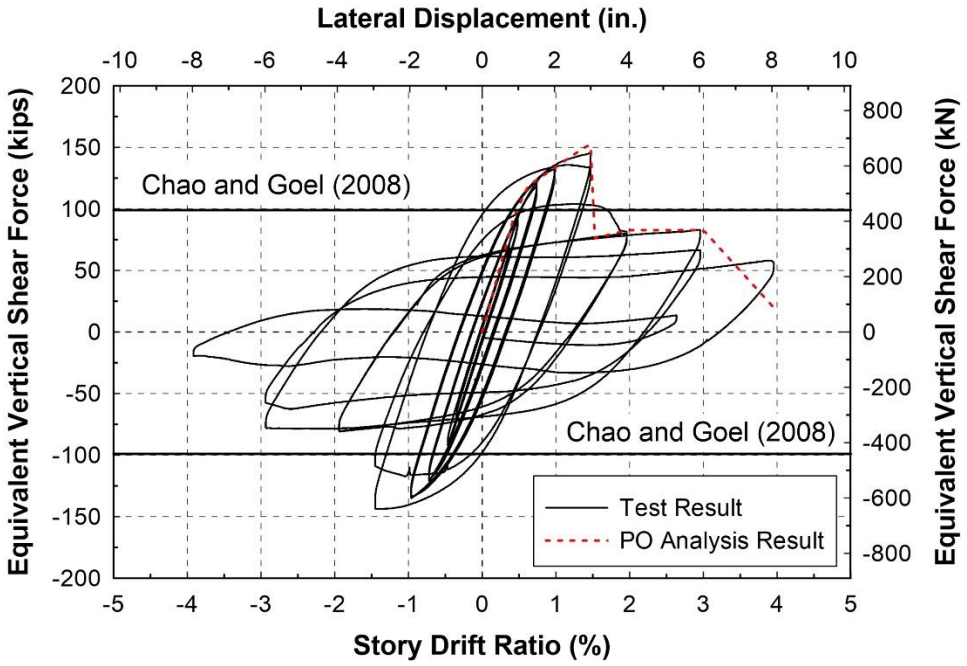

Figure 4-15 Equivalent shear force of STMF-2C8-2

Test results showed that the intermediate vertical members experienced inelastic deformation earlier than the chord members did. In other words, the rotational demand of intermediate members was higher than that of the chord members—the same as found in pushover analysis (discussed later). While different from the current practice shown in Figure 2-5 and 2-6, test results suggested that using intermediate vertical members that were smaller than the chord members could be advantageous. Because the damaged intermediate vertical members could be easily replaced in the case of minor to moderate earthquake events. Another advantage of STMFs with intermediate vertical members is the increase of strength and stiffness in STMFs. The size of chord member in the special

segment can be reduced because of the additional contribution from the intermediate vertical members.

4.2.3 STMF-2HSS8 Observations

The behavior of STMF-2HSS8 was stable and ductile up to approximately 3% story drift ratio. Plastic hinges formed at the expected locations (the ends of the chord members in the special segment) without any yielding in the members outside of the special segment. The lateral force at the crosshead versus drift responses of the specimens is close to the anticipated lateral force obtained from pushover analysis as shown in Figure 4-11. The revised pushover analyses, which were performed after the material properties of the actual HSS used in the full-scale experimental were obtained from a set of material tensile tests (discussed later), also gave almost identical results. The corresponding equivalent shear force at the center of the special segment was calculated by using the static equilibrium and is shown in Figure 4-16.

As shown in Figure 4-11, the specimen behaved elastically up to nearly 0.75% story drift ratio and exhibited stable and ductile behavior up to the first cycle of the 3% story drift ratio. Strength increased while stiffness gradually decreased from 1% to 3% story drift ratio. At the end of the first cycle of the 2% story drift ratio, small fractures began to appear at the end of the welds connecting the chord members to the gusset plates at the ends of the special segment; however, they did not affect the overall strength of the specimen. Fractures gradually propagated into the flanges of the chord members at the first cycle of 3% story drift ratio. After the first peak at 3% story drift ratio, large cracks formed on the tension side at the ends of chord members in the special segment and the specimen could not attain the same magnitude of lateral force when it underwent the peak displacement on the opposite direction. The strength dropped slightly during the second cycle of 3% story drift ratio. Strength of the specimen started to

degrade significantly at the first negative cycle of 4% story drift ratio, at which time the majority of the chord members in the special segment were torn and the capacity of the specimen drastically dropped to approximately 30% of the peak strength. In the second cycle of 4% story drift ratio, lateral force dropped to about 16% of the peak strength, and the experiment was terminated.

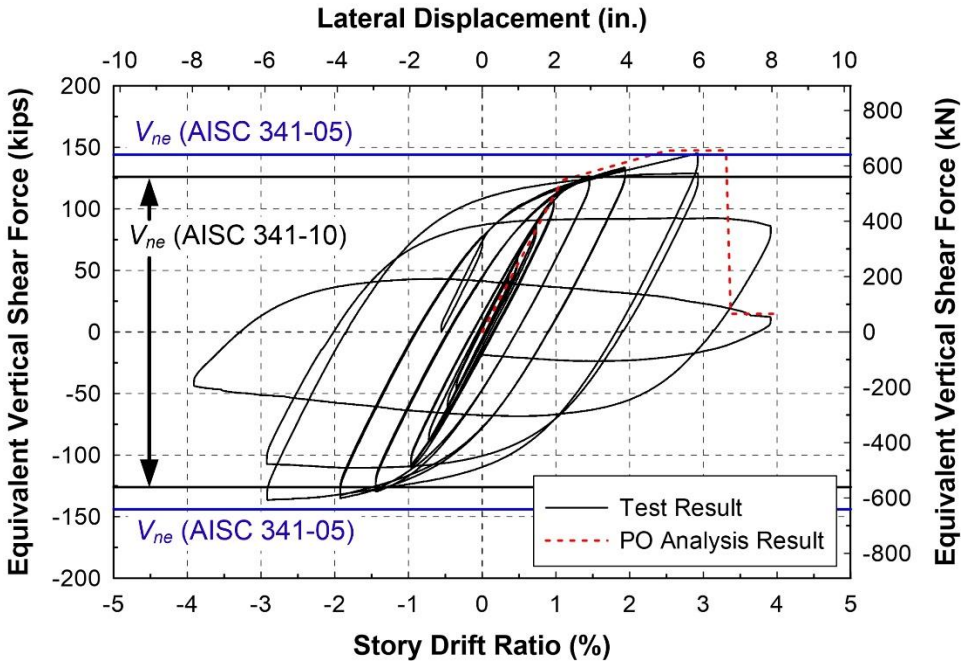

Figure 4-16 Equivalent shear force of STMF-2HSS8

Figure 4-17 shows the failure at the end of the chord members in the special segment of the subassemblage compared to the component test specimen. In both case, the failure was due to fracturing after low-cycle fatigue accompanied by slight necking of the section. No local buckling and lateral-torsional buckling was observed.

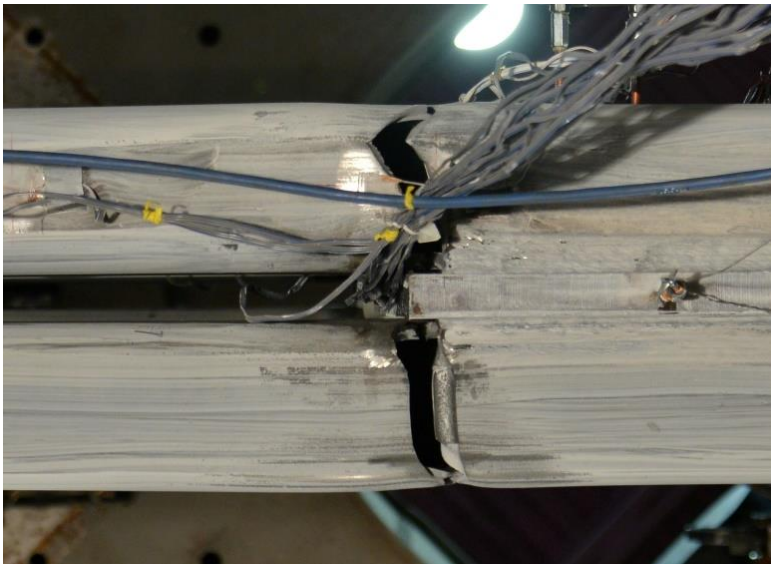

(a)

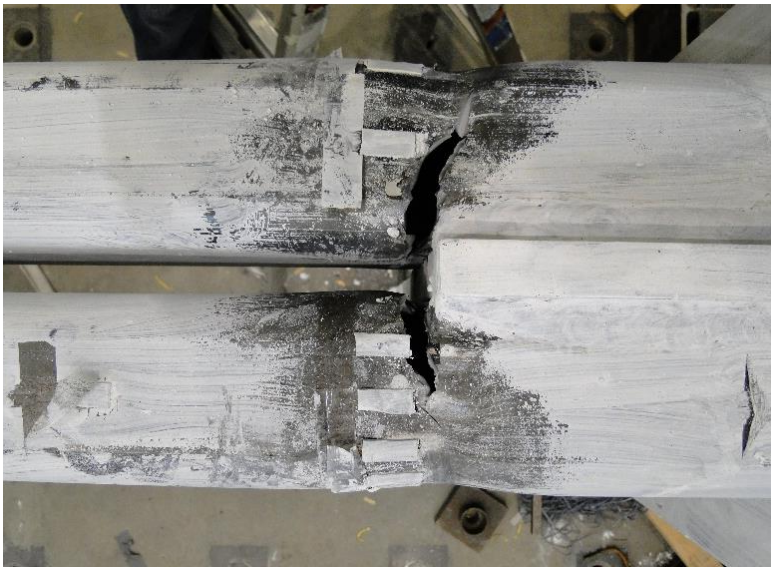

(b)

Figure 4-17 Failure of specimens: (a) at the end of chord members in the special segment of STMF-2HSS8 subassemblage specimen; (b) component test specimen C-2HSS8

Chapter 5

Part I : Discussion of Experimental Test Results

5.1 Special Detailing at the End of the Special Segment

Figure 5-1 shows the special detailing at the end of a chord member in the special segment of STMF-2C8-1 at the end of the test (4% story drift ratio). The “weld-free” area between the extended gusset plate and the chord member in the special segment allows the member to freely slide against the gusset plate while providing direct lateral support at the plastic hinge region. The plastic hinge zone extended greater than the depth of the chord members as indicated by flaking of the white wash on the members similar to the component test results from the first phase. It is evident that this proposed detailing configuration at the end of the special segment eliminated LTB at the plastic hinge. On the other hand, the chord members which had no lateral support (beyond the plastic hinge) showed significant LTB at large story drift (4%). It can also be observed that not connecting the vertical members to the chord members allows the inelastic deformation in the flanges of the chord members to develop without restraint along a much extended length. Strain gauge data shows that the maximum plastic hinge length of the chord members (from the end of weld between chord members and gusset plate) in STMF-2C8-1 was greater than 20.5 in. The maximum plastic hinge length in STMF-2C8-2 was even greater than 24.5 in. which is equivalent to 3.1 times the depth of the chord member (2C8×18.75 sections). Figure 5-2(a) shows the strain profile along the length of the chord member (from the end of weld) at the top right corner of the special segment in STMF-2C8-1 at each story drift level. The maximum strain levels at each corner of the special segment comparing to equivalent component test specimens are shown in Figure 5-2(b). Figure 5-3 shows the corresponding strain levels of

subassemblage specimen STMF-2C8-2. Similarly, Figure 5-4 shows the strain levels for STMF-2HSS8 specimen.

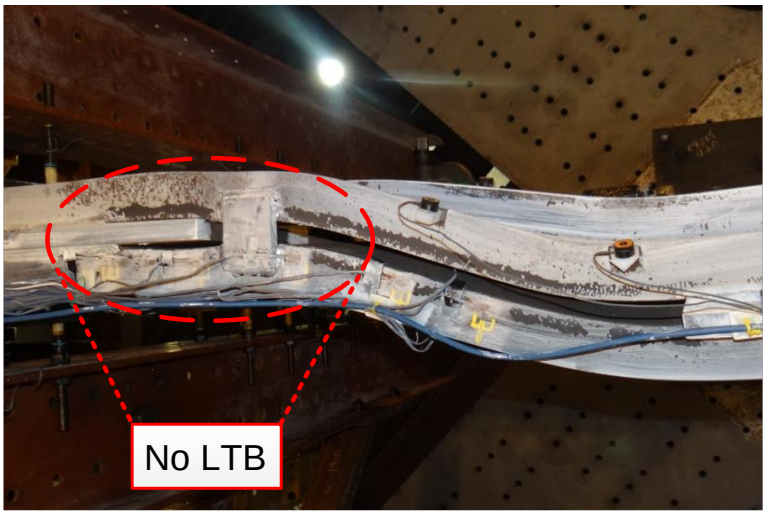

(a)

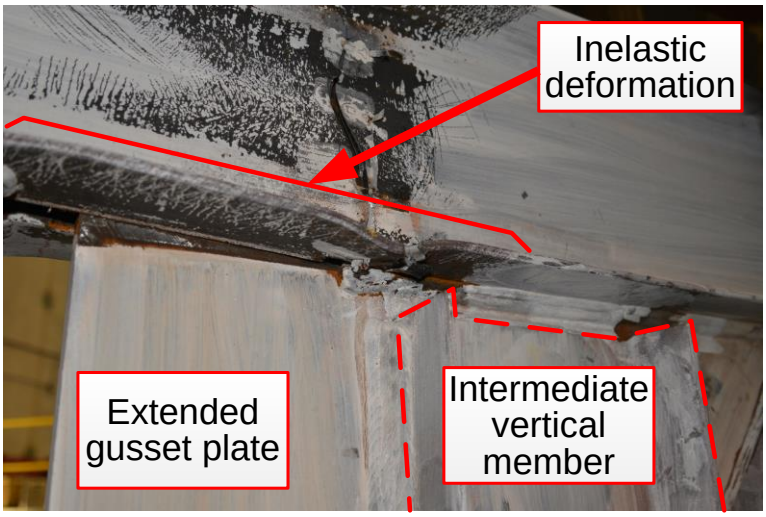

(b)

Figure 5-1 Special detailing at the end of a chord member in the special segment at 4% story drift ratio: (a) bottom view; (b) side view

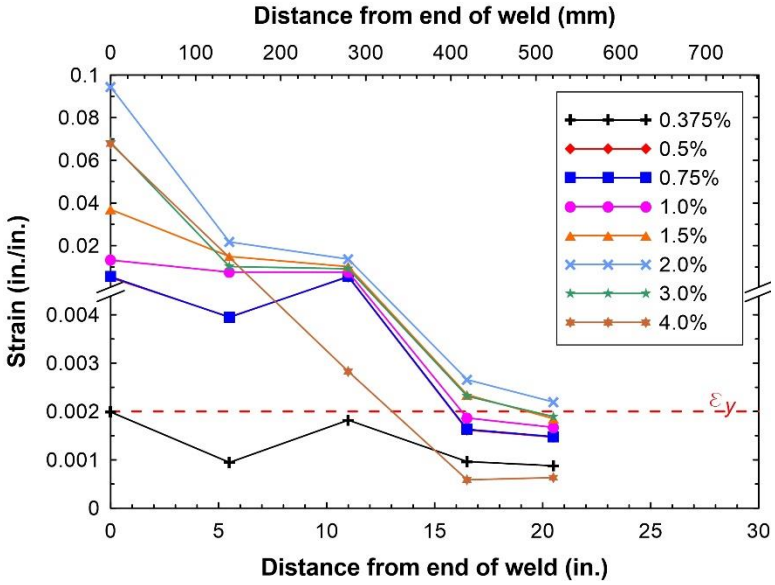

(a)

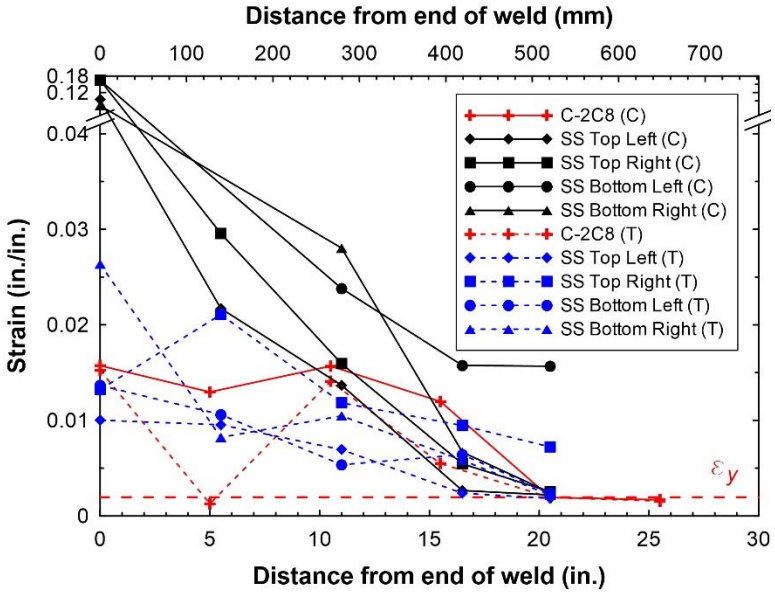

(b)

Figure 5-2 Strain profile along the length of chord members at the end of the special segment of STMF-2C8-1: (a) top right corner at different story drift levels; (b) maximum strain levels at each corner

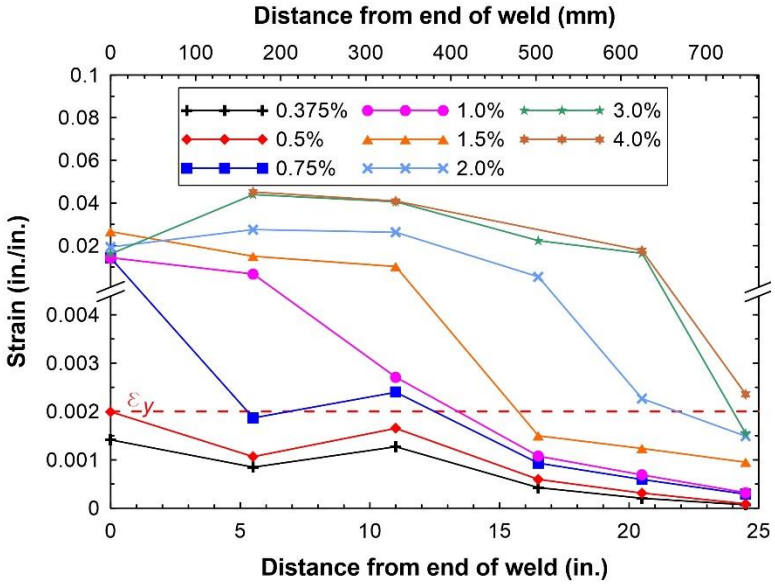

(a)

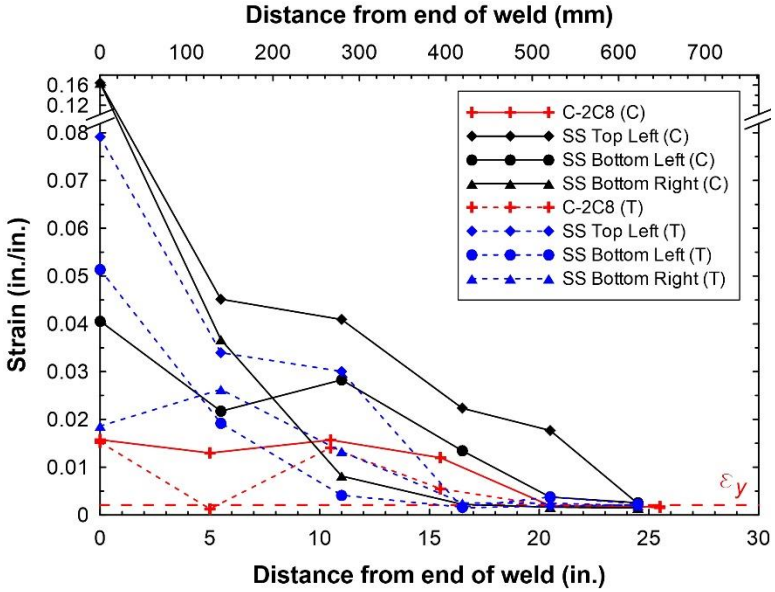

(b)

Figure 5-3 Strain profile along the length of chord members at the end of the special segment of STMF-2C8-2: (a) top right corner at different story drift levels; (b) maximum strain levels at each corner

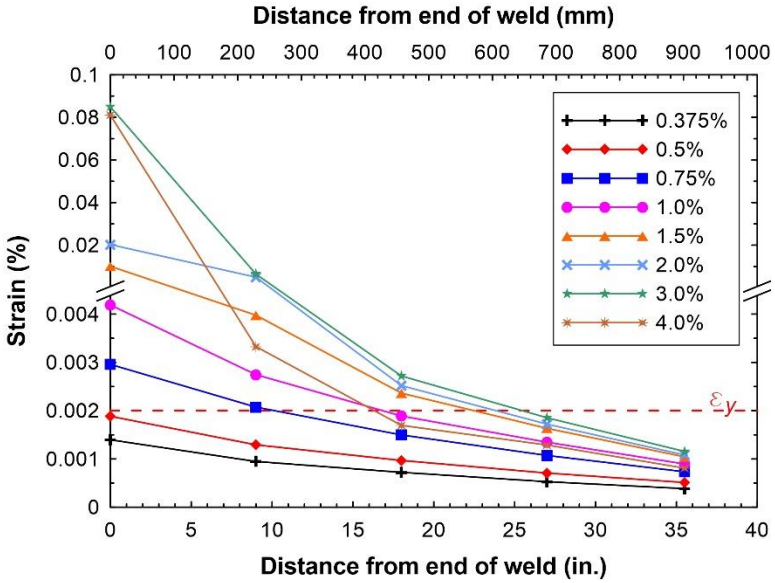

(a)

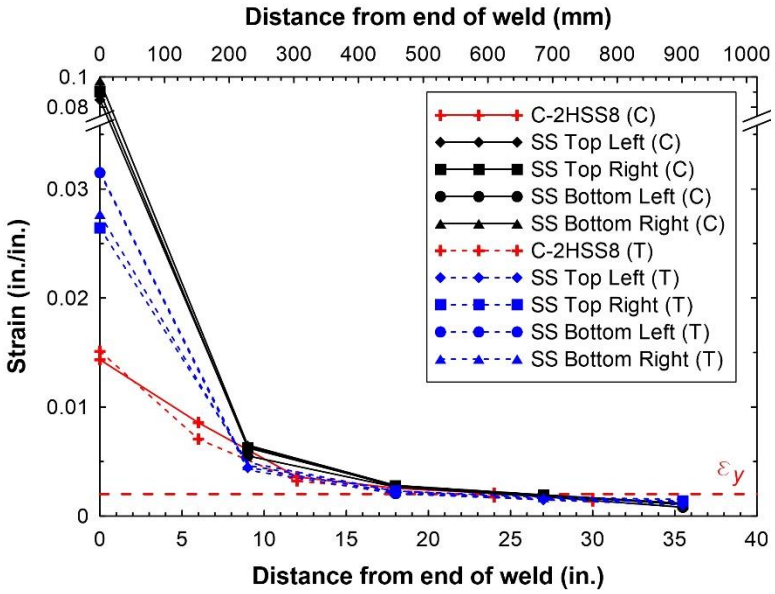

(b)

Figure 5-4 Strain profile along the length of chord members at the end of the special segment of STMF-2HSS8: (a) top right corner at different story drift levels; (b) maximum strain levels at each corner

5.2 Expected Vertical Shear Strength of STMFs with Intermediate Vertical Members

The presence of intermediate vertical members in the special segment contributed significant additional strength of STMF subassemblages as shown in Table 4-1. This was not considered in the current AISC V_{ne} equation (Eq. 2-3), which can result in considerable yielding in members outside of the special segment. A previously proposed V_{ne} equation for STMF with multiple Vierendeel panels (Eq. 2-4) assumed that both the chord members and the intermediate vertical members had the same plastic rotation when yield mechanism was reached (Chao and Goel, 2008a). A good illustration of the yield mechanism in STMFs with multiple Vierendeel panels can be seen in Figure 5-5.

In reality, because double-channel members had to be welded to gusset plates at truss joints, plastic hinges would not form at the end of the vertical members like the idealization shown in Figure 5-5. They would form where the welds between the members and the gusset plate ended which created an eccentricity, ℓ, shown in Figure 5-6 and Figure 5-7. Pushover analysis results performed prior to the experimental test took this eccentricity into account and showed that rotational demand of intermediate vertical members was substantially higher than that of the chord members. Moreover, because of the eccentricity, there was an additional contribution to the maximum vertical shear strength of the special segment coming from the shear force multiplied by this eccentricity in the vertical intermediate member. The expected maximum shear strength of the special segment with one intermediate vertical member (Figure 5-6) can be derived as:

$$V_{ne} = \frac{4\ M_{c\ \max}}{L_s} + \frac{4M'}{L_s} \qquad [5\text{-}1]$$

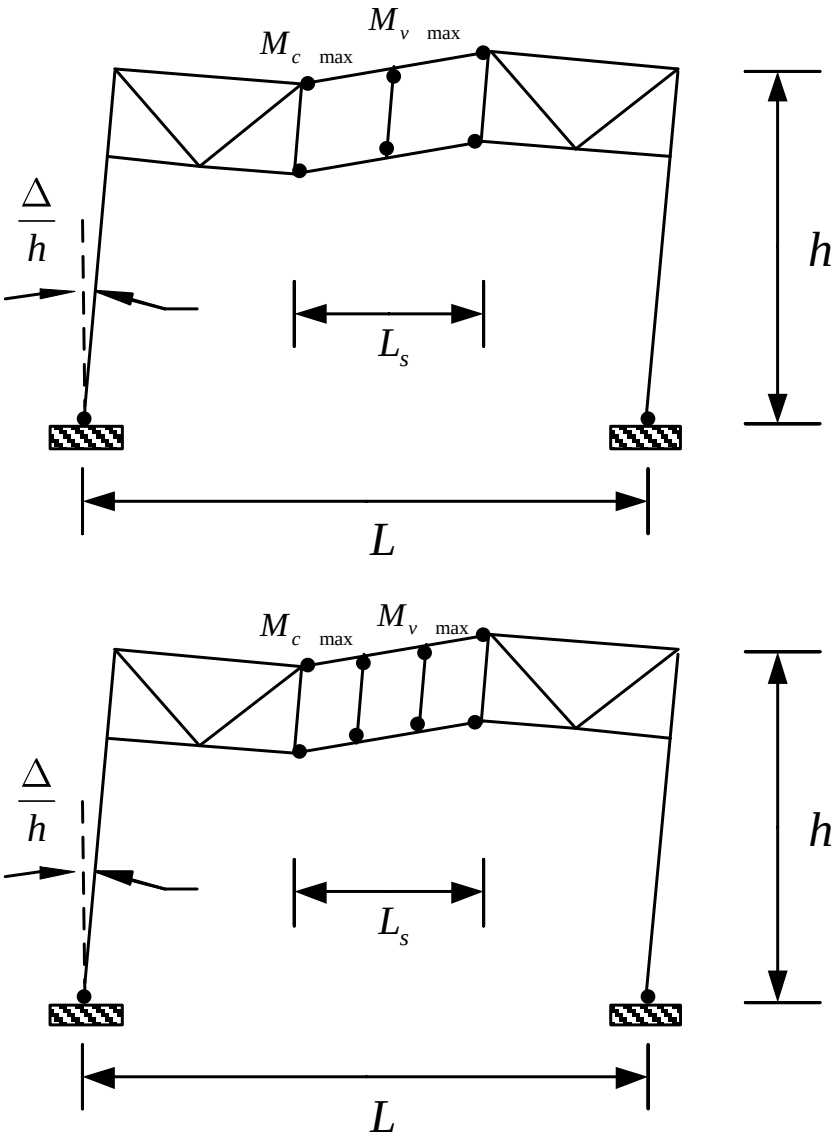

Figure 5-5 Yield mechanism of STMF with multiple Vierendeel panels

For a special segment with two intermediate vertical members as shown in Figure 5-7, the maximum shear strength can be derived as:

$$V_{ne} = \frac{4\ M_{c\ \max}}{L_s} + \frac{4\ 2M'}{L_s} \qquad [5\text{-}2]$$

$$\text{where } M' = \frac{(M_v)_{\max} + \dfrac{2\ M_{v\ \max}\ e}{l-2e}}{2}$$

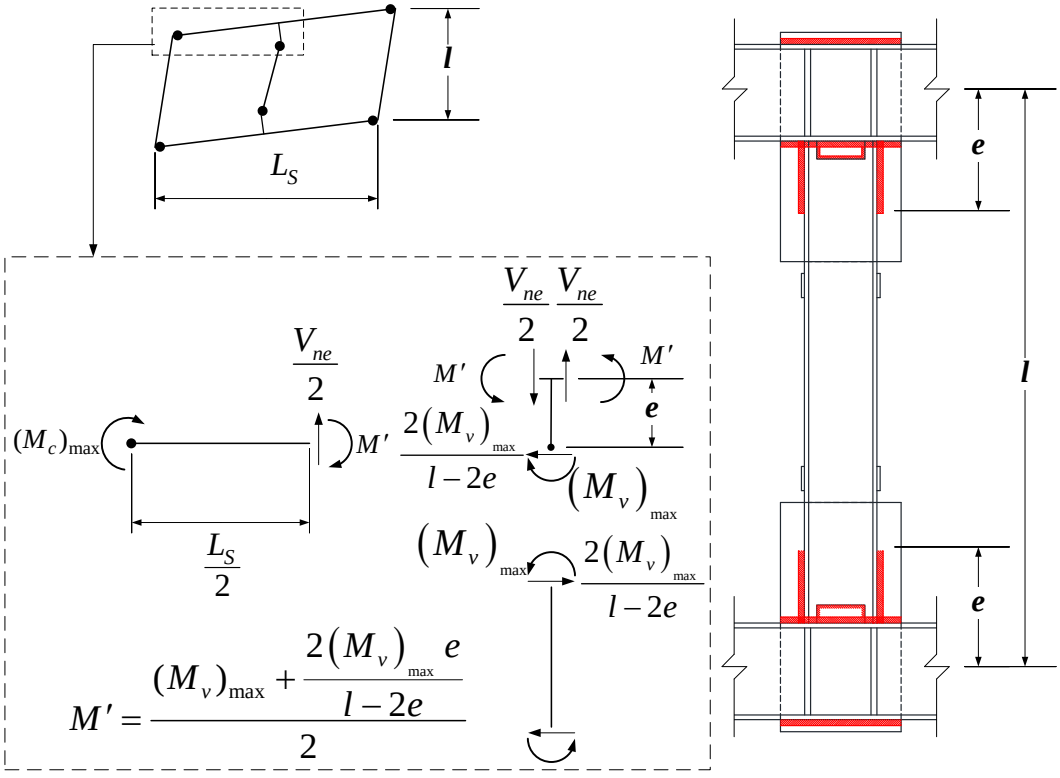

Figure 5-6 Calculation of V_{ne} for STMF with two Vierendeel panels

Using the maximum strain levels in the members outside of the special segment measured during the full-scale tests and R_y according to AISC 340-10 to substitute the maximum expected developed moments of the members, Eq. 5-2 becomes:

$$V_{ne} = \frac{5R_yM_{nc}}{L_s} + \frac{2.5mR_yM_{nv}}{L_s}\frac{l}{(l-2e)} \qquad [5\text{-}3]$$

where $m =$ number of intermediate vertical members

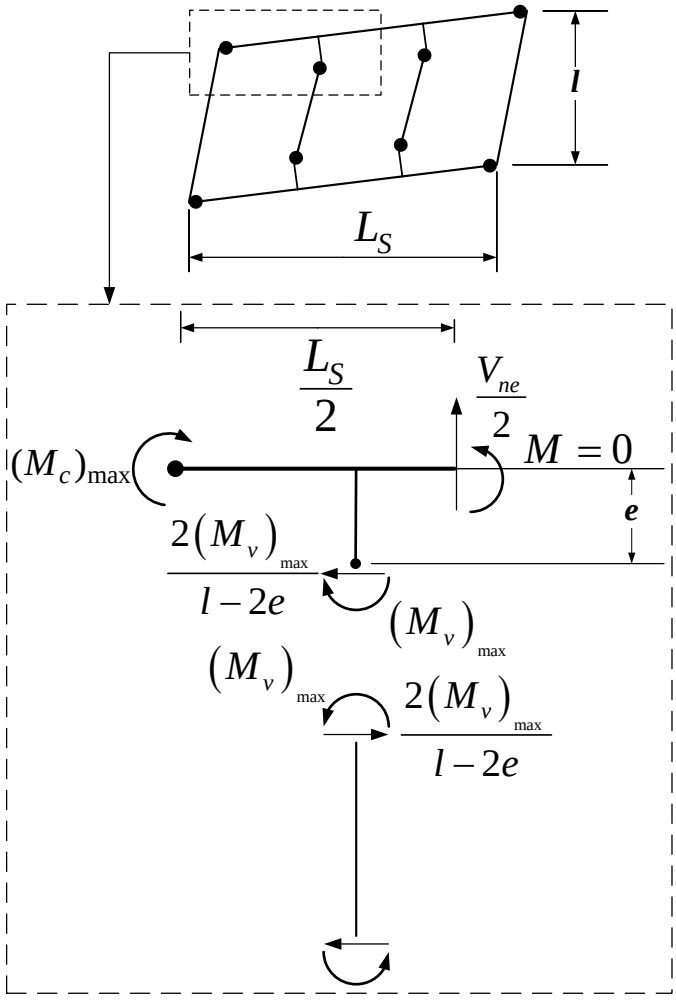

Figure 5-7 Calculation of V_{ne} for STMF with three Vierendeel panels

Eq. 5-3 eliminates two assumptions used in prior studies (Basha and Goel 1994; Chao and Goel 2008a): 1) the maximum expected developed moments of both the chord and the intermediate vertical members occur simultaneously at a 3% story drift ratio and 2) the strain-hardening ratio of both members are 10%. This strain-hardening ratio represents the ratio of the post-yield slope to the elastic slope based on the moment-

rotation relationship of the members. While previous studies found these values to be adequate, test results from this research showed that the maximum moment of the intermediate vertical members developed earlier than the chord members and greatly diminished before story drift ratio reached 3%.

Using Eq. 5-3, the contribution of the intermediate vertical members of STMF-2C8-2 to the V_{ne} (the second term of Eq. 5-3) was found to be 53%. At 1.5% story drift, the strength of STMF-2C8-2 peaked, and once the vertical members failed at 2% story drift, a drastic drop in strength was observed. Based on the observation, the strength ratio between the intermediate vertical members and the chord members were adequate because there was no major detrimental performance from the full-scale subassemblage test. However, a contribution from intermediate vertical member smaller than this ratio would yield a smoother strength degradation of the system.

5.3 Requirement for the Stability Bracing of Trusses

The lateral bracing system consisting of steel plates and threaded rods was instrumented with strain gauges to obtain the lateral forces (in transverse direction to the truss) at each corner of the special segments (Figure 5-8). The threaded rods were later tested to determine the force versus deformation relation (Figure 5-9). Lateral forces were then calculated based on the strain gauge response using a set of calibrated data from gauges on threaded rods. Examples of the strain response from individual thread rods are shown in Figure 5-10. It can be seen that the responses are significantly different from the theoretical values obtained by using the nominal area (0.44 in.^{2} for a 0.75-in. diameter threaded rod used in this experimental program).

Figure 5-8 Lateral bracing instrumentation

Figure 5-9 Lateral bracing threaded rod calibration test setup

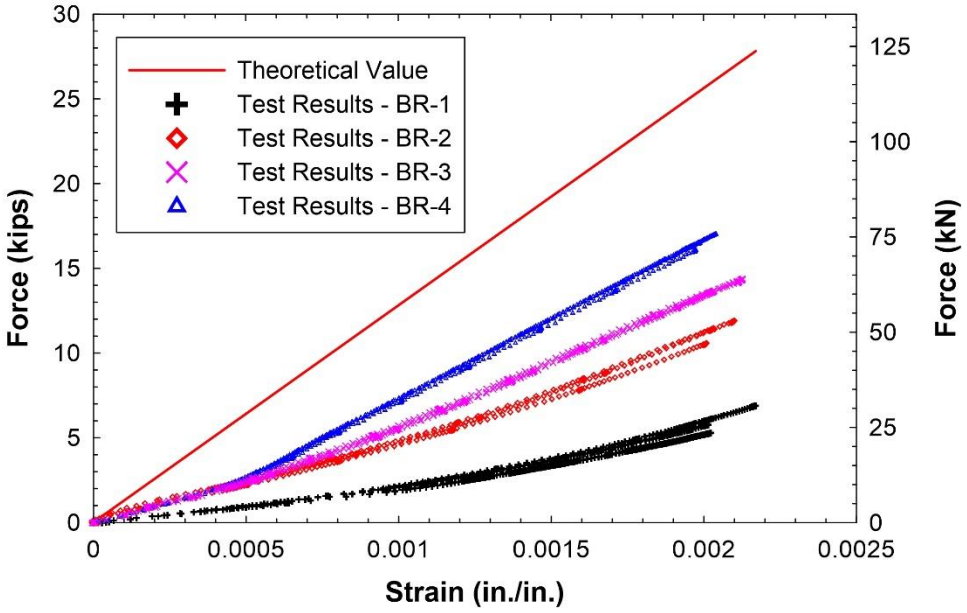

Figure 5-10 Lateral bracing threaded rod calibration test results

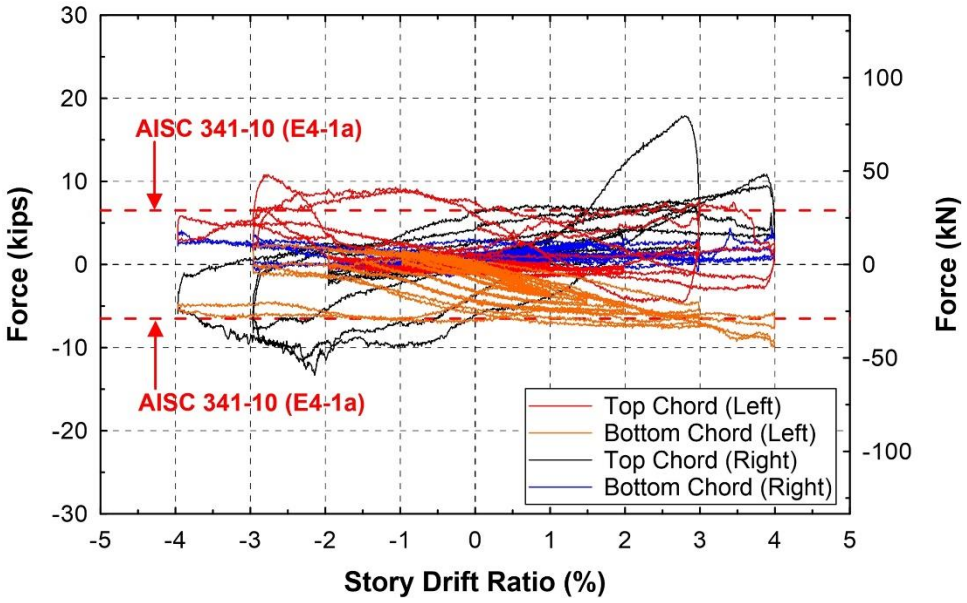

Figure 5-11 Lateral bracing forces at each corner of the special segment in STMF-2C8-1

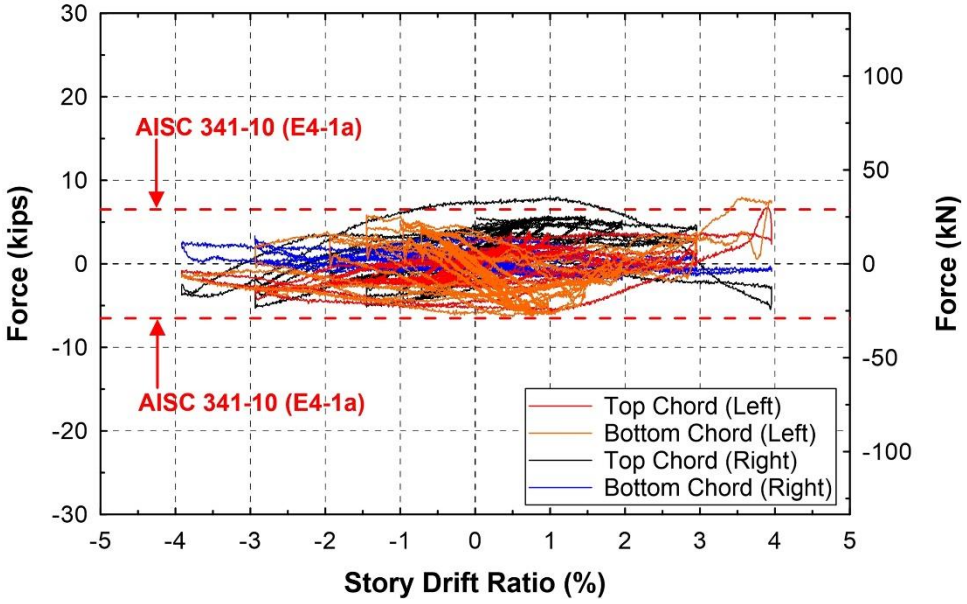

Figure 5-12 Lateral bracing forces at each corner of the special segment in STMF-2C8-2

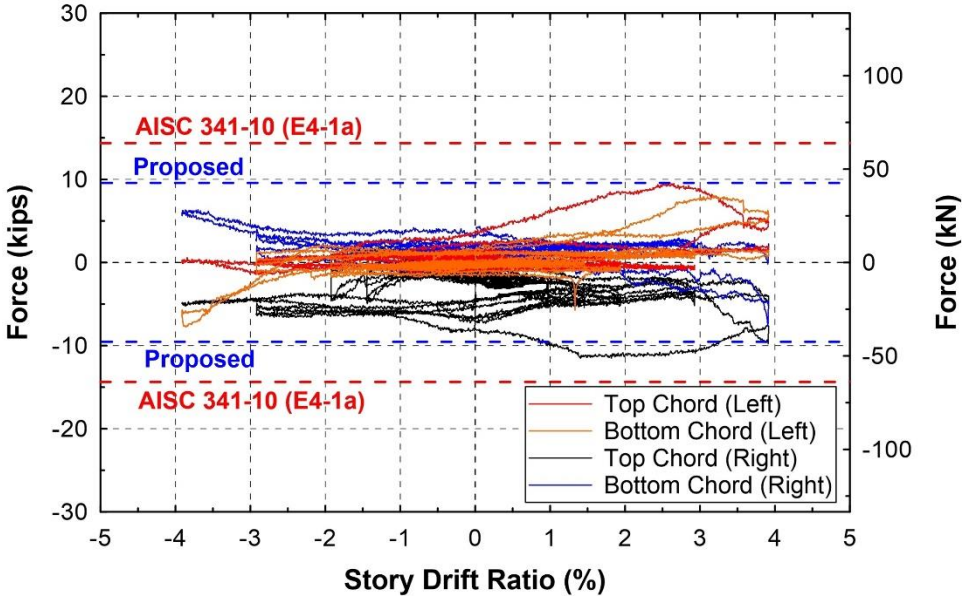

Figure 5-13 Lateral bracing forces at each corner of the special segment in STMF-2HSS8

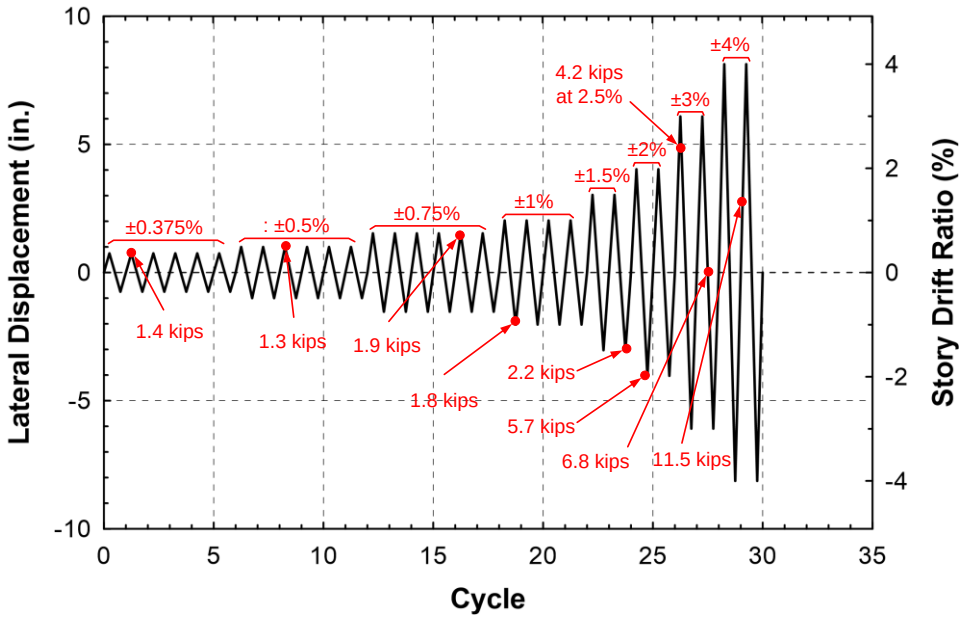

Figure 5-14 Maximum lateral bracing forces at different story drift levels of STMF-2HSS8

Figure 5-11 through Figure 5-13 shows the lateral bracing force responses at each corner of the special segment for the specimens. At first glance, it appears that the lateral forces were higher than the required strength of the lateral brace (AISC 341-10 Eq. E4-1a) for STMF-2C8-1 and STMF-2C82. Further investigation shows that the measured lateral forces were greater during the drift cycles at 3% and higher story drift ratios for STMF-2C8-1 and during 4% drift cycles for STMF-2C8-2. Those story drift levels are higher than the mean story drift ratios at design basis earthquakes (DBE) (10% probability of exceedance in 50 years) and maximum considered earthquakes (MCE) (2% probability of exceedance in 50 years) for a typical STMF system (Chao and Goel, 2008b). It is, then, concluded that the current requirement provides adequate strength for the lateral brace.

Figure 5-14 shows the maximum lateral bracing forces observed during the test at different targeted story drift ratios for STMF-2HSS8. The lateral bracing force gradually

increased from 1.4 kips during 0.375% story drift ratio cycles to 2.2 kips at the end of 1.5% story drift ratio cycles. It increased to 5.7 kips at the end of the first cycle of 2% story drift ratio and reached the maximum value of 11.5 kips during the second cycle of 4% story drift ratio. The maximum bracing forces typically occurred at the peak drift ratios, except when the drift ratios went beyond approximately 3% story drift. By this time, significant damage had occurred in the special segment causing the specimen to lose its lateral stability. Analytical studies indicated that, for typical STMF systems, the mean story drift ratios at design basis earthquakes (DBE) (10% probability of exceedance in 50 years) and maximum considered earthquakes (MCE) (2% probability of exceedance in 50 years) are approximately 1.5% and 2.5%, respectively (Chao and Goel, 2008b). It can be seen that the highest observed lateral bracing forces 6.8 kips at 3% story drift ratio are less than 50% of that required by AISC requirement (14.4 kips). It is worth mentioning that for STMFs using double-channel as chord members at the peak strength (2% story drift ratio), the maximum lateral force had already reached 98% of the AISC required strength of the lateral brace. This indicates that the current AISC requirement can be reduced for STMF with double-HSS built-up sections as chord members. This is due to the fact that HSS do not suffer from LTB and are more stable in the out-of-plane direction. Eq. 5-4 and Eq. 5-5 are suggested for the required strength of the lateral brace for STMF constructed with double-HSS as chord members for the load and resistance factor design (LRFD) method and allowable strength design (ASD) method, respectively.

$$P_u = 0.04 R_y F_y A_f \,(LRFD) \qquad [5\text{-}4]$$

$$P_u = (0.04/1.5) R_y F_y A_f \,(ASD) \qquad [5\text{-}5]$$

5.4 Predictive Formula and Strain Gauge Data

As previously shown, for STMF-2HSS8, the peak equivalent vertical shear forces obtained from test results (Figure 4-16) were close to the expected vertical shear strength, V_{ne} , predicted by AISC 341-05 (Eq. 2-2), but higher than that of AISC 341-10 (Eq. 2-3) by approximately 16%. This seems to indicate that AISC 341-10's equation underestimates the vertical shear strength of STMFs. However, further investigation indicates that the majority of the members outside of the special segment had strains much lower than the yield strain of steel, ε_y (see detailed strain analysis in next paragraph). This suggests that the AISC 341-10's equation (Eq. 2-3) still gives a safe design.

A portion of the HSS used in the chord members of the subassemblage specimen STMF-2HSS8 was cut off and set aside for the tensile test in order to obtain the material properties. Figure 5-15 shows the location of the cut locations for the tensile test coupon specimens. The average yielding strength of the section cut from the flange area was 65.1 ksi, which is significantly higher than the specified yield stress of 46 MPa. The average yielding strength of the web area was 59.8 ksi. Figure 5-16 shows the results from the tensile tests using the average strain of the gauge length (2 in.) obtained from a digital image correlation (DIC) measurement, shown in Figure 5-17, in accordance with ASTM E8/E8M standard (ASTM International, 2015) and compared to conventional strain gauges placed at the center and at both ends of the gauge length along the center line of the coupon specimens. The average yielding strength and tensile strength from the tensile test in conjunction with the member rotations obtained from component tests were used to represent the plastic hinge properties of the actual HSS used in the full-scale STMF subassemblage specimen. In other words, for example, the actual first

yielding moment was calculated using average yielding strength from coupon tests multiplied by the plastic modulus of the section.

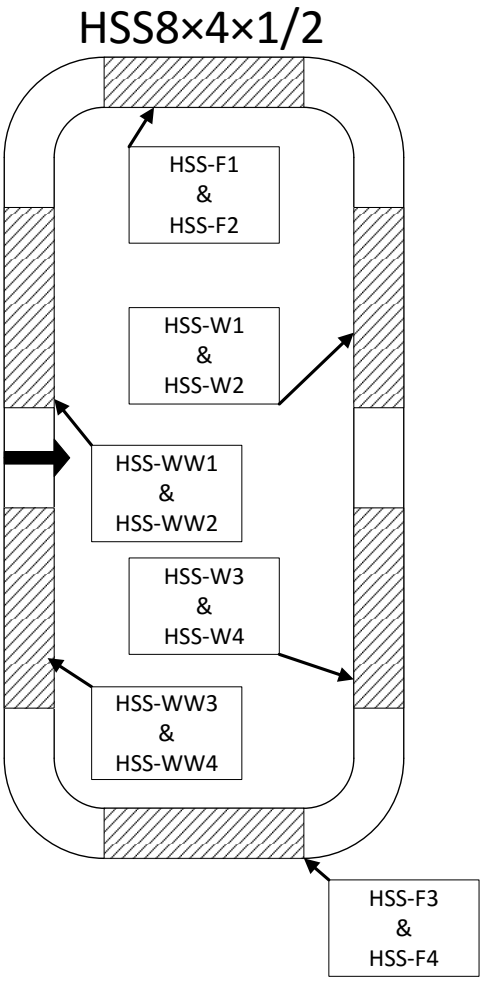

Figure 5-15 Cut locations for tensile test coupon specimens

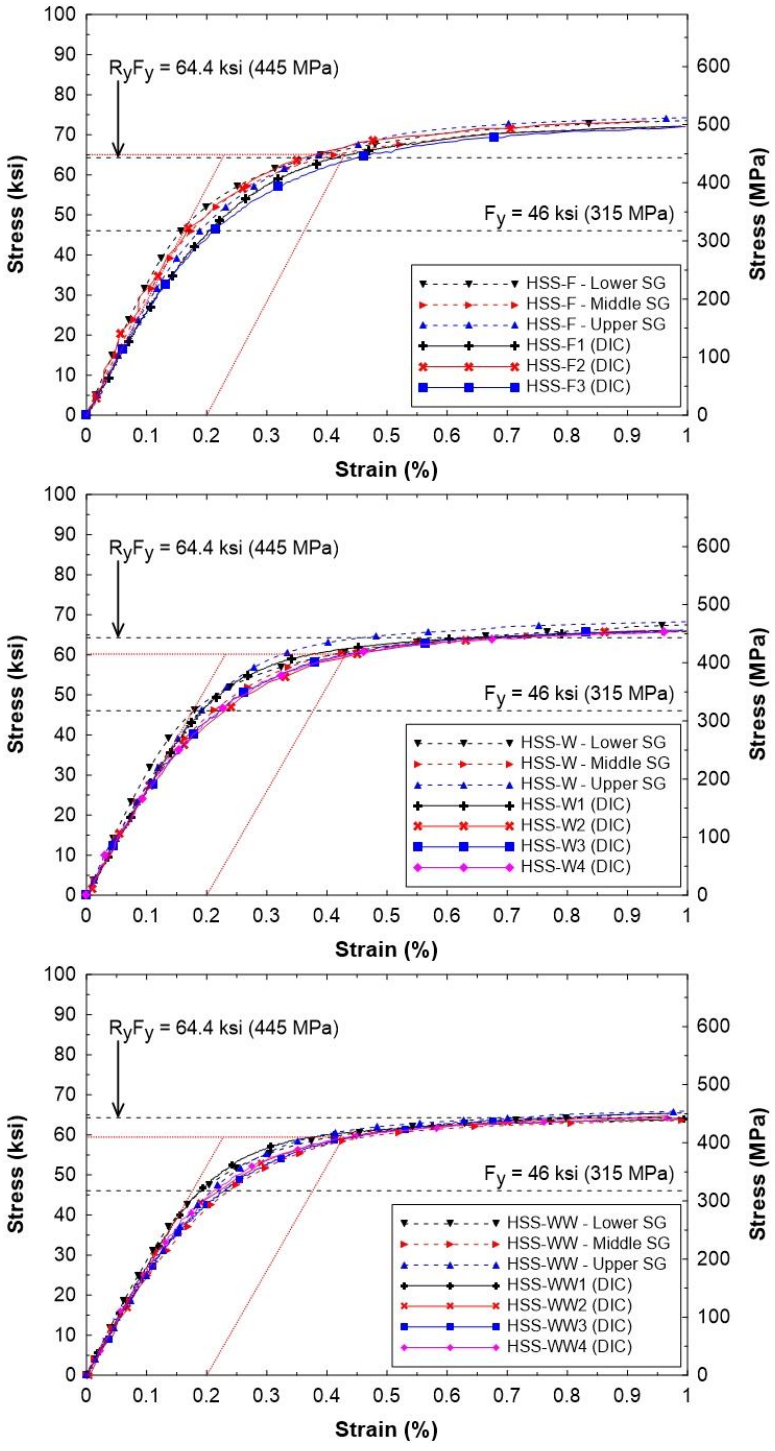

Figure 5-16 Tensile test results for HSS8×4×1/2 section

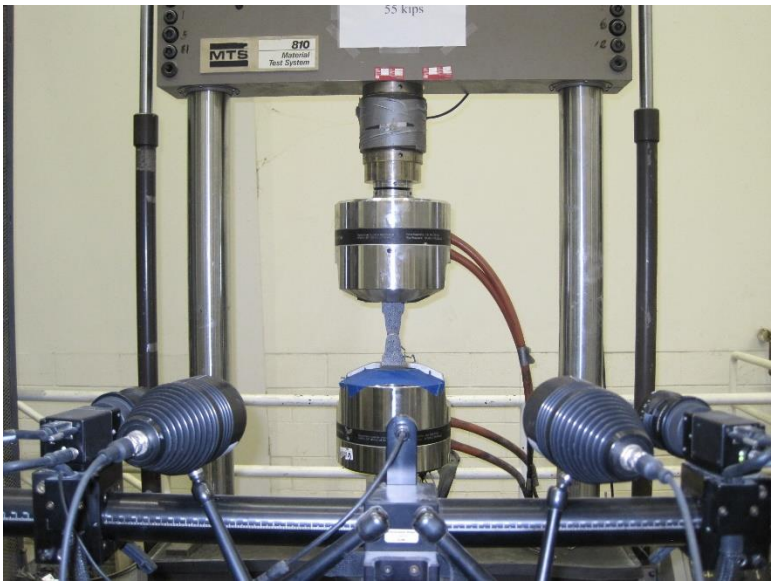

Figure 5-17 DIC test setup

Figure 5-18 shows the maximum strain levels observed during the test on members outside of the special segment.

Figure 5-19 shows the hysteretic strain response of strain gauges that recorded the maximum strain level in the member and gusset plate located outside of the special segment. The maximum strain occurred in members outside of the special segment was observed at 84% of the yield strain, assuming 2000 micro-strain (0.002 mm/mm) as the yielding point. This only occurred at one particular location (Strain Gauge M4-1-2) as shown in Figure 5-18. These data indicate that the predicted V_{ne} value from the AISC 341-10 is still conservative. For the vertical members at the ends of the special segment, the highest strain utilization was observed at 85% of the yield strain (

Figure 5-20).

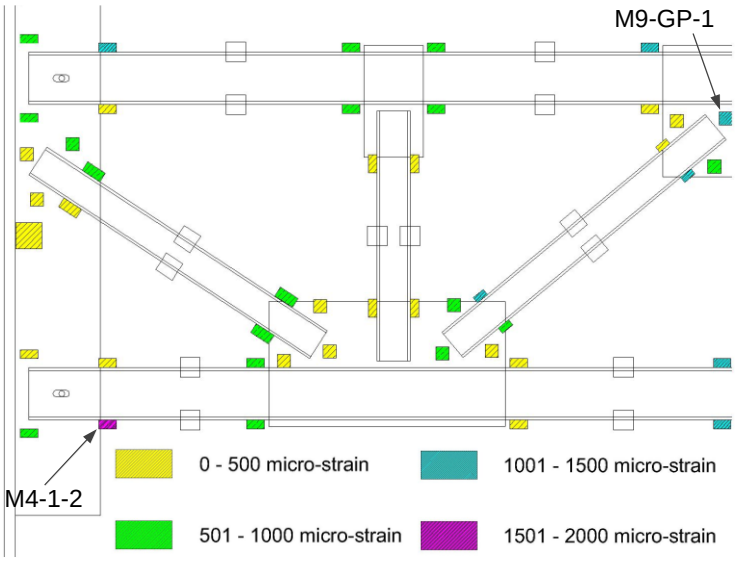

Figure 5-18 Maximum strain levels in exterior panels of specimen STMF-2HSS8

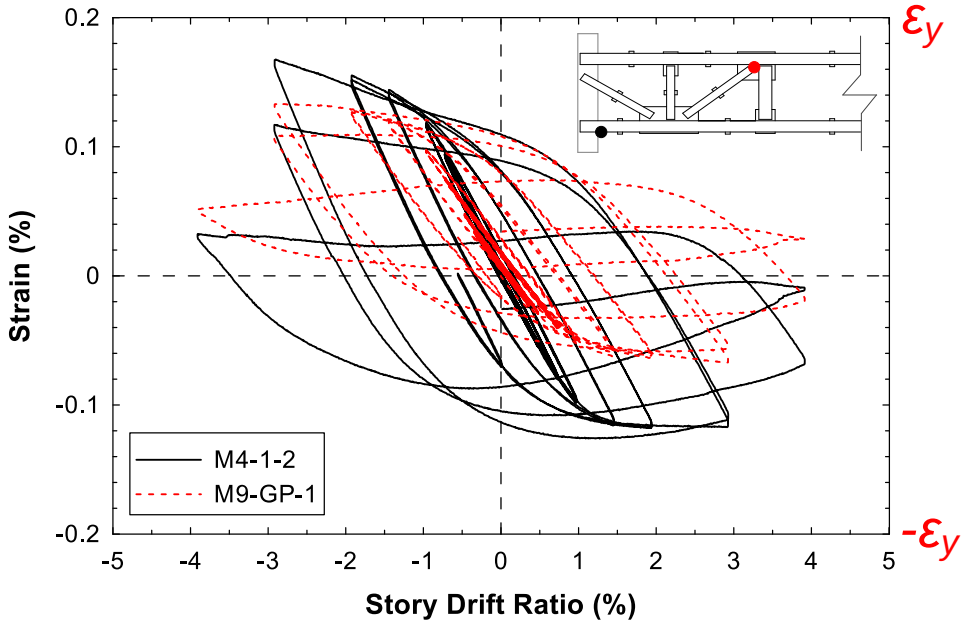

Figure 5-19 Hysteretic strain response of maximum strain level observed outside of the special segment of specimen STMF-2HSS8

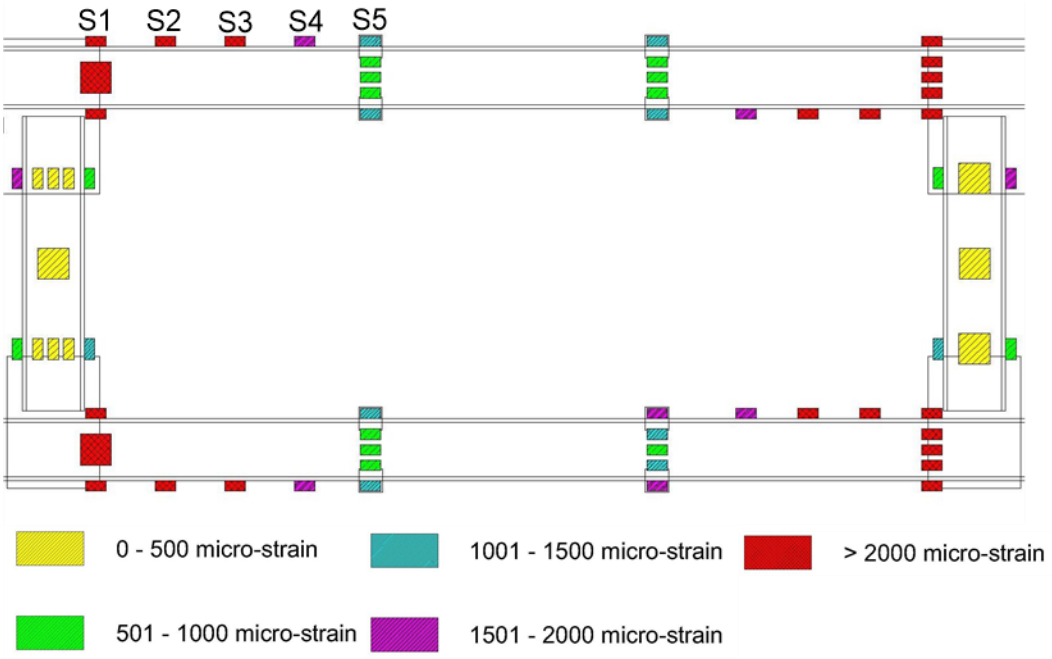

Figure 5-20 Maximum strain levels in the special segment panel of specimen STMF-2HSS8

Figure 5-21 shows that the first yielding of the chord member (at top flange) occurred at the story drift ratio slightly higher than 0.5%. Strain profiles along the length of the top chord members at the end of the special segment indicate that the length of the plastic hinge was approximately 25.5 in. (about three times the depth of the member) assuming the plastic hinge starts at the end of weld between the members and the gusset plate (location of strain gauge S1 as shown in

Figure 5-21) at the story drift ratio of 3.0%.

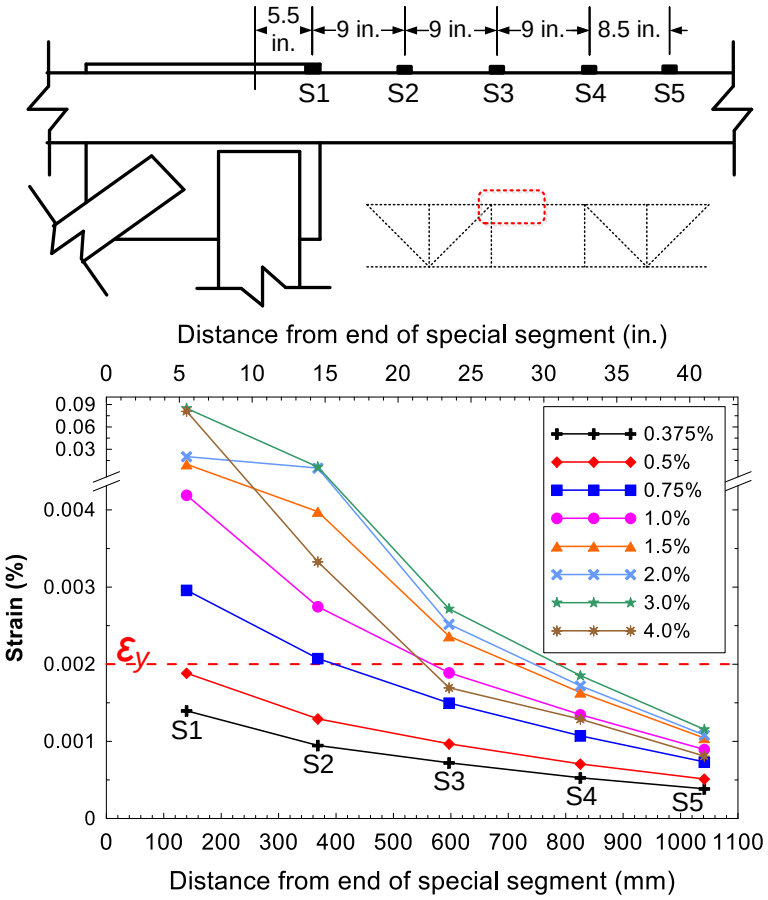

Figure 5-21 Strain profile on top of the flange and along the length of chord member at the end of the special segment of specimen STMF-2HSS8

5.5 Suggesting Design Approach for Non-Yielding Members Outside of the Special Segment

While AISC 341-10 (AISC, 2010) suggests a V_{ne} equation for the design of members outside of the special segment, it may not be the most direct and easy way to design those non-yielding members when the entire 3D building model is created by a computer software program. A more straightforward design could be done by directly modeling the plastic hinge properties of the chord members, then determining the forces

in the non-yielding members by a pushover analysis of the 3D model. The following design procedure and information is recommended:

Use the generalized moment-rotation relationship for plastic hinges in the chord member as shown in

1. Figure 5-22. Table 5-1 summarizes the values used for the plastic hinge properties used for the pushover analyses in this study using the test results and the recommended values for STMFs with double-HSS built-up sections as chord members. As shown in Figure 4-11, the recommended values give a reasonable force-displacement envelope (green dotted line) as compared to the cyclic testing of the full-scale specimen.
2. Carry out a pushover analysis until the story drift ratio reaches at least 1.5%. At that time, the maximum shear at the middle of the special segment reaches approximately the V_{ne} calculated by the AISC 341-10's V_{ne} value (Figure 4-16). Then use the forces in the non-yielding members to carry out the usual elastic design for these members.

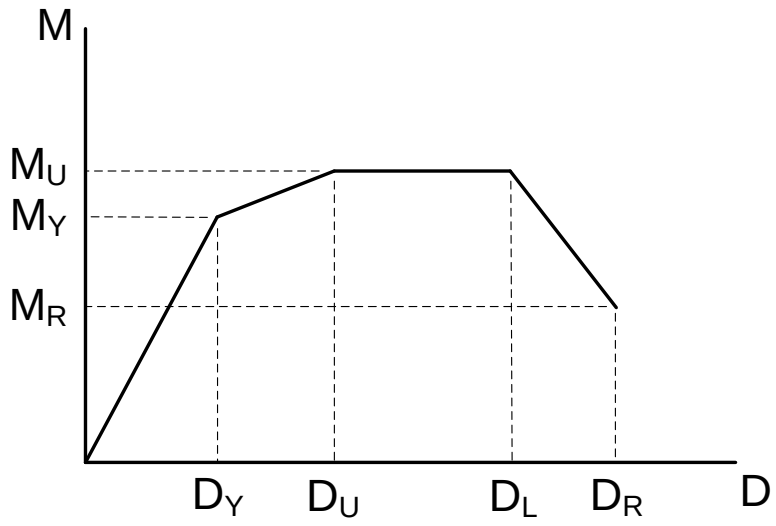

Figure 5-22 Generalized moment-rotation relation for plastic hinges

Table 5-1 Plastic hinge modeling parameters

	M_Y (kip-in.)	M_U (kip-in.)	M_R (kip-in.)	D_Y (rad)	D_U (rad)	D_L (rad)	D_R (rad)
Results from component test (2HSS8×4×1/2)	3340	3975	400	0.023	0.043	0.073	0.091
Recommended values for double-HSS built-up sections	$R_y F_y Z$	$1.3M_y$	$0.1M_u$	$\frac{M_Y L_S}{3.8EI}$	0.04	0.07	0.09

Chapter 6

Part I : Summary, Conclusions, and Design Recommendations

The major objectives reported in this research are:

1. Verifying whether larger sections (double-channel built-up members) could accommodate large rotational demand in full-scale STMF;
2. Investigating connection details of the joints at the end of the special segment;
3. Investigating seismic performance of STMF with special segment having multiple Vierendeel panels and suggesting a design equation considering the contribution of intermediate vertical members to V_{ne};
4. Verifying a new detailing configuration at plastic hinge region to minimize LTB.

6.1 STMF with Double-Channel as Chord Members

The results from the experimental tests of double-channel components and two full-scale STMF subassemblages with C8×18.75 section as chord members were compared to the current practice and AISC Seismic Provisions. The conclusions and design recommendations are drawn as follows:

1. Proposed special detailing: Extended gusset plates at the ends of the chord in the special segment and the intermediate vertical members with a weld-free zone (the plastic hinge region) can eliminate LTB and extend the plastic hinge length which, in turn, increase the ductility of the trusses.
2. Where intermediate vertical members are used, their contribution to both stiffness and strength of STMFs need to be explicitly considered in the design of members outside of the special segment. When the intermediate vertical members are smaller than the chord members, they yield and fail before the chord members due to their greater rotational

demands. In other words, they serve as the first elements that dissipate the majority of earthquake energy. Once they fail, an STMF's behavior follows that of an STMF without intermediate vertical members. This behavior could be beneficial because if only the intermediate vertical members are damaged in a low-to-moderate seismic event, they can be easily replaced. On the other hand, intermediate vertical members with high flexural capacity can lead to a drastic drop in an STMF's strength once they fail. To this end, it is suggested that the contribution of the intermediate vertical members to the V_{ne} is no more than 50% of the total V_{ne}. This contribution can be calculated from Eq. 5-3 with a reasonable accuracy. In current practice where the intermediate vertical members are larger than the chord members, which was not experimentally investigated in this study, an analysis should be done to confirm that the preferred yield mechanism can be achieved and their contribution to the V_{ne} would not cause detrimental degradation of strength, once they fail.

3. Although the current V_{ne} equation (AISC 341-10) slightly underestimates the maximum expected shear strength of STMF with a single Vierendeel panel, full-scale experiments show that members outside of the special segment did not experience any yielding even when the chord members in the special segment were completely fractured. A simpler and more accurate V_{ne} prediction equation for STMFs with a single Vierendeel panel is needed in order to better predict the expected vertical shear force in the special segment. This, in turn, will lead to a more economical design for members outside the special segment.

4. It is recommended that the end of vertical members at the end of the special segments should not be welded directly to the flanges of the chord members. This is to allow for a free spread of large inelastic deformation in plastic hinges, thus preventing undesirable early failure due to fractures.
5. Splicing of chord members within one-half the panel length from the ends of the special segment can be permitted.

6.2 STMF with Double-HSS as Chord Members

This research presents test results of an STMF subassemblage specimen constructed with double-HSS built-up chord members. Double-HSS members' high torsional rigidity eliminates lateral-torsional buckling, thereby eliminating the need for lateral bracing in beam-type members. They also effectively delay flange local buckling thereby enhancing rotational ductility due to the reduced width-to-thickness ratio (*b*/*t*) as compared to a single-HSS with the same flexural capacity. Only a simple connection detail utilizing gusset plate with direct welding between the gusset plate and the double-HSS is needed for the fabrication. The following conclusions can be drawn from the results of this study:

1. A full-scale STMF subassemblage test indicated that double-HSS members can be a viable option for the chord members in the special segments. They provide high rotational capacity up to nearly 0.09 radian before significant degradation occurs. This high rotational capacity is particularly critical for STMFs due to the high rotational demand in the special segments.
2. Although the current V_{ne} equation (AISC 341-10) slightly underestimates the maximum expected shear strength of the STMF subassemblage

using double-HSS chord members, test results show that members outside of the special segment did not experience any yielding even when the chord members in the special segment were completely fractured. Therefor the current Vne equation for STMFs is still valid.

3. The observed yield drift ratio (approximately 0.75%) of the full-scale specimen is nearly the same with the STMF with a special segment having a length-to-depth ratio of 2.0 (Chao and Goel, 2008b). Therefore, the upper limit for the length-to-depth ratio of any panel in the special segment could be increased to 2.5 without affecting the elastic lateral stiffness of STMFs.
4. The current requirement for the stability bracing of trusses (AISC 341-10, Eq. E4-1a and E4-1b) can be safely reduced for STMFs with double-HSS built-up chord members. Recommended equations (Eqs. 5-4 and 5-5) for the required strength of the lateral brace for STMF constructed with double HSS are proposed.
5. While the V_{ne} equation specified in AISC 341 is more convenient when a "column-tree" procedure is used to design the non-yielding members outside of the special segments, this paper suggests a moment-rotation model of the plastic hinges at chord members as well as a pushover analysis procedure to design the non-yielding members outside of the special segments. The suggested method can be more convenient when a 3D building model is built by computer which is typically done in modern design; hence, one does not have to carry out an additional column-tree analysis.

Chapter 7

Part II: Introduction

7.1 Overview

Steel staggered truss framing (STF) system was first developed as a result of a research project by a team of architects and engineers at Massachusetts Institute of Technology sponsored by the United States Steel Corporation in the late 1960s to compete with the reinforced concrete flat slab system (Goody et al., 1967; Scalzi, 1971). The system was developed to achieve a more efficient structural framing system to resist wind loads and at the same time provide versatility of floor layout with large open areas. The result was an economical steel framing system for mid- to high-rise buildings (6 to 25 stories tall) that was simple to fabricate and erect, with low floor-to-floor heights and large column-free spaces. A typical STF system, as shown in Figure 7-1, composes of a series of story-high steel trusses in a staggered pattern in the transverse direction serving as both gravity and lateral force-resisting system.

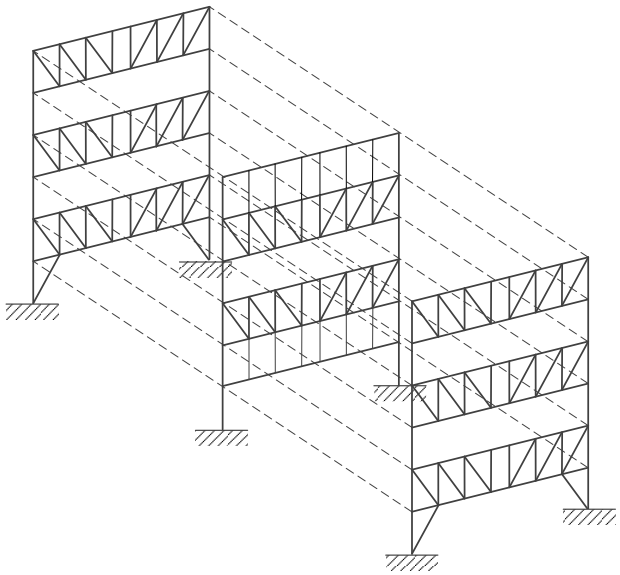

Figure 7-1 Schematic of a typical staggered truss framing system

The story-high trusses in a staggered pattern wherein trusses are placed at alternating levels at alternating column lines. This pattern provides large column-free areas and low floor-to-floor heights. The floor system serves as a diaphragm transferring the lateral shear forces between adjacent trusses. Key features of an STF system are:

(1) Story-height trusses are used in the transverse direction of the building to serve as both gravity and lateral force-resisting systems;

(2) Conventional moment or braced frames are used in the longitudinal direction of the building;

(2) Exterior columns support the ends of the truss and provide frame columns for the lateral force resisting system in the longitudinal direction of the building;

(3) Typically, the truss has one or more Vierendeel panels to allow an opening for a corridor or passageway perpendicular to the truss;

(4) Floor diaphragms are typically made of prestressed precast concrete hollow core planks spanning from the bottom chord of one truss to the top chord of the adjacent truss in the longitudinal direction;

7.2 Benefits of STF System

STF system was originally developed to achieve an efficient structural framing system to resist wind loads, and at the same time, provide versatility of floor layout with large open areas. Large column-free space of 60 to 80 ft can be achieved in both directions. It provides low floor-to-floor height (as low as 8 ft 8 in.) with fewer columns than other steel framing system which results in significant superstructure weight savings. Having fewer columns also offers faster fabrication and reduces foundation costs. It is reported that, on a relative basis, the structural unit costs per square foot of building area of the STF system is up to 40% less than other systems (Cohen, 1986). Other added benefits of the STF system include construction efficiency and effectiveness due to the

repetition of identical trusses and all-weather erection, increased design flexibility from the large column-free space, and semi-finished floor and ceiling that require little or no finishing. Using hollow core planks as flooring system also contributes to the weight reduction and the speed of construction. They are widely known for their low maintenance cost, economical spans, better control of deflection and flexural cracking, acoustical and heat transfer control, and excellent fire resistance. Figure 7-2 illustrates the benefits of STF system.

Because of the design flexibility, construction efficiency, and overall cost savings, STFs have become a popular system in the U.S. in regions of low seismicity for residential apartments, hotels, motels, dormitories, hospitals, and other structures for which a low floor-to-floor height is desirable (Brazil, 2000; Wexler and Lin, 2003).

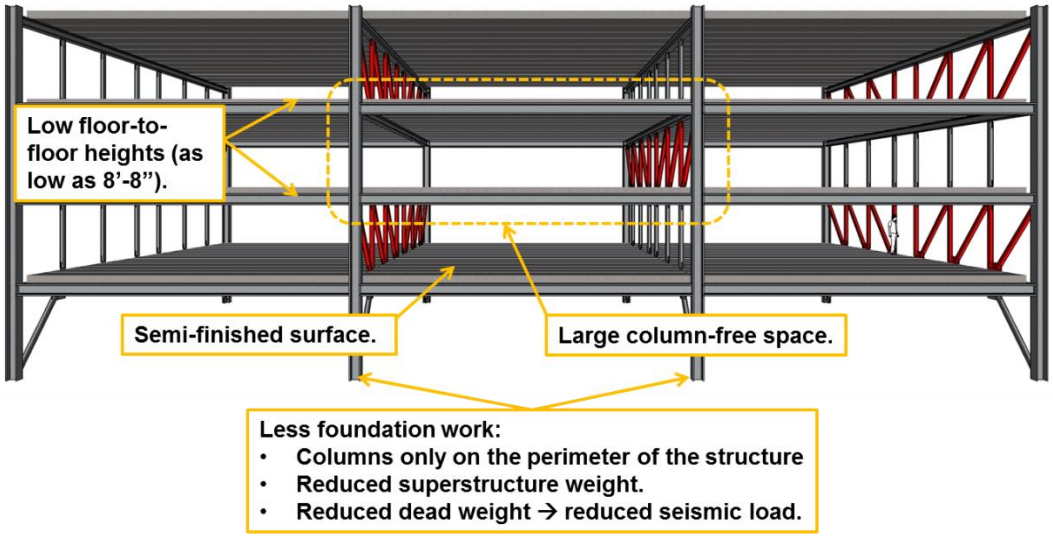

Figure 7-2 Benefits of STF system

Chapter 8

Part II: Research Objectives

8.1 Overview

While STF system was originally developed for low seismic regions, the high lateral stiffness and light weight structural frames make this system attractive for use in highly seismic regions. This research serves as a key step to understanding the seismic response and behavior of the STF systems. Limitations of the conventional STF system in seismically active areas are discussed. Subsequently, seismic performance of prototypes of mid-rise STF buildings with alternative structural layouts are investigated using pushover and nonlinear time-history analyses.

8.2 Limitations of STF System in Seismic Regions

Although STF system has been widely used in low-seismic regions because of the apparent benefits of the system, there are attributes that limit the use of STF system in areas of moderate to high seismicity such as the stability of gravity system due to the fact that the lateral and gravity force-resisting systems are one and the same and the increasingly large diaphragm shear force in the lower stories. Openings in the diaphragm (for stairwells and evaluator) can cause complex force transfer paths to form across the diaphragm. In addition to the issues in the diaphragm and its connections, there are attributes in the steel system that limit the use of STF system in areas of moderate to high seismicity such as a large “kink” in columns at the flexible non-truss level under lateral seismic loads and the large rotation at the ends of the chord members in the Vierendeel panels similar to the special segment in an STMF (Figure 2-4) which in turns limits the overall drift capacity of the system. Eq. 8-1 shows the approximate relationship between the story drift ratio and plastic hinge rotation of chord members in the center Vierendeel panel. For typical STFs with the ratio of truss girder span to the length of the

single Vierendeel panel of 9.0, the relationship between the story drift and the plastic rotation of the chord members is shown in Table 8-1. It can be seen that the plastic rotational demand of the chord member is as high as 0.17 radians at 2% story drift ratio.

$$\theta_p = \gamma + \beta \approx \frac{L}{L_s} * (story\ drift) - 0.015(rad) \quad [8\text{-}1]$$

where θ_p = plastic rotation of chord members

γ = rotation of the chord members in the Vierendeel panels with respect to the horizontal axis

β = rotation of the vertical member at the end of the Vierendeel panel with respect to the vertical axis

L = truss girder span length

L_s = length of the Vierendeel panel

Table 8-1 Plastic Rotation of Chord Members and Story Drift Ratio Relations

Story Drift Ratio (%)	Plastic Rotation (radian)
0.50	0.03
0.75	0.05
1.00	0.08
1.25	1.00
1.50	0.12
1.75	0.14
2.00	0.17
2.25	0.19
2.50	0.21
2.75	0.23
3.00	0.26

Limited studies have been conducted on the behavior of STFs under strong earthquake ground motions particularly on the high in-plane forces in the precast hollow-

core slab diaphragm typically utilized in STFs. To the author's best knowledge, there is no test data available on this subject. The shear force transfer between the precast hollow-core slab and steel truss in the exterior bay and the increasingly large diaphragm shear force in the lower stories, as shown in Figure 8-1, brings concerns regarding the cyclic behavior of diaphragm-to-truss connections. Due to rigidity of the connections, large moment would develop in the diaphragm-to-truss connections when the structure displaces along the longitudinal direction. The connections can be subjected to bi-axial bending. Large openings on the floor, e.g. stairwells or elevators, also affect the shear transfer across the diaphragms.

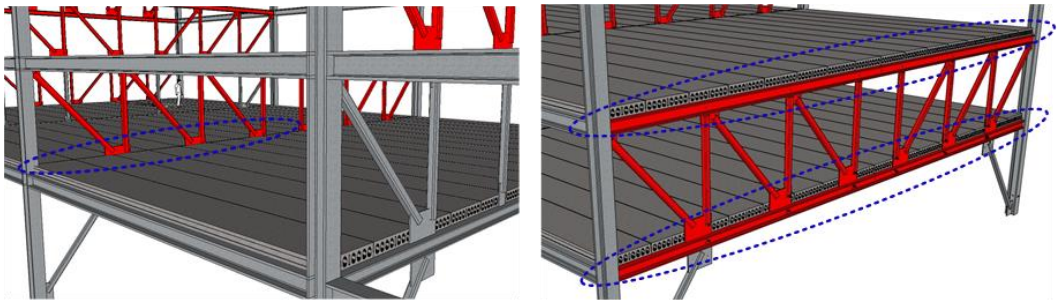

(a) (b)

Figure 8-1 Diaphragm-to-truss connections: (a) interior diaphragm; (b) exterior diaphragm

8.3 Objectives

This research presents an alternative layout of the STF system for moderate-to-high seismically active areas utilizing horizontal steel trusses to transfer the in-plane diaphragm forces and diagonal braces at the non-truss levels to alleviate the demand on columns. The conventional diaphragms composed of precast concrete planks are replaced by the horizontal steel truss to transmit the large diaphragm shear forces in the lower stories. Additional braces (called "kickers") are added in the story levels without floor-height trusses in order to minimize the column deformations that occur due to secondary bending and relatively smaller story stiffness as compared to stories with

story-height truss. Diagonal web members are added in the outermost panels of the posts and hangers. In addition, the Vierendeel panels in the center of the trusses are modified to span over three panels of the truss to increase the overall drift capacity of the structure (Gupta, 1974). In the conventional STF system, precast planks span in the longitudinal direction. If large openings in the floor are required, the shear transfer across the diaphragms is largely interrupted. For the modified system, because the horizontal trusses serve as transfer diaphragm, precast planks are arranged in the transverse direction. With this orientation, the gravity loads are resisted by the spandrel beams and the interior beams rather than directly on the trusses. Large openings in the floor can be arranged to accommodate for stairwells or elevators if needed. Figure 8-2 shows the three-dimensional models of the conventional and the modified STF systems with the precast plank orientation.

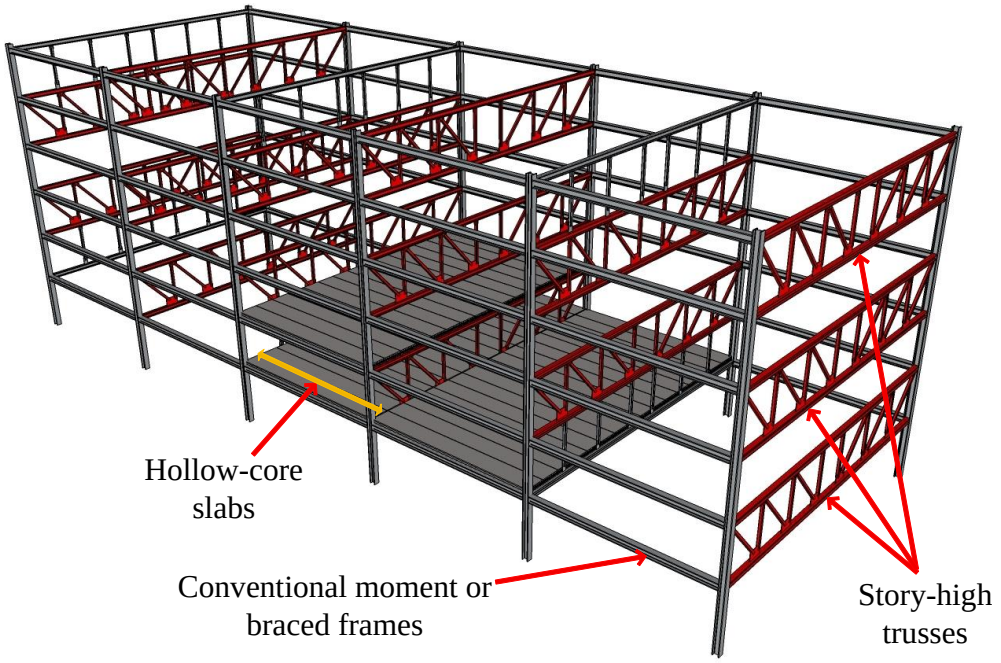

(a)

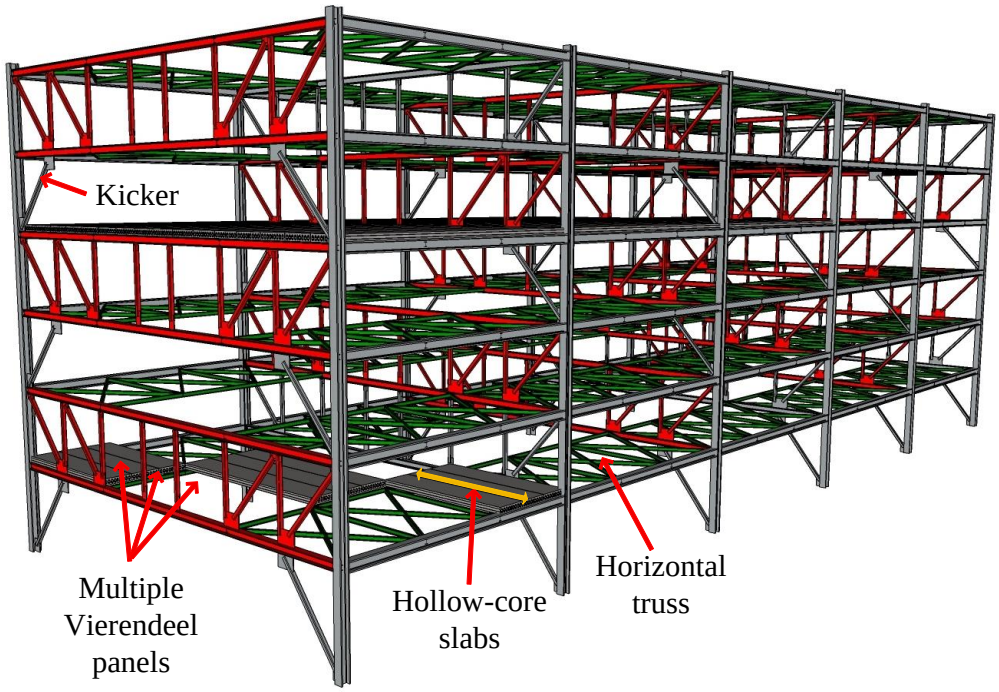

(b)

Figure 8-2 3D Models of STF systems: (a) conventional; (b) modified layout

Chapter 9

Part II: Prototypes STF Structures with Modified Structural Layouts

9.1 Overview

This chapter presents the design of prototypes STF structures with modified structural layouts. Kickers were added at the non-truss levels to alleviate the demand on columns. The single Vierendeel panel was modified to span over three panels of the truss to reduce the rotational demands in the chord members, thereby increasing the overall drift capacity of the structure. Horizontal steel trusses, with conventional precast hollow-core slabs spanning across the transverse direction, towards the ends of the STFs were chosen as floor diaphragms to effectively transfer the in-plane shear to STFs through direct axial forces in the truss members. The horizontal trusses are shifted to avoid the direct gravity loading on the Vierendeel panels so that the yielding members are not resisting gravity loads. Figure 9-1 shows the structure layouts and geometry of the prototype buildings. The structure was 64 ft 1½ in. by 180 ft in plan and 64 ft 6 in. in height. The floor height on the first level was 12 ft where the upper levels are 10 ft 6 in. There were six bays with 36 ft spacing on centers in the transverse direction. The STFs serve as the seismic force-resisting system in the transverse direction. In the longitudinal direction, conventional moment-resisting frames were used along the perimeter as the seismic force-resisting system. Pinned-connections, as shown in Figure 9-2, were modeled between the horizontal trusses and STFs to minimize bending moment induced by the lateral displacement in the longitudinal direction. With the horizontal trusses acting as floor diaphragm, the precast slabs, which are simply supported on the horizontal truss, only transfer their own inertia forces; therefore, the demand at the slab-to-truss connection reduced drastically.

First, a prototype mid-rise STF building, called “Base Model” was designed according to the spectrum specified in the 1997 NEHRP (FEMA, 1997). The structure was then redesigned with the lateral forces equal to those when the structure is pushed until the roof drift ratio is at one percent (explained later). This prototype structure is called the “Target Drift Model.” Figure 9-3 shows the elevation view along with the features of the Base and the Target Drift models, respectively. Another model, called “No Kicker Model” (Figure 9-4) was created by removing the diagonal braces at the upper non-truss levels (similar to the conventional STF) while keeping the member sections from the Base Model. An additional model, called “Single Vierendeel Panel” (SVP) Model (Figure 9-5), was also created by adding the diagonal web members with the same member sections as the diagonal web members from the Base Model to create a single Vierendeel panel for the trusses (similar to the conventional STF). Seismic performance of all the models was then evaluated by nonlinear pushover and time-history analyses. The prototype buildings were designed and analyzed for their seismic responses through a series of nonlinear time-history analyses for both the design basis earthquake (DBE, 10% probability of exceedance in 50 years) and the maximum considered earthquake (MCE, 2% probability of exceedance in 50 years) level ground motions in both the transverse and the longitudinal directions.

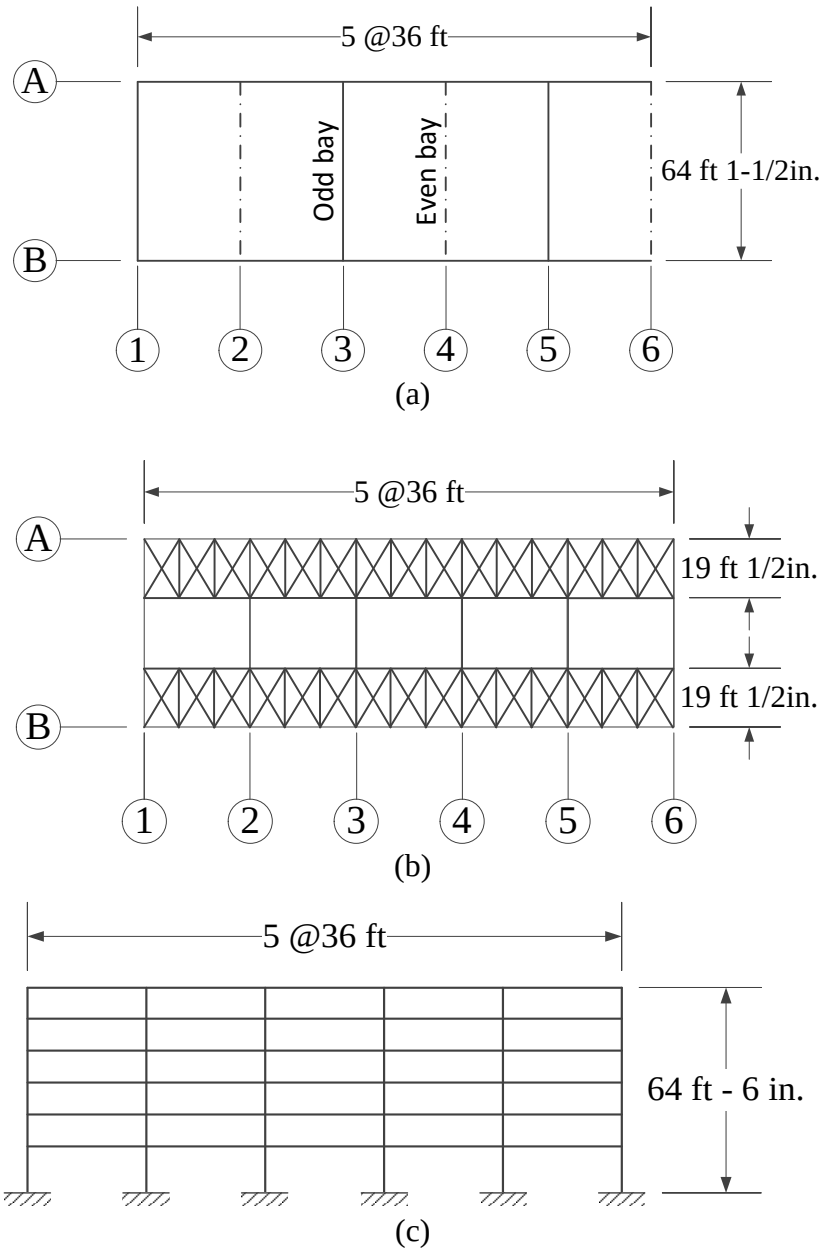

Figure 9-1 Structural geometry of the 6-story STF buildings: (a) plan view (horizontal trusses not shown for clarity); (b) horizontal trusses; (c) side view (moment frame)

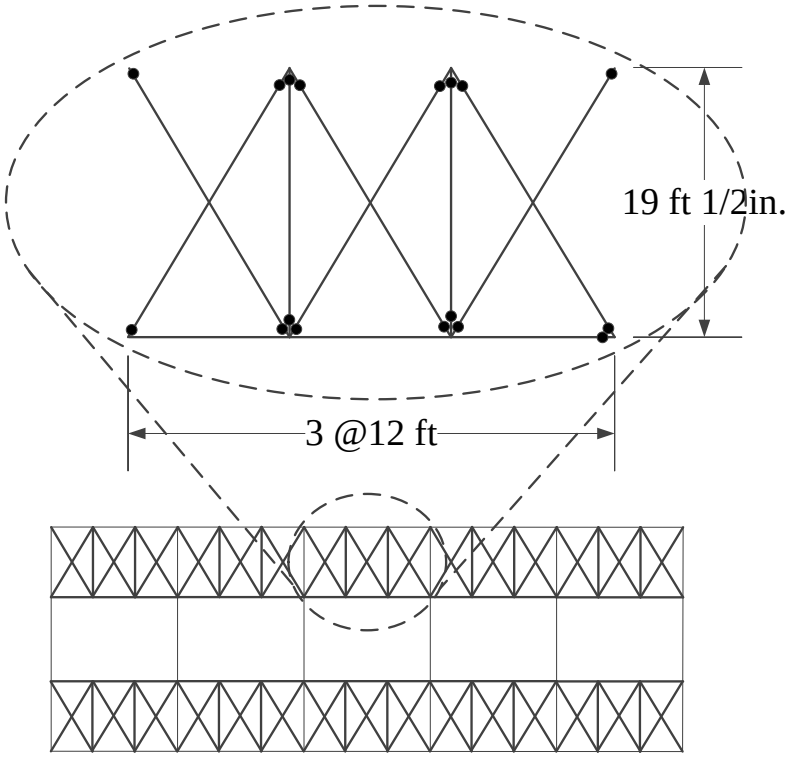

Figure 9-2 Pin connections at ends of horizontal truss members

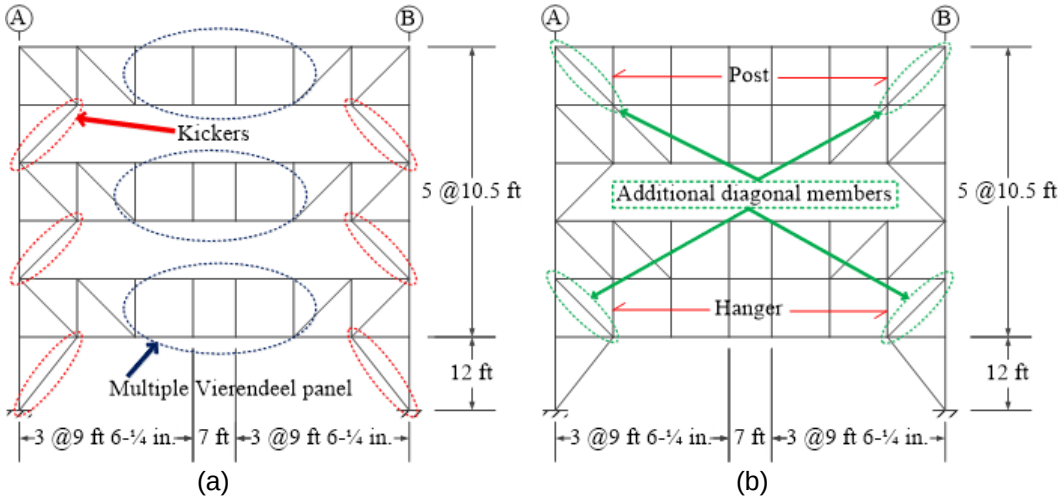

Figure 9-3 Elevation view of the Base and Target Drift Models: (a) odd bay; (b) even bay

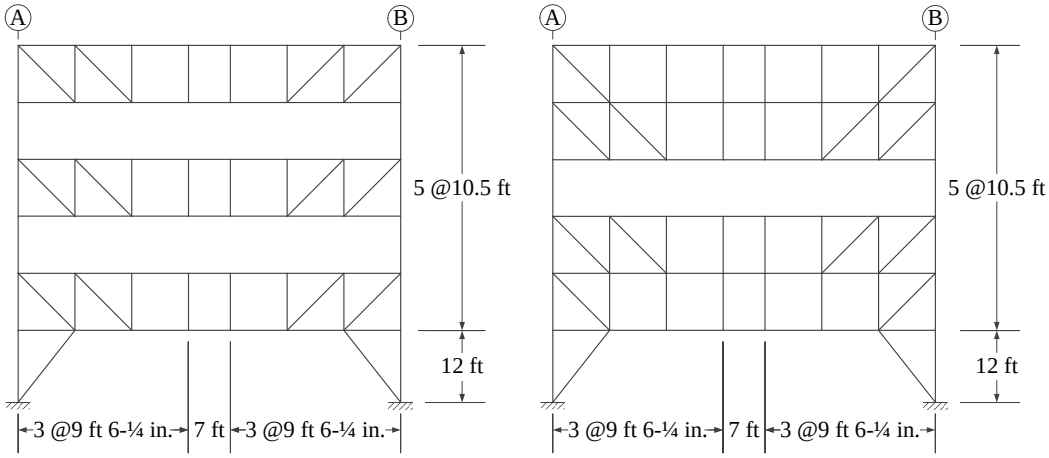

Figure 9-4 Elevation view of the No Kicker Model: (a) odd bay; (b) even bay

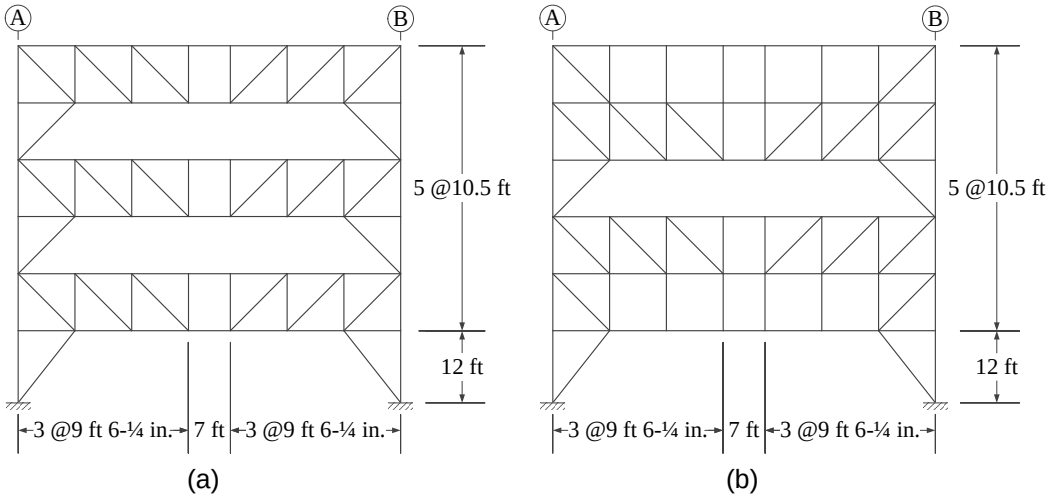

Figure 9-5 Elevation view of the SVP Models: (a) odd bay; (b) even bay

9.2 Design of Prototype Structures

Two prototype steel buildings with six-story STF, as explained previously, were designed using a computer program, SAP2000 (CSi, 2011b), to investigate the seismic behavior of the STFs. The first prototype building (Base Model) was elastically designed based on load combinations as defined in ASCE 7-10 (ASCE, 2010) with redundancy factor, ρ, and overstrength factor, Ω_o, equal to 1.0.

The design gravity loads for the model structures are similar to the loads used in AISC Steel Design Guide Series No.14 (Wexler, 2003). The dead load of 90 psf and live load of 40 psf were used as gravity load. Table 9-1 lists the loads used in the design of the structures. Structural member design was carried out according to the load and resistance factor design (LRFD) of AISC 360-10 (AISC, 2010b) with ASTM A992 Grade 50 steel. Because the STF system is not recognized as a seismic force-resisting system in ASCE 7-10 Table 12.14-1, a response modification factor, similar to that of steel special concentrically braced frames (SCBF), of 6.0 was conservatively applied in the seismic design. Table 9-2 lists the load cases used for the design of the models in this research.

Table 9-1 Loads Used in the Design of Structures

Dead Loads	**90 psf**
- 6” precast hollow core plank (with 2” minimum topping)	73 psf
- Structural steel	5 psf
- Partitions	12 psf
Live Loads	**40 psf**

Table 9-2 Loads Cases

Load Case	Basic Combinations
1	1.4D
2	1.2D + 1.6L
3	$(1.2 + 0.2S_{DS})D + \rho Q_E + 0.5L$
4	$(0.9 - 0.2S_{DS})D + \rho Q_E$

For the second prototype building (Target Drift Model), chord and vertical members of the Vierendeel panels were kept the same as the Base Model while the truss members outside the Vierendeel panels including horizontal truss members, interior and spandrel beams, and columns were redesigned using the capacity design approach based on lateral forces corresponding to 1% roof drift, as shown in Figure 9-6, from pushover analysis considering plastic hinge properties of the truss members in the

Vierendeel panels. Figure 9-7 shows the members in the Target Drift Models that were kept the same as those in the Base Model.

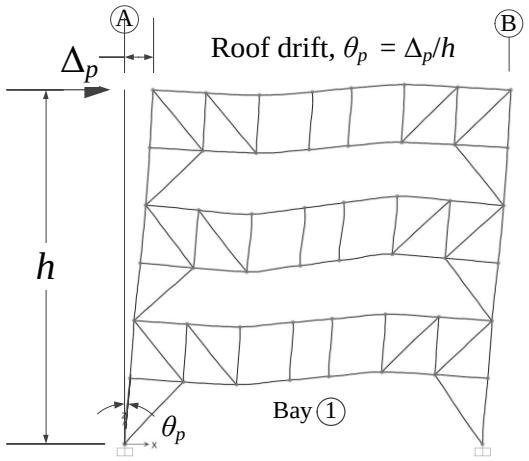

Figure 9-6 Roof drift calculation

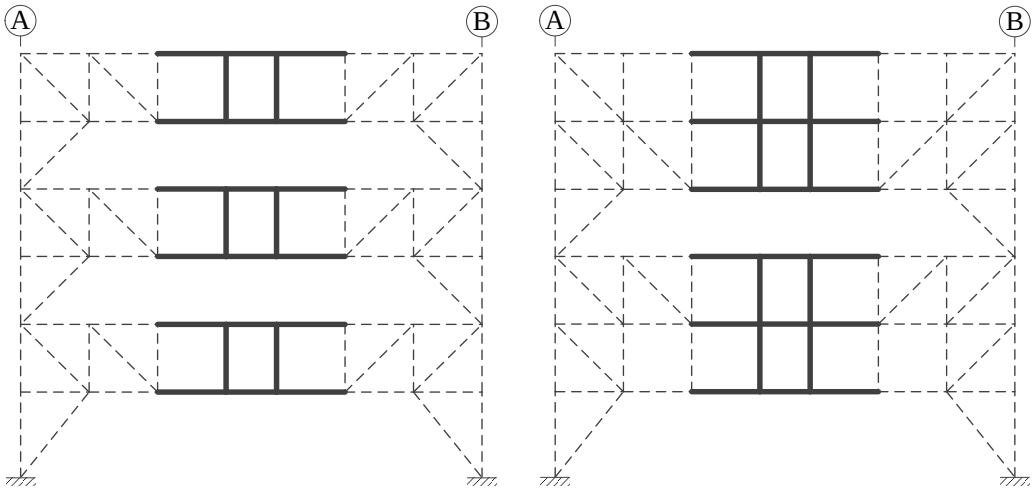

Figure 9-7 The Target Drift Model members that were kept the same sections as the Base Model: (a) odd bay; (b) even bay

The 1% value was selected based on preliminary nonlinear time-history analyses using the DBE level ground motions, which indicated that the average interstory drift

ratios were approximately 1%. This design approach was similar to that for the special segments with Vierendeel panels in STMFs (Chao and Goel, 2008b), in which the yielding of members is limited within the Vierendeel panels of the STFs under large lateral forces.

9.3 Design Procedures

A step-by-step design base shear and lateral force distribution calculation for seismic lateral forces used in the design procedure of the prototype buildings are as follows:

1. *Approximation of fundamental period (T)*:

During the initial design process, the approximate fundamental period (T_a), in second, was determined from the following equation as per ASCE 7-10:

$$T = T_a = C_t h_n^x$$

where the value of the coefficients C_t and x were taken as those from steel moment-resisting frames, 0.028 and 0.8 respectively. h_n (ft) is the structural height measured from the base to the highest level of the structure.

2. *Calculation of seismic base shear (V)*:

The seismic base shear, *V*, was determined in accordance with ASCE 7-10 with the following equation:

$$V = C_s W$$

where W is the effective seismic weight of the system. C_s, the seismic response coefficient, is determined in accordance with the following equation:

$$C_s = \frac{S_{DS}}{\left(\frac{R}{I_e}\right)}$$

where S_{DS} is the design spectral response acceleration parameter in the short period range, R is the importance factor, and I_e is the response modification factor. The value of C_s computed in accordance with the above equation need not exceed:

$$C_s = \frac{S_{D1}}{T\left(\frac{R}{I_e}\right)}$$

where S_{D1} is the design spectral response acceleration parameter at a period of 1.0 second and T is the fundamental period of the structure.

The design parameters S_{DS} and S_{D1} were selected based on 1997 NEHRP Provisions (FEMA, 1997). The design parameters for seismic lateral forces are presented in Table 9-3.

Table 9-3 Design Parameters for the 6-Story Prototype STF Buildings

Parameters	6-story STF
MCE Short Period Spectral Response Acc., S_s	2.09g
MCE One-second Spectral Response Acc., S_1	0.77g
Acceleration Site Coefficient, F_a	1.0
Velocity Site Coefficient, F_v	1.5
Short Period Design Spectral Response Acc., S_{DS}	1.393g
One-second Design Spectral Response Acc., S_{D1}	0.77g
Site Class	D
Occupancy Importance Factor, *I*	1.0
Seismic Design Category	D
Building Height	64.5 ft
Approximate Building Period, *T*	0.785 s
Response Modification Factor, *R*	6
Total Building Weight, *W*	6718 kips
Seismic Response Coefficient, *Cs = V/W*	0.163g

3. *Vertical distribution of seismic force*:

Vertical lateral seismic force distribution over the height of the structure was carried out according to the ASCE 7-10. The lateral force distribution for 6-Story STF is presented in Table 9-4.

Table 9-4 Lateral Force Distribution for 6-story Prototype Buildings

Level	h_i (ft)	w_i (kips)	$w_i h_i^k$ (kip-ft)	C_{vi}	F_i (kips)
2	12.0	1120	19144	0.0435	47.6
3	22.5	1120	39358	0.0892	97.7
4	33.0	1120	60809	0.1382	151.3
5	43.5	1120	83375	0.1895	207.4
6	54.0	1120	106739	0.2425	265.6
Roof	64.5	1120	130763	0.2971	325.4
Total	−	6718	440088	1.0000	1095.0

Note: k = 1.143 is used for this study.

4. Design of members:

4.1. Base model

The six-story STF building was designed in accordance with the LRFD of AISC 360-10 with W-shape steel sections for all of the members. Load combinations along with seismic load effects were as defined in ASCE 7-10. The top and bottom chords of the trusses were treated as continuous members. The web members were rigidly connected to the chord members. The chord members were assumed to be rigidly connected to the columns except where there was no diagonal web member connecting to the column at that location. In such case, typical construction details suggest that the chord members are more appropriately assumed to be pin-connected to the columns (Marstellar and Faraone, 2002). Figure 9-8 shows the location of the pin connections between the chord members and the columns. All of the horizontal truss members were considered pin-connected to the STFs and spandrel beams. Because the spandrel beams are part of the moment-resisting frames, they were treated as rigidly connected to the columns in their strong axis direction. Interior beams were considered pin-connected to the truss chords

to minimize force transfer from the horizontal trusses to the STFs when the building is displaced along the longitudinal direction. The column sizes were kept within the typical W-shape columns (W14). All of the members were selected such that all compression elements in the members were non-slender elements as defined in AISC 360-10. In addition, width-to-thickness ratios of the members were selected according to the requirement for highly ductile members ($0.30\sqrt{E/F_y} = 7.23$) specified in the 2010 AISC Seismic Provisions (AISC, 2010a). During the Base Model design, a preliminary pushover analysis was also carried out to identify the plastic hinge locations of the expected yield members.

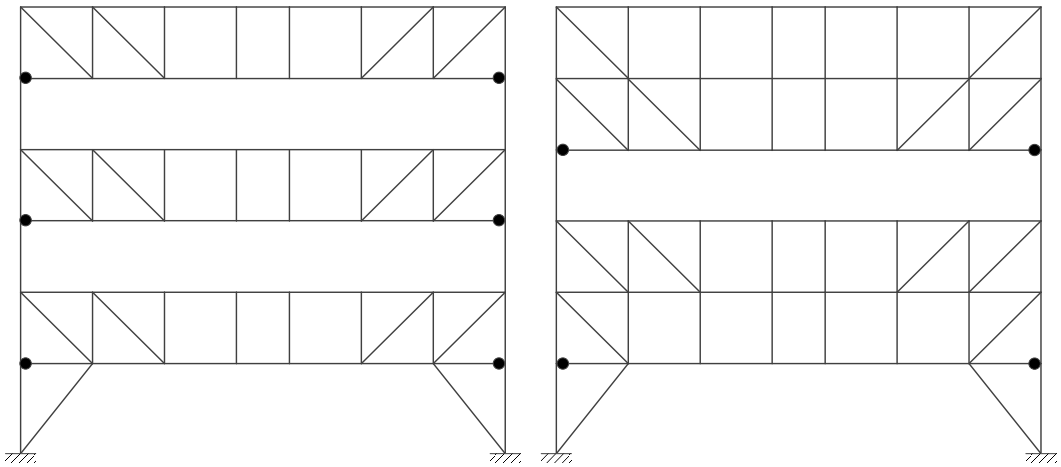

Figure 9-8 Locations of pin connections between chord members and columns in the Base Model: (a) odd bay; (b) even bay

4.2. Target drift model

The second prototype building was designed based on the capacity design philosophy with the lateral forces equal to those from the target 1% roof drift pushover analysis (discussed later). Top and bottom chords and vertical web members in the Vierendeel panels of the trusses, posts, and hangers were kept the same as those from

the base model. Plastic hinge models based on Table 5-6 in FEMA 356 (FEMA, 2000a) (partially shown in Figure 9-9) were introduced to the end of those members to account for the strain hardening and degradation of the expected yielding members. Figure 9-10 shows the moment-rotation curve according to Table 5-6 in FEMA 356. All the other members outside the Vierendeel panels were designed as non-yielding members for both the axial force and bending moment expected at the ultimate states of the members in Vierendeel panels. The reason of using the FEMA 356 plastic hinge models was because the design of all non-yielding members was done by somewhat automatic fashion through SAP2000, and the FEMA 356 model is the build-in option, which is sufficient for design purposes.

Table 5-6 Modeling Parameters and Acceptance Criteria for Nonlinear Procedures—Structural Steel Components

	Modeling Parameters			Acceptance Criteria				
	Plastic Rotation Angle, Radians		Residual Strength Ratio	Plastic Rotation Angle, Radians				
					Primary		Secondary	
Component/Action	a	b	c	IO	LS	CP	LS	CP
Beams—flexure								
a. $\frac{b_f}{2t_f} \le \frac{52}{\sqrt{F_{ye}}}$ and $\frac{h}{t_w} \le \frac{418}{\sqrt{F_{ye}}}$	$9\theta_y$	$11\theta_y$	0.6	$1\theta_y$	$6\theta_y$	$8\theta_y$	$9\theta_y$	$11\theta_y$
b. $\frac{b_f}{2t_f} \ge \frac{65}{\sqrt{F_{ye}}}$ or $\frac{h}{t_w} \ge \frac{640}{\sqrt{F_{ye}}}$	$4\theta_y$	$6\theta_y$	0.2	$0.25\theta_y$	$2\theta_y$	$3\theta_y$	$3\theta_y$	$4\theta_y$
c. Other	Linear interpolation between the values on lines a and b for both flange slenderness (first term) and web slenderness (second term) shall be performed, and the lowest resulting value shall be used							

Figure 9-9 Table 5-6 of FEMA 356 (partially shown)

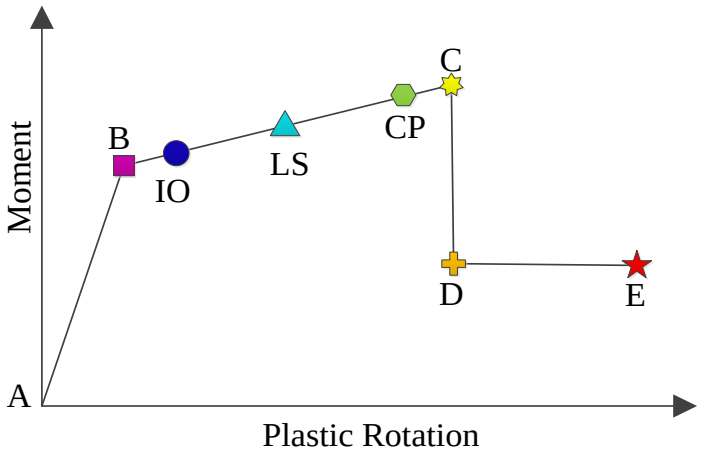

Figure 9-10 Table 5-6 of FEMA 356 (partially shown)

The moment frames in the longitudinal direction for both models were designed solely based on the ASCE 7-10 load combinations. In other words, the 1% target drift design approach is not applied to the structure in the longitudinal direction.

Figure 9-11 through Figure 9-14 show the typical designed truss member sections in both the transverse direction (trusses) including the pin connection locations and the longitudinal direction (moment frames) of the Base and Target Drift models, respectively. In order to utilize the repetition of identical trusses which is a great benefit of STF system, all truss members within the same story were designed such that they are the same within different bays. For example, the top chord members of the truss on the sixth floor are the same for bay 1, 3, and 5 as shown in Figure 9-11 (a), (c), and (e), respectively.

Table 9-5 lists the non-truss member sections which include the members in the longitudinal direction (interior and spandrel beams) and the horizontal truss members including the transverse beams in the horizontal truss. It can be seen that the non-yielding members in the Target Drift Model are heavier due to the use of capacity design

approach. However the column sizes are only slightly larger than that of the Base Model. It is observed that the column sizes are generally governed by the moment frames. It should be noted that the all columns are designed based on biaxial loading from the moment frames in the longitudinal direction and the STF frames in the transverse direction.

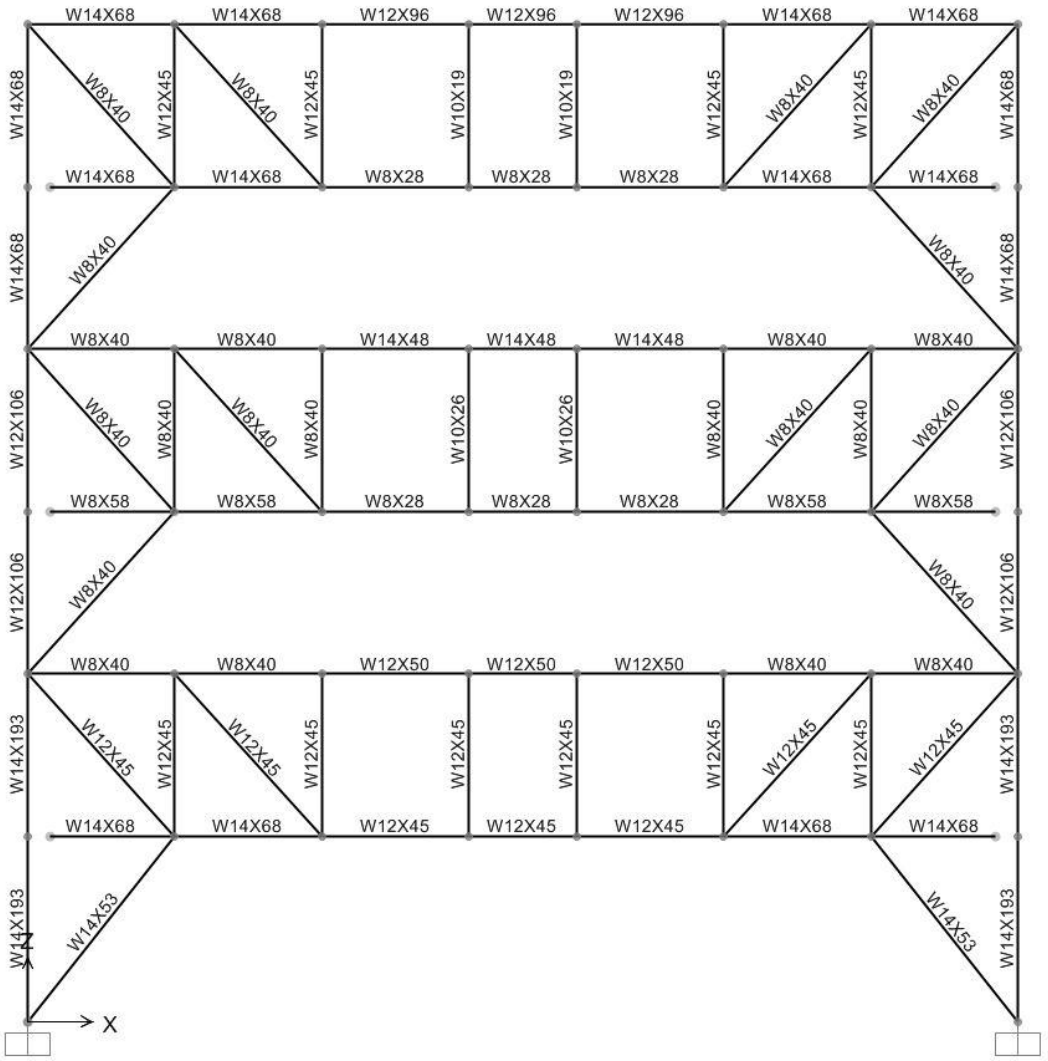

(a)

Figure 9-11 Truss member sections in the Base Model: (a) bay 1; (b) bay 2; (c) bay 3; (d) bay 4; (e) bay 5; (f) bay 6

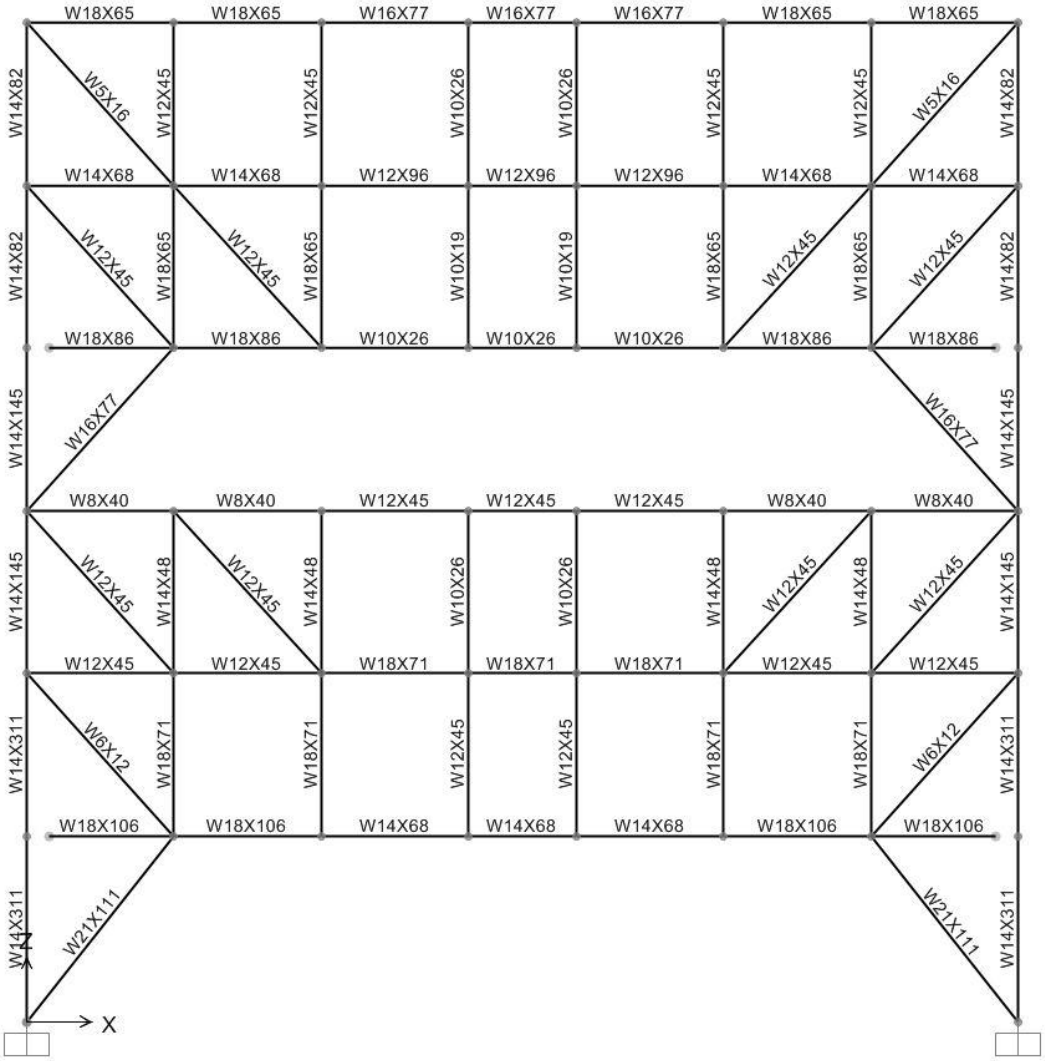

(b)

Figure 9-11—*Continued*

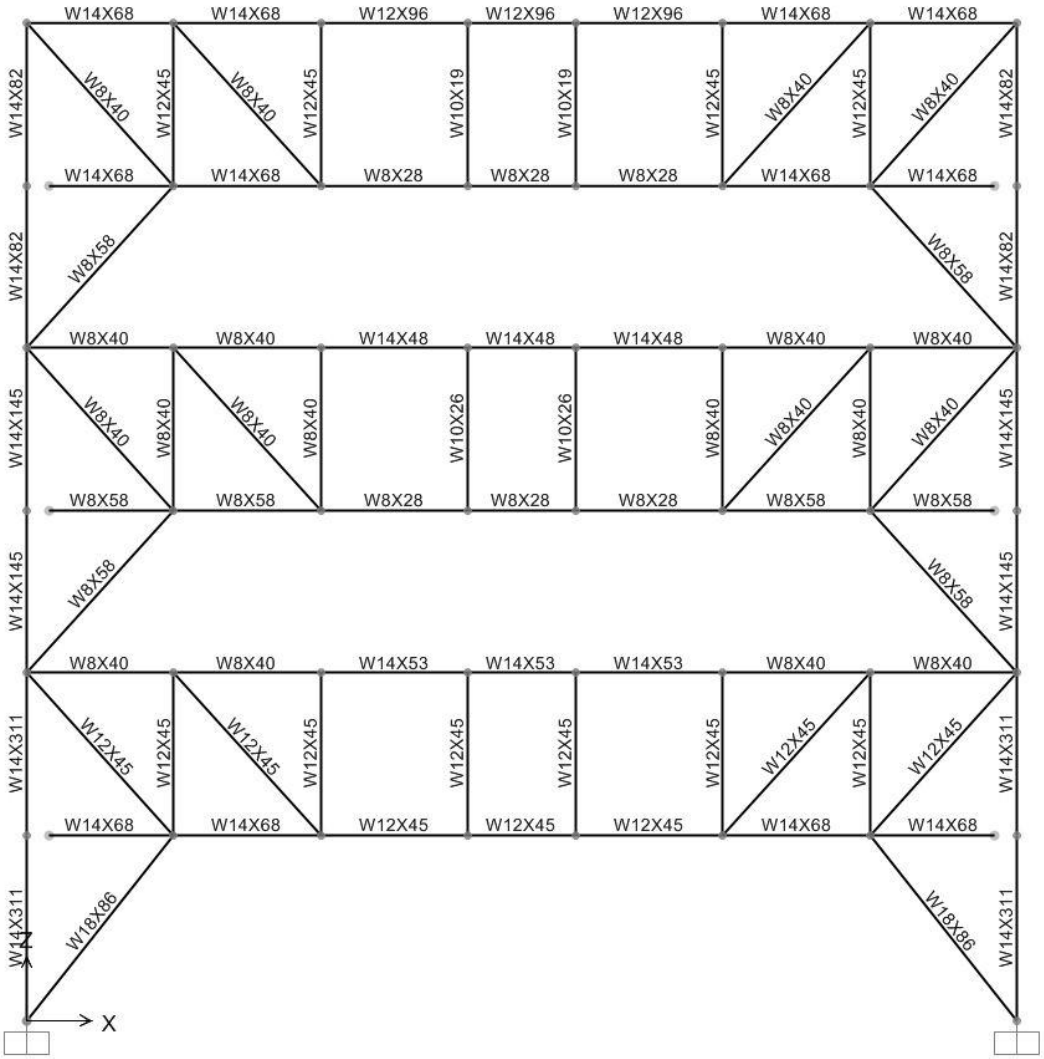

(c)

Figure 9-11—*Continued*

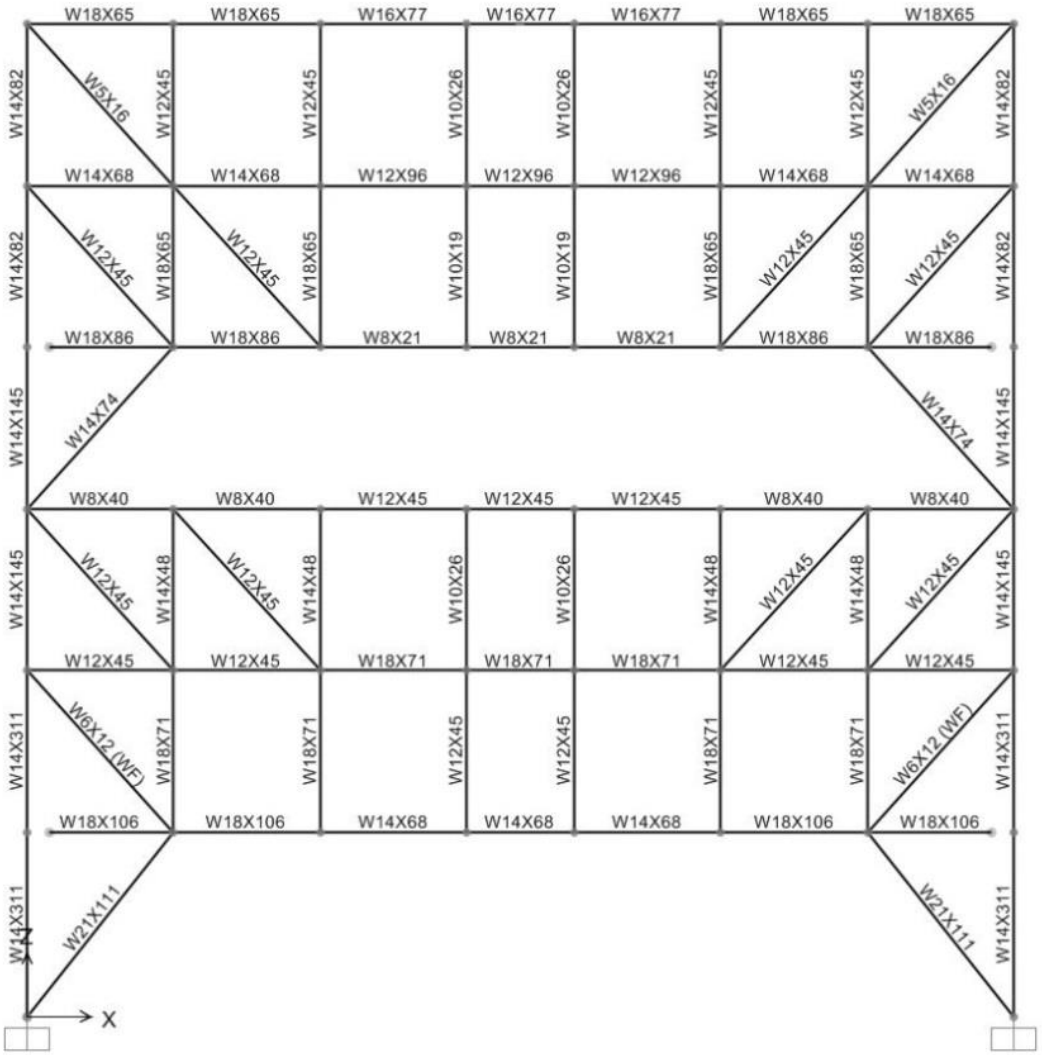

(d)

Figure 9-11—*Continued*

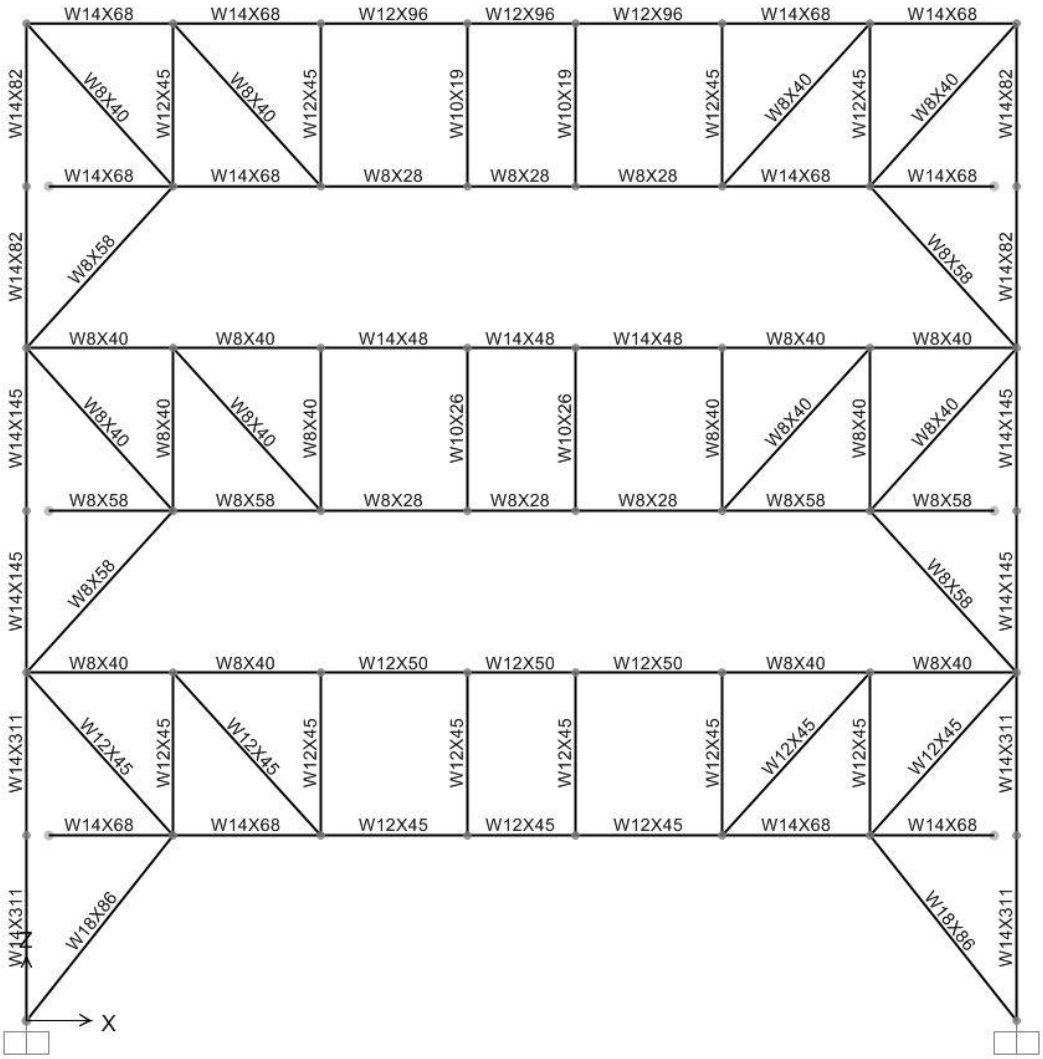

(e)

Figure 9-11—*Continued*

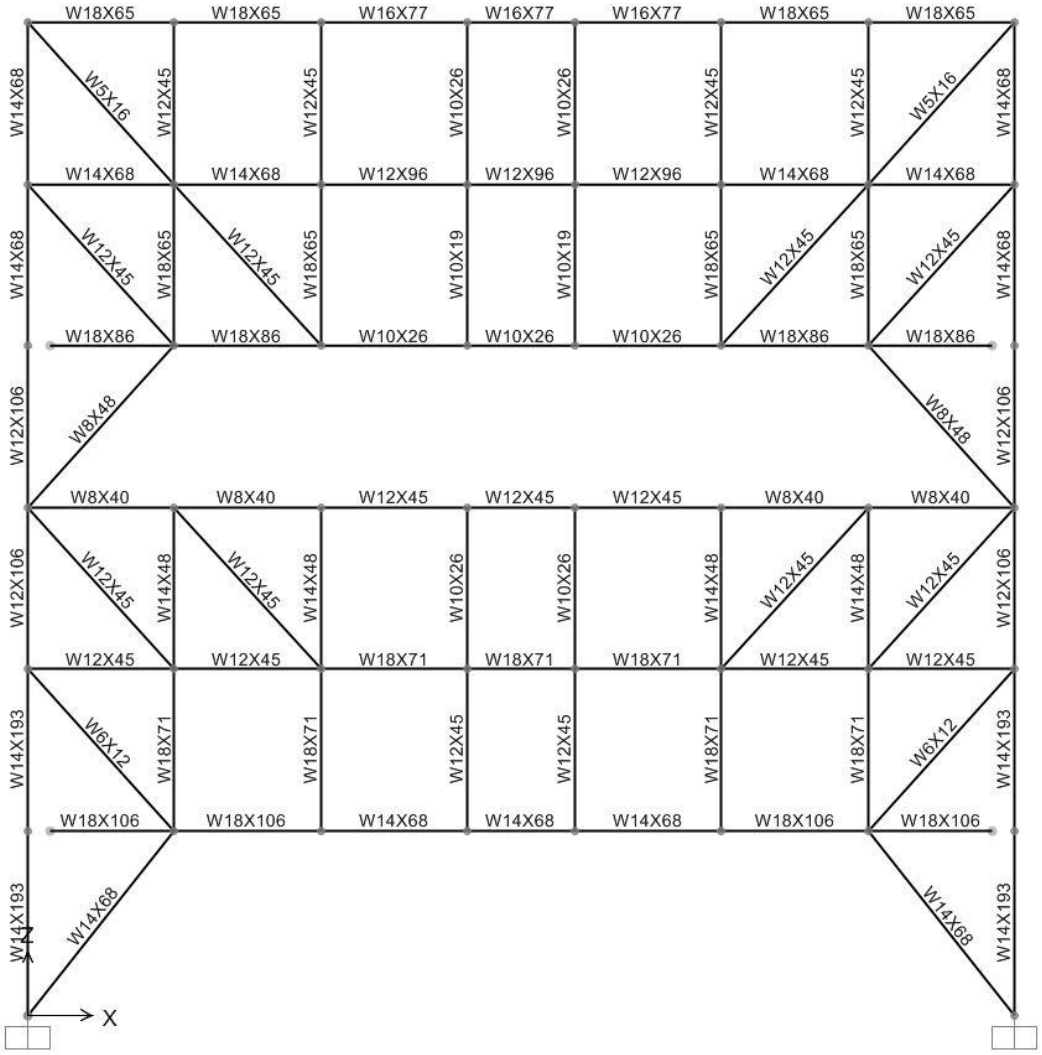

(f)

Figure 9-11—*Continued*

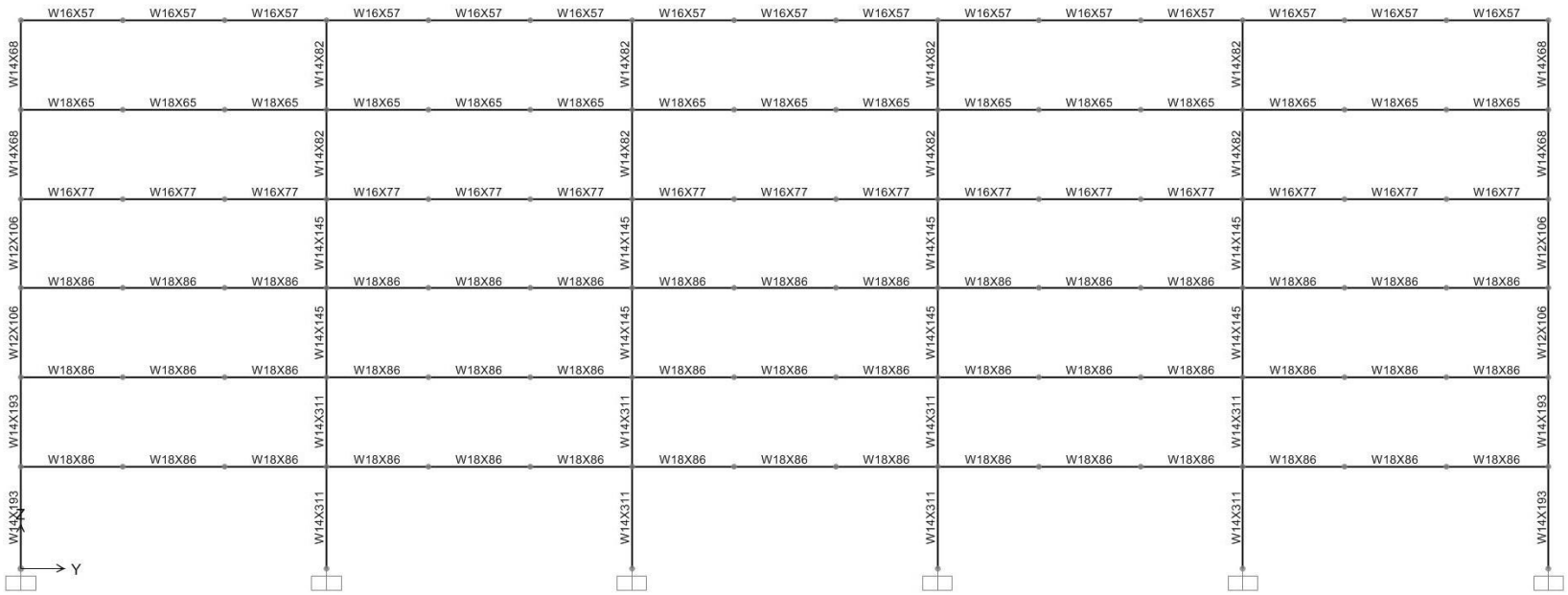

Figure 9-12 Typical moment frame member sections in the Base Model

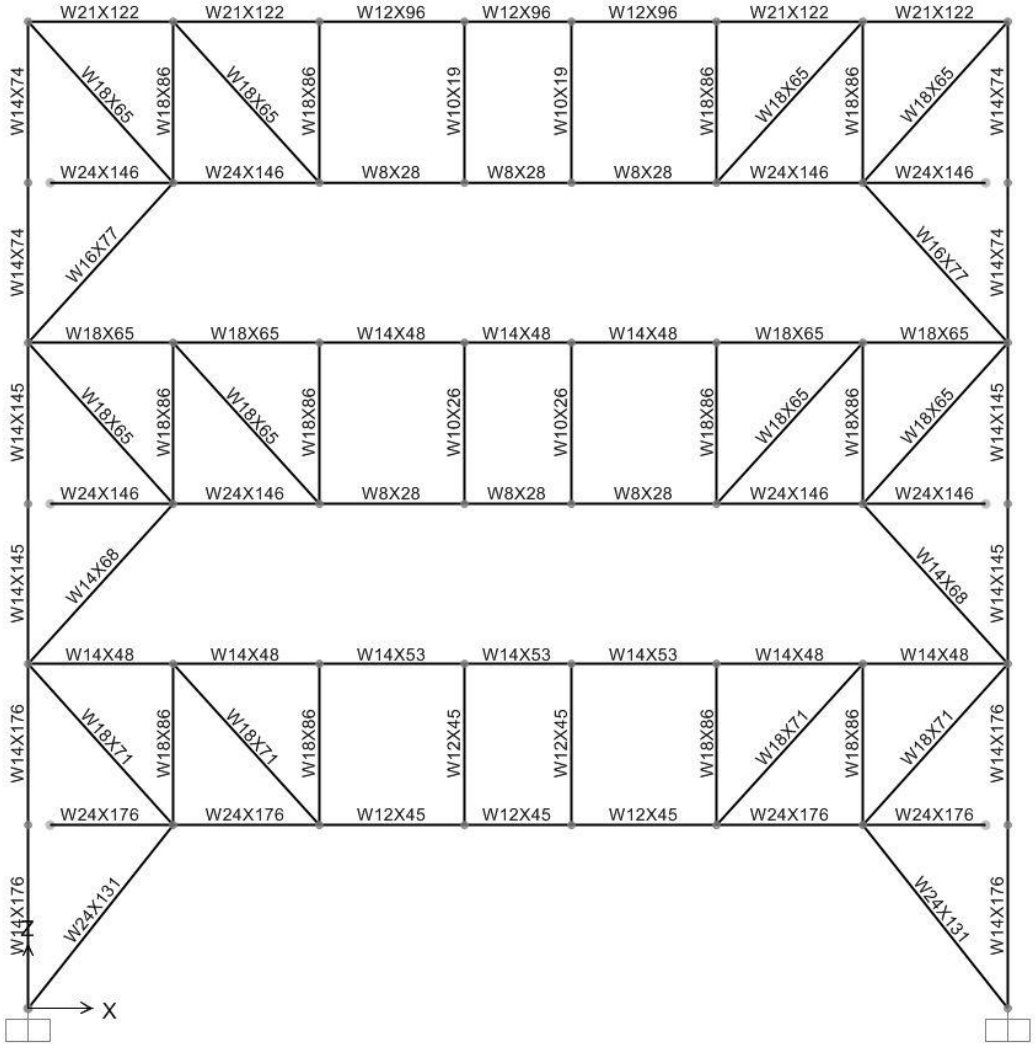

(a)

Figure 9-13 Truss member sections in the Target Drift Model: (a) bay 1; (b) bay 2; (c) bay 3; (d) bay 4; (e) bay 5; (f) bay 6

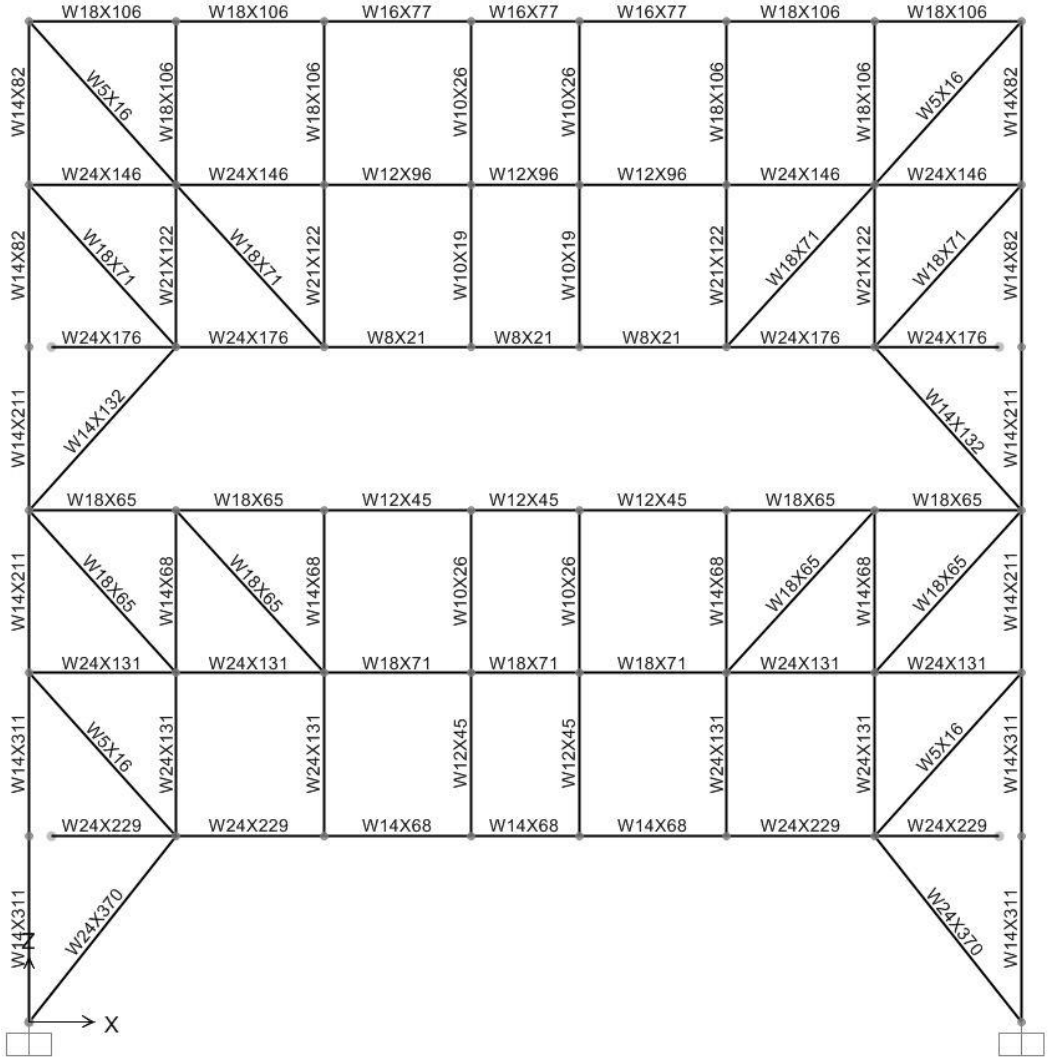

(b)

Figure 9-13—*Continued*

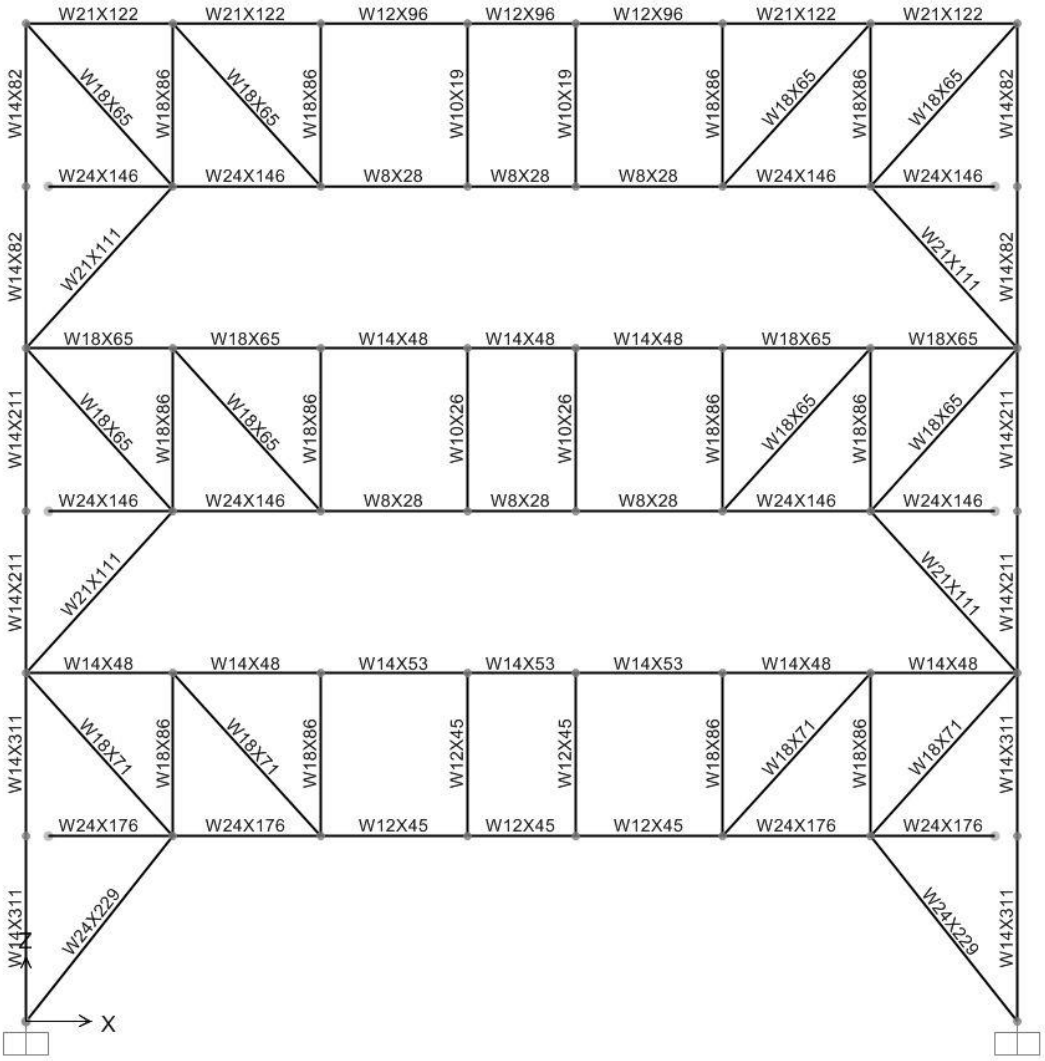

(c)

Figure 9-13—*Continued*

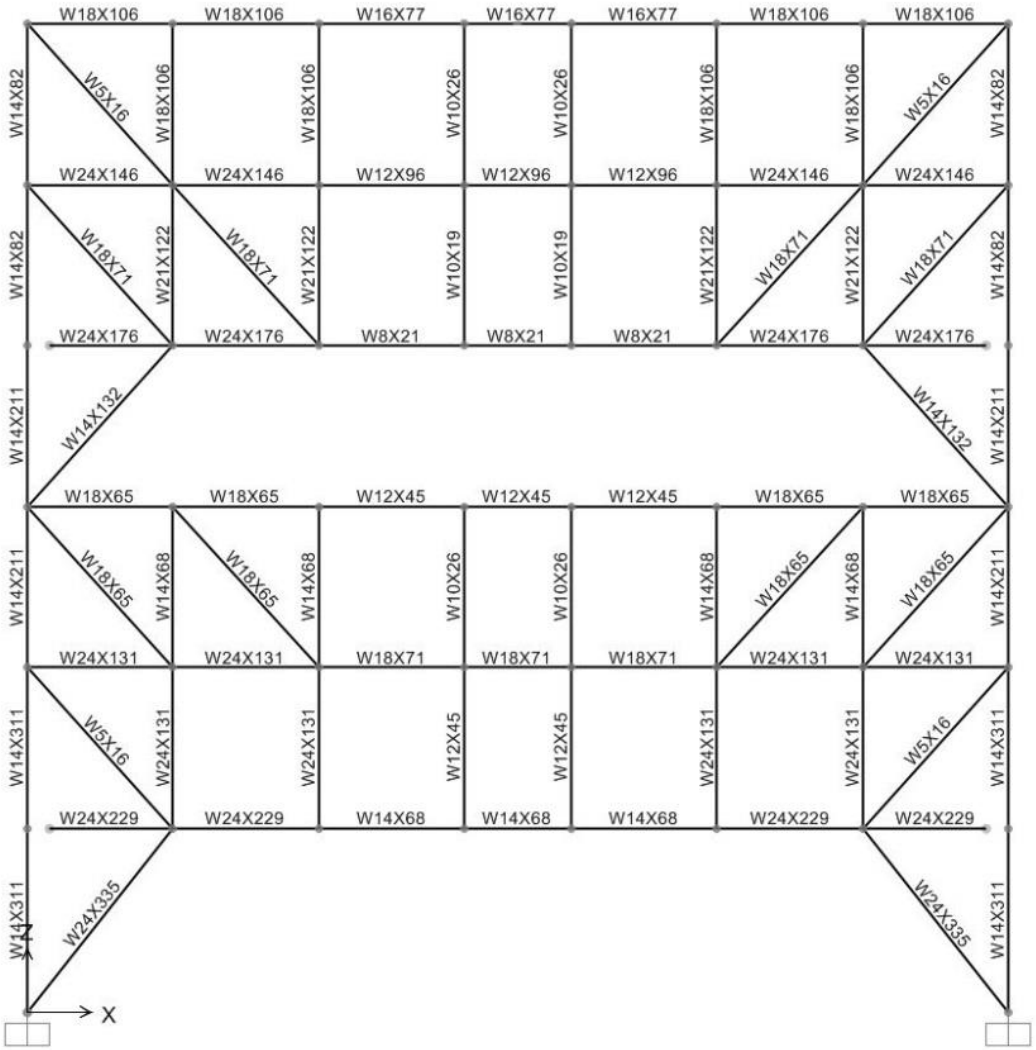

(d)

Figure 9-13—*Continued*

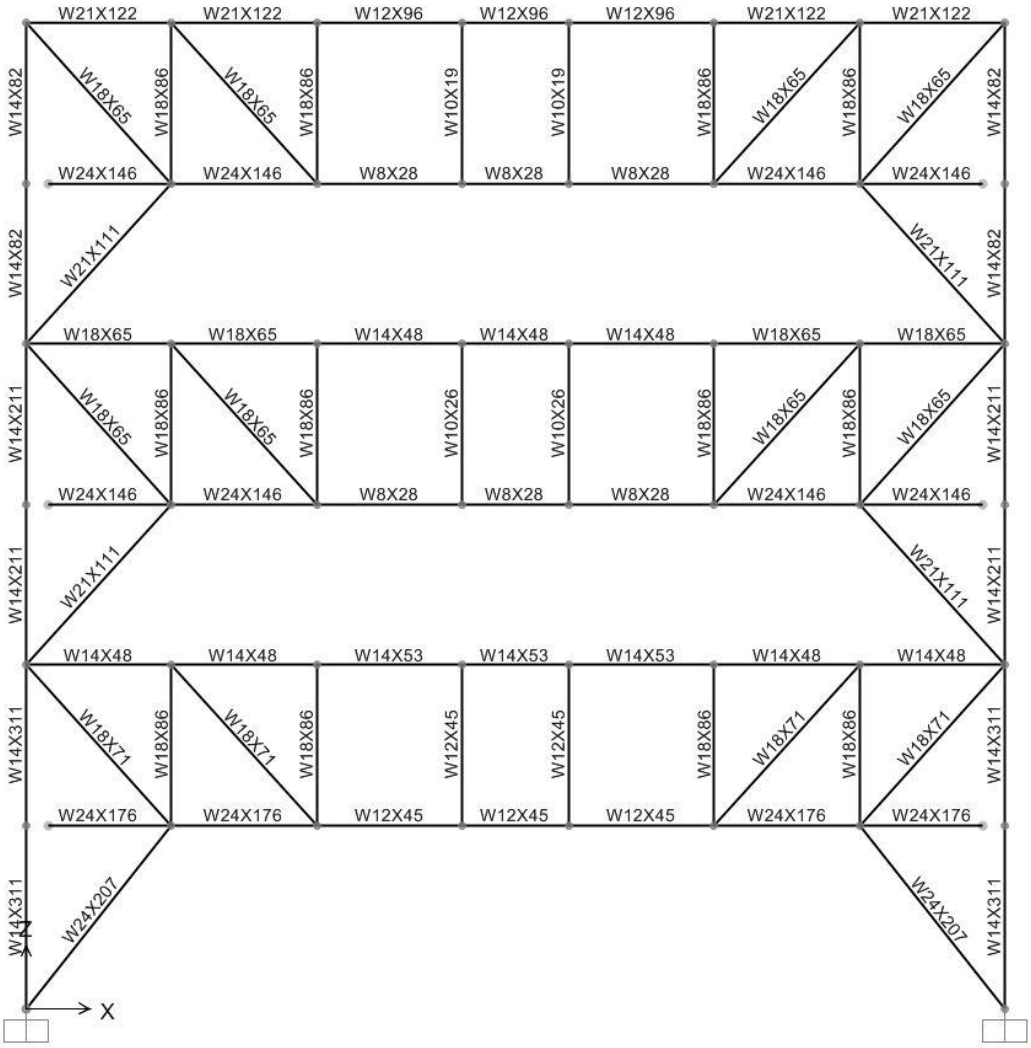

(e)

Figure 9-13—*Continued*

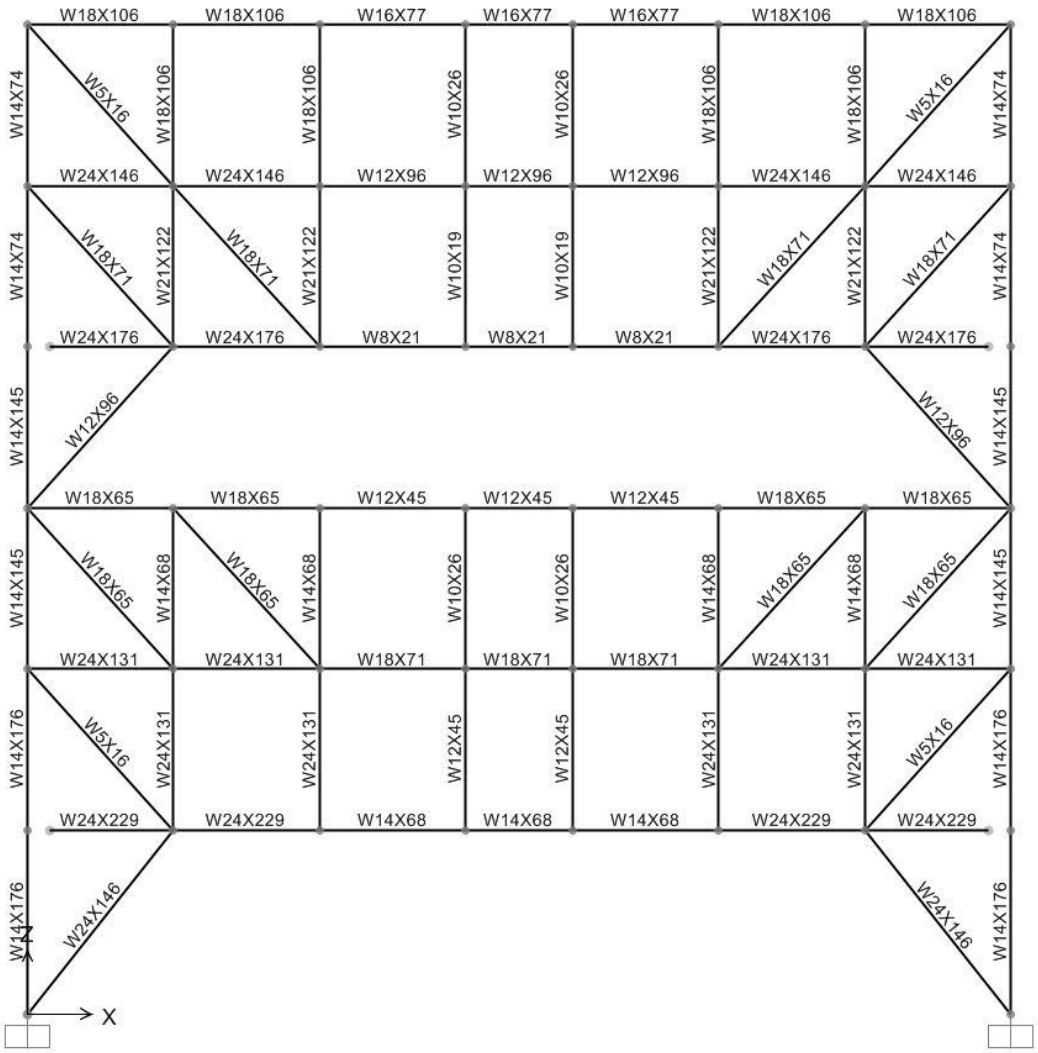

(f)

Figure 9-13—*Continued*

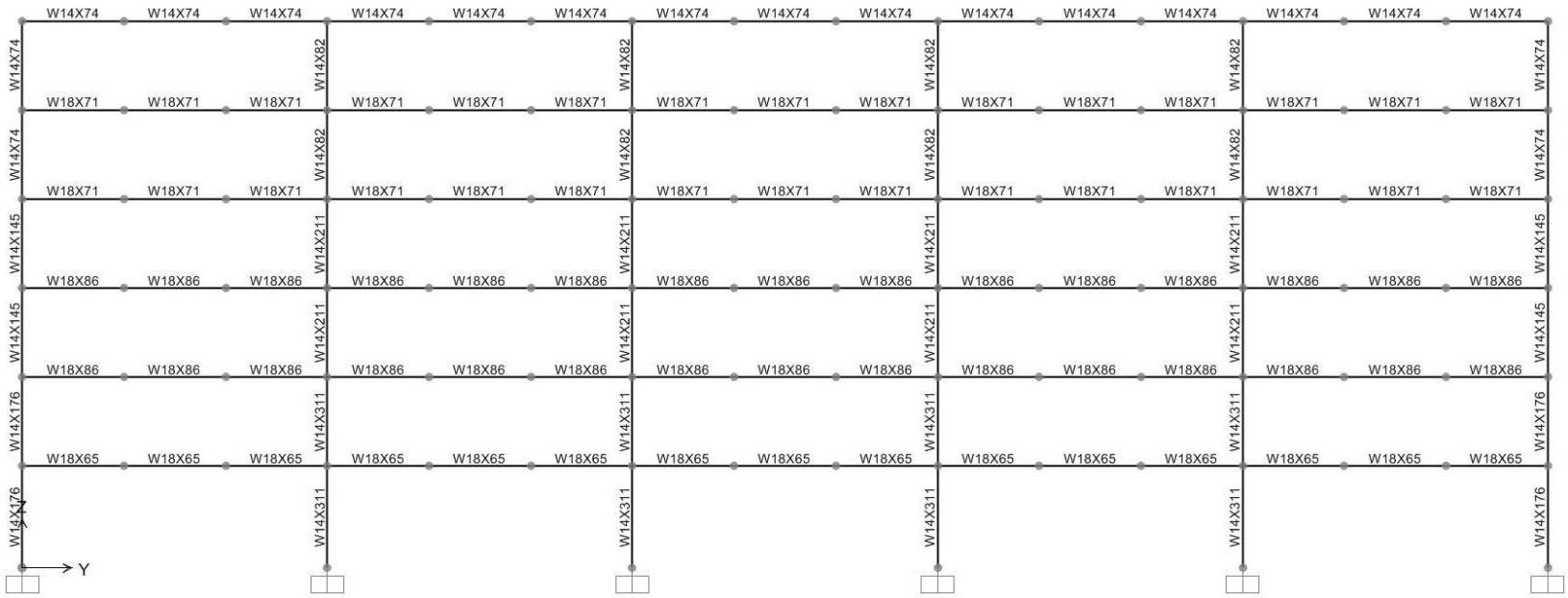

Figure 9-14 Typical moment frame member sections in the Target Drift Model

Table 9-5 Non-truss Member Sections

Members	Member Sections	
	Base Model	Target Drift Model
2nd Story Horizontal Truss	W6×25	W6×25
2nd Story Interior Beam	W21×93	W24×131
2nd Story Spandrel Beam	W18×86	W18×65
2nd Story Transverse Beam	W5×16	W5×16
3rd Story Horizontal Truss	W6×25	W6×25
3rd Story Interior Beam	W21×93	W24×146
3rd Story Spandrel Beam	W18×86	W18×86
3rd Story Transverse Beam	W5×16	W5×16
4th Story Horizontal Truss	W6×25	W6×25
4th Story Interior Beam	W21×93	W24×146
4th Story Spandrel Beam	W18×86	W18×86
4th Story Transverse Beam	W5×16	W5×16
5th Story Horizontal Truss	W6×25	W6×25
5th Story Interior Beam	W21×93	W24×146
5th Story Spandrel Beam	W16×77	W18×71
5th Story Transverse Beam	W5×16	W5×16
6th Story Horizontal Truss	W6×25	W8×40
6th Story Interior Beam	W21×93	W24×146
6th Story Spandrel Beam	W18×65	W18×71
6th Story Transverse Beam	W5×16	W5×16
Roof Horizontal Truss	W6×25	W6×25
Roof Interior Beam	W21×93	W24×146
Roof Spandrel Beam	W16×57	W14×74
Roof Transverse Beam	W5×16	W5×16

9.4 Analysis Model

Nonlinear static pushover and time-history analyses were carried out using a computer program, Perform-3D (CSi, 2011a), to evaluate the seismic performance of the structures. All of the members except the diagonal web members in the STF trusses, hangers, and posts and the diagonal braces in the non-truss level were modeled as standard frame (beam-column type) elements. In addition, the truss members and columns were modeled with both axial-moment (P-M-M) and moment-rotation plastic hinges at both ends. The flexure yielding properties also include the interaction between axial force and moment. The expected yield and ultimate strengths can be determined by

applying the material overstrength factor (R_y), and the strain hardening adjustment factor (ω). For this research, the respective values are considered to be 1.1 for both of them (AISC, 2010a). The column maximum total rotational capacity is considered to be 0.07 radian before strength degradations occur (Newell and Uang, 2008). Although the test results conducted by Newell and Uang (2008) were for the W14 columns bending about the strong axis, it was used for both the strong and weak-axis bending for this study. Note that for wide-flange shapes, the yield surfaces for the axial-moment interaction are different in major- (used in the moment frames along the longitudinal direction of the building) and minor-(used for the STFs along the transverse direction of the building) axis flexure. This is accounted for by using different yield surface parameters for the axial-moment interactions (El-Tawil and Deierlein, 2001a;2001b). The diagonal web members in the STF trusses, hangers, and posts and the diagonal braces in the non-truss level were modeled as buckling-type steel strut. The expected yield and ultimate strengths of those members were determined in accordance with brace members as per AISC 341-10. The lengths of yielding or buckling segments of the diagonal web members and the diagonal braces were taken as 85% of their working point lengths to account for the gusset plates and rigid zones of columns or chord members at the ends of those members. This effective length was used in the computation of the compressive strength of the buckling type members. P-Delta effect due to gravity loads was included in the analyses. The Rayleigh damping (combination of the mass and stiffness proportion damping) matrix suggested in Perform-3D's User Manual and the recommended damping ratio for welded steel structure of 2%, shown in Figure 9-15 and Table 9-6, is used throughout the analysis (Chopra, 2011).

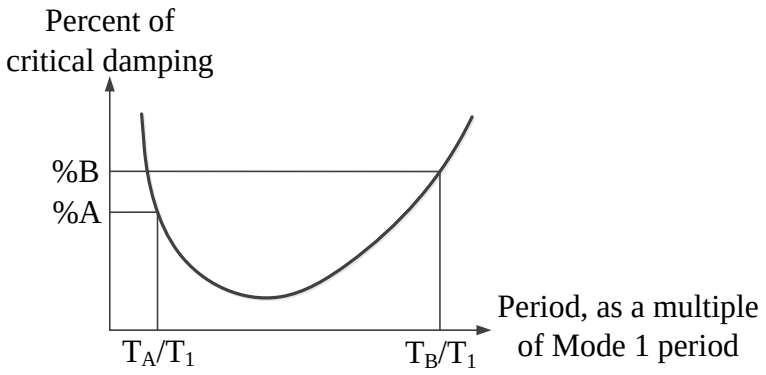

Figure 9-15 Rayleigh damping matrix

Table 9-6 Rayleigh Damping Matrix Values

	Point A	Point B
Damping, %	2	2
Period Ratio, T/T1	1	2

The member hysteresis model properties of typical beams, columns, and braces used in the nonlinear time-history analyses are shown in Figure 9-16. For the buckling material model used to simulate the behavior of braces or kickers, the tension stretch (additional tension strain in the subsequence tension cycles) on reloading is calculated by the stretch factor of 0.2 multiplied by the increase in buckling deformation in the current cycle. Also, when the material is reloaded in tension after it buckles in compression, the reloading line composes of three segments controlled by points A and B as shown in Figure 9-16(d). The forces, as a proportion of tension strength, are 0.01 and 0.4 for point A and B respectively. Similarly, the strains, as a proportion of strain range, are 0.3 for point A and 0.75 for point B. The value DL (strength degradation point) of each member was calculated assuming linear relation when the member is reloaded from compression. Figure 9-17 shows the joints where nodal lumped mass were applied, which was based

on the assumption that the hollow-core slabs are simply supported at two edges of the steel horizontal trusses.

As mentioned previously, the seismic response of the prototype buildings was evaluated under two earthquake hazard levels, namely, design basis earthquake (DBE), LA01 to LA20, and maximum considered earthquake (MCE), LA21 to LA40. Two suites of ground motion records (Somerville et al., 1997) for a hypothetical site in downtown Los Angeles with a probability of exceedance of 2% and 10% in 50 years were selected for nonlinear time-history analyses. These acceleration time histories were derived from historical recordings or from physical simulations and were scaled such that their mean response spectrum matches the 1997 NEHRP design spectrum. A total of forty records were obtained from twenty ground motions in both fault-parallel and fault-normal orientations. The magnitude of earthquakes ranges from 6.5 to 7.3 on Richter scale for DBE and 6.7 to 7.4 for MCE.

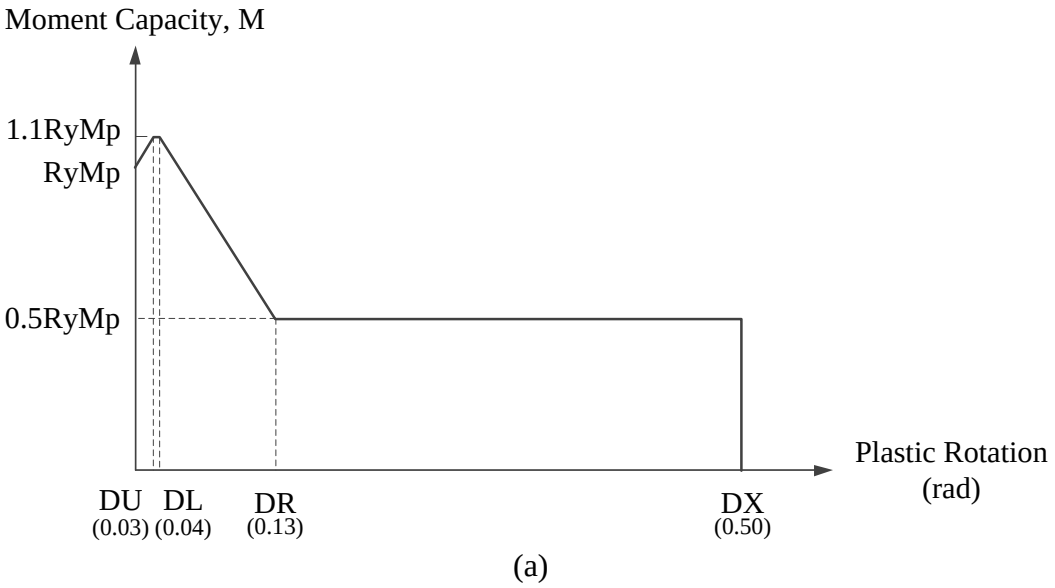

(a)

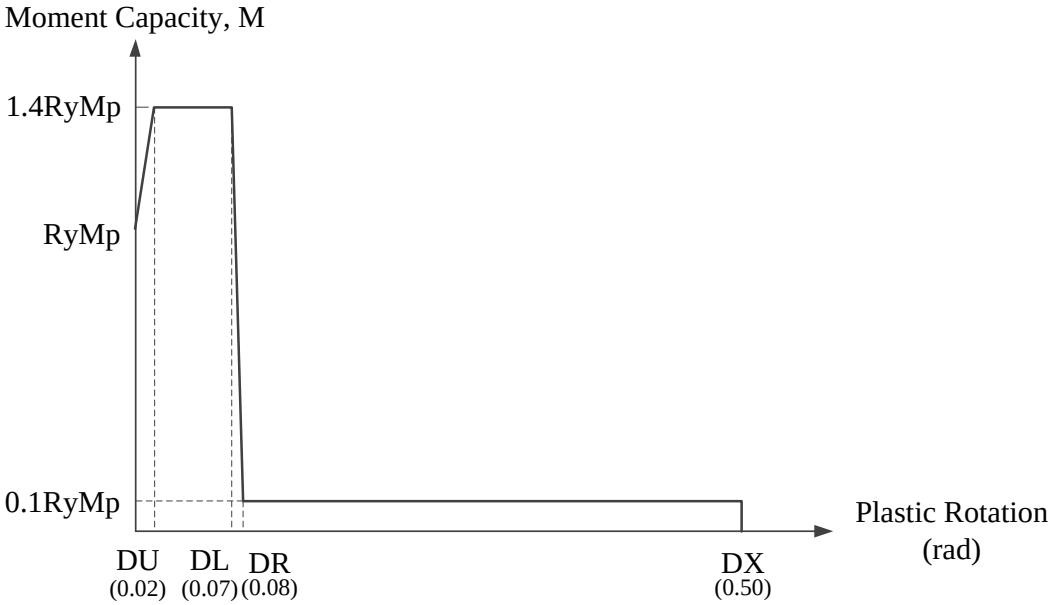

(b)

Figure 9-16 Member modeling properties: (a) beam element; (b) beam element in Vierendeel panels; (c) column element; (d) buckling-type element

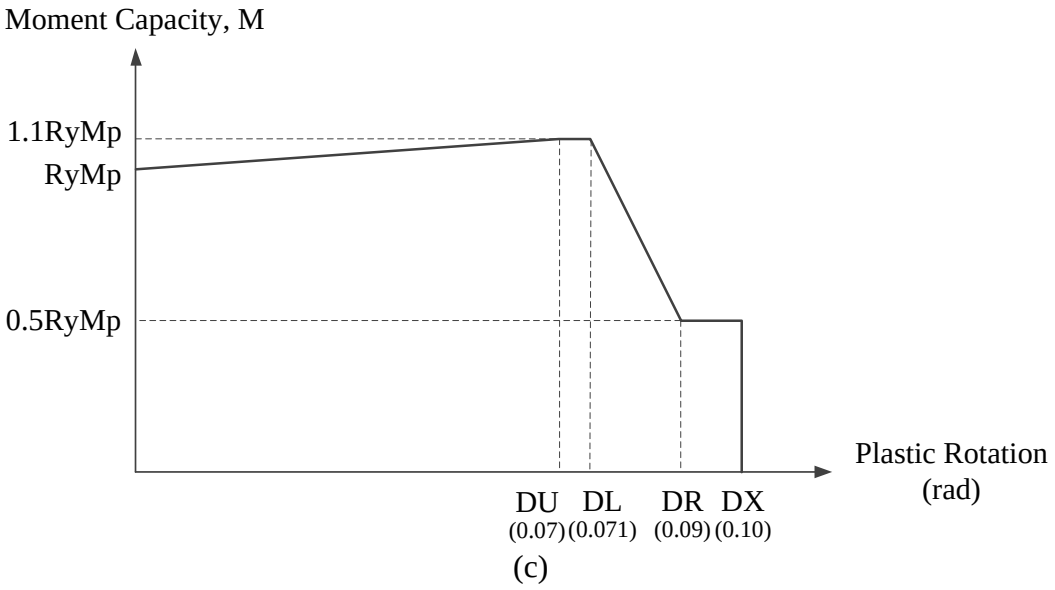

(c)

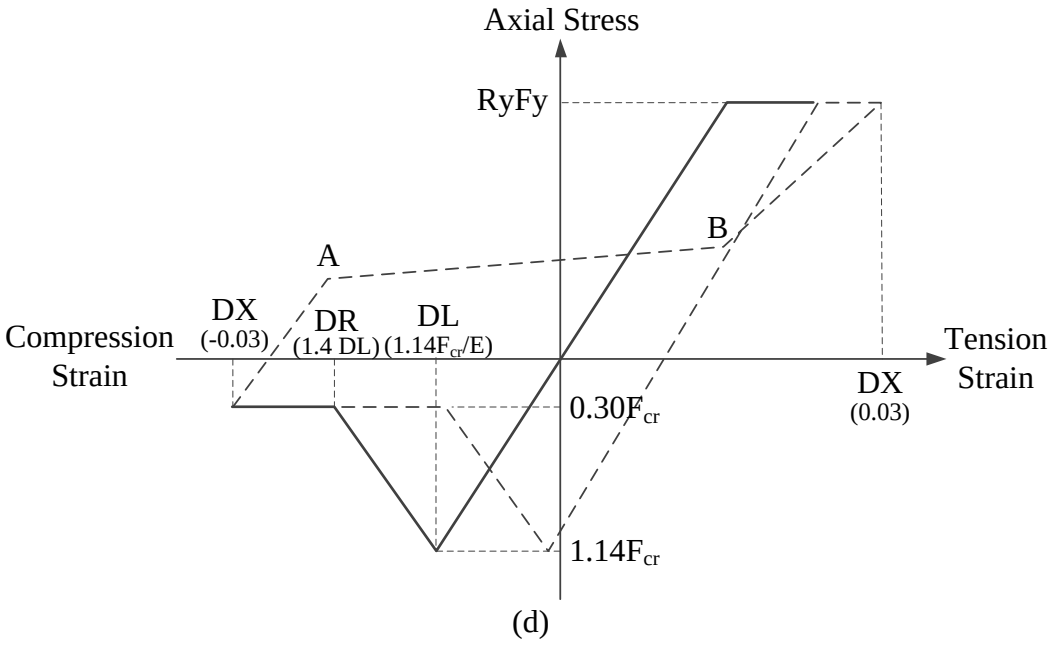

(d)

Figure 9-16—*Continued*

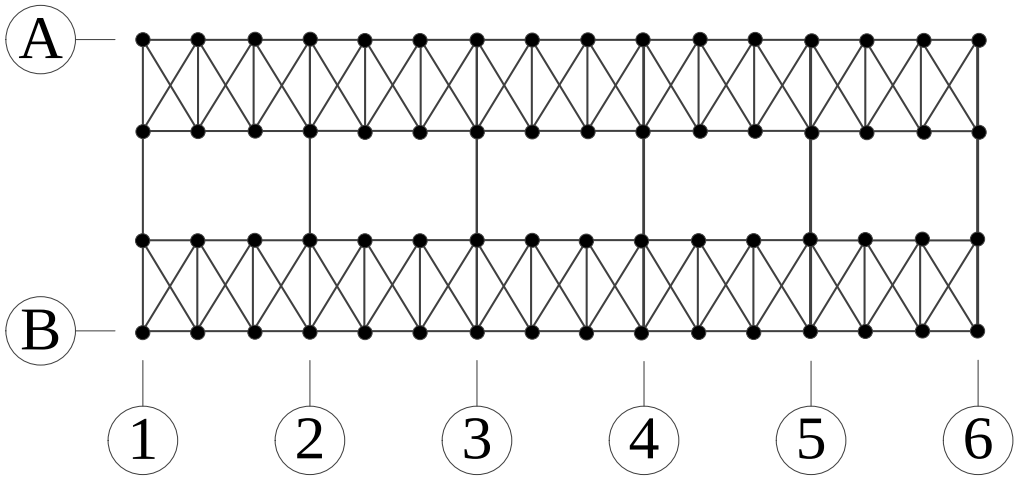

Figure 9-17 Locations of lumped nodal masses at the steel horizontal truss

Chapter 10

Part II: Analysis Results

10.1 Lateral Force Transfer Patterns

During the preliminary design process, it was observed that, when the diagonal braces are introduced to the STF system, the story shear forces were transferred in a more direct manner. In other words, the majority of lateral forces were transferred directly from upper truss to the lower non-truss and no longer primarily depended on staggered manner via the diaphragms to transfer the lateral forces as in the conventional STF system. This largely reduced the demands in the diaphragms as well as the connections between the diaphragms and STFs. In order to determine the story shear distributions in each bay of the conventional and the modified STF systems when subjected to code-specified lateral forces when the structural steel frames are still within the elastic region, the prototype buildings were modeled in RISA-3D program (RISA Technology, 2011). The rigid floor diaphragm was modeled to represent the story shear transfer mechanism of the hollow core planks in the conventional model whereas the horizontal truss was used as the shear diaphragm in the modified structural layouts of the STF. RISA-3D was chosen during the preliminary design process for its simplicity of obtaining the story shear forces. The story shear distributions are summarized in Table 10-1.

It is worth to mention that the total base shear of the conventional and the modified models are the same (1095 kips) which is the total lateral applied to the structures although the individual bays of the models had different base shear.

Table 10-1 Story Shear in Individual Bay (kips)

Story	Bay 1		Bay 2		Bay 3	
	Conventional	Modified	Conventional	Modified	Conventional	Modified
6	56	60	33	43	102	80
5	*28	*77	232	151	*9	*66
4	155	129	*11	*128	310	177
3	*36	*104	381	273	*10	*72
2	118	128	248	260	155	120
1	131	145	247	236	157	161
Story	Bay 4		Bay 5		Bay 6	
	Conventional	Modified	Conventional	Modified	Conventional	Modified
6	35	45	90	73	35	49
5	231	156	*9	*64	118	112
4	*9	*117	312	158	*35	123
3	343	267	*11	*68	193	189
2	237	250	125	107	176	194
1	248	222	128	139	185	192

Note: * indicates non-truss bay in the corresponding story.

10.2 Pushover Analysis Results and Discussions

Due to the horizontal irregularity of STF system, roof drifts of all of the bays were used during the time-history analysis as the drift limits. The analysis stopped when the displacement at roof elevation in any bay reached the 2% limit. For all models, the bay on grid 1 (as shown in Figure 9-1) reached 2% roof drift before other bays and was chosen as the controlling bay. Roof drift of this bay was then used as the control drift for the pushover analysis. Figure 9-6 shows the detail of how the roof drift was calculated for this study. Because roof drifts were varied from one bay to another due to the variation in the stiffness of each floor in different bays, roof drift from bay 1 was also used as the roof drift limit during the design process as previously mentioned in the design procedure section. Nonlinear pushover analysis results of all the models are shown in Figure 10-1.

From the pushover analysis result of the Base Model, it was observed that, under the 1% target roof drift, the members outside the Vierendeel panels experienced large rotation which leaded to undesired yielding of some of the members in the trusses. To prevent the undesired yielding of members outside the Vierendeel panels, the Target Drift Model was designed such that those member remain in elastic region as described in the member design section.

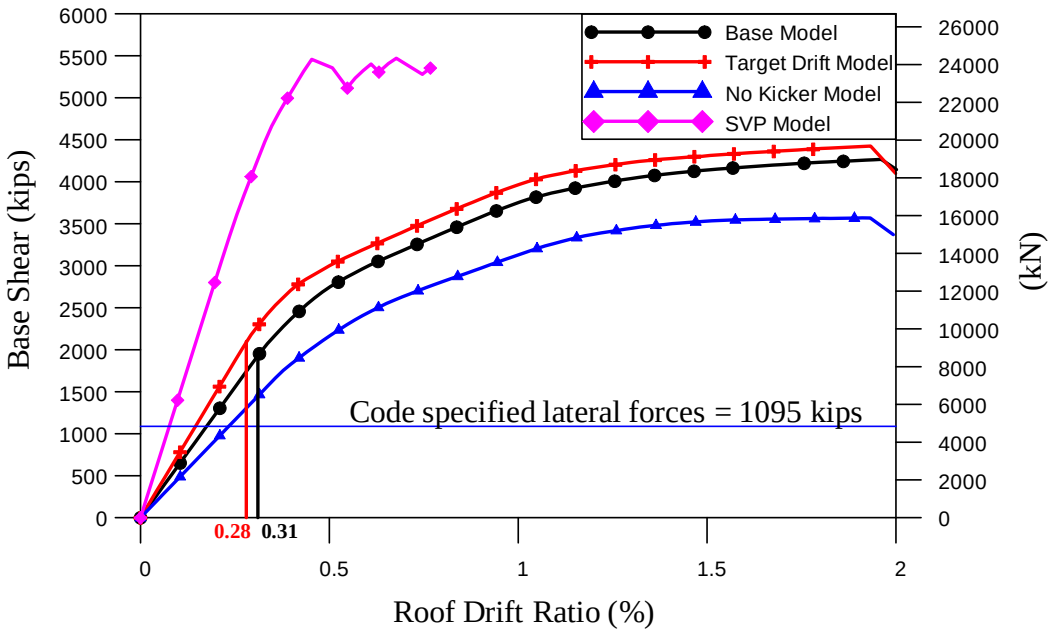

Figure 10-1 Base shear vs. roof drift response

It can be seen that the first yielding of the Base and the Target Drift STF models are at rather small story drifts of about 0.3% similar to that of a typical concentrically braced frame (AISC, 2010a). The story shear for individual bay in each story of all four models from the pushover analysis is summarized in Table 10-2.

Table 10-2 Story Shear in Individual Bay from Pushover Analysis (kips)

	Story	Bay 1	Bay 2	Bay 3	Bay 4	Bay 5	Bay 6	Total
Base Model	6th Story	150	64	193	67	153	95	636
	5th Story	190	287	167	289	150	264	1345
	4th Story	184	722	145	617	143	437	2008
	3rd Story	409	548	500	489	399	475	2684
	2nd Story	516	598	595	607	545	581	3434
	1st Story	565	894	590	891	608	725	4267
Target Drift Model	6th Story	183	64	233	64	180	95	659
	5th Story	227	278	193	277	165	284	1395
	4th Story	179	809	131	676	130	494	2082
	3rd Story	449	525	594	397	485	494	2783
	2nd Story	552	665	536	627	551	640	3562
	1st Story	642	914	553	907	625	797	4425
No Kicker Model	6th Story	61	111	103	101	75	82	532
	5th Story	33	452	3	454	3	245	1125
	4th Story	341	50	530	87	603	99	1679
	3rd Story	132	809	70	732	40	497	2245
	2nd Story	436	509	482	519	435	499	2873
	1st Story	553	601	603	615	619	581	3569
SVP Model	6th Story	16	97	48	93	38	115	394
	5th Story	243	131	229	134	227	86	1023
	4th Story	111	481	168	467	161	431	1725
	3rd Story	547	311	530	240	453	75	2030
	2nd Story	316	732	380	766	313	713	2990
	1st Story	734	1220	871	1137	851	915	5471

Note: The cell colors indicate story frame as shown below.

Truss
Hanger
Post
Column with kicker
Column without Kicker

In order to compare the plastic hinge rotation levels of the chord and vertical members in the trusses in bay 1 of all the models, some members of the truss are strategically selected for comparison purpose. The locations of the selected members are shown in Figure 10-2. It should be noted that the member locations are the same for all models even though the member layouts are different for the No Kicker Model and SVP Model. For example, the dash lines representing kickers on third and fifth story apply to the Base Model and Target Drift Model, but not to the No Kicker Model. The maximum plastic hinge rotations of the selected members are listed in Table 10-3.

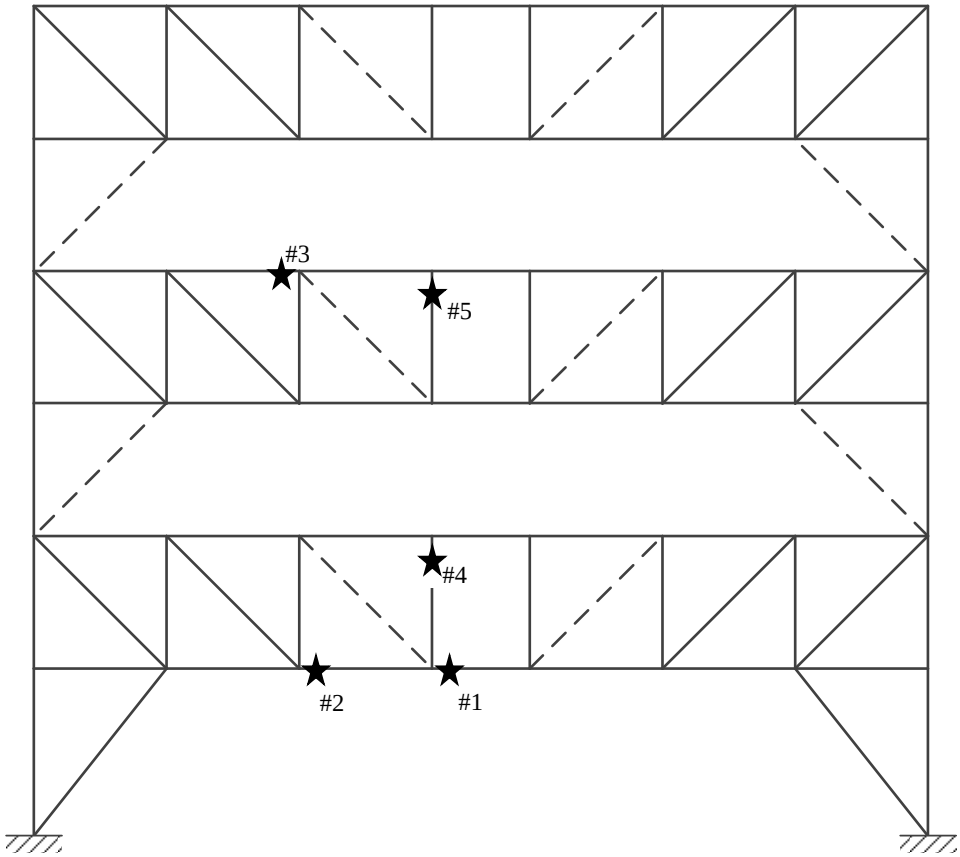

Figure 10-2 Locations of the selected chord and Vierendeel vertical members in bay 1

Table 10-3 Plastic hinge rotation of the selected members from pushover analysis

Member	Plastic Hinge Rotation (%)							
	Base Model		Target Drift Model		No Kicker Model		SVP Model	
	0.77% Drift	2% Drift	0.77% Drift	2% Drift	0.77% Drift	2% Drift	0.77% Drift	2% Drift
1	0.00	0.90	0.00	0.97	0.00	0.89	2.05	-
2	0.91	5.57	1.22	5.71	0.42	4.98	0.00	-
3	0.00	0.62	0.00	0.00	0.00	0.00	0.00	-
4	-1.46	-8.19	-1.82	-10.14	-0.74	-7.22	0.00	-
5	-1.45	-5.42	-1.75	-5.96	-0.17	-1.56	-0.25	-

Note: For the SVP Model, the analysis failed to converge due to excessive deformation and was prematurely terminated at 0.77% roof drift.

The plastic hinge rotational demand of the chord member at the end of Vierendeel panel at 0.77% roof drift for all of the models are plotted on the beam-type member model in Figure 10-3.

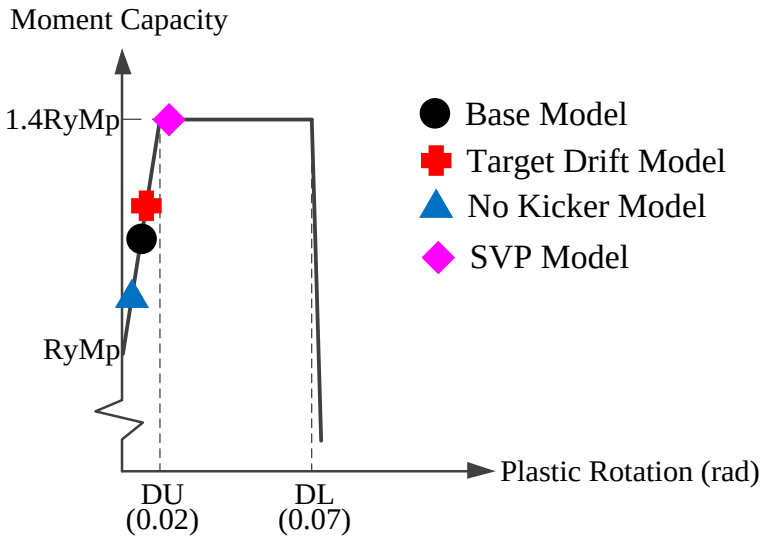

Figure 10-3 Plastic hinge rotational demand at the end of chord member in Vierendeel panel at 0.77% roof drift

It can be seen that the Vierendeel chord members of the SVP Model have relatively higher rotational and moment demand than the other models at the same level of roof drift. It should be noted that Figure 10-3 shows the plastic hinge rotation of the chord member at location #2, as shown in Figure 10-2, for the Base Model, the Target Drift Model, and the No Kicker Model. For the SVP Model, the plastic hinge rotation of the chord member is at location #1. The different locations were selected to compare the plastic hinge rotational demand of chord members at the ends of the Vierendeel panels. Figure 10-4 and Figure 10-5 also show that the early yielding in Vierendeel chord members in the SVP Model led to force redistribution to the kickers and the columns, thus much higher member force demands in the columns and the kickers at the same roof drift levels. This also leads to the failure of the SVP Model at much lower roof drift than the other three models. It can also be seen that the rotational demand in the chord members of the No Kicker Model is less than the Base Model and the Target Drift Model due to the early yielding of the columns, which prevents additional load from redistributing into the chord members.

Figure 10-6 through Figure 10-12 show the deflected shapes of the members in bay 1 for the Base Model, the Target Drift Model, and the No Kicker Model with the maximum interstory drift ratios, maximum plastic hinge rotations of the yielded members, and member minimum usage ratios at 0.77% and 2% roof drifts. For the SVP Model, only the deflected shape of bay 1 at 0.77% roof drift is included since the analysis failed to converge and was terminated at 0.77% roof drift. Deflected shapes of bay 2 through bay 6 can be found in the Appendix L.

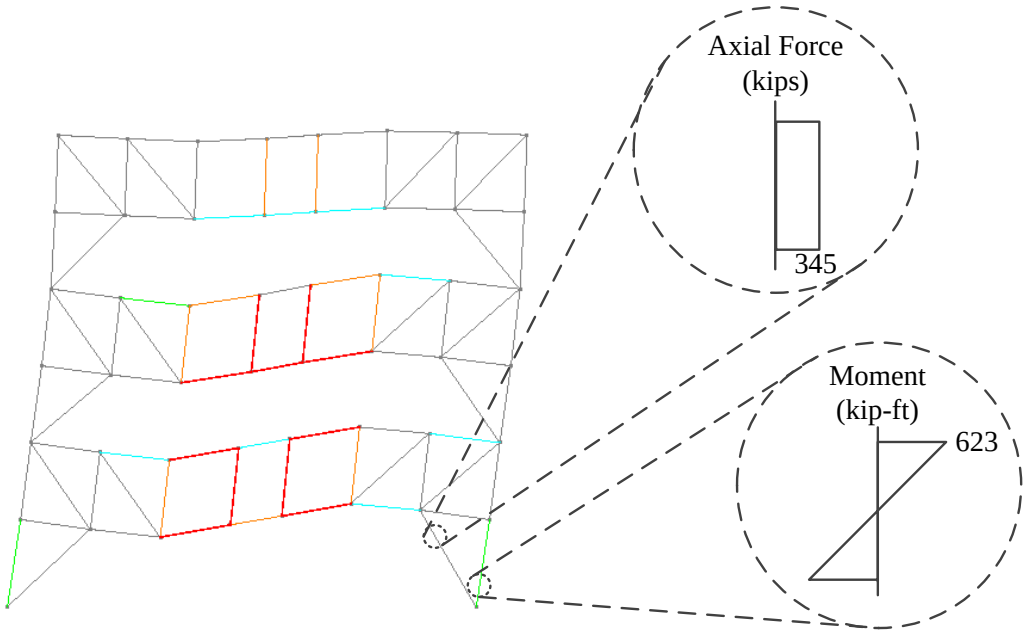

Figure 10-4 Member force demand at 0.77% roof drift in bay 1 of the Base Model

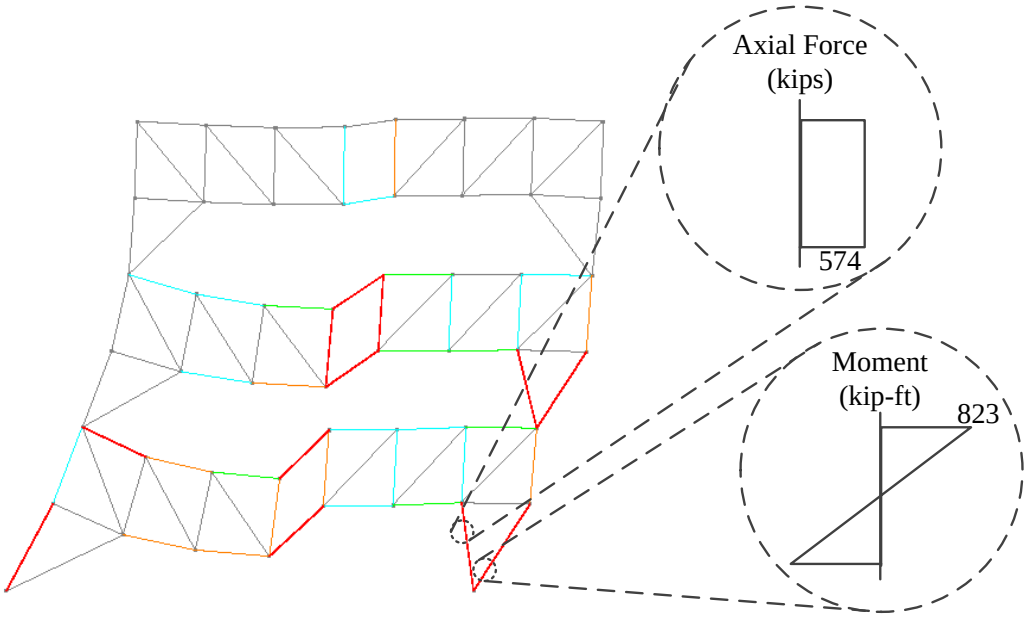

Figure 10-5 Member force demand at 0.77% roof drift in bay 1 of the SVP Model

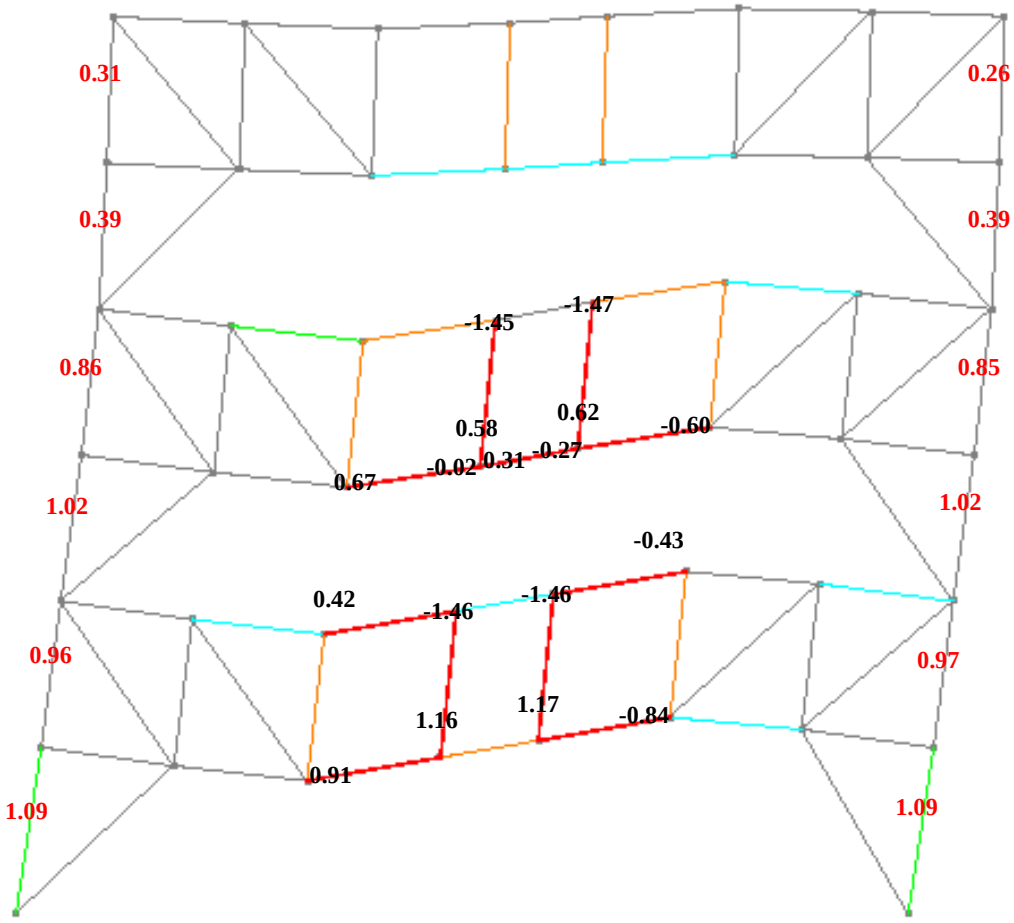

Figure 10-6 Bay 1 deflected shape with plastic hinge rotations (%) and interstory drift ratios (%) of the Base Model at 0.77% roof drift

Note: The plastic hinge rotations are indicated in **black** whereas the interstory drift ratios are indicated in **red**.
The member colors indicate the minimum usage ratio (demand versus capacity of the member) as followed:

Color	Usage Ratio
Grey	0.0
Teal	0.4
Green	0.6
Orange	0.8
Red	1.0

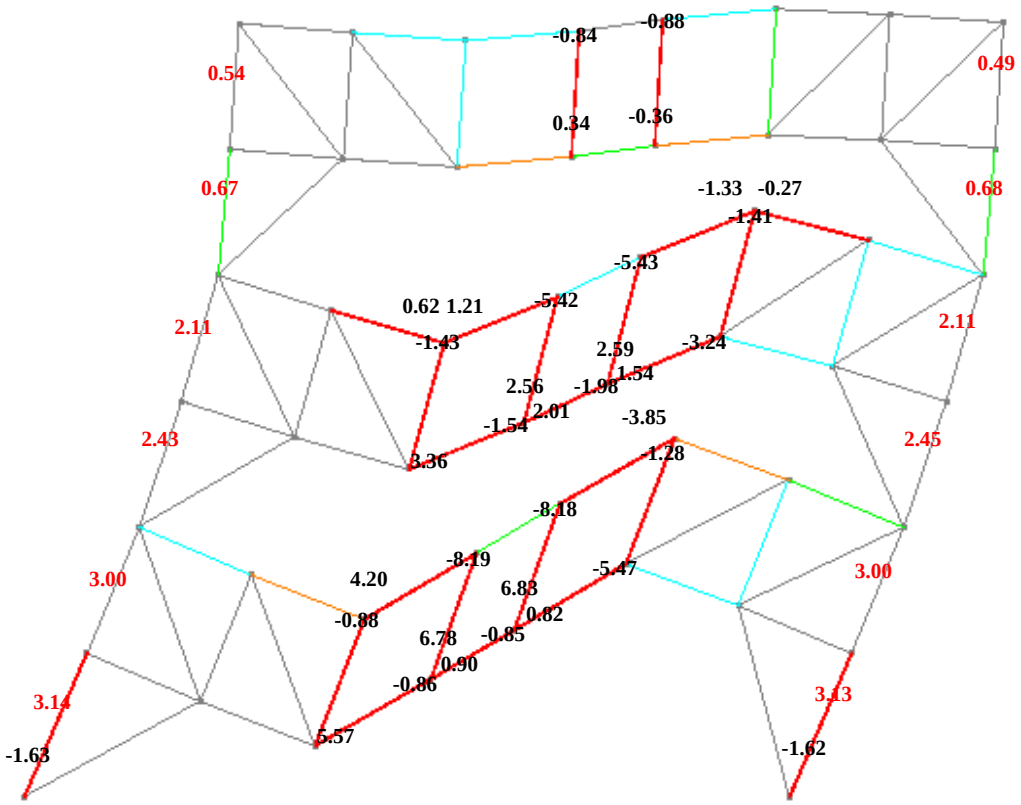

Figure 10-7 Bay 1 deflected shape with plastic hinge rotations (%) and interstory drift ratios (%) of the Base Model at 2% roof drift

Note: The plastic hinge rotations are indicated in **black** whereas the interstory drift ratios are indicated in **red**.
The member colors indicate the minimum usage ratio (demand versus capacity of the member) as followed:

Color	Usage Ratio
Grey	0.0
Teal	0.4
Green	0.6
Orange	0.8
Red	1.0

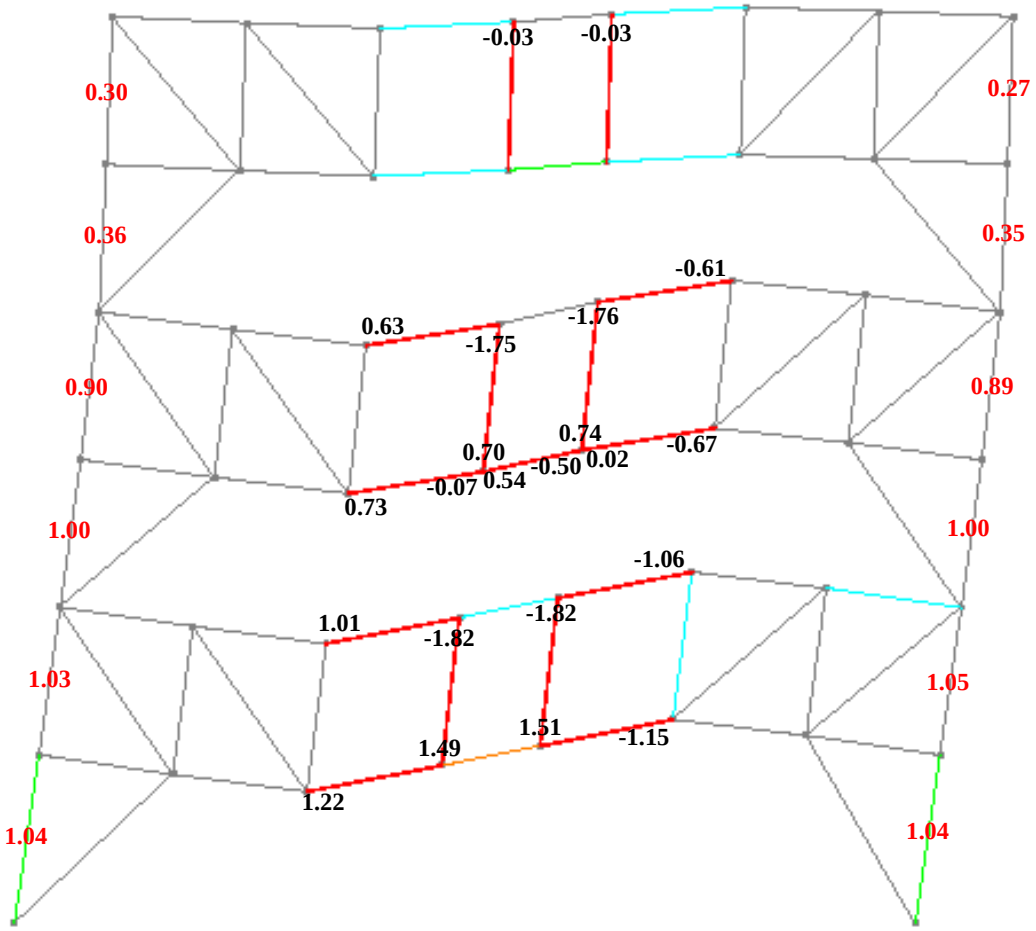

Figure 10-8 Bay 1 deflected shape with plastic hinge rotations (%) and interstory drift ratios (%) of the Target Drift Model at 0.77% roof drift

Note: The plastic hinge rotations are indicated in **black** whereas the interstory drift ratios are indicated in **red**.
The member colors indicate the minimum usage ratio (demand versus capacity of the member) as followed:

Color	Usage Ratio
Grey	0.0
Teal	0.4
Green	0.6
Orange	0.8
Red	1.0

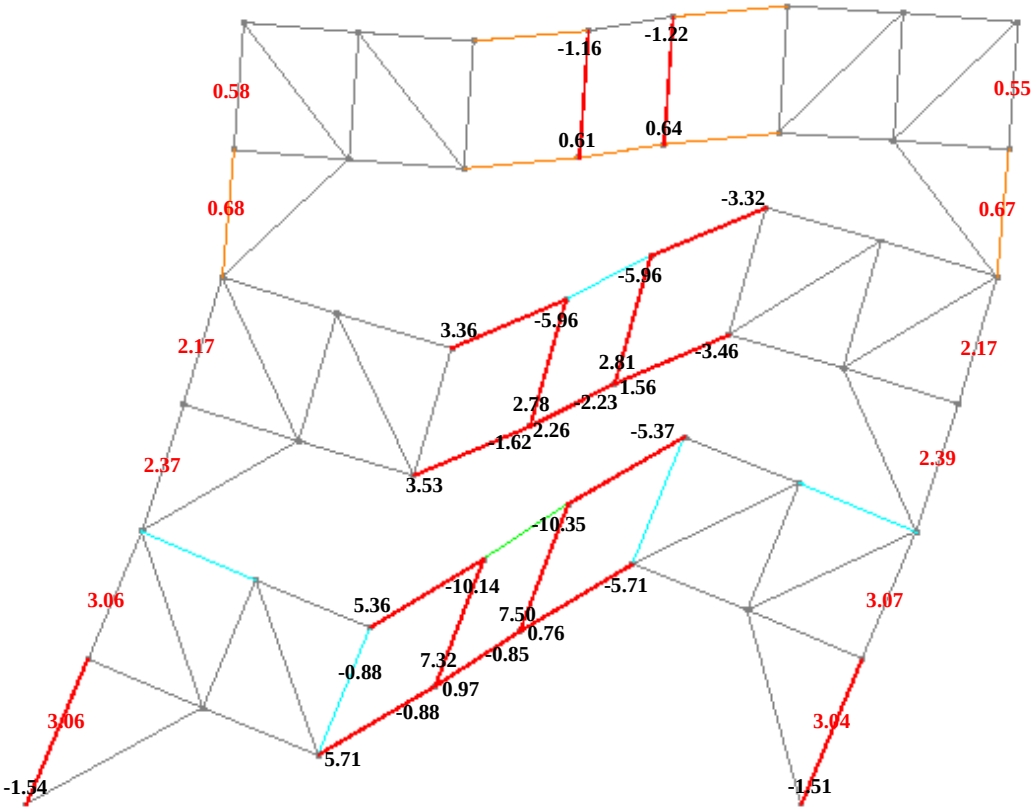

Figure 10-9 Bay 1 deflected shape with plastic hinge rotations (%) and interstory drift ratios (%) of the Target Drift Model at 2% roof drift

Note: The plastic hinge rotations are indicated in **black** whereas the interstory drift ratios are indicated in **red**.
The member colors indicate the minimum usage ratio (demand versus capacity of the member) as followed:

Color	Usage Ratio
Grey	0.0
Teal	0.4
Green	0.6
Orange	0.8
Red	1.0

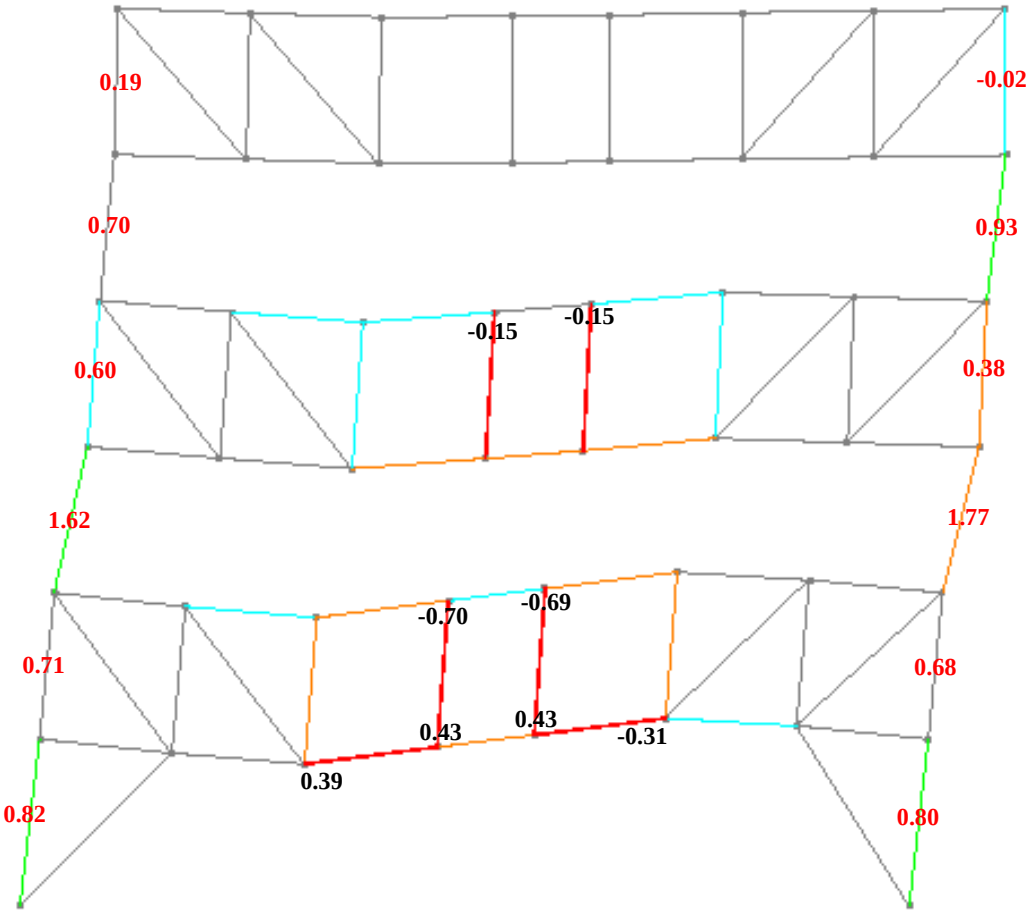

Figure 10-10 Bay 1 deflected shape with plastic hinge rotations (%) and interstory drift ratios (%) of the No Kicker Model at 0.77% roof drift

Note: The plastic hinge rotations are indicated in **black** whereas the interstory drift ratios are indicated in **red**.
The member colors indicate the minimum usage ratio (demand versus capacity of the member) as followed:

Color	Usage Ratio
Grey	0.0
Teal	0.4
Green	0.6
Orange	0.8
Red	1.0

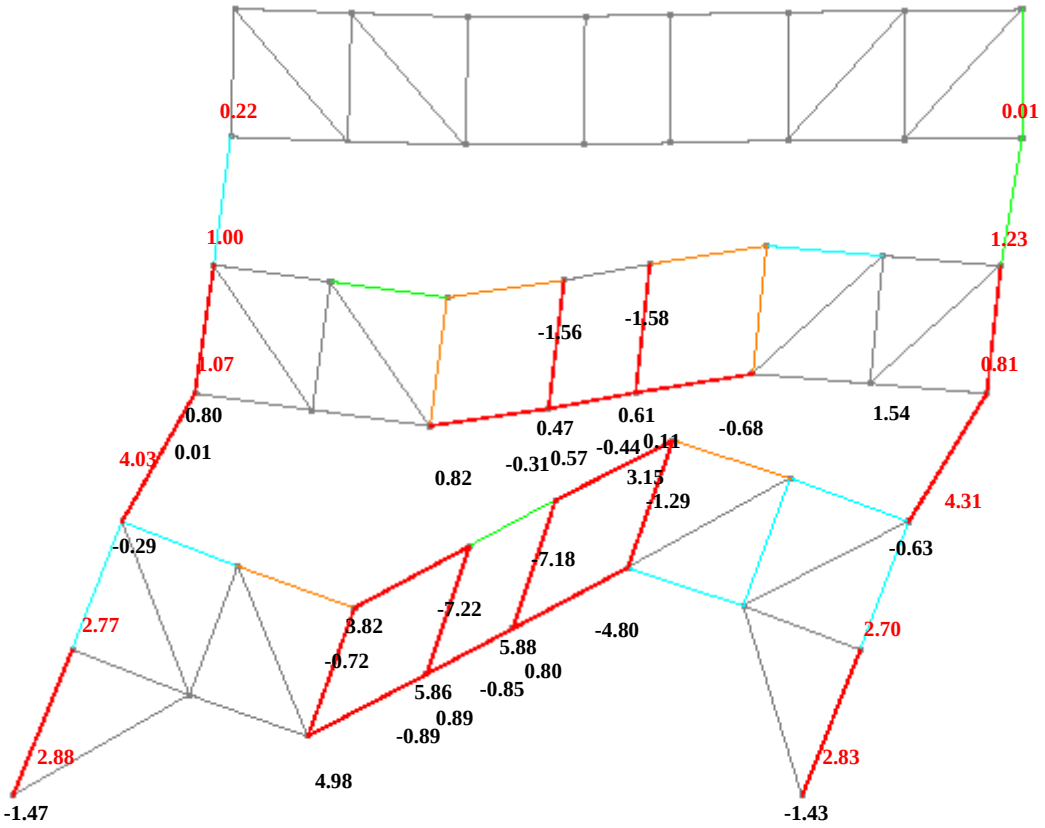

Figure 10-11 Bay 1 deflected shape with plastic hinge rotations (%) and interstory drift ratios (%) of the No Kicker Model at 2% roof drift

Note: The plastic hinge rotations are indicated in **black** whereas the interstory drift ratios are indicated in **red**.
The member colors indicate the minimum usage ratio (demand versus capacity of the member) as followed:

Color	Usage Ratio
Grey	0.0
Teal	0.4
Green	0.6
Orange	0.8
Red	1.0

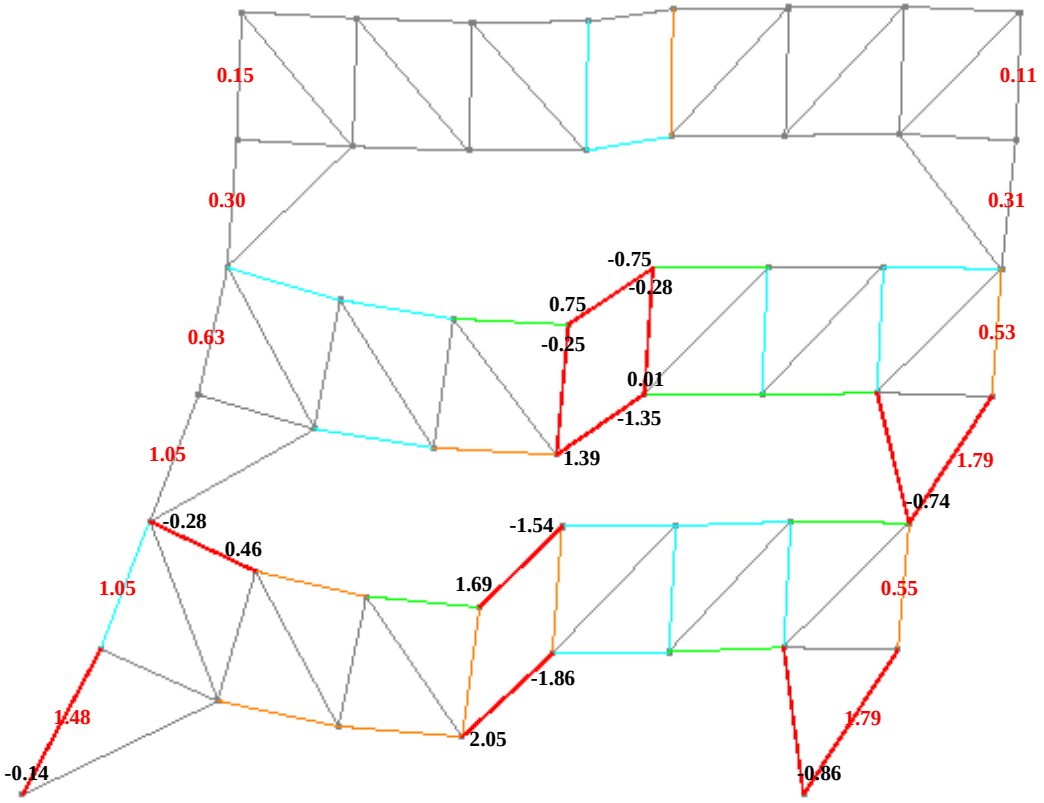

Figure 10-12 Bay 1 deflected shape with plastic hinge rotations (%) and interstory drift ratios (%) of the SVP Model at 0.77% roof drift

Note: The plastic hinge rotations are indicated in **black** whereas the interstory drift ratios are indicated in **red**.
The member colors indicate the minimum usage ratio (demand versus capacity of the member) as followed:

Color	Usage Ratio
Grey	0.0
Teal	0.4
Green	0.6
Orange	0.8
Red	1.0

The deflected shapes of the Base Model and the Target Drift Model are similar to those of K-braced Eccentrically Brace Frames (EBF) as shown in Figure 10-13. In those two models, the members in the Vierendeel panels of the STF deform while the members outside of the Vierendeel panels along with the adjacent columns and kickers at the lower floor act as one unit like the brace-beam-column units outside shear links in EBFs. In the modified STFs the non-truss (with kickers) and truss levels (with Vierendeel) act like one single story rather than two separate stories, as shown in Figure 10-13. This could be justified by the small relative rotations between columns of the two levels as shown in Figure 10-7 and Figure 10-9. It can also be seen that the plastic hinge rotation angles of the vertical members in the Vierendeel panels are larger than those of the chord members at the end of the Vierendeel panel. This is due to the long rigid end zones of the vertical members which are connected to the chord members via gusset plates as shown in Figure 10-13(a) and Figure 10-14.

Figure 10-15 shows the deflected shapes of the members in moment frame along the longitudinal direction of the Base Model and the Target Drift Model with the maximum interstory drift ratios, maximum plastic hinge rotations of the yielded members, and member minimum usage ratios at 2% roof drift. The results from the No Kicker Model and the SVP Model are excluded from this summary since the moment frame members of those two models are the same as in the Base Model.

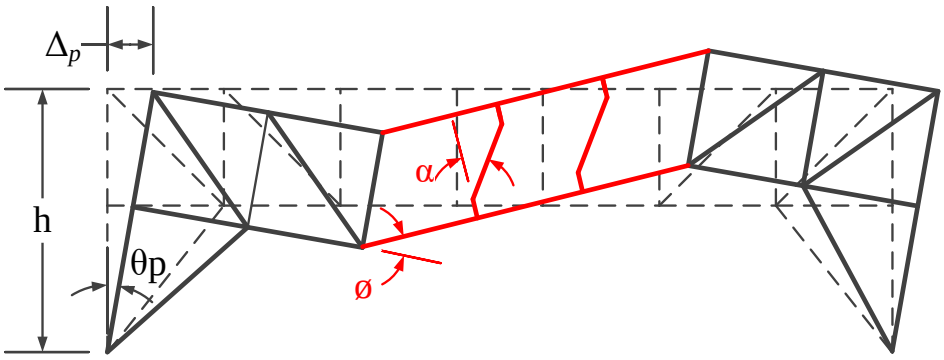

(a)

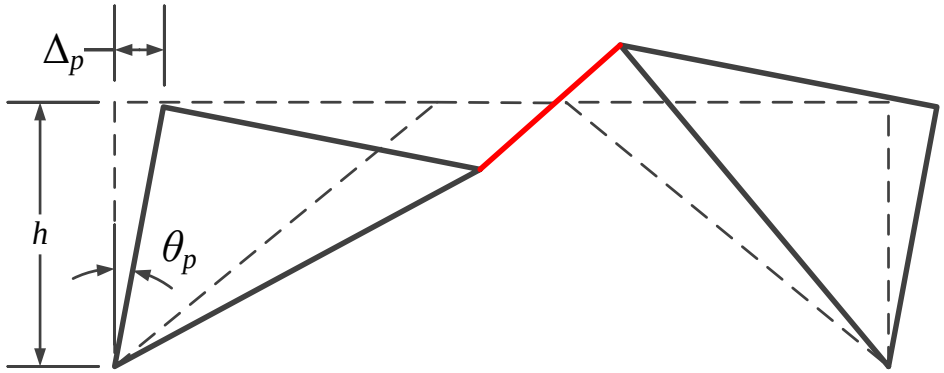

(b)

Figure 10-13 Deflected shapes: (a) STF; (b) K-braced EBF

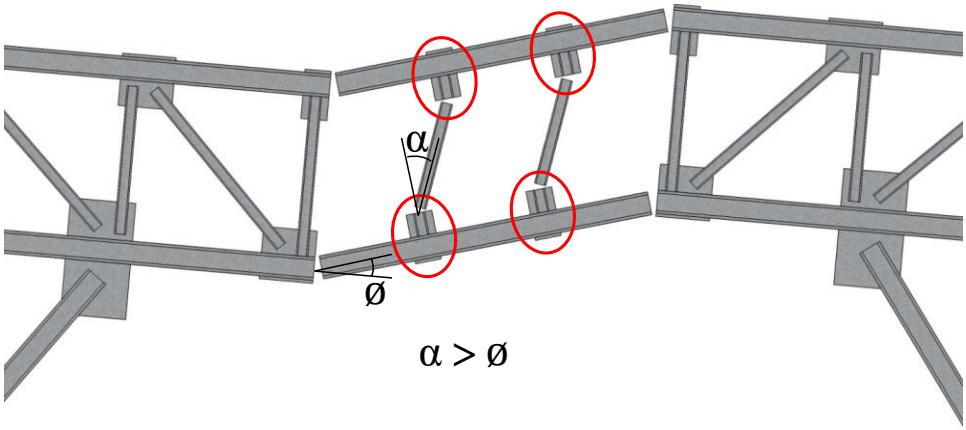

Figure 10-14 Rigid end zones of the vertical members in Vierendeel panels

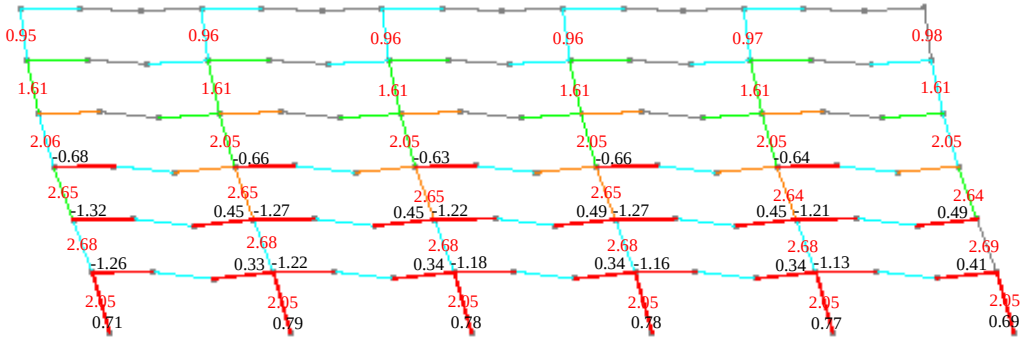

(a)

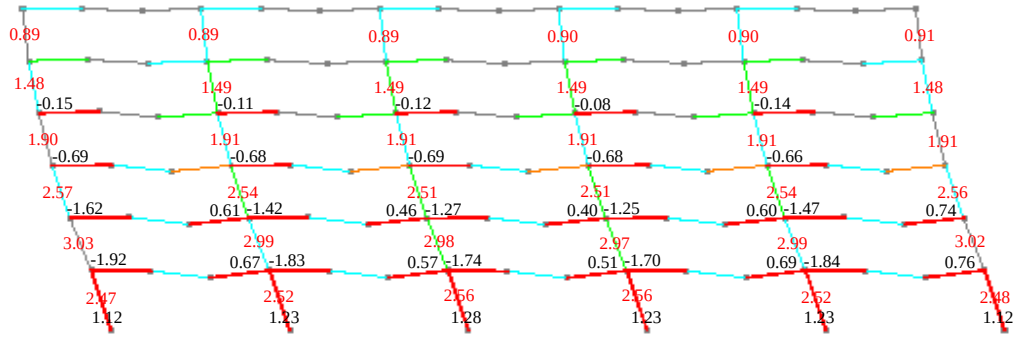

(b)

Figure 10-15 Deflected shapes of the moment frames with plastic hinge rotations (%) and interstory drift ratios (%) at 2% roof drift in the longitudinal direction: (a) Base Model; (b) Target Drift Model

Note: The plastic hinge rotations are indicated in **black** whereas the interstory drift ratios are indicated in **red**.
The member colors indicate the minimum usage ratio (demand versus capacity of the member) as followed:

Color	Usage Ratio
Grey	0.0
Teal	0.4
Green	0.6
Orange	0.8
Red	1.0

10.3 Nonlinear Time-History Analysis Results and Discussions

As stated previously, nonlinear time-history analyses of the prototype structures were carried out using Perfrom-3D computer program. All of the models were analyzed to evaluate the seismic performance under forty SAC recorded ground motions (Somerville et at., 1997) representing DBE and MCE hazard levels in both the transverse and the longitudinal directions. The main investigating parameter is the interstory drift ratio response in the direction of the truss (transverse direction of the structures). The fundamental periods of the structures obtained from Perform-3D modal analyses of all models are summarized in Table 10-4.

Table 10-4 Fundamental Periods of the Structures (seconds)

Model	Longitudinal Direction (Mode 1)	Transverse Direction (Mode 3)
Base Model	1.75	0.96
Target Drift Model	1.79	0.90
No Kicker Model	1.75	1.10
SVP Model	1.75	0.66

Due to the truss arrangement of the STF system, the stiffness varies greatly from bay to bay within the same floor. This results in significant differences in the story drifts of each bay in the same elevation. For the purpose of this study, the interstory drifts from all the bays on both sides of the frame (grid A and B as shown in Figure 9-1) were collected from the time-history analysis for each ground motion due to the aforementioned reason. The maximum interstory drift ratios (MIDR) of each ground motion are calculated using the greater of the absolute maximum or absolute minimum interstory drift ratios from all the bays within each story. The average values of MIDR for each hazard level were also calculated for all models. The results of the time-history analysis are shown in Figure 10-16 for the DBE hazard levels and in Figure 10-17 for the MCE hazard levels.

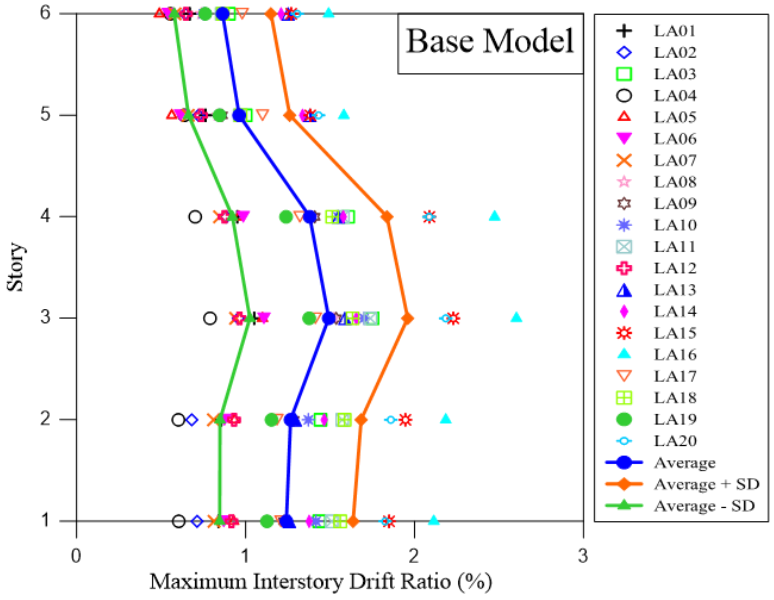

(a)

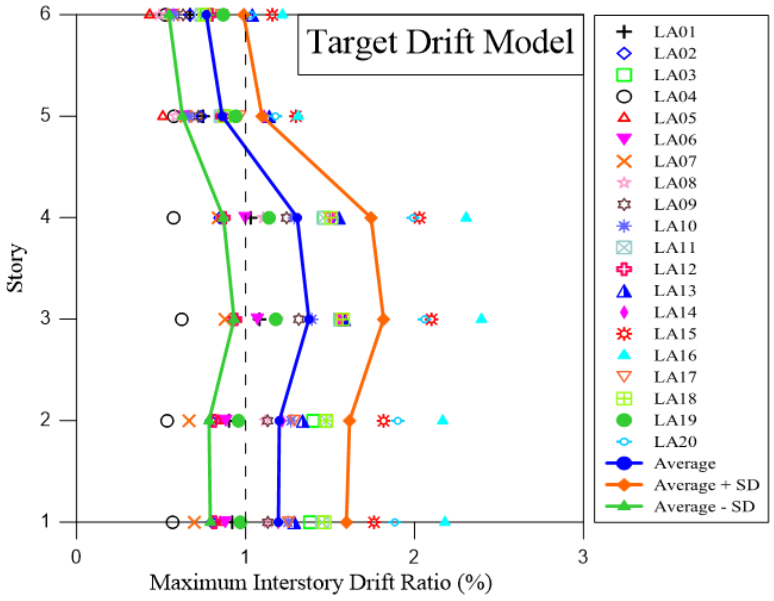

(b)

Figure 10-16 Maximum interstory drift ratios subjected to DBE level ground motions (LA01 to LA20): (a) Base Model; (b) Target Drift Model; (c) No Kicker Model; (d) SVP Model

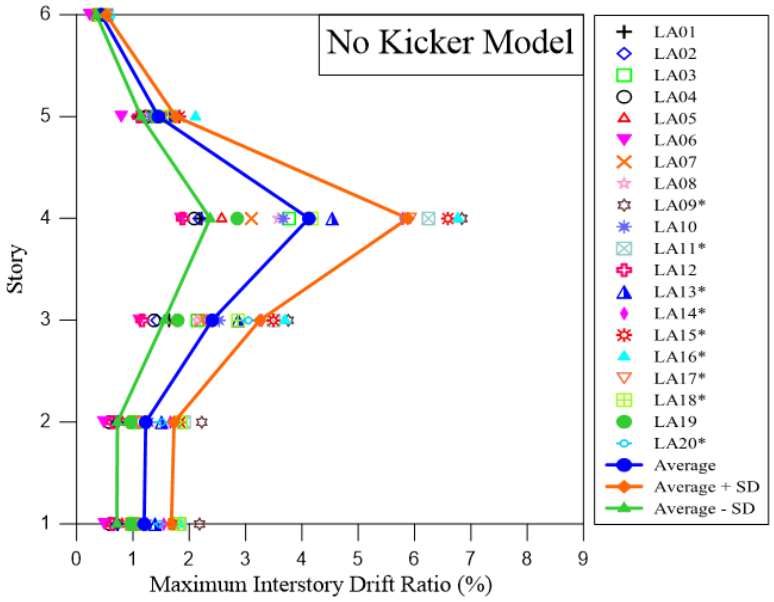

(c)

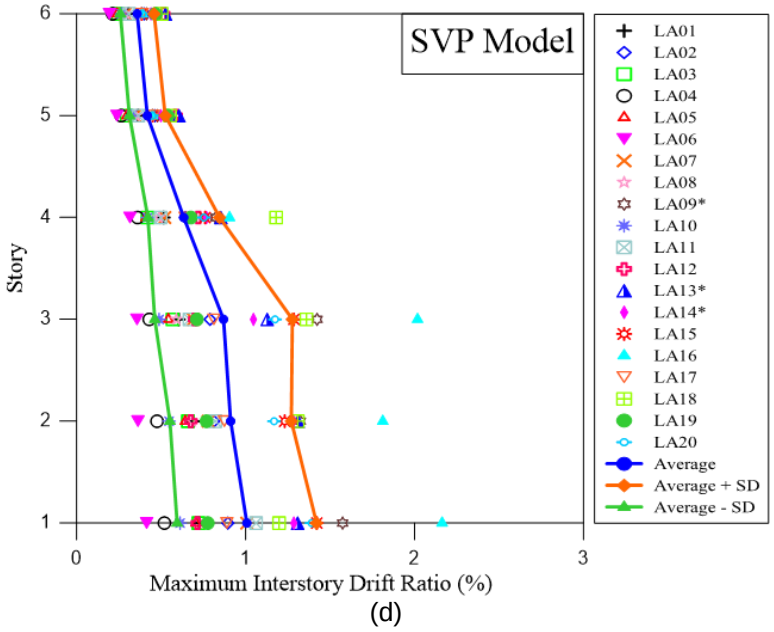

(d)

Figure 10-16—*Continued*

Note: * indicates the ground motions of which the analyses stopped before the end of the ground motion durations due to excessive damage of the yielded members.
The maximum interstory drift ratios of each ground motion are calculated using the greater of the absolute maximum or absolute minimum interstory drift ratios from all the bays within each story.

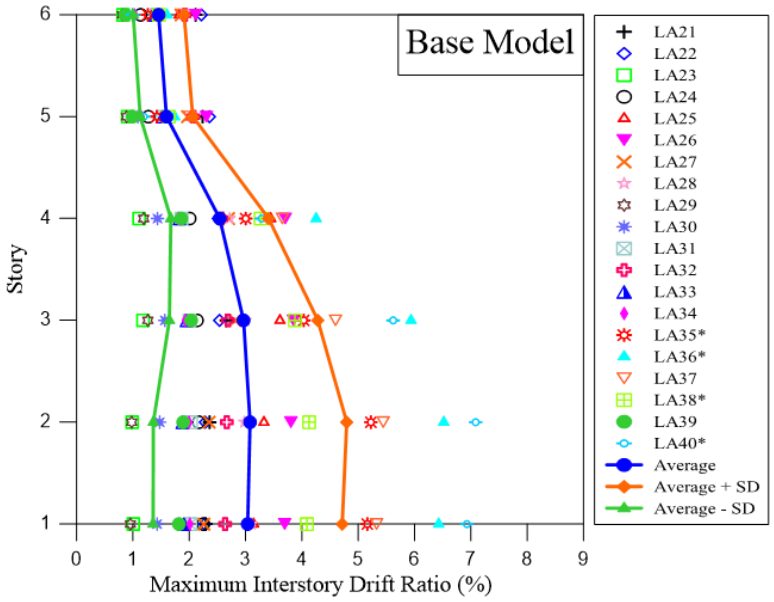

(a)

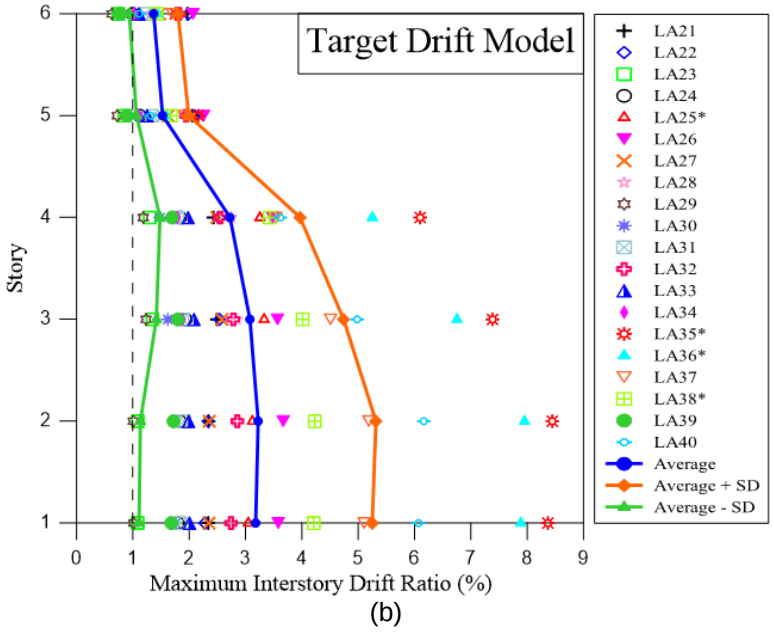

(b)

Figure 10-17 Maximum interstory drift ratios subjected to MCE level ground motions (LA21 to LA40): (a) Base Model; (b) Target Drift Model; (c) No Kicker Model; (d) SVP Model

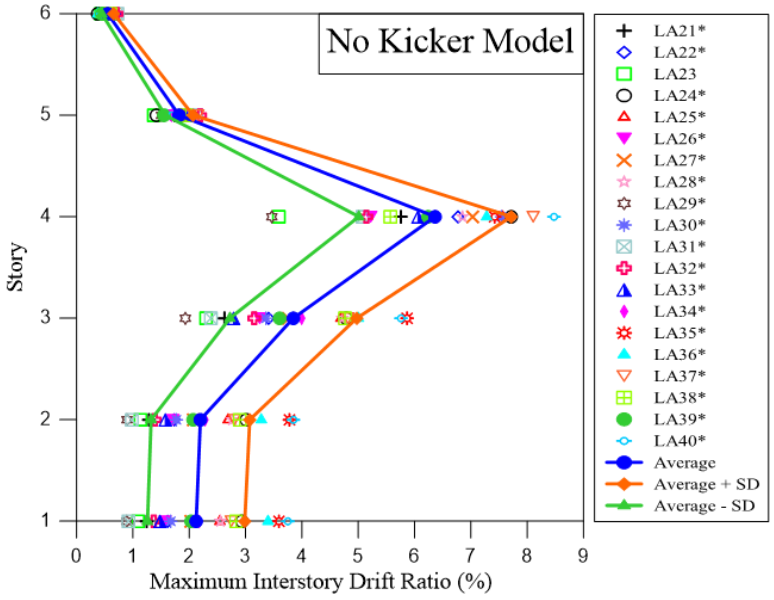

(c)

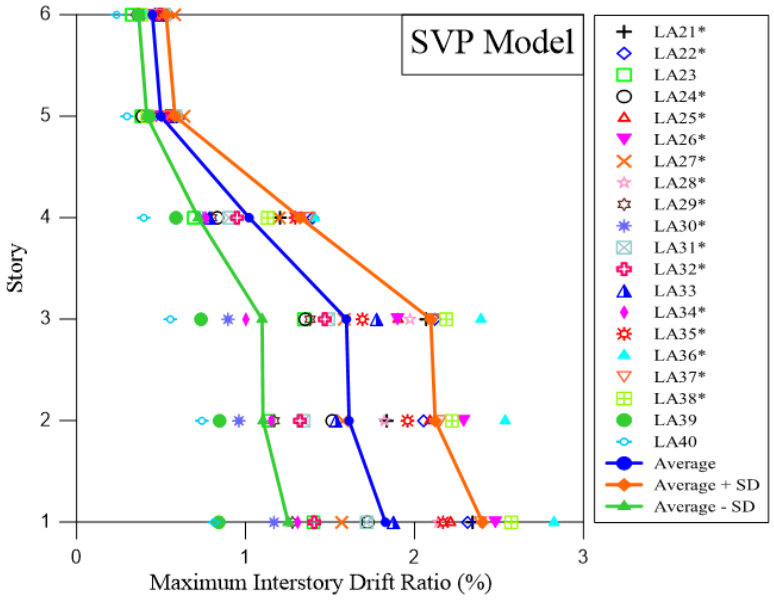

(d)

Figure 10-17—*Continued*

Note: * indicates the ground motions of which the analyses stopped before the end of the ground motion durations due to excessive damage of the yielded members.
The maximum interstory drift ratios of each ground motion are calculated using the greater of the absolute maximum or absolute minimum interstory drift ratios from all the bays within each story.

The analyses stopped before the end of some ground motions due to excessive damage in yielded members. Those ground motions are indicated with an asterisk (*) in the figures. Figure 10-18 and Figure 10-19 show the average MIDR of the DBE and MCE hazard levels, respectively.

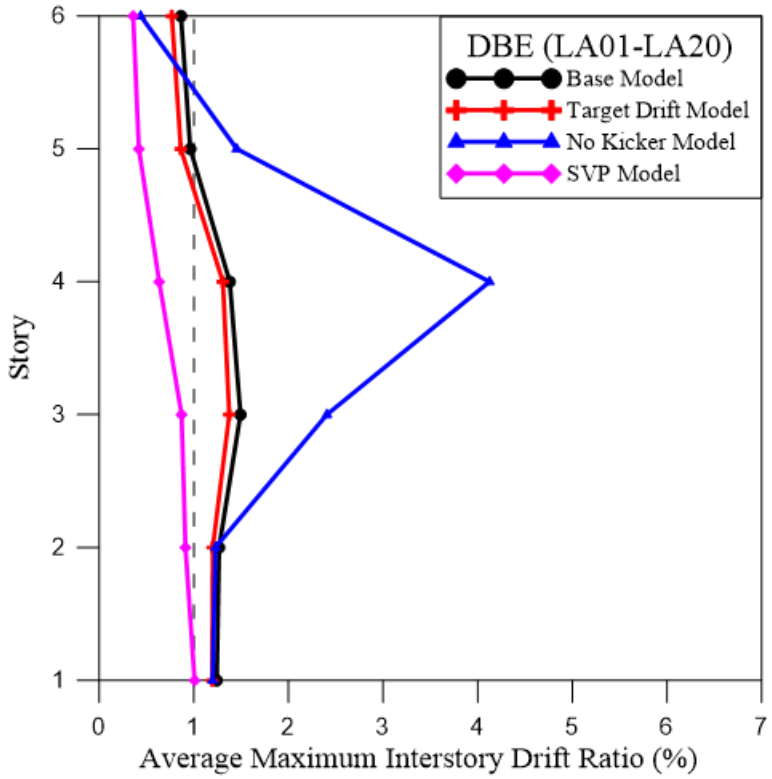

Figure 10-18 Average maximum interstory drift ratios subjected to DBE level ground motions (LA01 to LA20)

Note: The average maximum interstory drift ratios of the No Kicker Model and the SVP Model do not reflect the true behavior of the structures as the analyses stopped prematurely due to excessive member deformation.

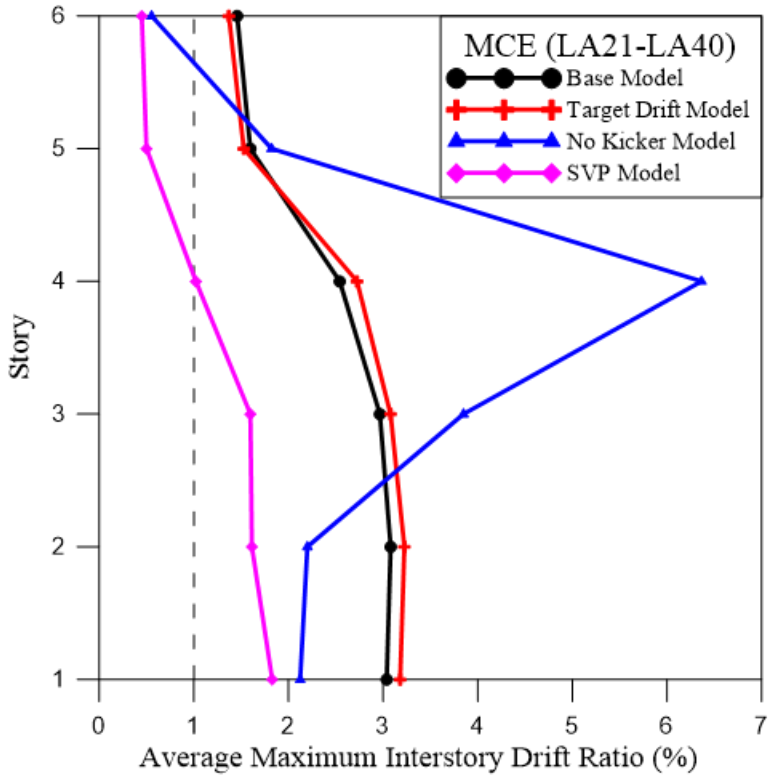

Figure 10-19 Average maximum interstory drift ratios subjected to MCE level ground motions (LA21 to LA40)

Note: The average maximum interstory drift ratios of the No Kicker Model and the SVP Model do not reflect the true behavior of the structures as the analyses stopped prematurely due to excessive member deformation.

The average values of MIDR of the Base Model range from 0.86-1.49% and 1.46-3.08% for the DBE and MCE hazard levels respectively, whereas the respective values of the Target Drift Model range from 0.77-1.37 and 1.37-3.22%. It can be seen that the average values of MIDR of the Base Model and Target Drift Model do not differ significantly. This is attributed to the yielding members in the Vierendeel panels which control the rotational capacity of the structures. It is worth noting that both models reach relatively small MIDR under DBE hazard levels. Comparing to the conventional STF

system (Kim et al., 2007), the modified STF system gives relatively uniformed MIDR throughout the height of the structure.

The average maximum plastic hinge rotations of the selected members as shown in Figure 10-2 from all ground motions are summarized in Table 10-5 and Table 10-6.

Table 10-5 Average maximum plastic hinge rotation of the selected members from nonlinear time-history analyses of DBE hazard levels (kips)

Member	Average Maximum Plastic Hinge Rotation (%)			
	Base Model	Target Drift Model	No Kicker Model	SVP Model
1	0.18	0.21	0.20	1.00
2	1.17	1.37	1.07	0.01
3	0.13	0.00	0.07	0.00
4	1.84	2.04	2.15	0.03
5	3.01	2.99	1.67	0.30

Table 10-6 Average maximum plastic hinge rotation of the selected members from nonlinear time-history analyses of MCE hazard levels (kips)

Member	Average Maximum Plastic Hinge Rotation (%)			
	Base Model	Target Drift Model	No Kicker Model	SVP Model
1	1.20	1.17	0.85	2.54
2	5.68	6.40	3.04	0.08
3	1.42	0.00	0.19	0.00
4	8.33	9.16	3.76	0.24
5	7.70	8.52	4.66	0.58

Figure 10-20 show the hysteresis loops of a buckling-type element (the right kicker – towards grid B – on the third floor) from LA23 ground motion for the Base Model, the Target Drift Model, and the SVP Model to illustrate the severe local deformation of the kicker in the SVP Model which leads to the failure of the structure before the end of the ground motion duration. On the other hand, kickers in both the Base Model and Target Drift Model remained essentially elastic which prevented the column from suffering large rotations.

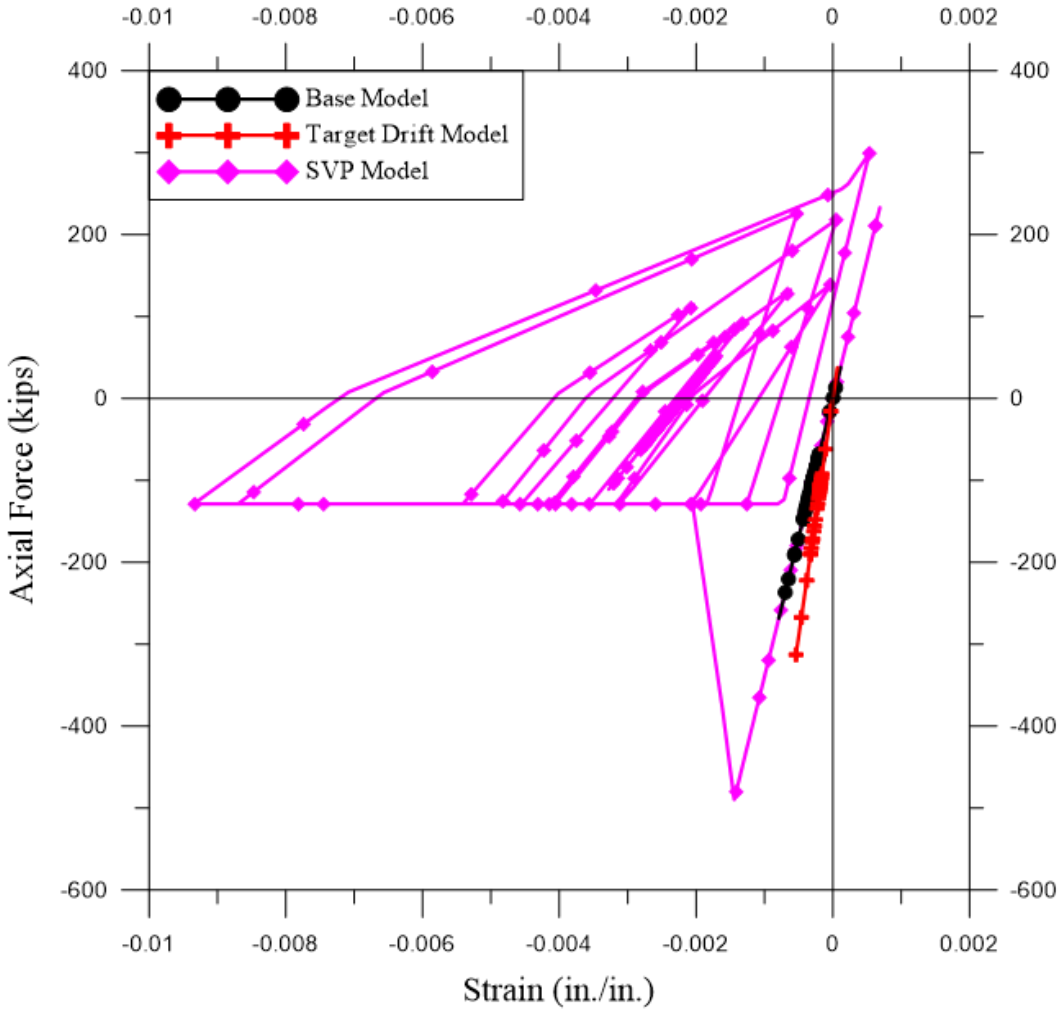

Figure 10-20 Hysteresis loops of the right kicker on third floor of bay 1

Table 10-7 and Table 10-8 list the maximum absolute roof drift values in the truss (along the transverse) direction for all models from all forty ground motions and the average of the maximum absolute roof drifts for DBE and MCE hazard levels respectively. For the ground motions of which the analyses stopped before the end of the ground motion durations due to excessive member deformations, the values are taken from when the analyses stopped.

Table 10-7 Maximum absolute roof drift (%) under DBE ground motions

Ground Motion	Base Model	Target Drift Model	No Kicker Model	SVP Model
LA01	0.72	0.78	0.77	0.43
LA02	0.66	0.69	0.62	0.52
LA03	1.26	1.15	1.03	0.41
LA04	0.55	0.45	0.64	0.29
LA05	0.79	0.71	0.84	0.38
LA06	0.79	0.78	0.53	0.24
LA07	0.66	0.61	1.03	0.49
LA08	1.07	0.85	1.04	0.41
LA09	1.08	0.95	**1.83**	**0.82**
LA10	1.17	1.01	1.22	0.34
LA11	1.27	1.17	**1.70**	0.47
LA12	0.65	0.69	0.53	0.43
LA13	1.15	1.14	**1.23**	**0.71**
LA14	1.19	1.13	**1.63**	**0.66**
LA15	1.64	1.55	**1.75**	0.72
LA16	1.93	1.82	**1.95**	1.08
LA17	1.02	1.13	**1.15**	0.52
LA18	1.14	1.13	**1.30**	0.70
LA19	0.94	0.88	0.80	0.48
LA20	1.61	1.53	**1.53**	0.66
Average Maximum Absolute	**1.06**	**1.01**	**1.16**	**0.54**

Note: The numbers in red indicate that the analyses for the corresponding models and ground motions stopped before the end of the ground motion durations due to excessive member deformation.

Table 10-8 Maximum absolute roof drift (%) under MCE ground motions

Ground Motion	Base Model	Target Drift Model	No Kicker Model	SVP Model
LA21	1.86	1.79	**1.38**	**1.11**
LA22	1.90	1.93	**1.75**	**1.17**
LA23	0.80	0.95	1.09	0.71
LA24	1.60	1.47	**2.26**	**0.81**
LA25	2.66	2.54	**2.41**	**1.12**
LA26	2.93	2.85	**1.52**	**1.17**
LA27	2.16	2.00	**1.99**	**0.89**
LA28	2.12	2.12	**2.21**	**1.06**
LA29	0.88	0.86	**0.92**	**0.70**
LA30	1.13	1.22	**1.64**	**0.57**
LA31	1.46	1.37	**1.24**	**0.81**
LA32	1.98	2.03	**1.59**	**0.79**
LA33	1.42	1.59	**1.35**	0.92
LA34	1.48	1.37	**1.91**	**0.69**
LA35	**3.07**	**5.30**	**2.80**	**0.96**
LA36	**4.06**	**4.83**	**2.34**	**1.31**
LA37	3.32	3.26	**2.50**	**1.19**
LA38	**2.88**	**2.93**	**2.25**	**1.21**
LA39	1.48	1.33	**1.80**	0.49
LA40	**3.81**	3.54	**2.79**	0.41
Average Maximum Absolute	**1.06**	**1.01**	**1.16**	**0.54**

Note: The numbers in red indicate that the analyses for the corresponding models and ground motions stopped before the end of the ground motion durations due to excessive member deformation.

x.4 Discussion on Time-History Response of Interstory Drift Ratio under Selected Ground Motions

For comparison purposes, time-history analysis results from two severe ground motions – one each from DBE and MCE levels – are presented in this report. LA16 and LA36 ground motions are selected for DBE and MCE levels respectively. For the DBE level, the analyses finished through the end of the ground motion period for all models except the No Kicker Model.

It was observed that majority of the horizontal truss members remained elastic under DBE ground motions except a few members in the No Kicker Model and SVP Model. The analysis results also show that the horizontal truss members effectively transfer the seismic force. Figure 10-21 and Figure 10-22 show the deflected shapes and the member usage ratios of the horizontal truss members on the fourth story from LA16 and LA36 ground motions respectively. The fourth story was chosen to represent the analysis results because the yielding members are almost entirely on this floor. For LA16 ground motion, the analysis for the No Kicker Model stopped before the end of the ground motion duration due to the excessive member deformations of the yielded members. For LA36 ground motion, all models experienced excessive member deformations of the yielded members. The Target Drift Model sustained the highest roof drift among all models at the end of analysis.

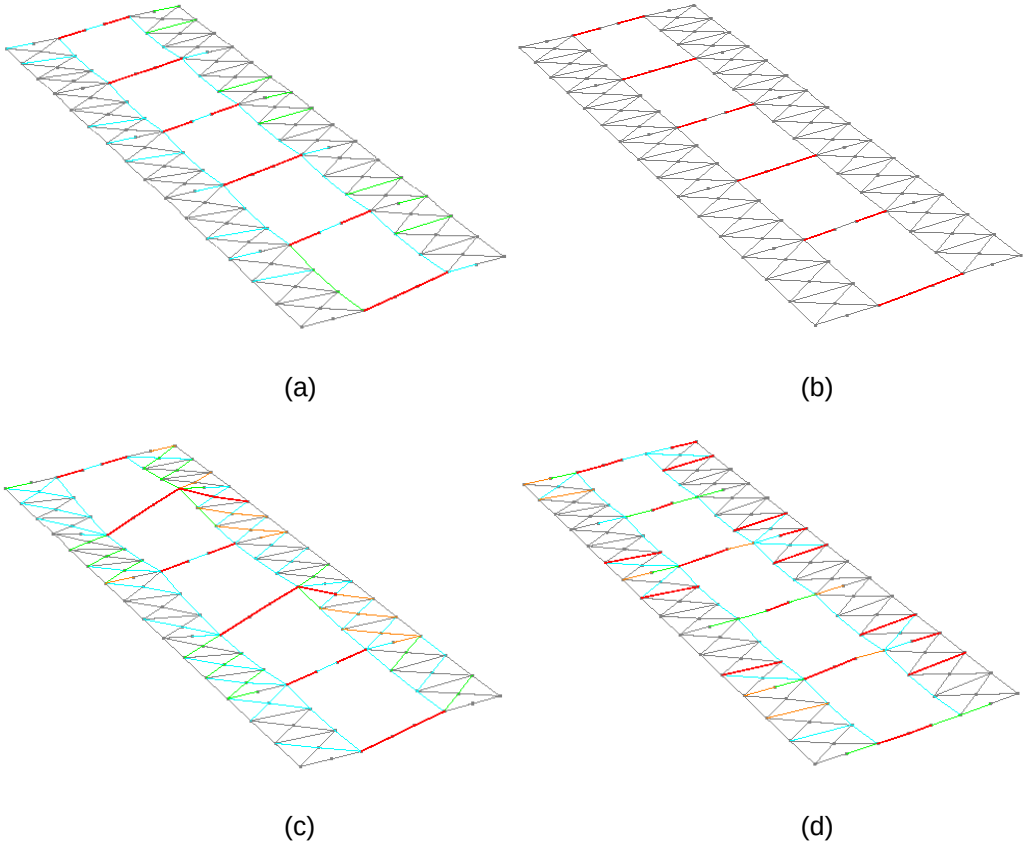

Figure 10-21 Deflected shapes and the color-coded member usage ratios of the horizontal truss members on the fourth floor under LA16 ground motion: (a) Base Model; (b) Target Drift Model; (c) No Kicker Model*; (d) SVP Model

Note: *The time-history analysis was terminated before the end of the LA16 ground motion duration for the No Kicker Model due to excessive deformation of the yielded members.

The member colors indicate the minimum usage ratio (demand versus capacity of the member) as followed:

Color	Usage Ratio
Grey	0.0
Teal	0.4
Green	0.6
Orange	0.8
Red	1.0

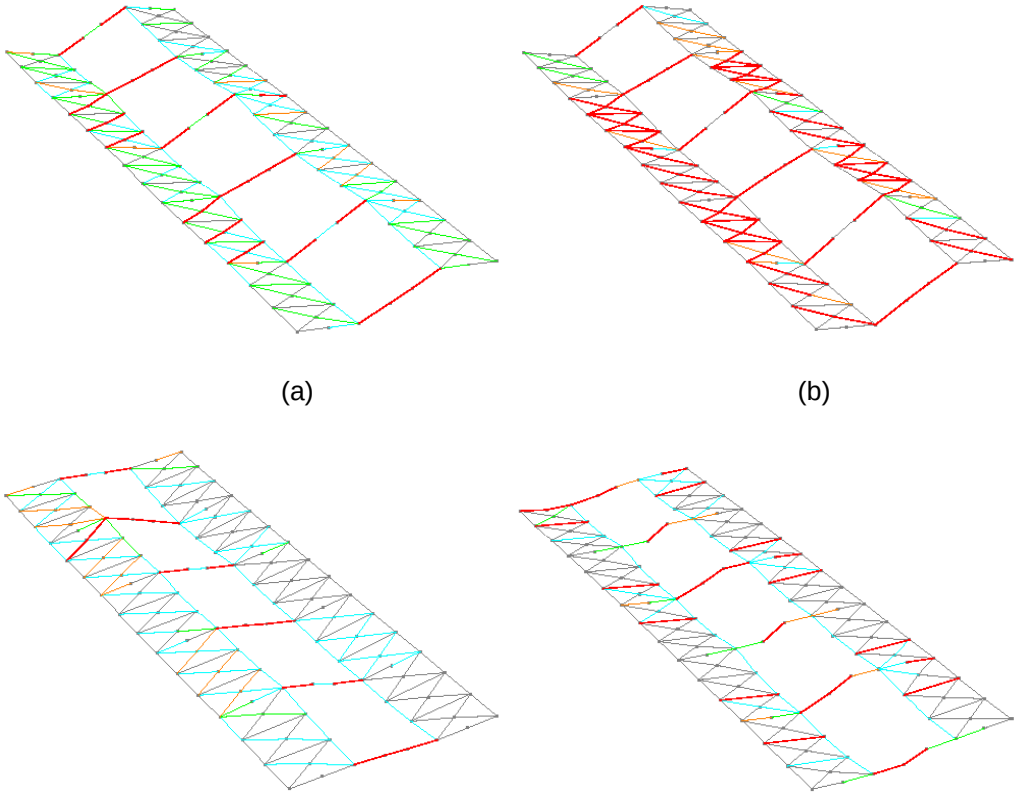

(a) (b)

(c) (d)

Figure 10-22 Deflected shapes and the color-coded member usage ratios of the horizontal truss members on the fourth floor under LA36 ground motion: (a) Base Model; (b) Target Drift Model; (c) No Kicker Model*; (d) SVP Model

Note: *The time-history analysis was terminated before the end of the LA16 ground motion duration for the No Kicker Model due to excessive deformation of the yielded members.

The member colors indicate the minimum usage ratio (demand versus capacity of the member) as followed:

Color	Usage Ratio
Grey	0.0
Teal	0.4
Green	0.6
Orange	0.8
Red	1.0

Figure 10-23 through Figure 10-26 show plastic hinge locations, the maximum plastic hinge rotations, and the maximum interstory drift ratios along with the minimum usage ratios of the members in the deflected shape of bay 1 at the maximum roof drift ratio under LA16 (DBE) ground motion for the Base Model, the Target Drift Model, the No Kicker Model, and the SVP Model, respectively. The hysteresis loops of the kickers subjected to severe deformations (right kickers on first and third story) in the SVP Model are shown in Figure 10-27. Similarly, Figure 10-28 through Figure 10-31 show the results from LA36 (MCE) ground motion and Figure 10-32 show the hysteresis loops of the kickers of the SVP Model subjected to severe deformation under LA36 ground motion. It is worth noting that the maximum plastic hinge rotations and the maximum interstory drift ratios do not necessarily occur at the same time as the maximum roof drift ratios during the ground motions except when the analyses stopped before the end of the ground motion duration due to excessive damage in the yielded members.

For the Target Drift Model under DBE level, the plastic hinge locations are confined within the Vierendeel panels which is the preferred yielding mechanism (Moore, 2005). First floor column plastic hinge rotations of the Target Drift Model are slightly smaller than those of the Base Model. The time-history roof drift ratios of all models subjected to DBE and MCE levels are shown in Figure 10-33 and Figure 10-34 respectively. The residual roof drift ratio of the Target Drift Model is slightly smaller than that of the Base Model. It can be seen that under LA36 ground motion, the plastic hinge rotations of the Vierendeel panel members exceed the residual strength point of 0.08 as defined during the modeling step.

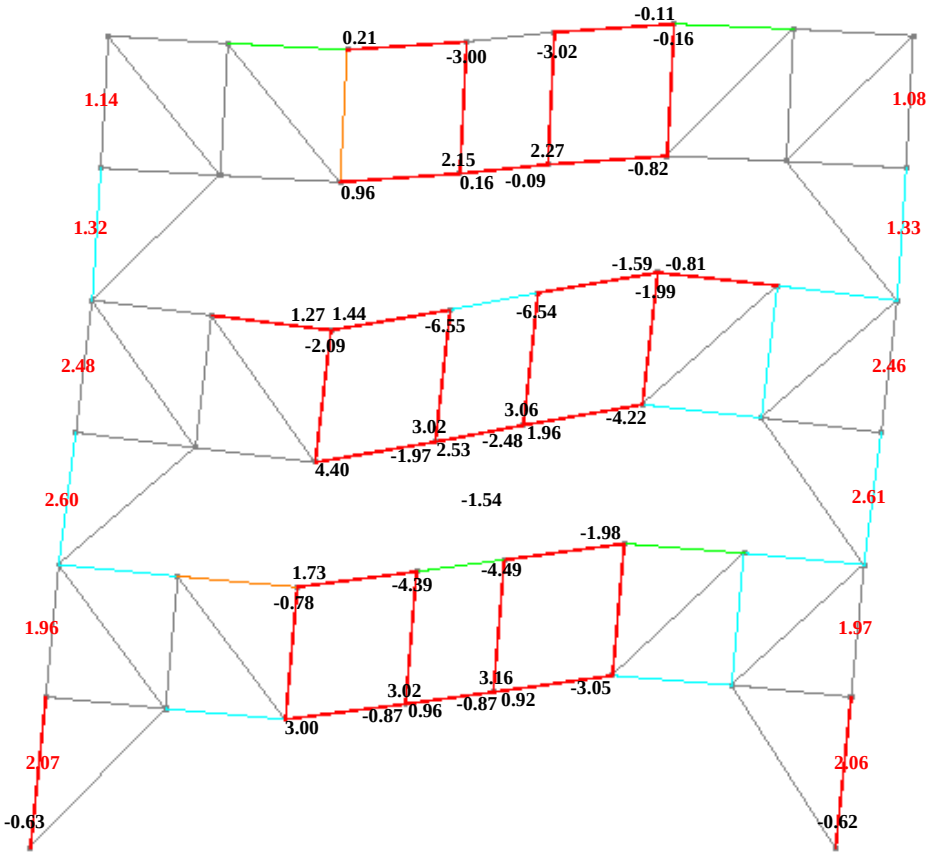

Figure 10-23 Bay 1 deflected shape at the maximum roof drift with maximum plastic hinge rotations (%) and maximum interstory drift ratios (%) of the Base Model under LA16 ground motion

Note: The plastic hinge rotations are indicated in **black** whereas the interstory drift ratios are indicated in **red**.
The member colors indicate the minimum usage ratio (demand versus capacity of the member) as followed:

Color	Usage Ratio
Grey	0.0
Teal	0.4
Green	0.6
Orange	0.8
Red	1.0

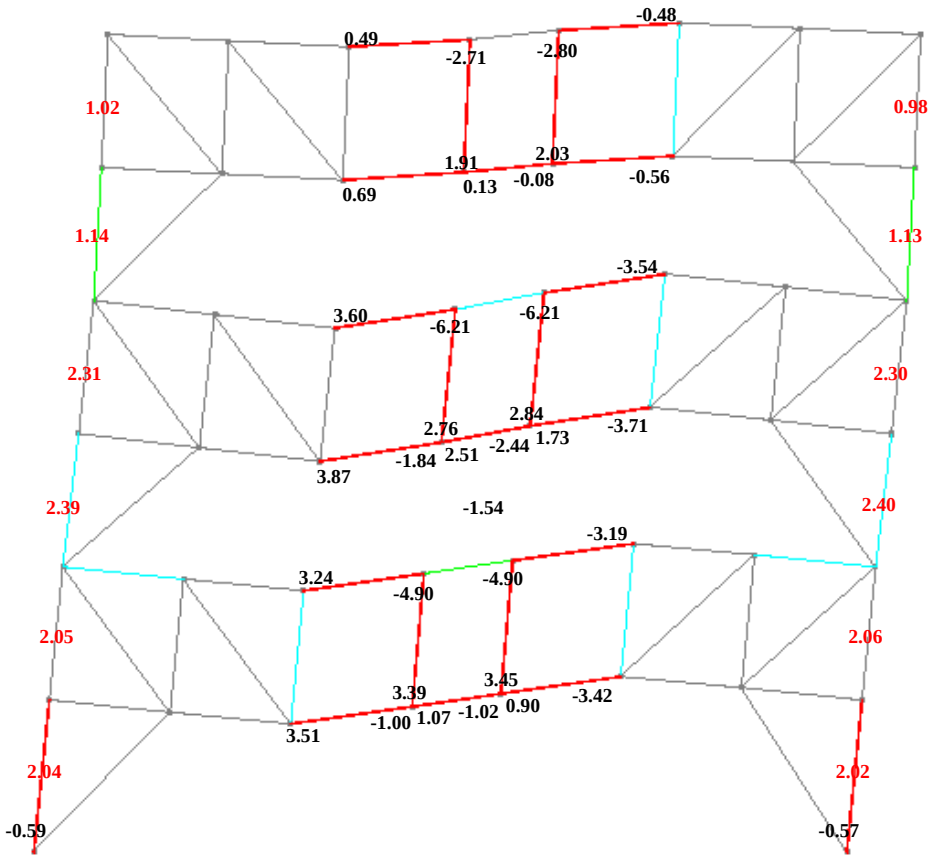

Figure 10-24 Bay 1 deflected shape at the maximum roof drift with maximum plastic hinge rotations (%) and maximum interstory drift ratios (%) of the Target Drift Model under LA16 ground motion

Note: The plastic hinge rotations are indicated in **black** whereas the interstory drift ratios are indicated in **red**.
The member colors indicate the minimum usage ratio (demand versus capacity of the member) as followed:

Color	Usage Ratio
Grey	0.0
Teal	0.4
Green	0.6
Orange	0.8
Red	1.0

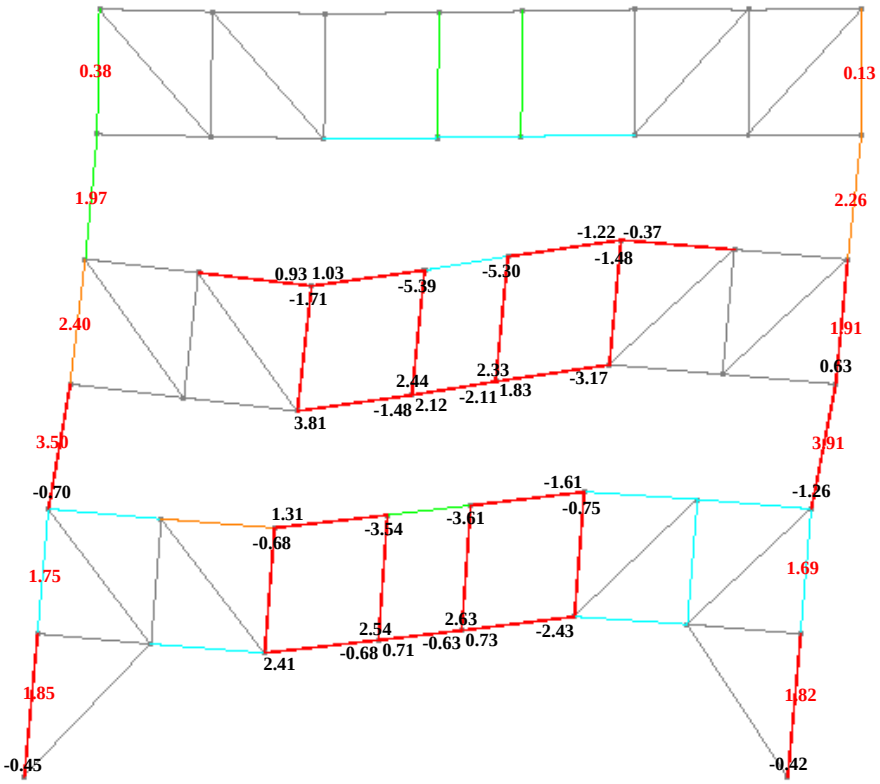

Figure 10-25 Bay 1 deflected shape at the maximum roof drift with maximum plastic hinge rotations (%) and maximum interstory drift ratios (%) of the No Kicker Model under LA16 ground motion*

Note: *The time-history analysis was terminated before the end of the LA16 ground motion duration due to excessive deformation of the yielded members of the No Kicker Model.
The plastic hinge rotations are indicated in **black** whereas the interstory drift ratios are indicated in **red**.
The member colors indicate the minimum usage ratio (demand versus capacity of the member) as followed:

Color	Usage Ratio
Grey	0.0
Teal	0.4
Green	0.6
Orange	0.8
Red	1.0

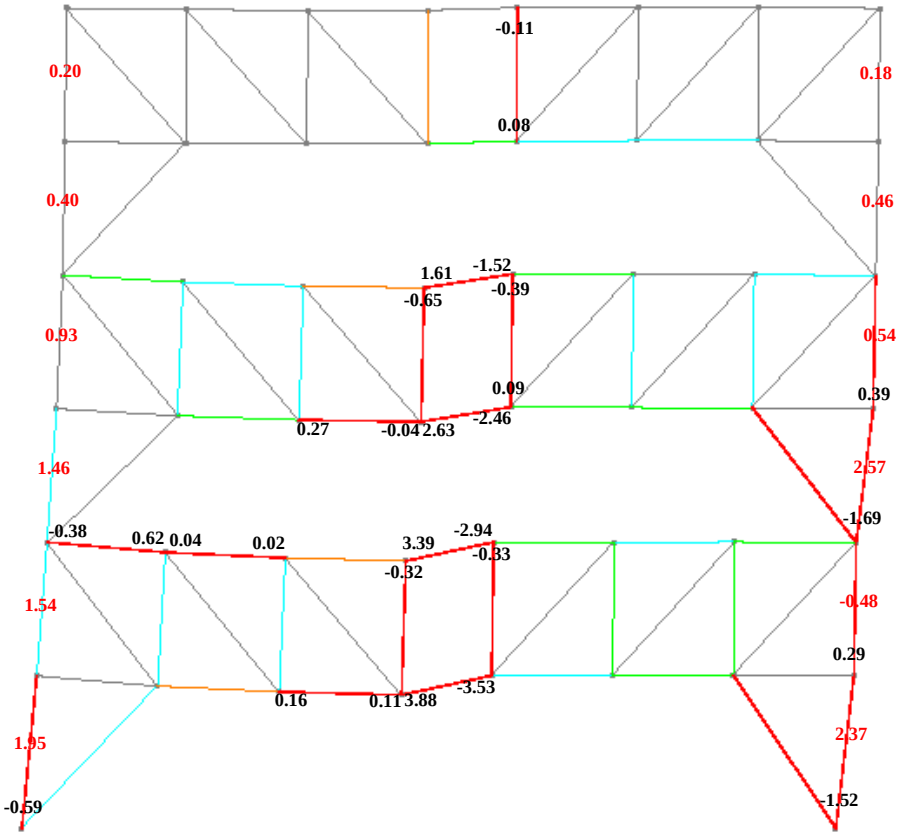

Figure 10-26 Bay 1 deflected shape at the maximum roof drift with maximum plastic hinge rotations (%) and maximum interstory drift ratios (%) of the SVP Model under LA16 ground motion

Note: The plastic hinge rotations are indicated in **black** whereas the interstory drift ratios are indicated in **red**.
The member colors indicate the minimum usage ratio (demand versus capacity of the member) as followed:

Color	Usage Ratio
Grey	0.0
Teal	0.4
Green	0.6
Orange	0.8
Red	1.0

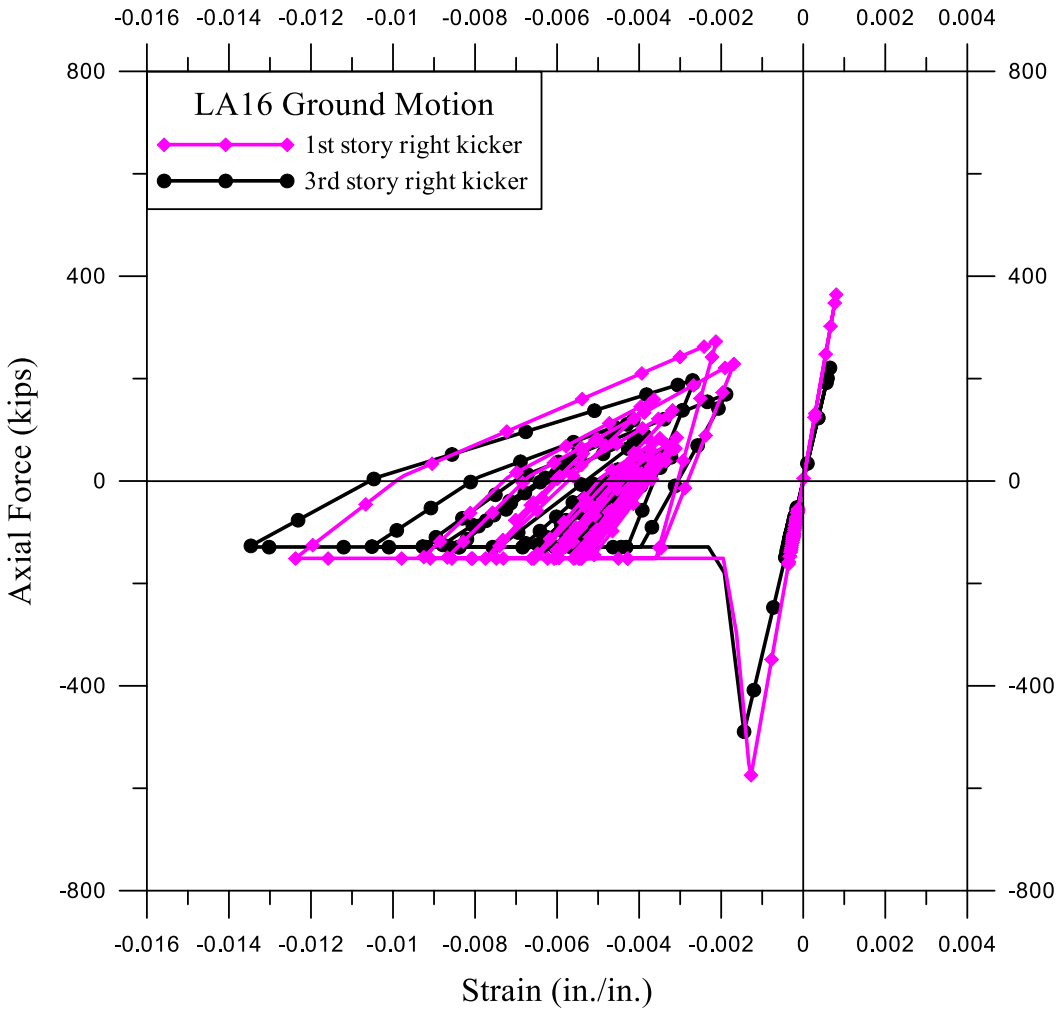

Figure 10-27 Hysteresis loops of the yielded kickers of the SVP Model in bay 1 under LA16 ground motion

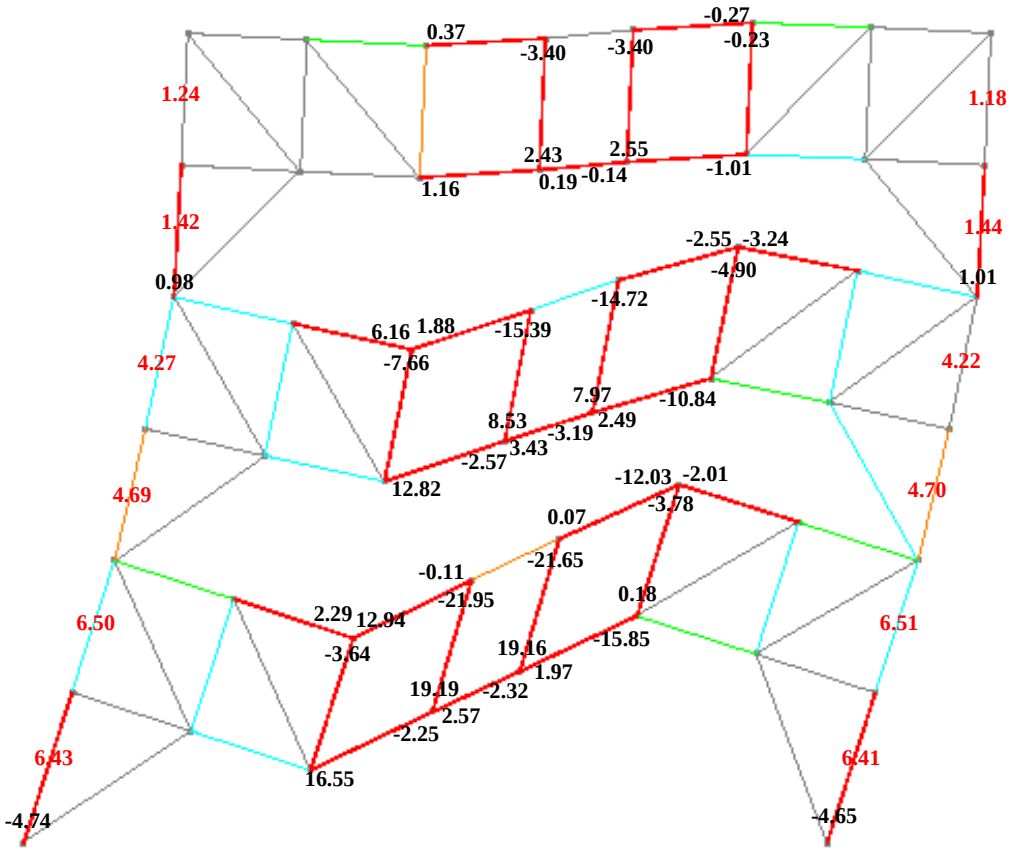

Figure 10-28 Bay 1 deflected shape at the maximum roof drift with maximum plastic hinge rotations (%) and maximum interstory drift ratios (%) of the Base Model under LA36 ground motion

Note: The plastic hinge rotations are indicated in **black** whereas the interstory drift ratios are indicated in **red**.
The member colors indicate the minimum usage ratio (demand versus capacity of the member) as followed:

Color	Usage Ratio
Grey	0.0
Teal	0.4
Green	0.6
Orange	0.8
Red	1.0

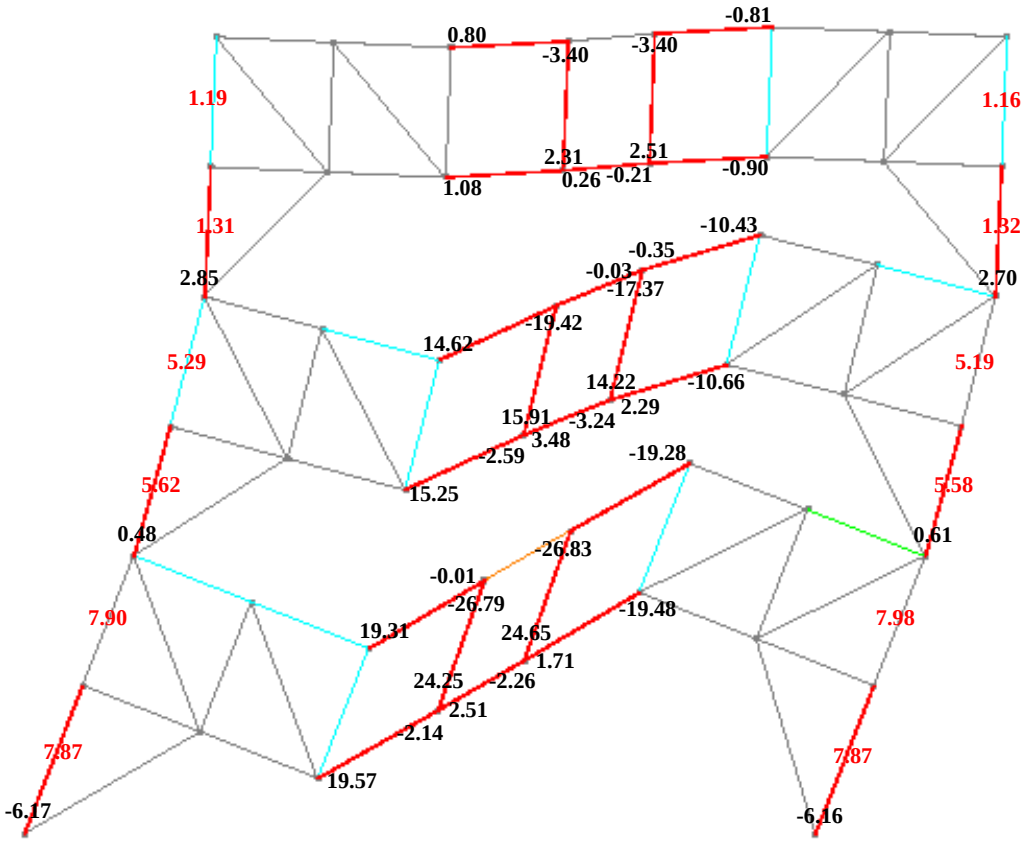

Figure 10-29 Bay 1 deflected shape at the maximum roof drift with maximum plastic hinge rotations (%) and maximum interstory drift ratios (%) of the Target Drift Model under LA36 ground motion

Note: The plastic hinge rotations are indicated in **black** whereas the interstory drift ratios are indicated in **red**.
The member colors indicate the minimum usage ratio (demand versus capacity of the member) as followed:

Color	Usage Ratio
Grey	0.0
Teal	0.4
Green	0.6
Orange	0.8
Red	1.0

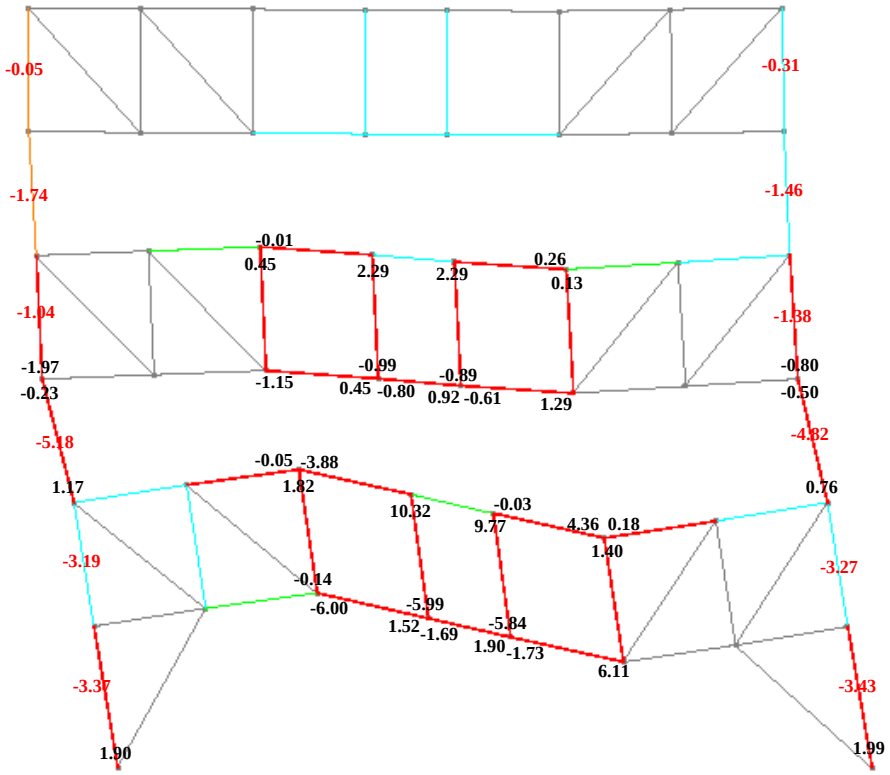

Figure 10-30 Bay 1 deflected shape at the maximum roof drift with maximum plastic hinge rotations (%) and maximum interstory drift ratios (%) of the No Kicker Model under LA36 ground motion*

Note: *The time-history analysis was terminated before the end of the LA16 ground motion duration due to excessive deformation of the yielded members of the No Kicker Model.
The plastic hinge rotations are indicated in **black** whereas the interstory drift ratios are indicated in **red**.
The member colors indicate the minimum usage ratio (demand versus capacity of the member) as followed:

Color	Usage Ratio
Grey	0.0
Teal	0.4
Green	0.6
Orange	0.8
Red	1.0

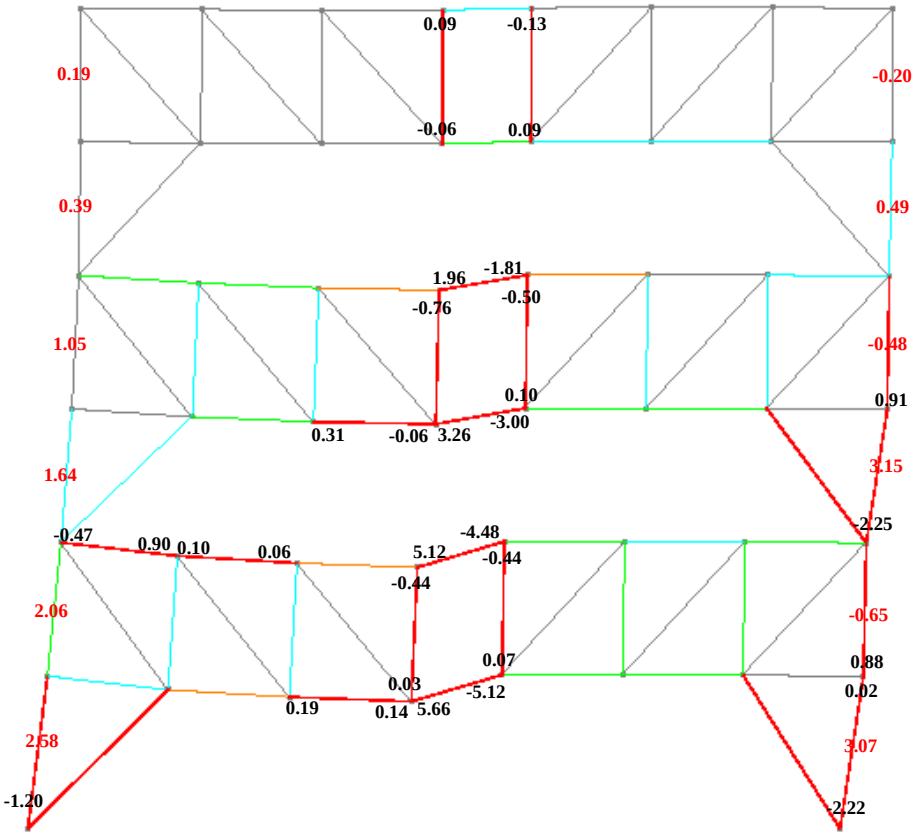

Figure 10-31 Bay 1 deflected shape at the maximum roof drift with maximum plastic hinge rotations (%) and maximum interstory drift ratios (%) of the SVP Model under LA36 ground motion

Note: The plastic hinge rotations are indicated in **black** whereas the interstory drift ratios are indicated in **red**.
The member colors indicate the minimum usage ratio (demand versus capacity of the member) as followed:

Color	Usage Ratio
Grey	0.0
Teal	0.4
Green	0.6
Orange	0.8
Red	1.0

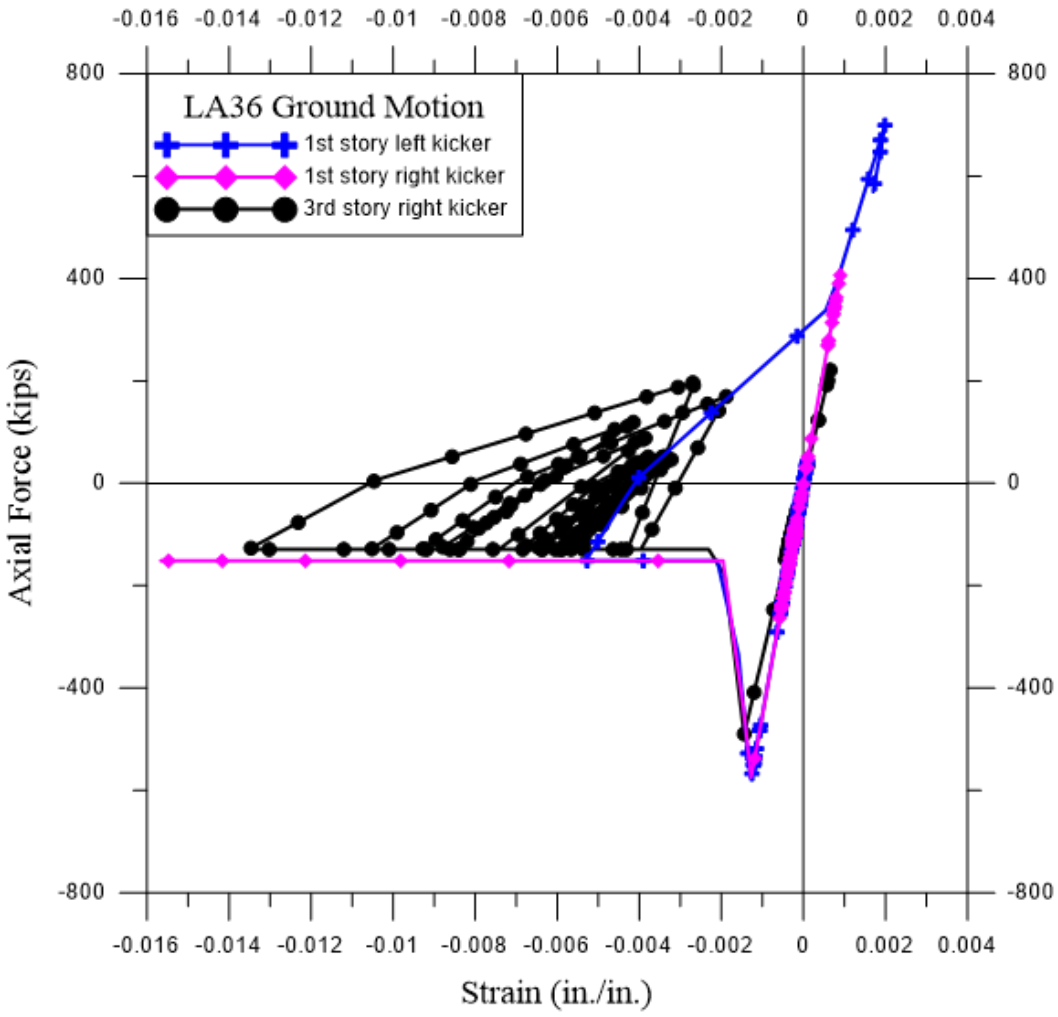

Figure 10-32 Hysteresis loops of the yielded kickers of the SVP Model in bay 1 under LA36 ground motion

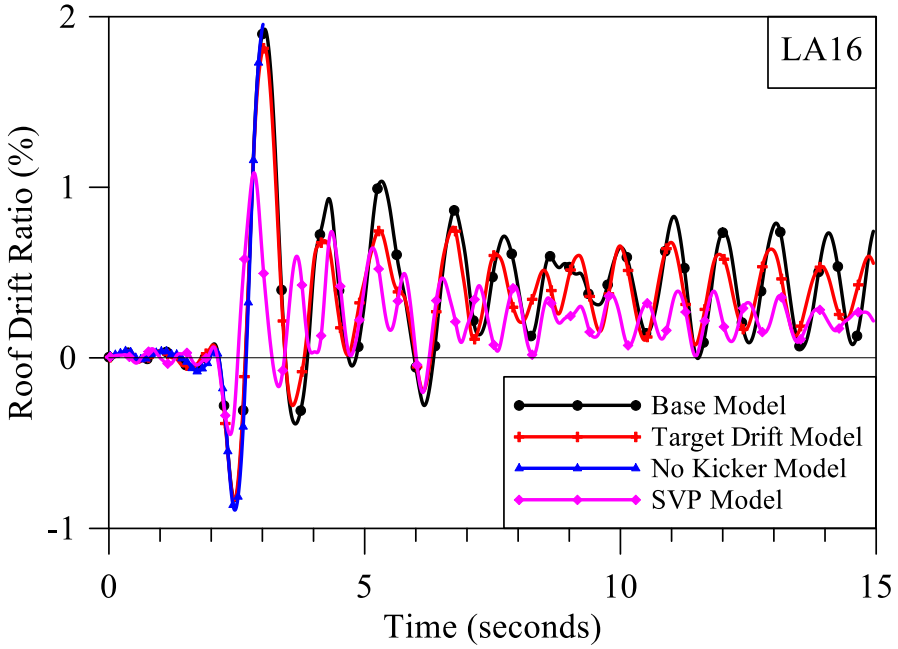

Figure 10-33 Time-history roof drift ratio (%) of the LA16 ground motion

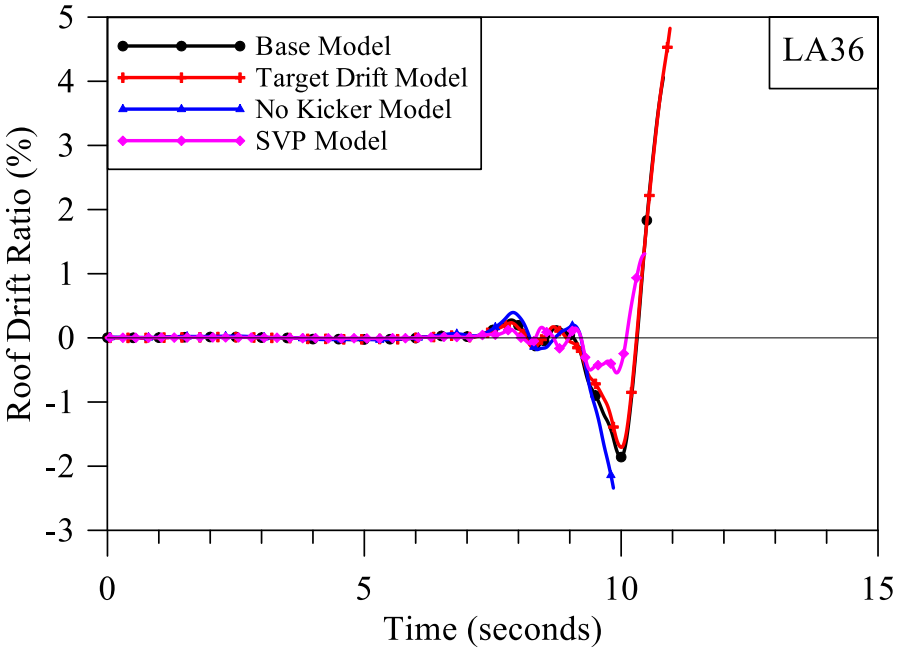

Figure 10-34 Time-history roof drift ratio (%) of the LA36 ground motion

The deflected shapes of the Base Model and the Target Drift Model in the longitudinal (moment frame) direction ,the maximum plastic hinge rotations, and the maximum interstory drift ratios along with the minimum usage ratios of the members under LA16 and LA36 ground motions are shown in Figure 10-35 and Figure 10-36 respectively. The results for the No Kicker Model and the SVP Model are omitted because the member sections in the longitudinal direction are the same as those in the Base Model.

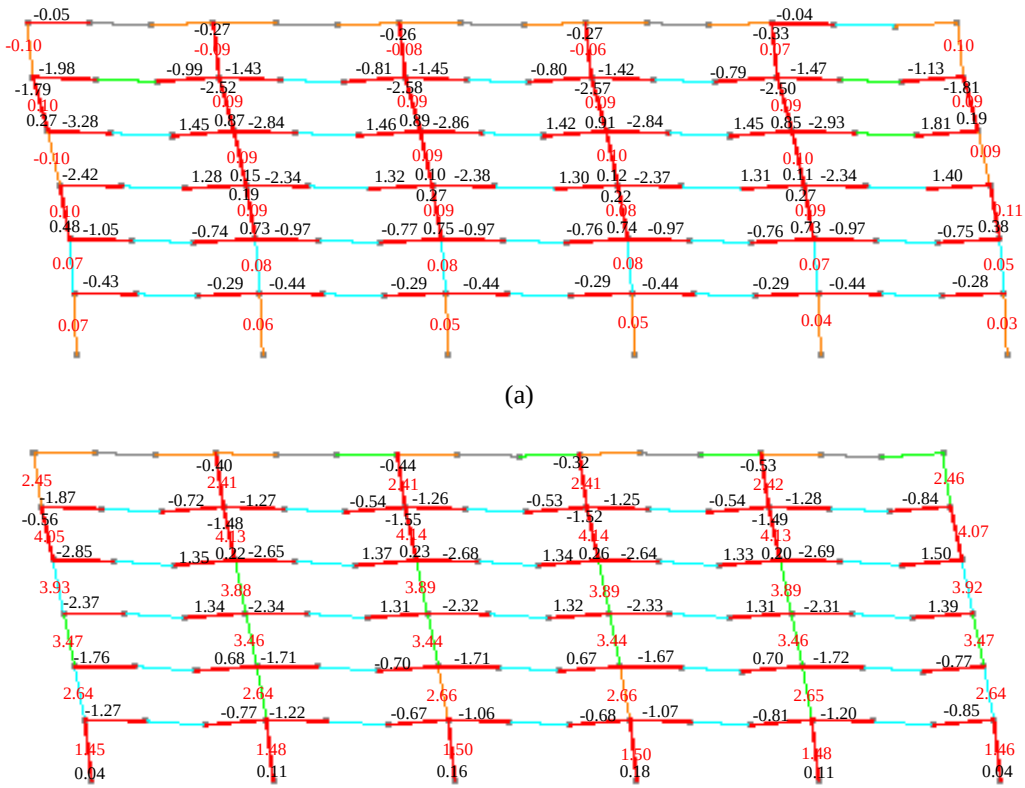

(a)

(b)

Figure 10-35 Deflected shape at the maximum roof drift with maximum plastic hinge rotations (%) and maximum interstory drift ratios (%) under LA16 ground motion: (a)Base Model; (b) Target Drift Model

Note: The plastic hinge rotations are indicated in **black** whereas the interstory drift ratios are indicated in **red**.
The member colors indicate the minimum usage ratio (demand versus capacity of the member) as followed:

Color	Usage Ratio
Grey	0.0
Teal	0.4
Green	0.6
Orange	0.8
Red	1.0

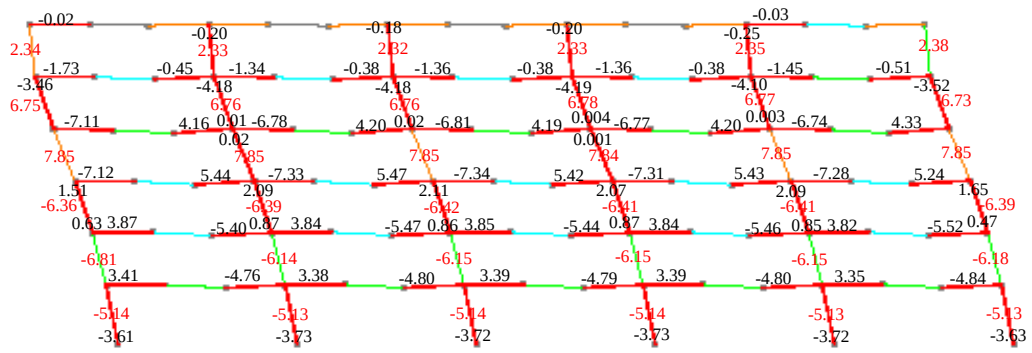

(a)

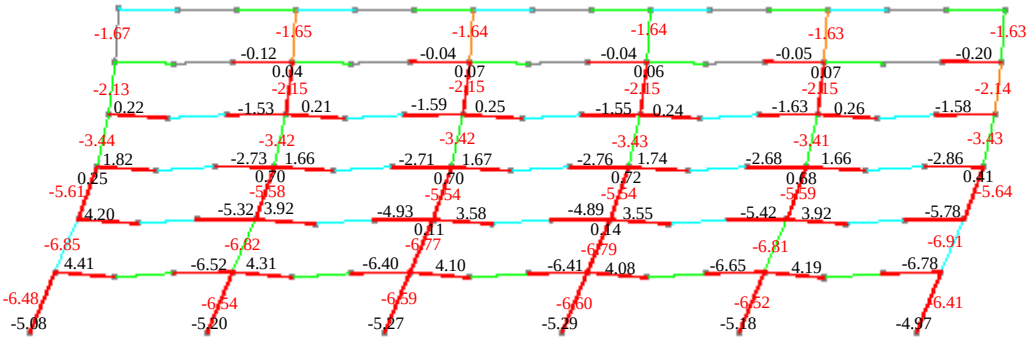

(b)

Figure 10-36 Deflected shape at the maximum roof drift with maximum plastic hinge rotations (%) and maximum interstory drift ratios (%) under LA36 ground motion*:

(a)Base Model; (b) Target Drift Model *

Note: **The time-history analysis was terminated before the end of the LA36 ground motion duration due to excessive deformation of the yielded members in both models.
The plastic hinge rotations are indicated in **black** whereas the interstory drift ratios are indicated in **red**.
The member colors indicate the minimum usage ratio (demand versus capacity of the member) as followed:

Color	Usage Ratio
Grey	0.0
Teal	0.4
Green	0.6
Orange	0.8
Red	1.0

10.4 Seismic Behavior of Structural Floor Diaphragm in STFs

A key to the lateral load resisting mechanism of STFs is the active participation of the floor diaphragms (typically consisting of precast prestressed concrete hollow core planks) to transfer the inertial forces cumulating in a staggered manner across the height of the structure as previously discussed. The increasingly large diaphragm shear force transfer between the precast hollow core slab and steel truss in the lower stories, as shown in Figure 10-37, brings concerns regarding the cyclic behavior of diaphragm-to-truss connections as well as local stress demand in the diaphragms under in-plane force and out-of-plane displacement. Due to rigidity of the connections, large bending moment would develop in the diaphragm-to-truss connections when the structure displaces. The connections can be subjected to bending along different directions.

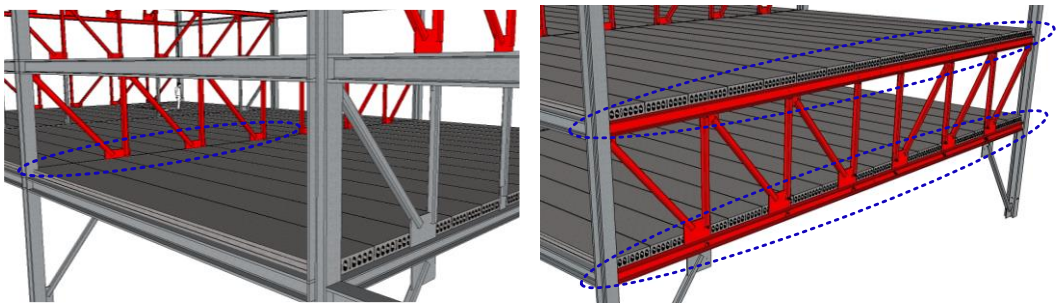

(a) (b)

Figure 10-37 Diaphragm-to-truss connection: (a) Interior; (b) Exterior connection

Nonlinear time-history analyses of the prototype STF buildings indicated that the hollow core slab diaphragms and the diaphragm-to-truss connections are primarily subject to three types of deformations under earthquake loads. The first type of deformation is the in-plane shear deformation (γ) due to relative lateral drifts between steel trusses (Figure 10-38 (a)) and the second type is the out-of-plane twist (φ) due to relative vertical displacement of the adjacent trusses (the red and green lines in Figure 10-38 (b)). Nonlinear time-history analyses of the prototype STF buildings with rigid floor

diaphragm based on design basis earthquake (DBE) [10% probability of exceedance in 50 years] level ground motions indicated that γ and φ have maximum values of approximately 0.2% and 0.5%, respectively. These values are expected to be larger for hollow core slabs because they are not completely rigid.

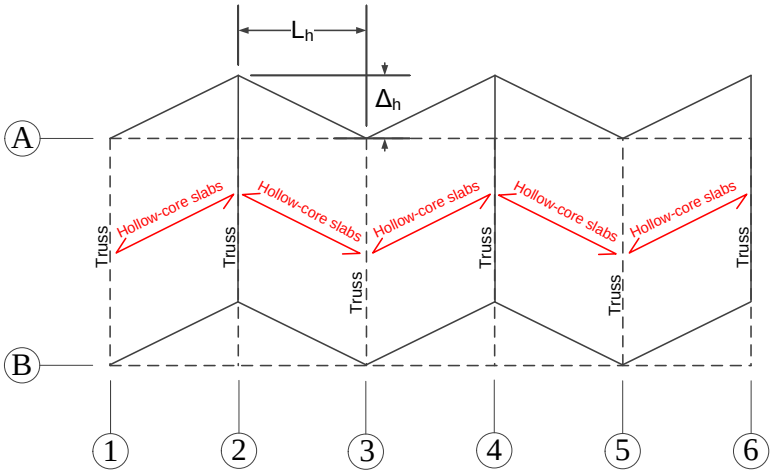

$$\text{Lateral drift ratio} = \frac{\Delta_h}{L_h}$$

(a)

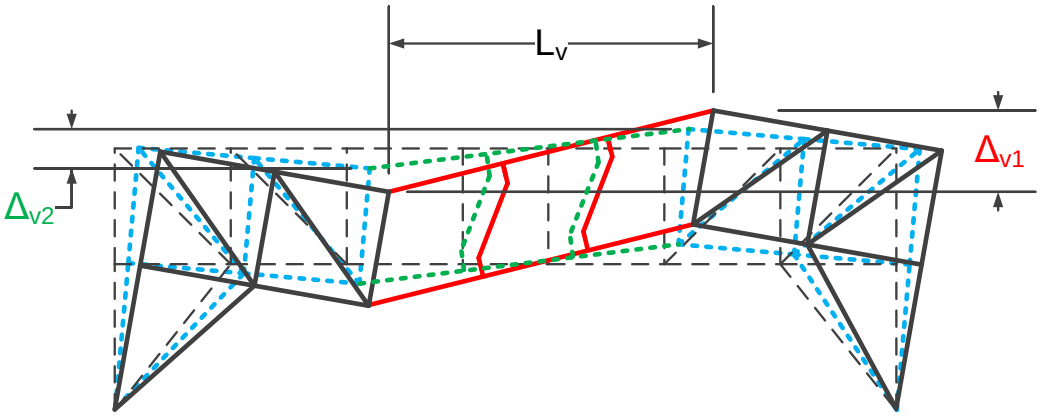

$$\text{Twist angle} \simeq \frac{\Delta_{v1} - \Delta_{v2}}{L_v}$$

(b)

Figure 10-38 Major deformations in the hollow core slab diaphragms and the diaphragm-to-truss connections: (a) In-plane shear deformation; (b) Out-of-plane twist

Figure 10-39 and Figure 10-40 show the time-history results obtained from SAC LA02 and LA16 ground motions on the fourth floor of the Base Model for the in-plane shear deformation. The out-of-plane twist of the same ground motions of the fourth floor for the Base Model are shown in Figure 10-41 and Figure 10-42.

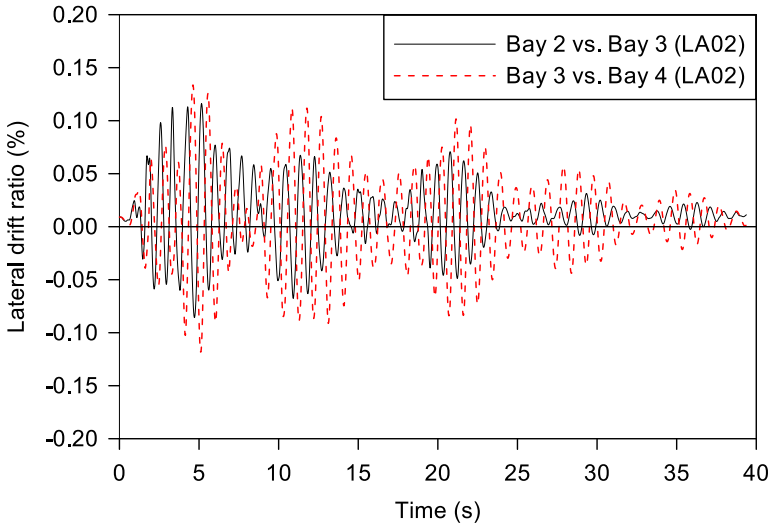

Lateral drift ratio vs. time under LA02 ground motion

Figure 10-39 In-plane shear deformation (γ) versus time history for SAC LA02 ground motion of the Base Model

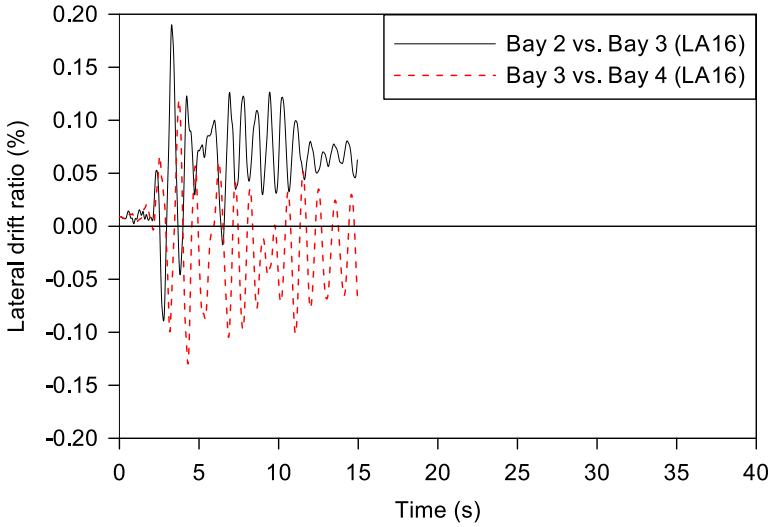

Figure 10-40 In-plane shear deformation (γ) versus time history for SAC LA16 ground motion of the Base Model

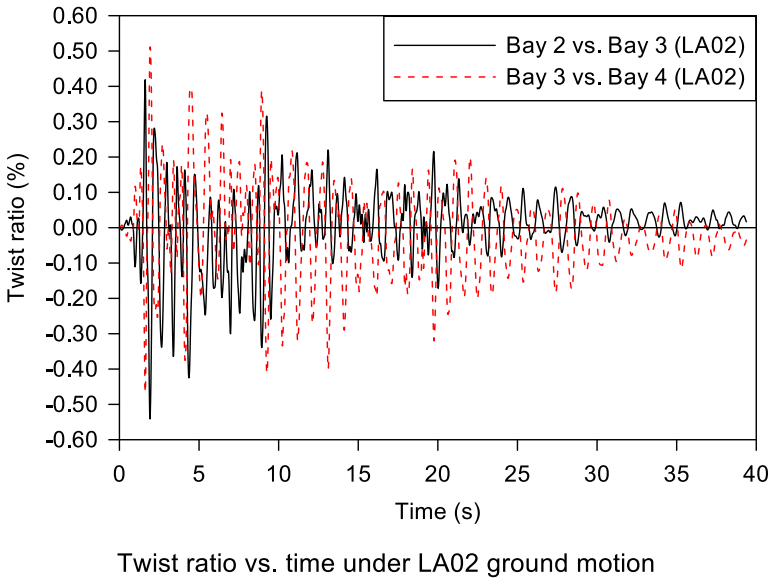

Figure 10-41 Out-of-plane twist (φ) versus time history for SAC LA02 ground motion of the Base Model

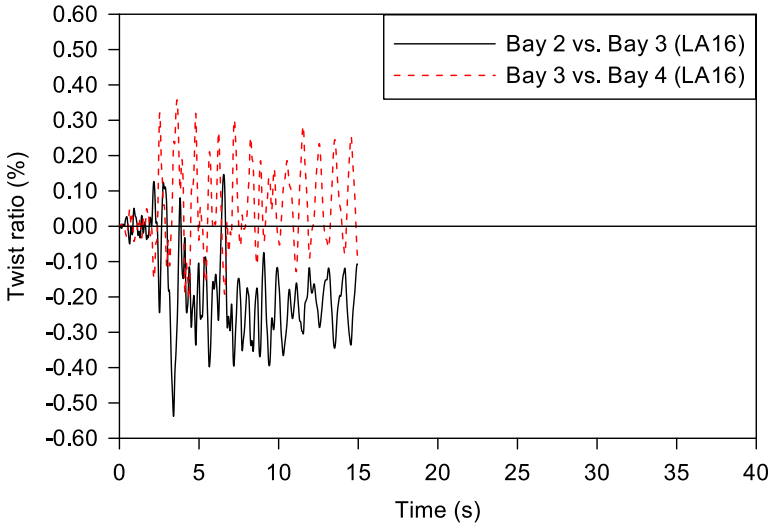

Figure 10-42 Out-of-plane twist (φ) versus time history for SAC LA16 ground motion of the Base Model

The third deformation comes from the lateral displacement along the moment (or braced) frame in the longitudinal direction of the building as shown in Figure 10-43. The bending rotation, θ, is resulting from the compatibility deformation and its magnitude is close to the story drift ratio of the moment frame (or braced frame) in the longitudinal direction. In general this rotation ratio can be close to 1 to 2% under DBE ground motions.

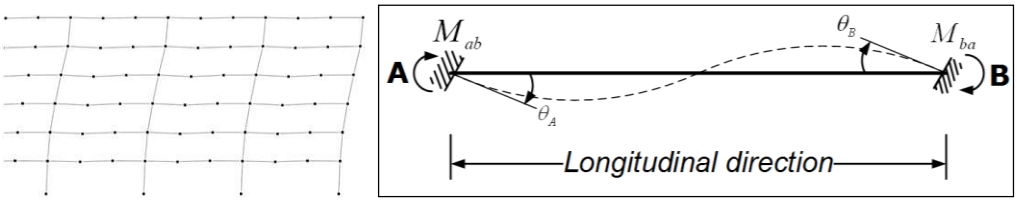

Figure 10-43 Bending rotation, θ, of the hollow core diaphragm and its connections due to the lateral displacement along the moment frame in longitudinal direction

Chapter 11

Part II: Summary and Conclusions

A modified STF system in which the diagonal braces are added in the non-truss frames to alleviate the demand on columns along with horizontal trusses serving as in-plane shear diaphragm is proposed to improve the seismic response of the STF system. The preferred yield mechanism of the STF system is where plastic hinges form only within Vierendeel panels located at the center of the truss similar to that in the “special segments” of the Special Truss Moment Frames (STMFs). In order to increase the overall drift capacity of the structure, the Vierendeel panels are expanded over three panels. This reduces the rotational demand at the ends of the chord members in the truss and allows the structure to reach larger drifts.

Following conclusions are drawn from the analysis results:

1. STFs with the modified configurations showed stable responses under severe ground motions. Nonlinear time-history analyses indicated that the modified STF could be used in seismically active areas.
2. The addition of “kickers” and multi-panel Vierendeel panels can effectively reduce the demands in the non-truss stories. Using a single Vierendeel panel would lead to extreme high rotational demands in the chord members even at small roof drift ratios. The early yielding of the chord members in the single Vierendeel panel in turn leads to force redistribution and failure of the non-truss level due to the failure in the kickers and columns.
3. The addition of kickers alters the seismic load transfer path from a staggered pattern via diaphragms to a more direct path from upper truss

to the non-truss at lower level. This in turn relieves the high force demands in the diaphragms and the diaphragm-to-truss connections.

4. Analysis results show that the horizontal trusses can effectively transfer the seismic force. The demands in members of the horizontal trusses are generally small. Further modification of the horizontal truss is possible to simplify the configuration and fabrication.
5. Nonlinear analyses also showed that the horizontal trusses can effectively transfer the seismic forces along the longitudinal direction, as evidenced by the yielding of the members in the moment frames.
6. Surprisingly, the Base Model in which the non-yielding members were not designed based on capacity design approach had very similar performance and suffered limited damage in the non-yielding members as compared to the Target Drift Model in which all the non-yielding members were designed based on the maximum capacity of the Vierendeel panel. The kickers in the Base Model are subjected to yielding deformation only under a few MCE ground motions even though they were also not designed with the capacity design approach. Redesigning the STF by using a target roof drift ratio of 0.5% might be an economical alternative.
7. The story drift at first yield of the modified STF is similar to that of a typical concentrically braced frame. Design using a period equation for the CBFs and an R factor value of 7 or 8 is warranted.

11.1 Recommendations for Future Study

The three types of deformations (γ, φ, and θ) could occur simultaneously which makes the behavior of the hollow core slab diaphragms and the diaphragm-to-truss connections complicated. Openings in the diaphragm can also make the force transfer paths more complicated. Further experimental testing program is needed in order to understand the interaction of the three major deformations in the hollow core slab diaphragms and the diaphragm-to-truss connection.

Also, STF system is currently identified as an “undefined structural system” and not allowed to be used in seismic prone areas per the 2001 California Building Code section 1629.9.2 and subsequent editions (CBSC, 2001).

In addition to the issues discussed above, the Seismology Committee of SEAOC (SEAOC, 2006) lists the following design and performance issues that need to be addressed by adequate testing and analysis:

- Identification of predictable inelastic mechanisms;
- Design forces and deformations in yielding Vierendeel panels and adjacent truss members;
- Design forces related to diaphragm-truss interaction, considering expected strength, stiffness, and ductility;
- Force distribution and inelasticity in precast diaphragms and topping slabs under high in-plane forces;
- Force distribution and inelasticity in diaphragms under vertical displacements related to truss deflections and link deformation;
- Design of diaphragm-to-truss connections, considering cyclic loading and diaphragm or truss overstrength;
- Column design forces and ductility demands, considering dynamic truss-column interaction and sharing of columns by lateral and transverse systems;
- Vulnerability of the gravity system to failure of seismic-force-resisting members;
- Effects of openings and discontinuities in highly loaded diaphragms;
- Disproportionate effects of atypical and irregular building configuration;
- Axial and flexural interaction in truss chords, diagonals, and connectors.

SEAOC (2006) also notes: “Because the system’s load path involves an out-of-plane offset at every floor level, testing must consider the interaction of yielding (and possibly degrading) diaphragms, trusses, and connections, as opposed to just the behavior of individual components. Even the testing of an entire truss frame would not capture the essential aspect of shear transfer between adjacent frames.”

In order to confidently use STF in seismic areas, both experimental cyclic test data and analytical studies are required to quantify its seismic performance factors (R, C_d, and Ω_0). Extensive analytical studies need to be carried out through reliable procedure to determine those seismic design parameters. FEMA P695 (FEMA, 2009) collapse assessment methodology is suggested for analytical investigations because it is the official methodology for gaining approval of a new structure system in the ASCE 7 building code.

Appendix A

Subassemblage Specimen STMF-2C8-1 Photos

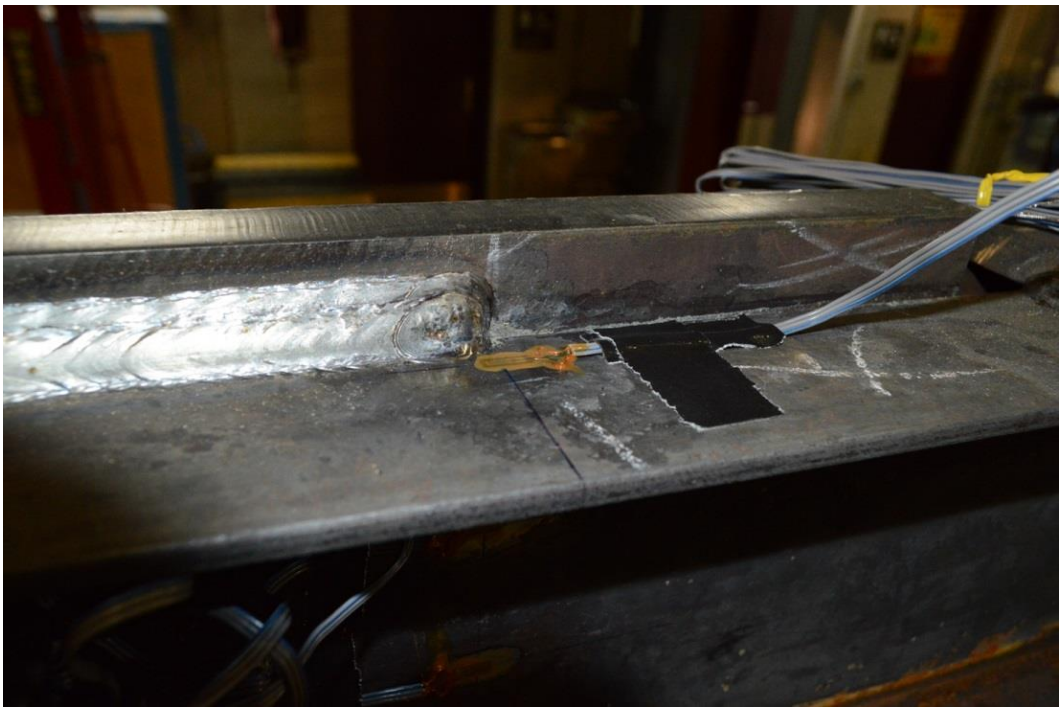

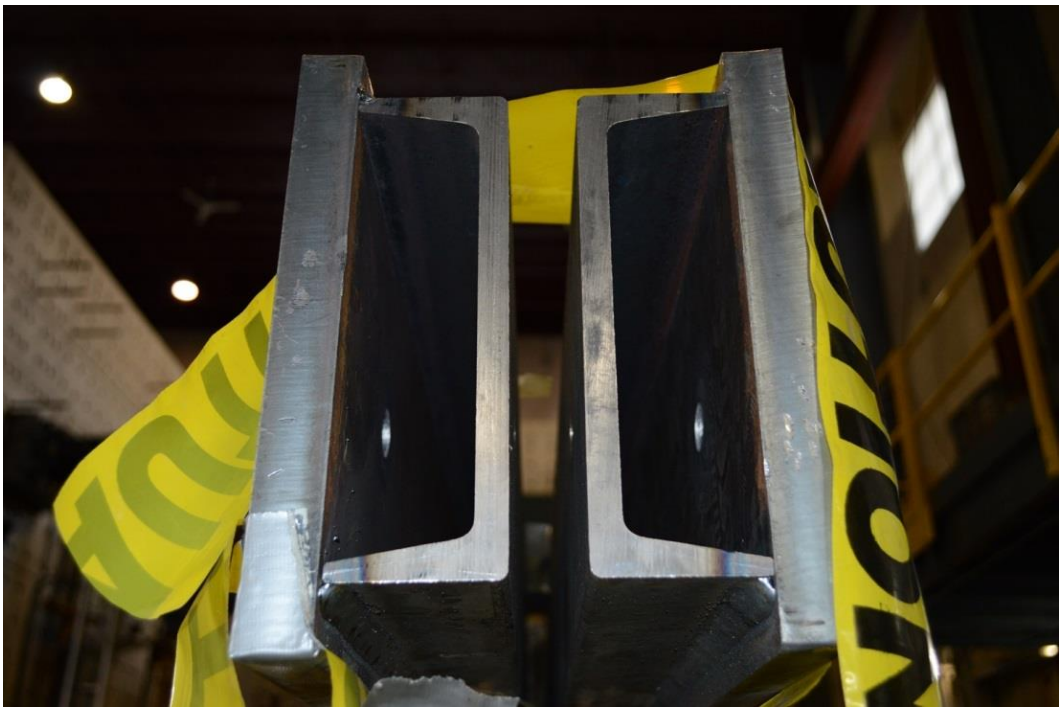

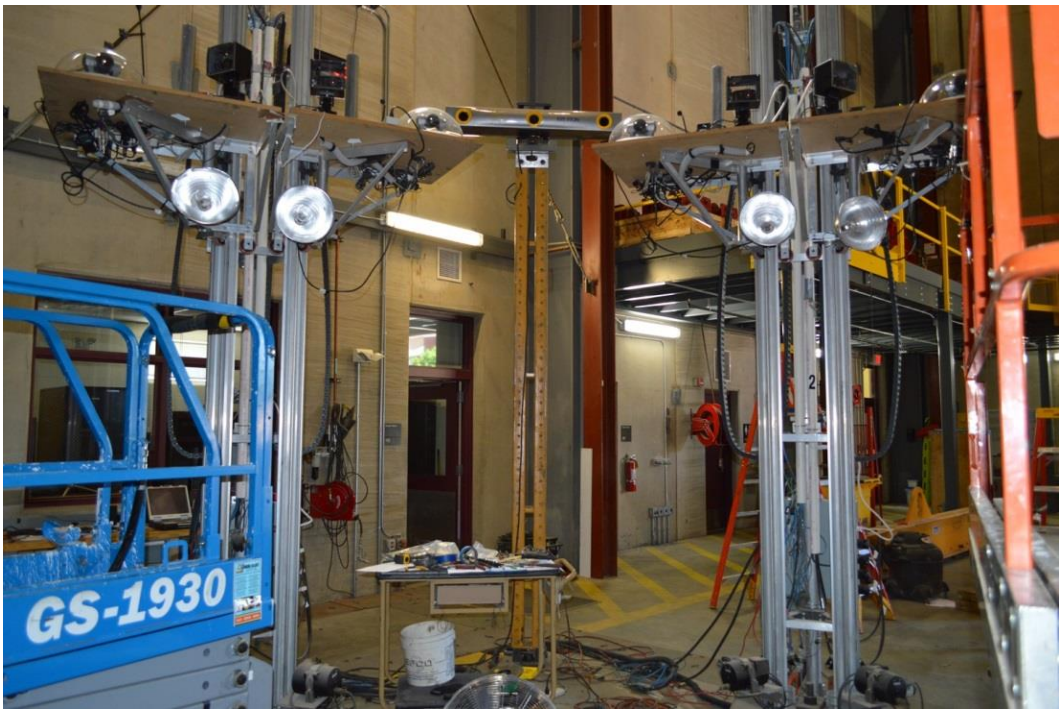
GS-1930

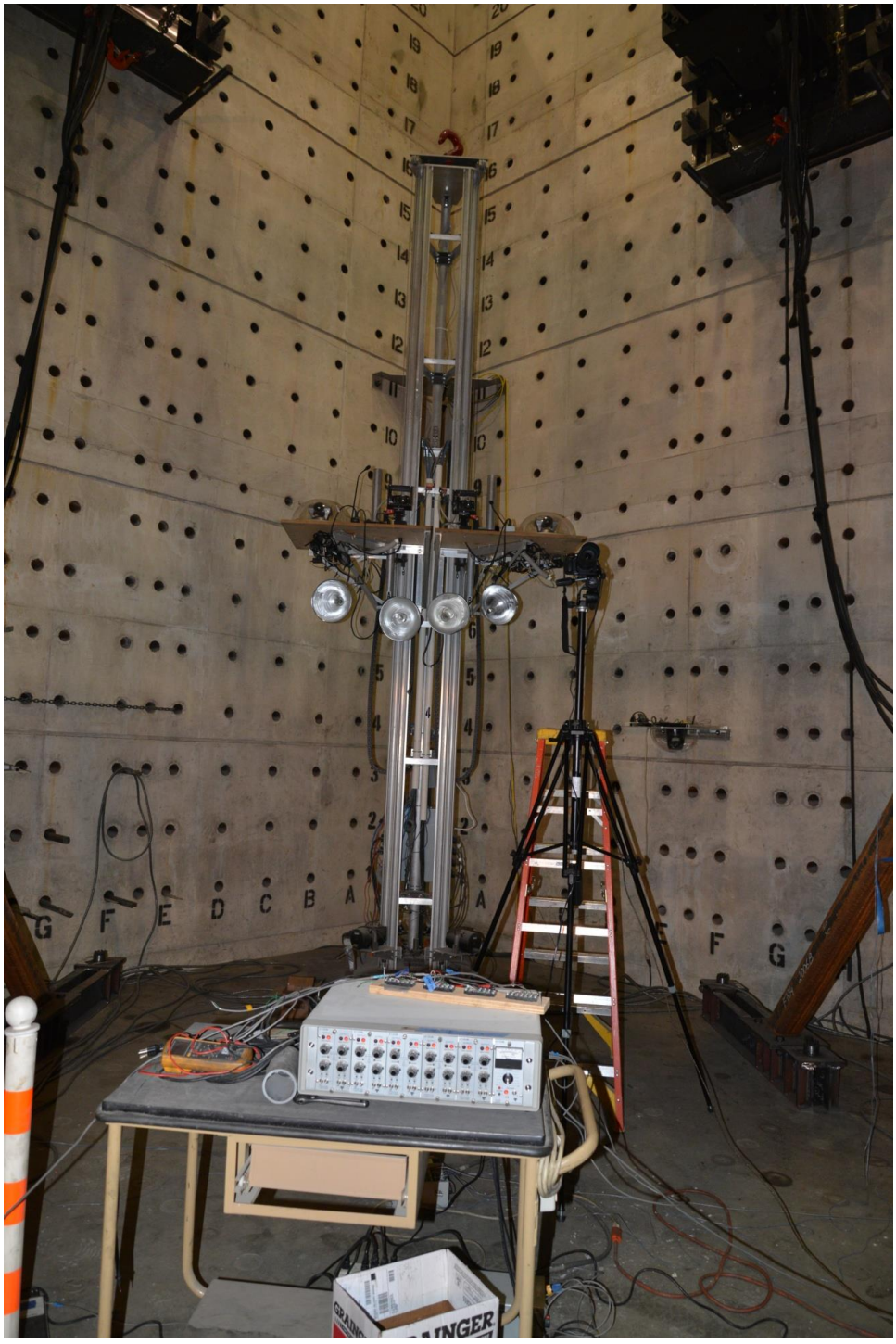
G F E D C B A
A B C D E F G
GRAINGER

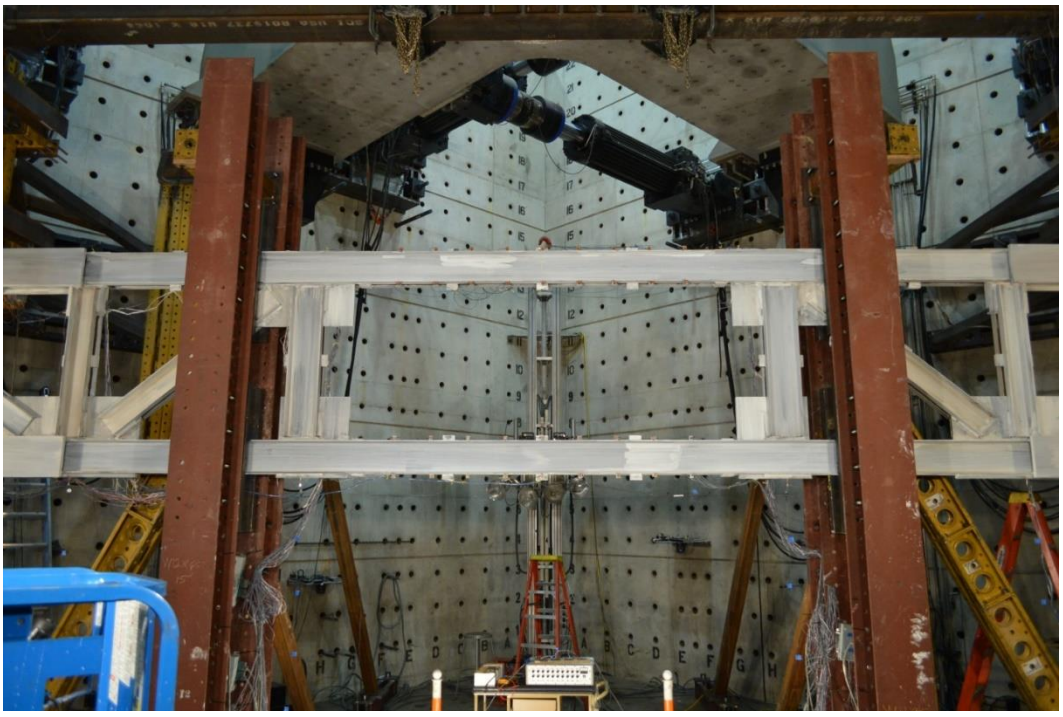

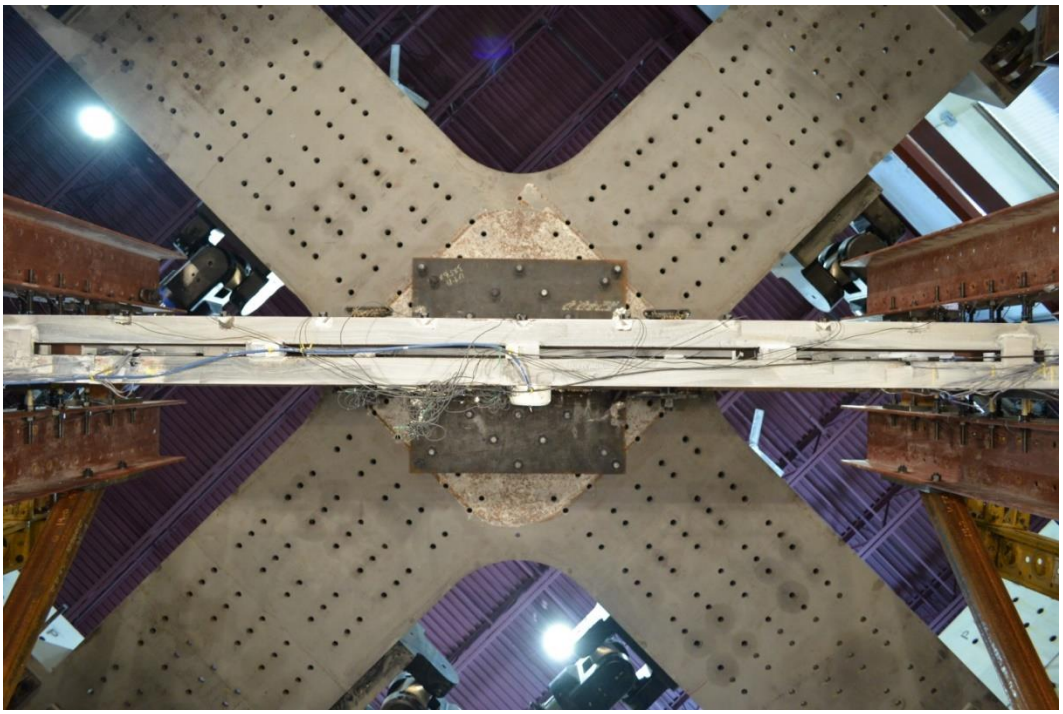

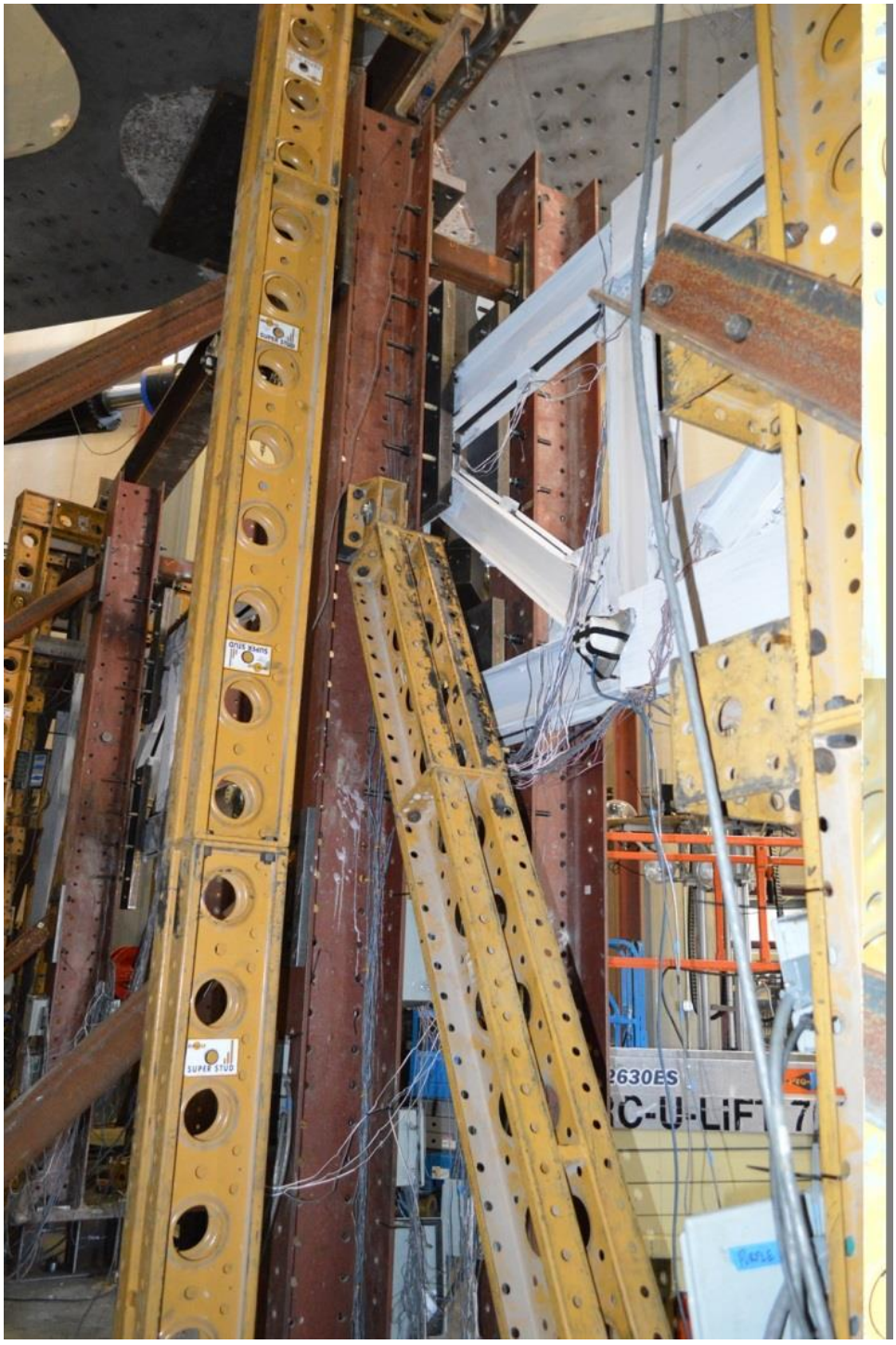
SUPER STUD
2630ES

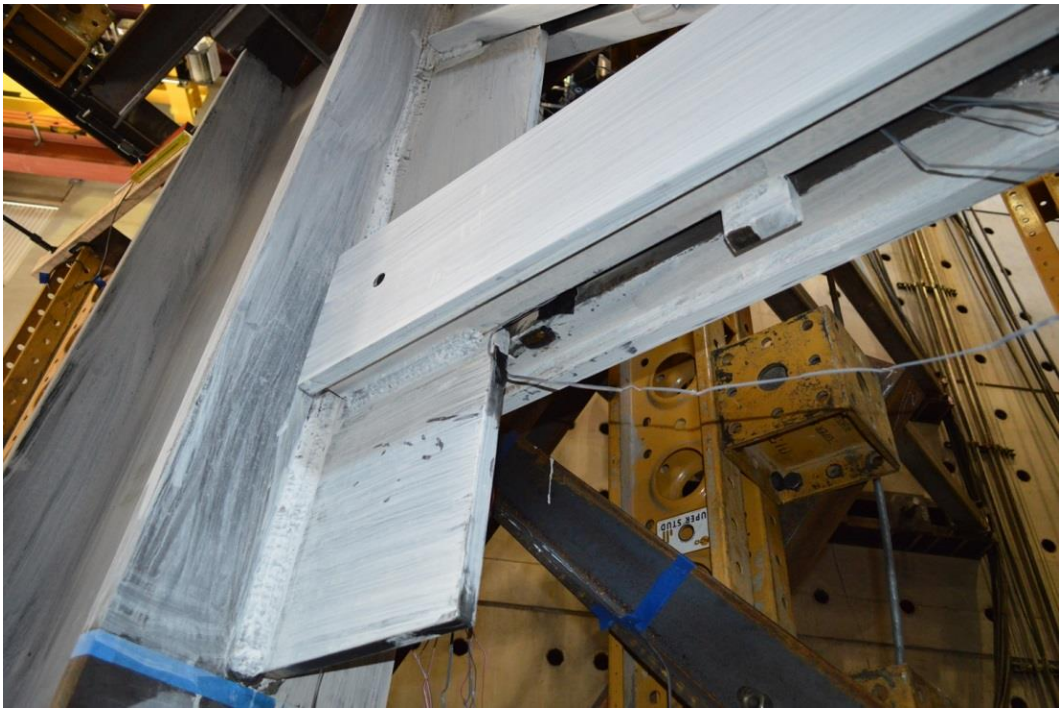

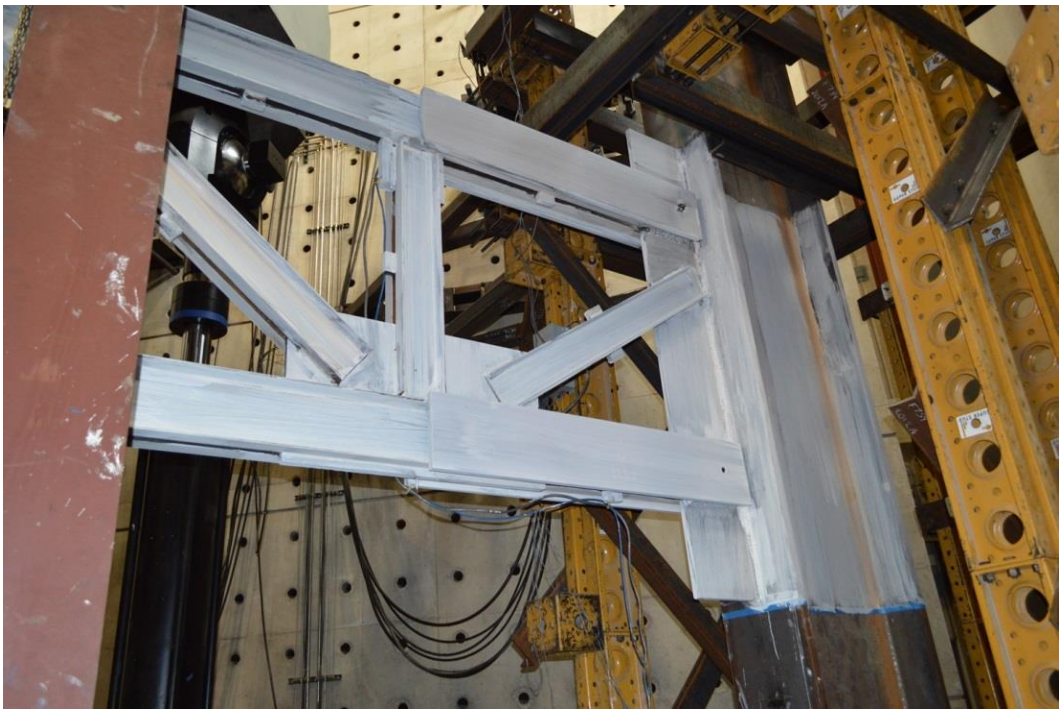

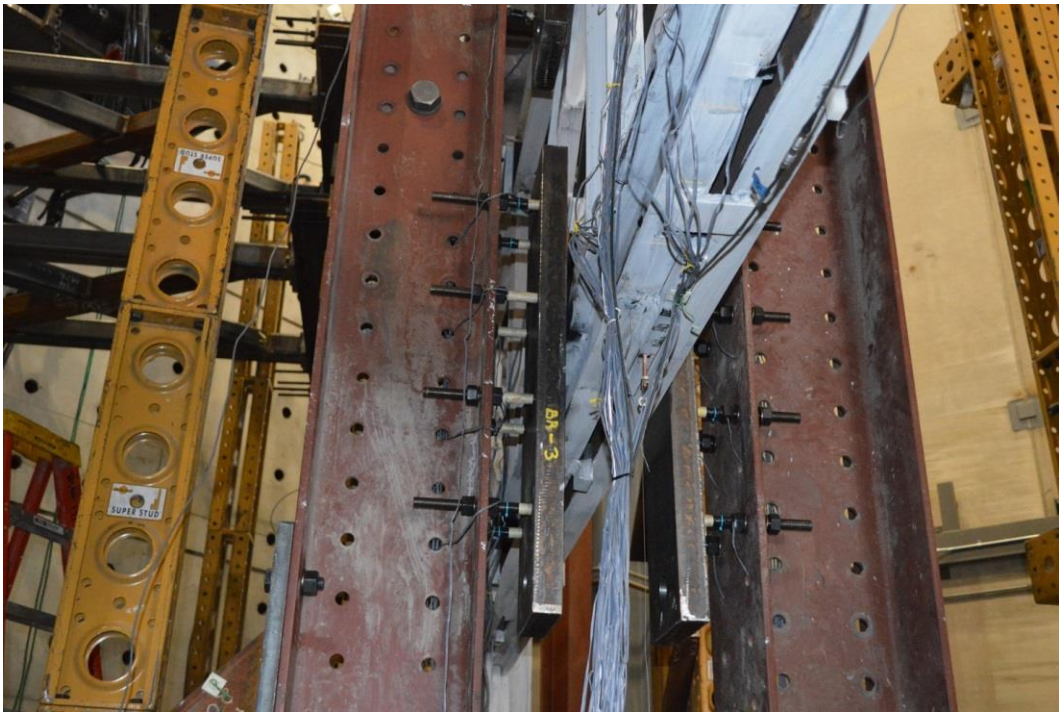
SUPER STUD
BR-3

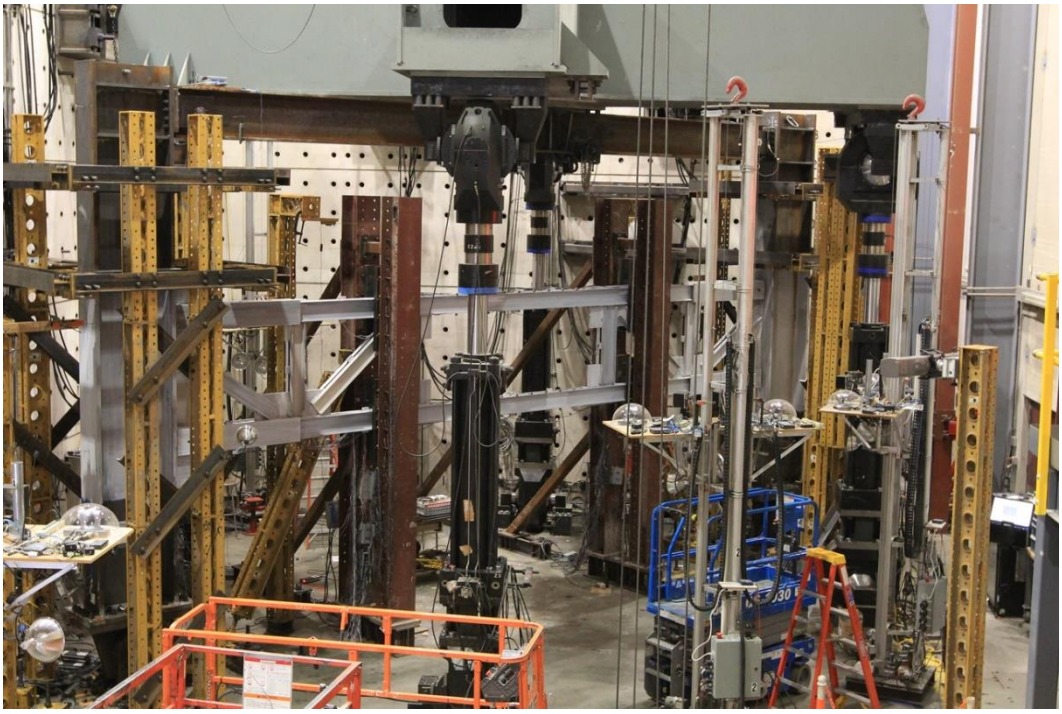

Appendix B

Subassemblage Specimen STMF-2C8-2 Photos


763-479-2501

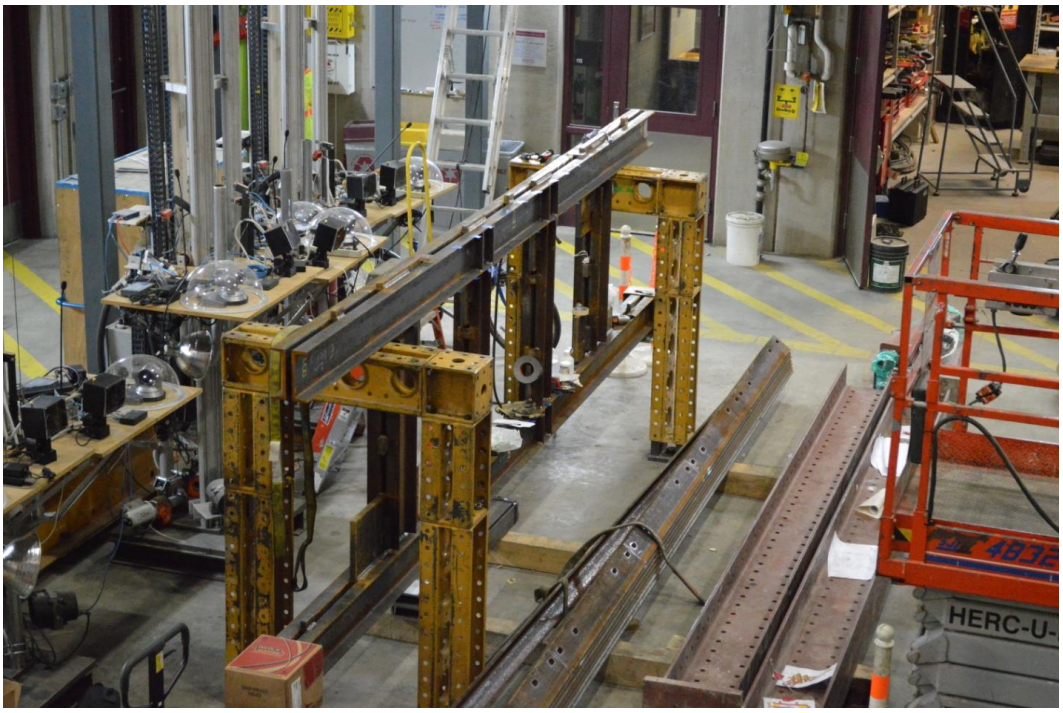
HERC-U-


HUSKY

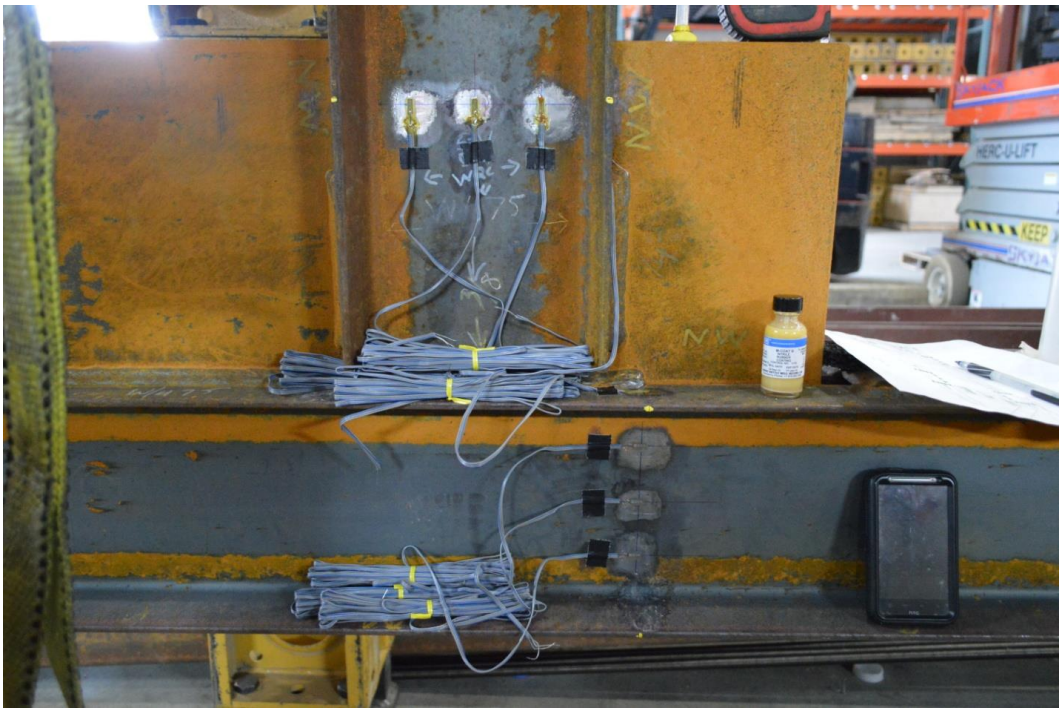
HERC-U-LIFT
KEEP

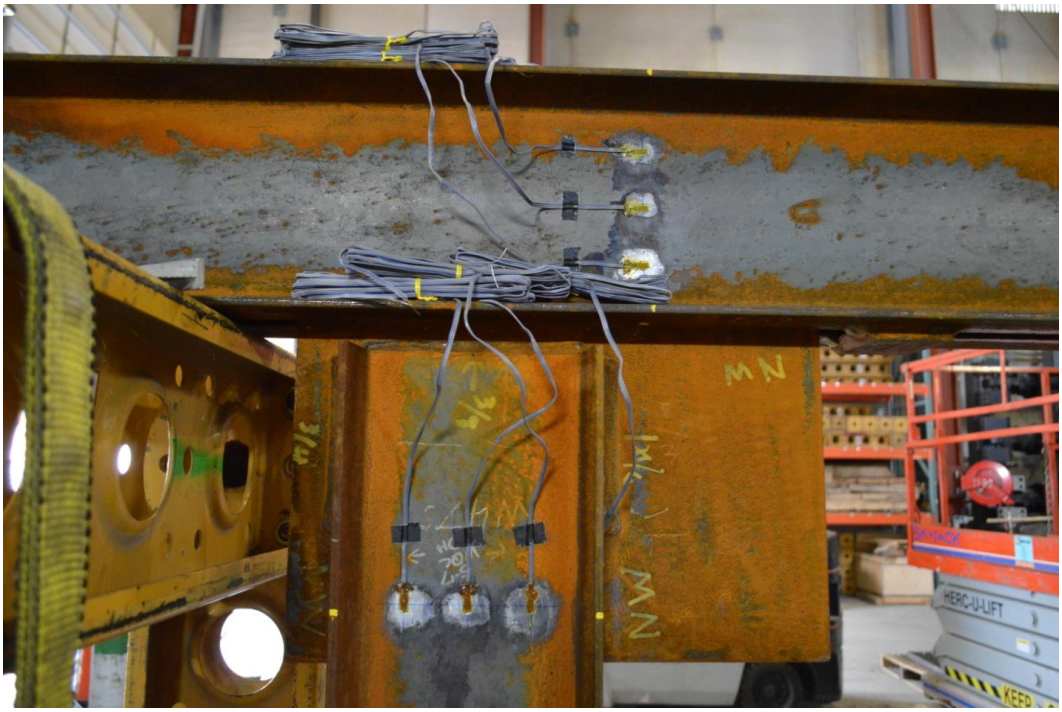
HERC-U-LIFT


SUPER STUD


NW


F734


DCCI
COMMITTED TO SAFETY
WERNER

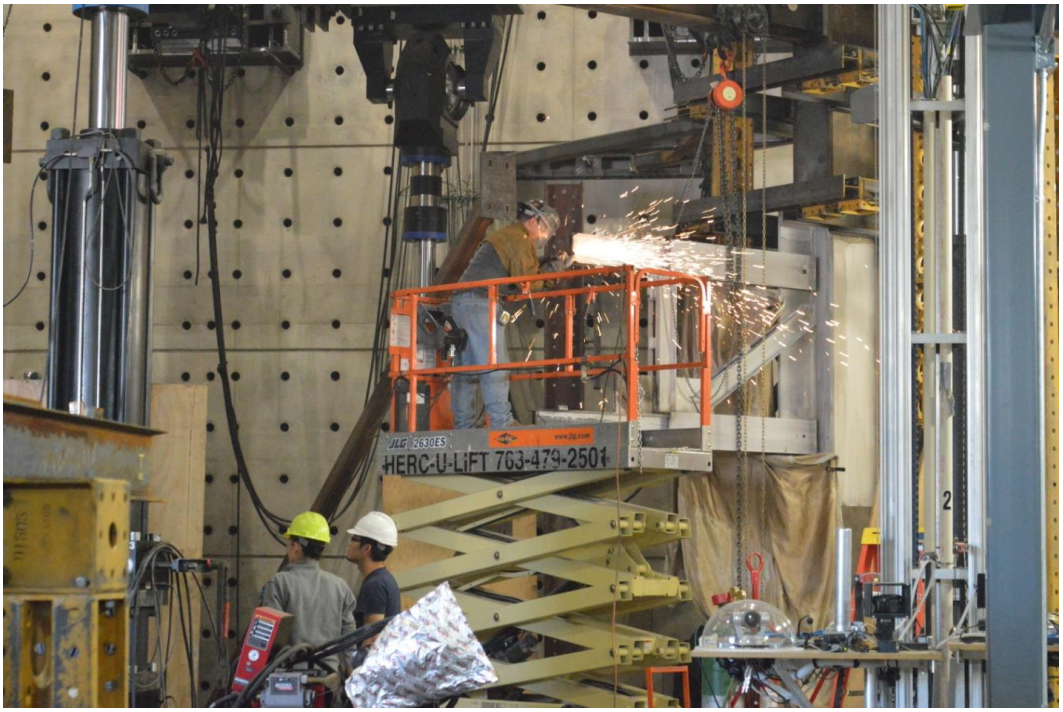
JLG 2630ES
HERC-U-LIFT 763-479-2501

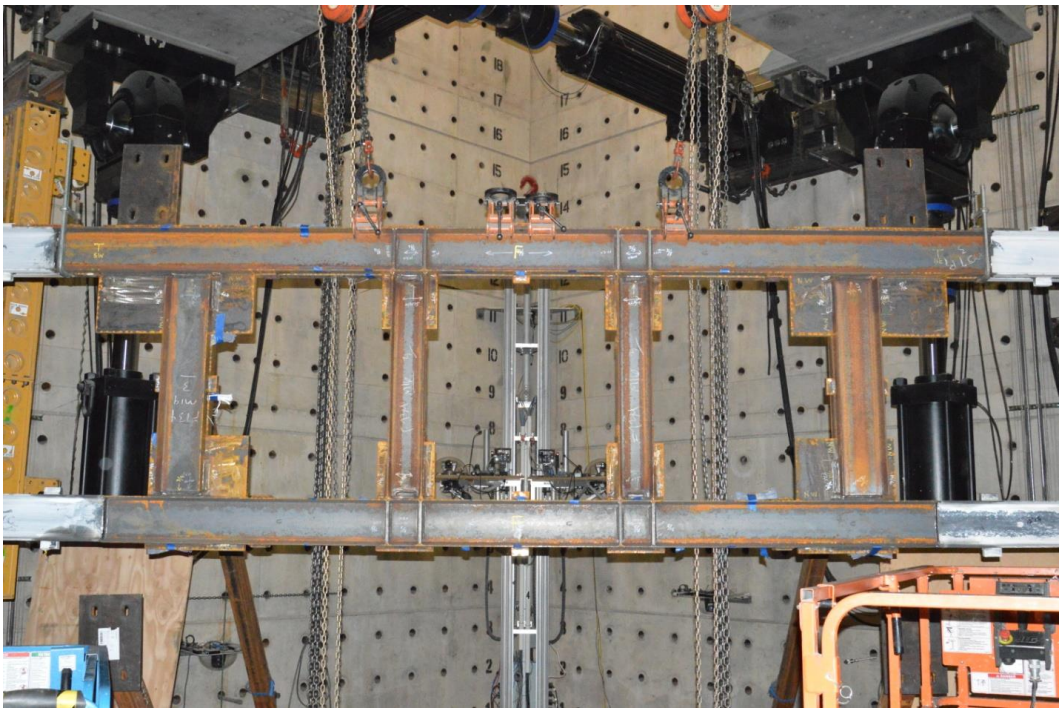


NE
NW

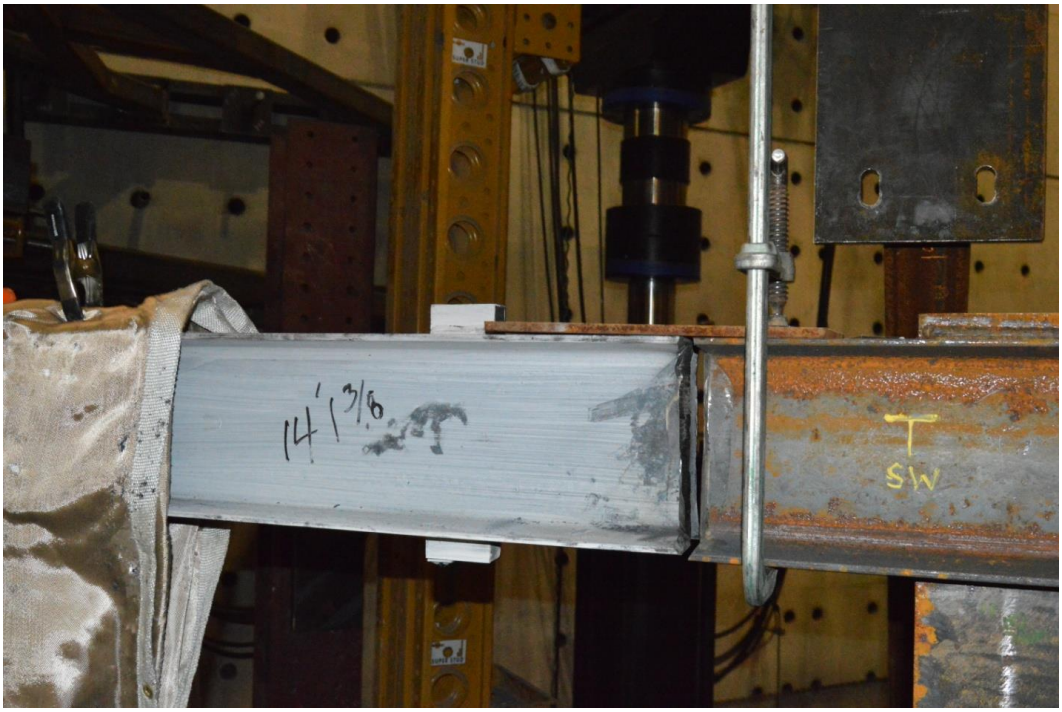
14' 1 3/8"
T
SW

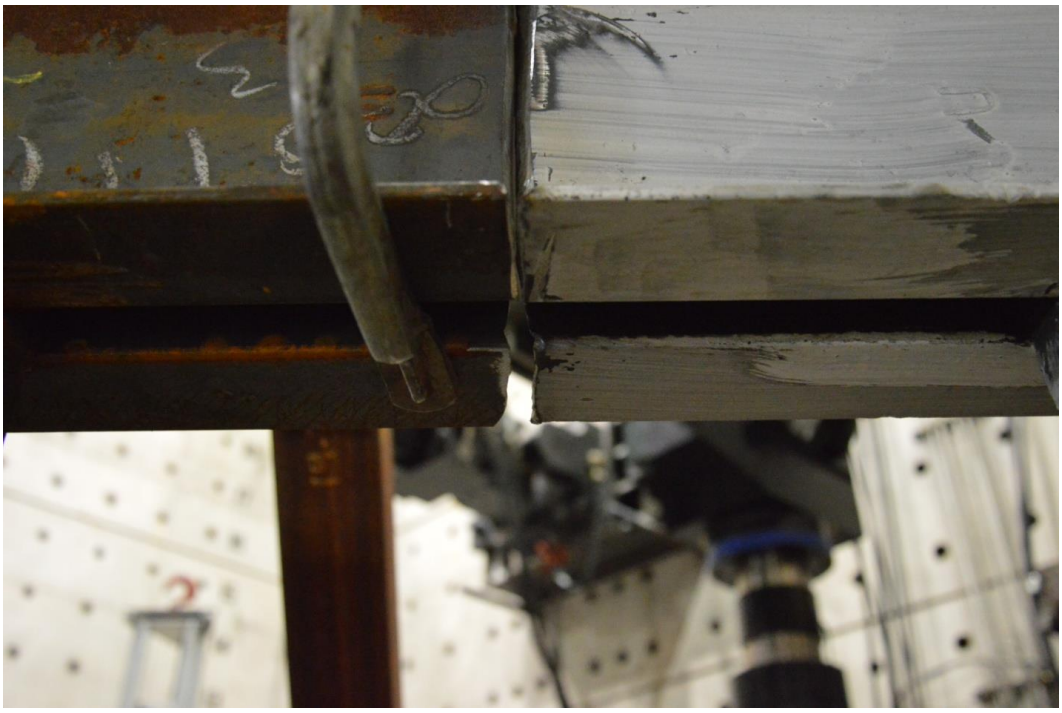

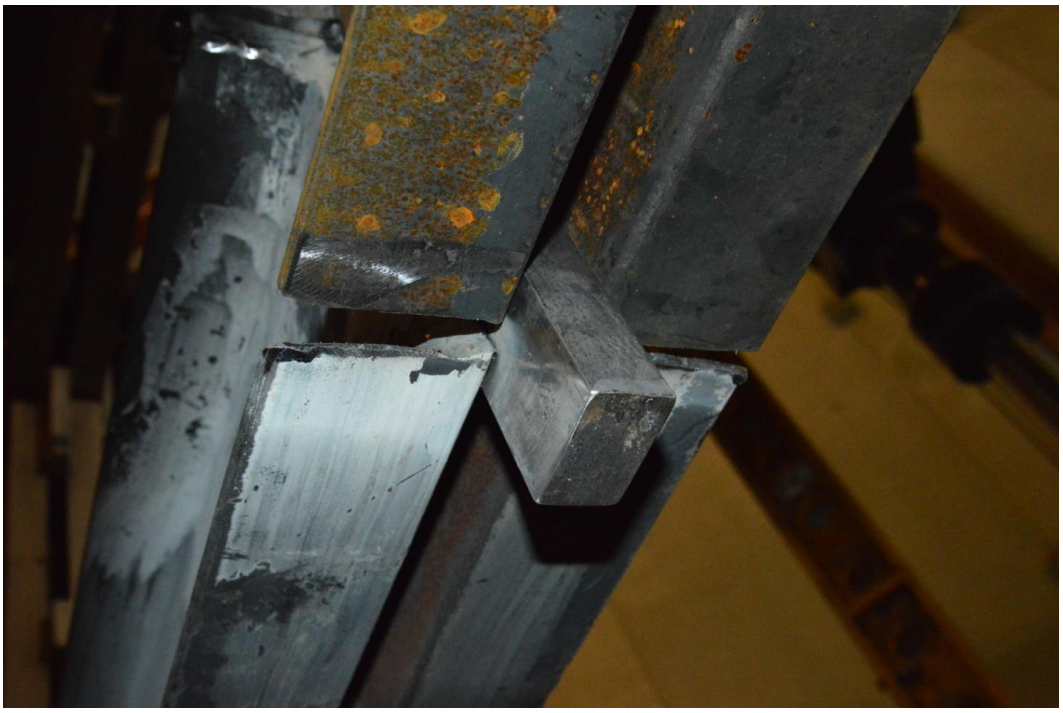


1
2
3
49
50
5

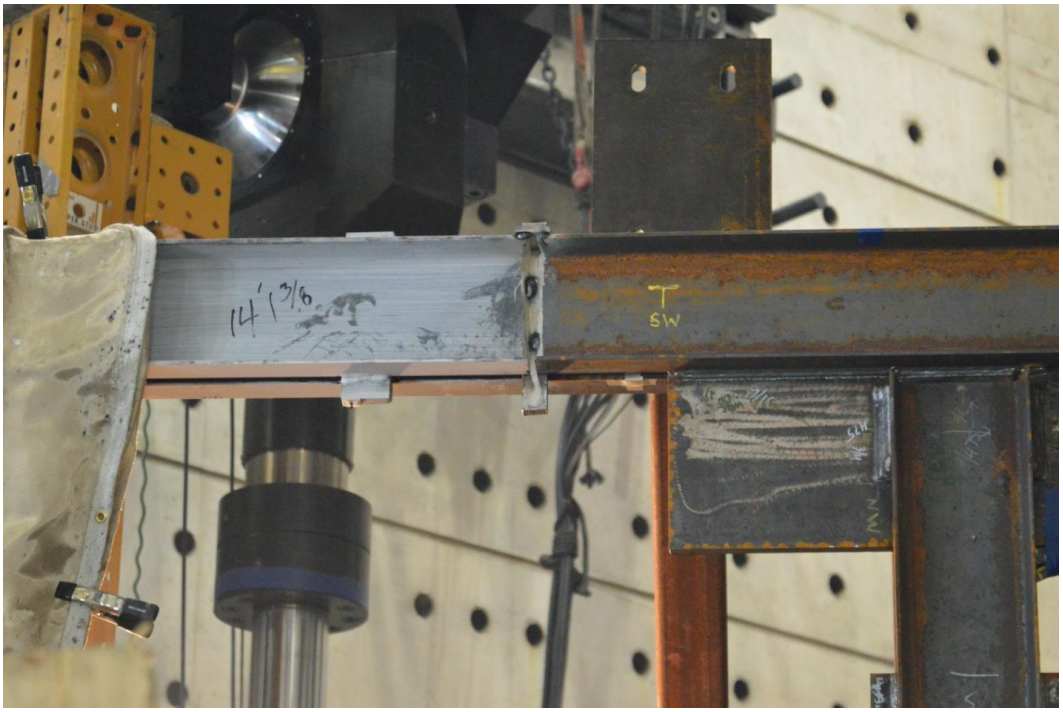
14' 1 3/8
SW

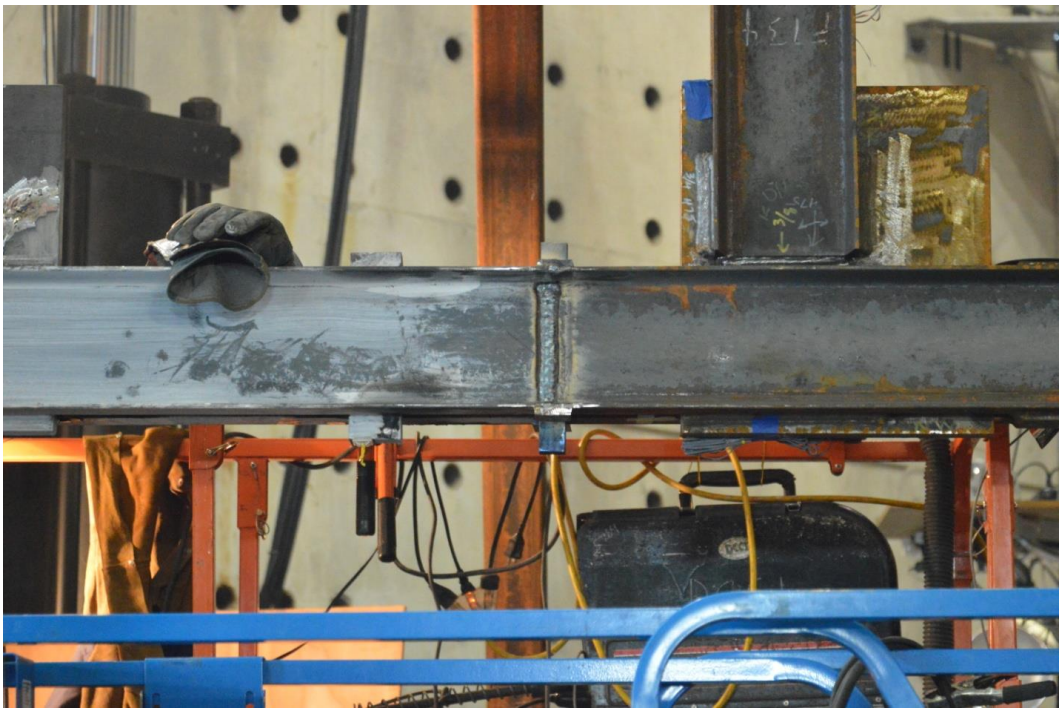

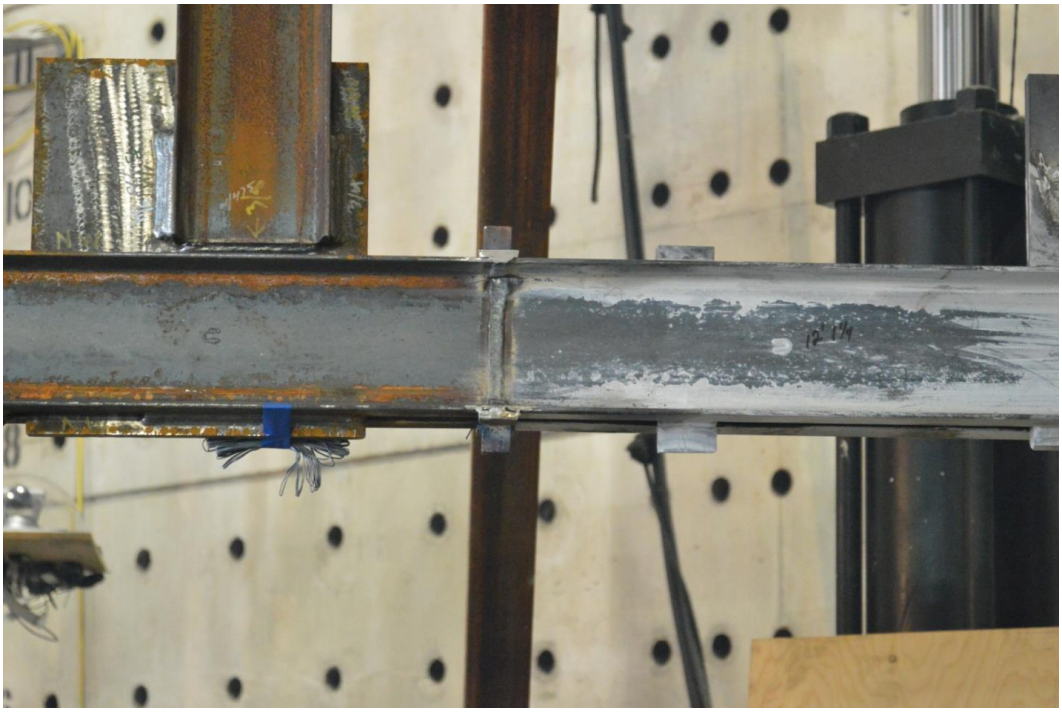

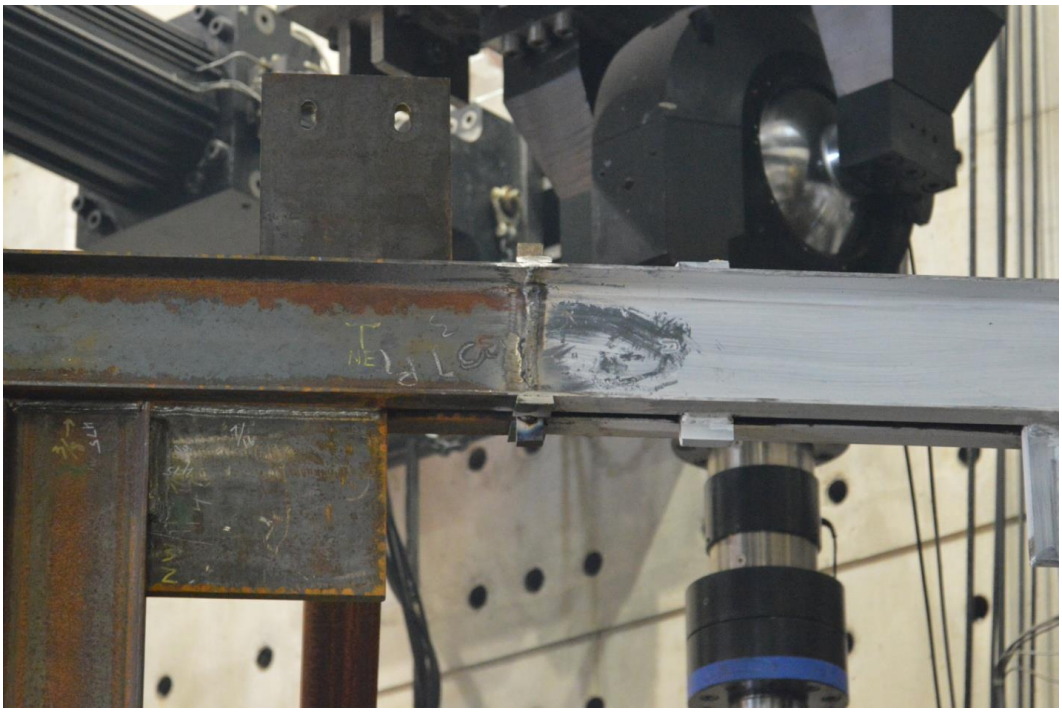


C-U-LIFT 763-479-2501

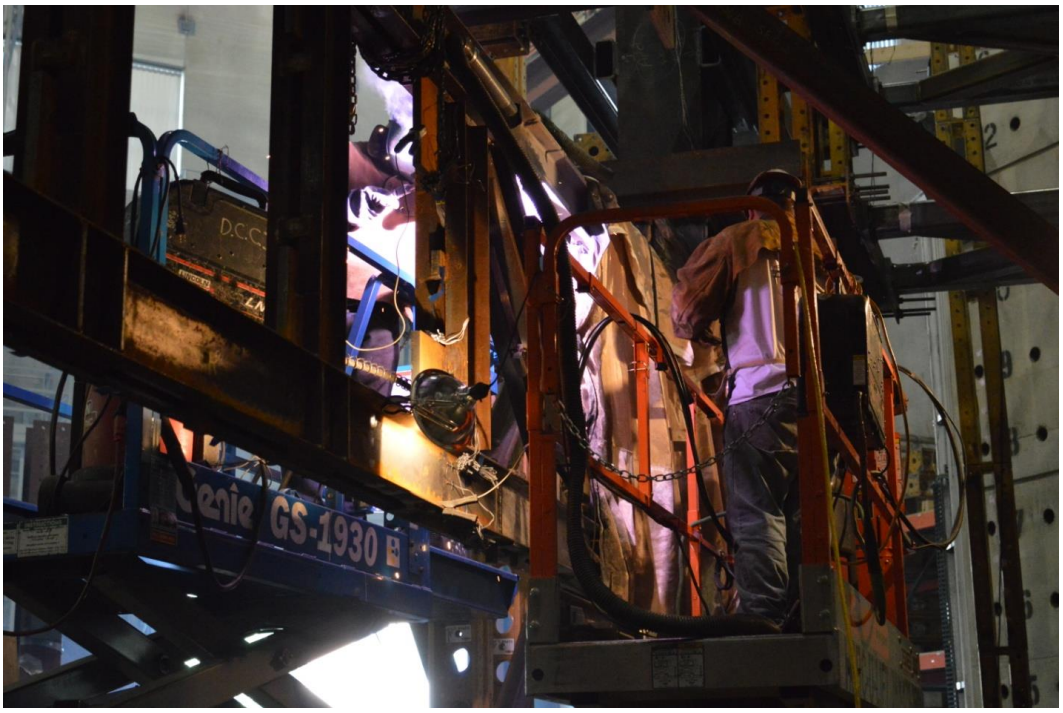
Genie GS-1930

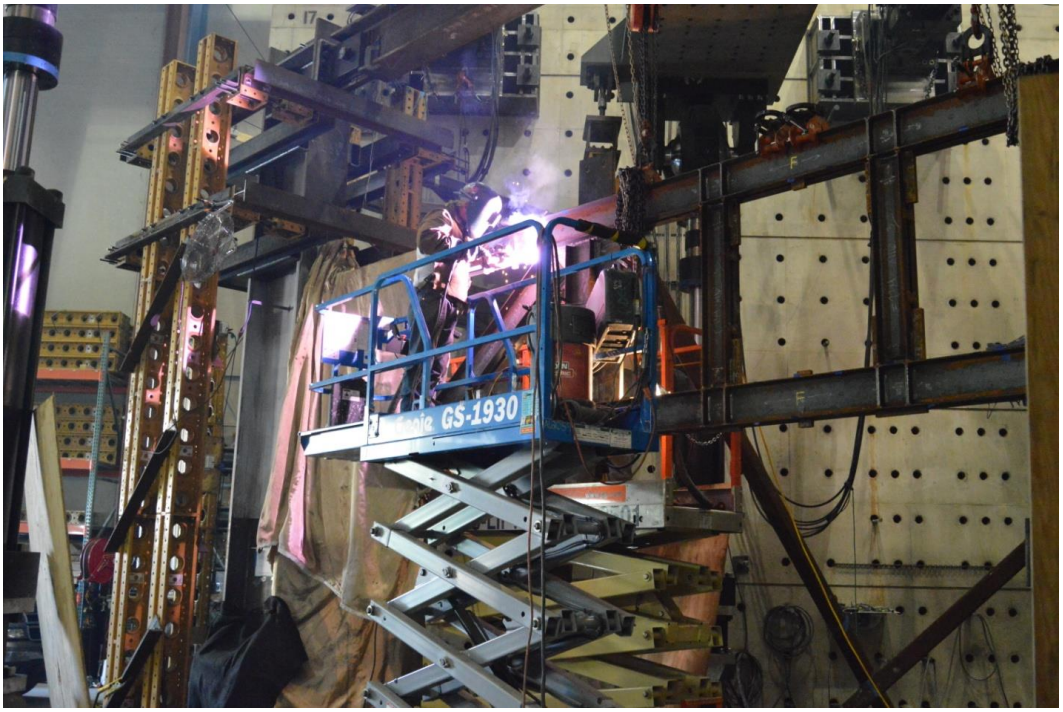
GS-1930

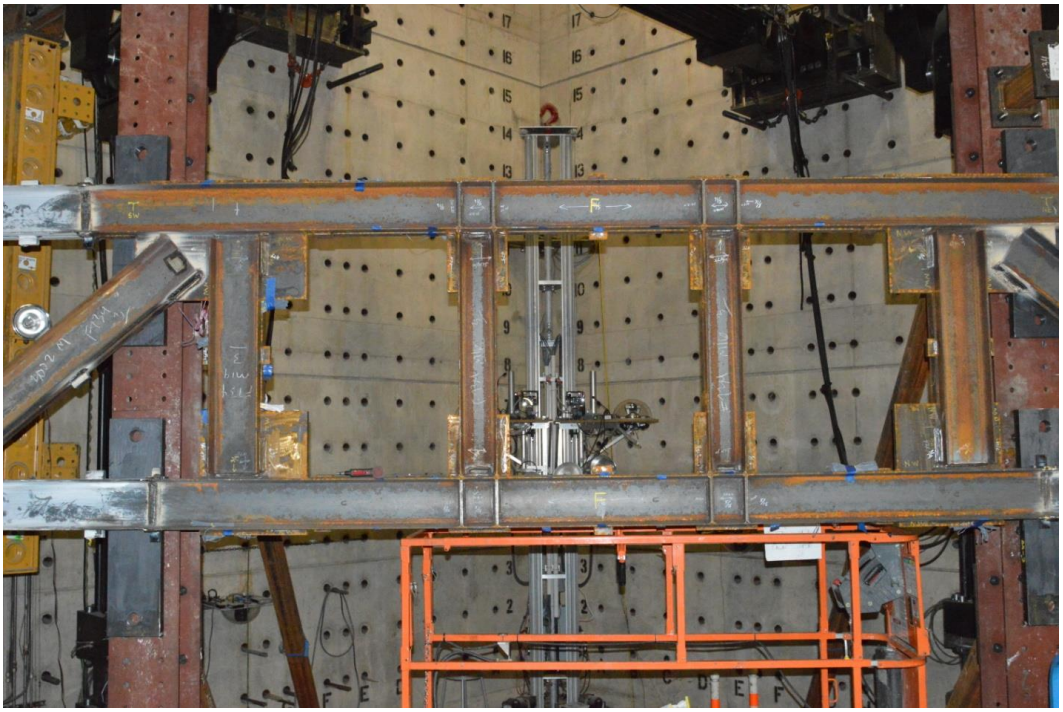

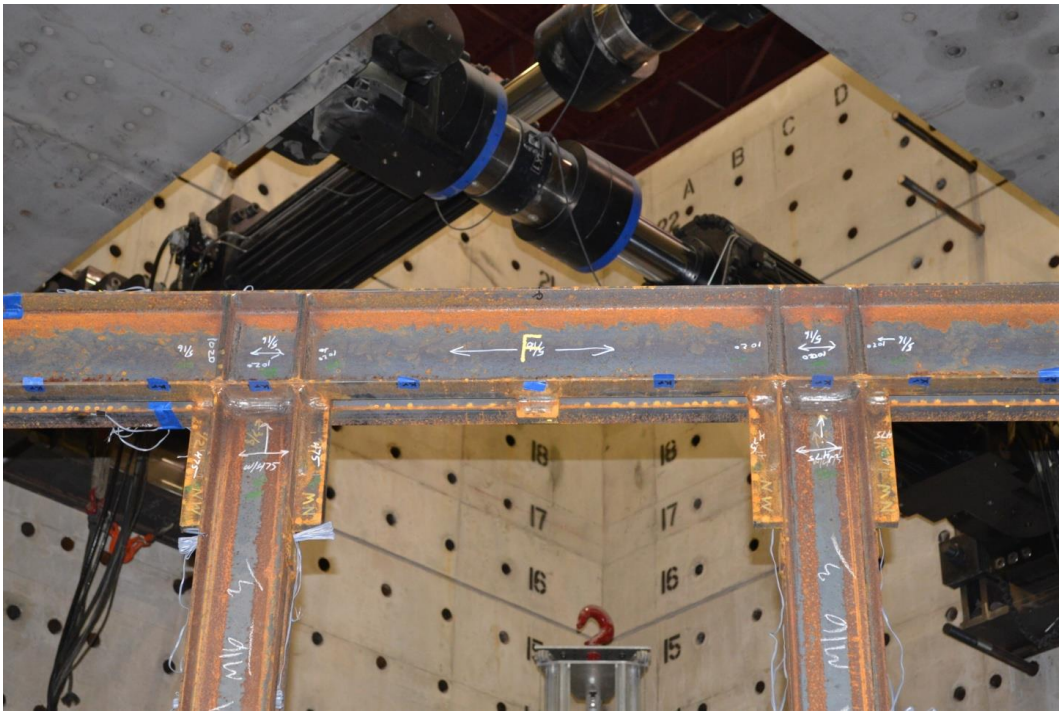
A
B
C
D
18
17
16
15

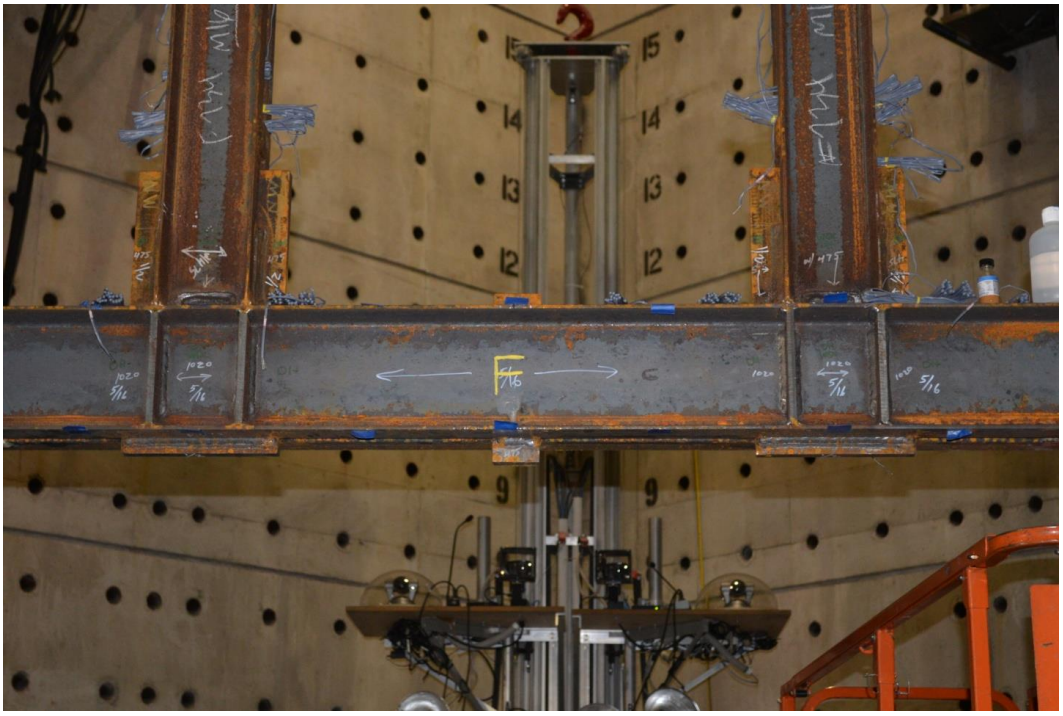
15
14
13
12
9

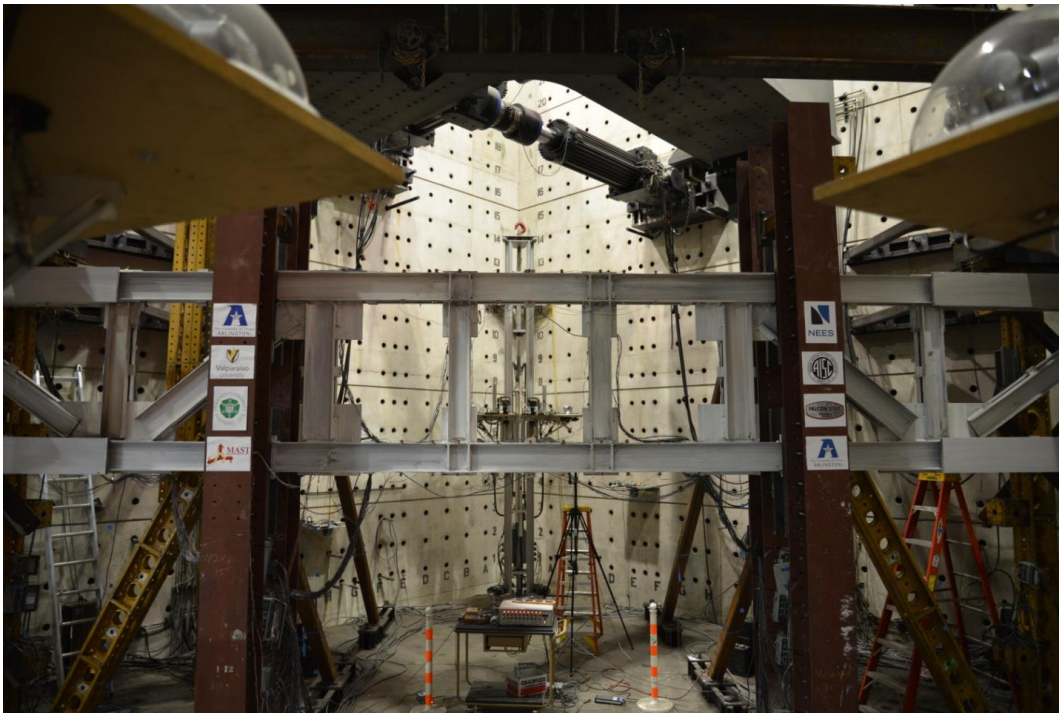
NEES


Valparaiso University
MAST
W12X65
15'


NEES
AISC
FALCON STEEL Company
The University of Texas ARLINGTON

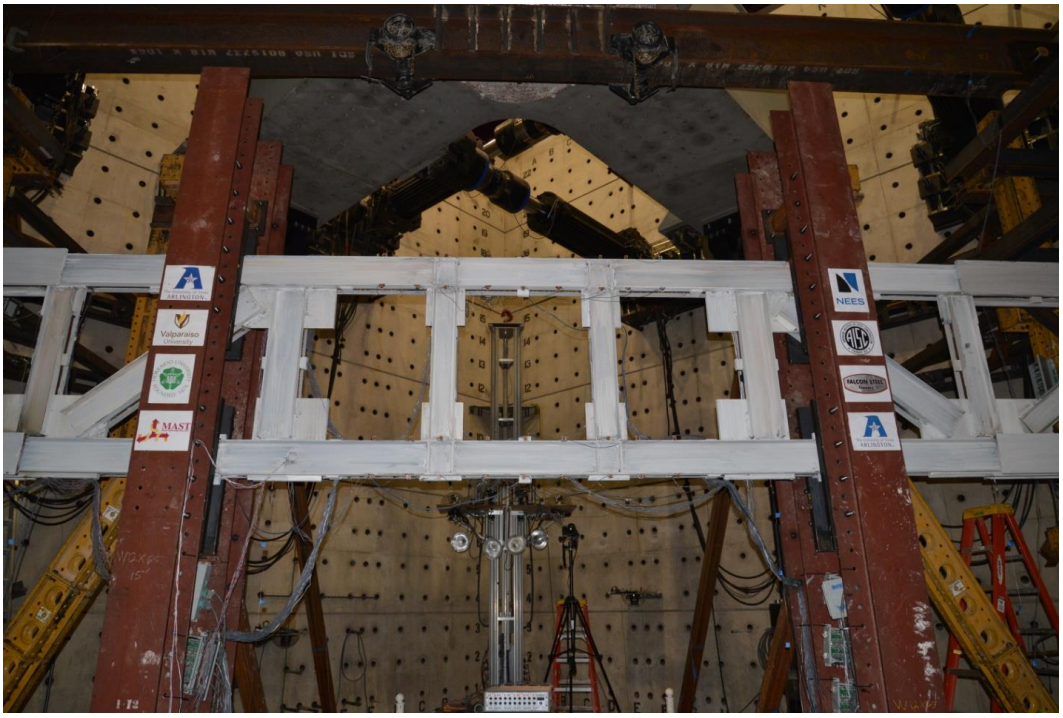
NEES
MAST

Appendix C

Subassemblage Specimen STMF-2HSS8 Photos

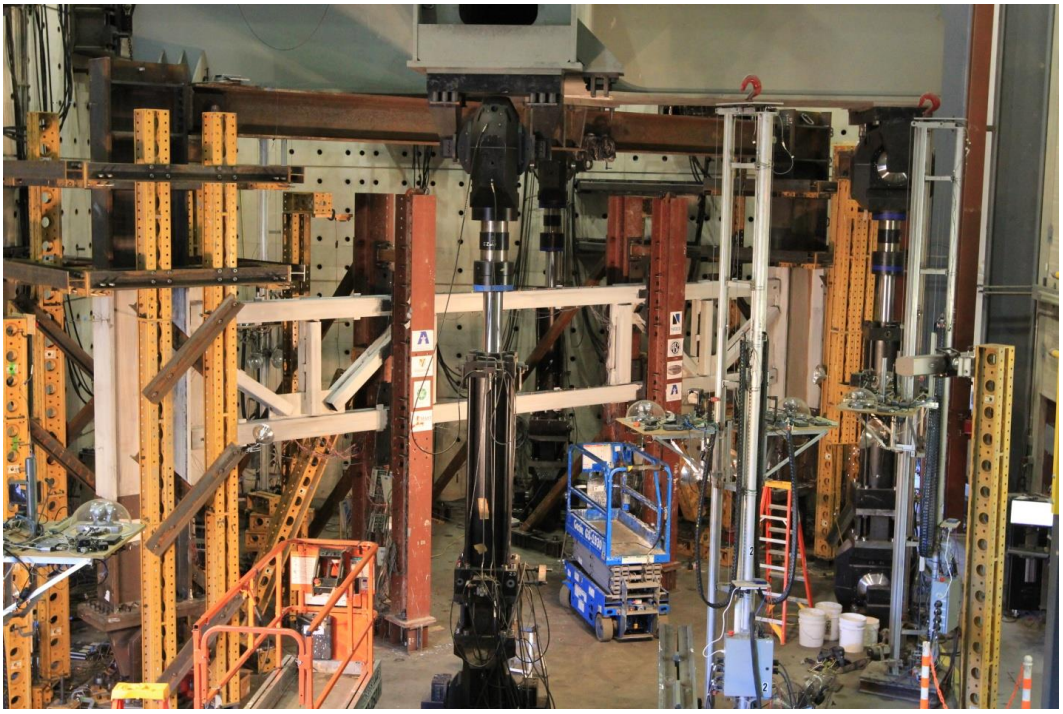

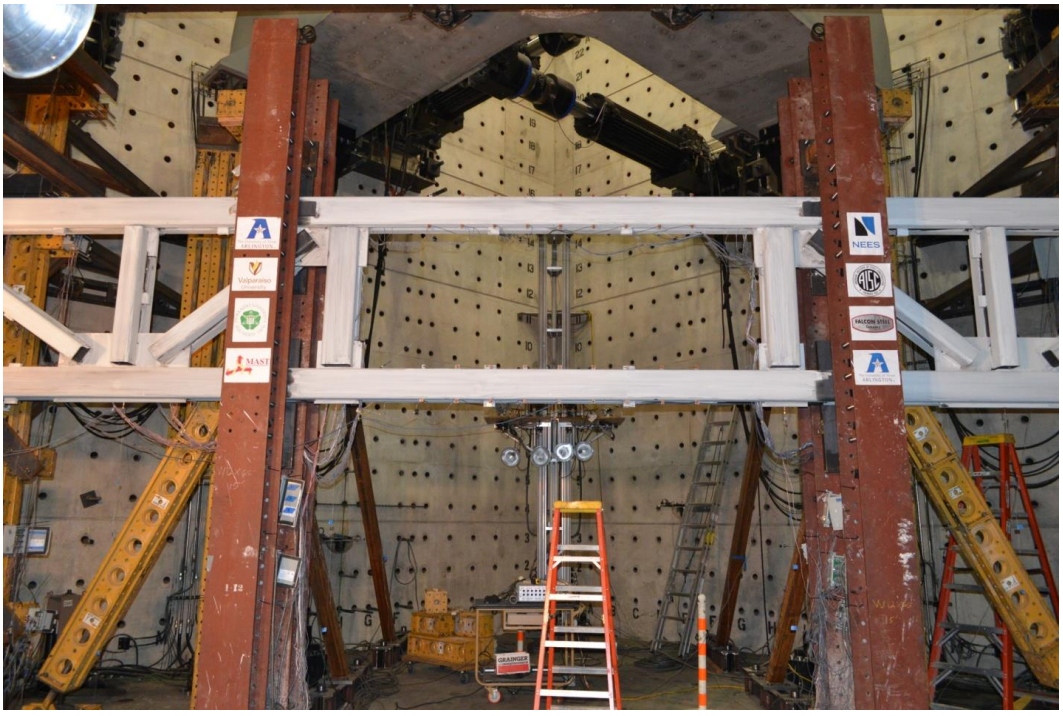
NEES

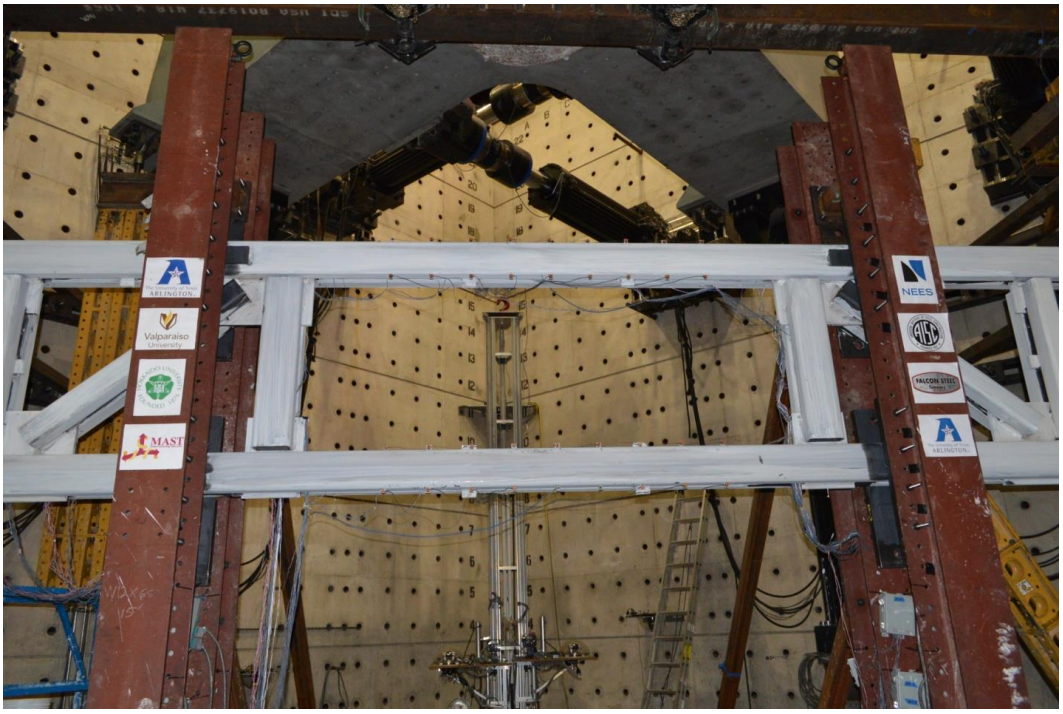
NEES
MAST


Valparaiso
MAST


NEES
AISC

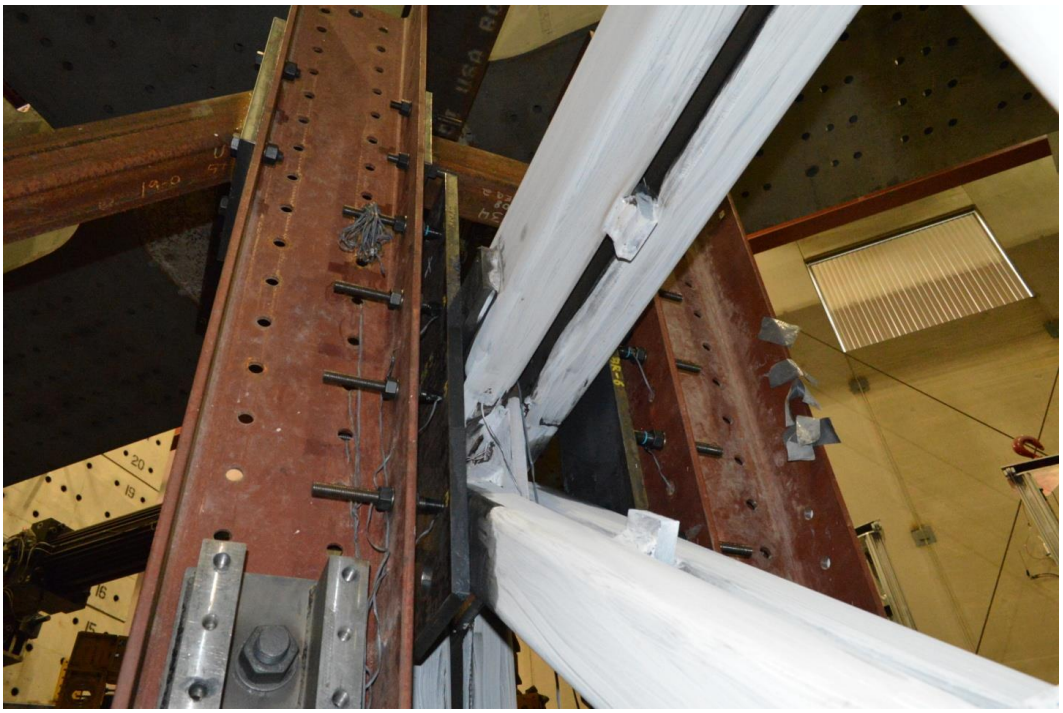

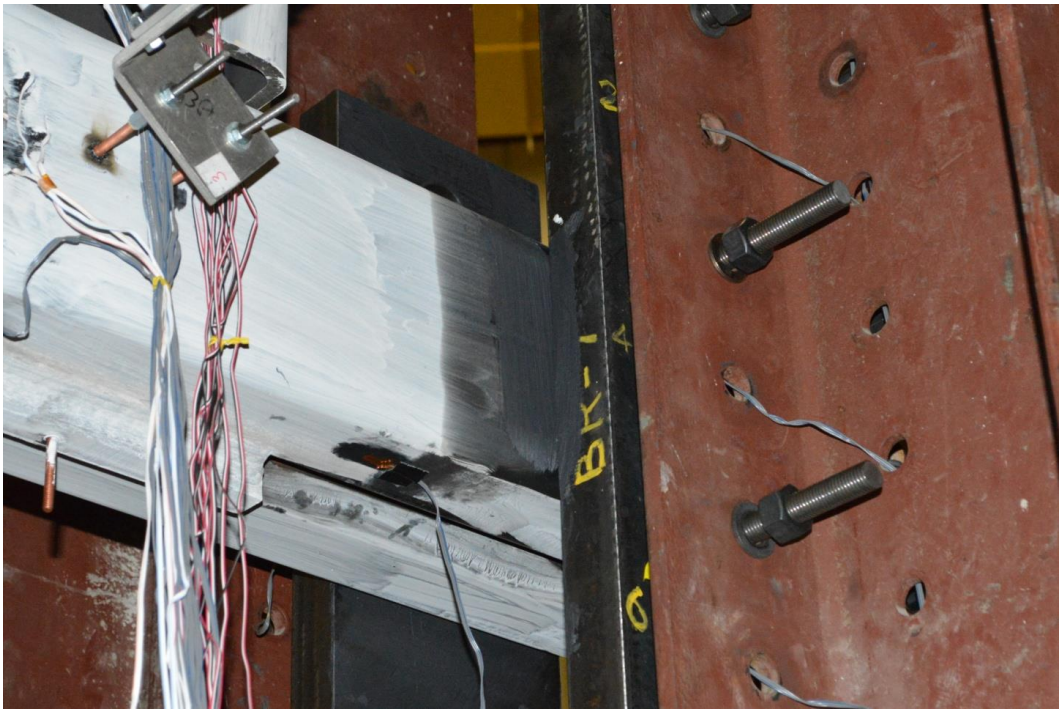
BK-1


T
SW


B
SW


SW


SW
B
SW

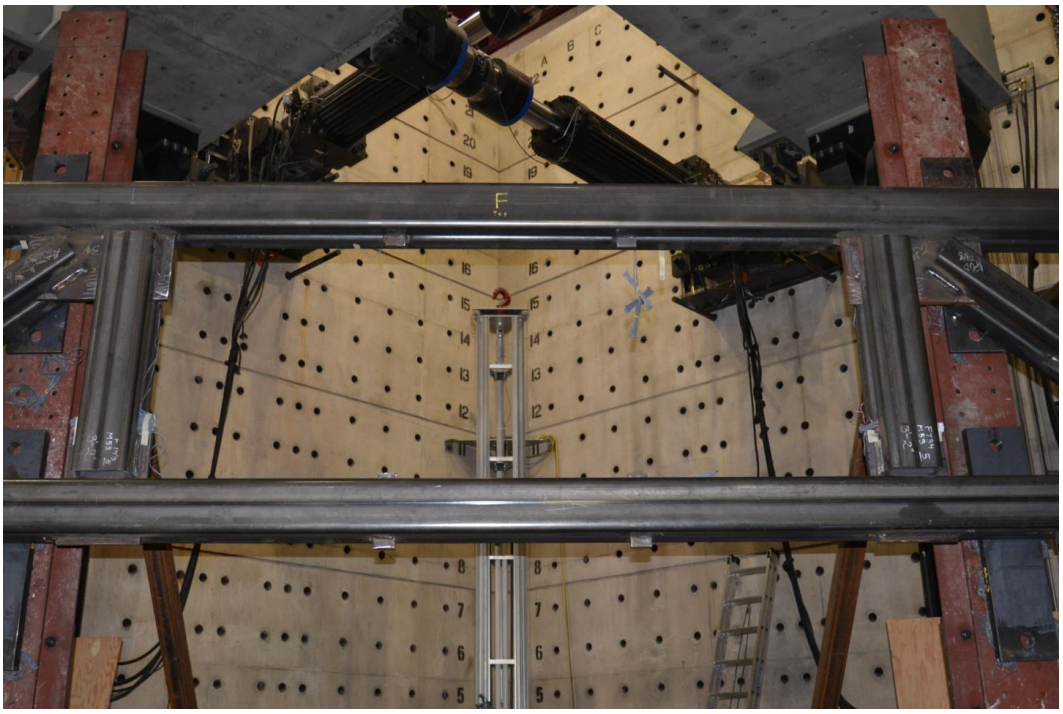

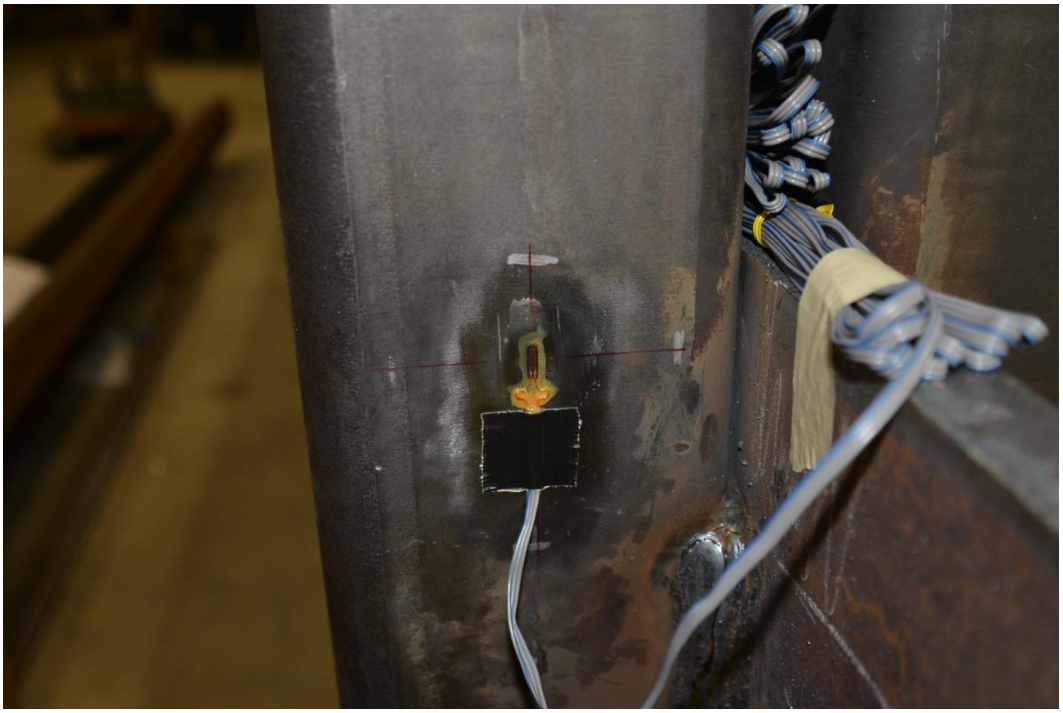

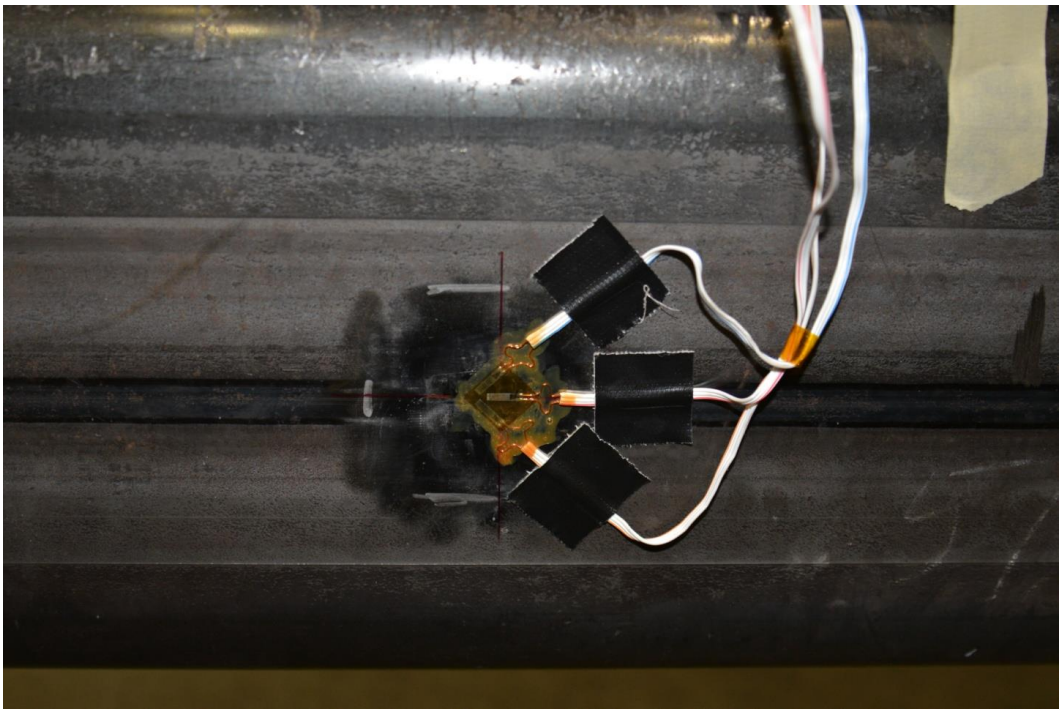

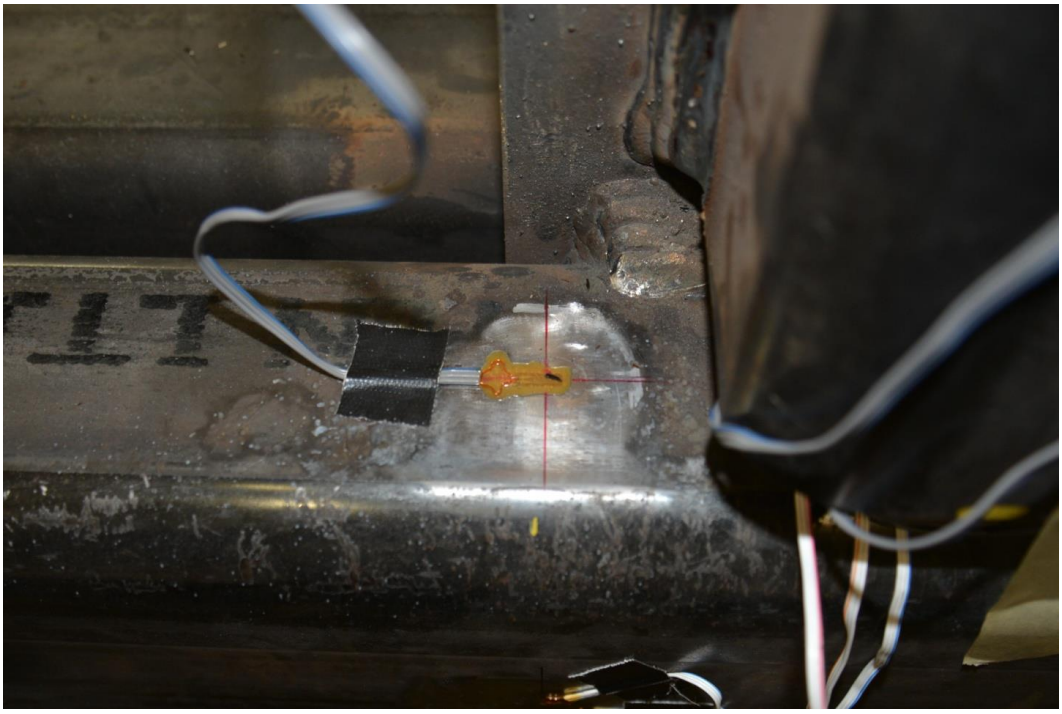

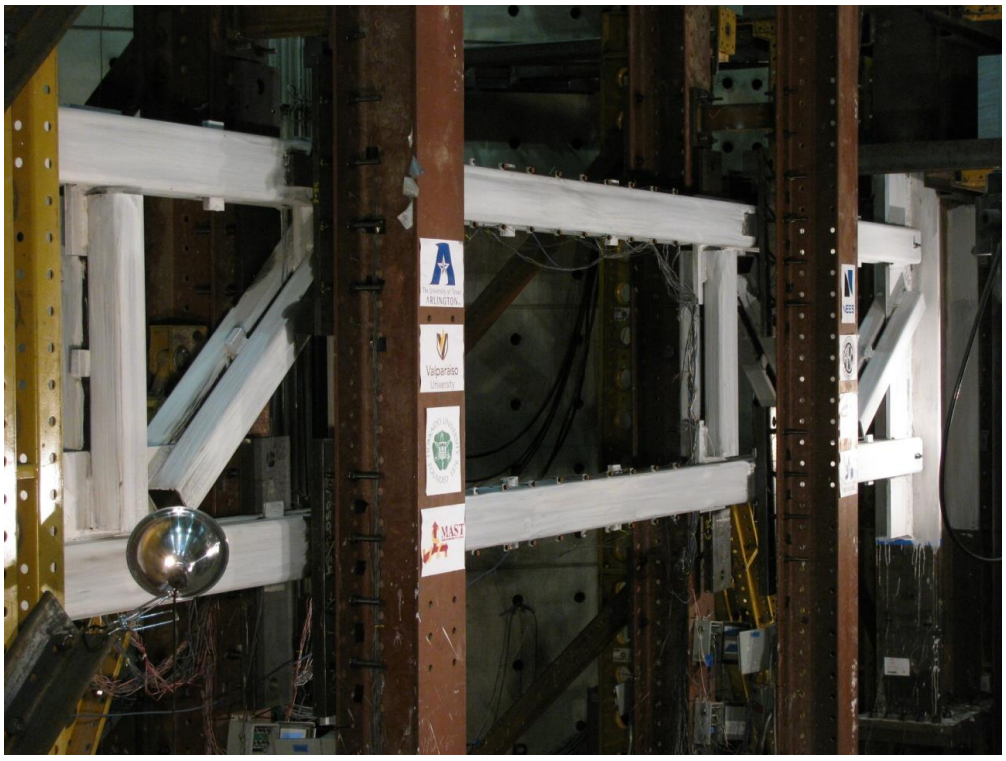
Valparaiso

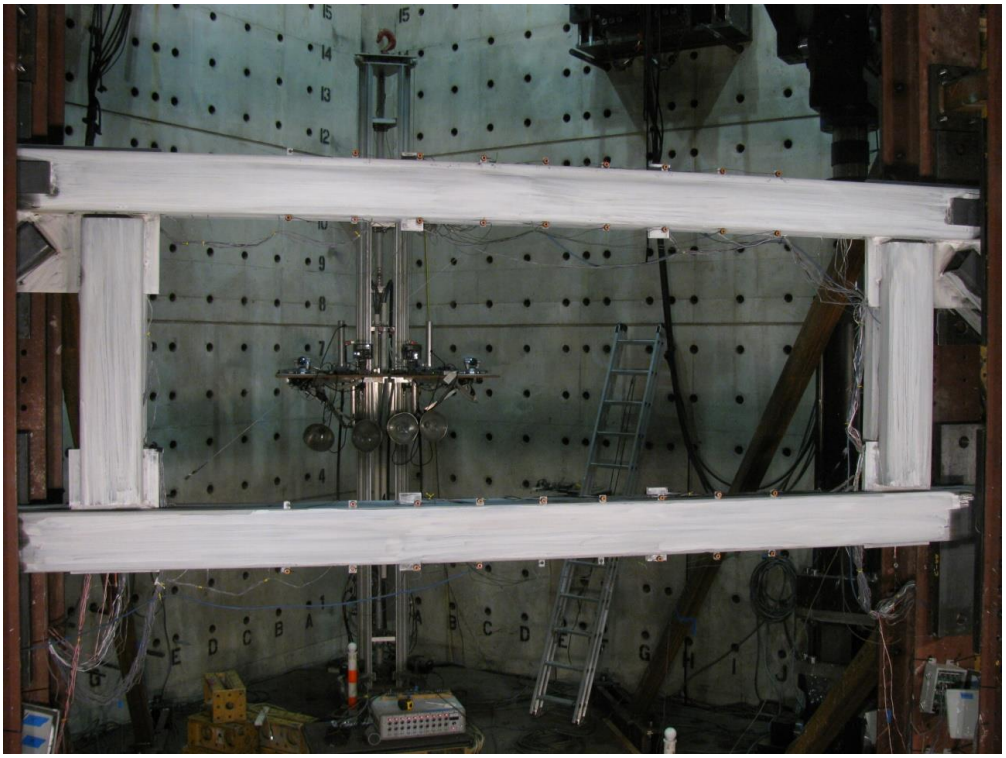


The University of Texas
ARLINGTON
Valparaiso
University
HOKKAIDO UNIVERSITY
FOUNDED 1876
MAST


NEES
AISC
FALCON STEEL
Company
The University of Texas
ARLINGTON

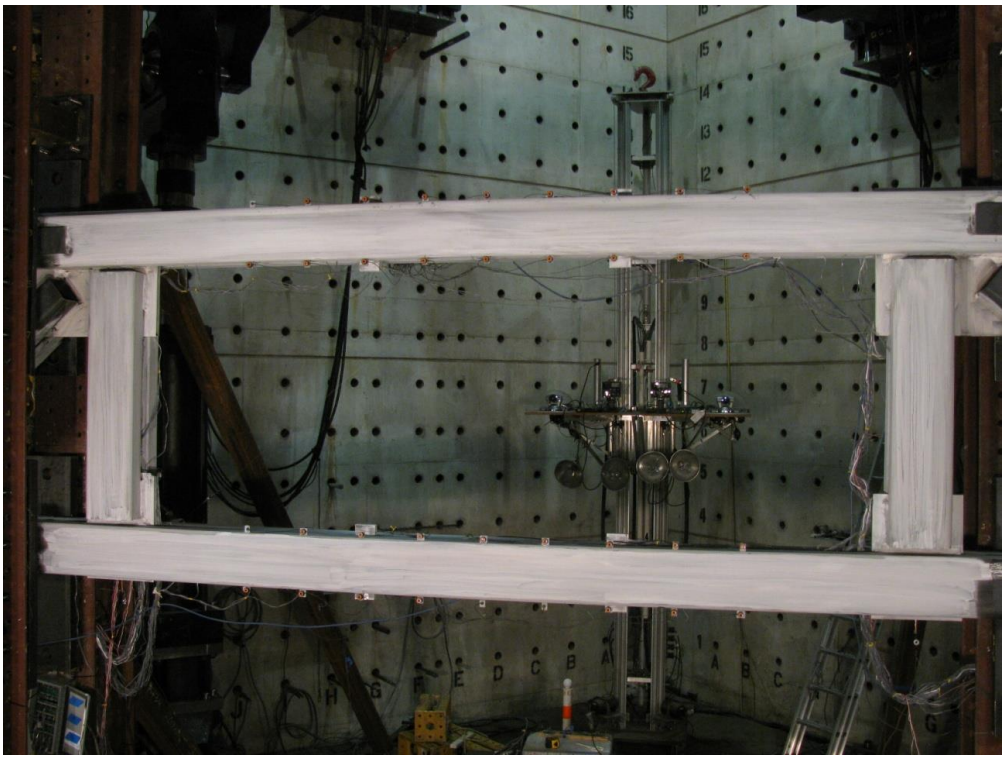

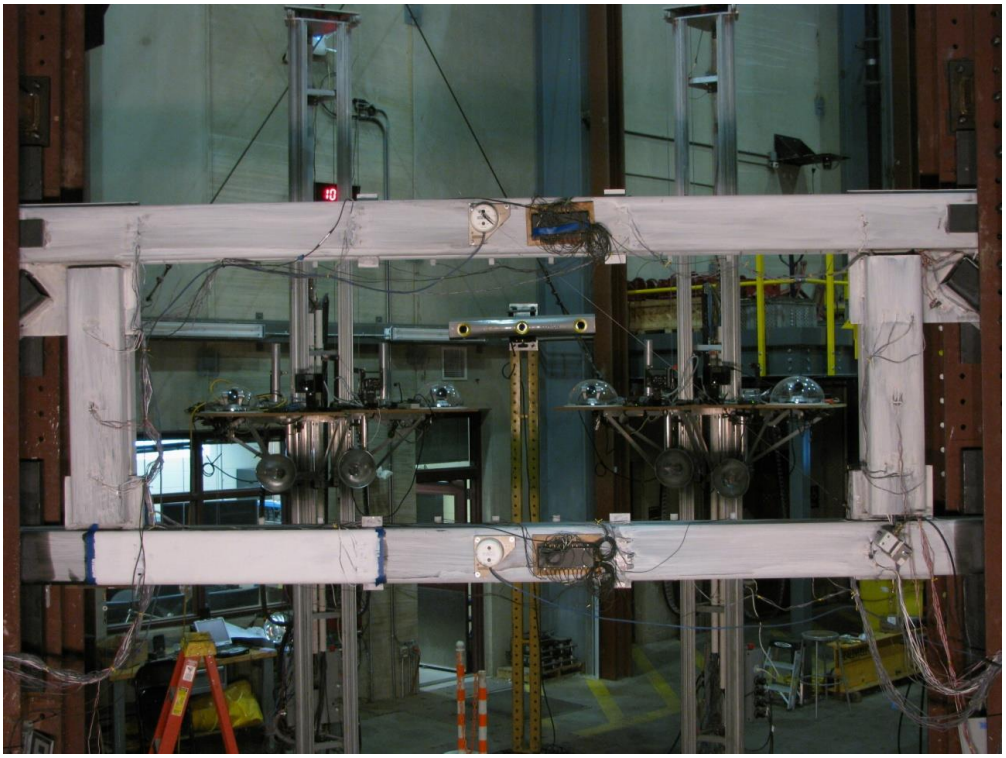

Appendix D

Test Procedures for STMF Subassemblage Specimens

Test Procedures

1. Apply lateral displacements in a reversed cyclic manner at a rate of 1 in./min, according to the displacement history given in Figure D1. The displacement is to be controlled according to the displacement measured at crosshead. Each drift level consists of either six, four, or two cycles.
2. Still images will be taken by using the 8 MAST telepresence cameras at the beginning of the test. Also at the drift levels (pause the loading) specified in Figure D1.
3. Continue loading and pausing, as described in steps 1) and 2), until (a) the Cycle Step #11 is completed (Table D1), or (b) the MAST crosshead reaches the maximum displacement allowed, or (c) the lateral resistance of the specimen degrades to 20% or less of the peak resistance exhibited during the test in both directions.
4. Unload the specimen at a rate of 1 in./min without pausing for pictures until the crosshead returns to the initial (undeflected) configuration and STOP.

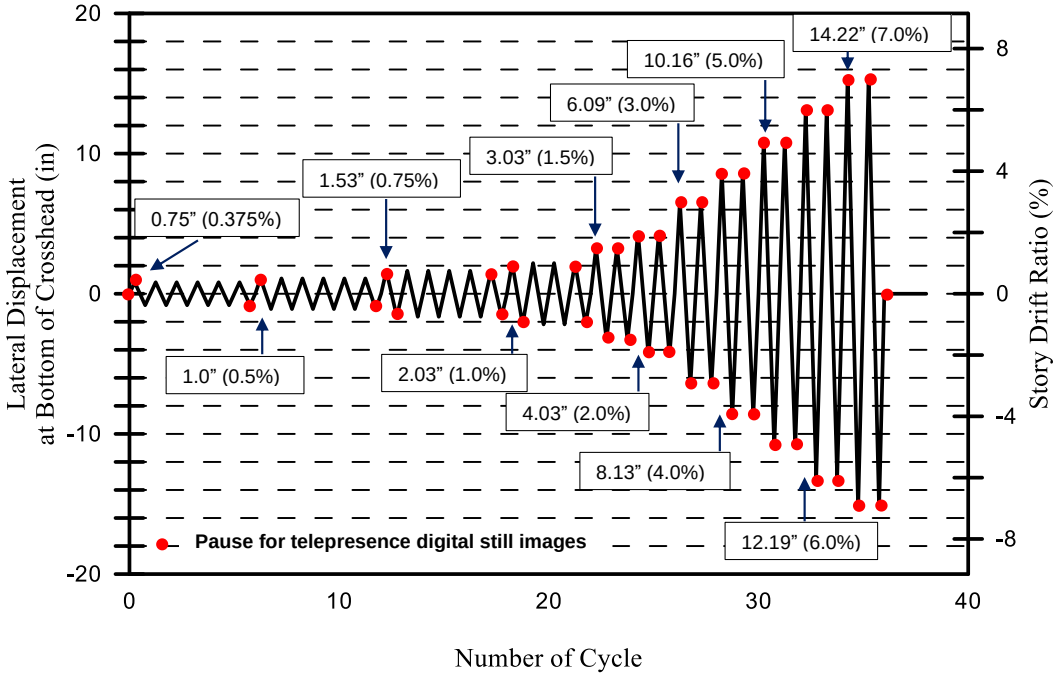

Figure D1. Displacement protocol

Table D1. Displacement History

Load Step #	Peak Lateral Displacement at Bottom of Crosshead (in.)	Peak Drift (%), θ	Number of Cycles, n
	Baby Cycles*		
1	0.75	0.375	6
2	1.00	0.5	6
3	1.53	0.75	6
4	2.03	1	4
5	3.03	1.5	2
6	4.03	2	2
7	6.09	3	2
8	8.13	4	2
9	10.16	5	2
10	12.19	6	2
11	14.22	7	2

Notes for STMF-2C8-1:

1. Peak lateral displacement (required by displacement protocol) is measured at the center of the bottom of crosshead (at the bottom flange plate) when the crosshead is at the 19’-9” standard elevation in neutral position.
2. Maximum lateral displacement for the structure (limited by test setup) in the X’ direction at the bottom of the crosshead is 25 in.
3. For baby cycles: a small displacement cycle (0.2-in.) in both +/- X’-directions. This would give an approximate lateral force of 20 kips.
4. The measured heights of the load transfer plate at 4 corners are: 19' 6-0", 19' 5-15/16", 19' 5-7/8", 19' 5-7/8". When adding the thickness of the plate, the bottom of the cross head will be at, 19' 9-1/16", 19' 9-0", 19' 8-15/16", 19' 8'15/16". It is safe to say that the bottom of crosshead is at 19'-9".
5. The bottom of the bottom chord of the truss is supposed to be 7'-10 5/8" high from the floor in the design drawing. The bottom of the front channel is measured as 7'-10 11/16" while the back is 7'-10 5/8". The truss from back of the top chord to the bottom of the bottom chord is 55-31/32" in the front and 56-1/16" in the back (theoretically is 56"). It is calculated that center of the top chord is at 12'-2 21/32" and the back is 12'-2 11/16" above the floor. From the drawing, the center of the top chord is at 12'-2 5/8" above the ground – it is within 1/16" tolerance. As a result, it is assumed that the top chord is at the exact height specified in the drawing.

Notes for STMF-2C8-2:

1. Peak lateral displacement (required by displacement protocol) is measured at the center of the bottom of crosshead (at the bottom flange plate) when the crosshead is at the 19’-9” standard elevation in neutral position.
2. Maximum lateral displacement for the structure (limited by test setup) in the X’ direction at the bottom of the crosshead is 25 in.
3. For baby cycles: a small displacement cycle (0.1-in.) in both +/- X’-directions. This would give an approximate lateral force of 20 kips.
4. The measured heights of the load transfer plate at 4 corners are: 19' 6-0", 19' 5-15/16", 19' 6-0", 19' 5-7/8". When adding the thickness of the plate, the bottom of the cross head will be at, 19' 9-1/16", 19' 9-0", 19' 9-1/16", 19' 8'15/16". It is safe to say that the bottom of crosshead is at 19'-9".
5. For the existing part of the truss (STMF-2C8-1), the bottom of the bottom chord of the truss is supposed to be 7'-10 5/8" high from the floor in the design drawing. The bottom of the front channel is measured as 7'-10 11/16" while the back is 7'-10 5/8". The truss from back of the top chord to the bottom of the bottom chord is 55-31/32" in the front and 56-1/16" in the back (theoretically is 56"). It is calculated that center of the top chord is at 12'-2 21/32" and the back is 12'-2 11/16" above the floor. From the drawing, the center of the top chord is at 12'-2 5/8" above the ground which is within 1/16" tolerance. As for the splicing part (STMF-2C8-2), the front and back of the NE corner is measured at 7'-10 5/8" while the SW corner is measured at 7'-10 9/16" respectively. The truss from back of the top chord to the bottom of the bottom chord is 56-1/16" in the front and 56-0" in the back (theoretically is 56"). It is calculated that center of the top chord is at 12'-2 21/32" and the back is 12'-2 19/32" above the floor. From the drawing, the center of the top chord is at 12'-2 5/8" above the ground which

is within 1/16" tolerance. As a result it is assumed that the top chord is at the exact height specified in the drawing.

Notes for STMF-2HSS8:

1. Peak lateral displacement (required by displacement protocol) is measured at the center of the bottom of crosshead (at the bottom flange plate) when the crosshead is at the 19’-9” standard elevation in neutral position.
2. Maximum lateral displacement for the structure (limited by test setup) in the X’ direction at the bottom of the crosshead is 25 in.
3. For baby cycles: a small displacement cycle (0.16-in.) in both +/- X’-directions. This would give an approximate lateral force of 20 kips.
4. The measured heights of the plate at 4 corners are: 19' 6-0", 19' 5-15/16", 19' 5-13/16", 19' 5-15/16". When adding the thickness of the plate, the bottom of the cross head will be at, 19' 9-1/16", 19' 9-0", 19' 8-7/8", 19' 9-0". It is safe to say that the bottom of crosshead is at 19'-9".
5. The bottom of the bottom chord of the truss is supposed to be 7'-10 5/8" high from the floor in the design drawing. The bottom of the front tube is measured as 7'-10 5/8" while the back is 7'-10 11/16". The truss from bottom of the top chord to the back of the bottom chord is 40-1/8" in the front and the back (theoretically is 40"). It is calculated that center of the top chords are at 12'-2 3/4" in the front and 12'-2 13/16" in the back above the floor. From the drawing, the center of the top chord is at 12'-2 5/8" above the ground which it is within 1/8” and 3/16" tolerances in the front and back respectively. As a result it is assumed that the top chord is at the exact height specified in the drawing.

Appendix E

Instrumentation Drawings for STMF Subassemblage Testing Program

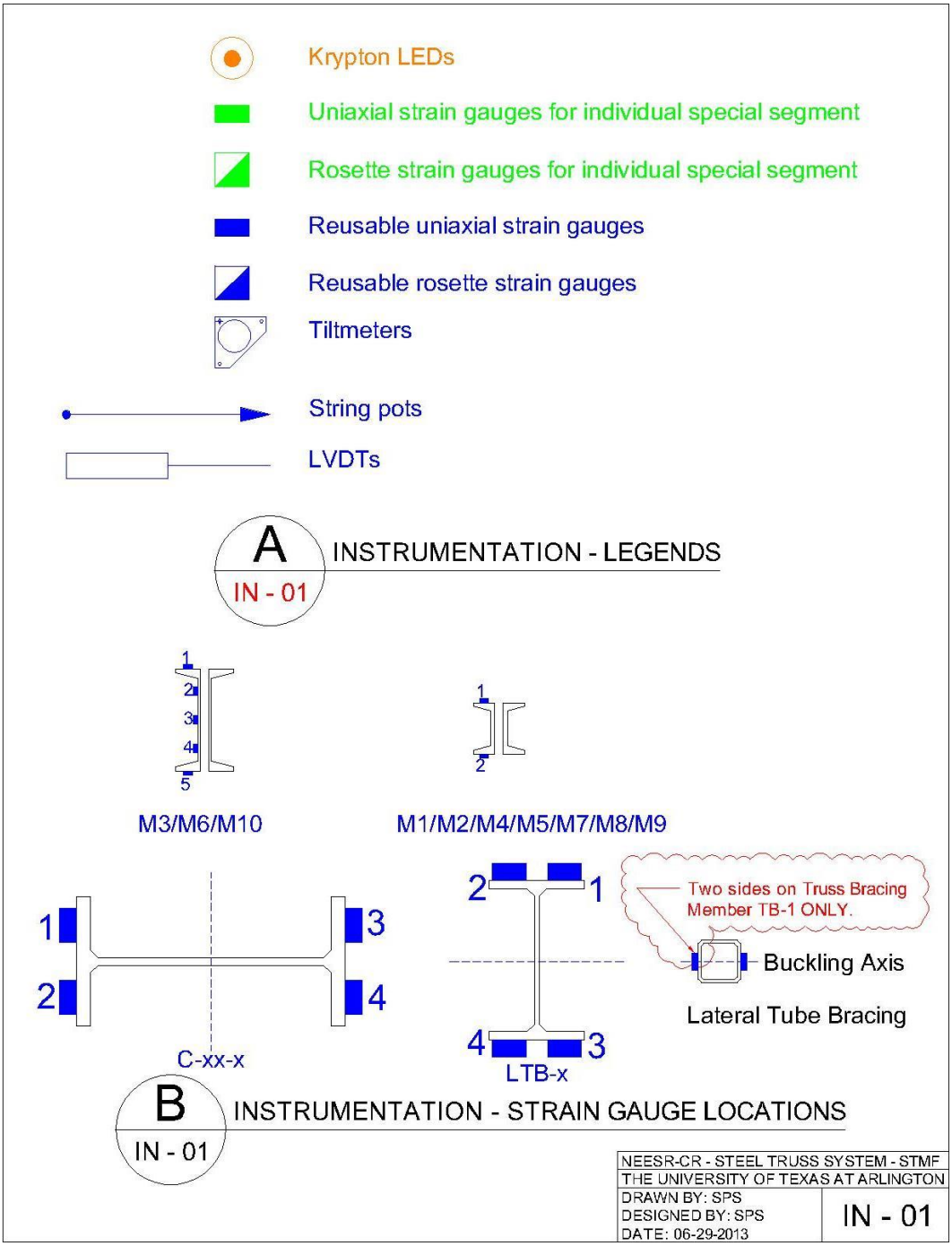
Krypton LEDs
Uniaxial strain gauges for individual special segment
Rosette strain gauges for individual special segment
Reusable uniaxial strain gauges
Reusable rosette strain gauges
Tiltmeters
String pots
LVDTs
A
IN - 01
INSTRUMENTATION - LEGENDS
1
2
3
4
5
M3/M6/M10
1
2
M1/M2/M4/M5/M7/M8/M9
1
2
3
4
C-xx-x
2
1
4
3
LTB-x
Two sides on Truss Bracing Member TB-1 ONLY.
Buckling Axis
Lateral Tube Bracing
B
IN - 01
INSTRUMENTATION - STRAIN GAUGE LOCATIONS
NEESR-CR - STEEL TRUSS SYSTEM - STMF
THE UNIVERSITY OF TEXAS AT ARLINGTON
DRAWN BY: SPS
DESIGNED BY: SPS
DATE: 06-29-2013
IN - 01

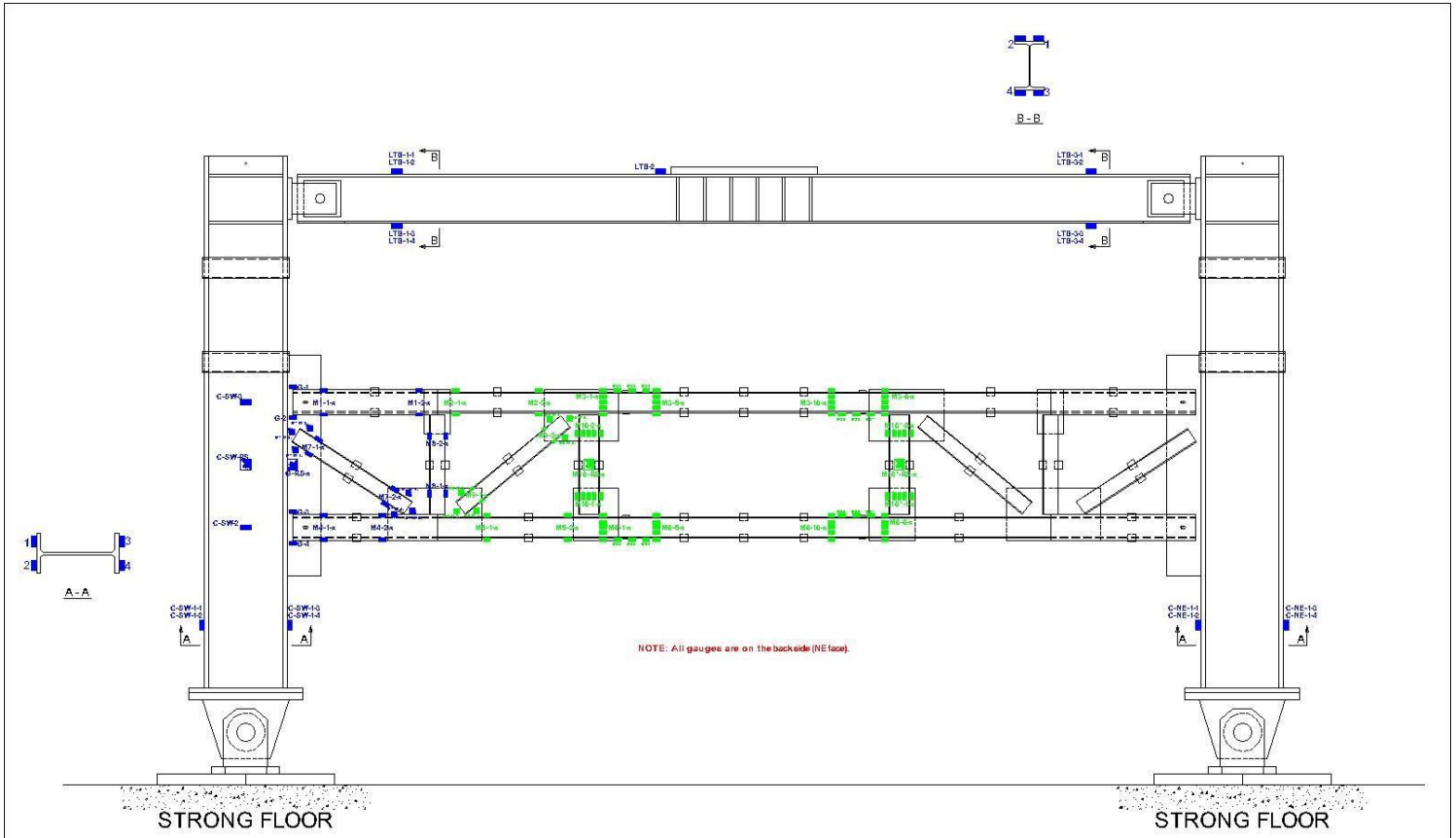

A
IN - 02a

INSTRUMENTATION - STRAIN GAUGES

NEESR-CR - STEEL TRUSS SYSTEM - STMF	
THE UNIVERSITY OF TEXAS AT ARLINGTON	
DRAWN BY: SPS DESIGNED BY: SPS DATE: 06-29-2013	IN - 02a

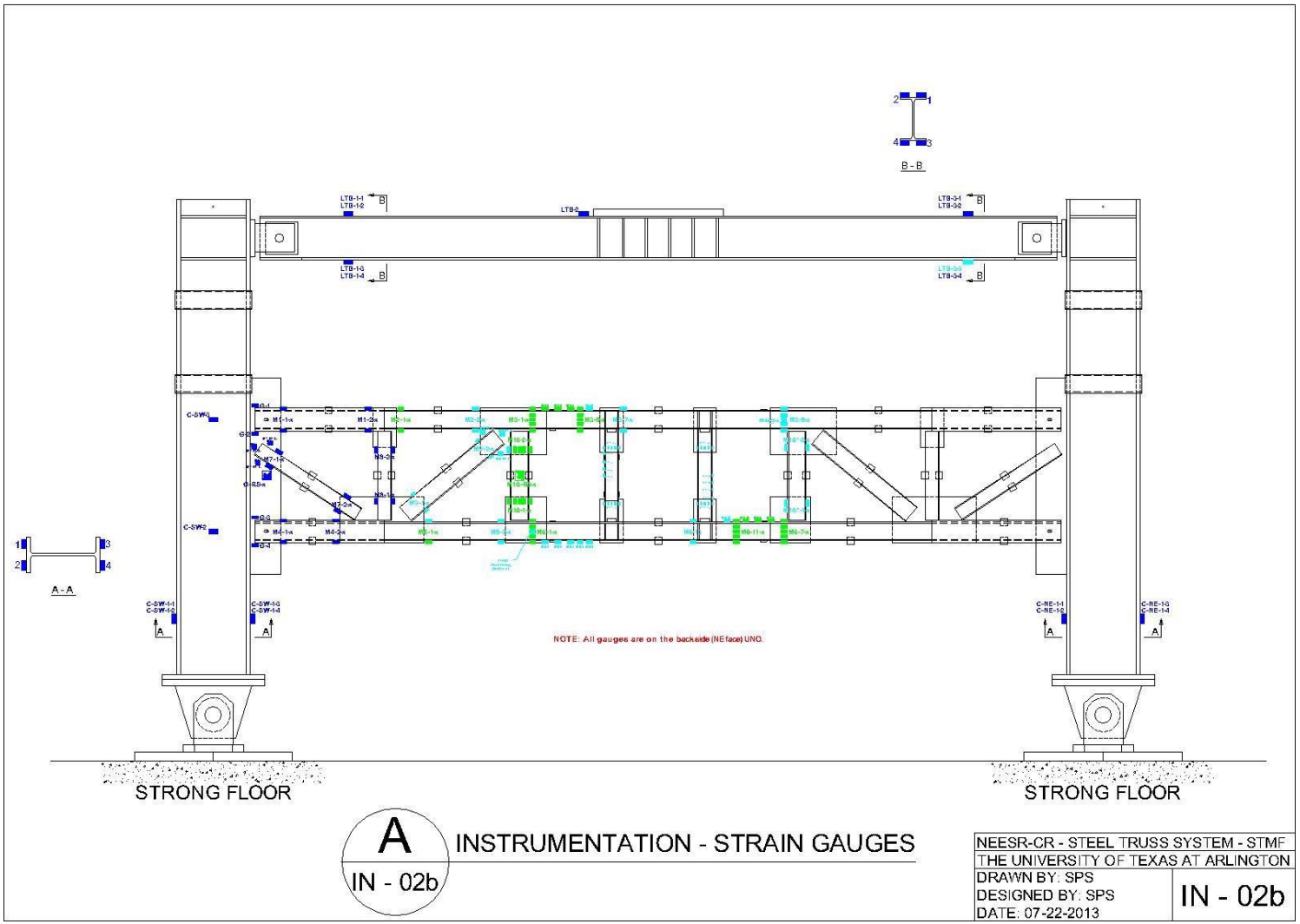

A
IN - 02b
INSTRUMENTATION - STRAIN GAUGES

NEESR-CR - STEEL TRUSS SYSTEM - STMF	
THE UNIVERSITY OF TEXAS AT ARLINGTON	
DRAWN BY: SPS DESIGNED BY: SPS DATE: 07-22-2013	IN - 02b

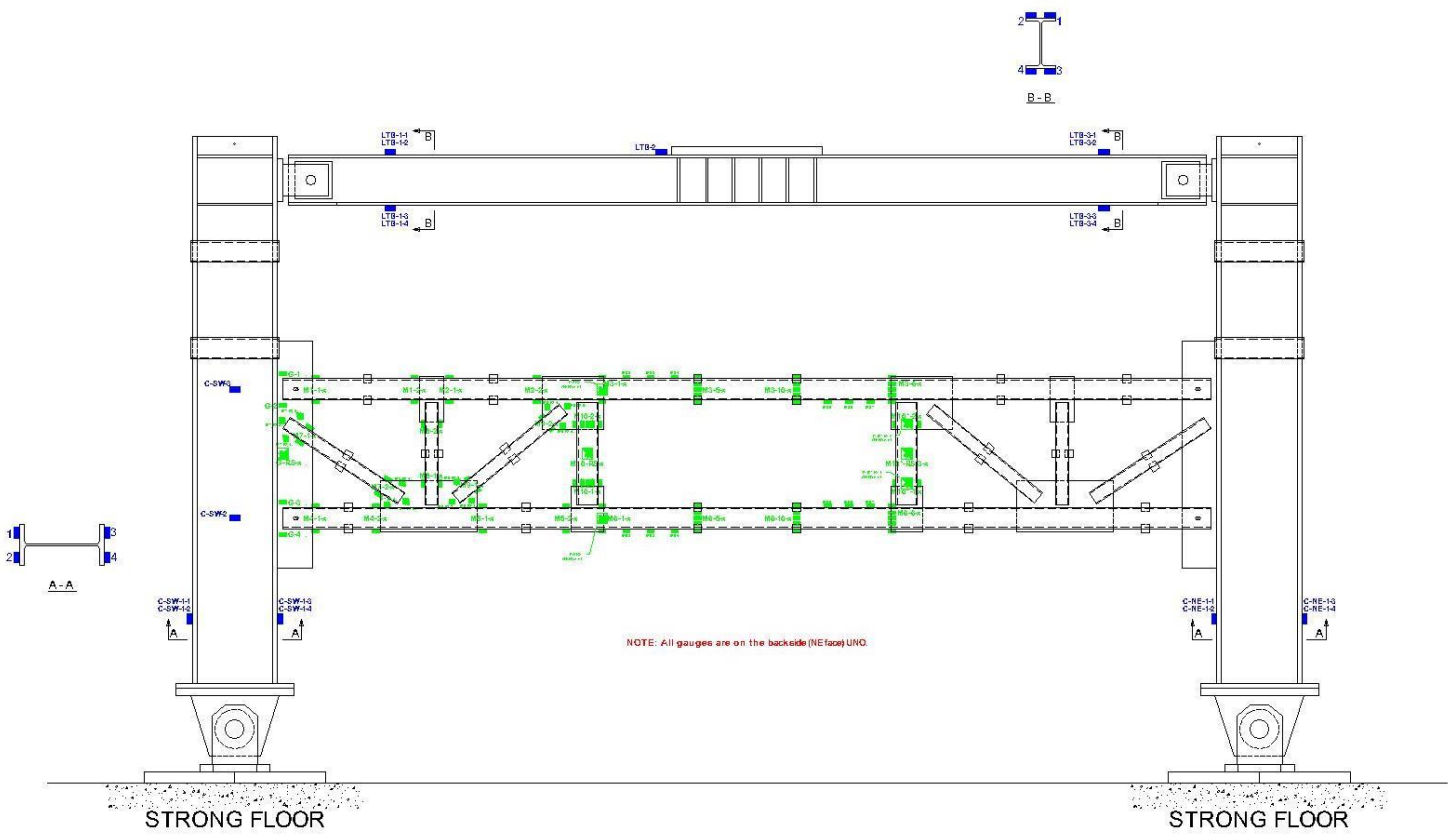

A
IN - 02c

INSTRUMENTATION - STRAIN GAUGES

NEESR-CR - STEEL TRUSS SYSTEM - STMF	
THE UNIVERSITY OF TEXAS AT ARLINGTON	
DRAWN BY: SPS DESIGNED BY: SPS DATE: 09-06-2013	IN - 02c

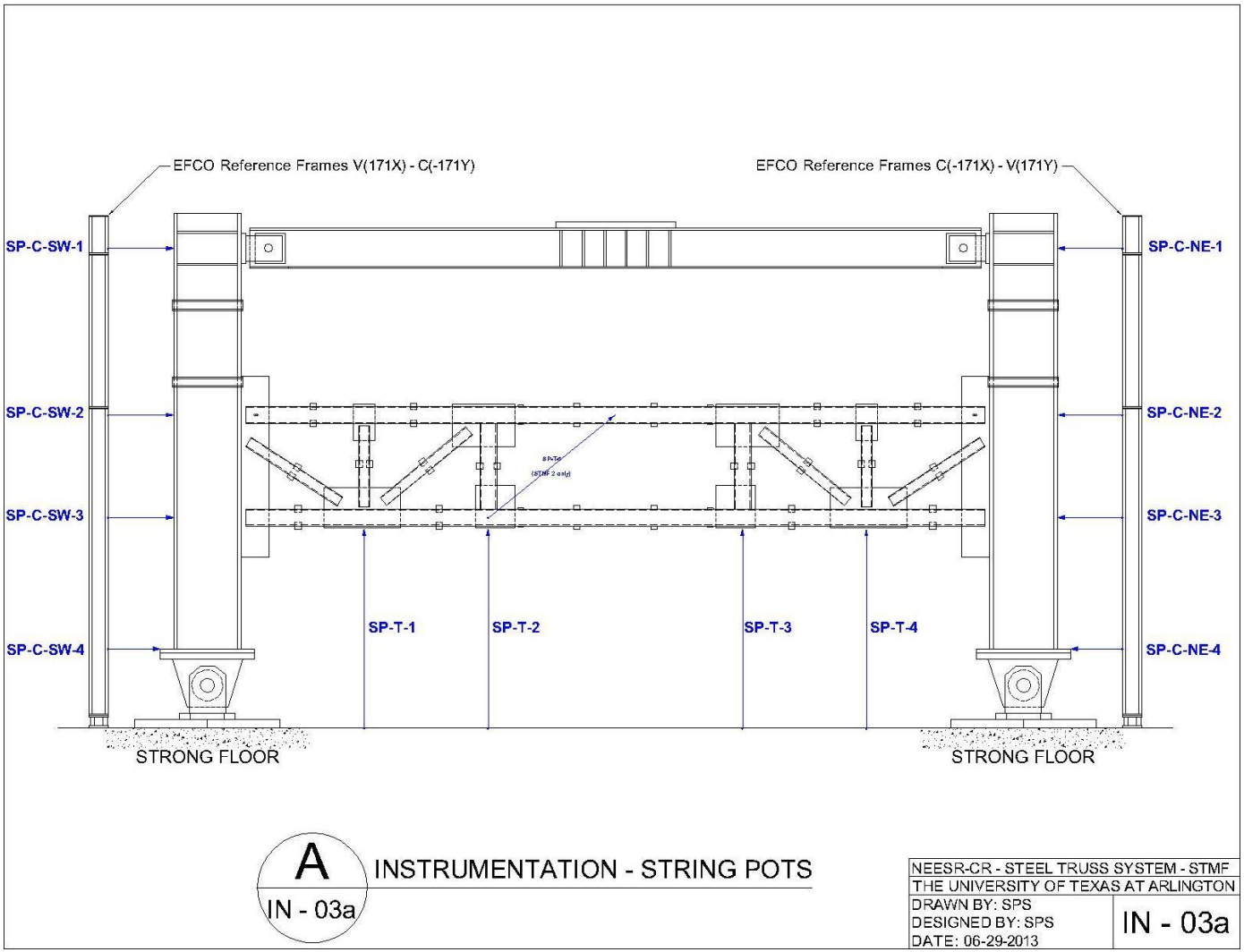

A
IN - 03a
INSTRUMENTATION - STRING POTS

NEESR-CR - STEEL TRUSS SYSTEM - STMF	
THE UNIVERSITY OF TEXAS AT ARLINGTON	
DRAWN BY: SPS DESIGNED BY: SPS DATE: 06-29-2013	IN - 03a

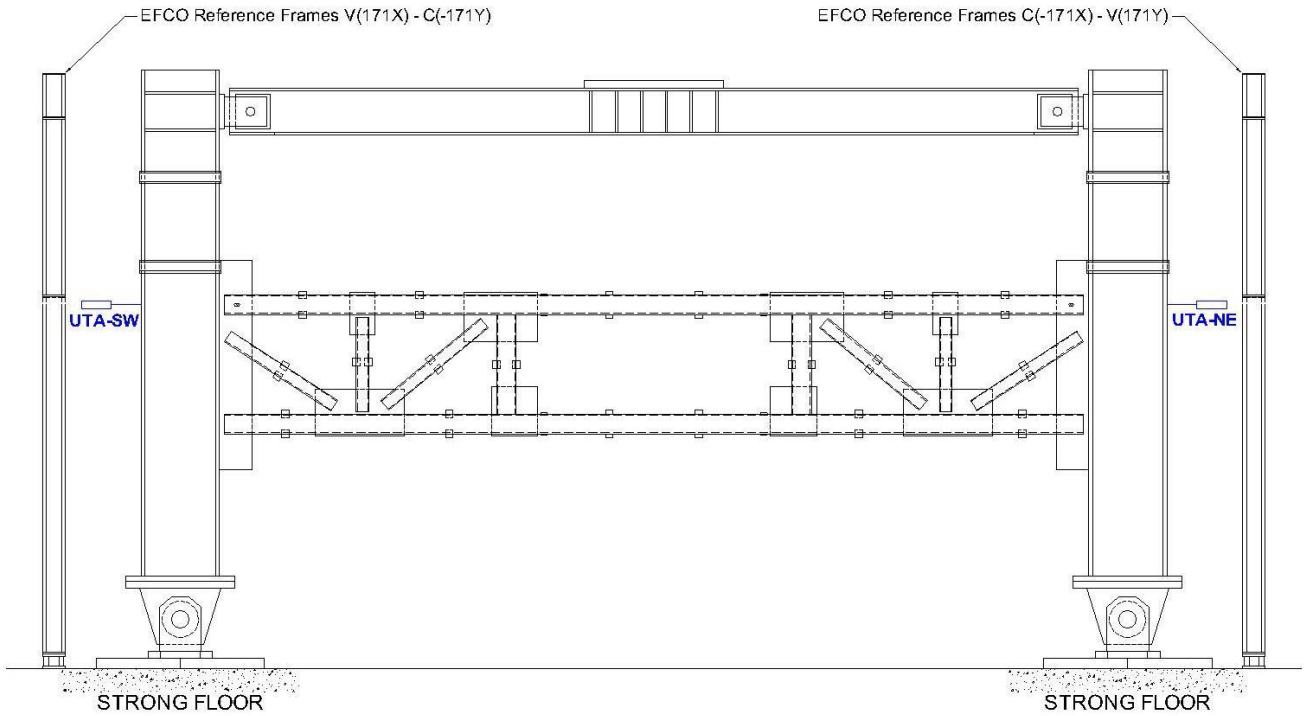

A
IN - 03b

INSTRUMENTATION - ADDITIONAL LVDTs

NEESR-CR - STEEL TRUSS SYSTEM - STMF	
THE UNIVERSITY OF TEXAS AT ARLINGTON	
DRAWN BY: SPS DESIGNED BY: SPS DATE: 06-29-2013	IN - 03b

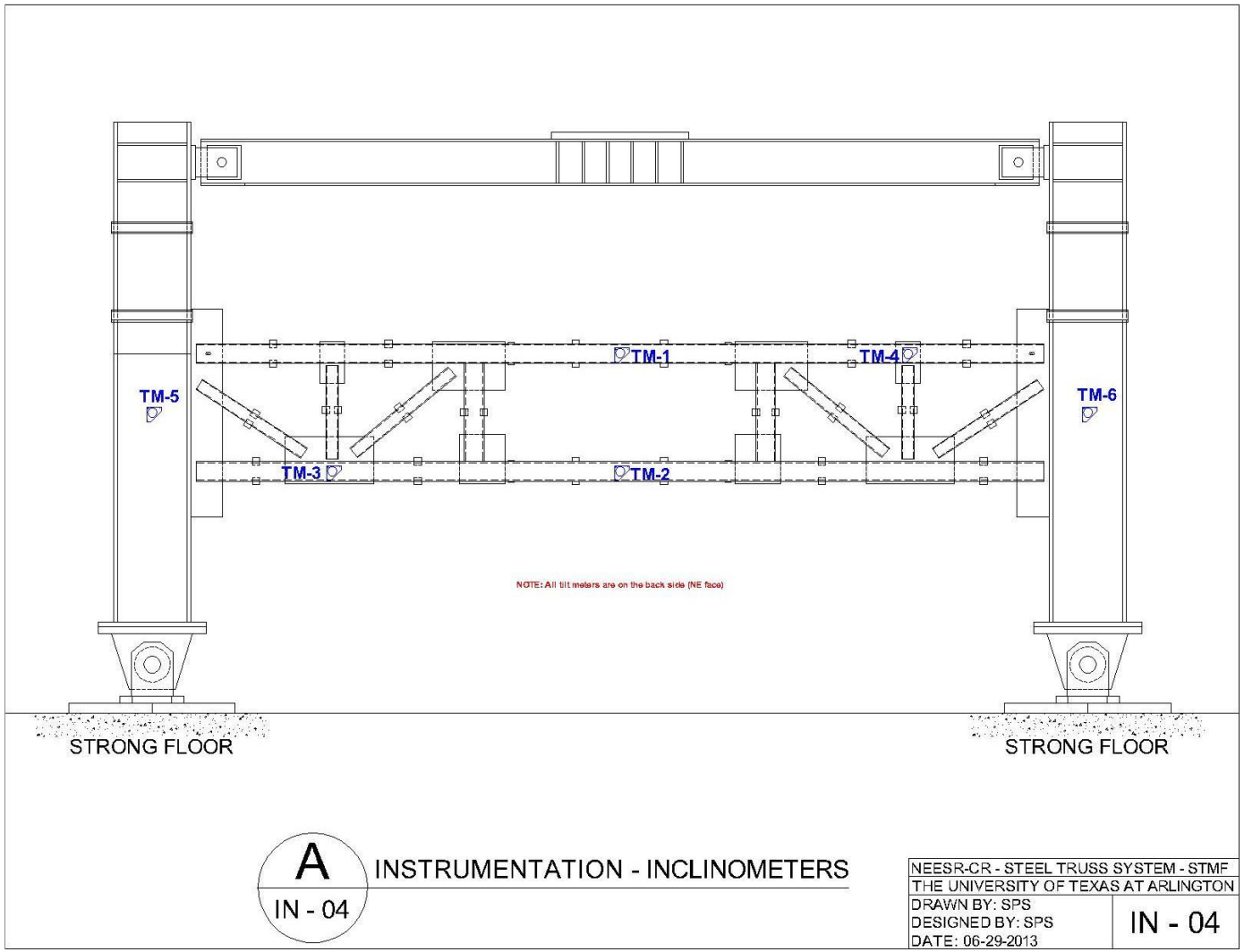

A
IN - 04

INSTRUMENTATION - INCLINOMETERS

NEESR-CR - STEEL TRUSS SYSTEM - STMF	
THE UNIVERSITY OF TEXAS AT ARLINGTON	
DRAWN BY: SPS DESIGNED BY: SPS DATE: 06-29-2013	IN - 04

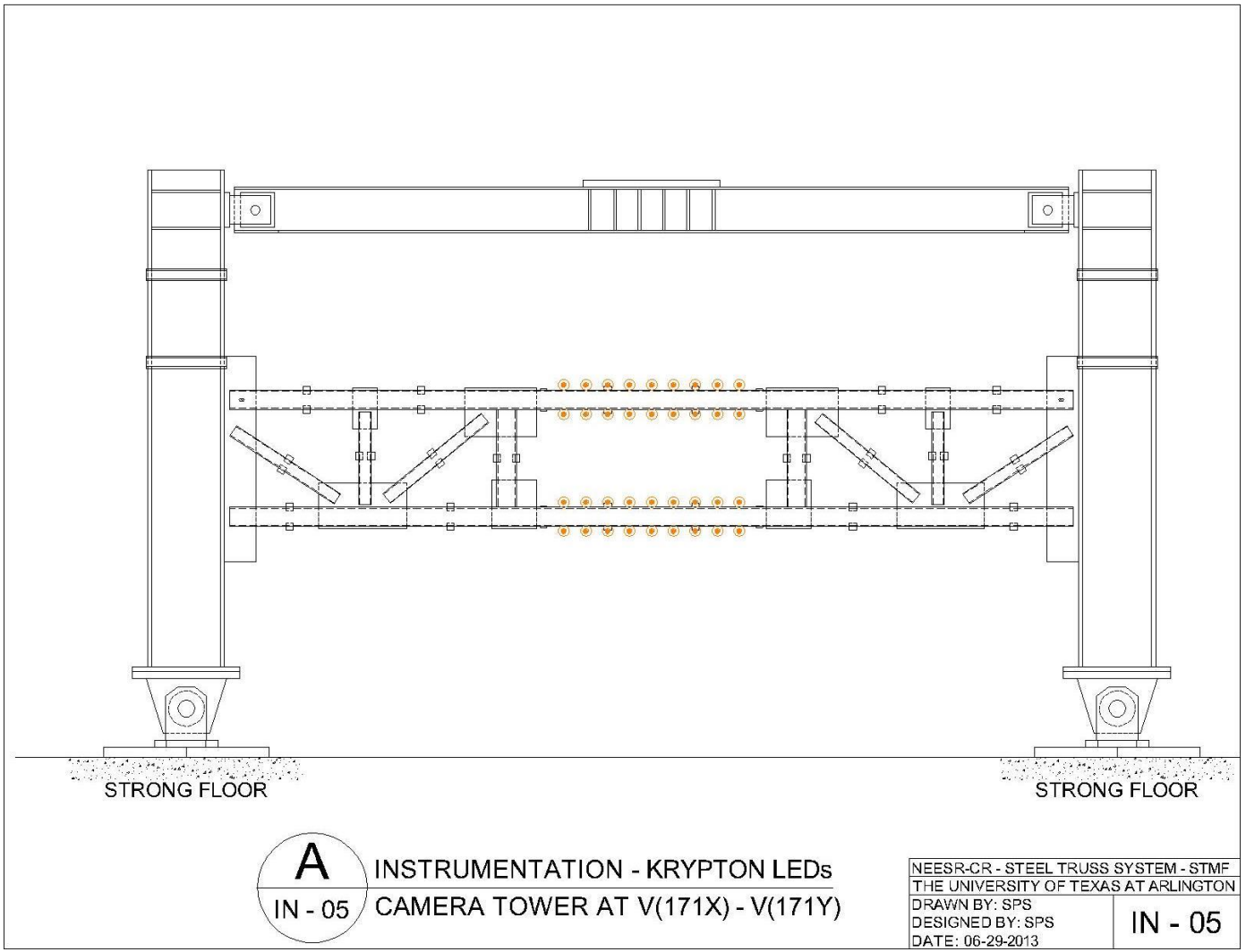
STRONG FLOOR
STRONG FLOOR
A
IN - 05
INSTRUMENTATION - KRYPTON LEDs
CAMERA TOWER AT V(171X) - V(171Y)
NEESR-CR - STEEL TRUSS SYSTEM - STMF
THE UNIVERSITY OF TEXAS AT ARLINGTON
DRAWN BY: SPS
DESIGNED BY: SPS
DATE: 06-29-2013
IN - 05

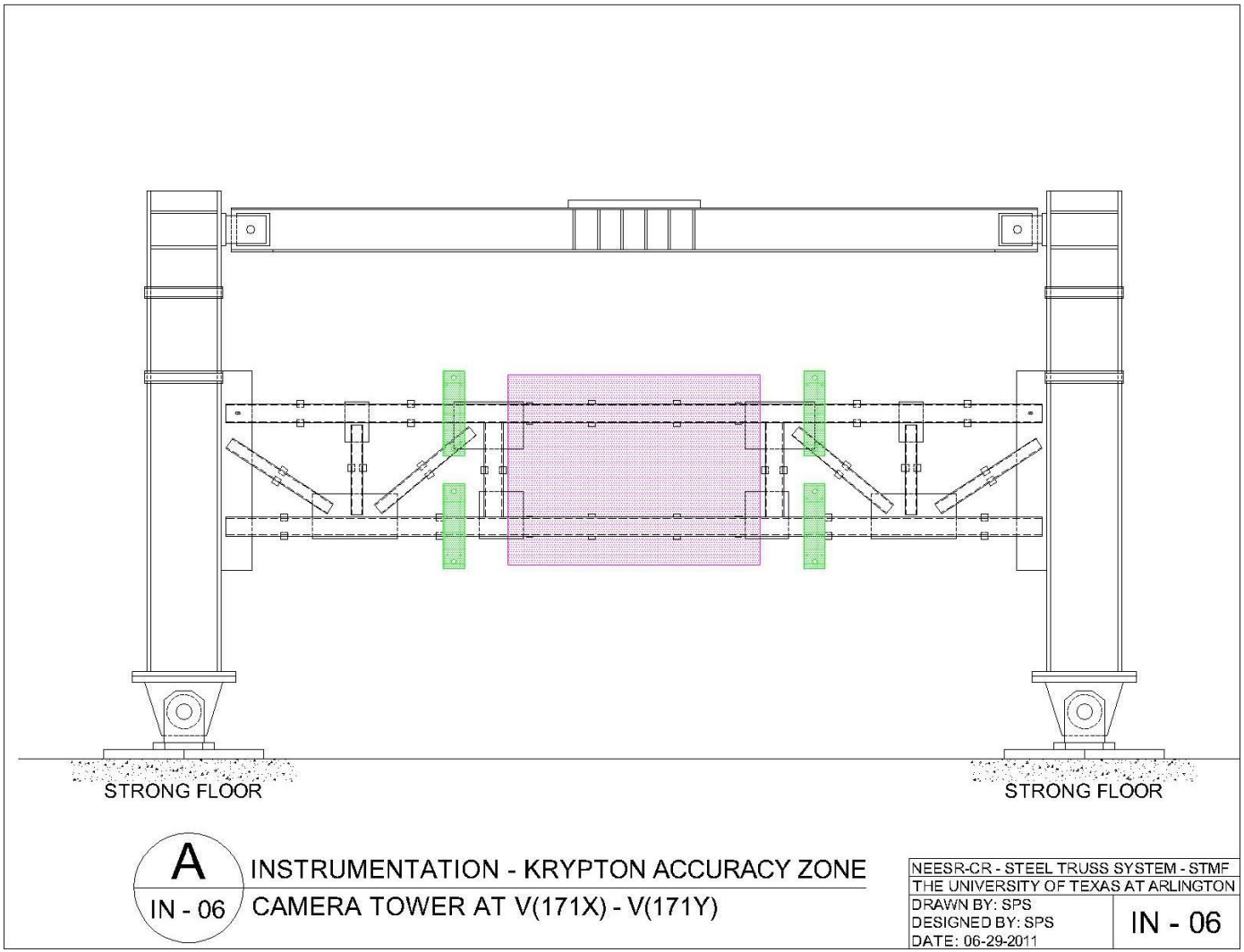

A
IN - 06

INSTRUMENTATION - KRYPTON ACCURACY ZONE
CAMERA TOWER AT V(171X) - V(171Y)

NEESR-CR - STEEL TRUSS SYSTEM - STMF	
THE UNIVERSITY OF TEXAS AT ARLINGTON	
DRAWN BY: SPS DESIGNED BY: SPS DATE: 06-29-2011	IN - 06

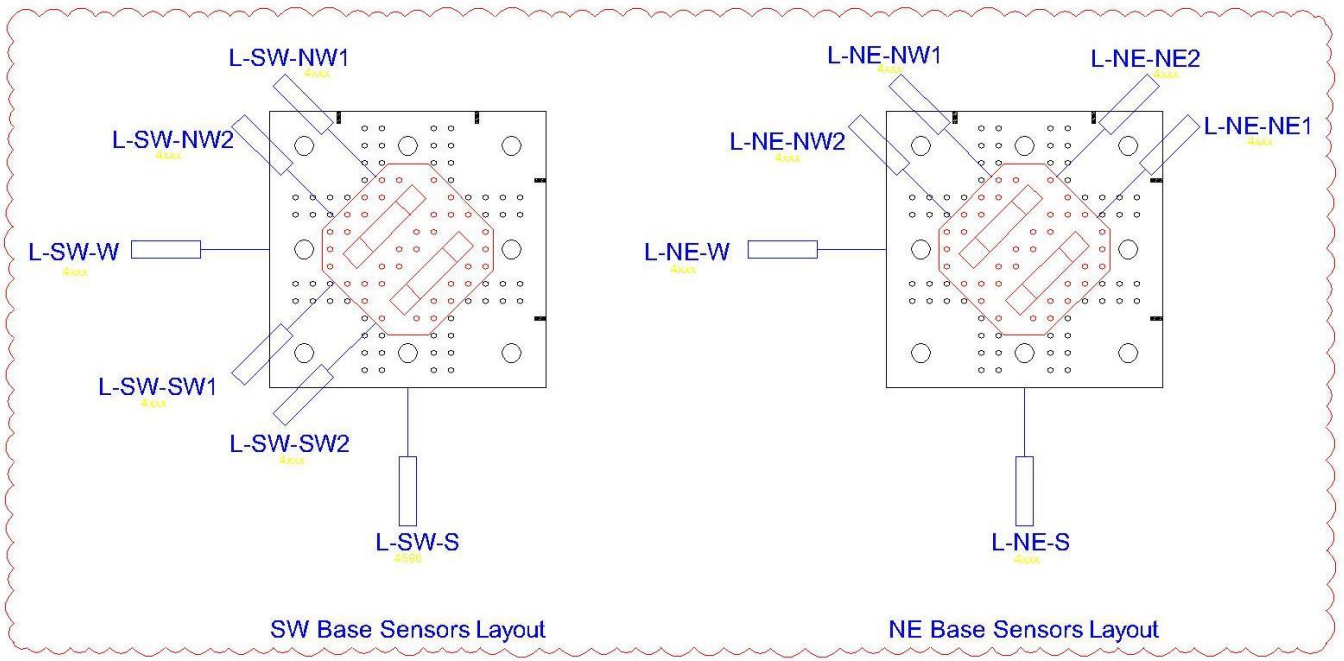

A
IN - 07

INSTRUMENTATION - LVDT LOCATIONS

NEESR-CR - STEEL TRUSS SYSTEM - STMF	
THE UNIVERSITY OF TEXAS AT ARLINGTON	
DRAWN BY: SPS DESIGNED BY: SPS DATE: 06-29-2013	IN - 07

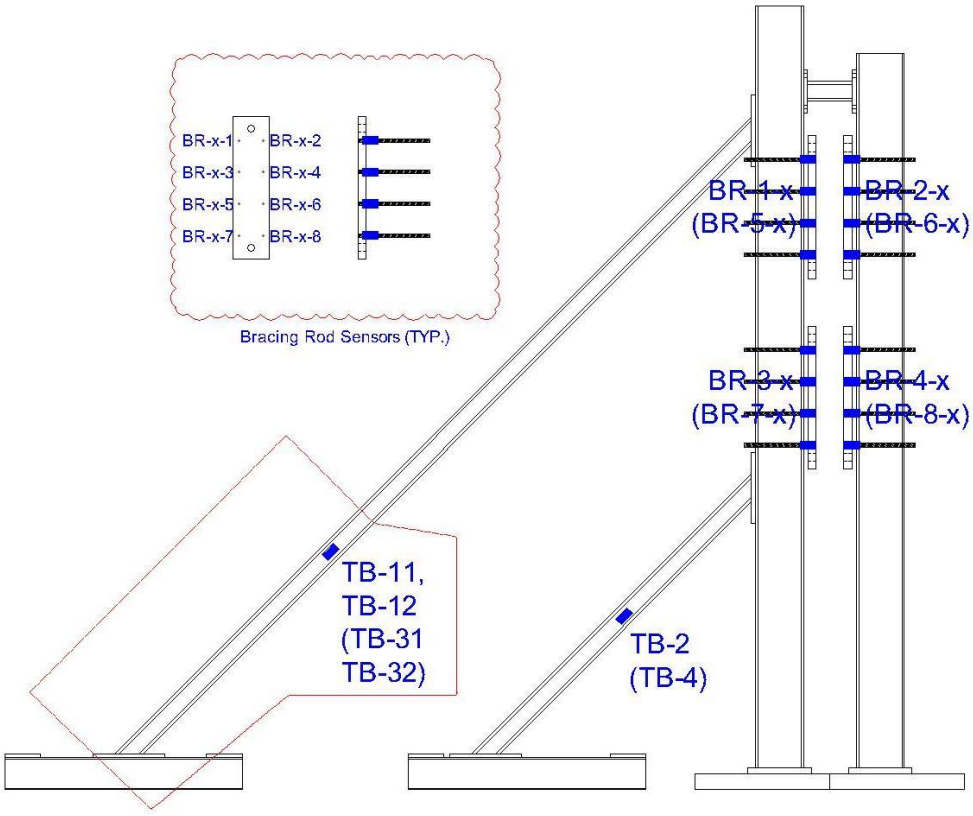

NE Truss Bracing - Strain Gauge Labels
Note: Strain Gauge Labels for SW Truss Bracing Shown in Parentheses

A
IN - 08

INSTRUMENTATION - TRUSS BRACING STRAIN GAUGE LOCATIONS

NEESR-CR - STEEL TRUSS SYSTEM - STMF	
THE UNIVERSITY OF TEXAS AT ARLINGTON	
DRAWN BY: SPS DESIGNED BY: SPS DATE: 06-29-2013	IN - 08

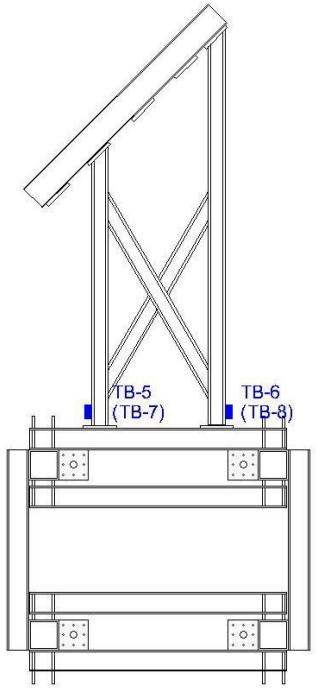

SW Column Lateral Support Bracing - Strain Gauge Labels
Note: Strain Gauge Labels for Lower Bracing Shown in Parentheses

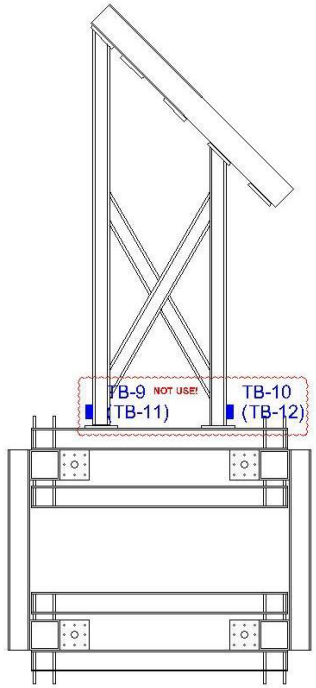

NE Column Lateral Support Bracing - Strain Gauge Labels
Note: Strain Gauge Labels for Lower Bracing Shown in Parentheses

A
IN - 09

INSTRUMENTATION - COLUMN BRACING
STRAIN GAUGE LOCATIONS

NEESR-CR - STEEL TRUSS SYSTEM - STMF	
THE UNIVERSITY OF TEXAS AT ARLINGTON	
DRAWN BY: SPS DESIGNED BY: SPS DATE: 06-29-2013	IN - 09

Appendix F

Strain vs. Story Drift Ratio Response of Strain Gauges on Threaded Rods in Lateral Bracing System

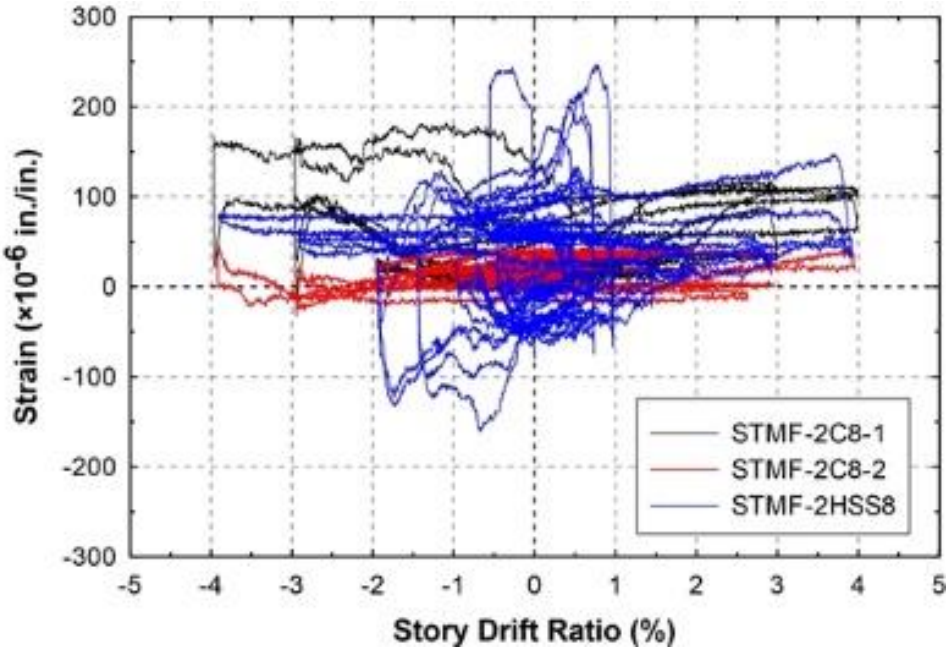
300
200
100
0
-100
-200
-300
-5
-4
-3
-2
-1
0
1
2
3
4
5
Strain (×10-6 in./in.)
Story Drift Ratio (%)
STMF-2C8-1
STMF-2C8-2
STMF-2HSS8

BR-1-1

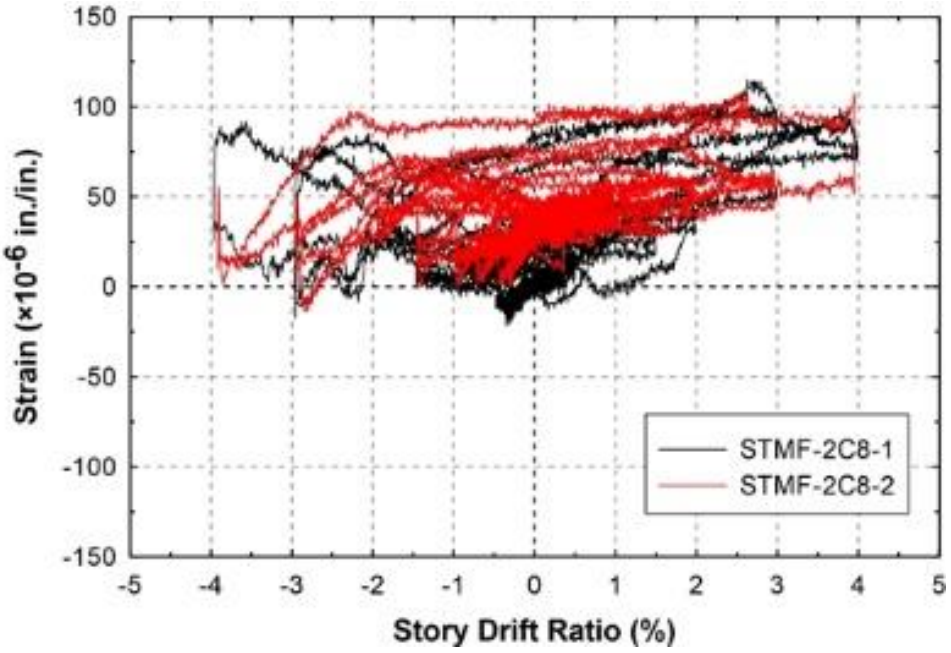
150
100
50
0
-50
-100
-150
-5
-4
-3
-2
-1
0
1
2
3
4
5
Strain (×10-6 in./in.)
Story Drift Ratio (%)
STMF-2C8-1
STMF-2C8-2

BR-1-2

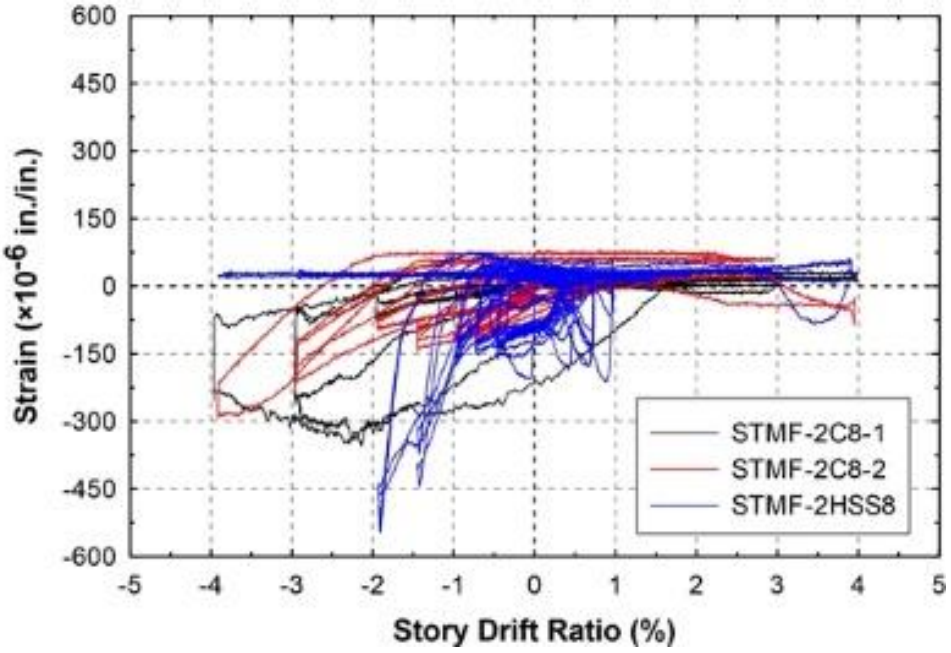
600
450
300
150
0
-150
-300
-450
-600
-5
-4
-3
-2
-1
0
1
2
3
4
5
Strain (×10-6 in./in.)
Story Drift Ratio (%)
STMF-2C8-1
STMF-2C8-2
STMF-2HSS8

BR-1-3

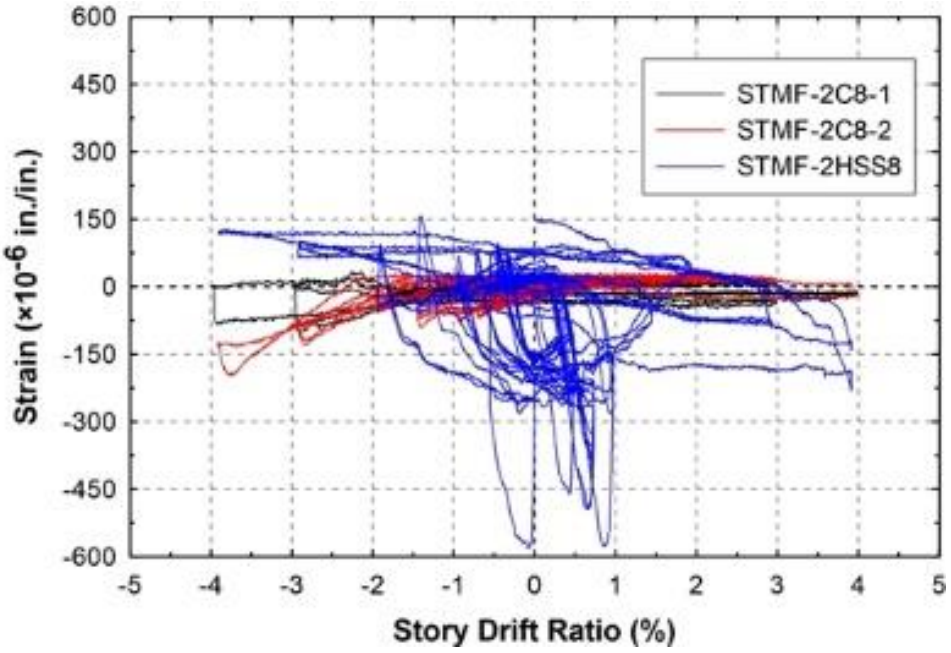
600
450
300
150
0
-150
-300
-450
-600
-5
-4
-3
-2
-1
0
1
2
3
4
5
Strain (×10-6 in./in.)
Story Drift Ratio (%)
STMF-2C8-1
STMF-2C8-2
STMF-2HSS8

BR-1-4

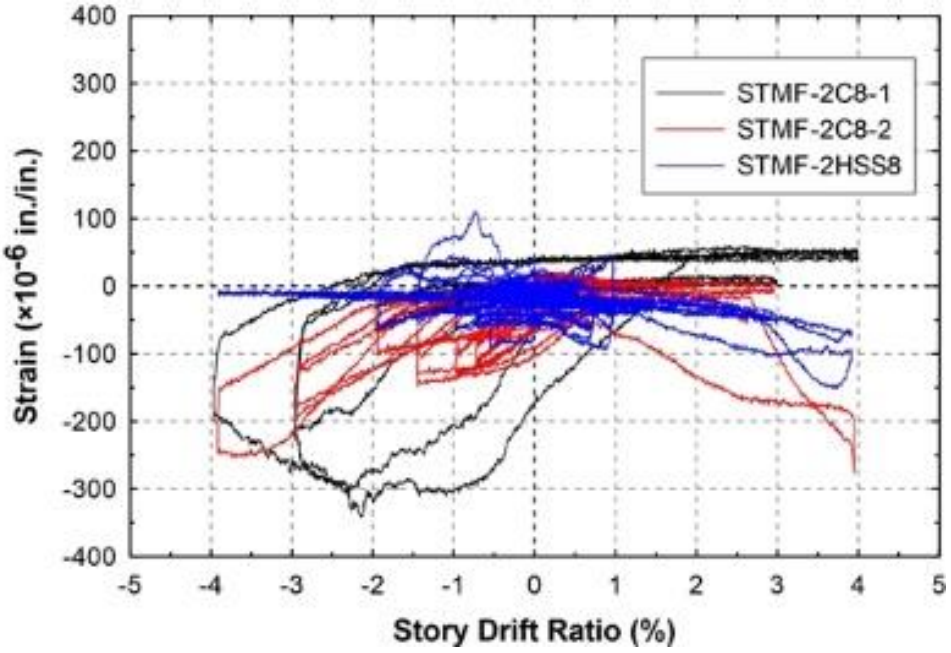
STMF-2C8-1
STMF-2C8-2
STMF-2HSS8
Strain (×10-6 in./in.)
Story Drift Ratio (%)

BR-1-5

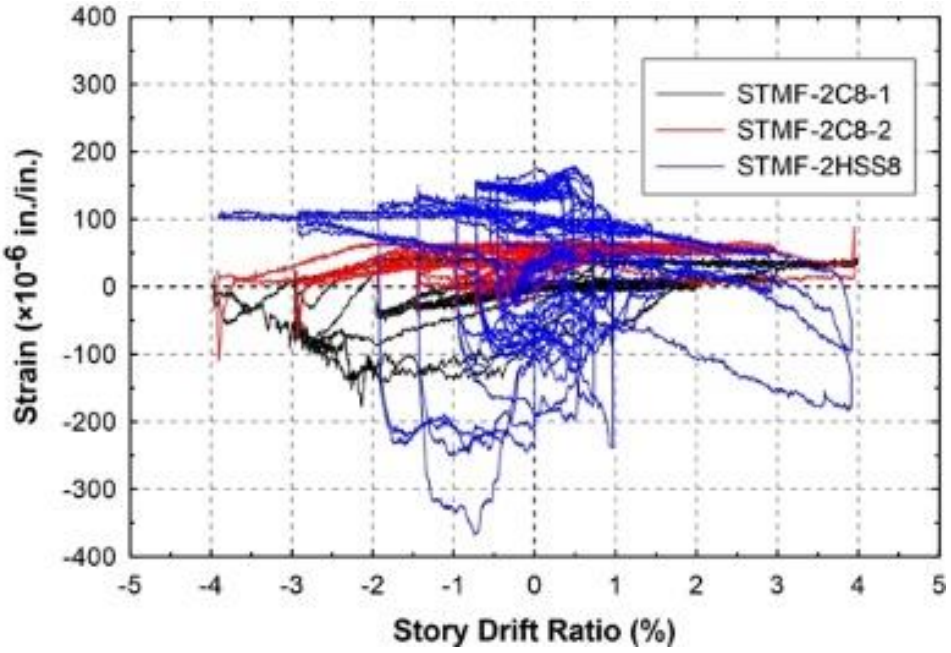
STMF-2C8-1
STMF-2C8-2
STMF-2HSS8
Strain (×10-6 in./in.)
Story Drift Ratio (%)

BR-1-6

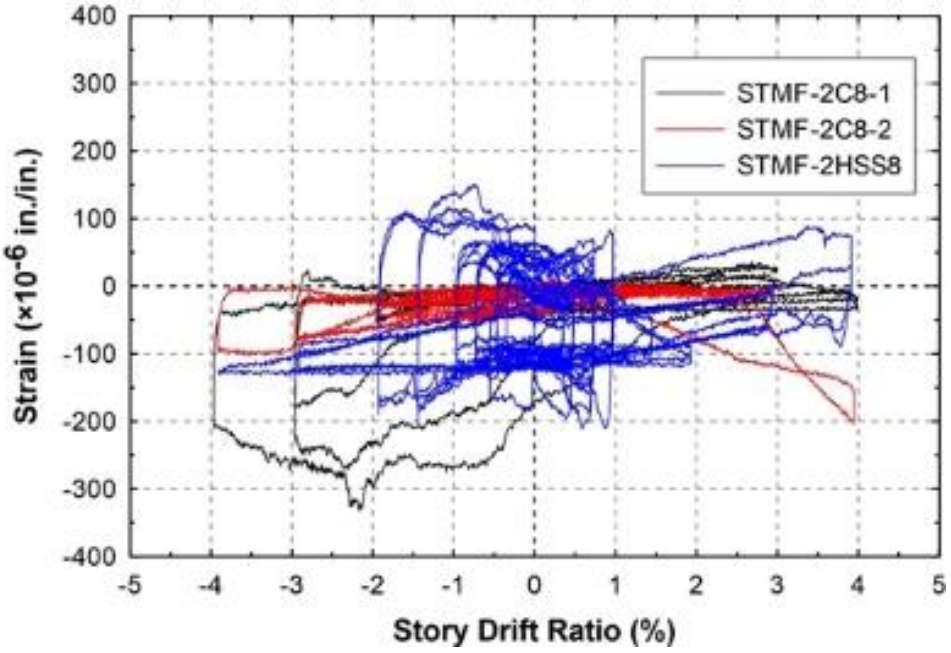
STMF-2C8-1
STMF-2C8-2
STMF-2HSS8
Strain (×10-6 in./in.)
Story Drift Ratio (%)

BR-1-7

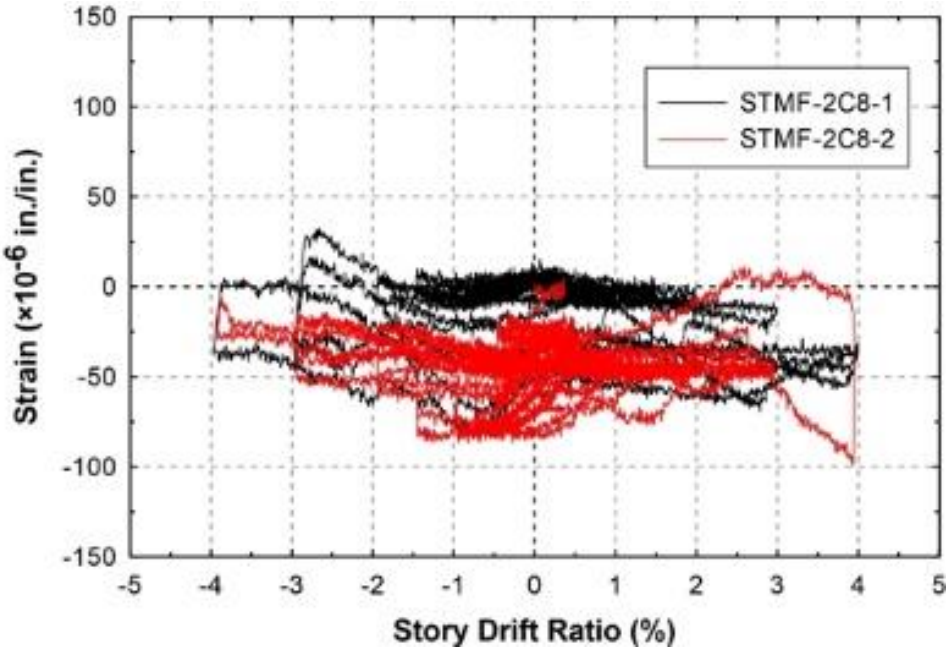
STMF-2C8-1
STMF-2C8-2
Strain (×10-6 in./in.)
Story Drift Ratio (%)

BR-1-8

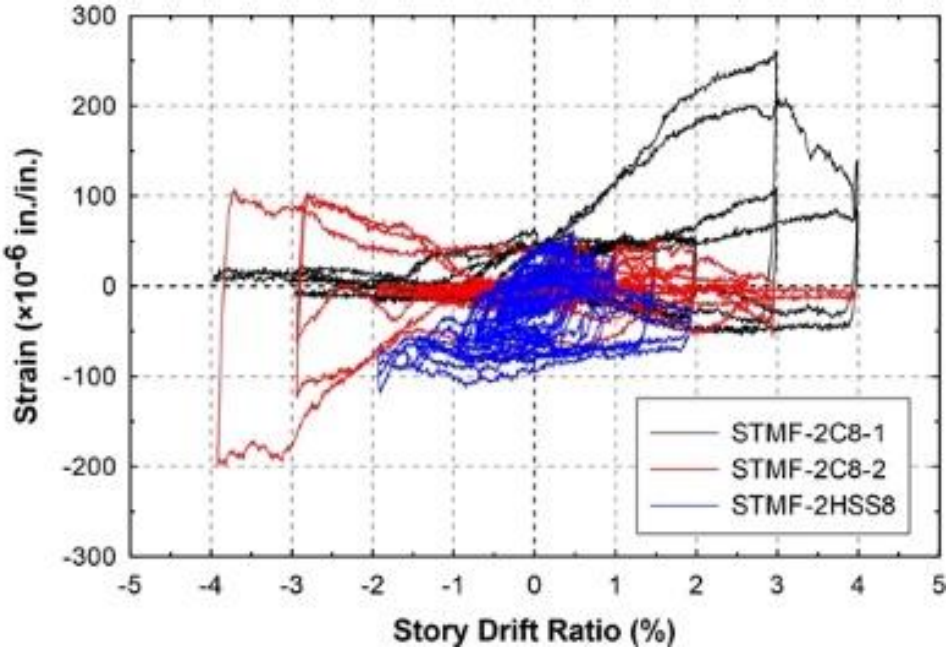
300
200
100
0
-100
-200
-300
-5
-4
-3
-2
-1
0
1
2
3
4
5
Strain (×10-6 in./in.)
Story Drift Ratio (%)
STMF-2C8-1
STMF-2C8-2
STMF-2HSS8

BR-2-1

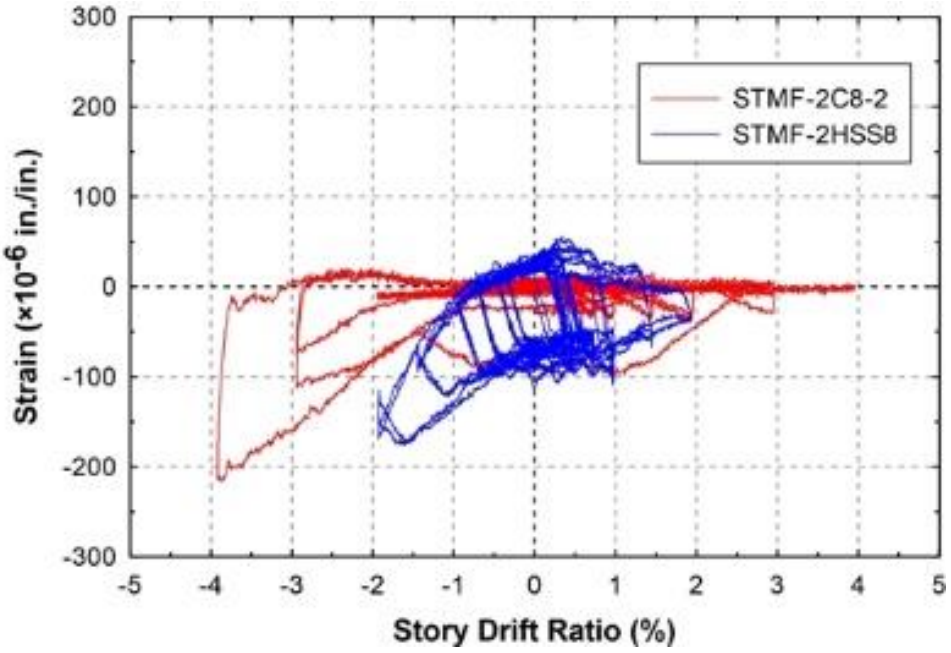
300
200
100
0
-100
-200
-300
-5
-4
-3
-2
-1
0
1
2
3
4
5
Strain (×10-6 in./in.)
Story Drift Ratio (%)
STMF-2C8-2
STMF-2HSS8

BR-2-2

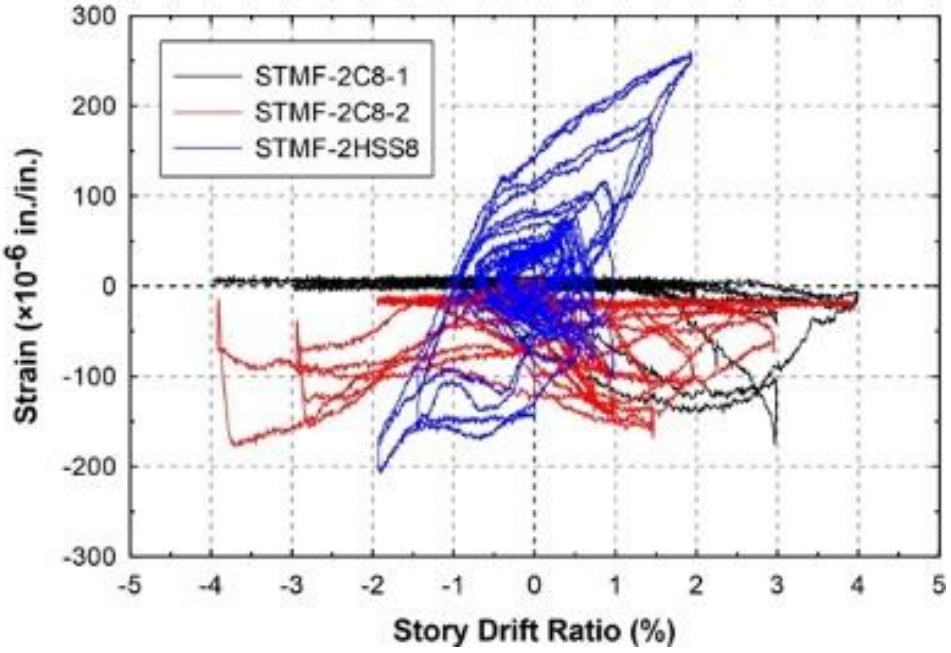
STMF-2C8-1
STMF-2C8-2
STMF-2HSS8
Strain (×10-6 in./in.)
Story Drift Ratio (%)

BR-2-3

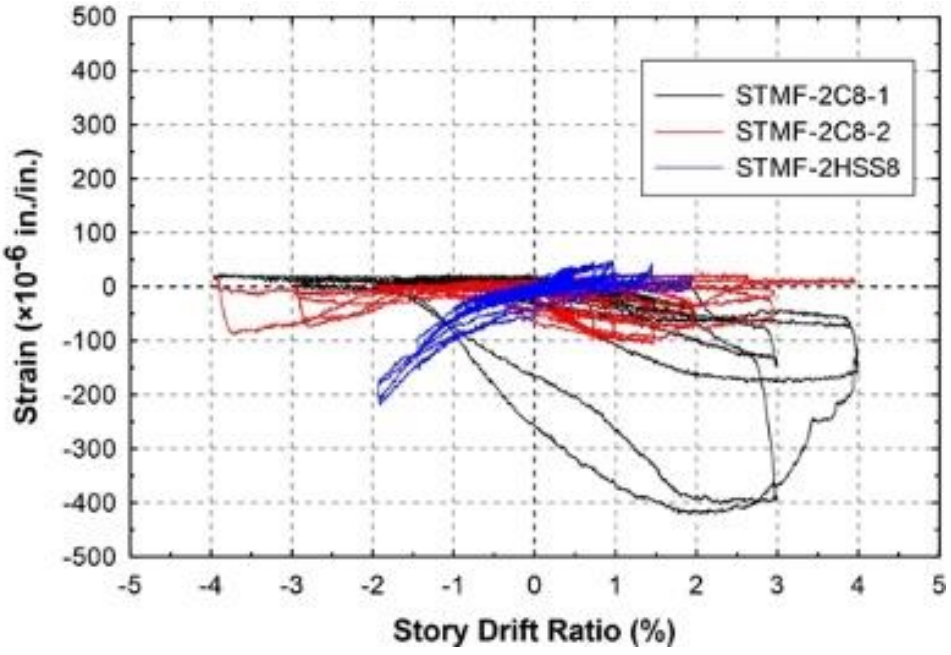
STMF-2C8-1
STMF-2C8-2
STMF-2HSS8
Strain (×10-6 in./in.)
Story Drift Ratio (%)

BR-2-4

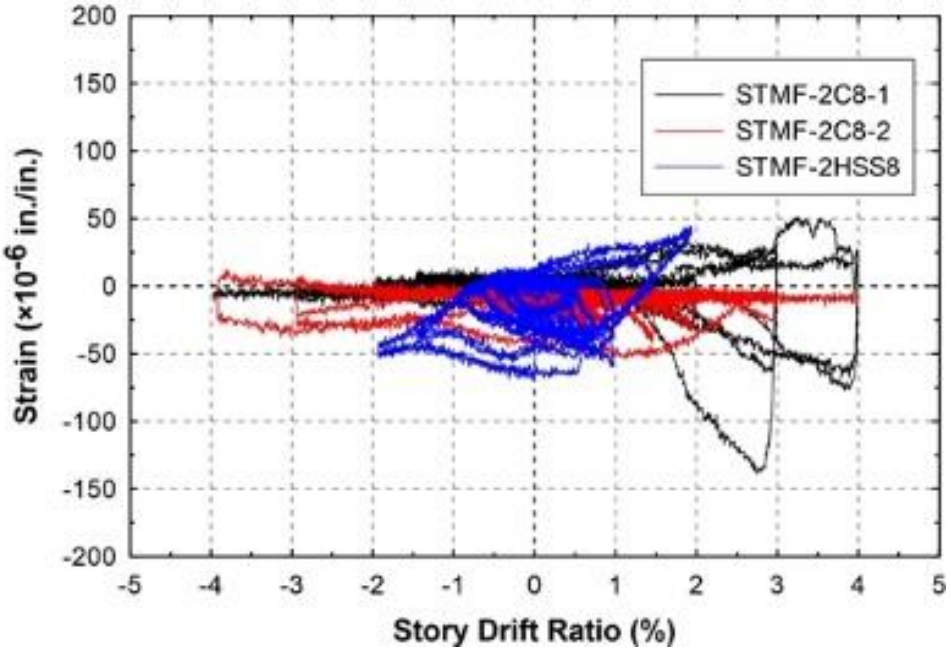
STMF-2C8-1
STMF-2C8-2
STMF-2HSS8
Strain (×10-6 in./in.)
Story Drift Ratio (%)

BR-2-5

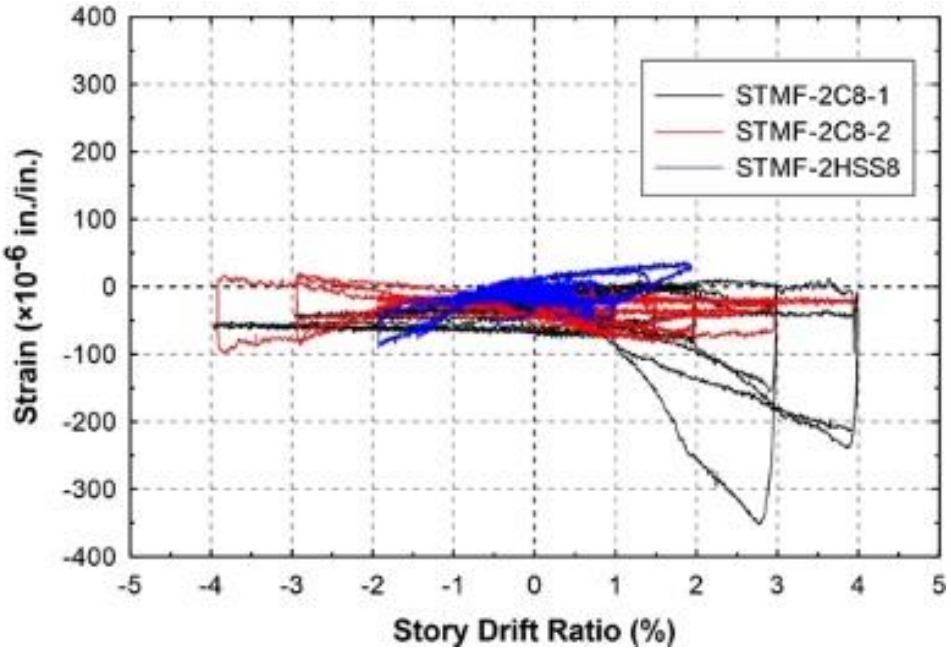
STMF-2C8-1
STMF-2C8-2
STMF-2HSS8
Strain (×10-6 in./in.)
Story Drift Ratio (%)

BR-2-6

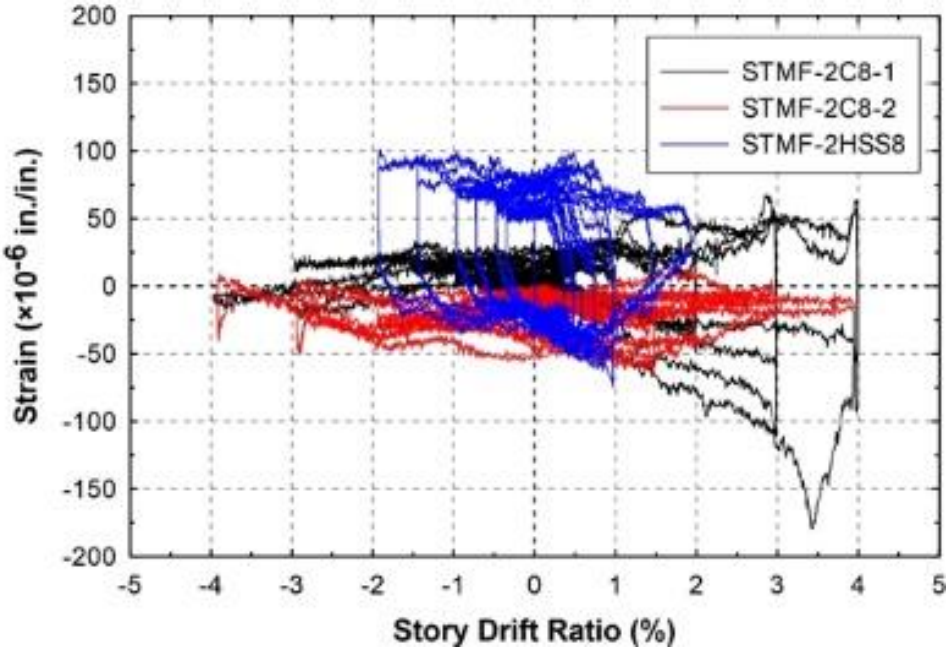
STMF-2C8-1
STMF-2C8-2
STMF-2HSS8
Strain (×10-6 in./in.)
Story Drift Ratio (%)

BR-2-7

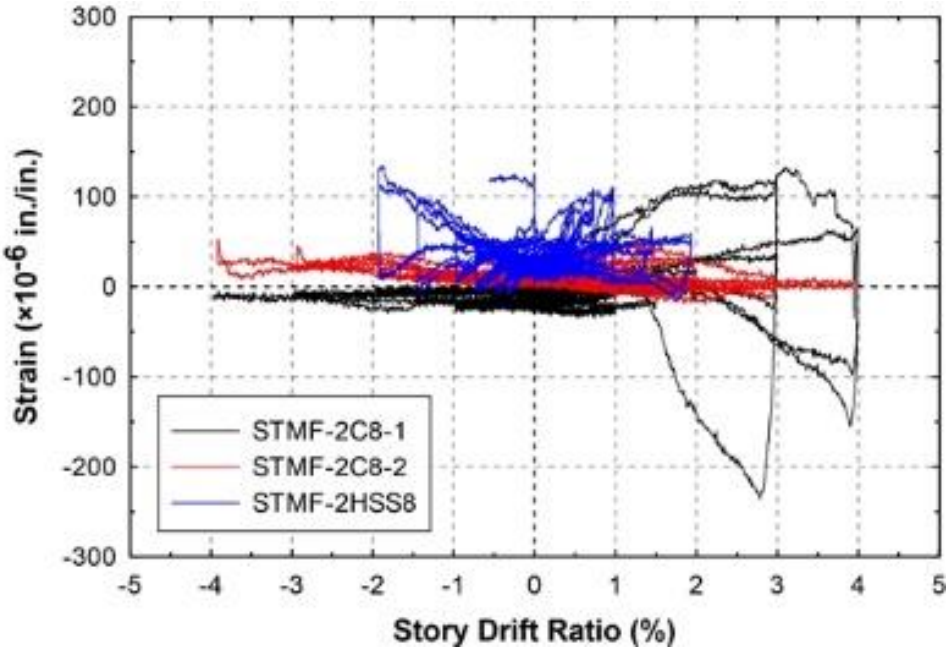
STMF-2C8-1
STMF-2C8-2
STMF-2HSS8
Strain (×10-6 in./in.)
Story Drift Ratio (%)

BR-2-8

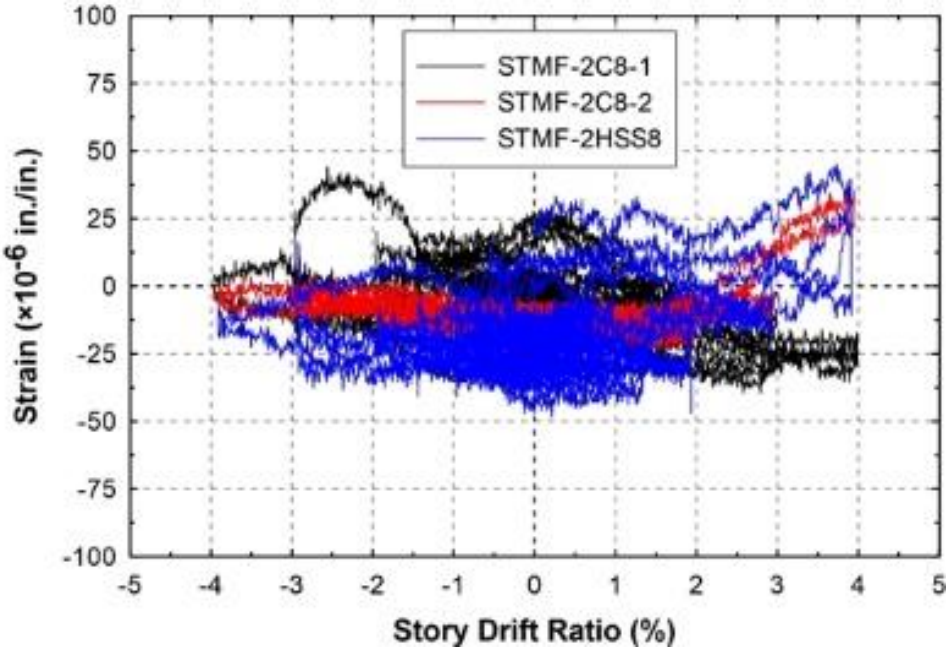
STMF-2C8-1
STMF-2C8-2
STMF-2HSS8
Strain (×10-6 in./in.)
Story Drift Ratio (%)
100
75
50
25
0
-25
-50
-75
-100
-5
-4
-3
-2
-1
0
1
2
3
4
5

BR-3-1

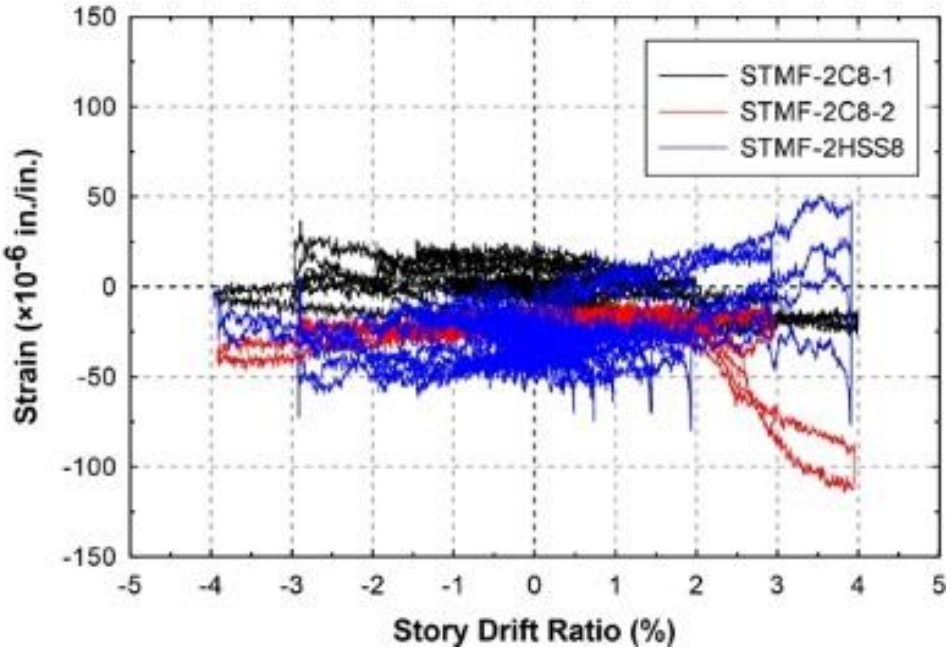
STMF-2C8-1
STMF-2C8-2
STMF-2HSS8
Strain (×10-6 in./in.)
Story Drift Ratio (%)
150
100
50
0
-50
-100
-150
-5
-4
-3
-2
-1
0
1
2
3
4
5

BR-3-2

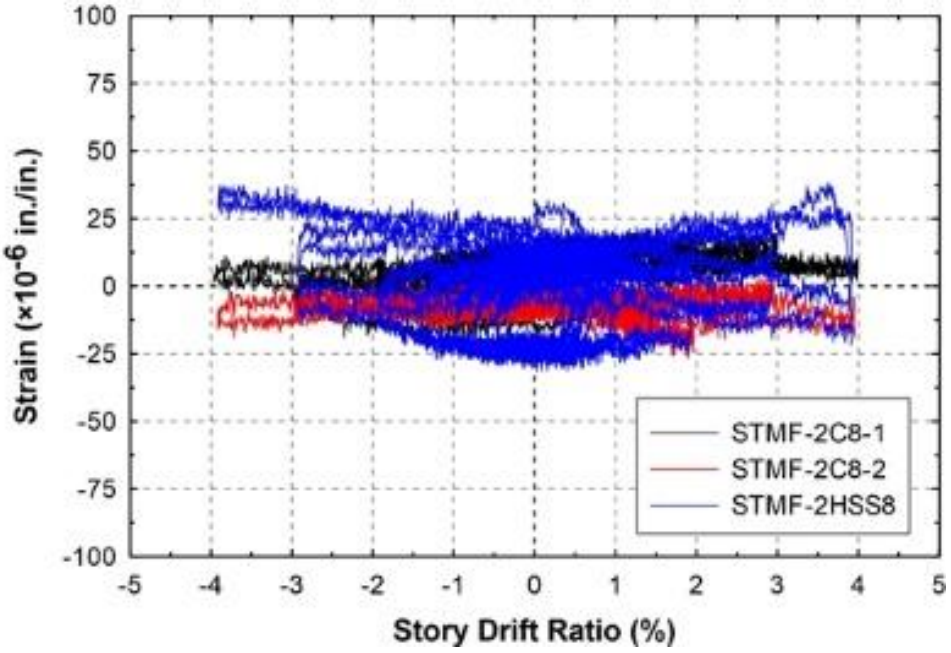
Strain (×10-6 in./in.)
Story Drift Ratio (%)
STMF-2C8-1
STMF-2C8-2
STMF-2HSS8

BR-3-3

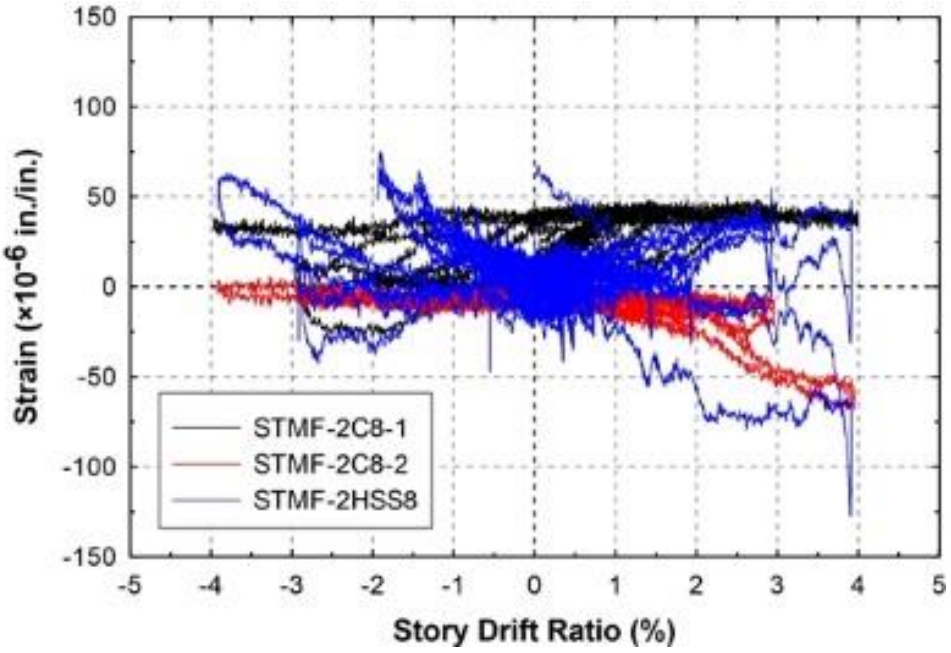
Strain (×10-6 in./in.)
Story Drift Ratio (%)
STMF-2C8-1
STMF-2C8-2
STMF-2HSS8

BR-3-4

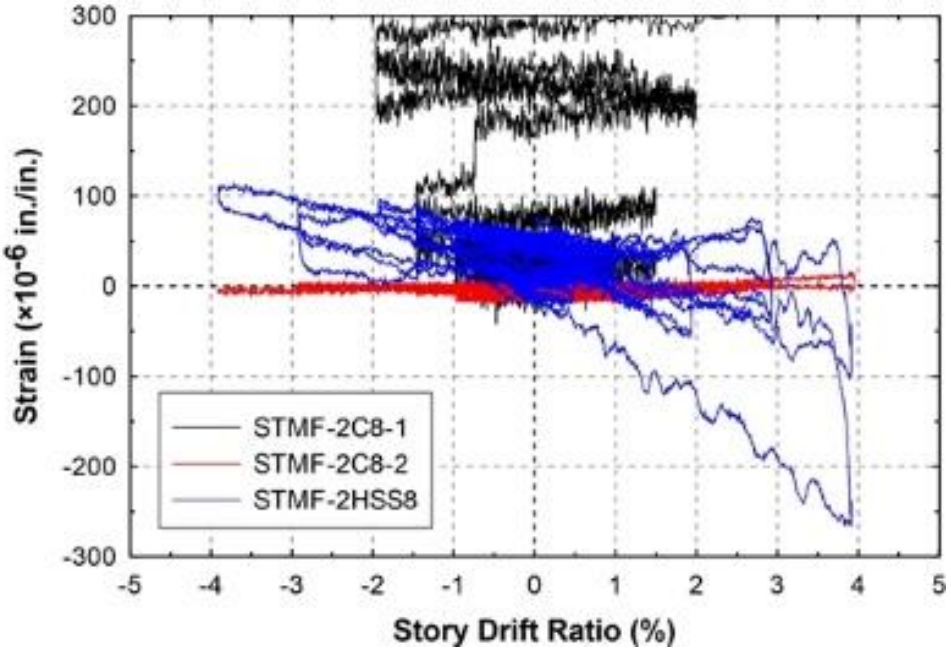
300
200
100
0
-100
-200
-300
-5
-4
-3
-2
-1
0
1
2
3
4
5
Strain (×10-6 in./in.)
Story Drift Ratio (%)
STMF-2C8-1
STMF-2C8-2
STMF-2HSS8

BR-3-5

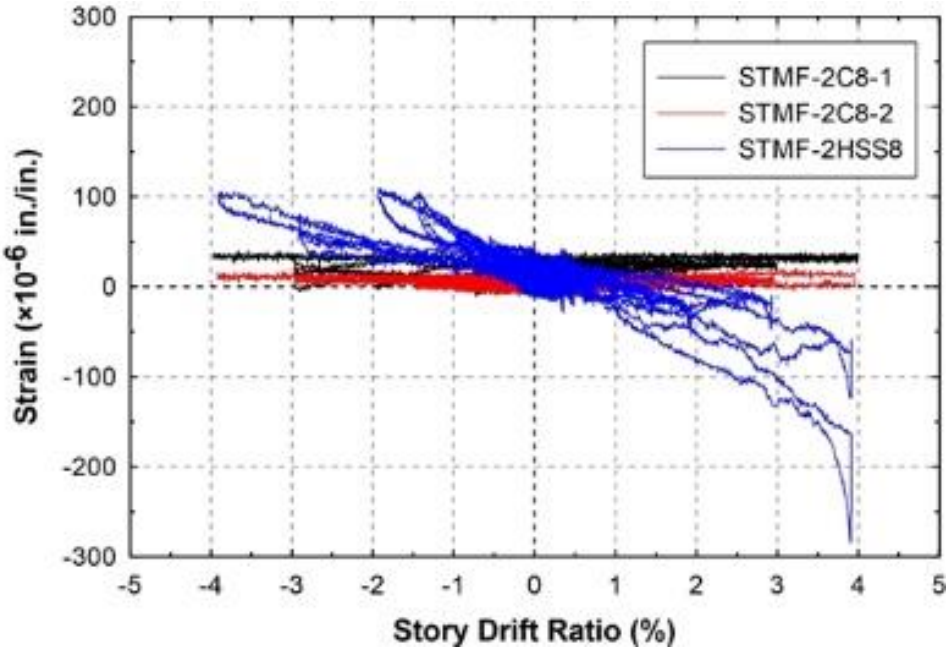
300
200
100
0
-100
-200
-300
-5
-4
-3
-2
-1
0
1
2
3
4
5
Strain (×10-6 in./in.)
Story Drift Ratio (%)
STMF-2C8-1
STMF-2C8-2
STMF-2HSS8

BR-3-6

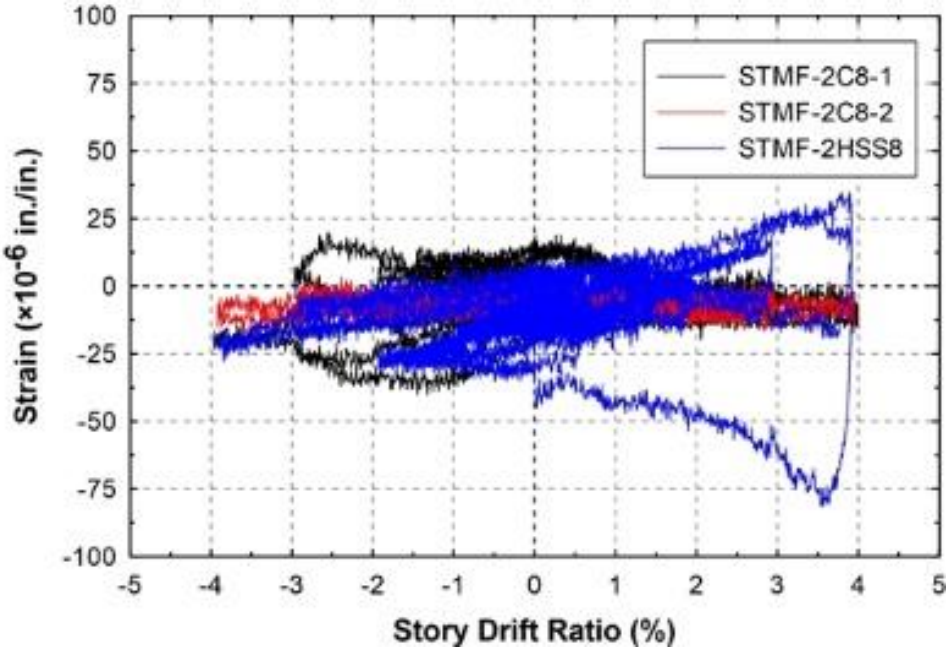
STMF-2C8-1
STMF-2C8-2
STMF-2HSS8
Strain (×10-6 in./in.)
Story Drift Ratio (%)
100
75
50
25
0
-25
-50
-75
-100
-5
-4
-3
-2
-1
0
1
2
3
4
5

BR-3-7

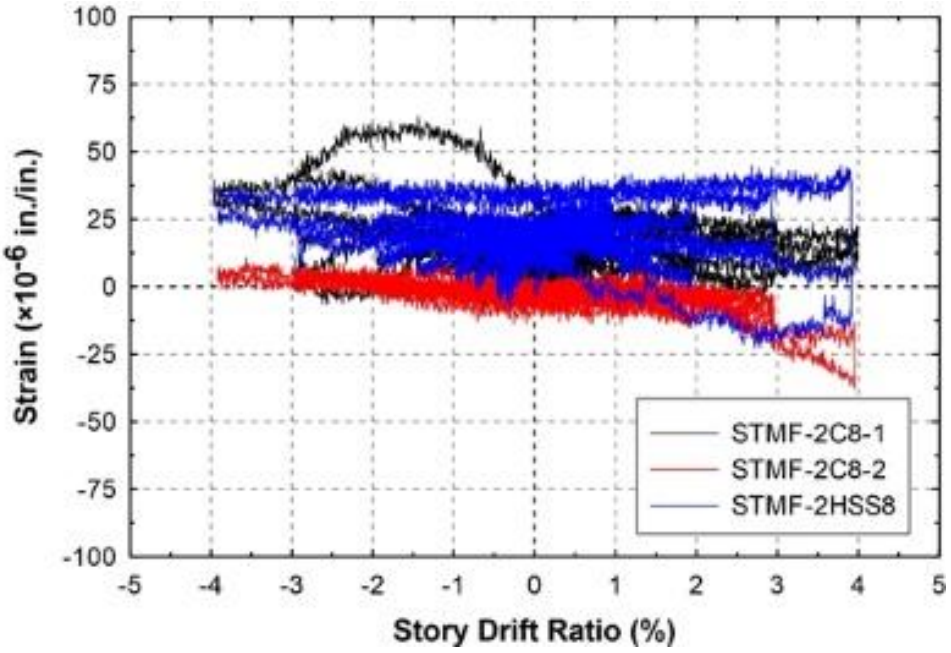
STMF-2C8-1
STMF-2C8-2
STMF-2HSS8
Strain (×10-6 in./in.)
Story Drift Ratio (%)
100
75
50
25
0
-25
-50
-75
-100
-5
-4
-3
-2
-1
0
1
2
3
4
5

BR-3-8

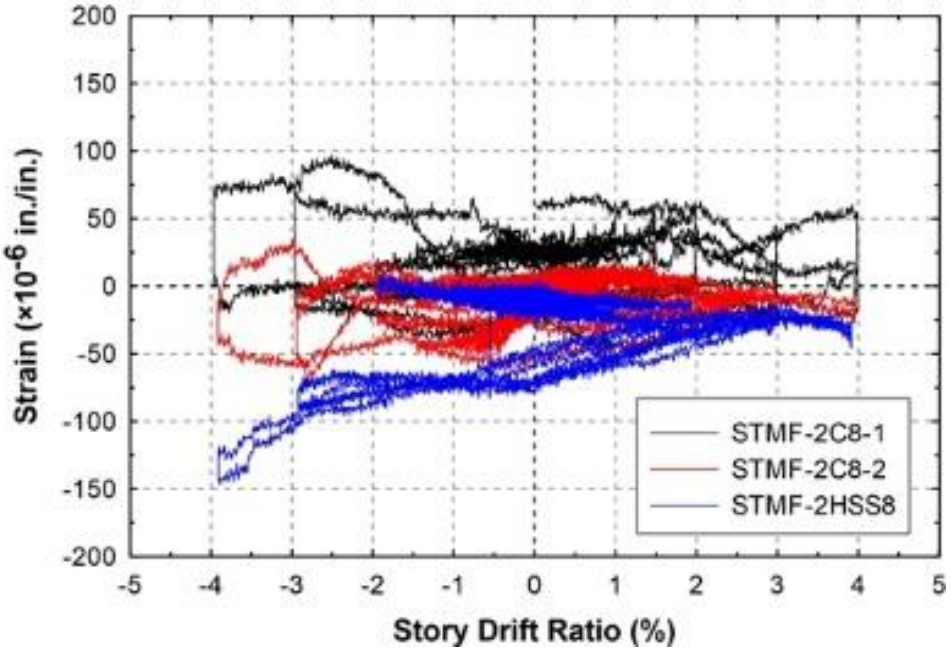
Strain (×10-6 in./in.)
Story Drift Ratio (%)
STMF-2C8-1
STMF-2C8-2
STMF-2HSS8

BR-4-1

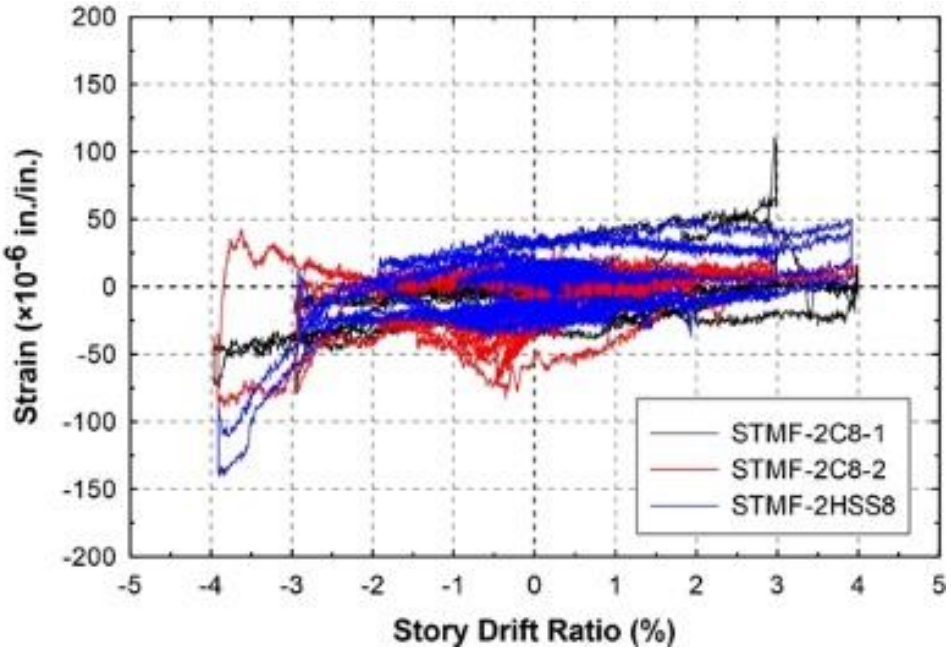
Strain (×10-6 in./in.)
Story Drift Ratio (%)
STMF-2C8-1
STMF-2C8-2
STMF-2HSS8

BR-4-2

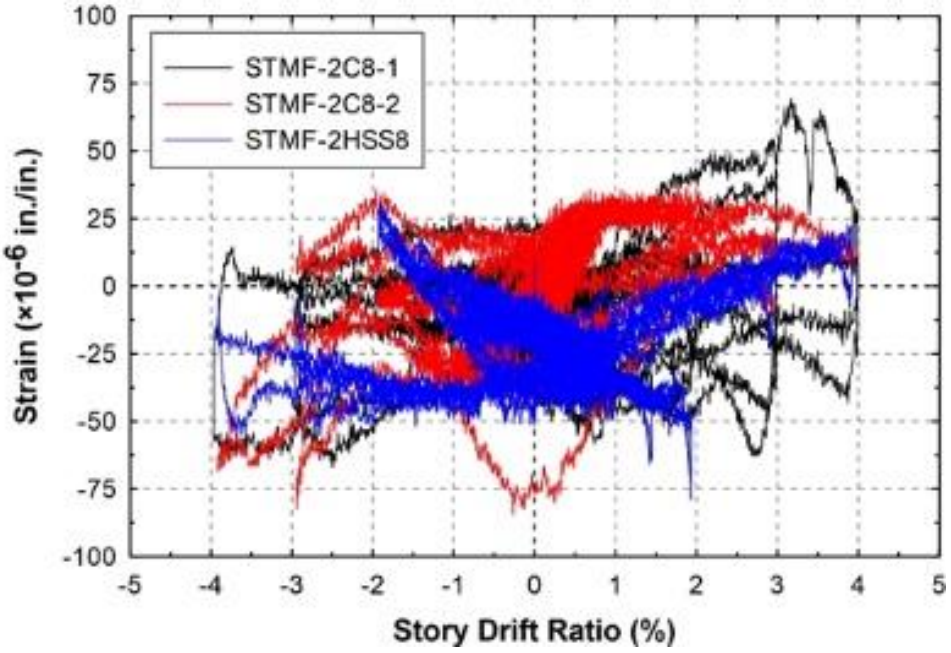
STMF-2C8-1
STMF-2C8-2
STMF-2HSS8
Strain (×10-6 in./in.)
Story Drift Ratio (%)
100
75
50
25
0
-25
-50
-75
-100
-5
-4
-3
-2
-1
0
1
2
3
4
5

BR-4-3

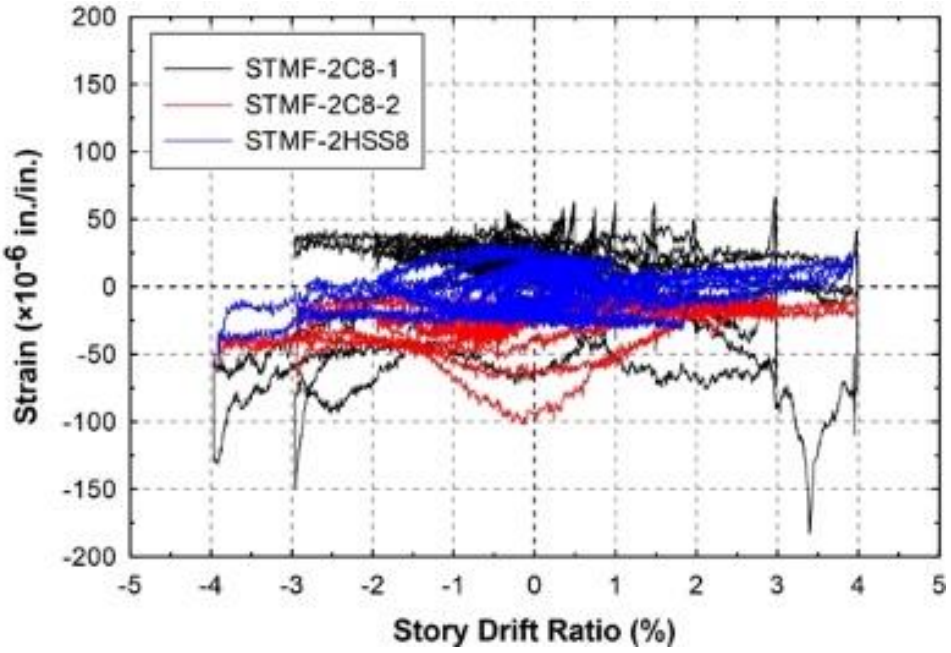
STMF-2C8-1
STMF-2C8-2
STMF-2HSS8
Strain (×10-6 in./in.)
Story Drift Ratio (%)
200
150
100
50
0
-50
-100
-150
-200
-5
-4
-3
-2
-1
0
1
2
3
4
5

BR-4-4

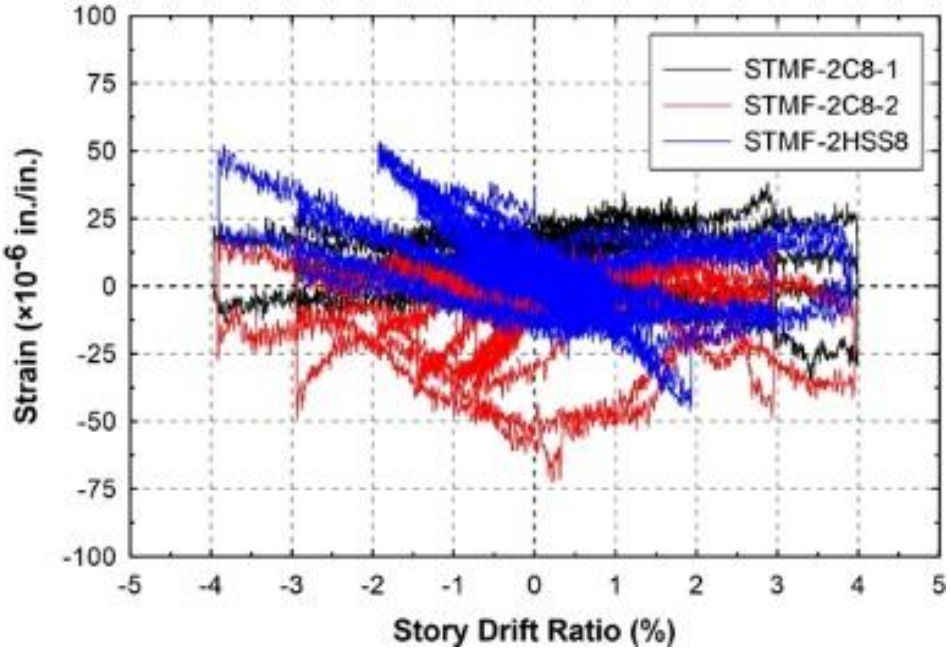
STMF-2C8-1
STMF-2C8-2
STMF-2HSS8
Strain (×10-6 in./in.)
Story Drift Ratio (%)
100
75
50
25
0
-25
-50
-75
-100
-5
-4
-3
-2
-1
0
1
2
3
4
5

BR-4-5

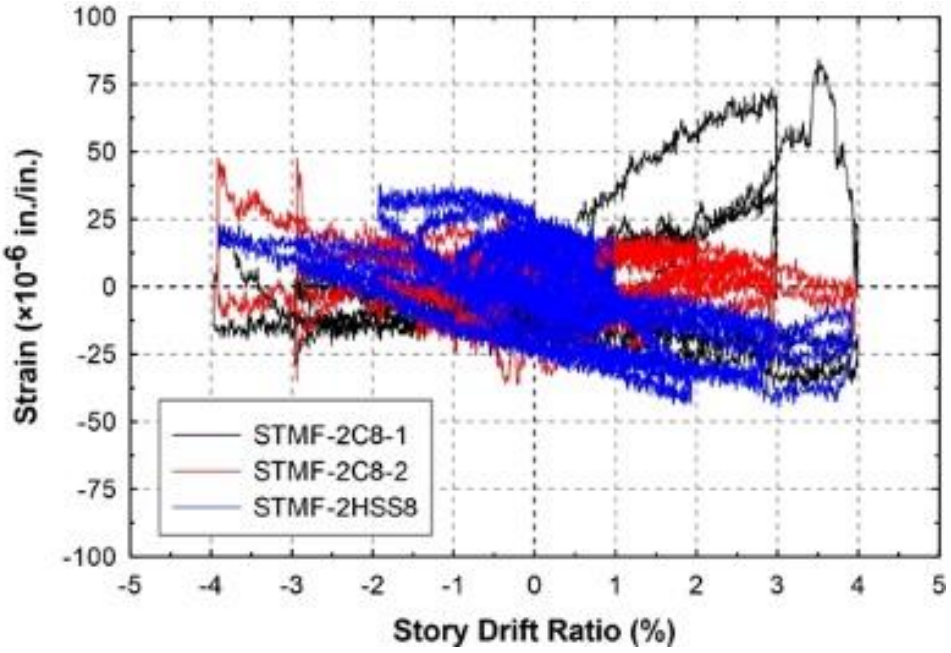
STMF-2C8-1
STMF-2C8-2
STMF-2HSS8
Strain (×10-6 in./in.)
Story Drift Ratio (%)
100
75
50
25
0
-25
-50
-75
-100
-5
-4
-3
-2
-1
0
1
2
3
4
5

BR-4-6

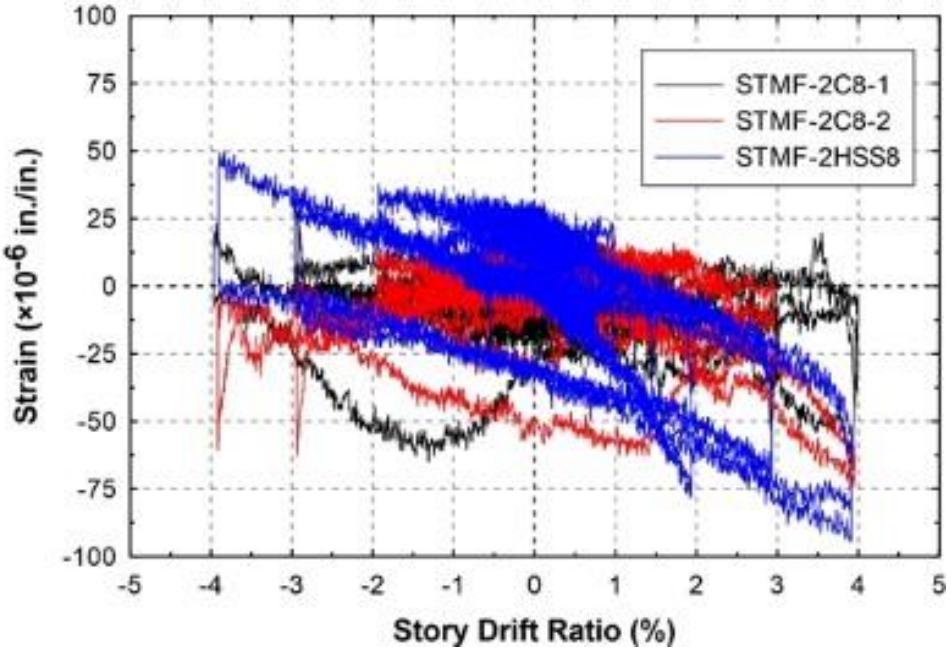
STMF-2C8-1
STMF-2C8-2
STMF-2HSS8
Strain (×10-6 in./in.)
Story Drift Ratio (%)

BR-4-7

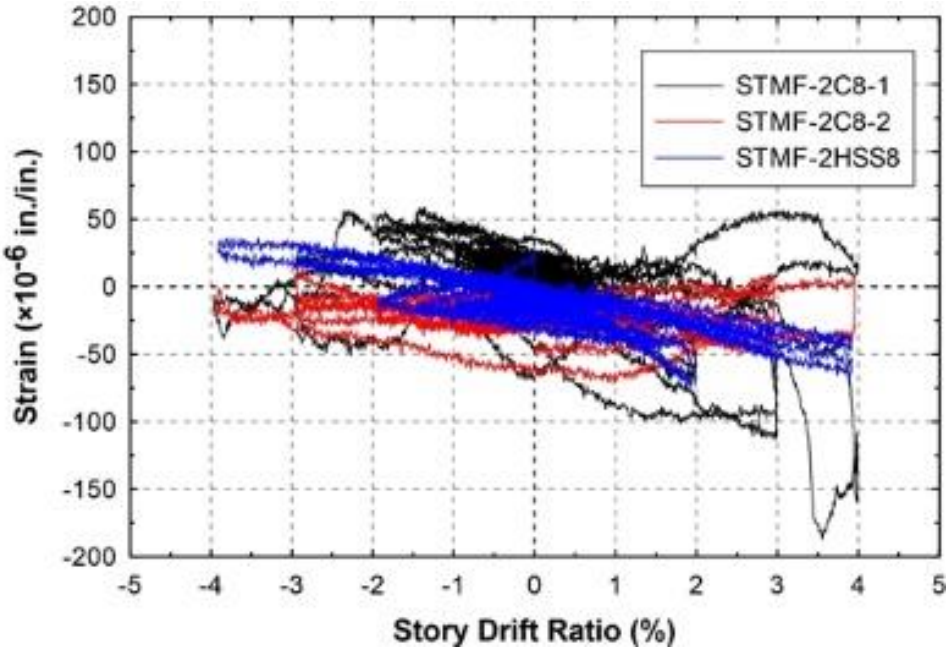
STMF-2C8-1
STMF-2C8-2
STMF-2HSS8
Strain (×10-6 in./in.)
Story Drift Ratio (%)

BR-4-8

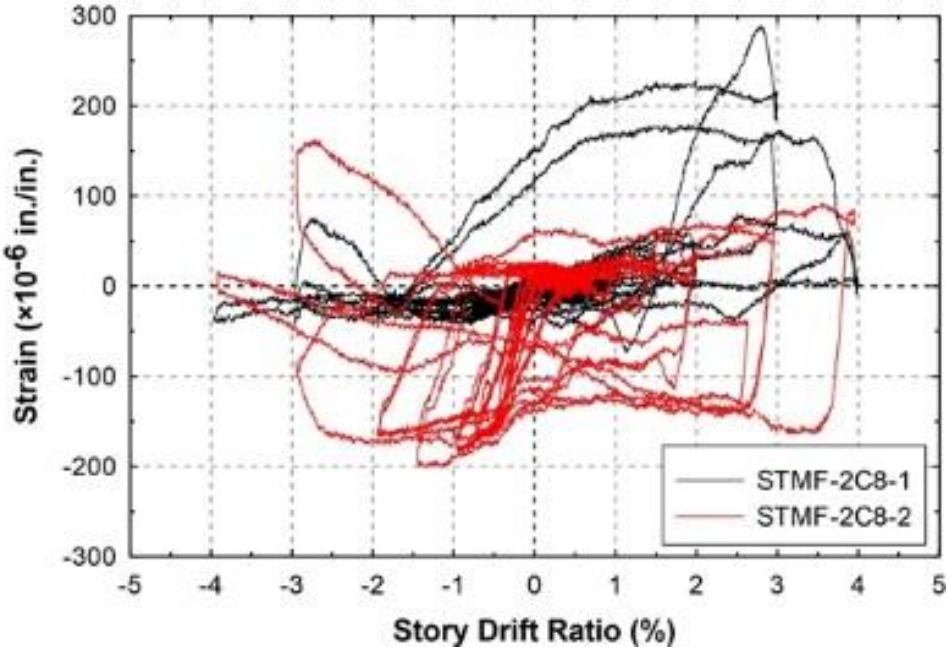
Strain (×10-6 in./in.)
Story Drift Ratio (%)
STMF-2C8-1
STMF-2C8-2

BR-5-1

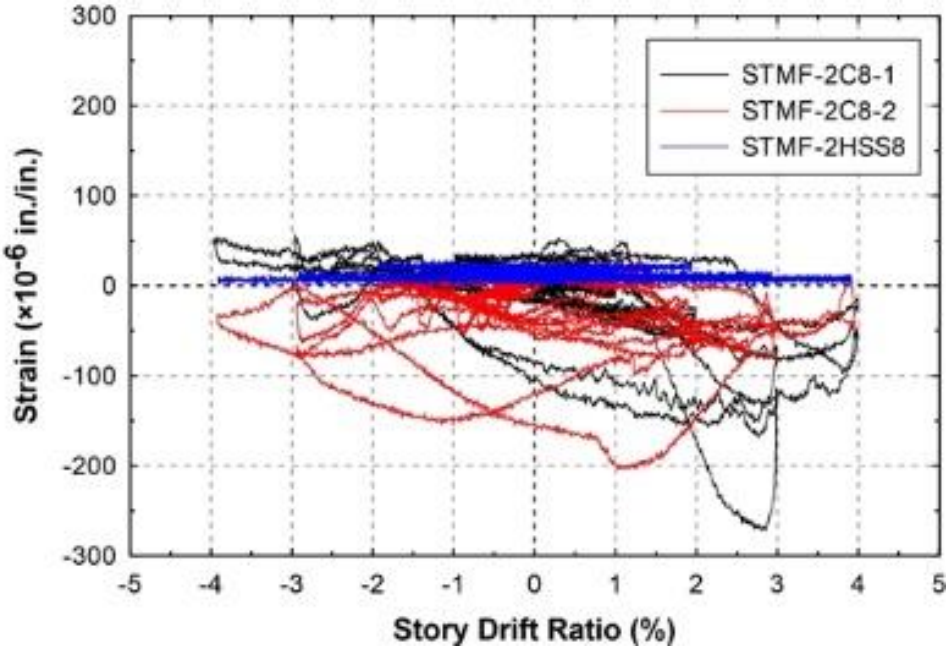
Strain (×10-6 in./in.)
Story Drift Ratio (%)
STMF-2C8-1
STMF-2C8-2
STMF-2HSS8

BR-5-2

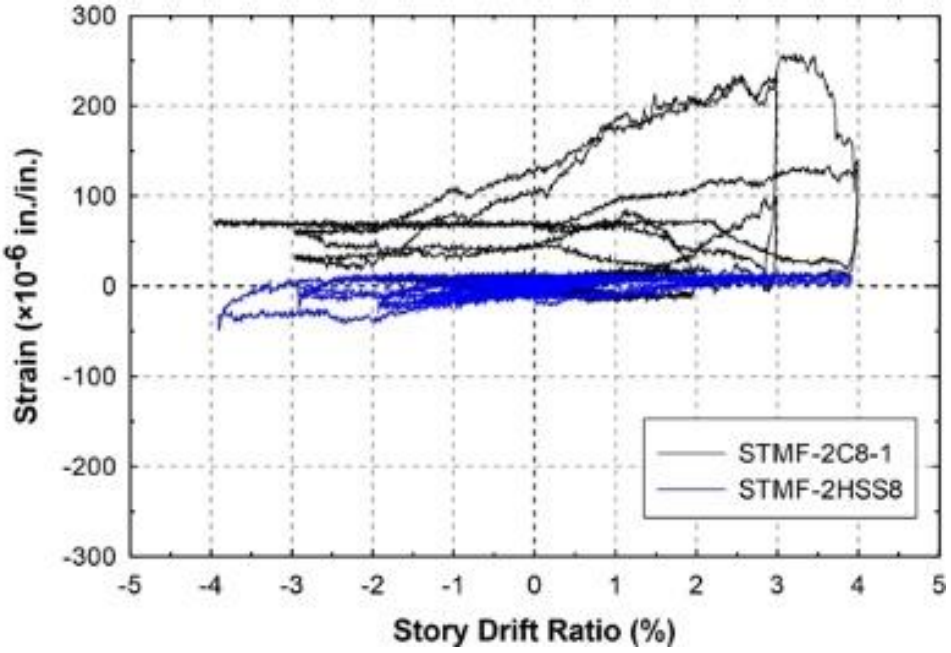
300
200
100
0
-100
-200
-300
-5
-4
-3
-2
-1
0
1
2
3
4
5
Strain (×10-6 in./in.)
Story Drift Ratio (%)
STMF-2C8-1
STMF-2HSS8

BR-5-3

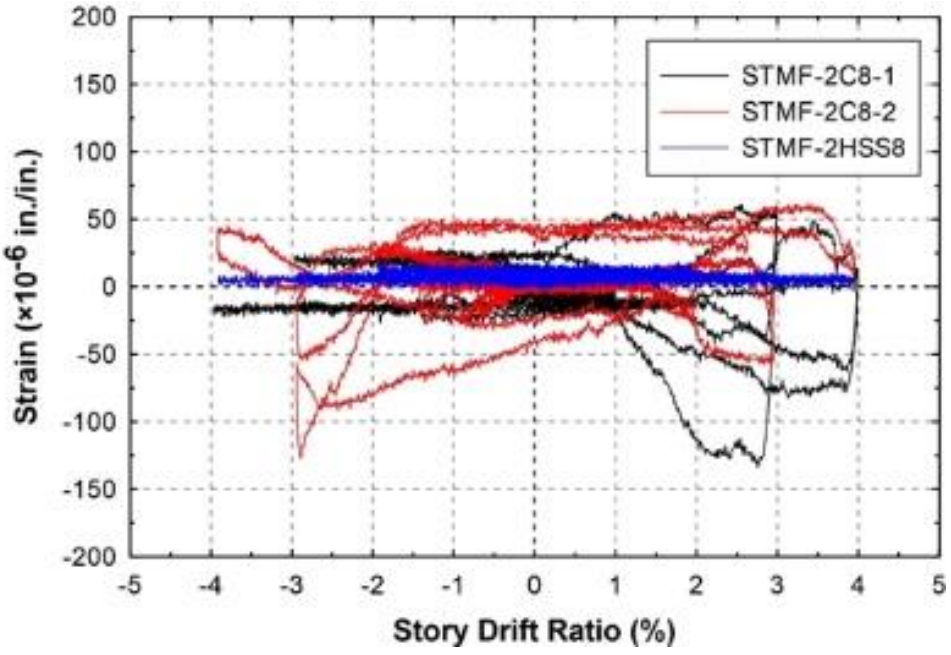
200
150
100
50
0
-50
-100
-150
-200
-5
-4
-3
-2
-1
0
1
2
3
4
5
Strain (×10-6 in./in.)
Story Drift Ratio (%)
STMF-2C8-1
STMF-2C8-2
STMF-2HSS8

BR-5-4

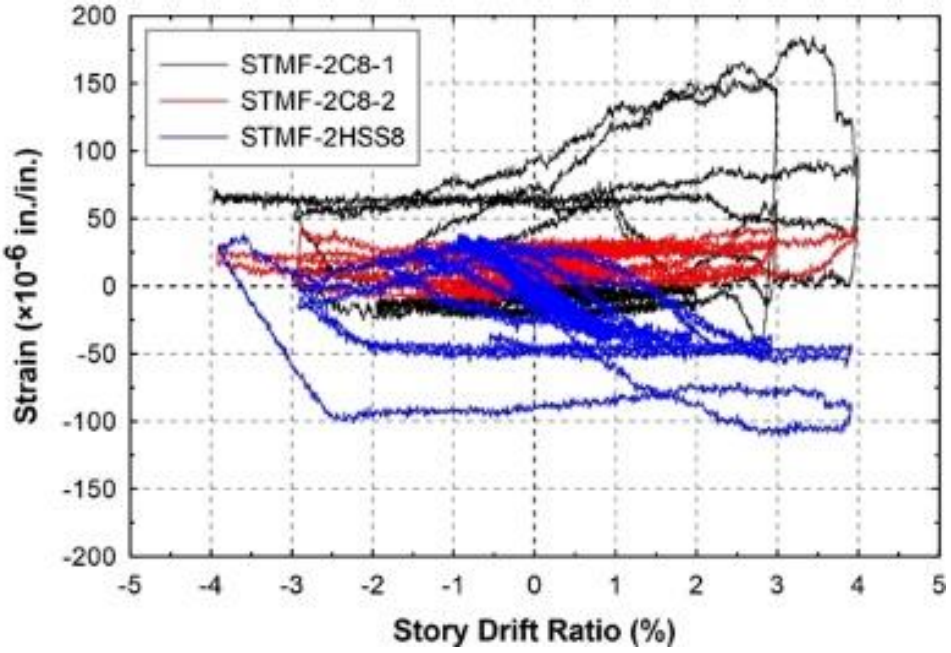
STMF-2C8-1
STMF-2C8-2
STMF-2HSS8
Strain (×10-6 in./in.)
Story Drift Ratio (%)
200
150
100
50
0
-50
-100
-150
-200
-5
-4
-3
-2
-1
0
1
2
3
4
5

BR-5-5

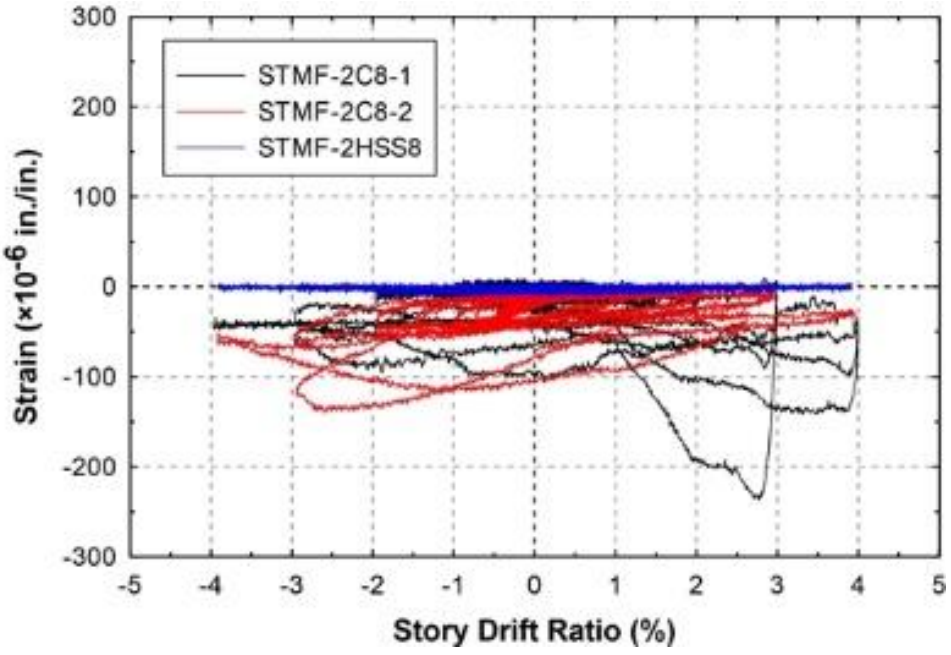
STMF-2C8-1
STMF-2C8-2
STMF-2HSS8
Strain (×10-6 in./in.)
Story Drift Ratio (%)
300
200
100
0
-100
-200
-300
-5
-4
-3
-2
-1
0
1
2
3
4
5

BR-5-6

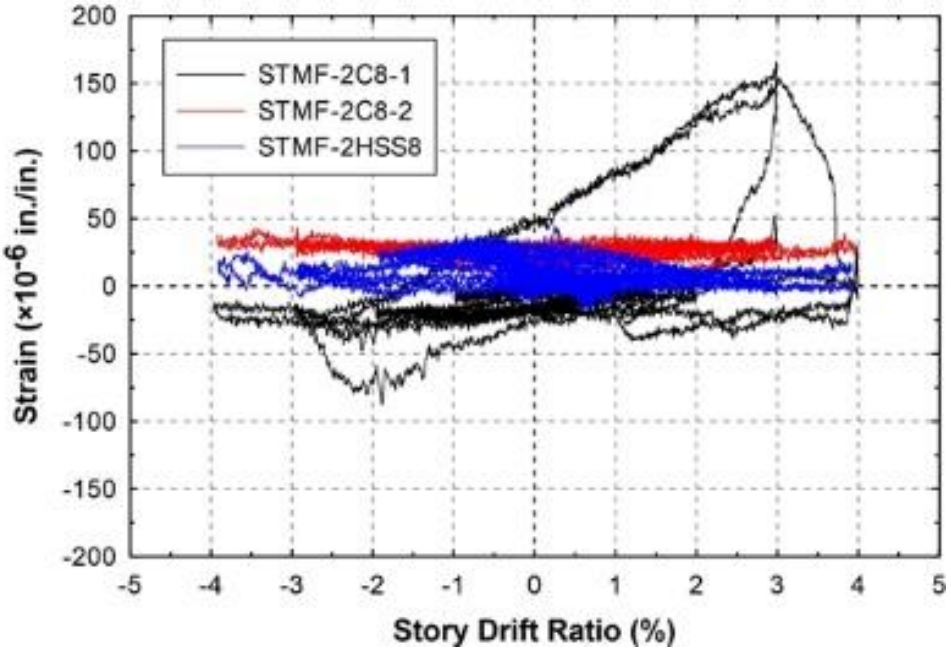
STMF-2C8-1
STMF-2C8-2
STMF-2HSS8
Strain (×10-6 in./in.)
Story Drift Ratio (%)

BR-5-7

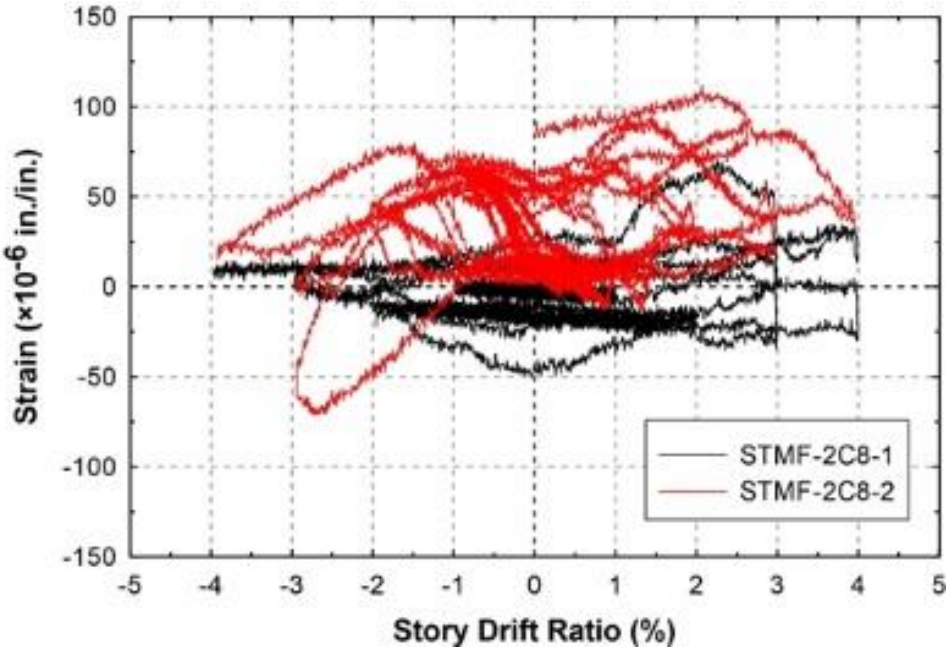
STMF-2C8-1
STMF-2C8-2
Strain (×10-6 in./in.)
Story Drift Ratio (%)

BR-5-8

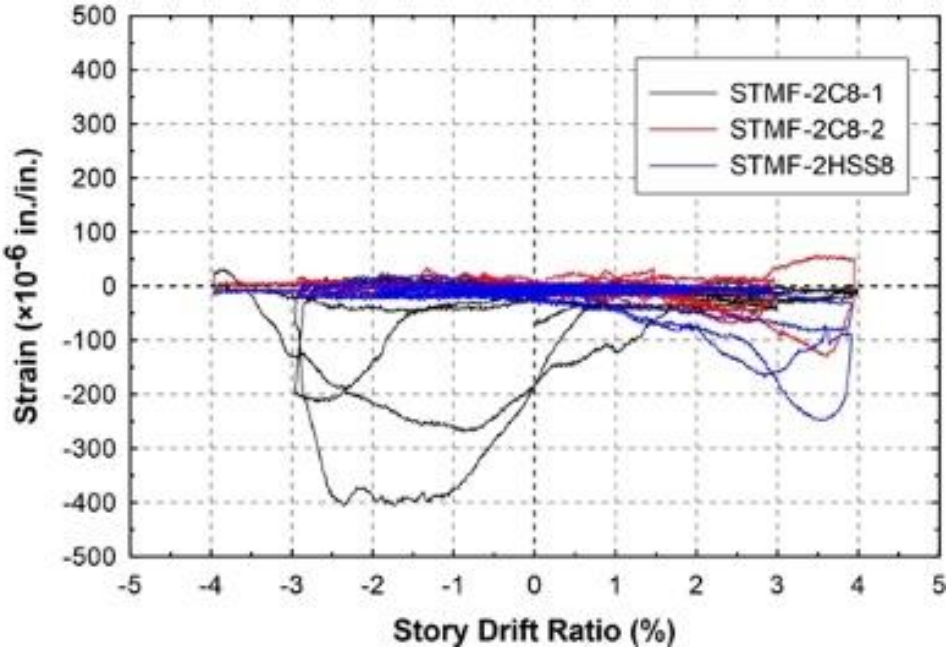
STMF-2C8-1
STMF-2C8-2
STMF-2HSS8
Strain (×10-6 in./in.)
Story Drift Ratio (%)

BR-6-1

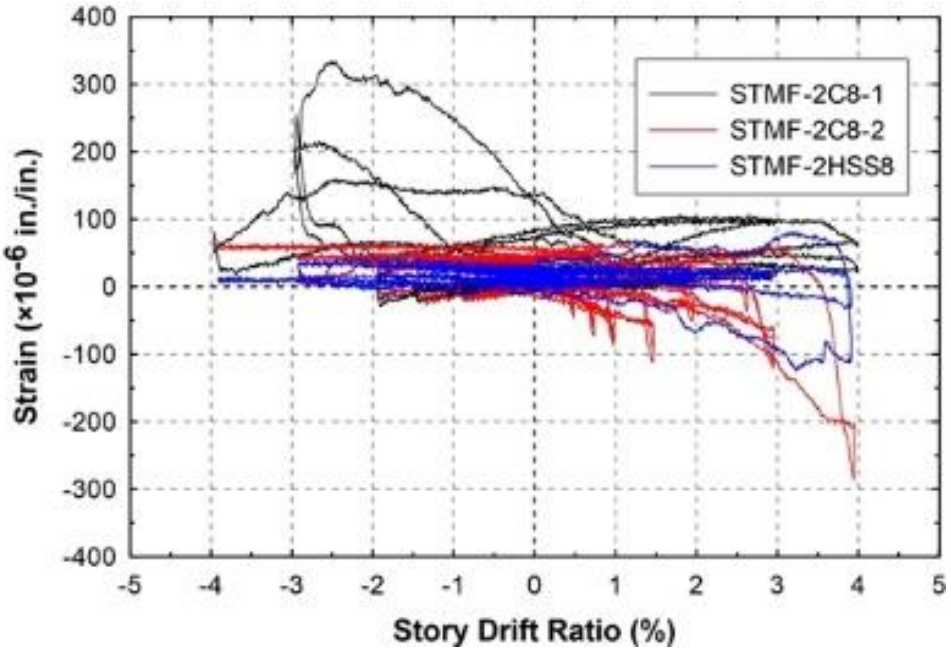
STMF-2C8-1
STMF-2C8-2
STMF-2HSS8
Strain (×10-6 in./in.)
Story Drift Ratio (%)

BR-6-2

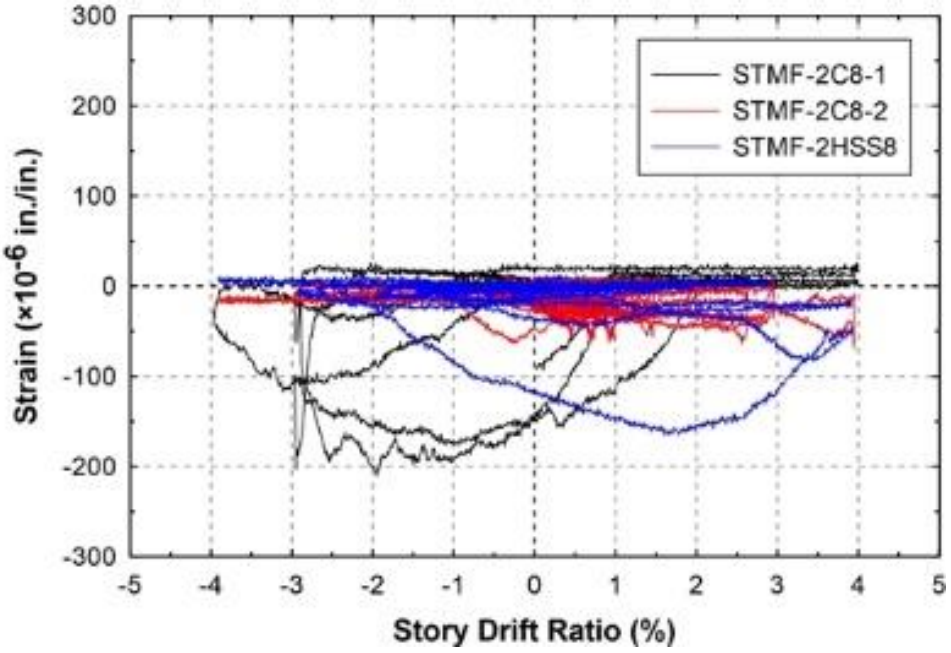
STMF-2C8-1
STMF-2C8-2
STMF-2HSS8
Strain (×10-6 in./in.)
Story Drift Ratio (%)
300
200
100
0
-100
-200
-300
-5
-4
-3
-2
-1
0
1
2
3
4
5

BR-6-3

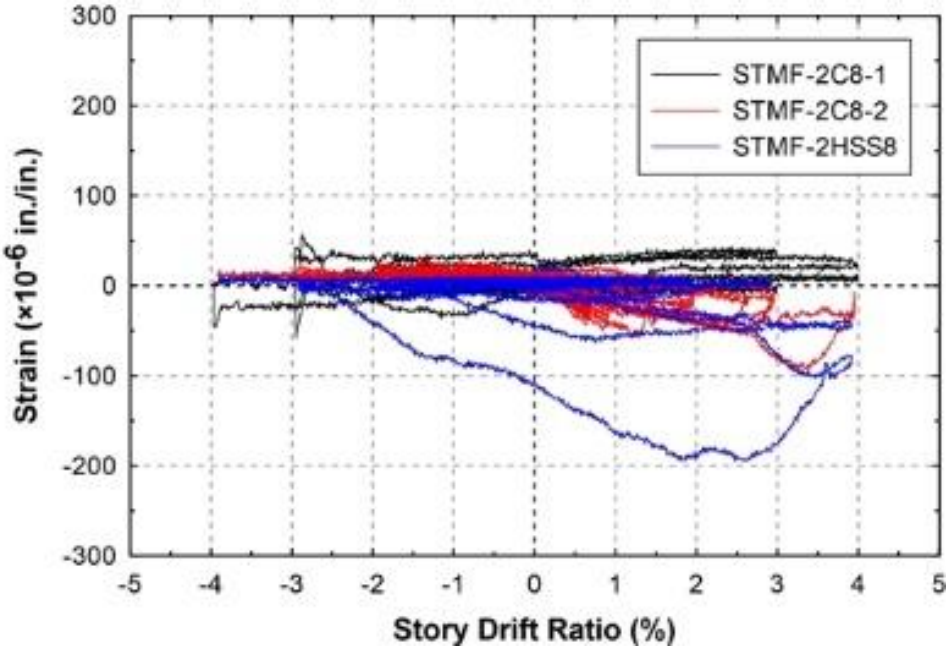
STMF-2C8-1
STMF-2C8-2
STMF-2HSS8
Strain (×10-6 in./in.)
Story Drift Ratio (%)
300
200
100
0
-100
-200
-300
-5
-4
-3
-2
-1
0
1
2
3
4
5

BR-6-4

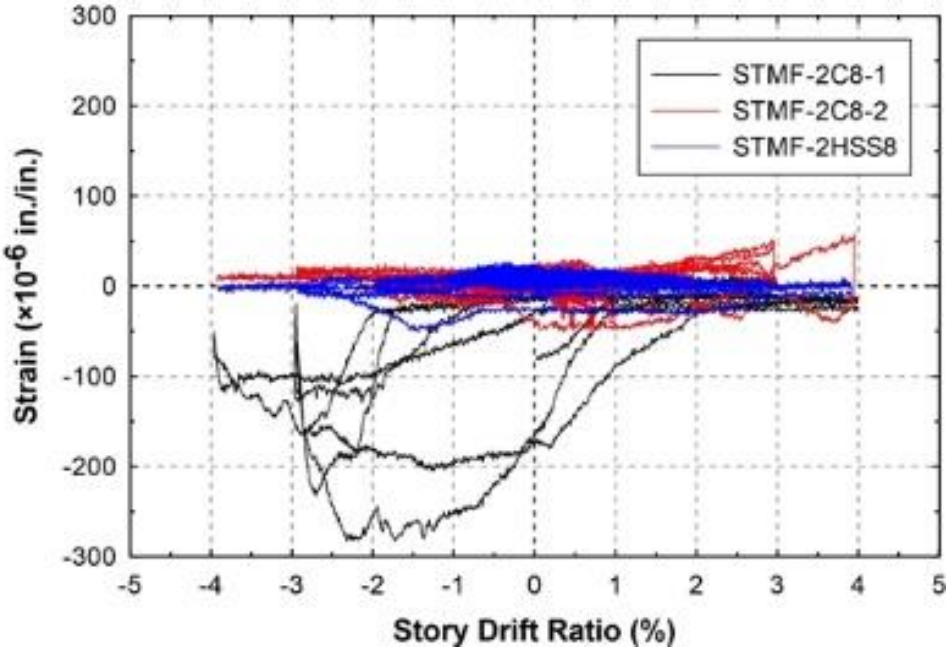
STMF-2C8-1
STMF-2C8-2
STMF-2HSS8
Strain (×10-6 in./in.)
Story Drift Ratio (%)

BR-6-5

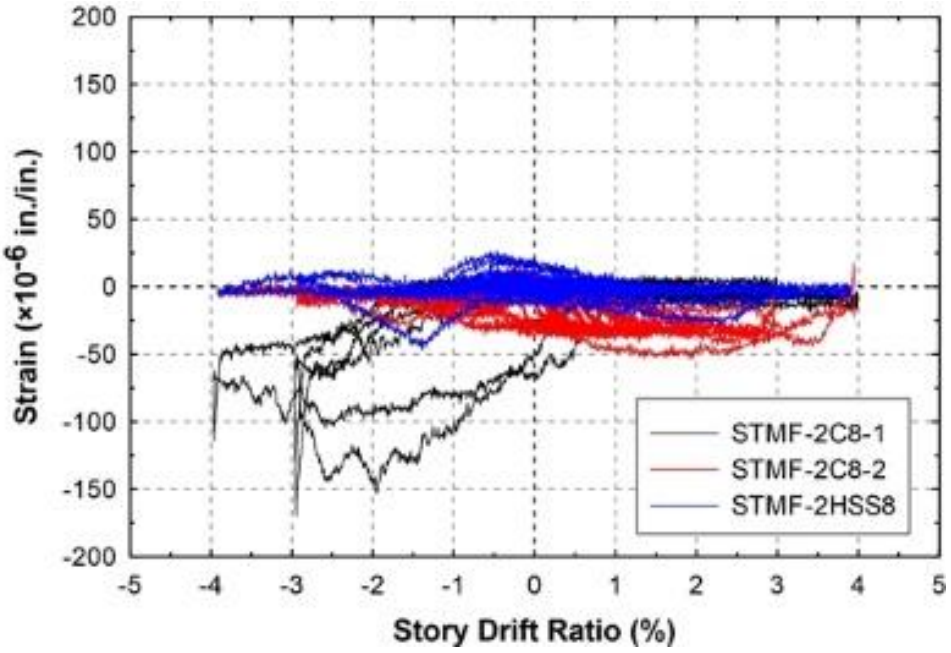
STMF-2C8-1
STMF-2C8-2
STMF-2HSS8
Strain (×10-6 in./in.)
Story Drift Ratio (%)

BR-6-6

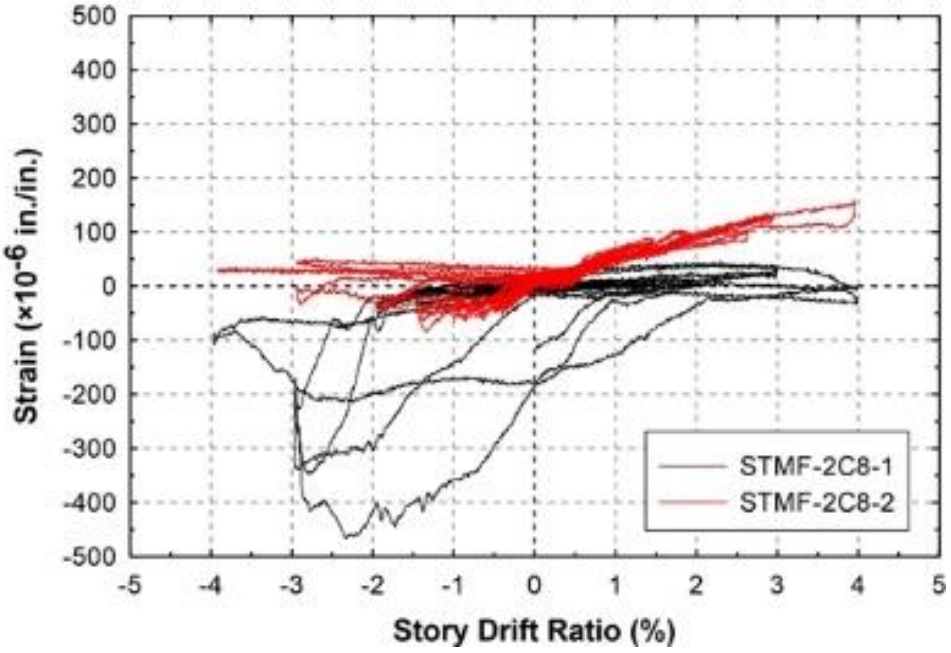
Strain (×10-6 in./in.)
Story Drift Ratio (%)
STMF-2C8-1
STMF-2C8-2

BR-6-7

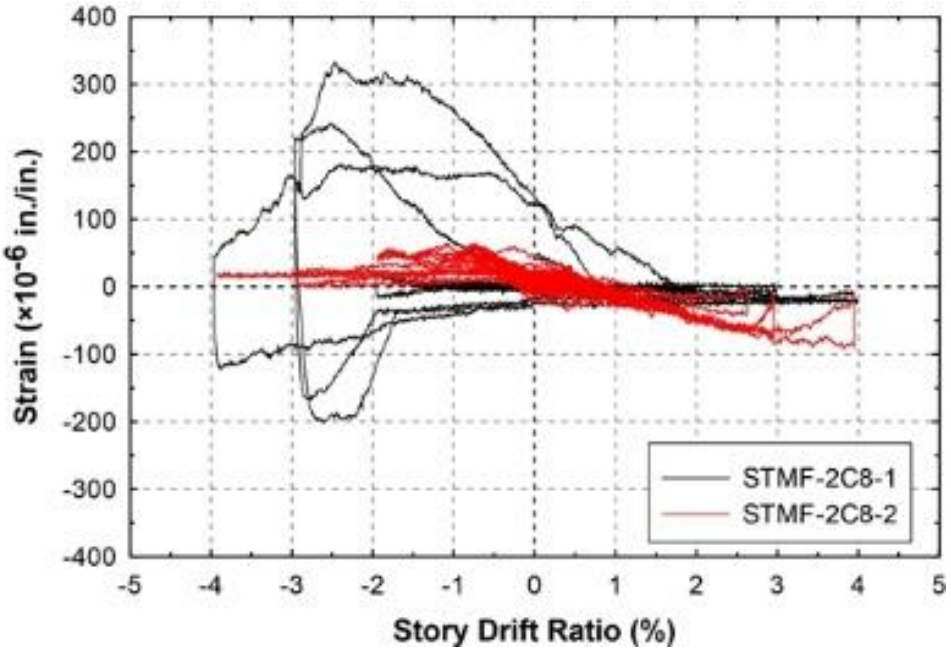
Strain (×10-6 in./in.)
Story Drift Ratio (%)
STMF-2C8-1
STMF-2C8-2

BR-6-8

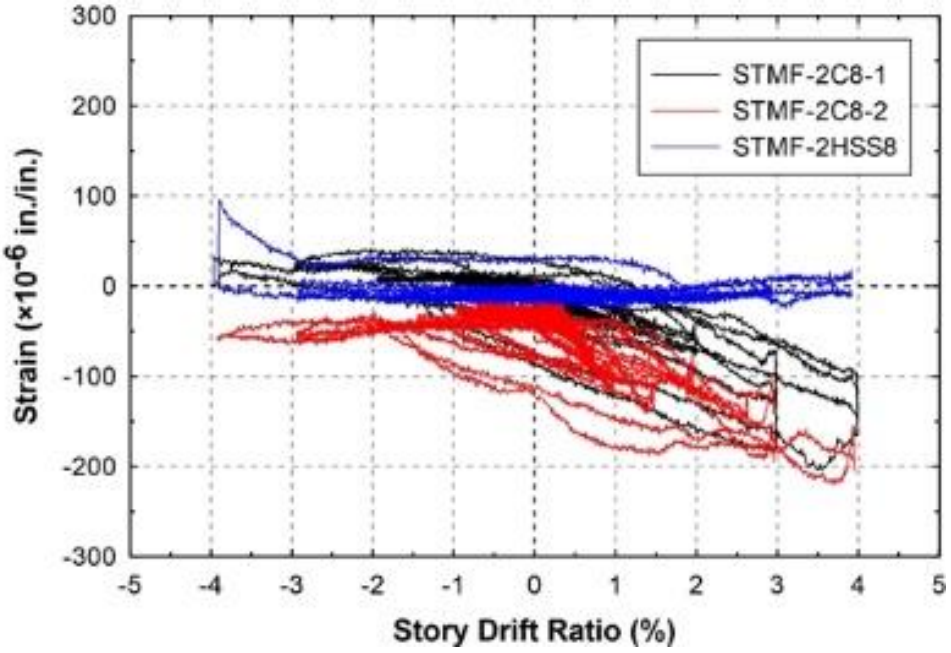
STMF-2C8-1
STMF-2C8-2
STMF-2HSS8
Strain (×10-6 in./in.)
Story Drift Ratio (%)
300
200
100
0
-100
-200
-300
-5
-4
-3
-2
-1
0
1
2
3
4
5

BR-7-1

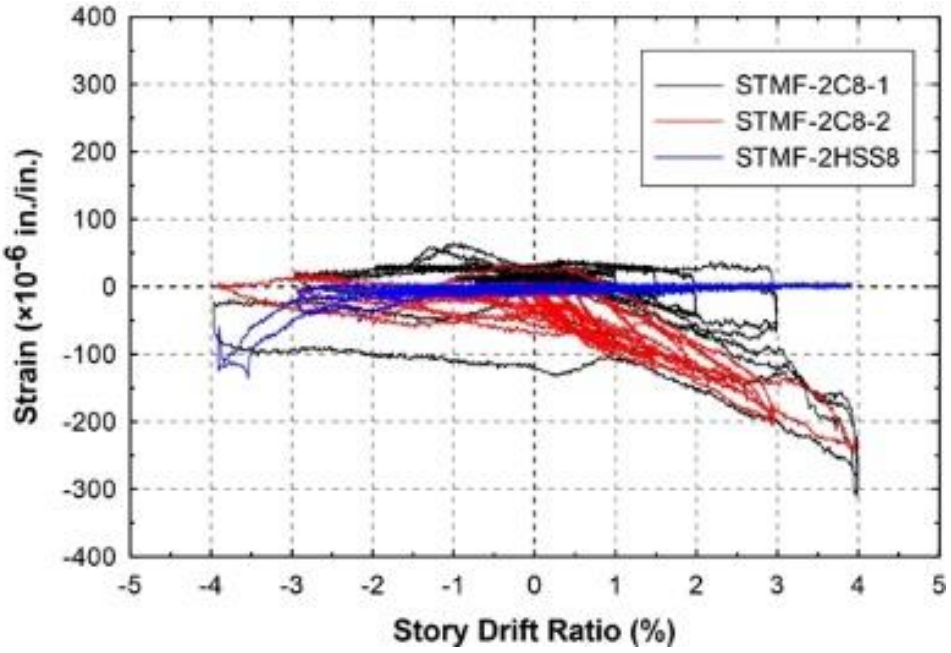
STMF-2C8-1
STMF-2C8-2
STMF-2HSS8
Strain (×10-6 in./in.)
Story Drift Ratio (%)
400
300
200
100
0
-100
-200
-300
-400
-5
-4
-3
-2
-1
0
1
2
3
4
5

BR-7-2

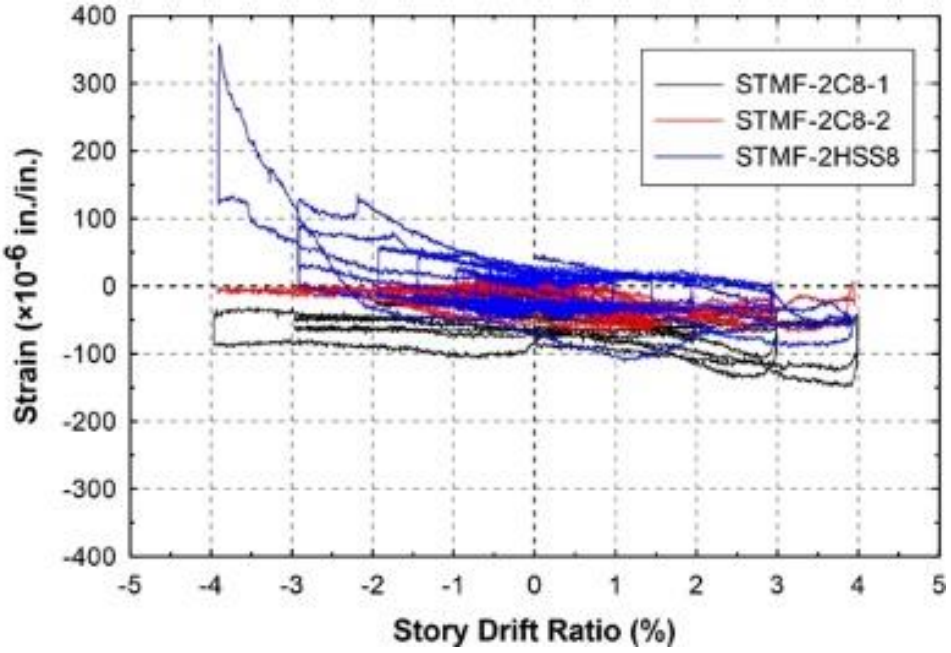
STMF-2C8-1
STMF-2C8-2
STMF-2HSS8
Strain (×10-6 in./in.)
Story Drift Ratio (%)

BR-7-3

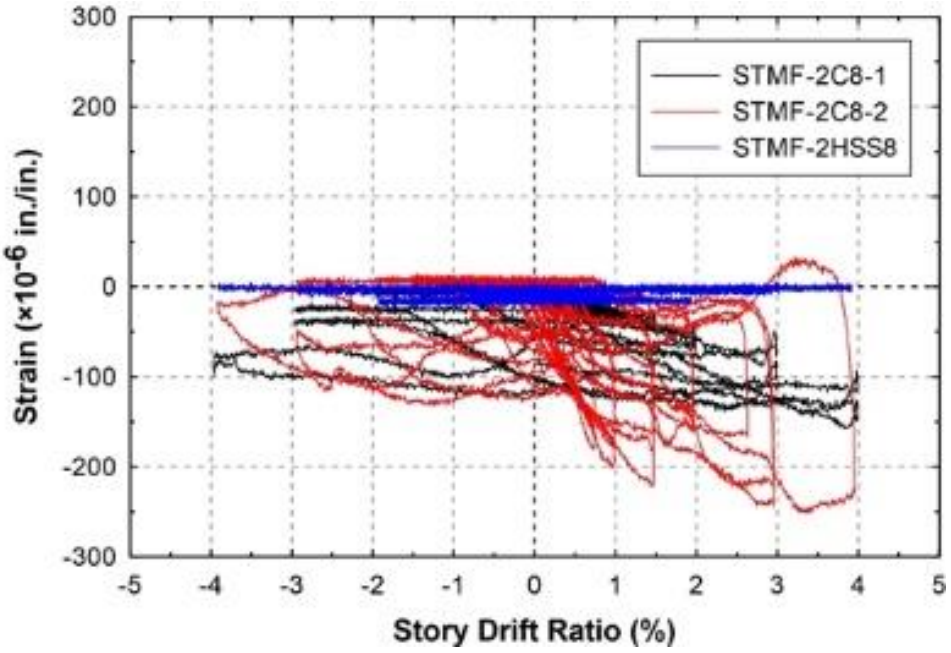
STMF-2C8-1
STMF-2C8-2
STMF-2HSS8
Strain (×10-6 in./in.)
Story Drift Ratio (%)

BR-7-4

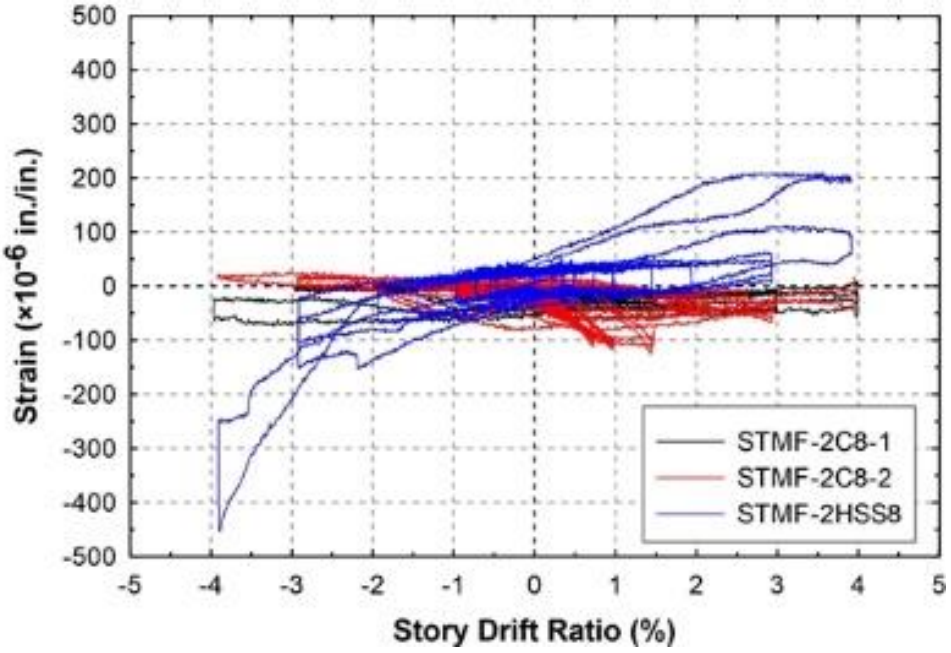
Strain (×10-6 in./in.)
Story Drift Ratio (%)
STMF-2C8-1
STMF-2C8-2
STMF-2HSS8

BR-7-5

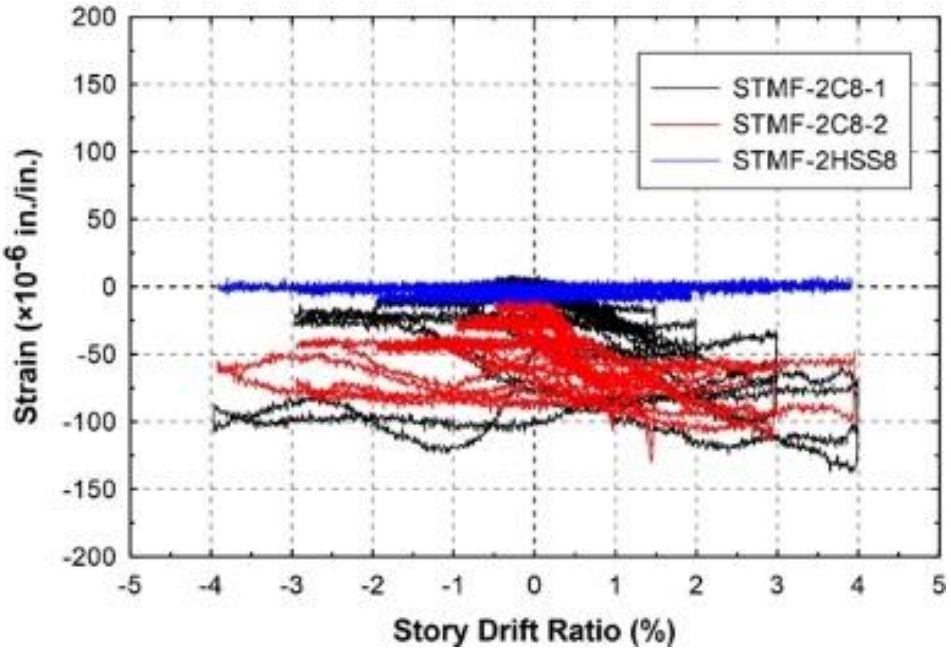
Strain (×10-6 in./in.)
Story Drift Ratio (%)
STMF-2C8-1
STMF-2C8-2
STMF-2HSS8

BR-7-6

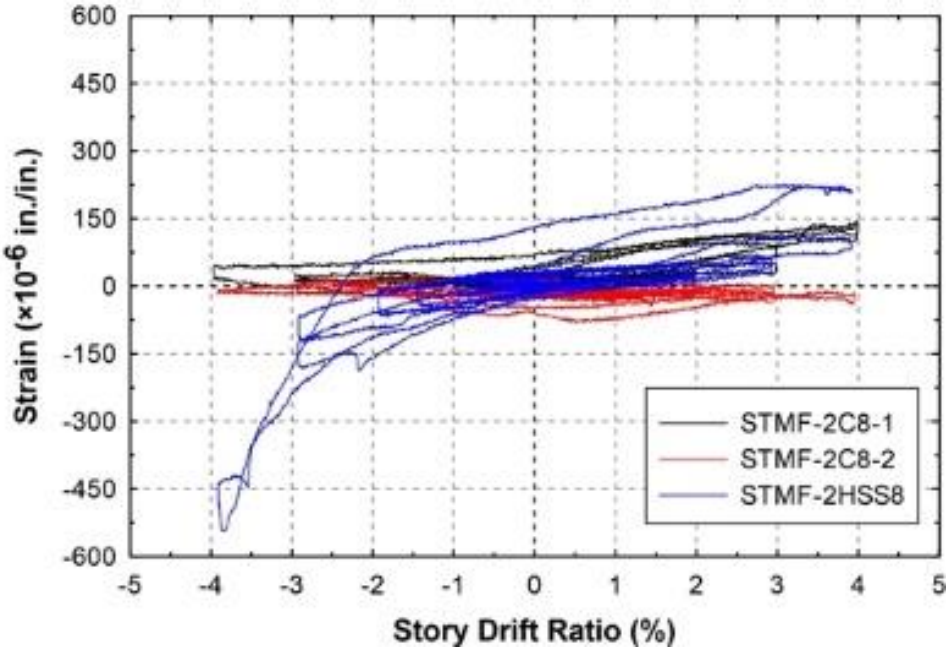
600
450
300
150
0
-150
-300
-450
-600
-5
-4
-3
-2
-1
0
1
2
3
4
5
Strain (×10-6 in./in.)
Story Drift Ratio (%)
STMF-2C8-1
STMF-2C8-2
STMF-2HSS8

BR-7-7

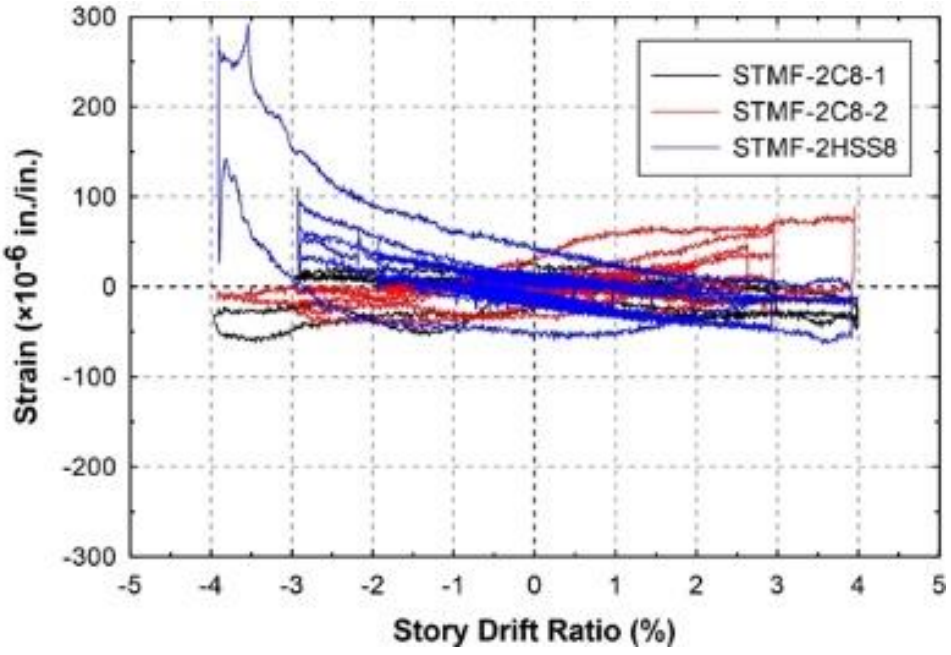
300
200
100
0
-100
-200
-300
-5
-4
-3
-2
-1
0
1
2
3
4
5
Strain (×10-6 in./in.)
Story Drift Ratio (%)
STMF-2C8-1
STMF-2C8-2
STMF-2HSS8

BR-7-8

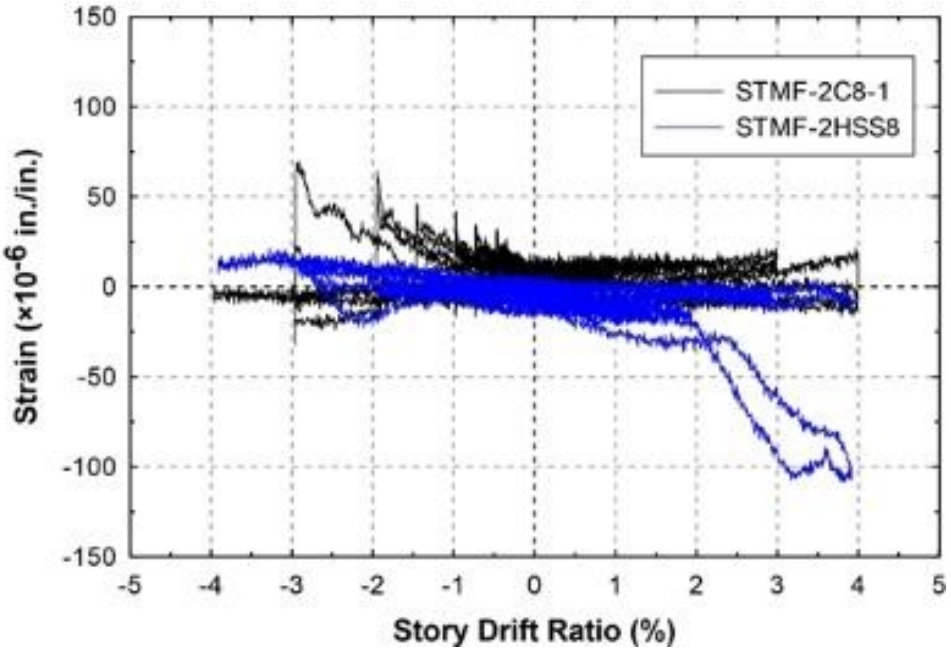
STMF-2C8-1
STMF-2HSS8
Strain (×10-6 in./in.)
Story Drift Ratio (%)

BR-8-1

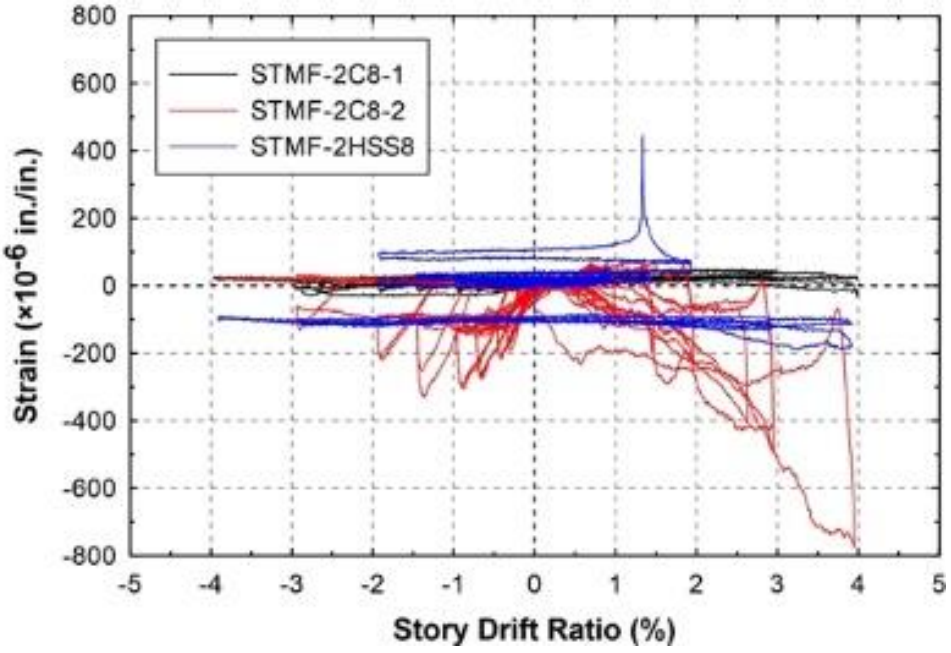
STMF-2C8-1
STMF-2C8-2
STMF-2HSS8
Strain (×10-6 in./in.)
Story Drift Ratio (%)

BR-8-2

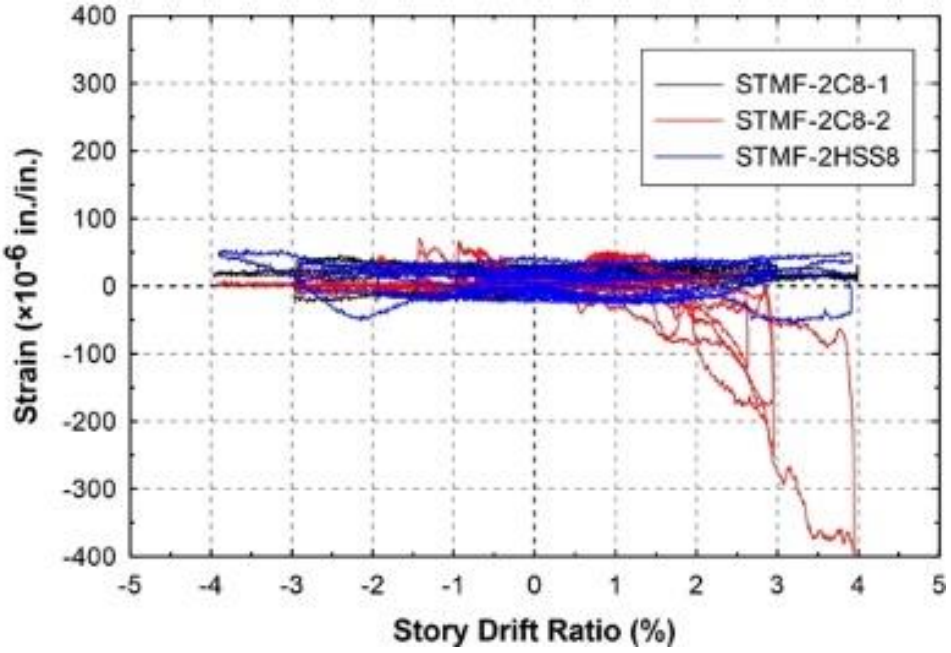
STMF-2C8-1
STMF-2C8-2
STMF-2HSS8
Strain (×10-6 in./in.)
Story Drift Ratio (%)

BR-8-3

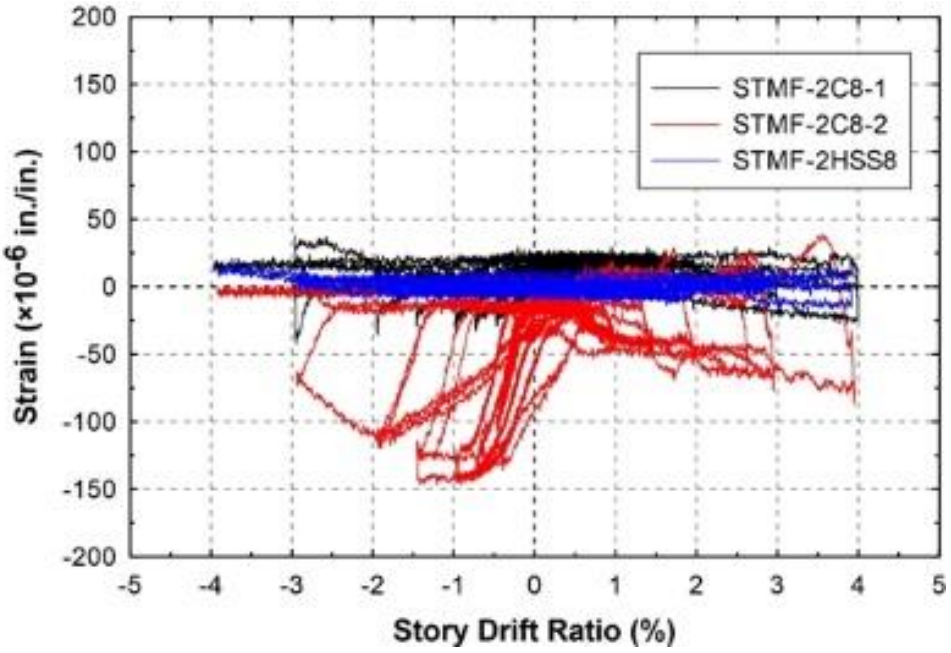
STMF-2C8-1
STMF-2C8-2
STMF-2HSS8
Strain (×10-6 in./in.)
Story Drift Ratio (%)

BR-8-4

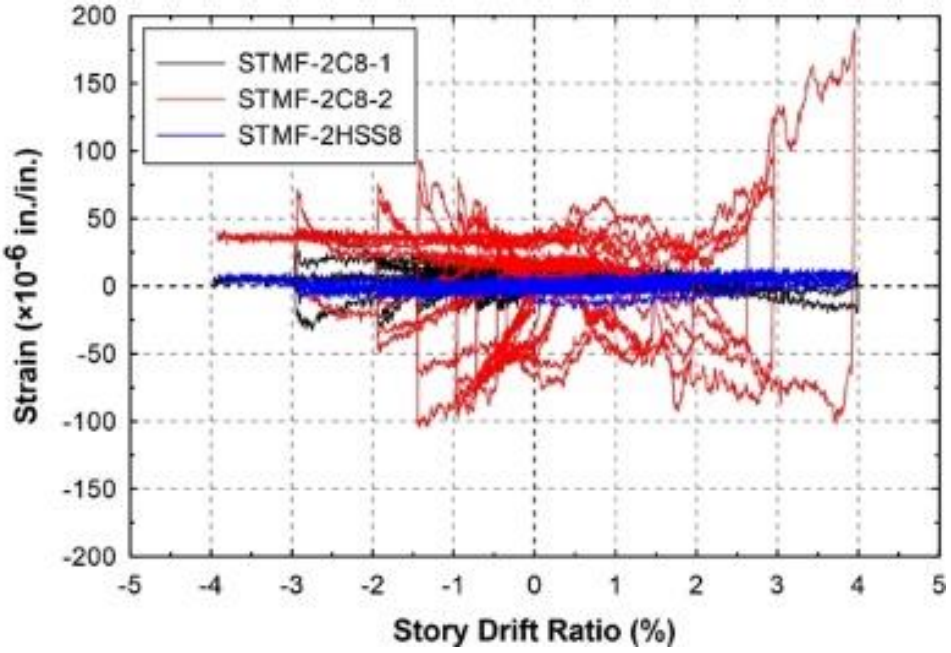
STMF-2C8-1
STMF-2C8-2
STMF-2HSS8
Strain (×10-6 in./in.)
Story Drift Ratio (%)
200
150
100
50
0
-50
-100
-150
-200
-5
-4
-3
-2
-1
0
1
2
3
4
5

BR-8-5

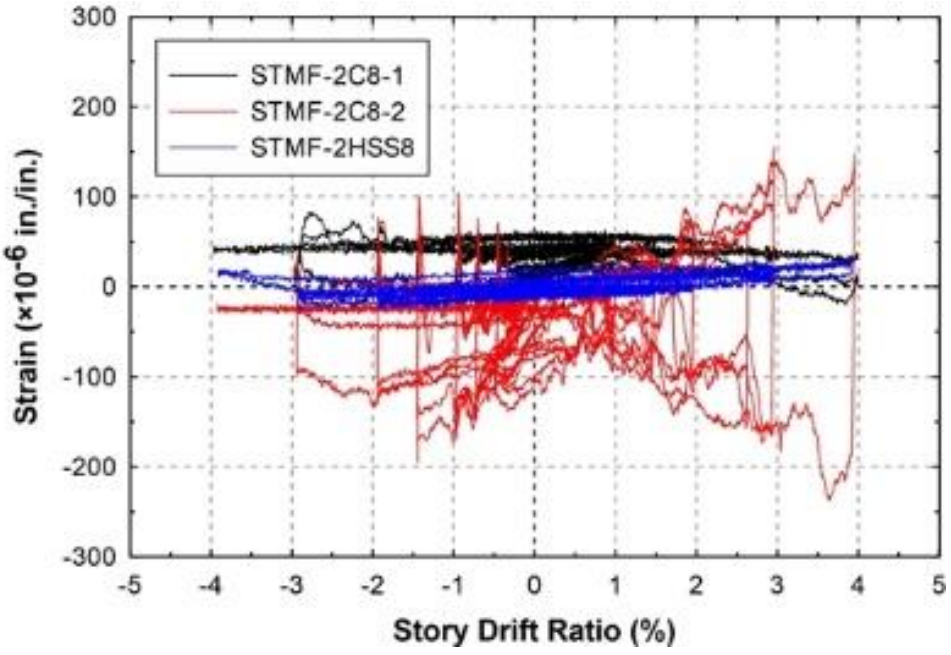
STMF-2C8-1
STMF-2C8-2
STMF-2HSS8
Strain (×10-6 in./in.)
Story Drift Ratio (%)
300
200
100
0
-100
-200
-300
-5
-4
-3
-2
-1
0
1
2
3
4
5

BR-8-6

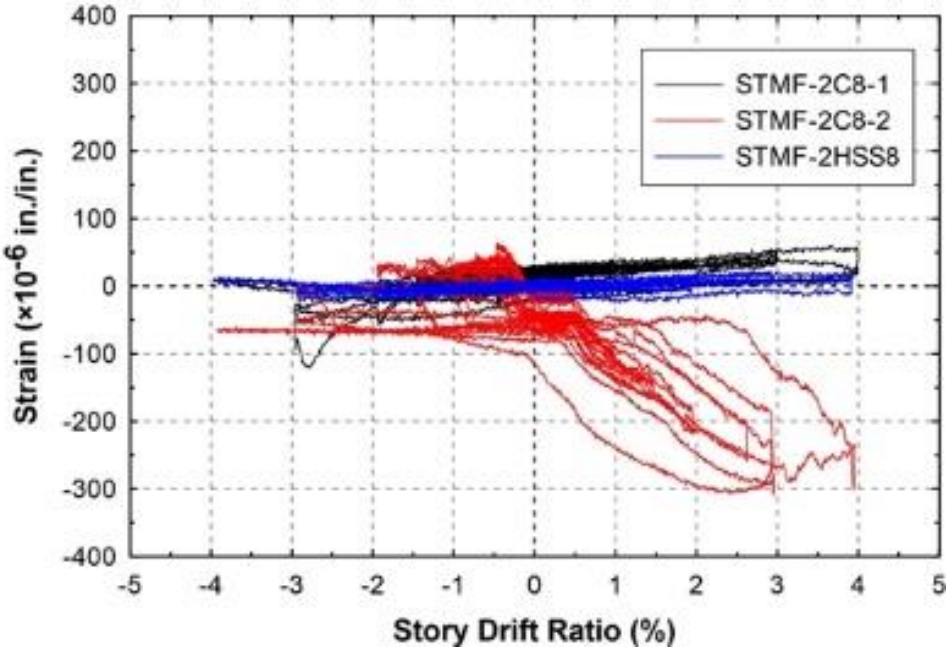
STMF-2C8-1
STMF-2C8-2
STMF-2HSS8
Strain (×10-6 in./in.)
Story Drift Ratio (%)

BR-8-7

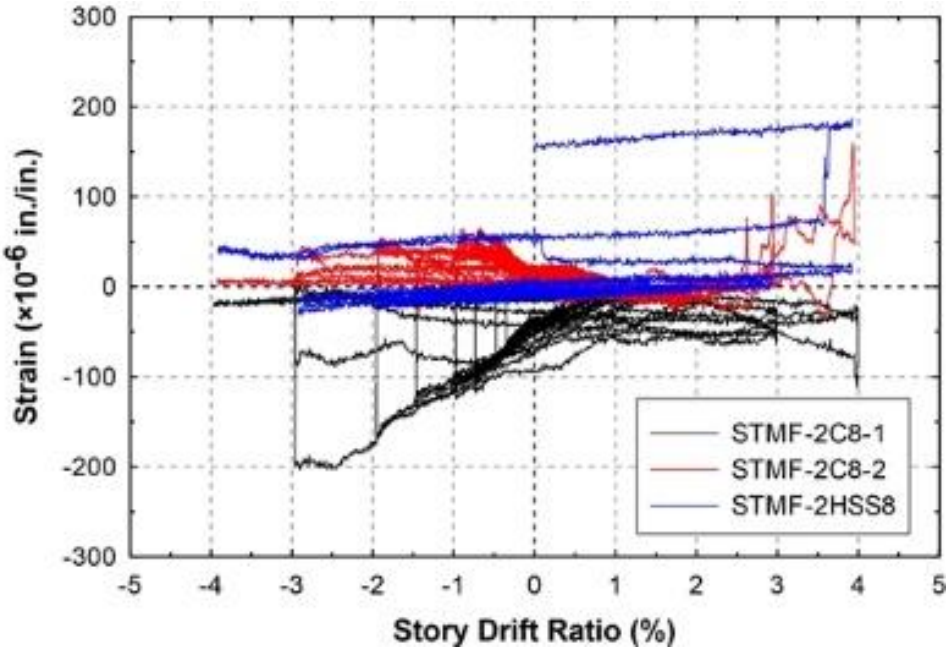
STMF-2C8-1
STMF-2C8-2
STMF-2HSS8
Strain (×10-6 in./in.)
Story Drift Ratio (%)

BR-8-8

Appendix G

Force vs. Story Drift Ratio Response of Lateral Bracing System

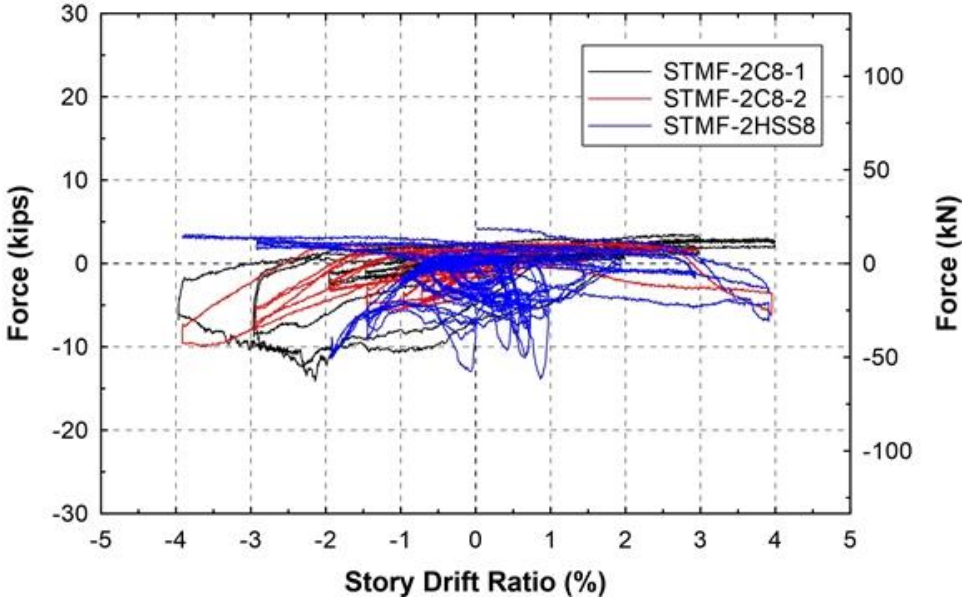
STMF-2C8-1
STMF-2C8-2
STMF-2HSS8
Force (kips)
Force (kN)
Story Drift Ratio (%)
30
20
10
0
-10
-20
-30
100
50
0
-50
-100
-5
-4
-3
-2
-1
0
1
2
3
4
5

BR-1

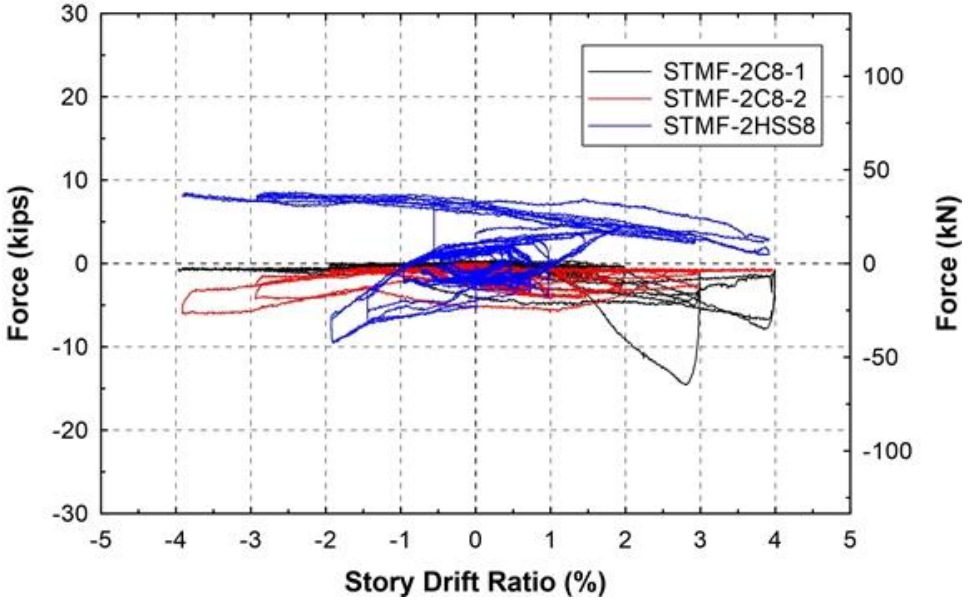
STMF-2C8-1
STMF-2C8-2
STMF-2HSS8
Force (kips)
Force (kN)
Story Drift Ratio (%)
30
20
10
0
-10
-20
-30
100
50
0
-50
-100
-5
-4
-3
-2
-1
0
1
2
3
4
5

BR-2

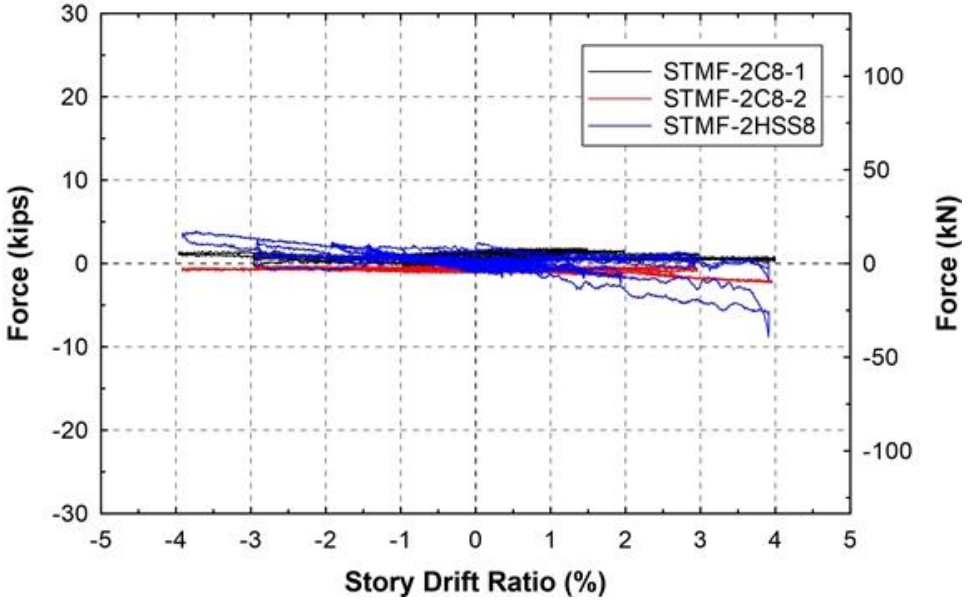
STMF-2C8-1
STMF-2C8-2
STMF-2HSS8
Force (kips)
Force (kN)
Story Drift Ratio (%)
30
20
10
0
-10
-20
-30
100
50
0
-50
-100
-5
-4
-3
-2
-1
0
1
2
3
4
5

BR-3

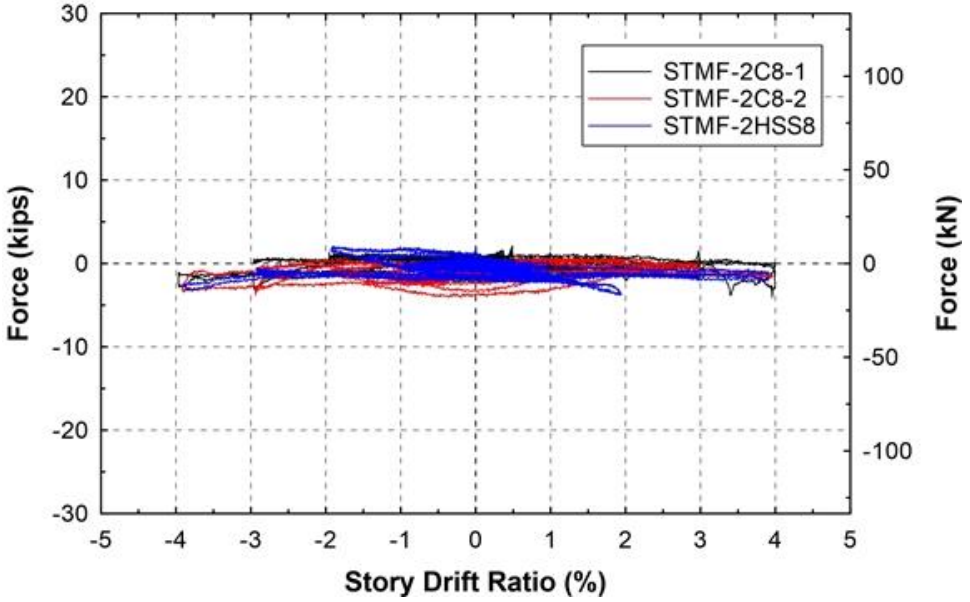
STMF-2C8-1
STMF-2C8-2
STMF-2HSS8
Force (kips)
Force (kN)
Story Drift Ratio (%)
30
20
10
0
-10
-20
-30
100
50
0
-50
-100
-5
-4
-3
-2
-1
0
1
2
3
4
5

BR-4

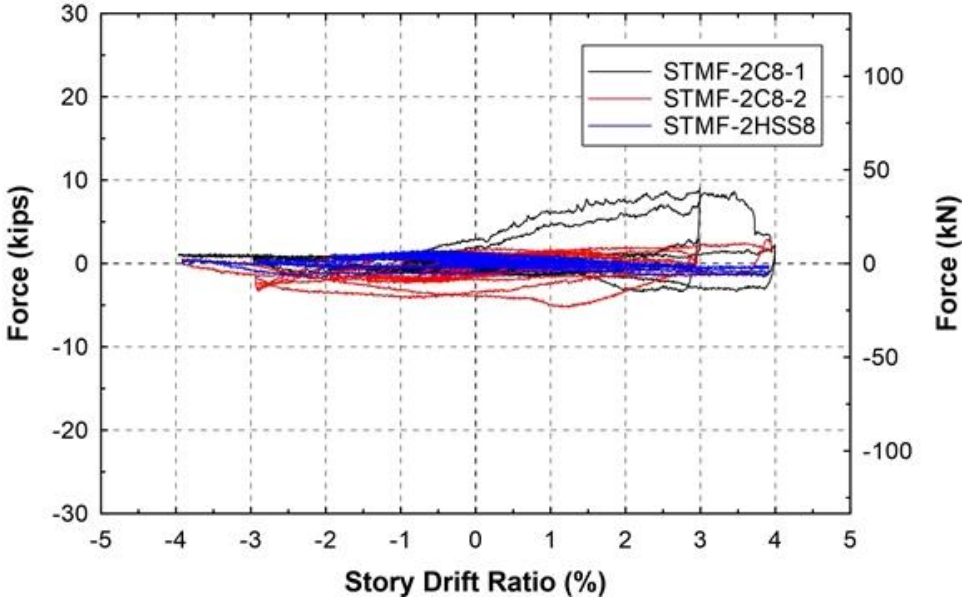
STMF-2C8-1
STMF-2C8-2
STMF-2HSS8
Force (kips)
Force (kN)
Story Drift Ratio (%)
30
20
10
0
-10
-20
-30
100
50
0
-50
-100
-5
-4
-3
-2
-1
0
1
2
3
4
5

BR-5

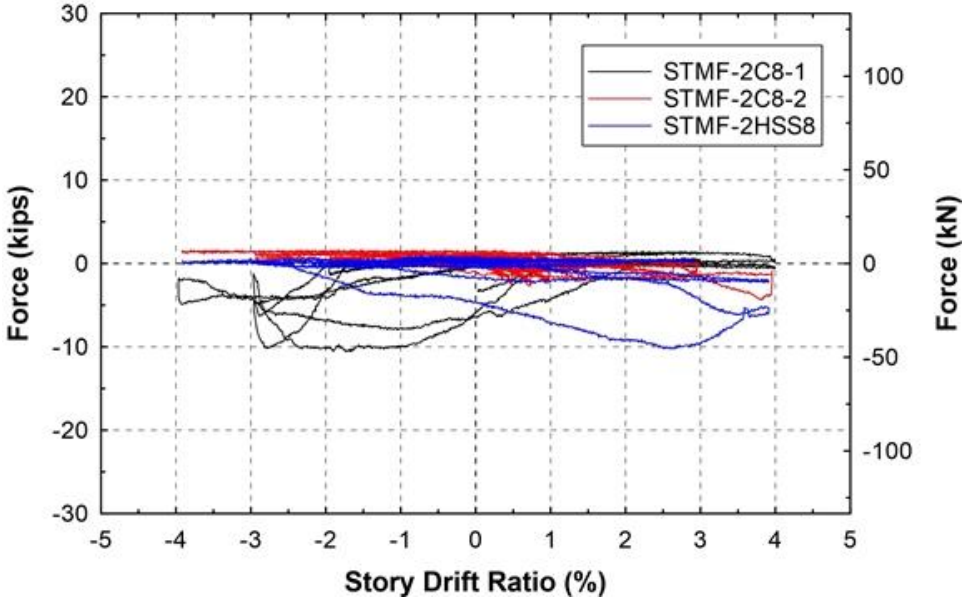
STMF-2C8-1
STMF-2C8-2
STMF-2HSS8
Force (kips)
Force (kN)
Story Drift Ratio (%)
30
20
10
0
-10
-20
-30
100
50
0
-50
-100
-5
-4
-3
-2
-1
0
1
2
3
4
5

BR-6

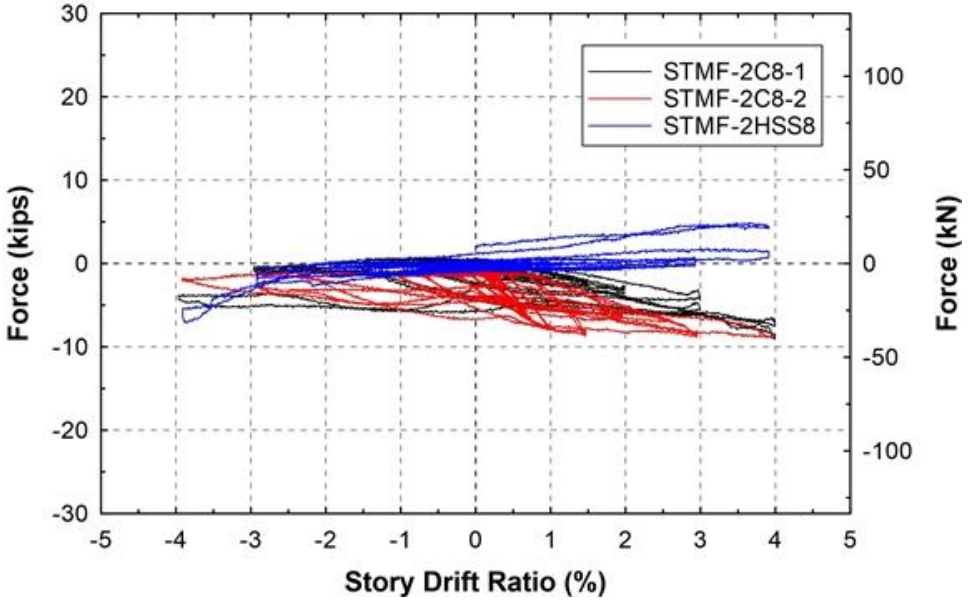
STMF-2C8-1
STMF-2C8-2
STMF-2HSS8
Force (kips)
Force (kN)
Story Drift Ratio (%)

BR-7

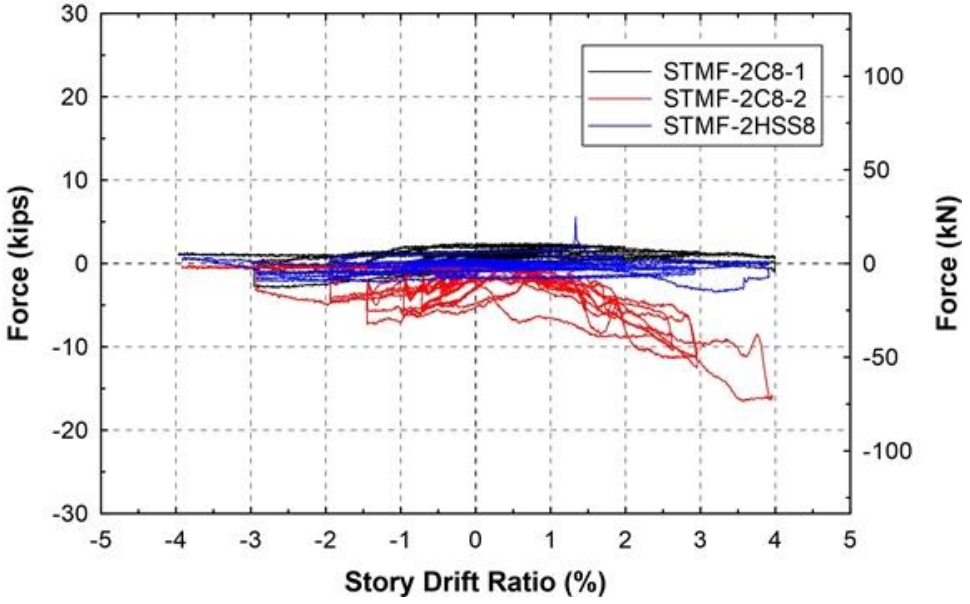
STMF-2C8-1
STMF-2C8-2
STMF-2HSS8
Force (kips)
Force (kN)
Story Drift Ratio (%)

BR-8

Appendix H

Displacement vs. Story Drift Ratio Response of LVDTs at the Base of Test Setup Column

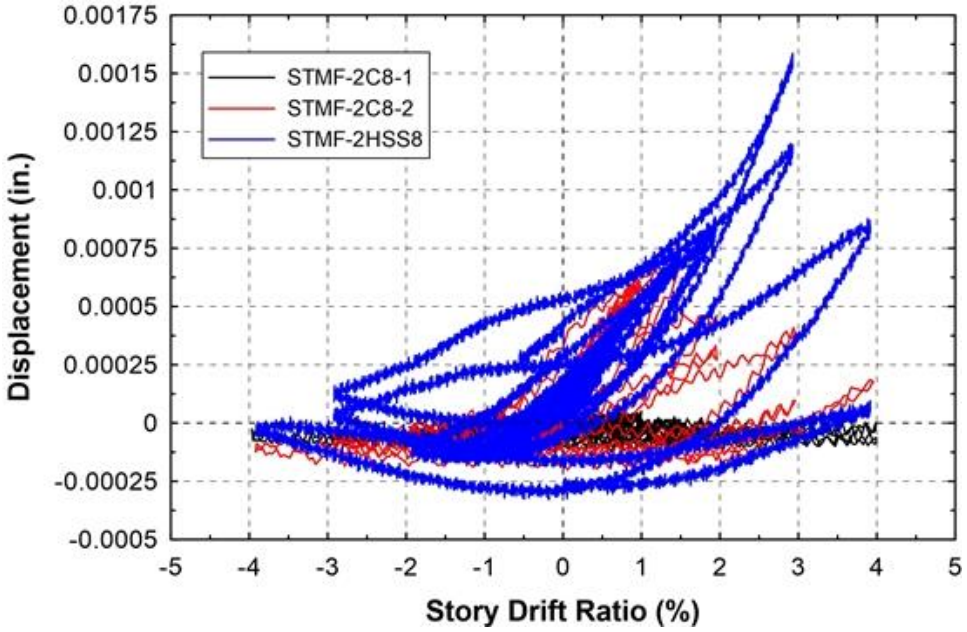

L-NE-NE1

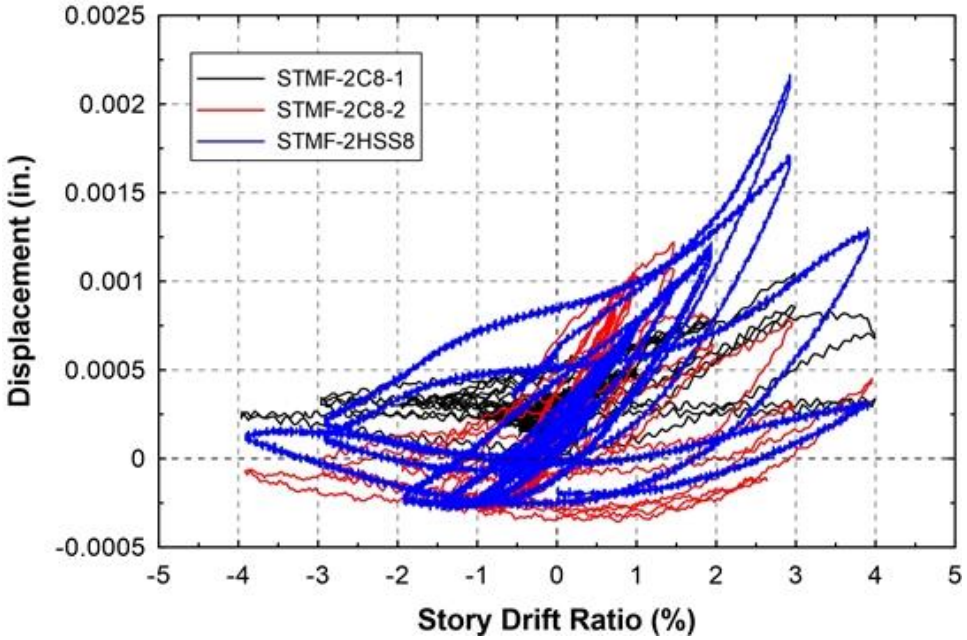

L-NE-NE2

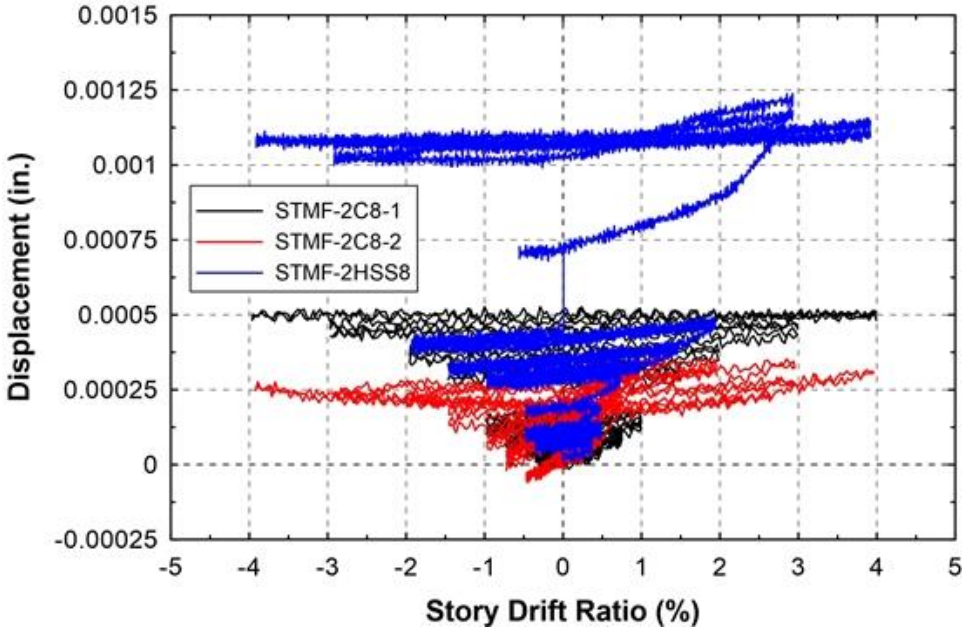

L-NE-NW1

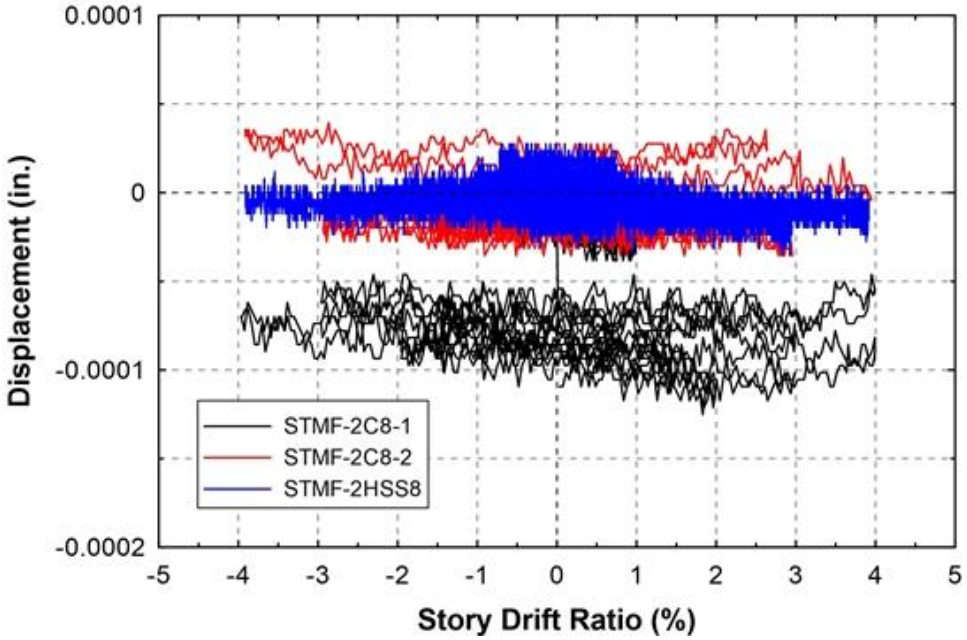

L-NE-NW 2

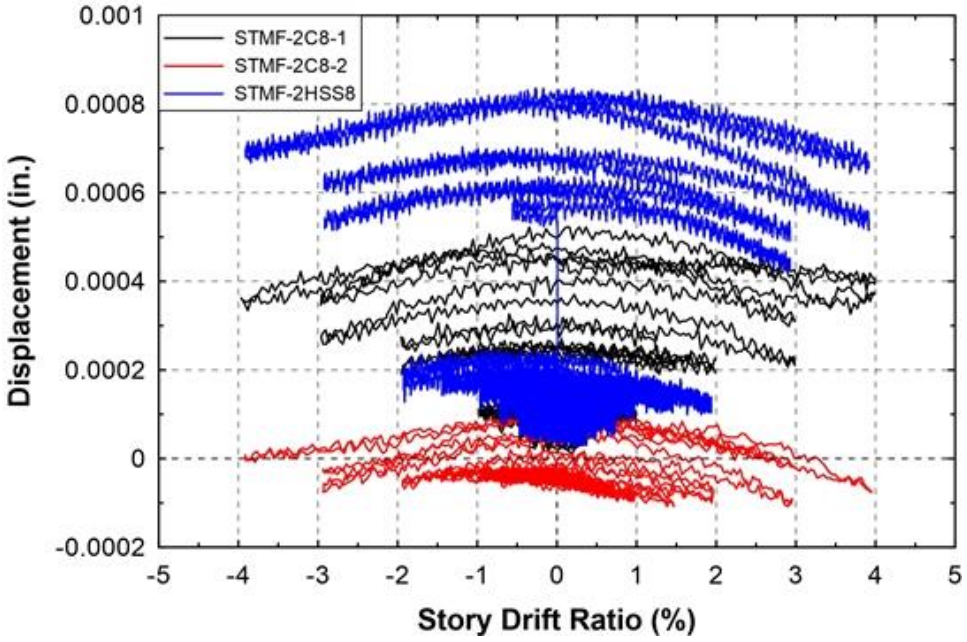
STMF-2C8-1
STMF-2C8-2
STMF-2HSS8
Displacement (in.)
0.001
0.0008
0.0006
0.0004
0.0002
0
-0.0002
-5
-4
-3
-2
-1
0
1
2
3
4
5
Story Drift Ratio (%)

L-NE-S

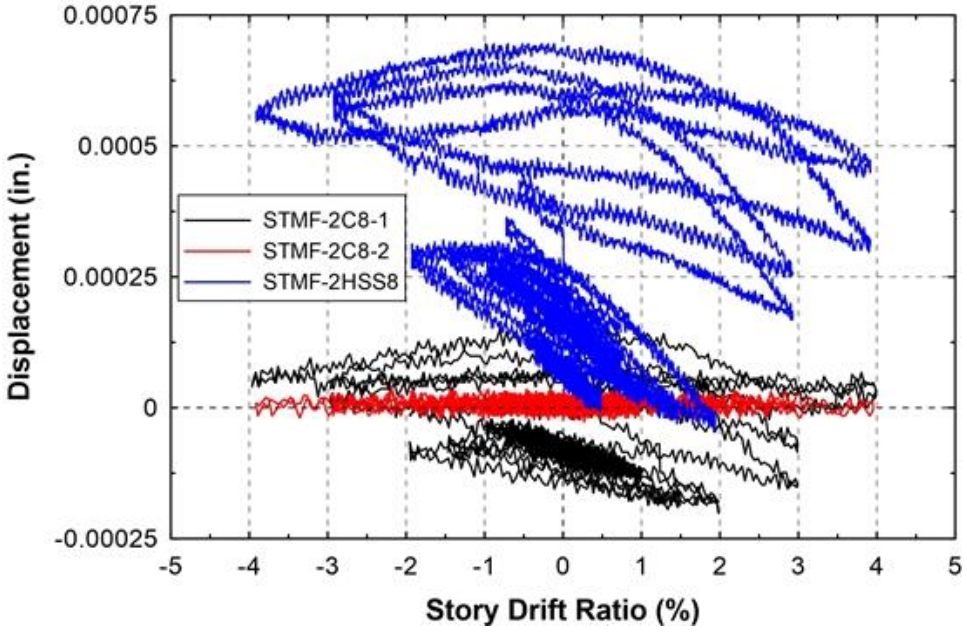
STMF-2C8-1
STMF-2C8-2
STMF-2HSS8
Displacement (in.)
0.00075
0.0005
0.00025
0
-0.00025
-5
-4
-3
-2
-1
0
1
2
3
4
5
Story Drift Ratio (%)

L-NE-W

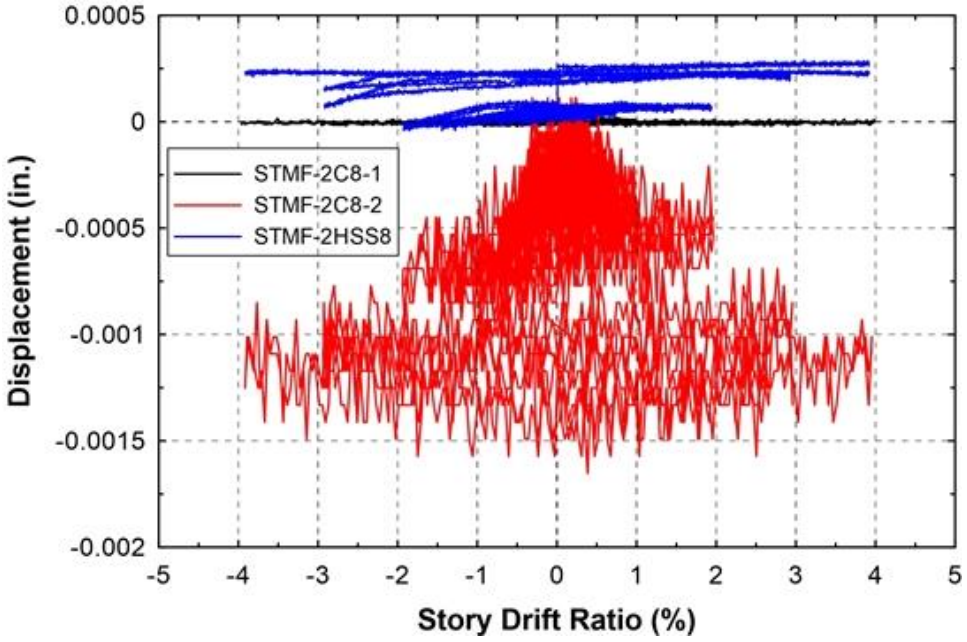

L-SW-NW1

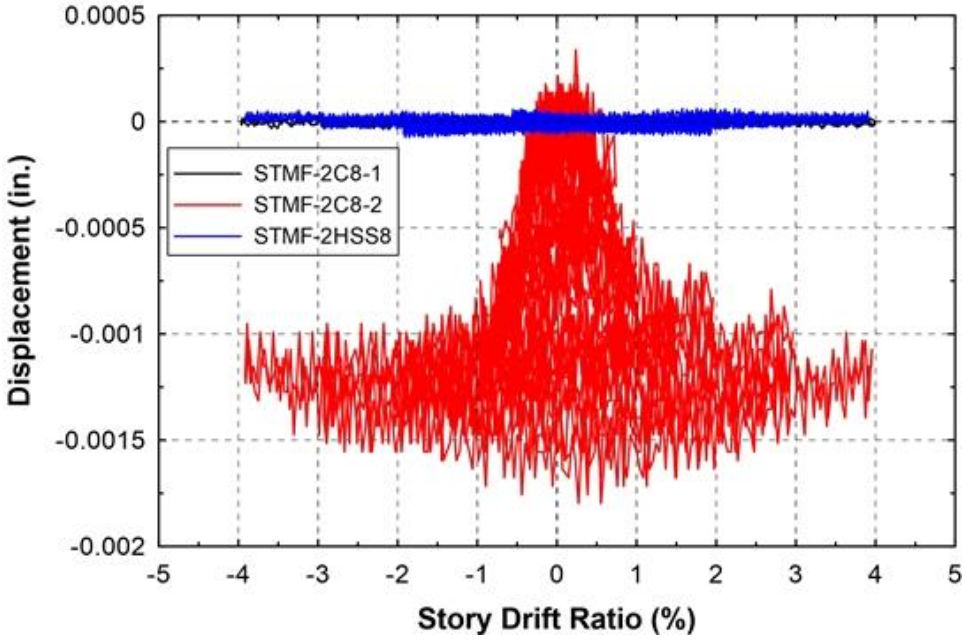

L-SW-NW2

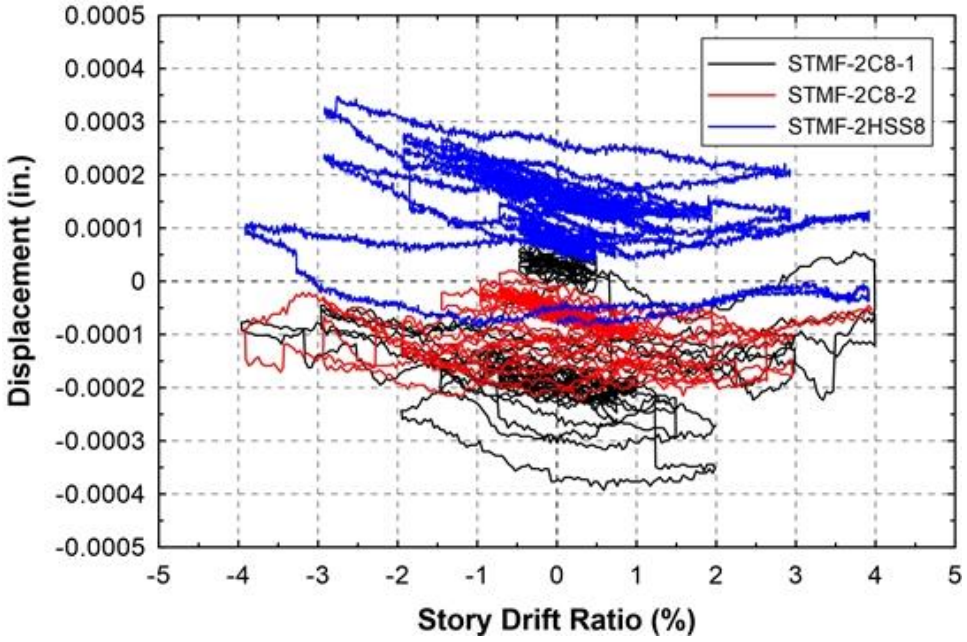
STMF-2C8-1
STMF-2C8-2
STMF-2HSS8
Displacement (in.)
Story Drift Ratio (%)
0.0005
0.0004
0.0003
0.0002
0.0001
0
-0.0001
-0.0002
-0.0003
-0.0004
-0.0005
-5
-4
-3
-2
-1
0
1
2
3
4
5

L-SW-S

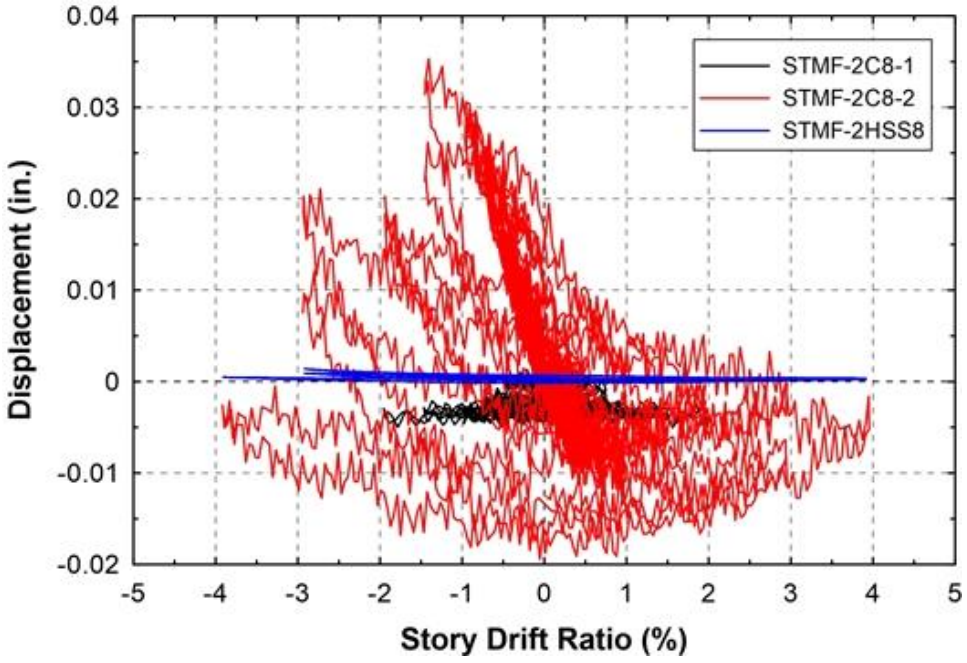
STMF-2C8-1
STMF-2C8-2
STMF-2HSS8
Displacement (in.)
Story Drift Ratio (%)
0.04
0.03
0.02
0.01
0
-0.01
-0.02
-5
-4
-3
-2
-1
0
1
2
3
4
5

L-SW-SW1

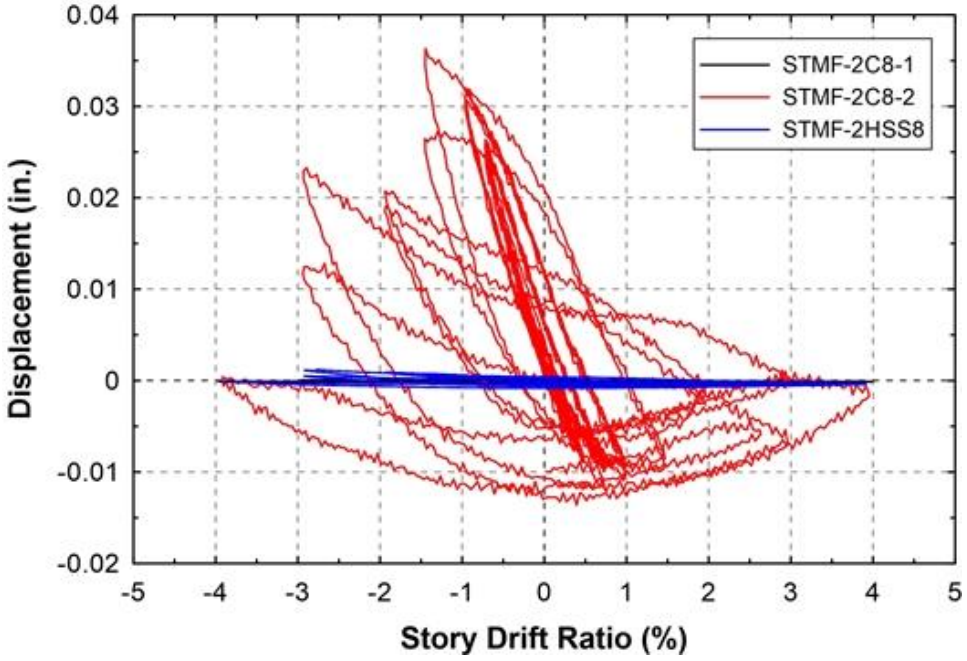
0.04
0.03
0.02
0.01
0
-0.01
-0.02
Displacement (in.)
-5
-4
-3
-2
-1
0
1
2
3
4
5
Story Drift Ratio (%)
STMF-2C8-1
STMF-2C8-2
STMF-2HSS8

L-SW-SW2

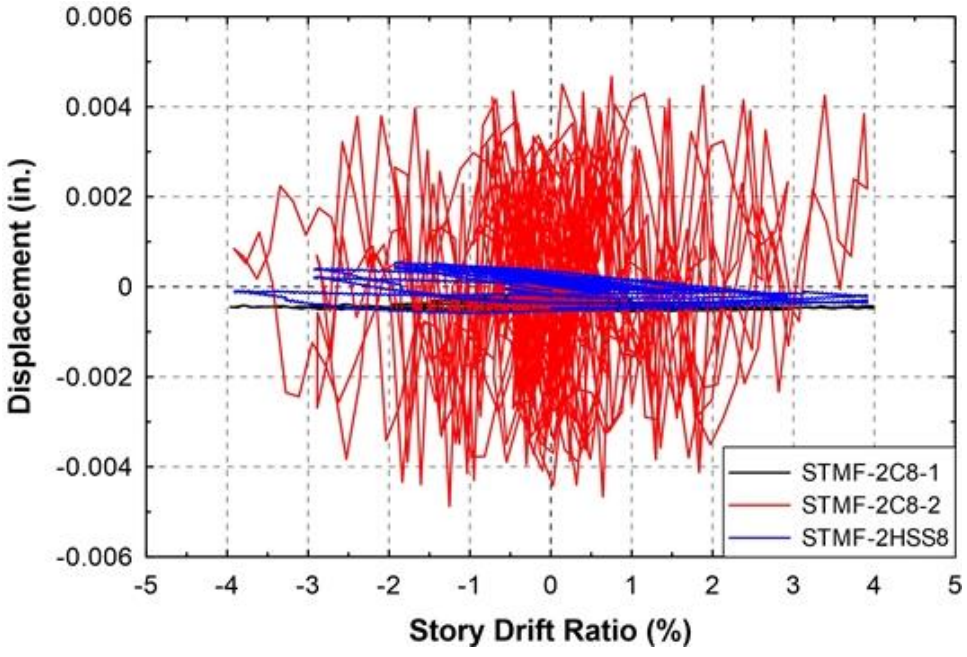
0.006
0.004
0.002
0
-0.002
-0.004
-0.006
Displacement (in.)
-5
-4
-3
-2
-1
0
1
2
3
4
5
Story Drift Ratio (%)
STMF-2C8-1
STMF-2C8-2
STMF-2HSS8

L-SW-W

Appendix I

Strain vs. Story Drift Ratio Response of Test Setup Strain Gauges

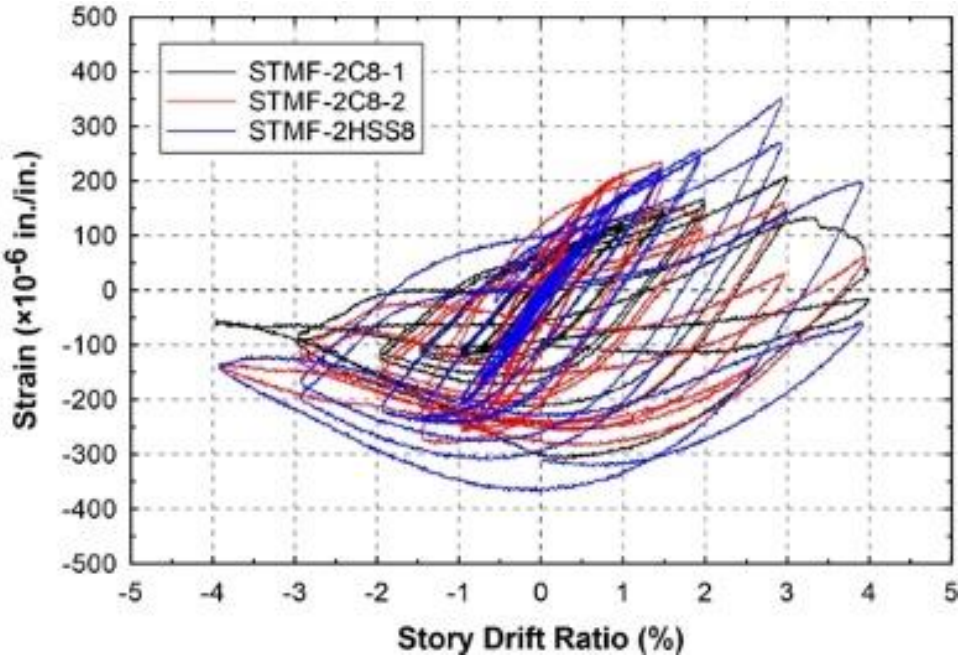
STMF-2C8-1
STMF-2C8-2
STMF-2HSS8
Strain (×10-6 in./in.)
Story Drift Ratio (%)
500
400
300
200
100
0
-100
-200
-300
-400
-500
-5
-4
-3
-2
-1
0
1
2
3
4
5

C-NE-1-1

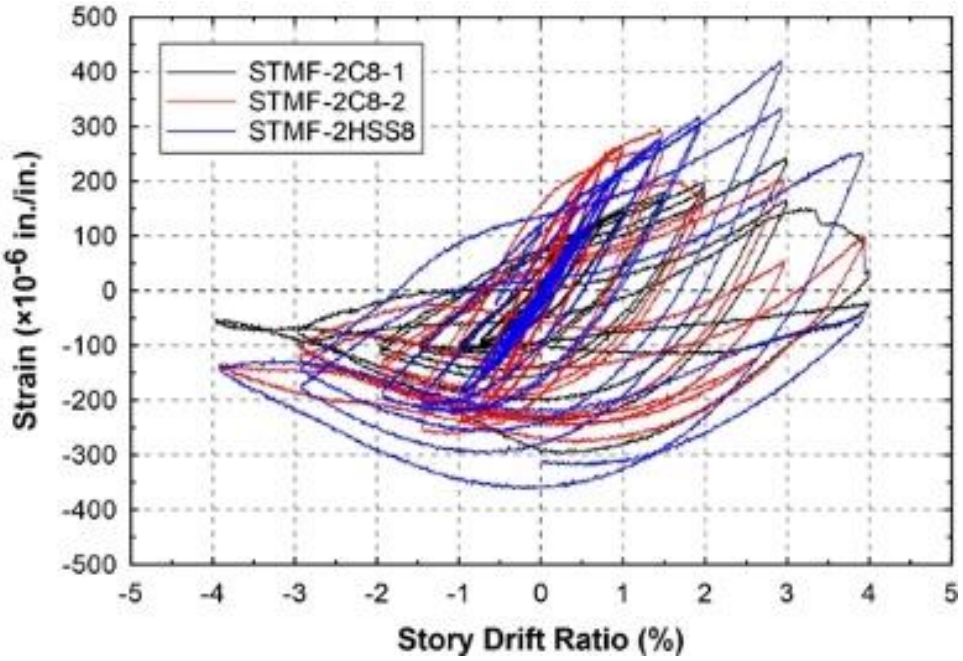
STMF-2C8-1
STMF-2C8-2
STMF-2HSS8
Strain (×10-6 in./in.)
Story Drift Ratio (%)
500
400
300
200
100
0
-100
-200
-300
-400
-500
-5
-4
-3
-2
-1
0
1
2
3
4
5

C-NE-1-2

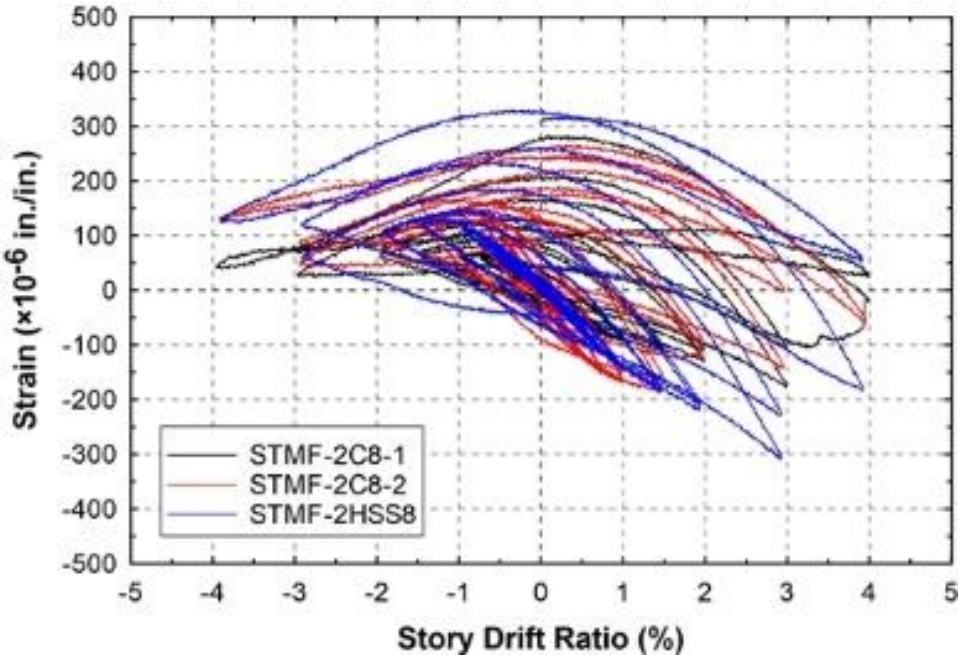
Strain (×10-6 in./in.)
Story Drift Ratio (%)
STMF-2C8-1
STMF-2C8-2
STMF-2HSS8

C-NE-1-3

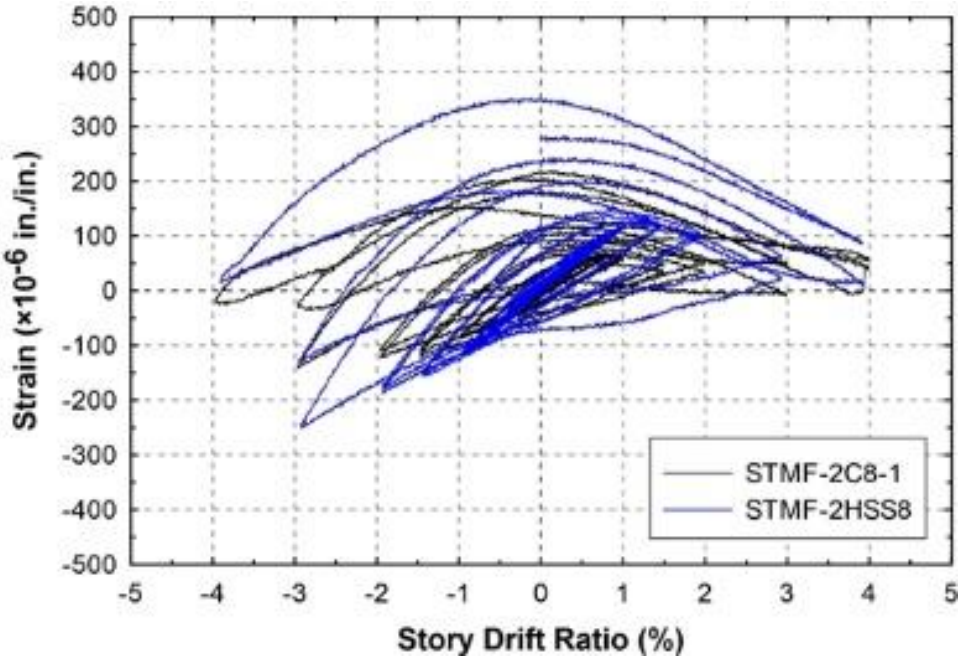
Strain (×10-6 in./in.)
Story Drift Ratio (%)
STMF-2C8-1
STMF-2HSS8

C-SW-1-1

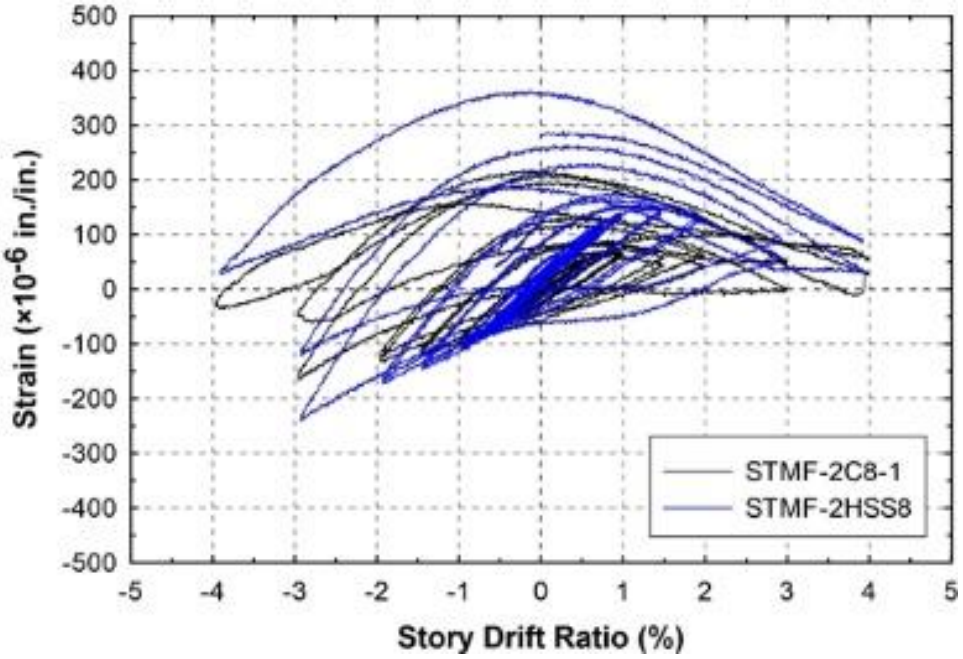
Strain (×10-6 in./in.)
Story Drift Ratio (%)
STMF-2C8-1
STMF-2HSS8

C-SW-1-2

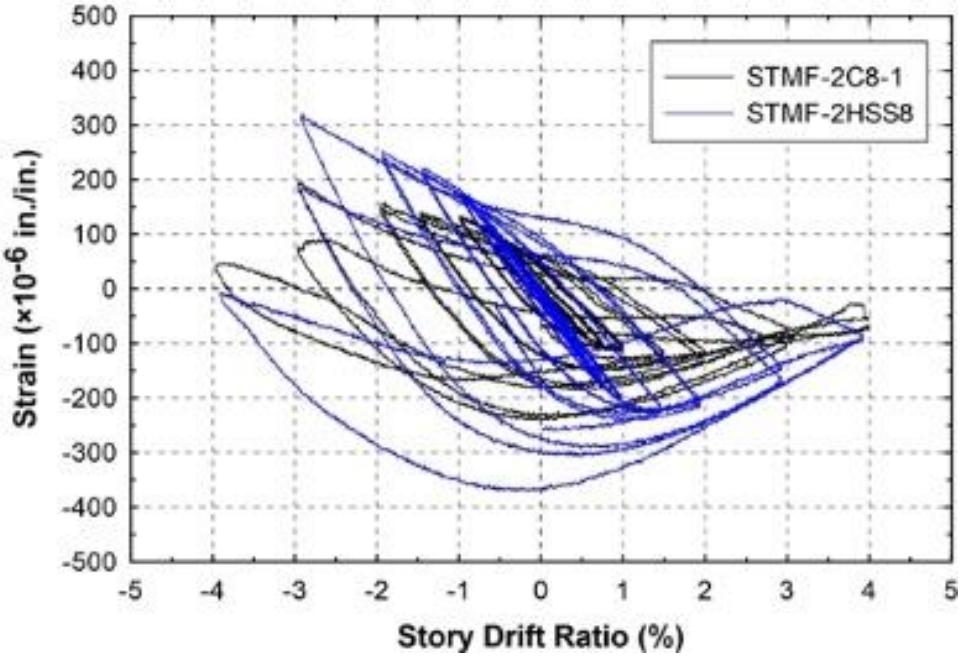
Strain (×10-6 in./in.)
Story Drift Ratio (%)
STMF-2C8-1
STMF-2HSS8

C-SW-1-3

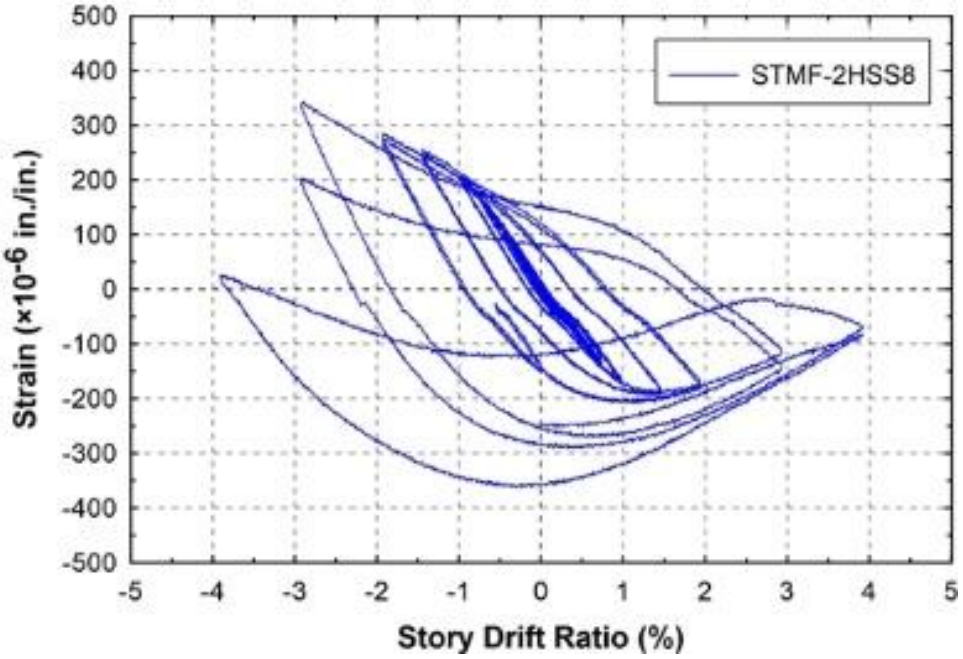
STMF-2HSS8
Strain (×10-6 in./in.)
Story Drift Ratio (%)
500
400
300
200
100
0
-100
-200
-300
-400
-500
-5
-4
-3
-2
-1
0
1
2
3
4
5

C-SW-1-4

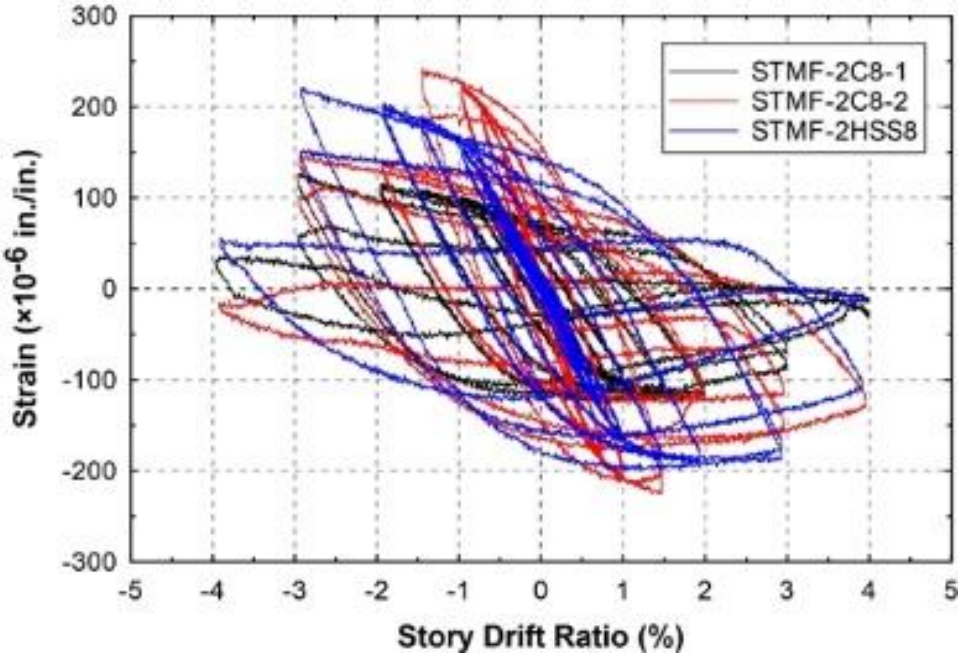
STMF-2C8-1
STMF-2C8-2
STMF-2HSS8
Strain (×10-6 in./in.)
Story Drift Ratio (%)
300
200
100
0
-100
-200
-300
-5
-4
-3
-2
-1
0
1
2
3
4
5

C-SW-2

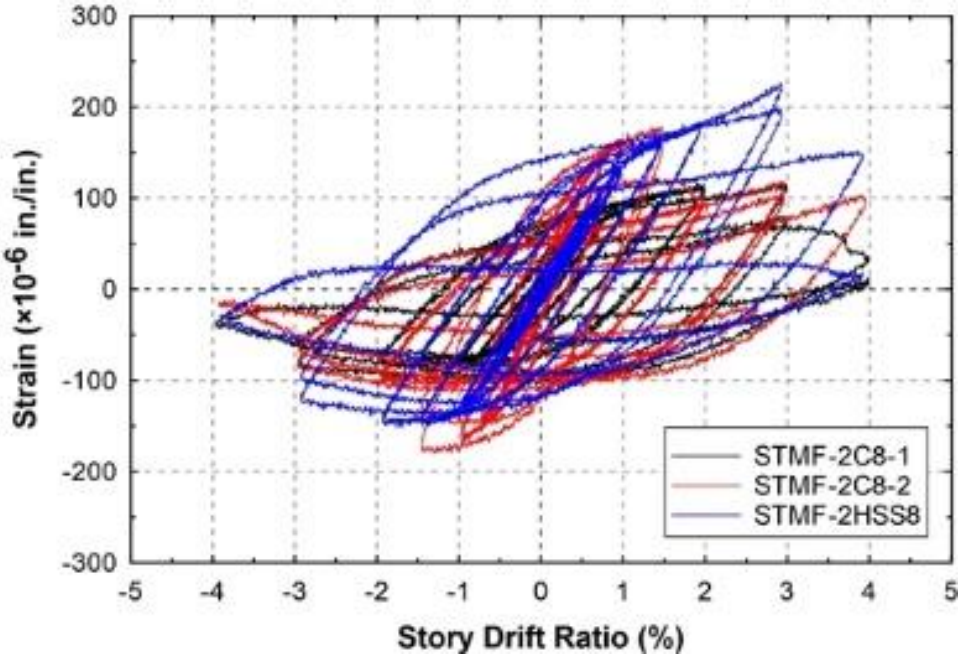
Strain (×10-6 in./in.)
Story Drift Ratio (%)
STMF-2C8-1
STMF-2C8-2
STMF-2HSS8

C-SW-3

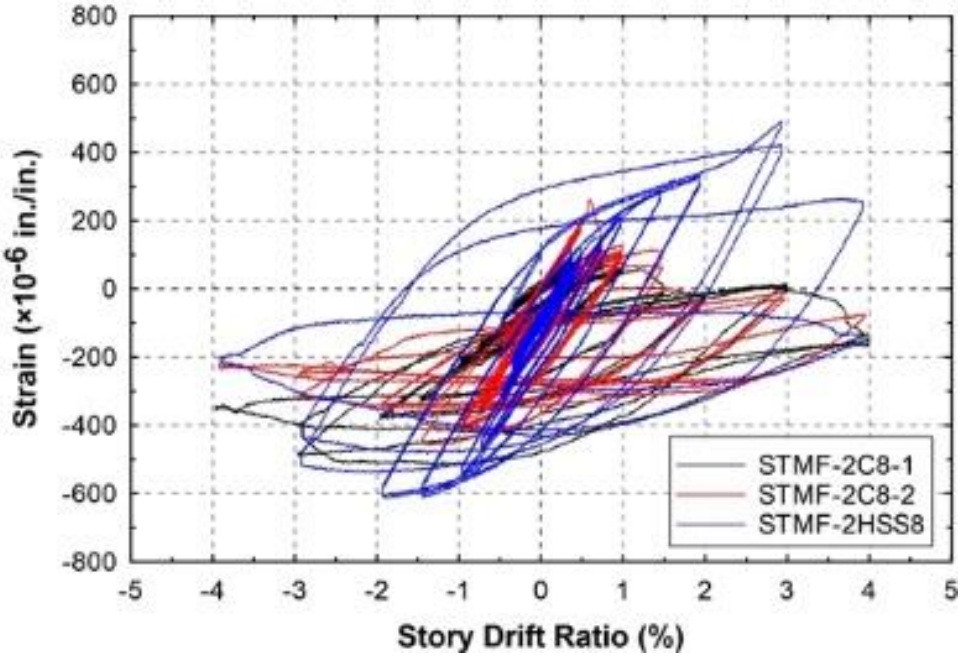
Strain (×10-6 in./in.)
Story Drift Ratio (%)
STMF-2C8-1
STMF-2C8-2
STMF-2HSS8

G-1

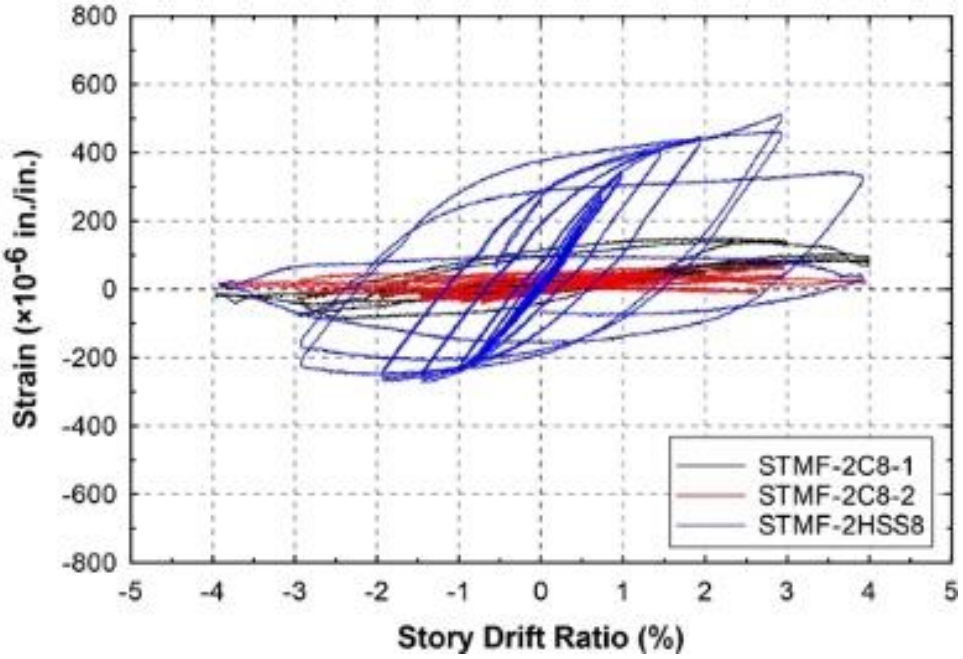
Strain (×10-6 in./in.)
Story Drift Ratio (%)
STMF-2C8-1
STMF-2C8-2
STMF-2HSS8

G-2

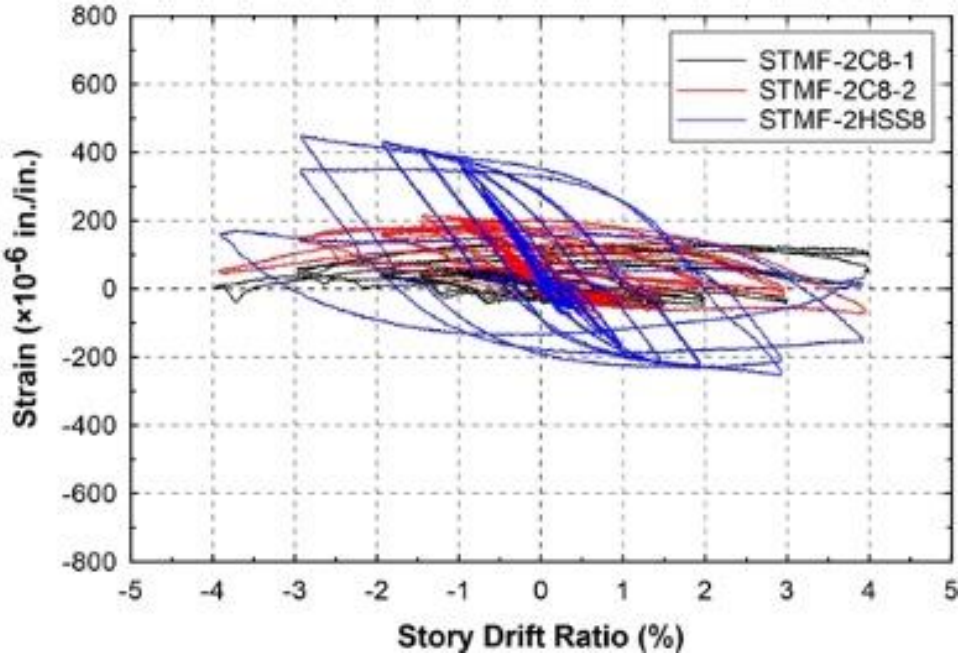
Strain (×10-6 in./in.)
Story Drift Ratio (%)
STMF-2C8-1
STMF-2C8-2
STMF-2HSS8

G-3

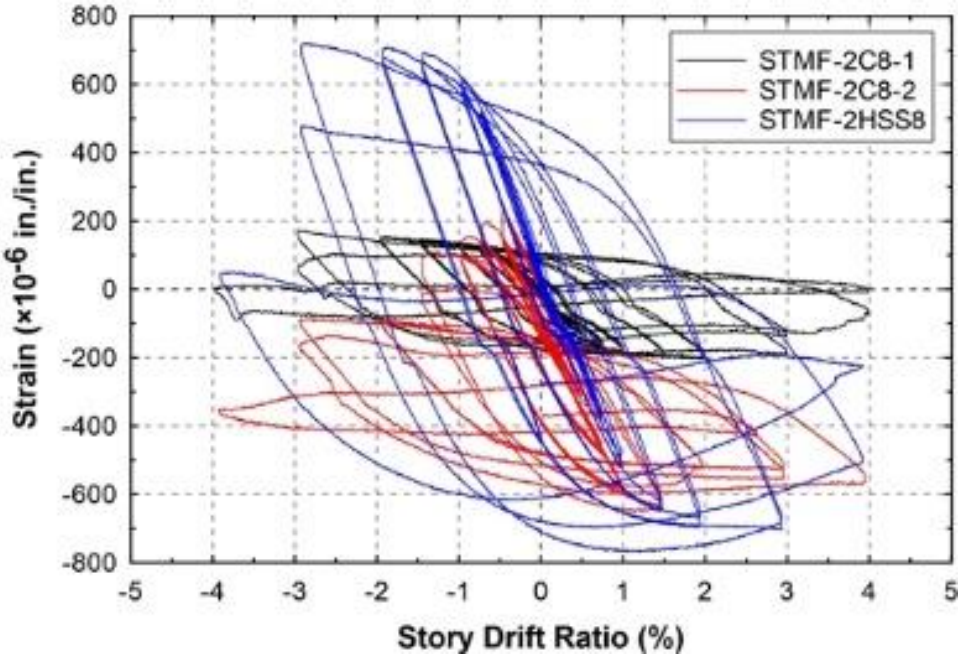
STMF-2C8-1
STMF-2C8-2
STMF-2HSS8
Strain (×10-6 in./in.)
Story Drift Ratio (%)

G-4

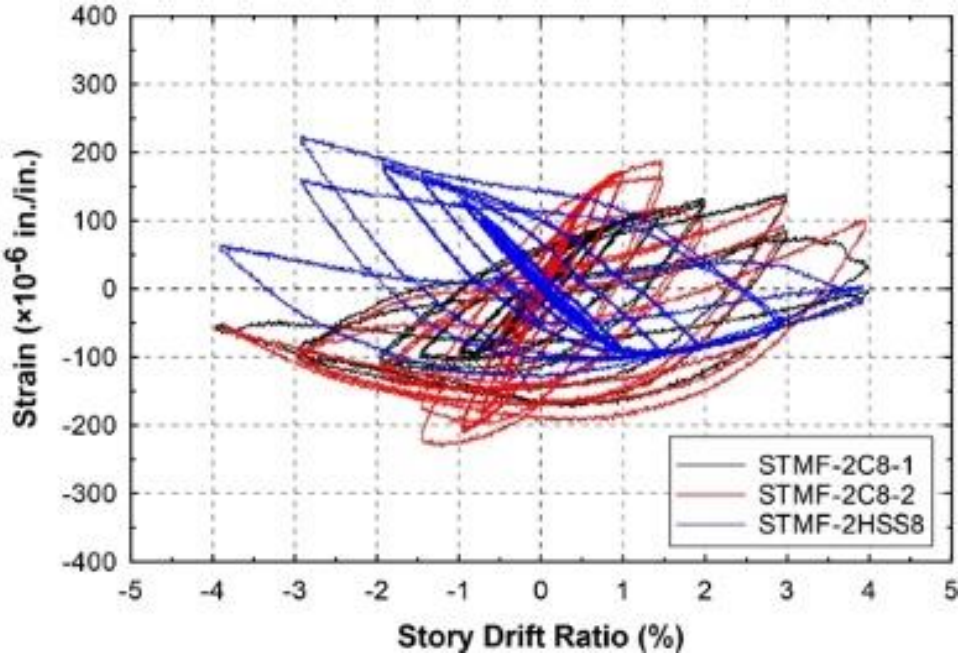
STMF-2C8-1
STMF-2C8-2
STMF-2HSS8
Strain (×10-6 in./in.)
Story Drift Ratio (%)

G-RS-1

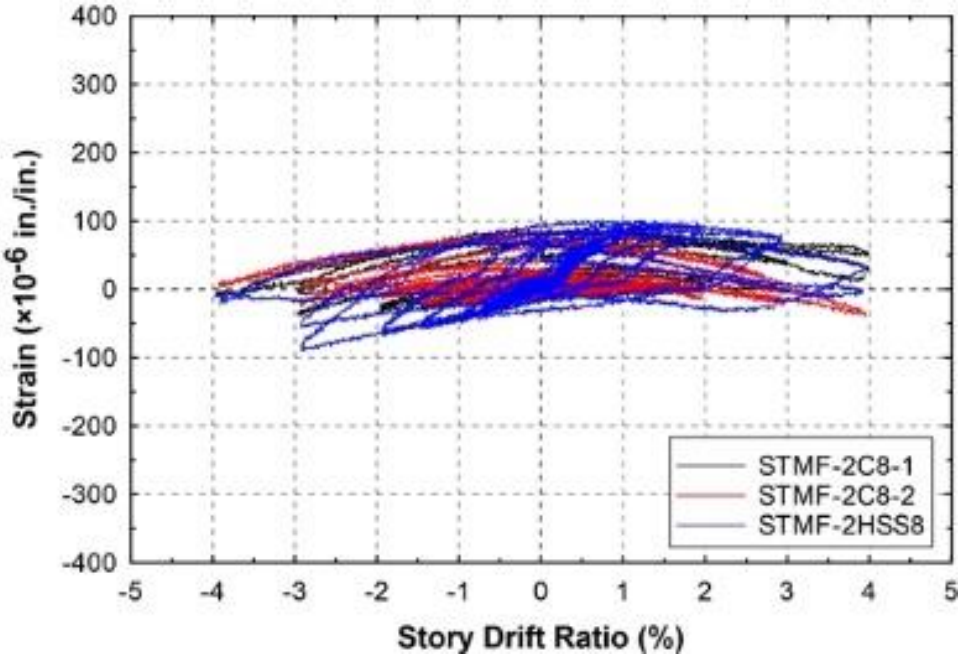
Strain (×10-6 in./in.)
Story Drift Ratio (%)
STMF-2C8-1
STMF-2C8-2
STMF-2HSS8

G-RS-2

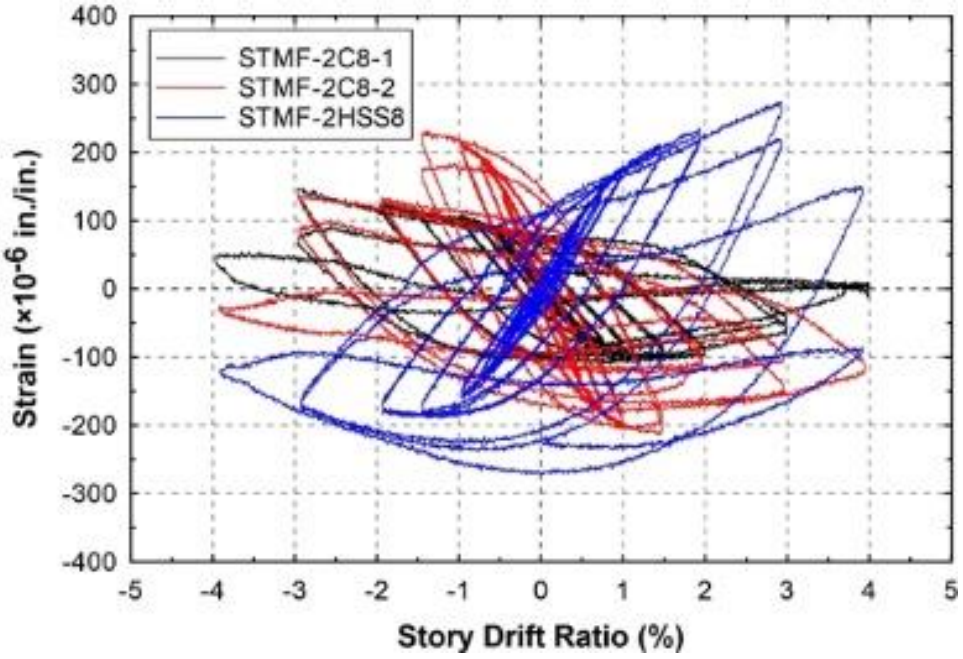
Strain (×10-6 in./in.)
Story Drift Ratio (%)
STMF-2C8-1
STMF-2C8-2
STMF-2HSS8

G-RS-3

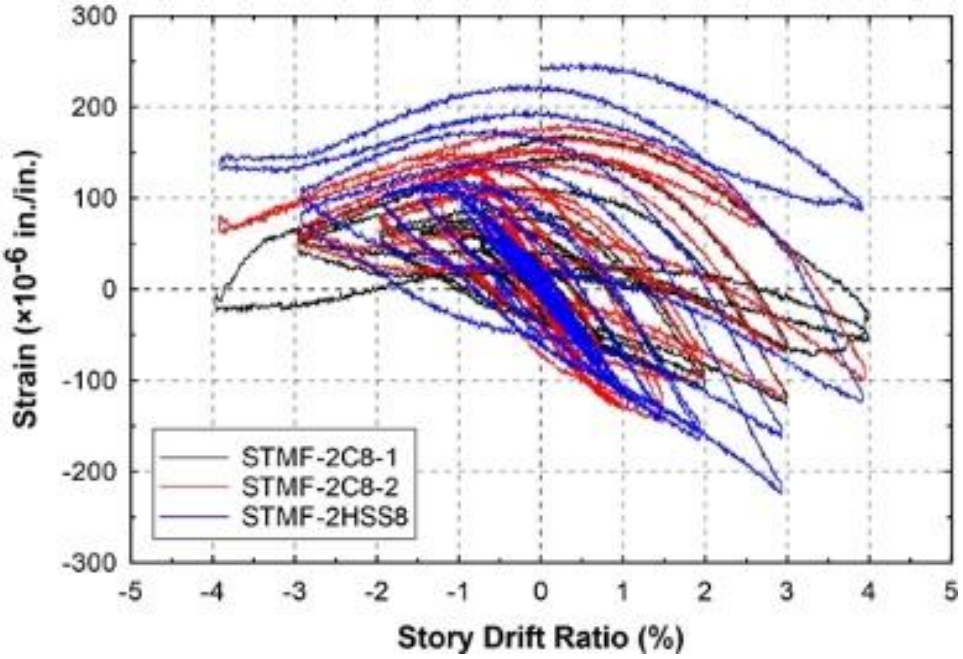
Strain (×10-6 in./in.)
Story Drift Ratio (%)
STMF-2C8-1
STMF-2C8-2
STMF-2HSS8

LTB-1-1

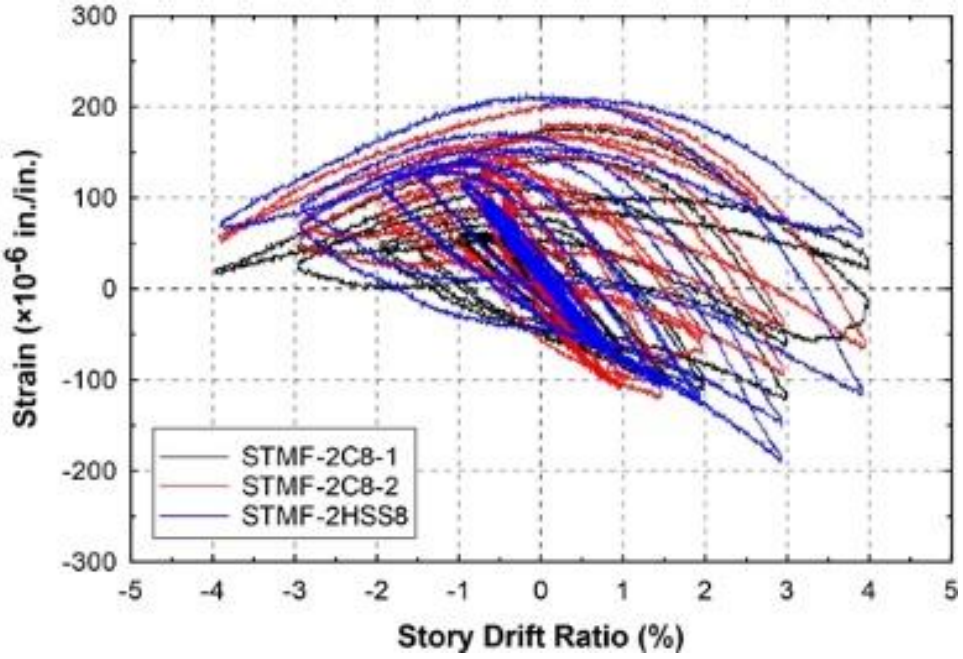
Strain (×10-6 in./in.)
Story Drift Ratio (%)
STMF-2C8-1
STMF-2C8-2
STMF-2HSS8

LTB-1-2

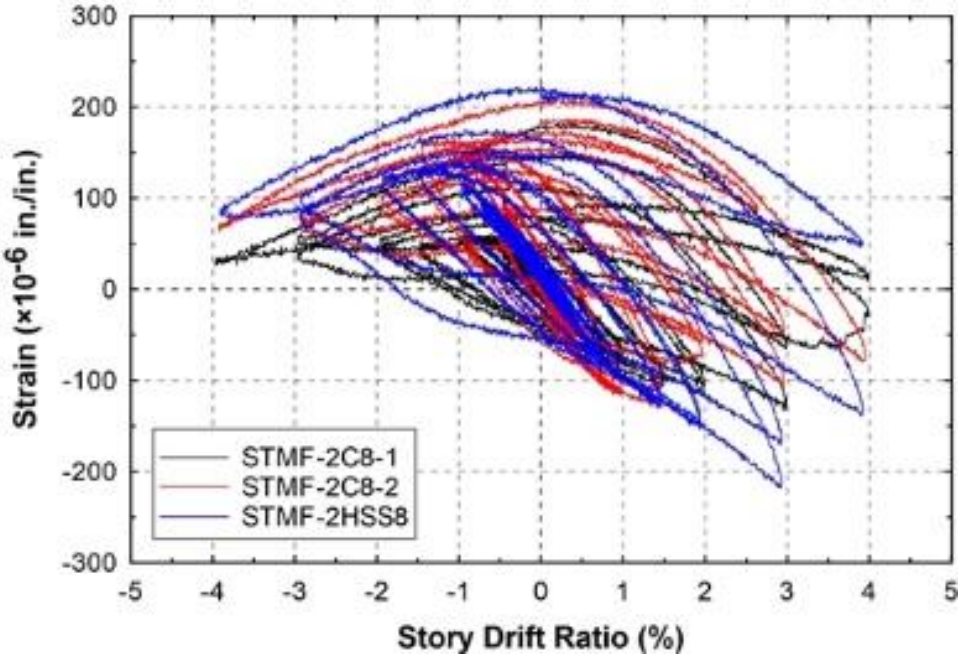
300
200
100
0
-100
-200
-300
-5
-4
-3
-2
-1
0
1
2
3
4
5
Strain (×10-6 in./in.)
Story Drift Ratio (%)
STMF-2C8-1
STMF-2C8-2
STMF-2HSS8

LTB-1-3

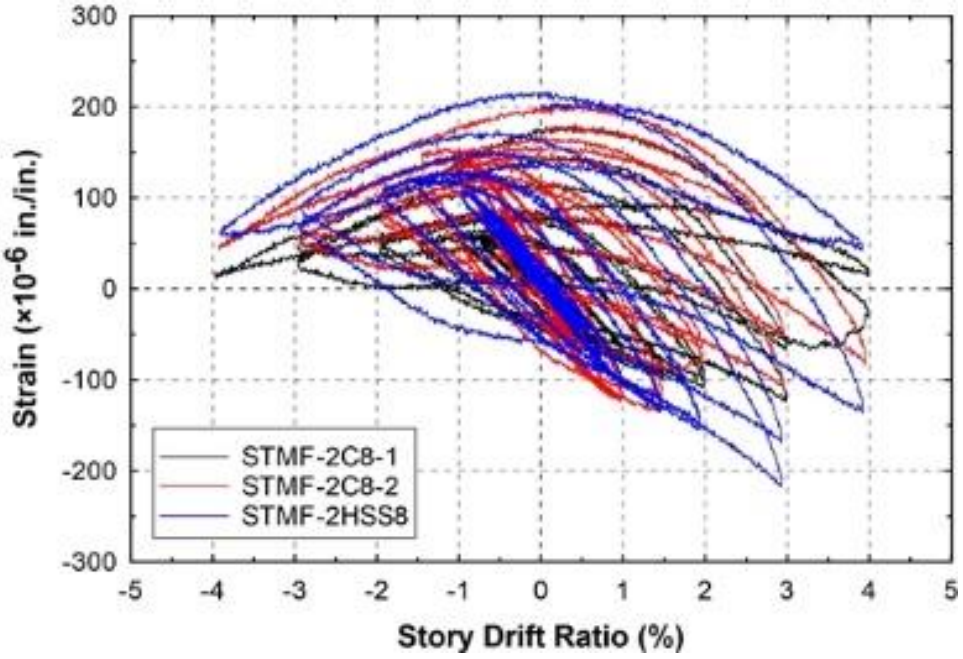
300
200
100
0
-100
-200
-300
-5
-4
-3
-2
-1
0
1
2
3
4
5
Strain (×10-6 in./in.)
Story Drift Ratio (%)
STMF-2C8-1
STMF-2C8-2
STMF-2HSS8

LTB-1-4

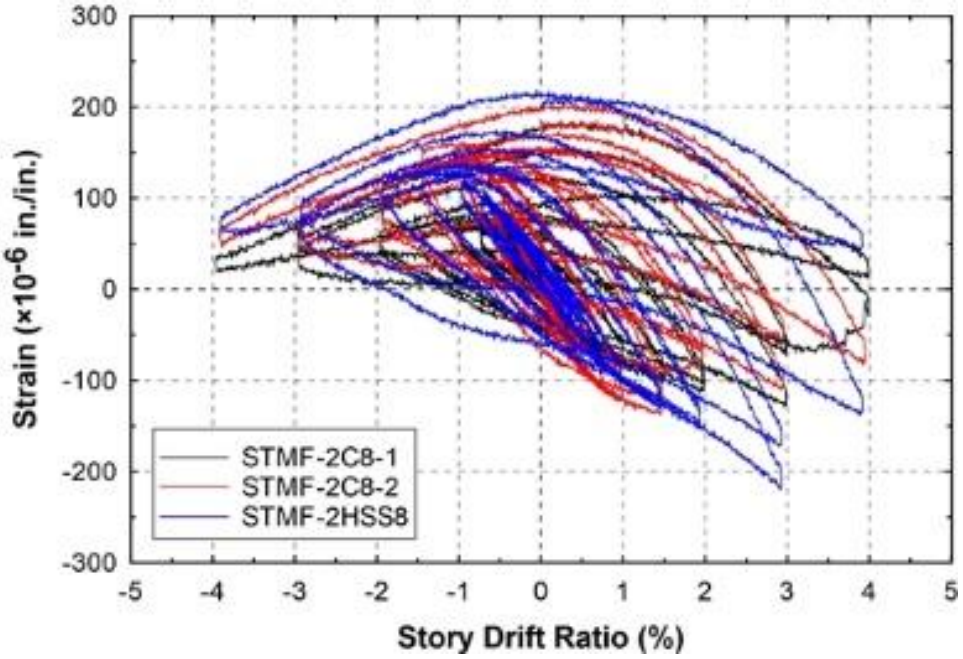
300
200
100
0
-100
-200
-300
-5
-4
-3
-2
-1
0
1
2
3
4
5
Strain (×10-6 in./in.)
Story Drift Ratio (%)
STMF-2C8-1
STMF-2C8-2
STMF-2HSS8

LTB-2

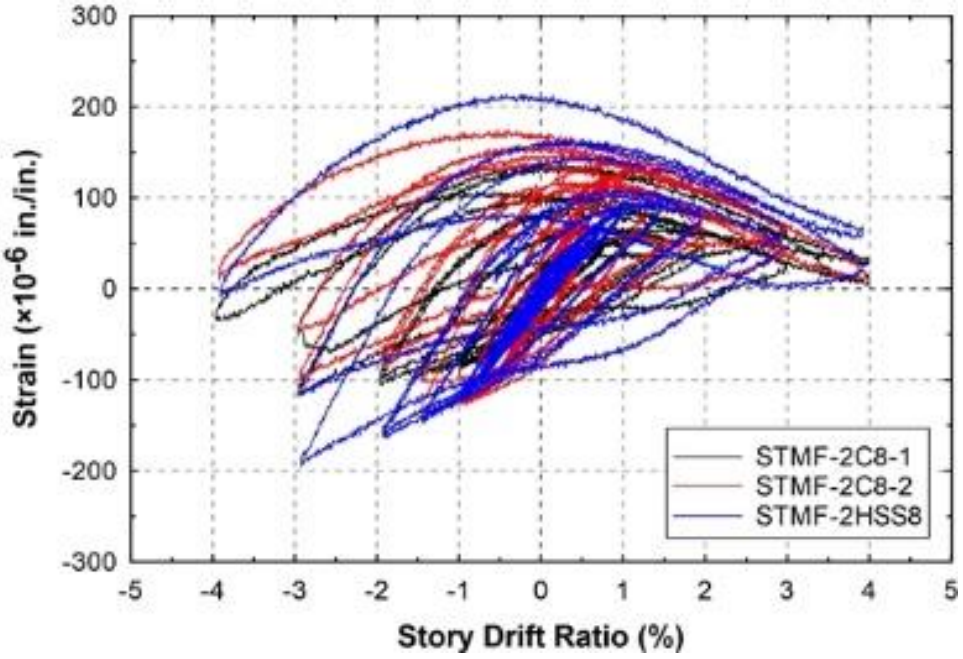
300
200
100
0
-100
-200
-300
-5
-4
-3
-2
-1
0
1
2
3
4
5
Strain (×10-6 in./in.)
Story Drift Ratio (%)
STMF-2C8-1
STMF-2C8-2
STMF-2HSS8

LTB-3-1

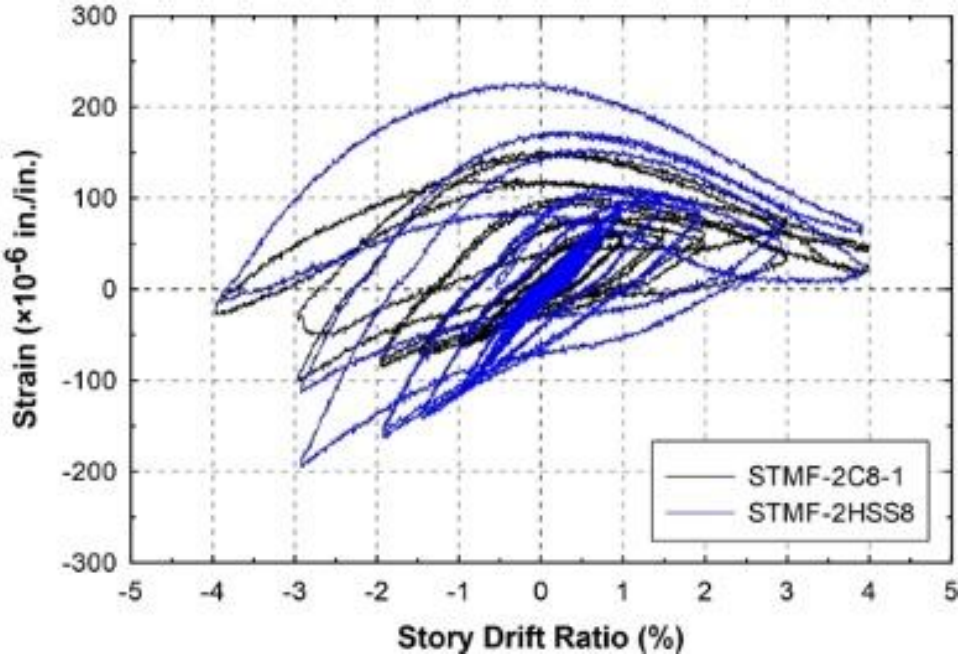
Strain (×10-6 in./in.)
Story Drift Ratio (%)
STMF-2C8-1
STMF-2HSS8

LTB-3-2

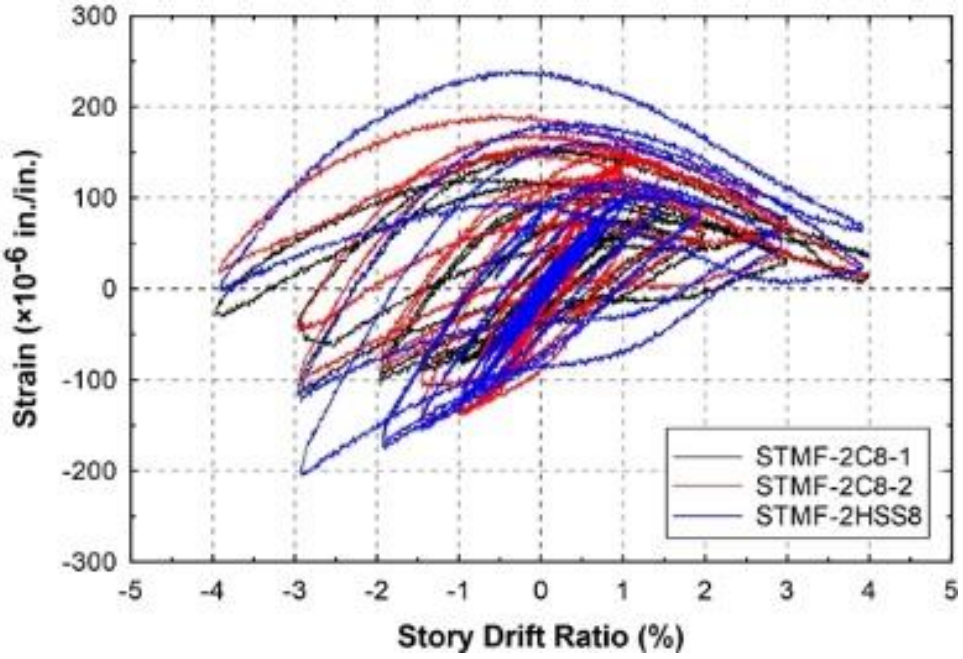
Strain (×10-6 in./in.)
Story Drift Ratio (%)
STMF-2C8-1
STMF-2C8-2
STMF-2HSS8

LTB-3-3

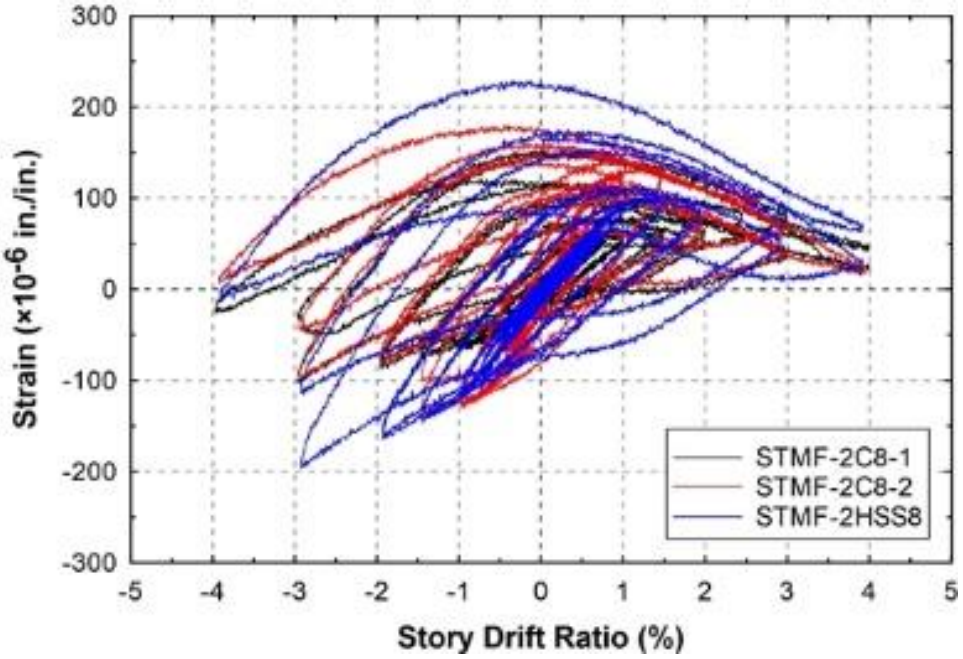

LTB-3-4

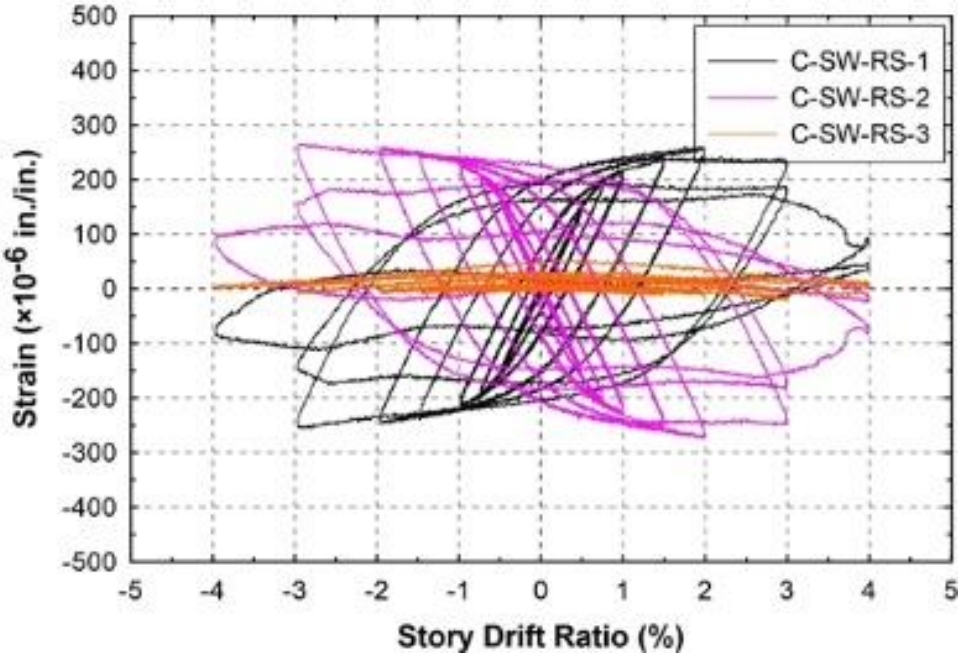

STMF 1-1 - C-SW-RS-x

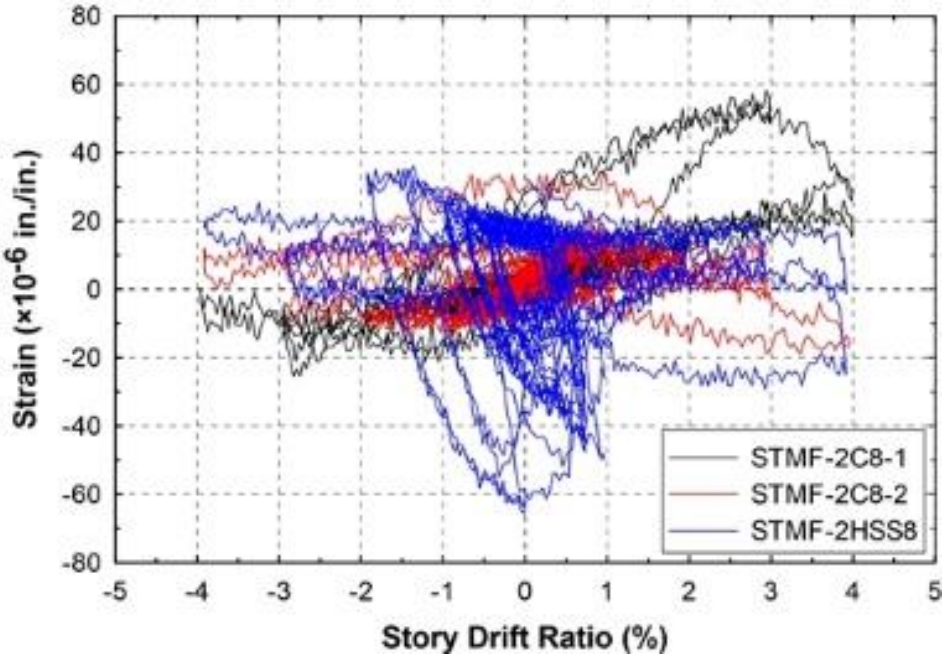
Strain (×10-6 in./in.)
Story Drift Ratio (%)
STMF-2C8-1
STMF-2C8-2
STMF-2HSS8

TB-1-1

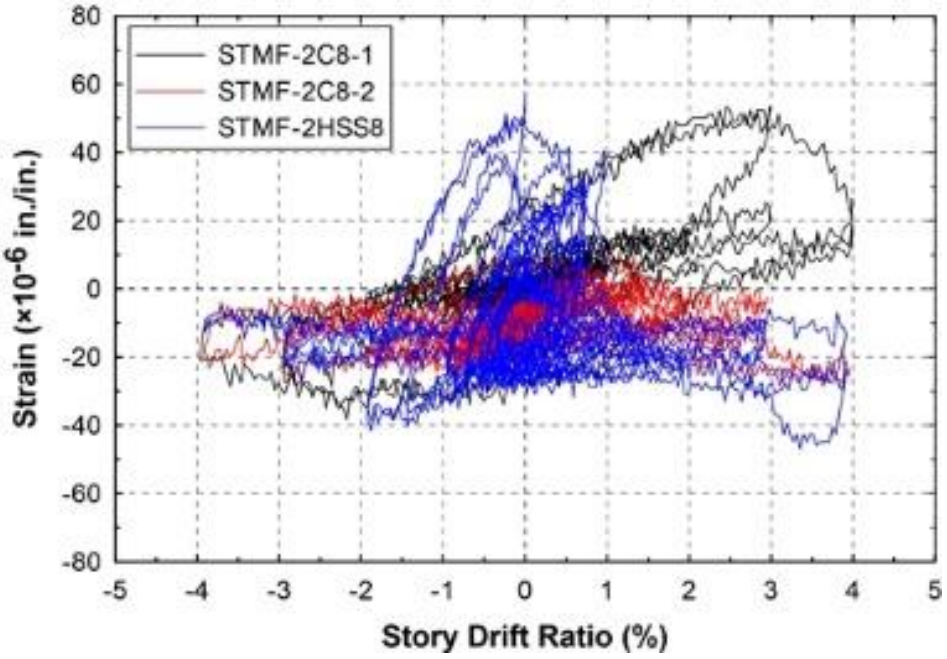
Strain (×10-6 in./in.)
Story Drift Ratio (%)
STMF-2C8-1
STMF-2C8-2
STMF-2HSS8

TB-1-2

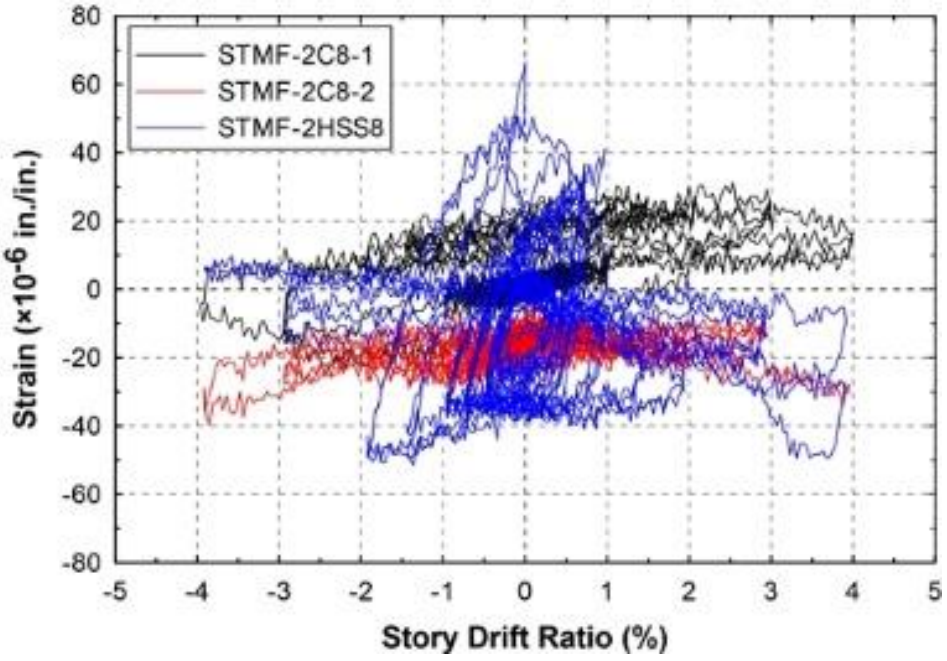
STMF-2C8-1
STMF-2C8-2
STMF-2HSS8
Strain (×10-6 in./in.)
Story Drift Ratio (%)

TB-2

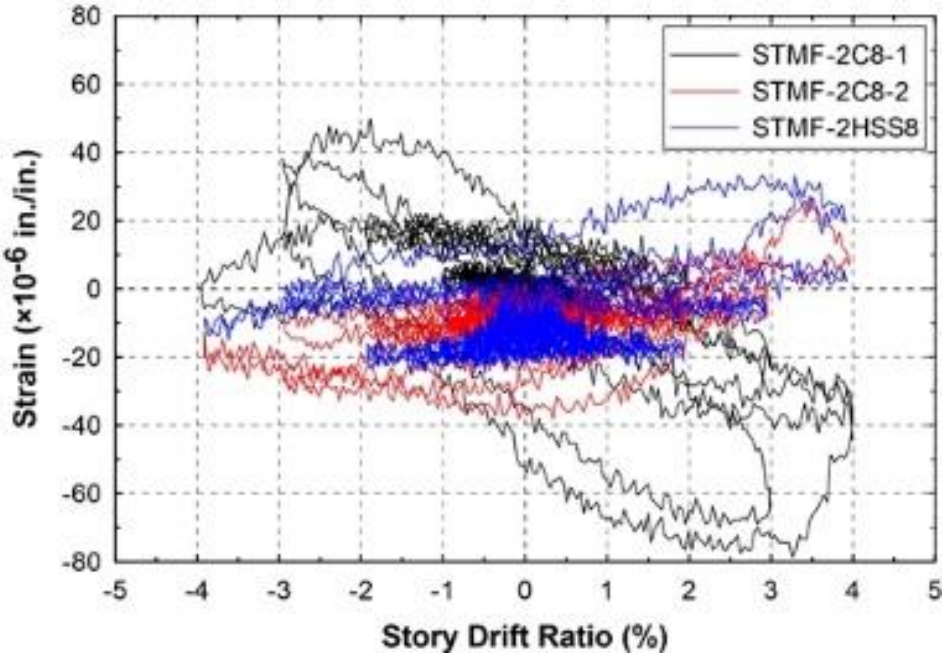
STMF-2C8-1
STMF-2C8-2
STMF-2HSS8
Strain (×10-6 in./in.)
Story Drift Ratio (%)

TB-3-1

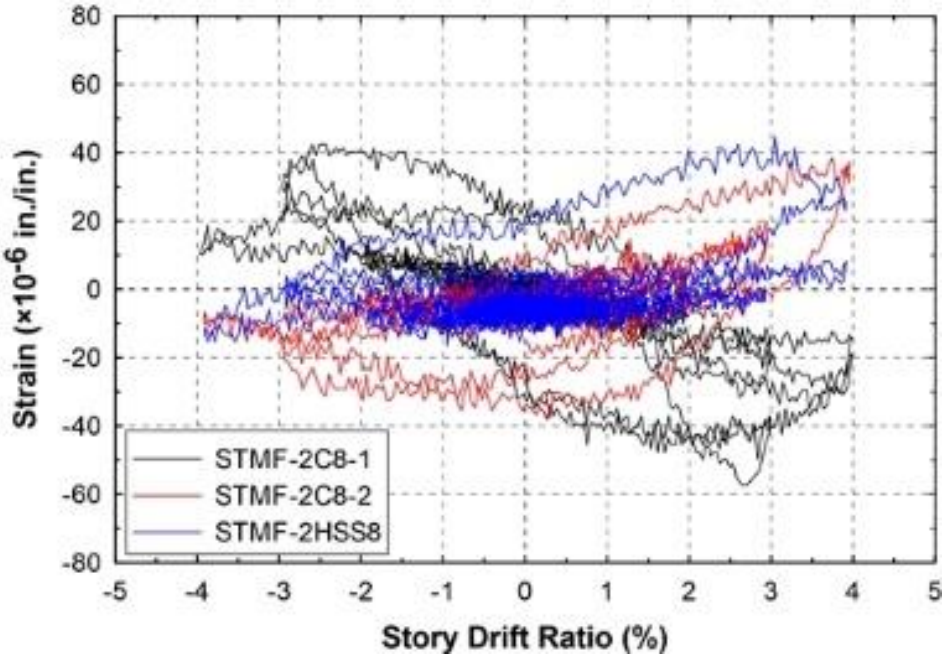
Strain (×10-6 in./in.)
Story Drift Ratio (%)
STMF-2C8-1
STMF-2C8-2
STMF-2HSS8

TB-3-2

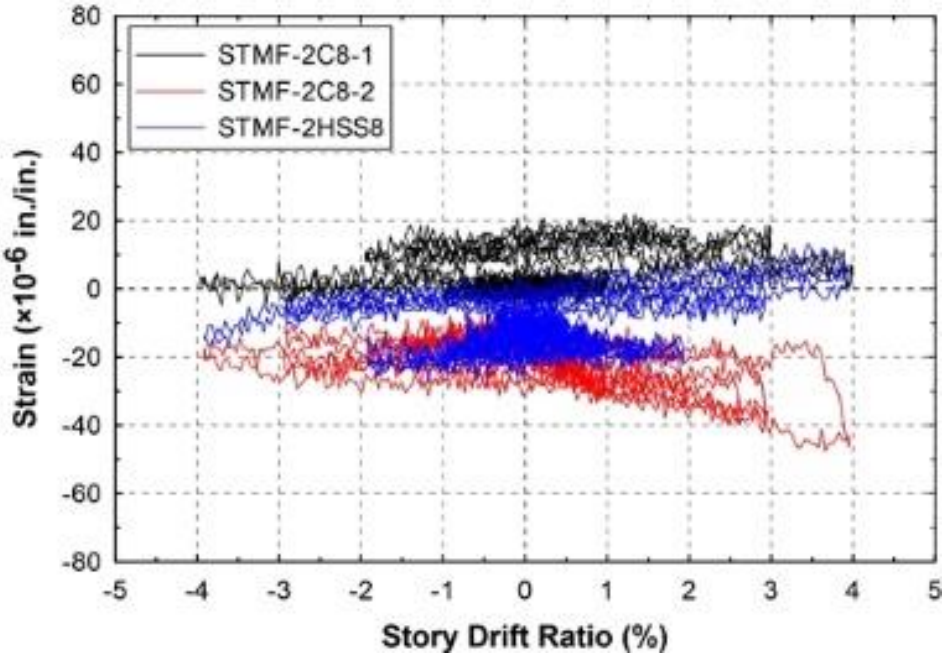
Strain (×10-6 in./in.)
Story Drift Ratio (%)
STMF-2C8-1
STMF-2C8-2
STMF-2HSS8

TB-4

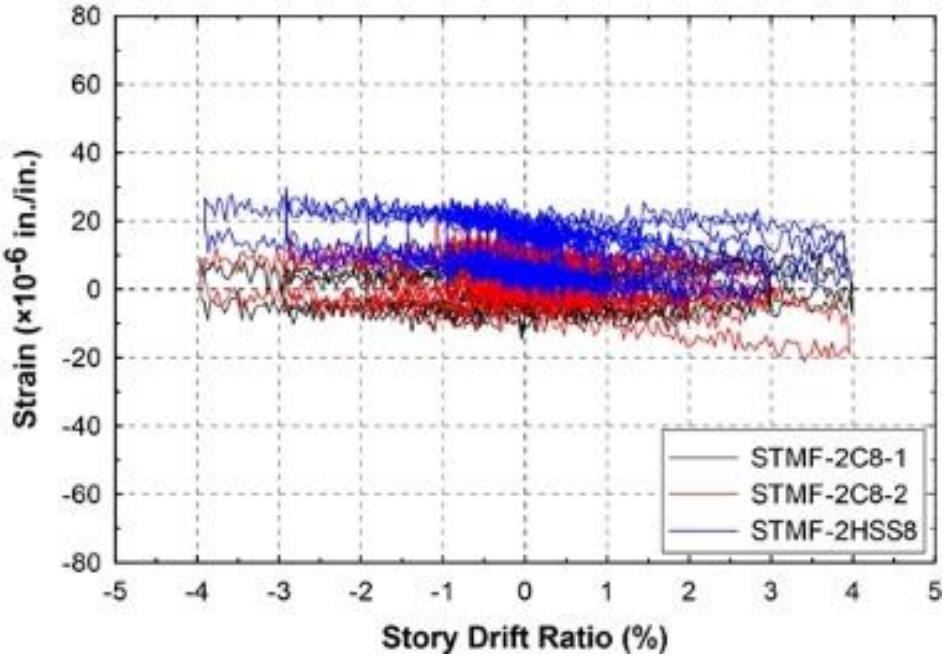
Strain (×10-6 in./in.)
Story Drift Ratio (%)
STMF-2C8-1
STMF-2C8-2
STMF-2HSS8

TB-5

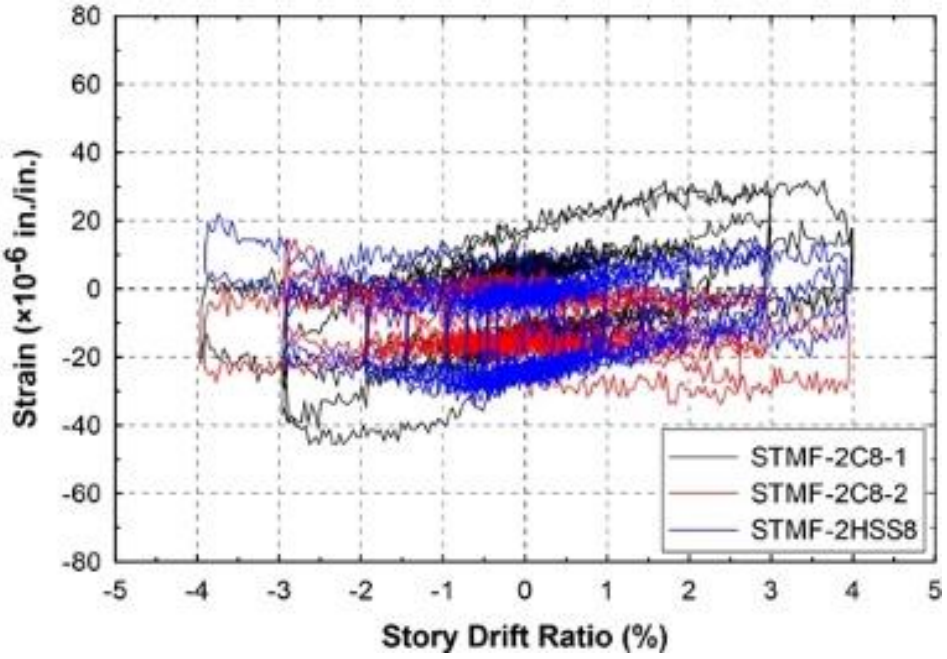
Strain (×10-6 in./in.)
Story Drift Ratio (%)
STMF-2C8-1
STMF-2C8-2
STMF-2HSS8

TB-6

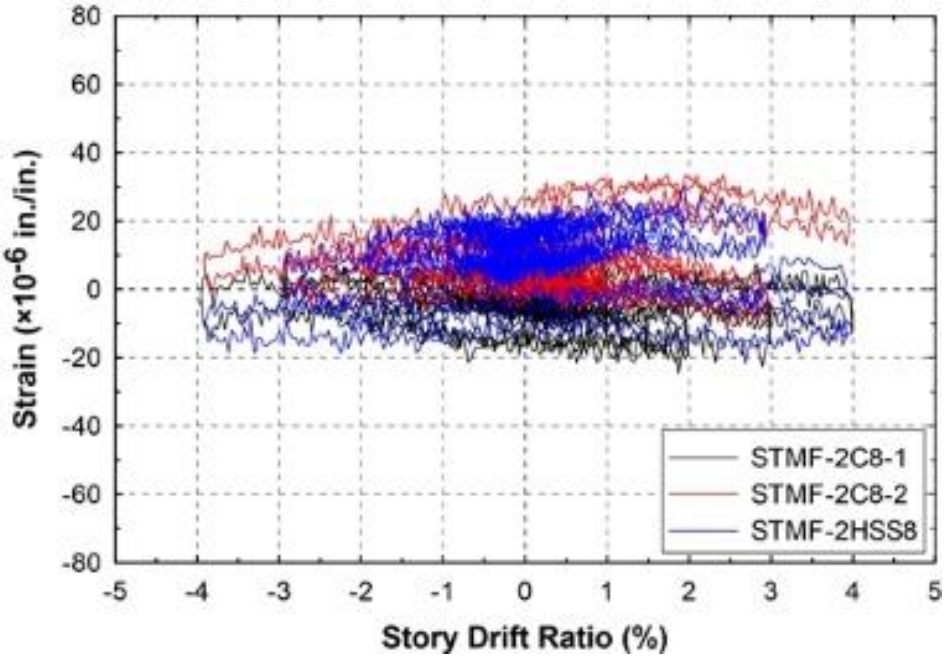
Strain (×10-6 in./in.)
Story Drift Ratio (%)
STMF-2C8-1
STMF-2C8-2
STMF-2HSS8

TB-7

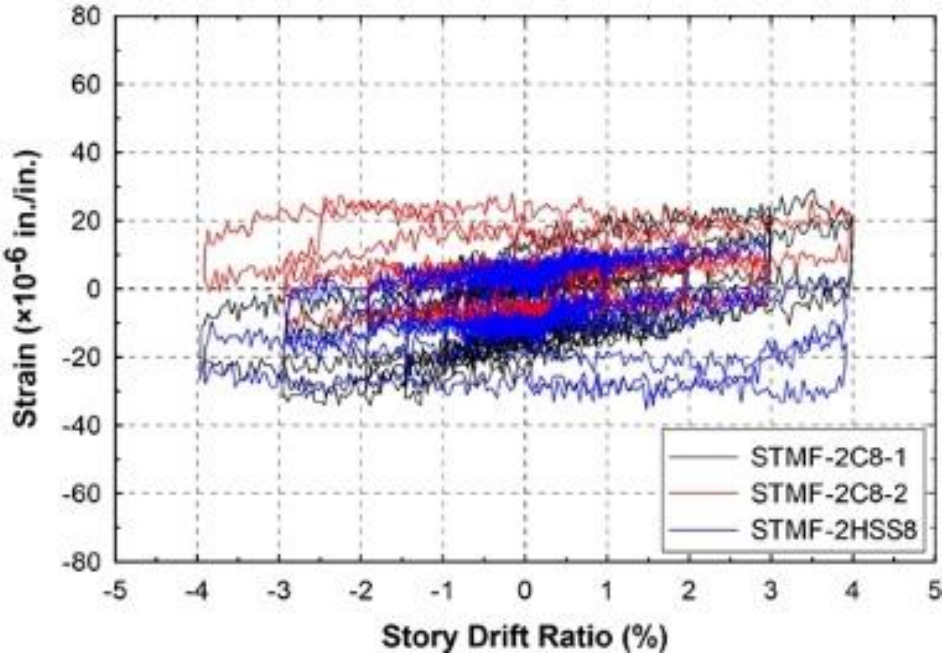
Strain (×10-6 in./in.)
Story Drift Ratio (%)
STMF-2C8-1
STMF-2C8-2
STMF-2HSS8

TB-8

Appendix J

Strain vs. Story Drift Ratio Response of Member Strain Gauges

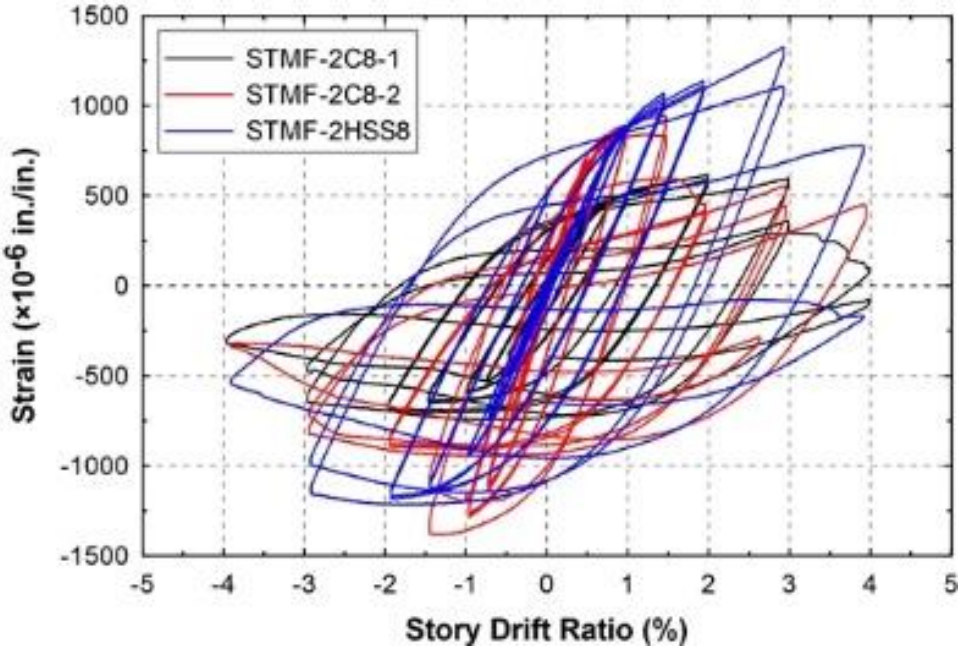
STMF-2C8-1
STMF-2C8-2
STMF-2HSS8
Strain (×10-6 in./in.)
Story Drift Ratio (%)
1500
1000
500
0
-500
-1000
-1500
-5
-4
-3
-2
-1
0
1
2
3
4
5

M1-1-1

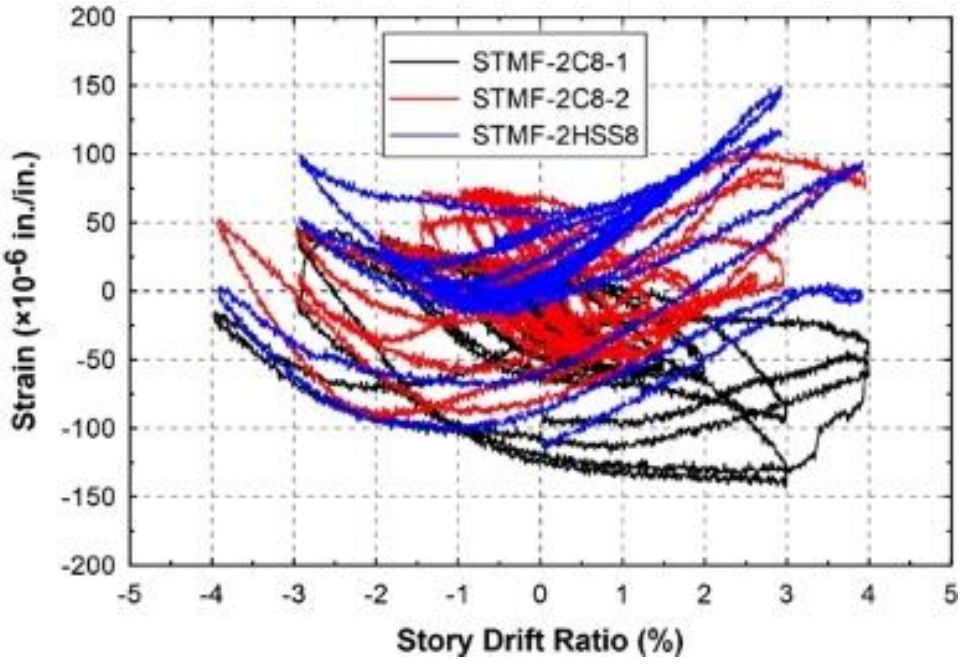
STMF-2C8-1
STMF-2C8-2
STMF-2HSS8
Strain (×10-6 in./in.)
Story Drift Ratio (%)
200
150
100
50
0
-50
-100
-150
-200
-5
-4
-3
-2
-1
0
1
2
3
4
5

M1-1-2

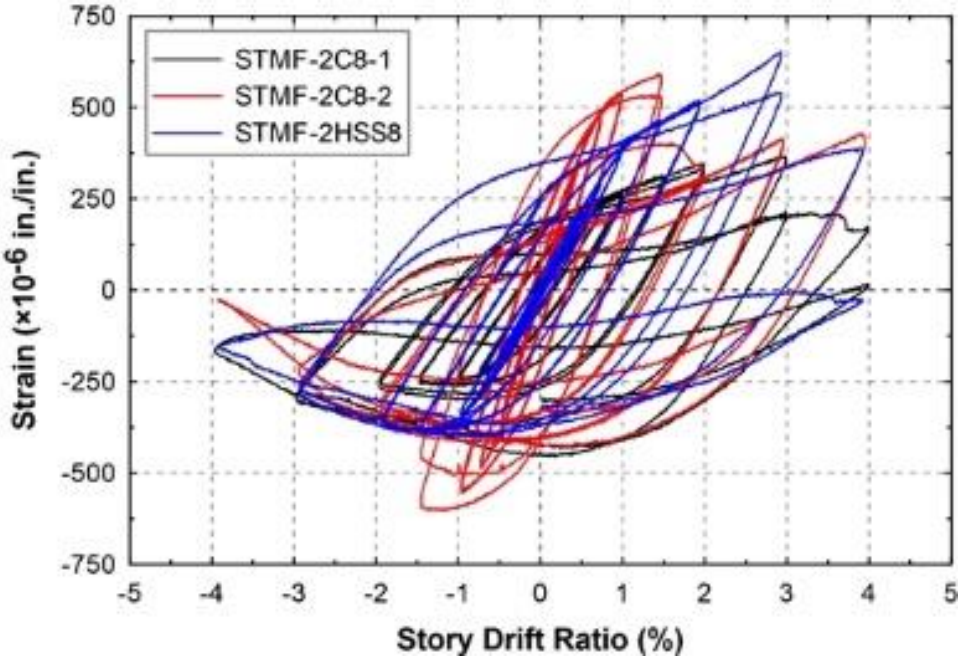
STMF-2C8-1
STMF-2C8-2
STMF-2HSS8
Strain (×10-6 in./in.)
Story Drift Ratio (%)
750
500
250
0
-250
-500
-750
-5
-4
-3
-2
-1
0
1
2
3
4
5

M1-2-1

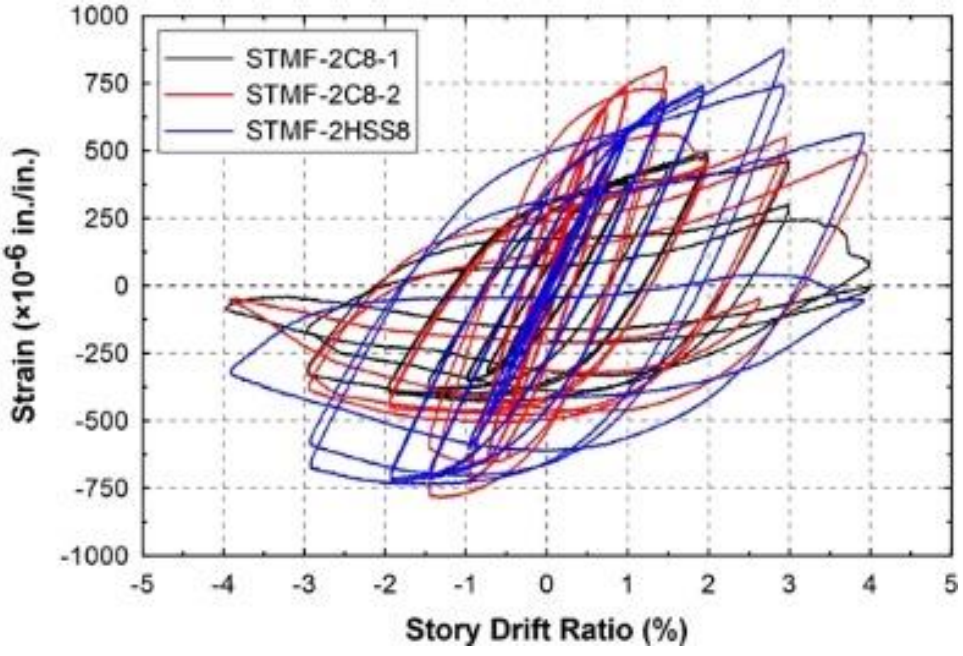
STMF-2C8-1
STMF-2C8-2
STMF-2HSS8
Strain (×10-6 in./in.)
Story Drift Ratio (%)
1000
750
500
250
0
-250
-500
-750
-1000
-5
-4
-3
-2
-1
0
1
2
3
4
5

M1-2-2

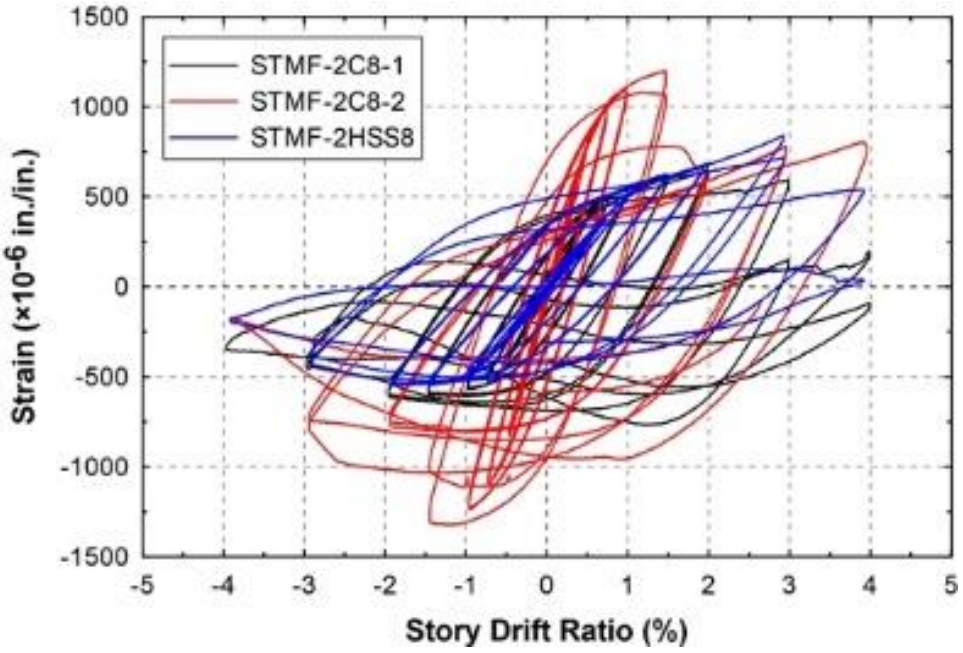
STMF-2C8-1
STMF-2C8-2
STMF-2HSS8
Strain (×10-6 in./in.)
Story Drift Ratio (%)
1500
1000
500
0
-500
-1000
-1500
-5
-4
-3
-2
-1
0
1
2
3
4
5

M2-1-1

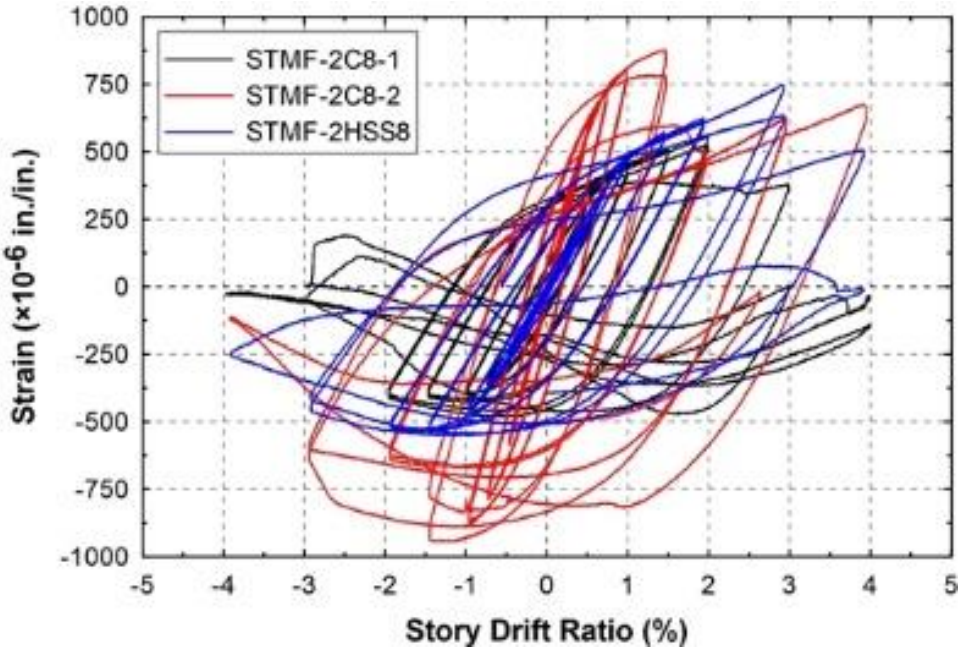
STMF-2C8-1
STMF-2C8-2
STMF-2HSS8
Strain (×10-6 in./in.)
Story Drift Ratio (%)
1000
750
500
250
0
-250
-500
-750
-1000
-5
-4
-3
-2
-1
0
1
2
3
4
5

M2-1-2

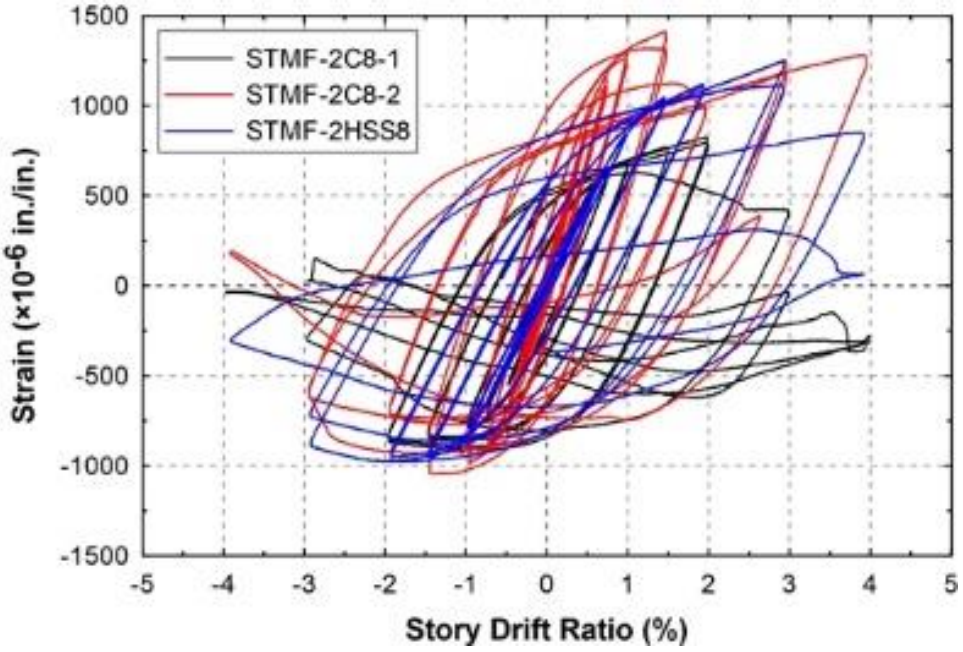
STMF-2C8-1
STMF-2C8-2
STMF-2HSS8
Strain (×10-6 in./in.)
Story Drift Ratio (%)
1500
1000
500
0
-500
-1000
-1500
-5
-4
-3
-2
-1
0
1
2
3
4
5

M2-2-1

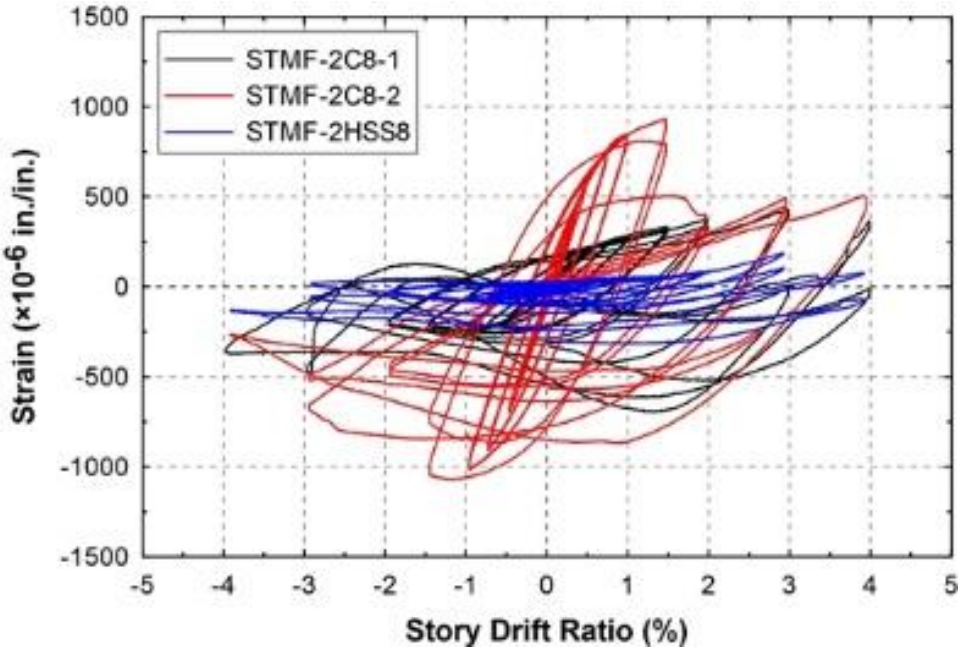
STMF-2C8-1
STMF-2C8-2
STMF-2HSS8
Strain (×10-6 in./in.)
Story Drift Ratio (%)
1500
1000
500
0
-500
-1000
-1500
-5
-4
-3
-2
-1
0
1
2
3
4
5

M2-2-2

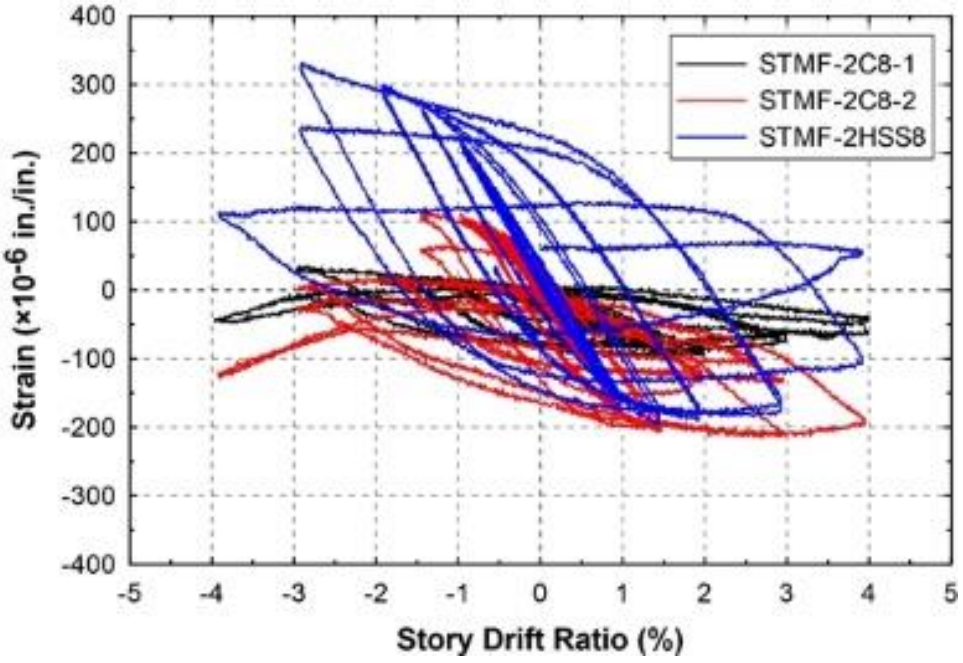
STMF-2C8-1
STMF-2C8-2
STMF-2HSS8
Strain (×10-6 in./in.)
Story Drift Ratio (%)
400
300
200
100
0
-100
-200
-300
-400
-5
-4
-3
-2
-1
0
1
2
3
4
5

M4-1-1

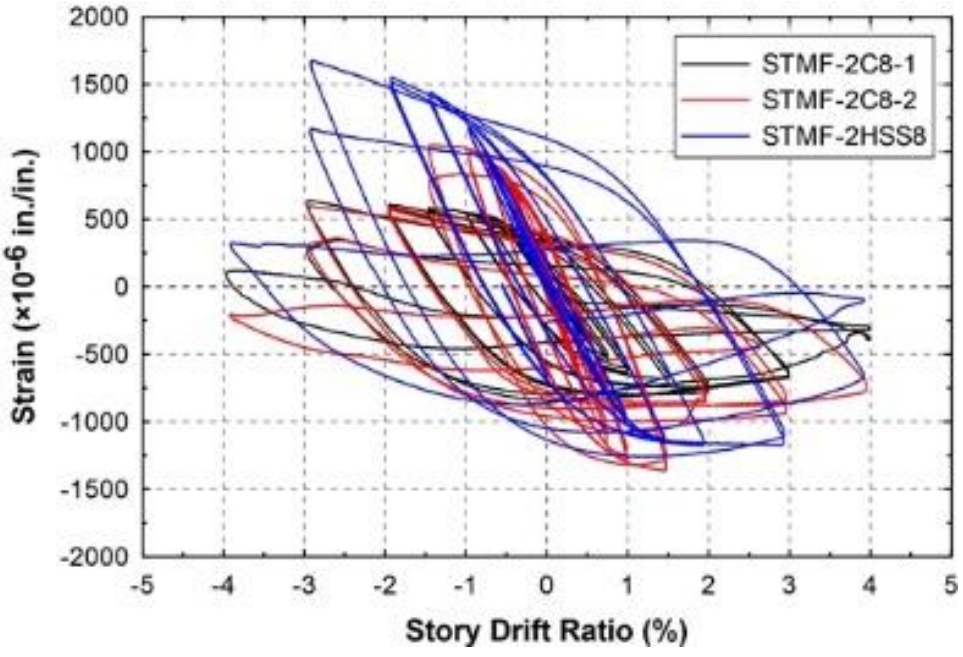
STMF-2C8-1
STMF-2C8-2
STMF-2HSS8
Strain (×10-6 in./in.)
Story Drift Ratio (%)
2000
1500
1000
500
0
-500
-1000
-1500
-2000
-5
-4
-3
-2
-1
0
1
2
3
4
5

M4-1-2

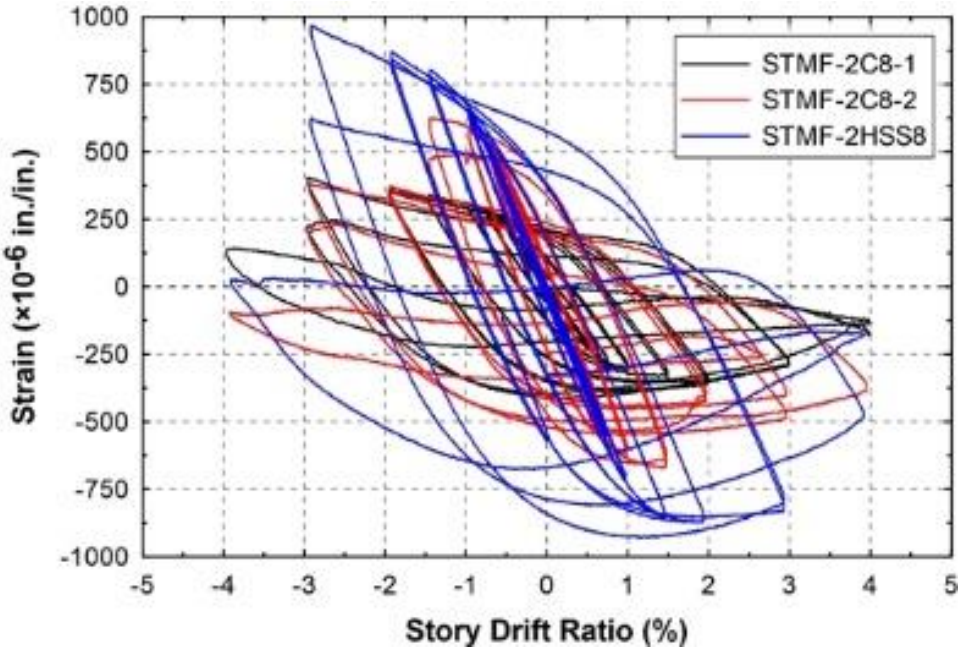
STMF-2C8-1
STMF-2C8-2
STMF-2HSS8
Strain (×10-6 in./in.)
Story Drift Ratio (%)
1000
750
500
250
0
-250
-500
-750
-1000
-5
-4
-3
-2
-1
0
1
2
3
4
5

M4-2-1

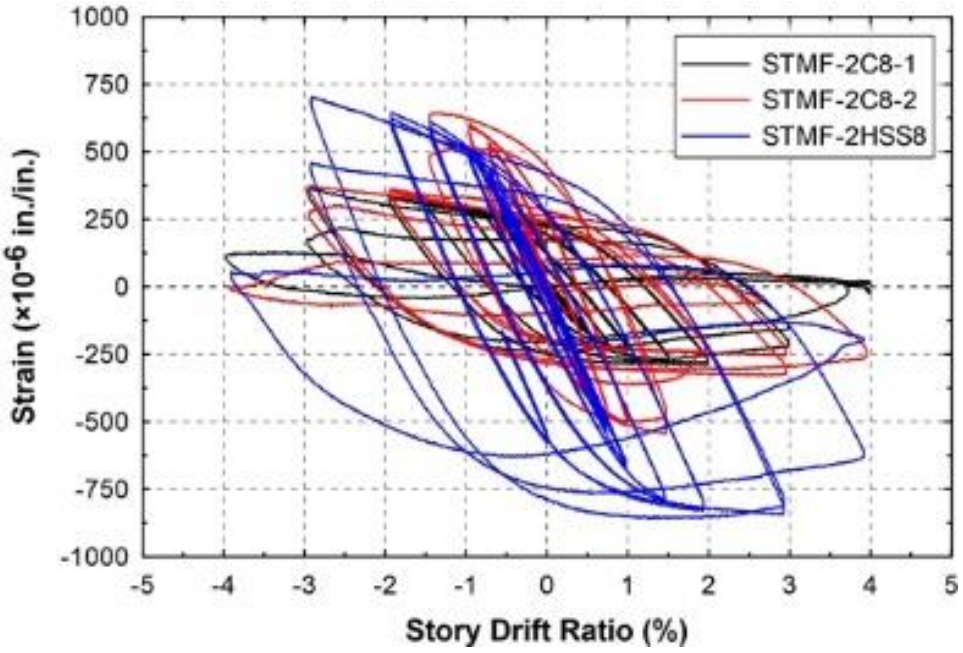
STMF-2C8-1
STMF-2C8-2
STMF-2HSS8
Strain (×10-6 in./in.)
Story Drift Ratio (%)
1000
750
500
250
0
-250
-500
-750
-1000
-5
-4
-3
-2
-1
0
1
2
3
4
5

M4-2-2

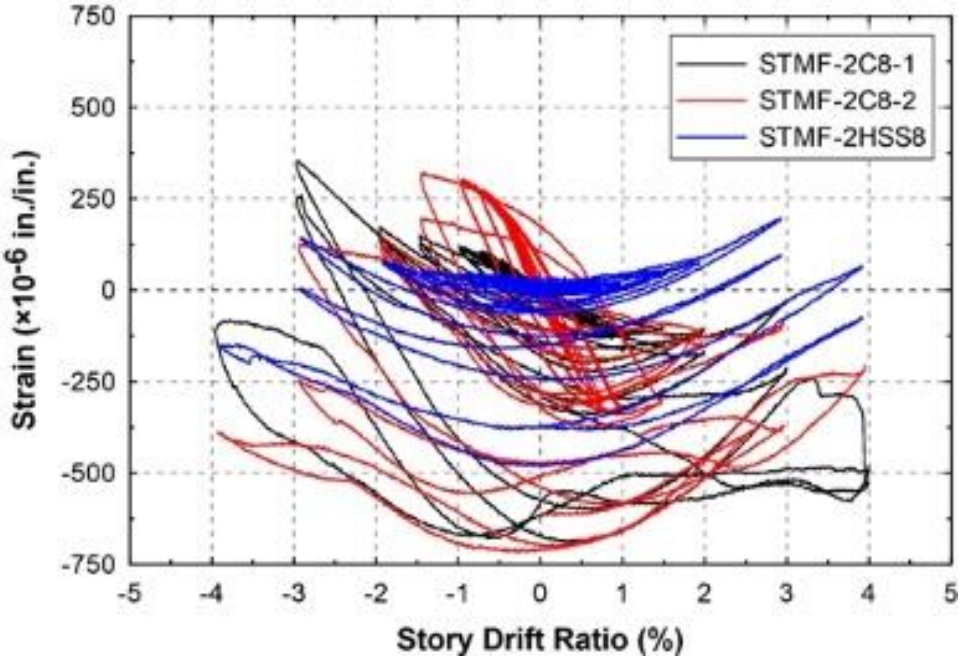
STMF-2C8-1
STMF-2C8-2
STMF-2HSS8
Strain (×10-6 in./in.)
Story Drift Ratio (%)
750
500
250
0
-250
-500
-750
-5
-4
-3
-2
-1
0
1
2
3
4
5

M5-1-1

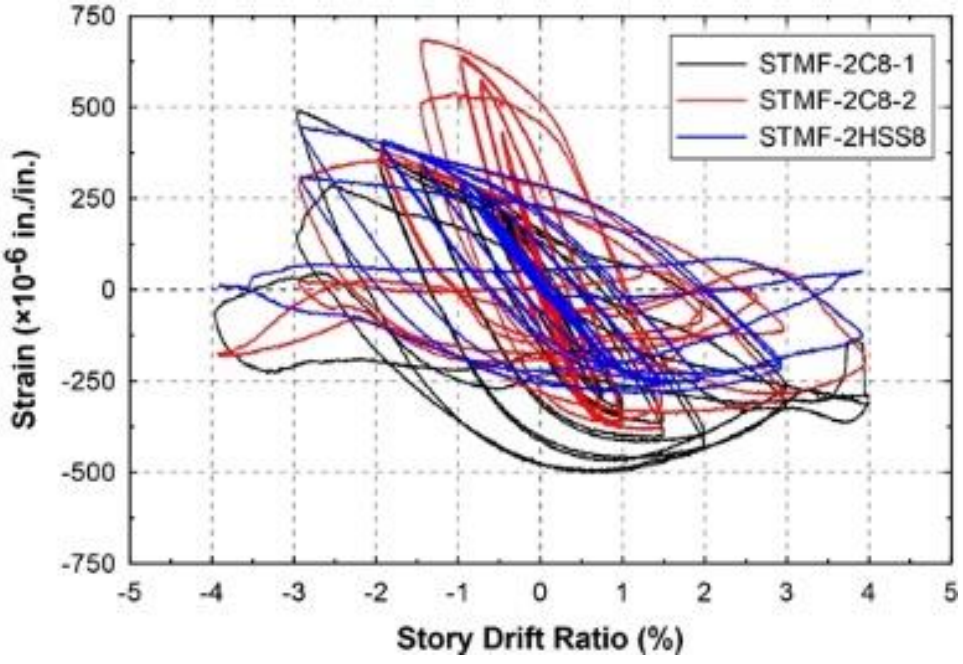
STMF-2C8-1
STMF-2C8-2
STMF-2HSS8
Strain (×10-6 in./in.)
Story Drift Ratio (%)
750
500
250
0
-250
-500
-750
-5
-4
-3
-2
-1
0
1
2
3
4
5

M5-1-2

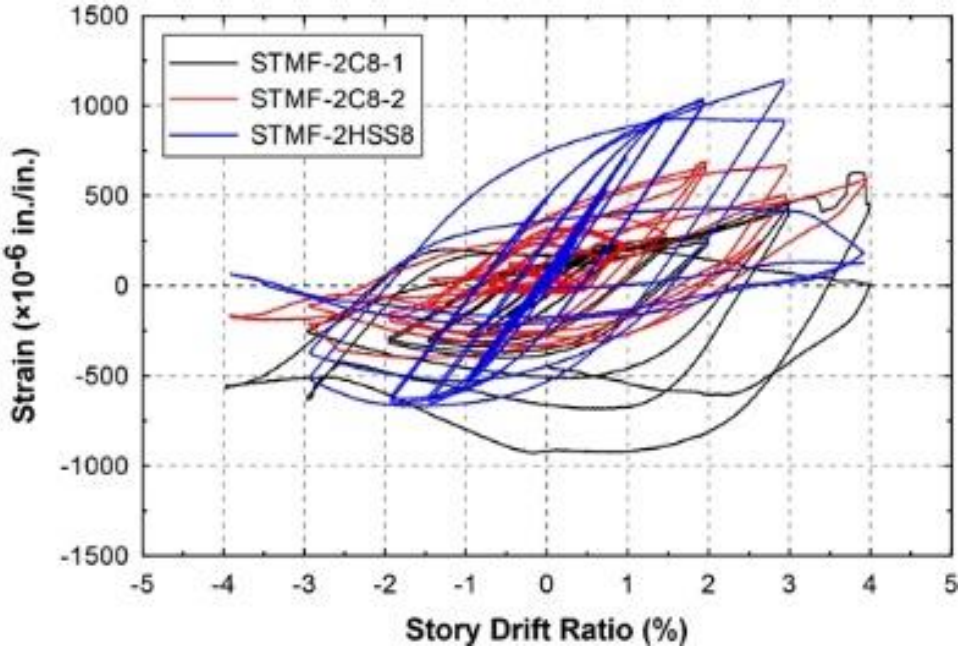
STMF-2C8-1
STMF-2C8-2
STMF-2HSS8
Strain (×10-6 in./in.)
Story Drift Ratio (%)
1500
1000
500
0
-500
-1000
-1500
-5
-4
-3
-2
-1
0
1
2
3
4
5

M5-2-1

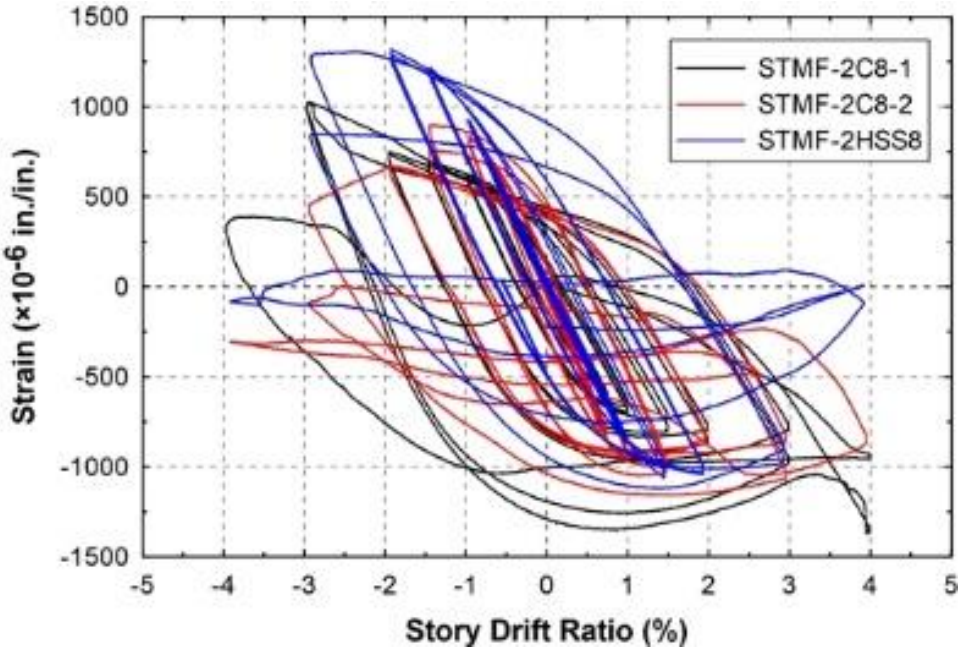
STMF-2C8-1
STMF-2C8-2
STMF-2HSS8
Strain (×10-6 in./in.)
Story Drift Ratio (%)
1500
1000
500
0
-500
-1000
-1500
-5
-4
-3
-2
-1
0
1
2
3
4
5

M5-2-2

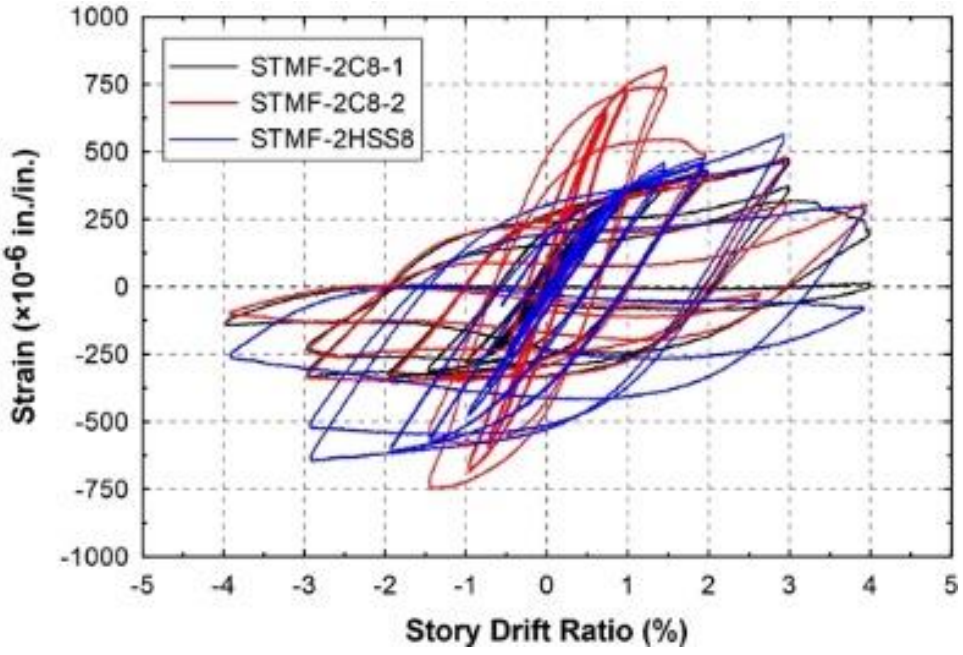
STMF-2C8-1
STMF-2C8-2
STMF-2HSS8
Strain (×10-6 in./in.)
Story Drift Ratio (%)
1000
750
500
250
0
-250
-500
-750
-1000
-5
-4
-3
-2
-1
0
1
2
3
4
5

M7-1-1

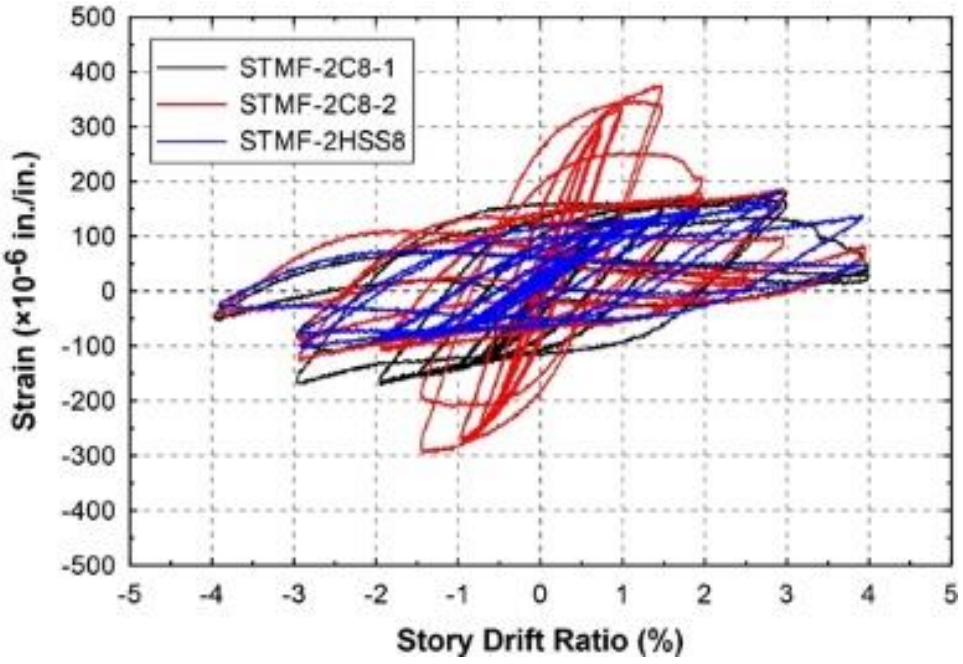
STMF-2C8-1
STMF-2C8-2
STMF-2HSS8
Strain (×10-6 in./in.)
Story Drift Ratio (%)
500
400
300
200
100
0
-100
-200
-300
-400
-500
-5
-4
-3
-2
-1
0
1
2
3
4
5

M7-1-2

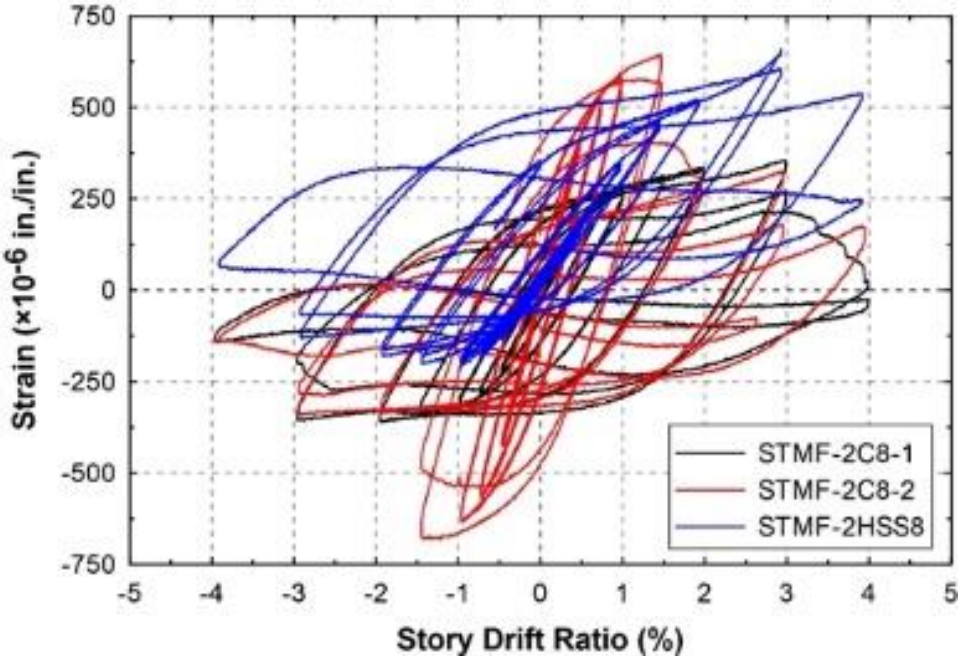
750
500
250
0
-250
-500
-750
-5
-4
-3
-2
-1
0
1
2
3
4
5
Strain (×10-6 in./in.)
Story Drift Ratio (%)
STMF-2C8-1
STMF-2C8-2
STMF-2HSS8

M7-2-1

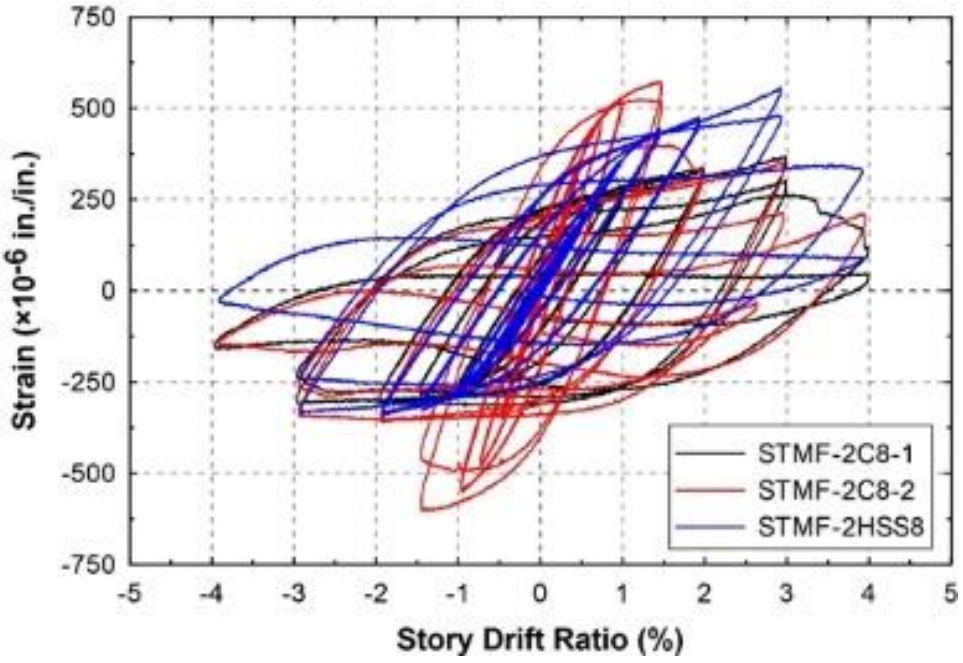
750
500
250
0
-250
-500
-750
-5
-4
-3
-2
-1
0
1
2
3
4
5
Strain (×10-6 in./in.)
Story Drift Ratio (%)
STMF-2C8-1
STMF-2C8-2
STMF-2HSS8

M7-2-2

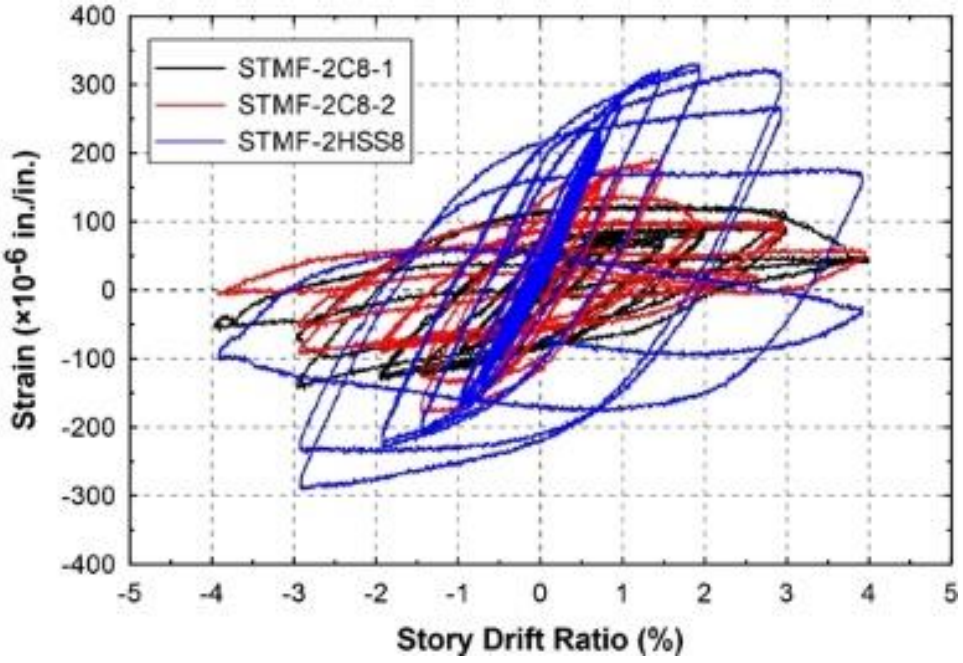

M7-RS-1-1

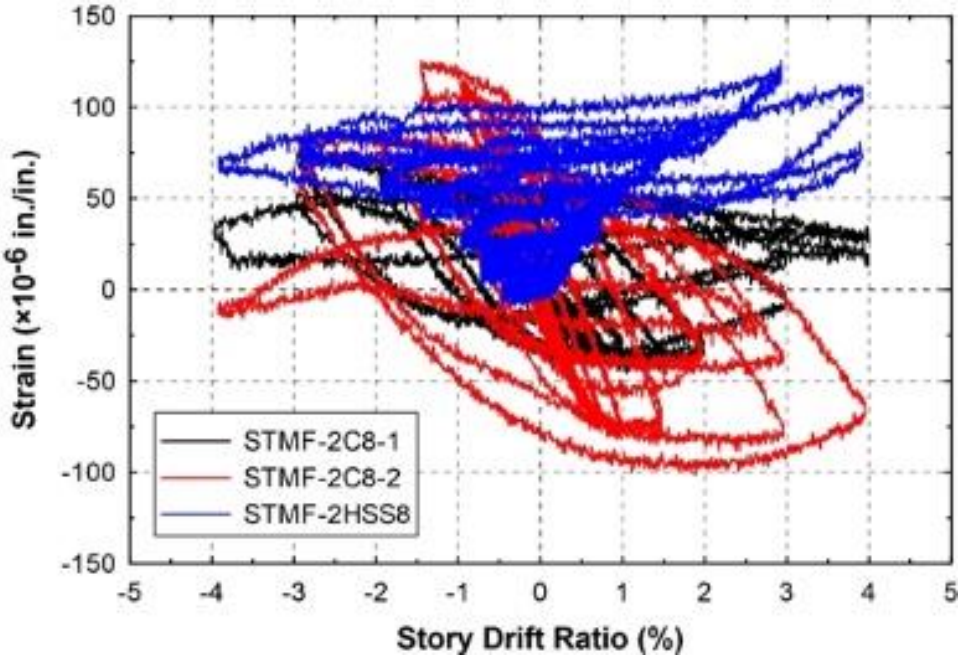

M7-RS-1-2

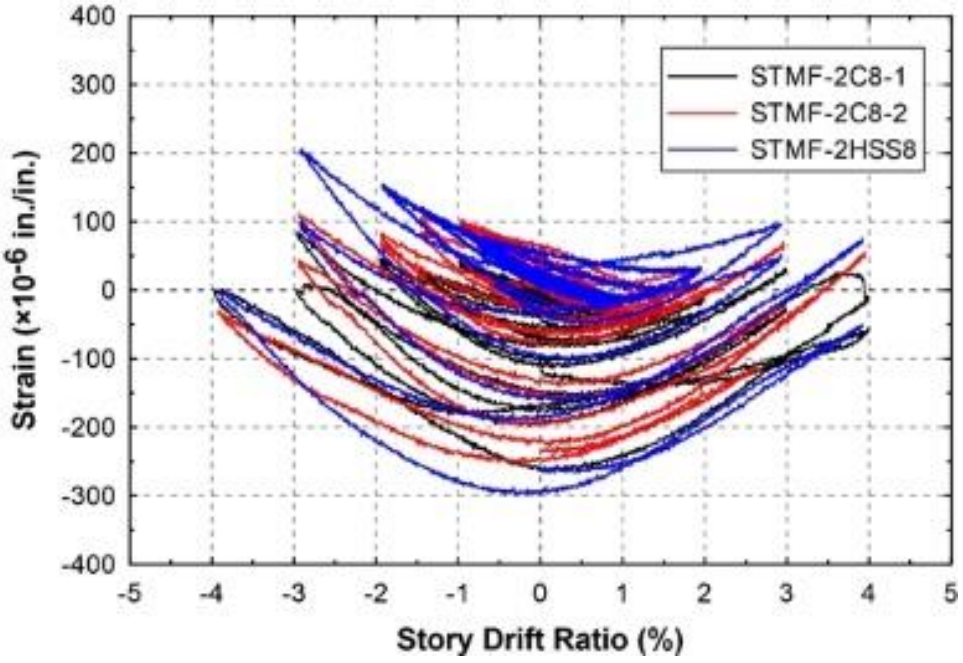

M7-RS-1-3

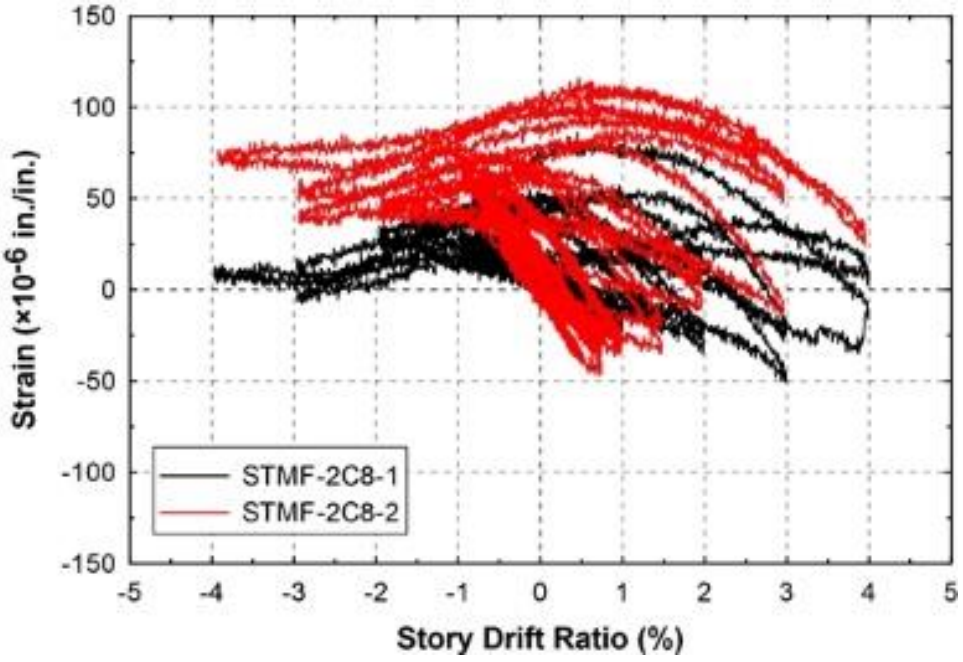

M7-RS-2-1

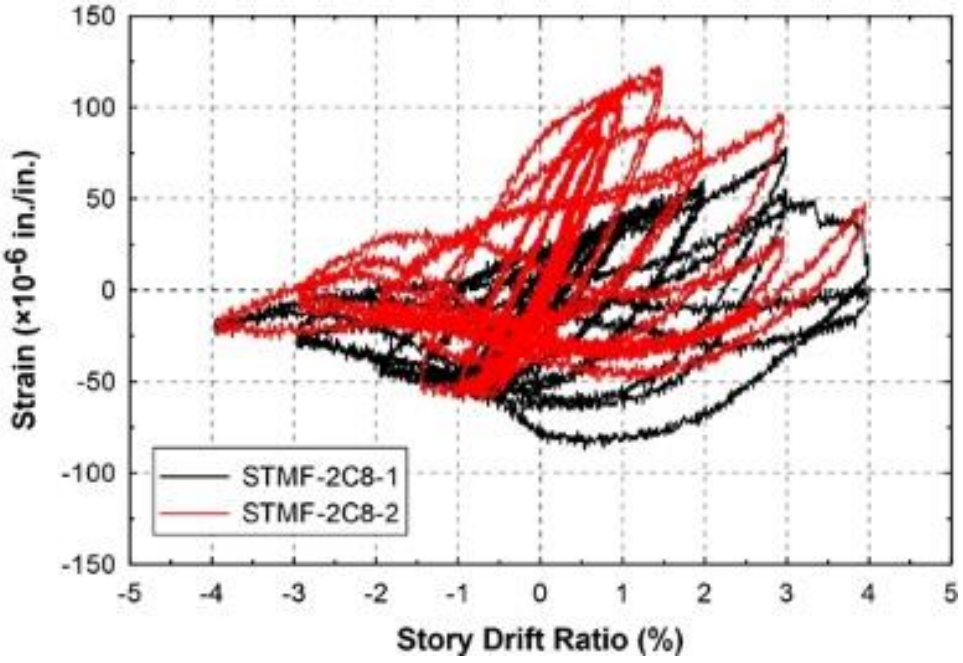

M7-RS-2-2

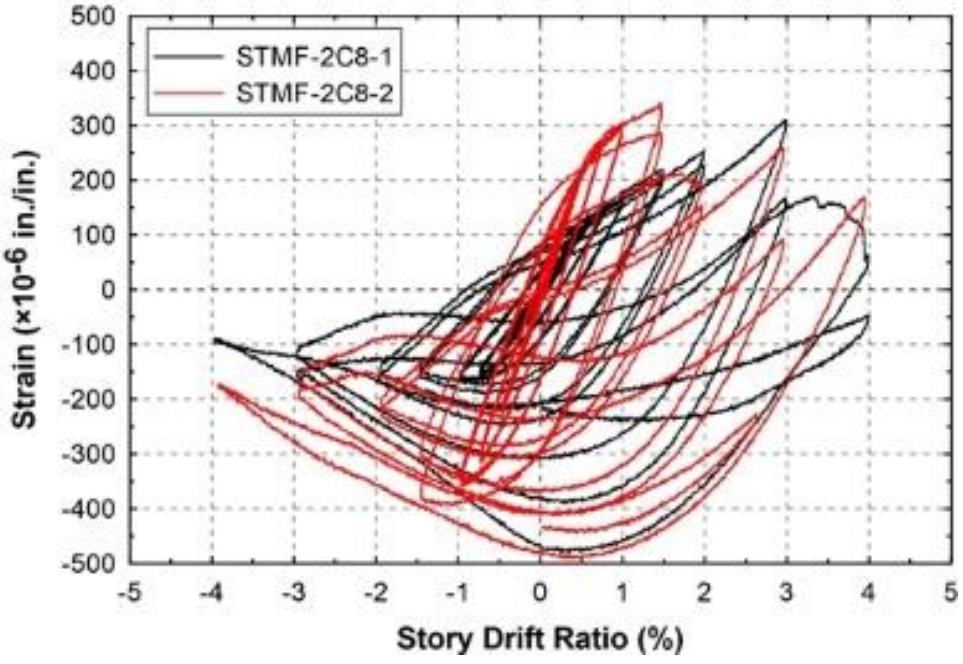

M7-RS-2-3

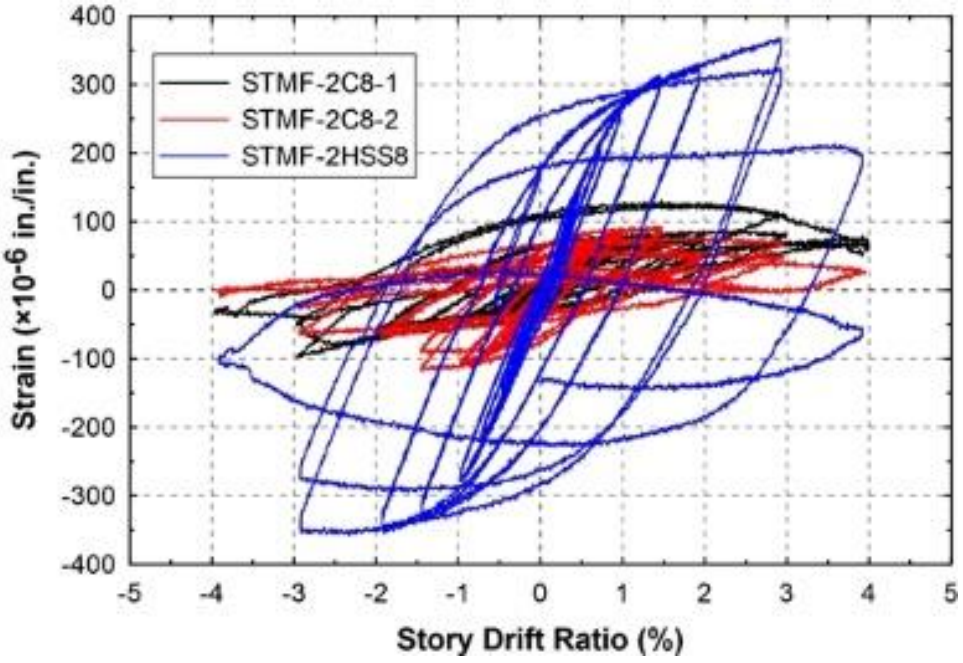

M7-RS-3-1

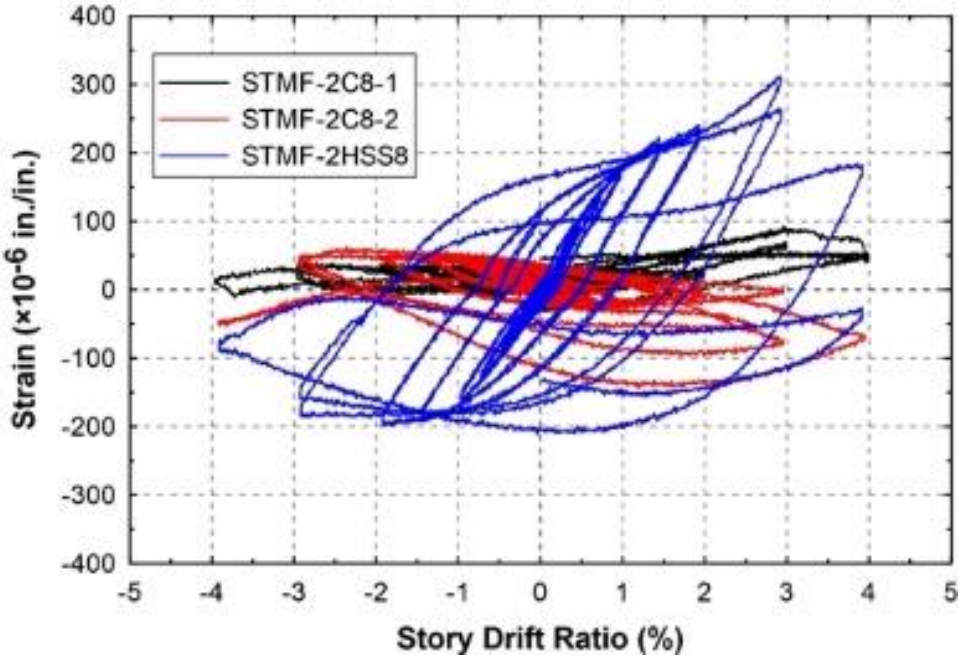

M7-RS-3-2

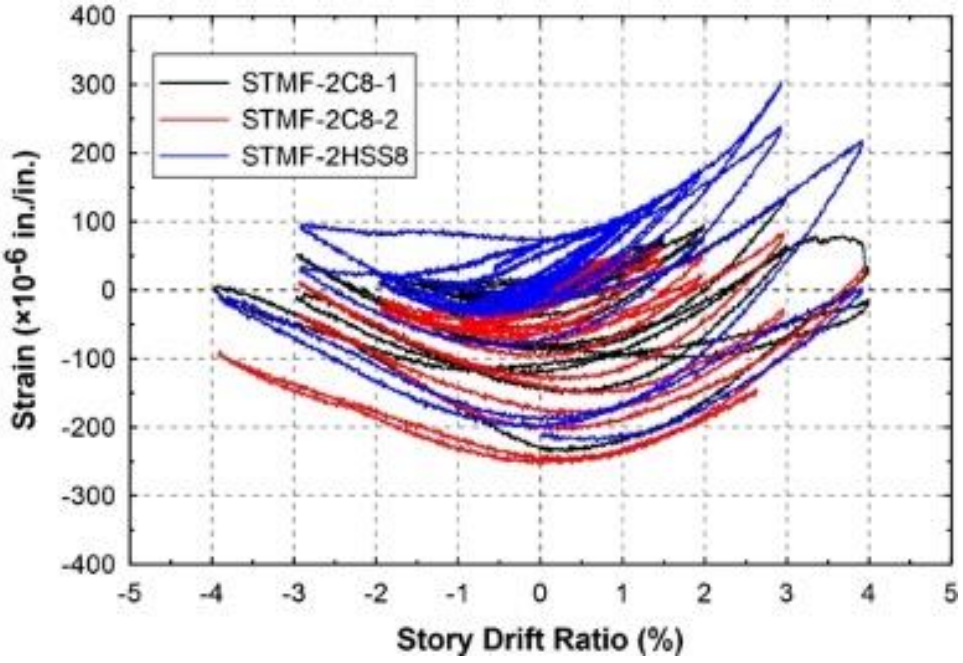

M7-RS-3-3

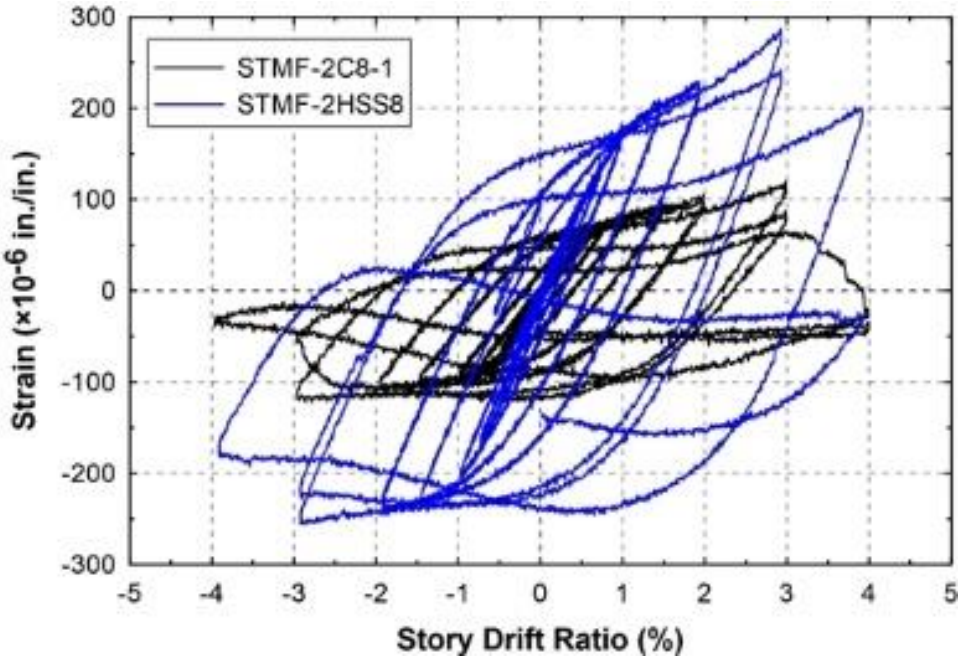

M7-RS-4-1

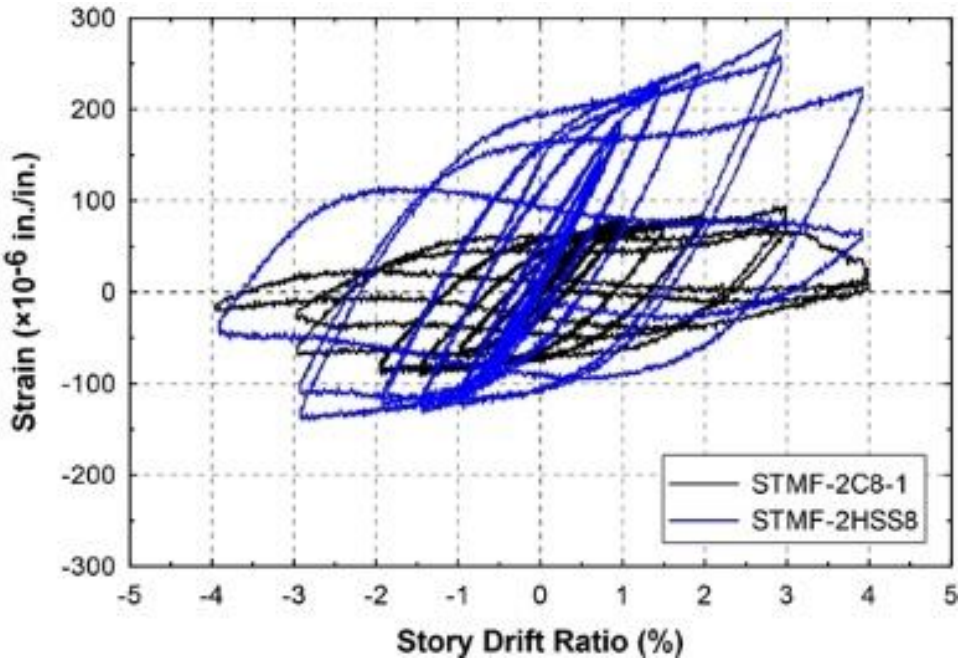

M7-RS-4-2

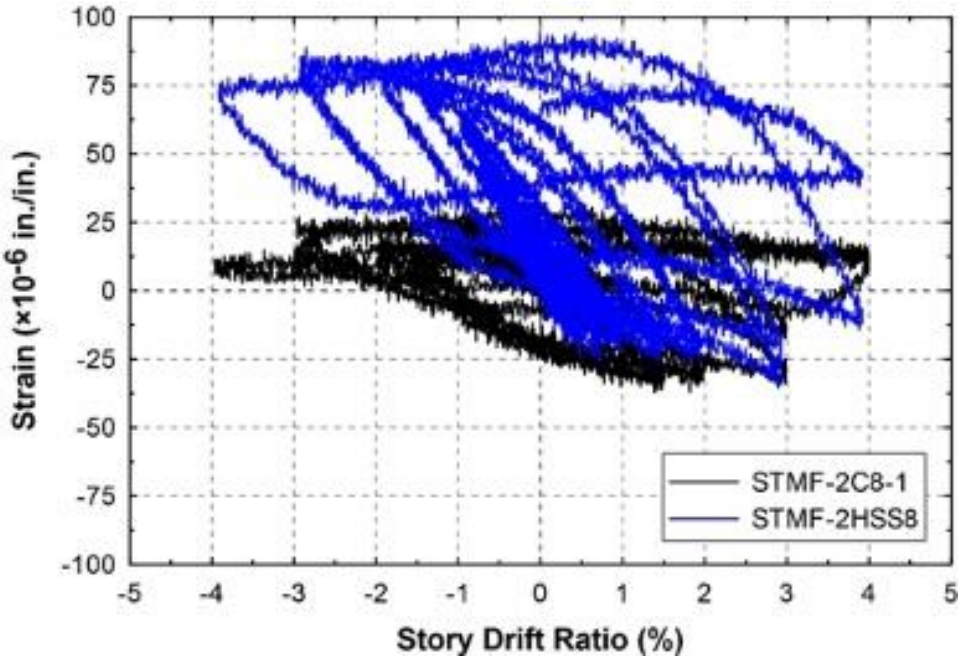

M7-RS-4-3

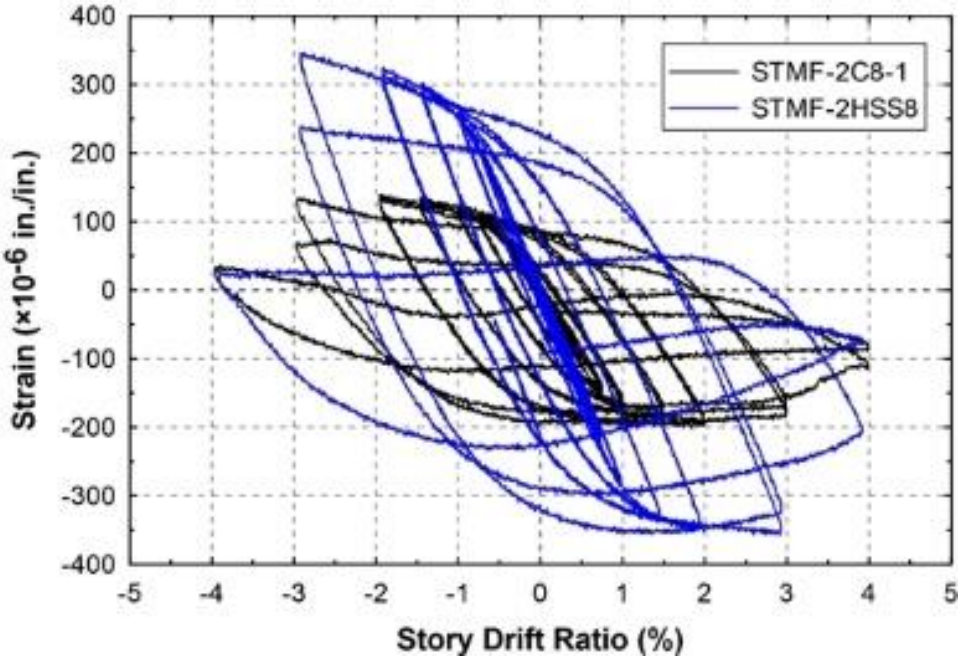

M7-RS-5-1

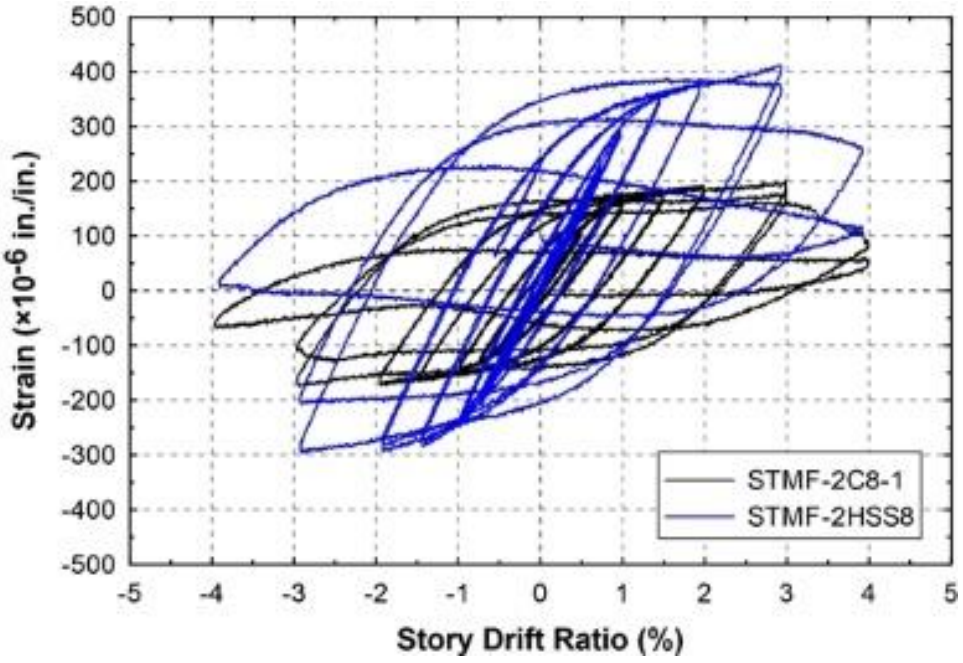

M7-RS-5-2

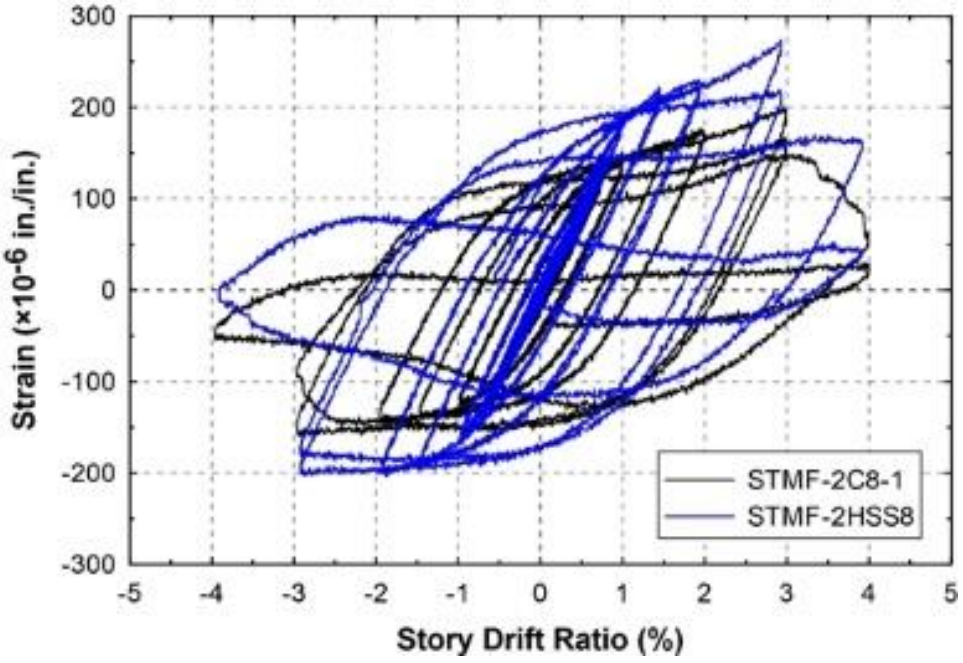

M7-RS-5-3

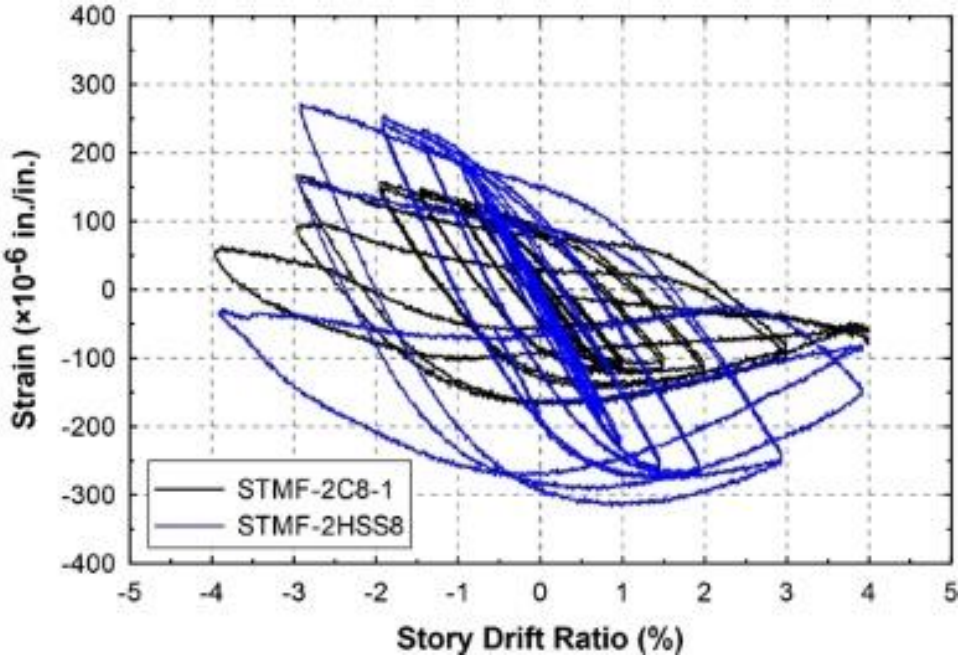

M7-RS-6-1

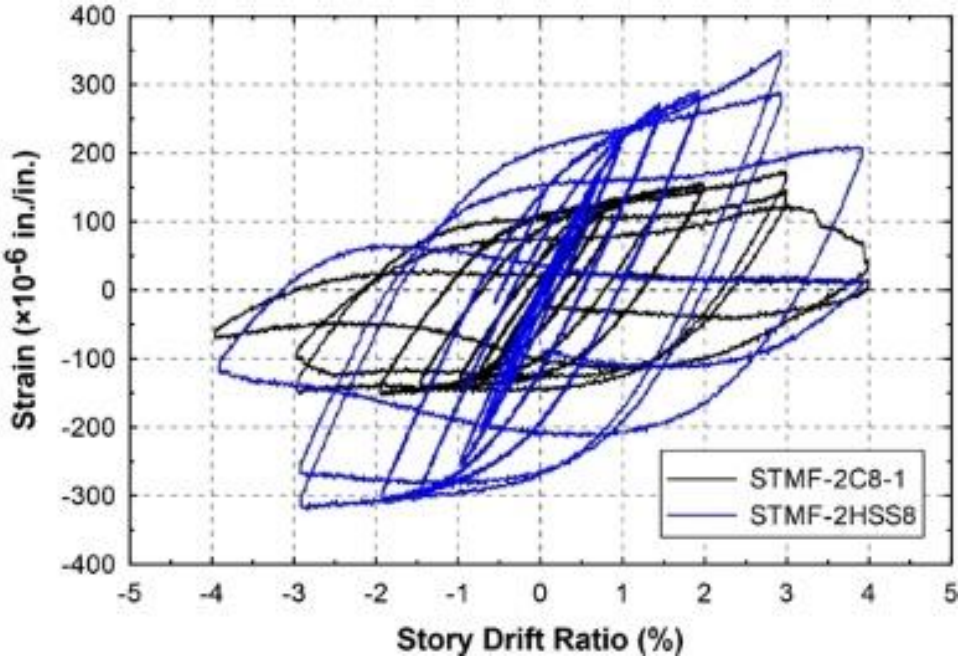

M7-RS-6-2

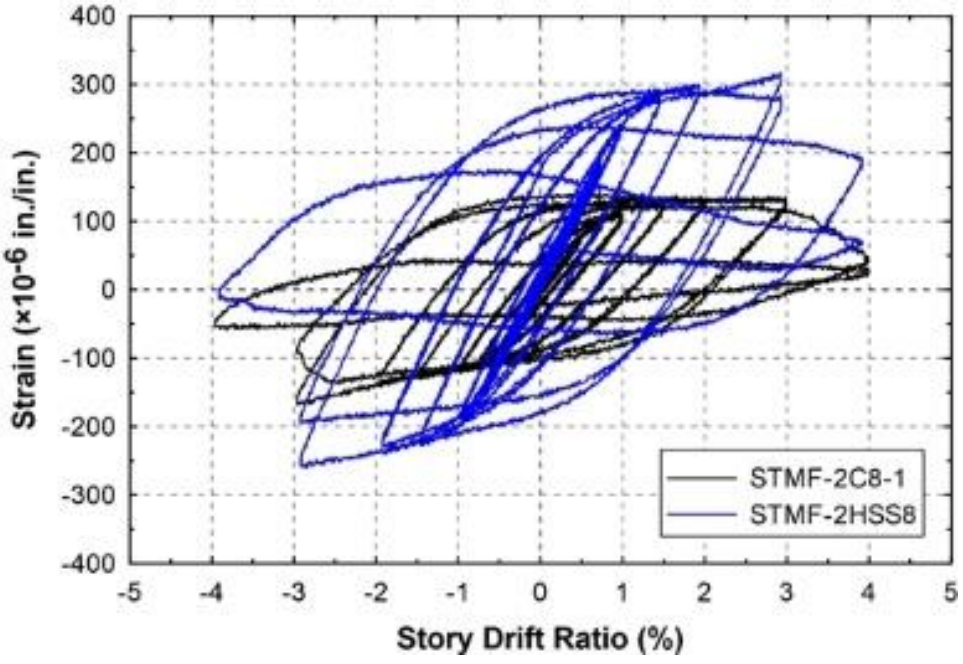

M7-RS-6-3

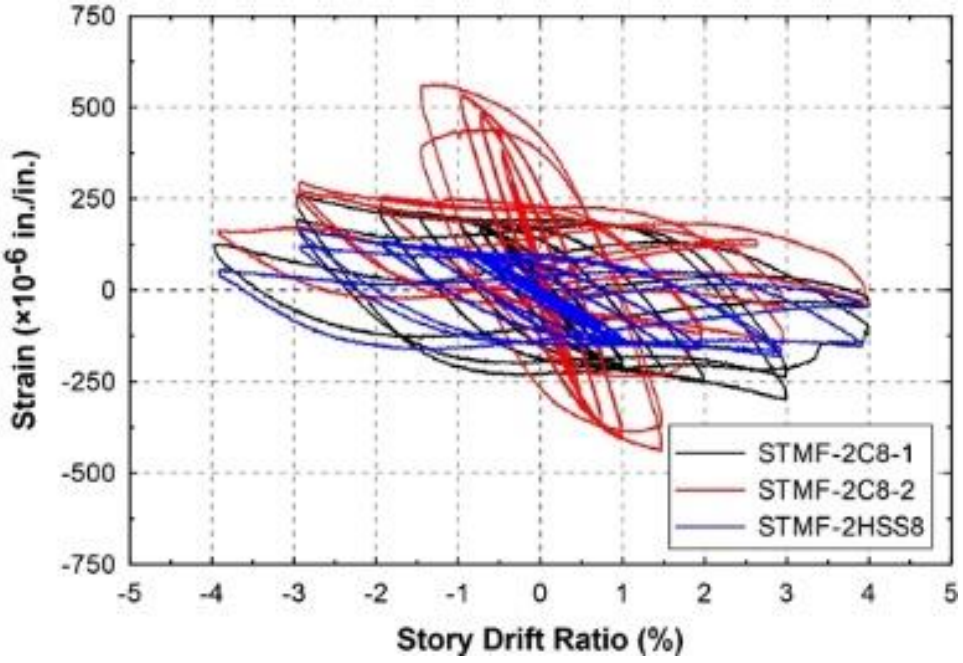
750
500
250
0
-250
-500
-750
-5
-4
-3
-2
-1
0
1
2
3
4
5
Strain (×10-6 in./in.)
Story Drift Ratio (%)
STMF-2C8-1
STMF-2C8-2
STMF-2HSS8

M8-1-1

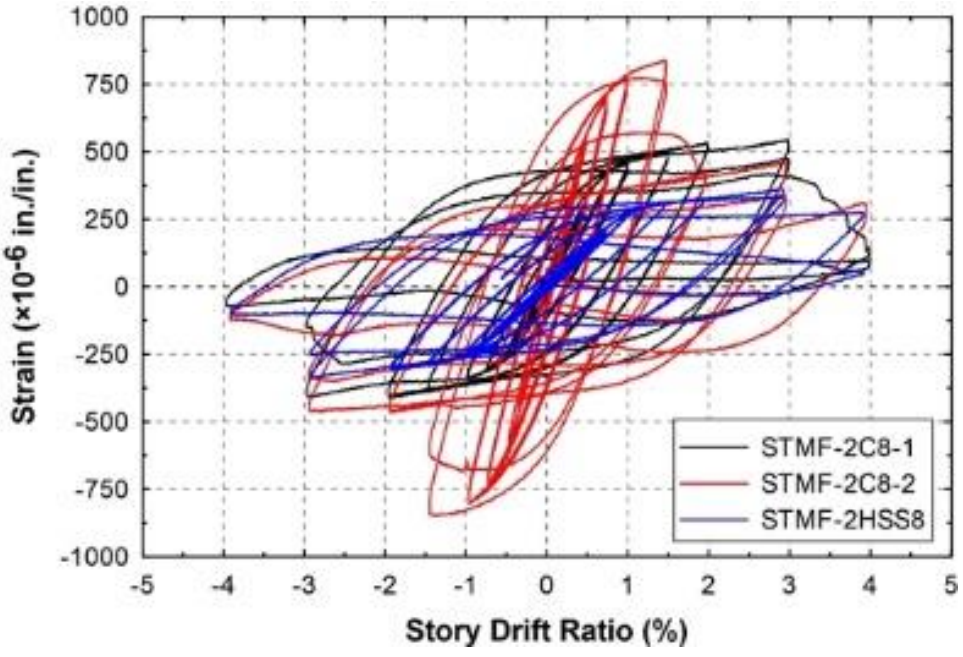
1000
750
500
250
0
-250
-500
-750
-1000
-5
-4
-3
-2
-1
0
1
2
3
4
5
Strain (×10-6 in./in.)
Story Drift Ratio (%)
STMF-2C8-1
STMF-2C8-2
STMF-2HSS8

M8-1-2

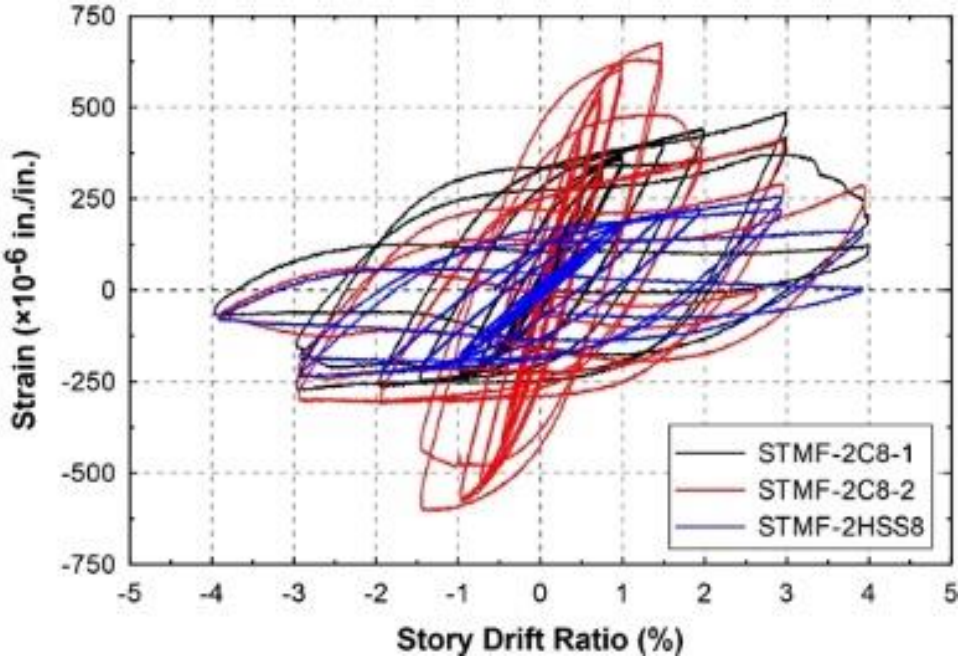
750
500
250
0
-250
-500
-750
-5
-4
-3
-2
-1
0
1
2
3
4
5
Strain (×10-6 in./in.)
Story Drift Ratio (%)
STMF-2C8-1
STMF-2C8-2
STMF-2HSS8

M8-2-1

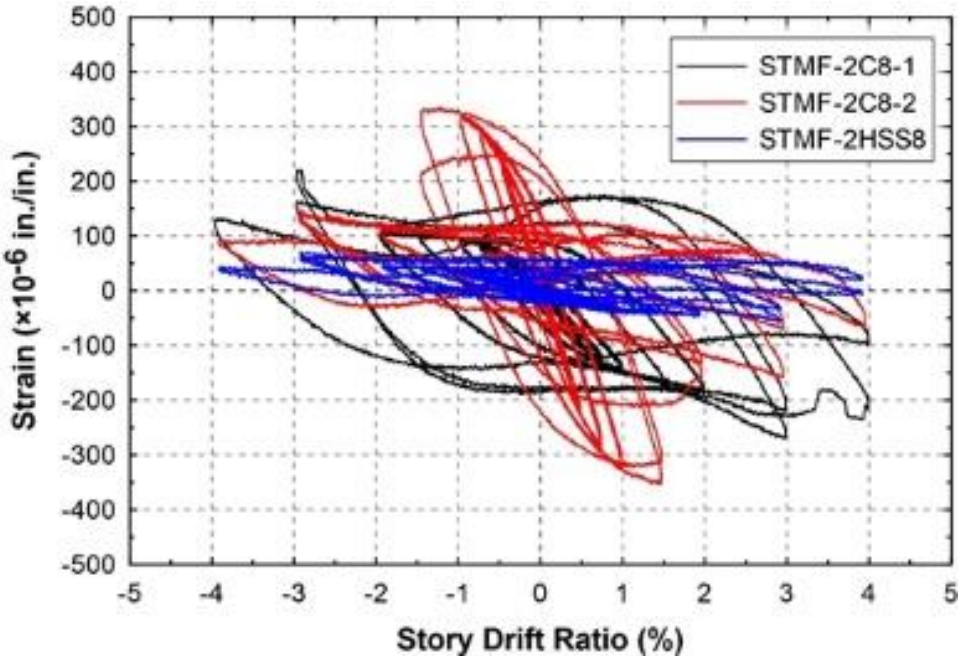
500
400
300
200
100
0
-100
-200
-300
-400
-500
-5
-4
-3
-2
-1
0
1
2
3
4
5
Strain (×10-6 in./in.)
Story Drift Ratio (%)
STMF-2C8-1
STMF-2C8-2
STMF-2HSS8

M8-2-2

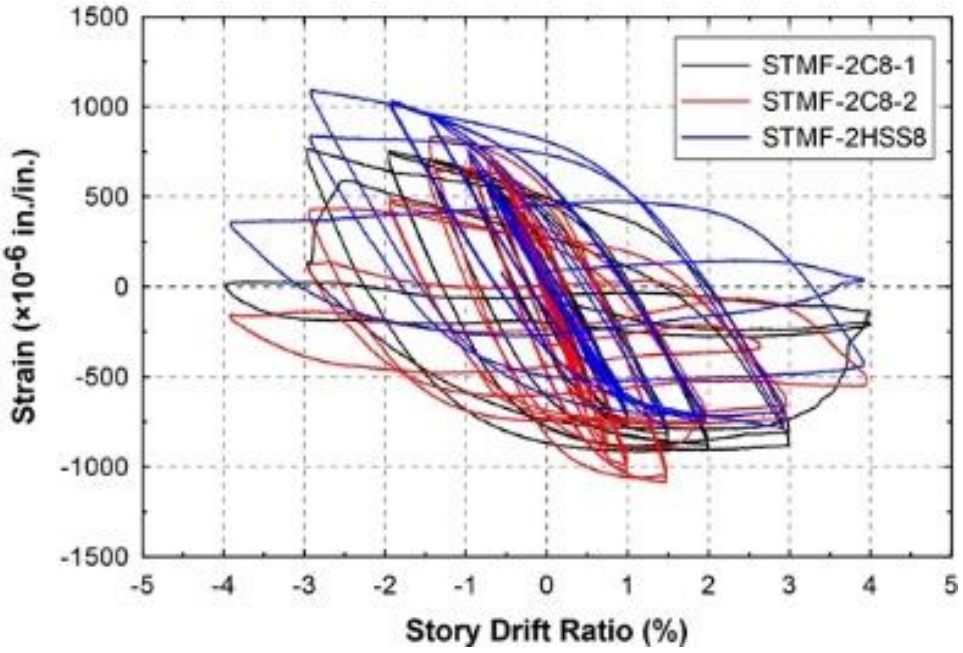
STMF-2C8-1
STMF-2C8-2
STMF-2HSS8
Strain (×10-6 in./in.)
Story Drift Ratio (%)
1500
1000
500
0
-500
-1000
-1500
-5
-4
-3
-2
-1
0
1
2
3
4
5

M9-1-1

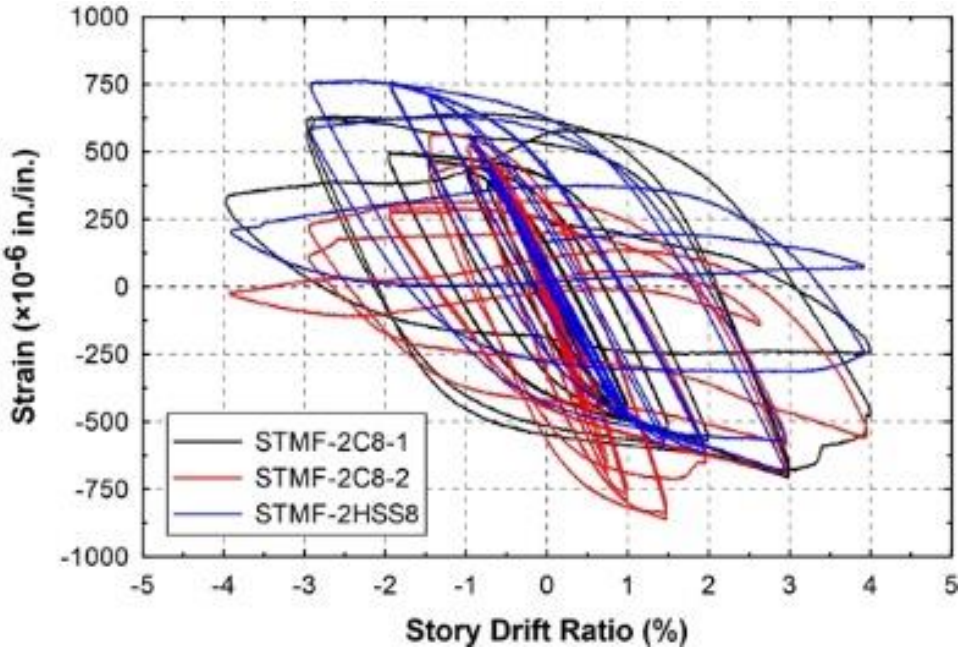
STMF-2C8-1
STMF-2C8-2
STMF-2HSS8
Strain (×10-6 in./in.)
Story Drift Ratio (%)
1000
750
500
250
0
-250
-500
-750
-1000
-5
-4
-3
-2
-1
0
1
2
3
4
5

M9-1-2

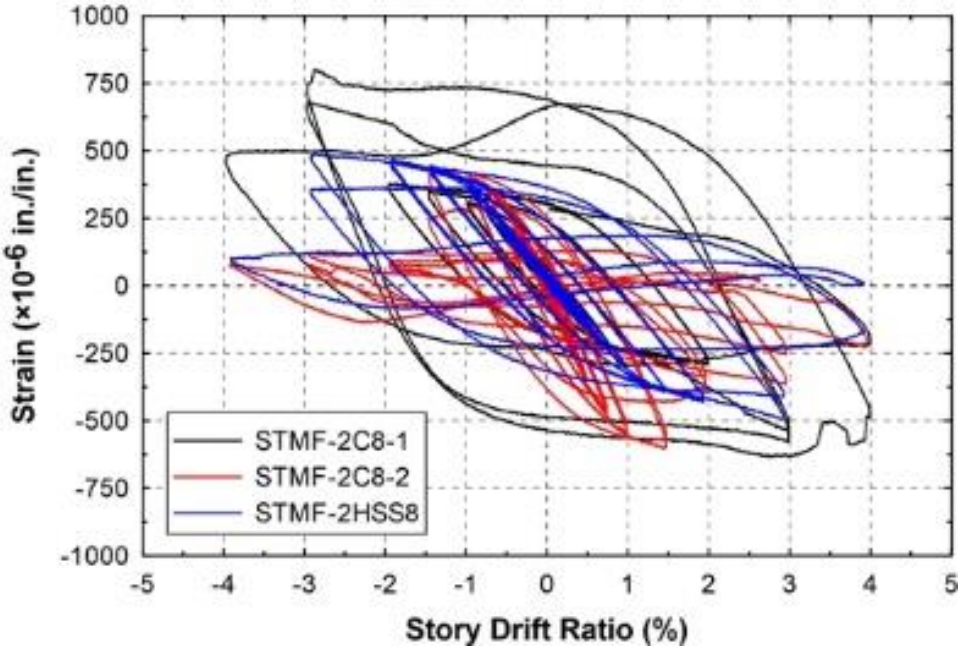
1000
750
500
250
0
-250
-500
-750
-1000
-5
-4
-3
-2
-1
0
1
2
3
4
5
Strain (×10-6 in./in.)
Story Drift Ratio (%)
STMF-2C8-1
STMF-2C8-2
STMF-2HSS8

M9-2-1

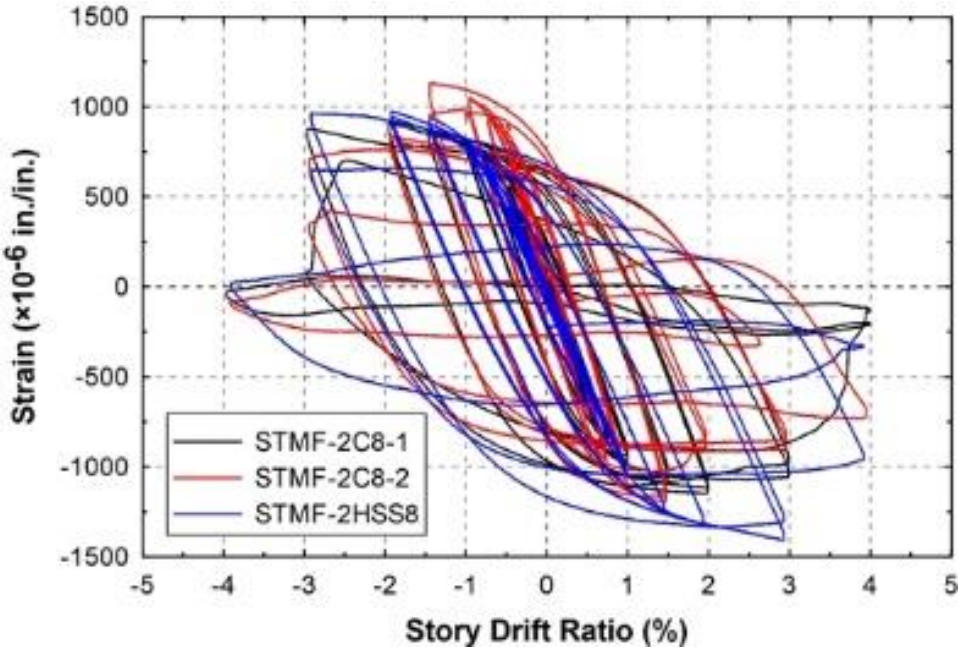
1500
1000
500
0
-500
-1000
-1500
-5
-4
-3
-2
-1
0
1
2
3
4
5
Strain (×10-6 in./in.)
Story Drift Ratio (%)
STMF-2C8-1
STMF-2C8-2
STMF-2HSS8

M9-2-2

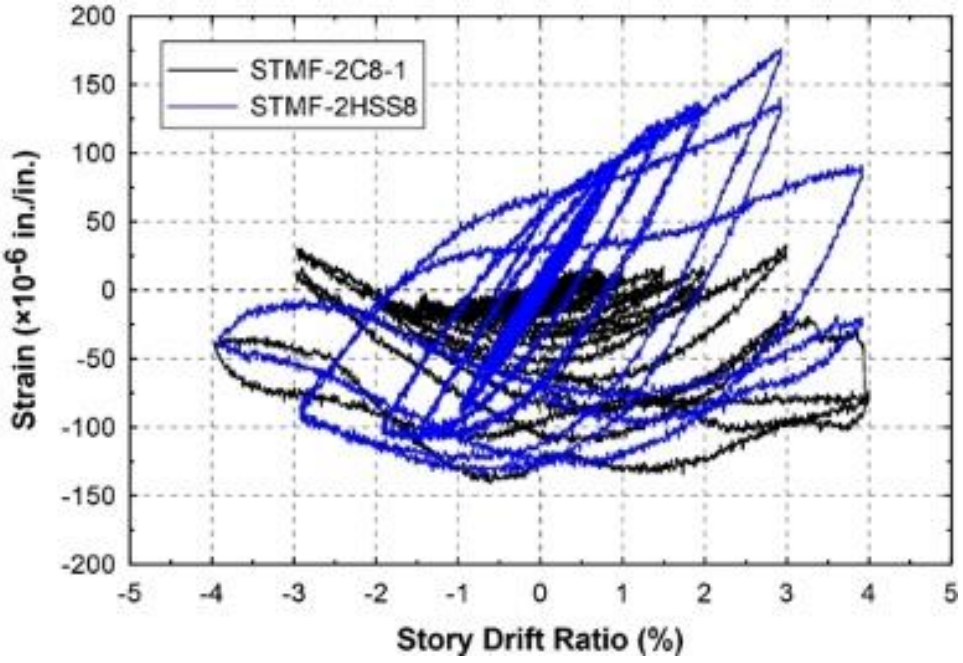

M9-RS-1-1

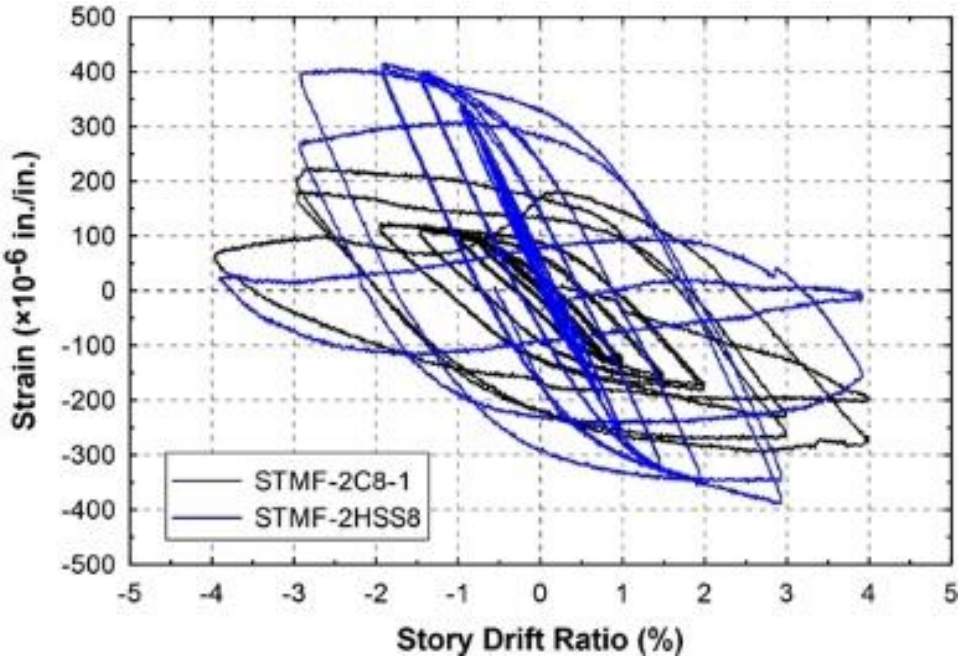

M9-RS-1-2

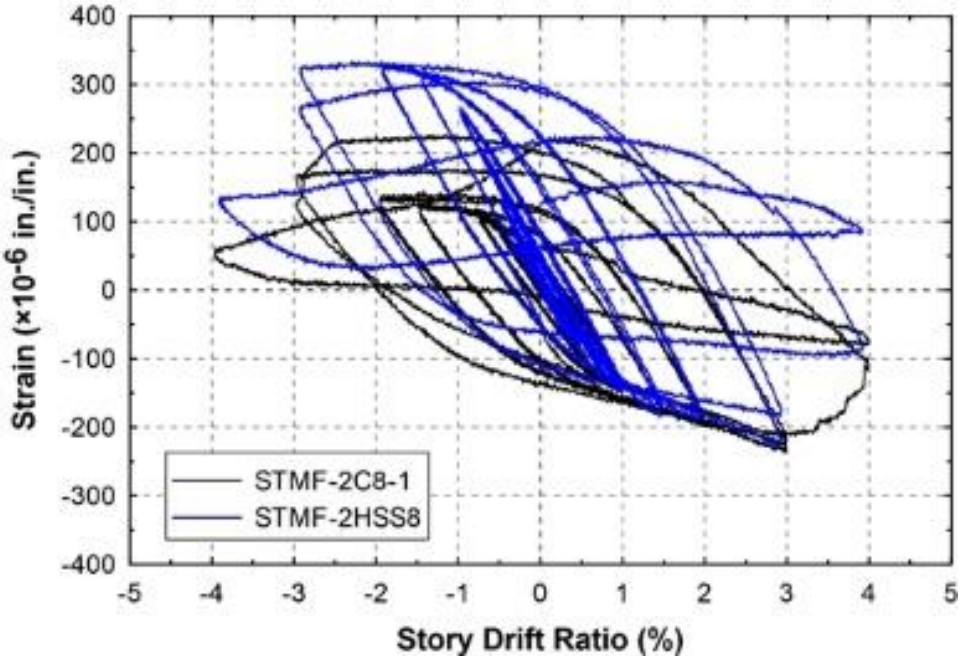

M9-RS-1-3

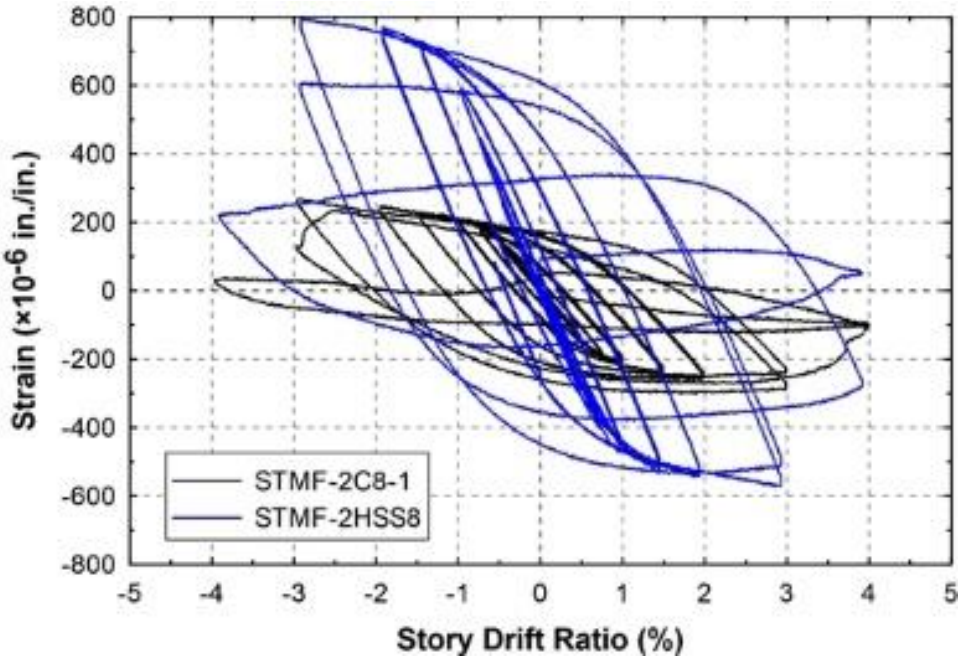

M9-RS-2-1

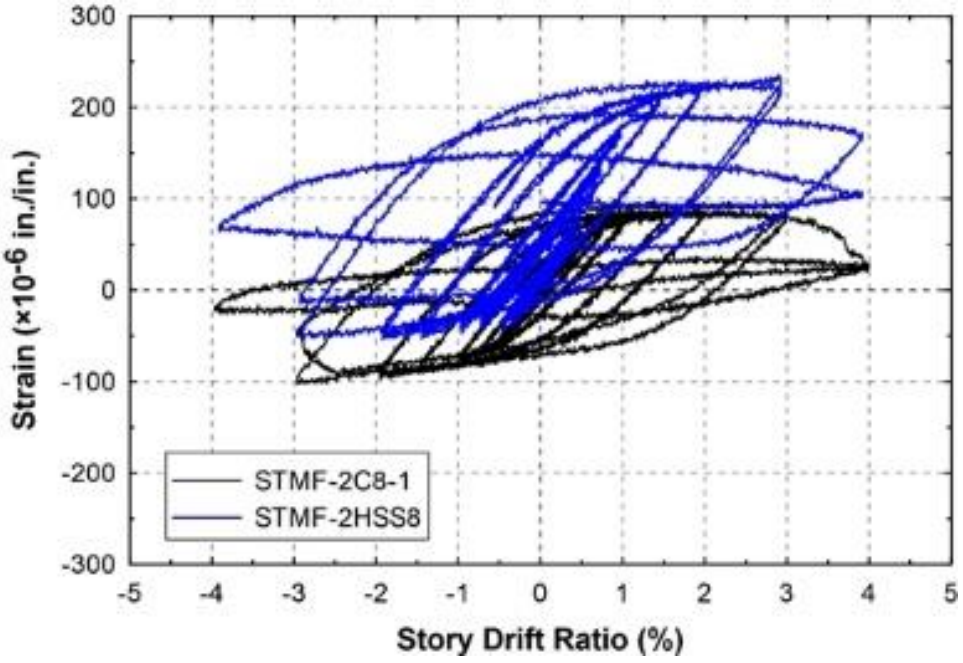

M9-RS-2-2

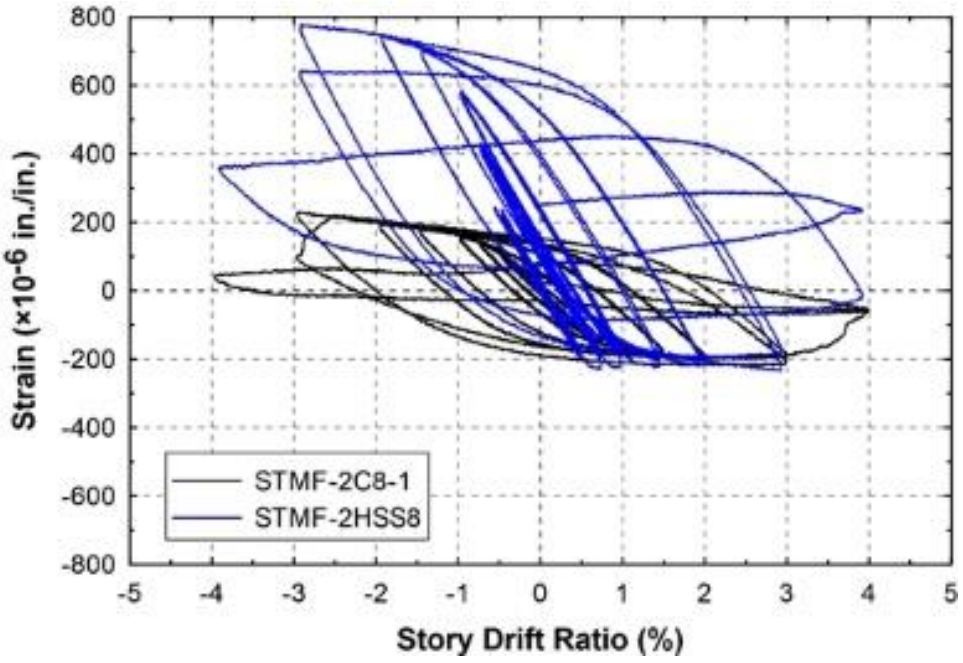

M9-RS-2-3

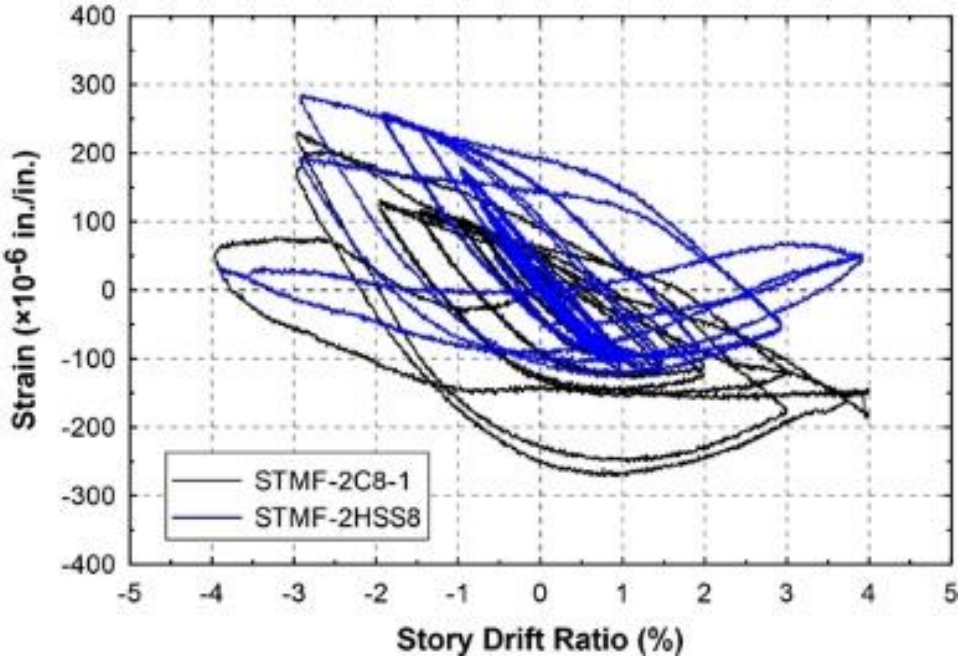

M9-RS-3-1

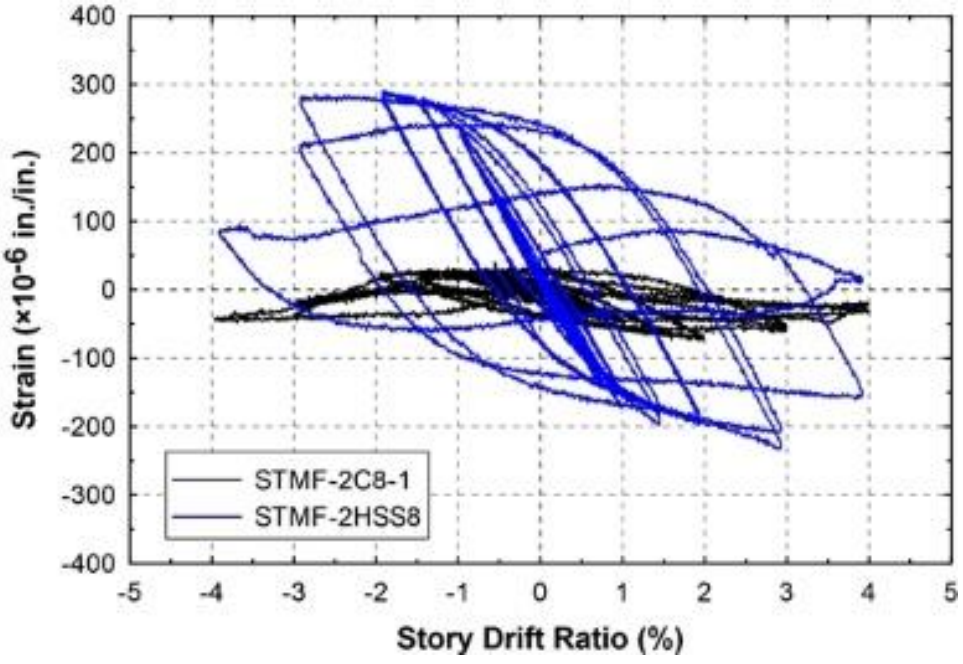

M9-RS-3-2

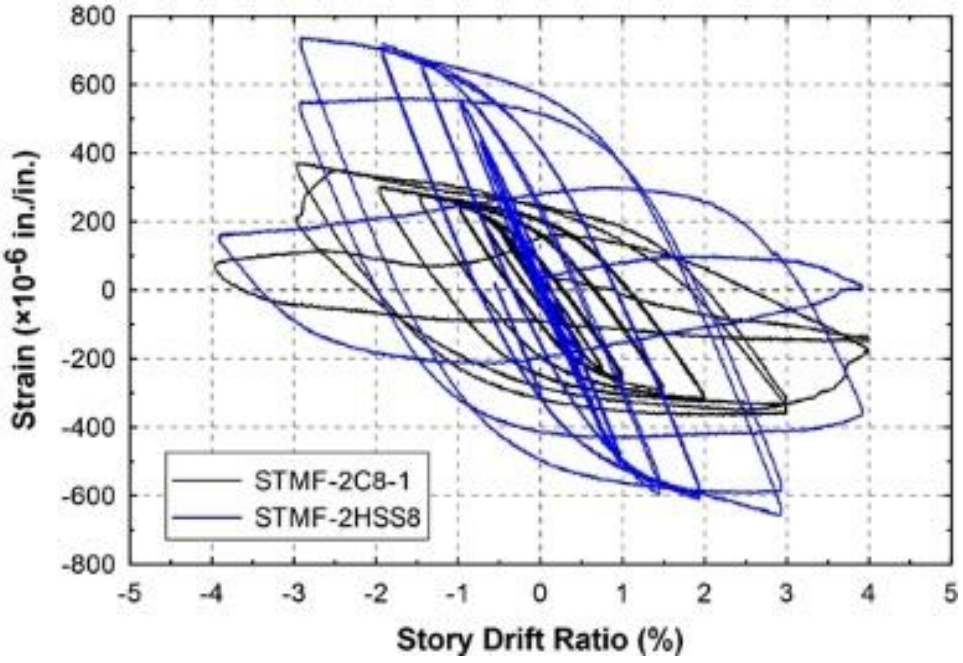

M9-RS-3-3

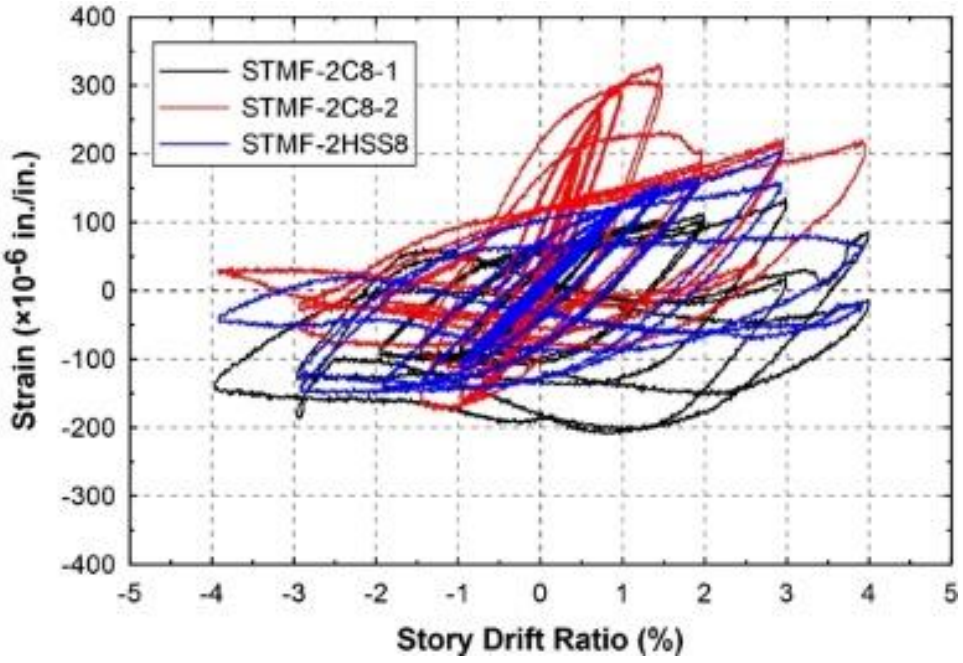

M9-RS-4-1

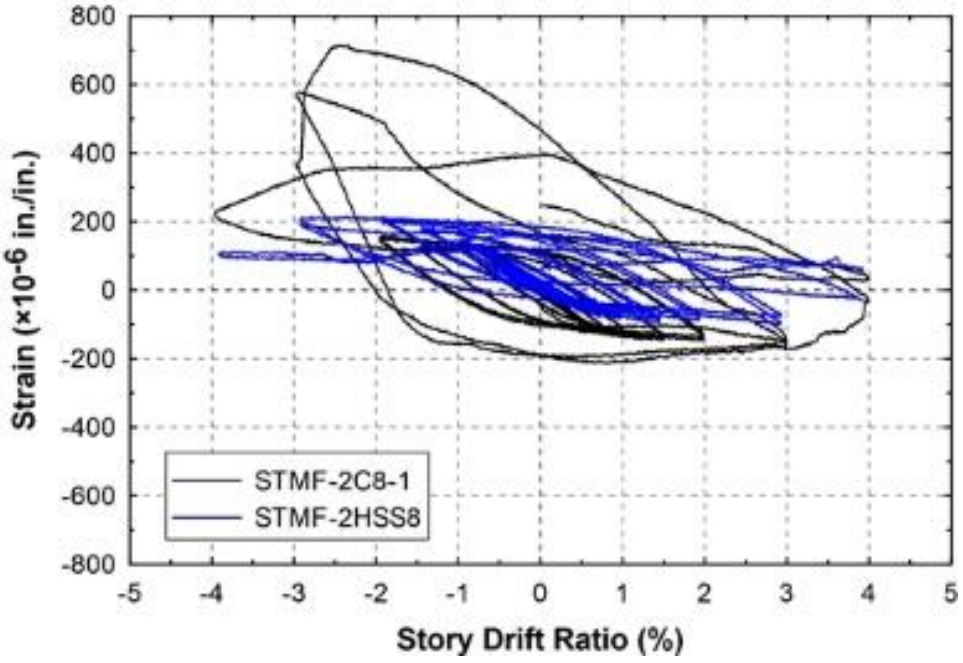

M9-RS-4-2

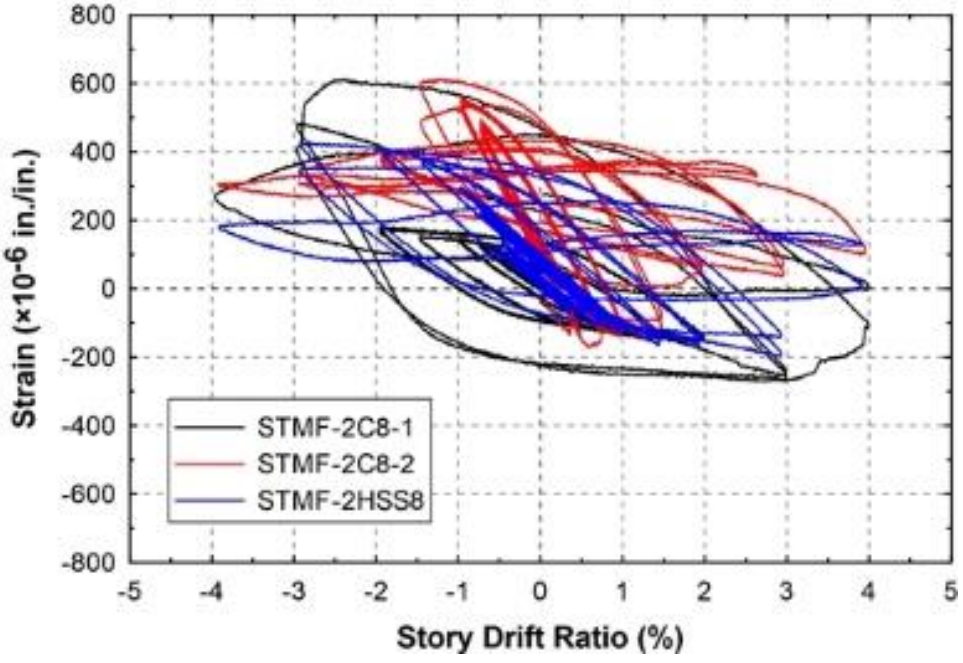

M9-RS-4-3

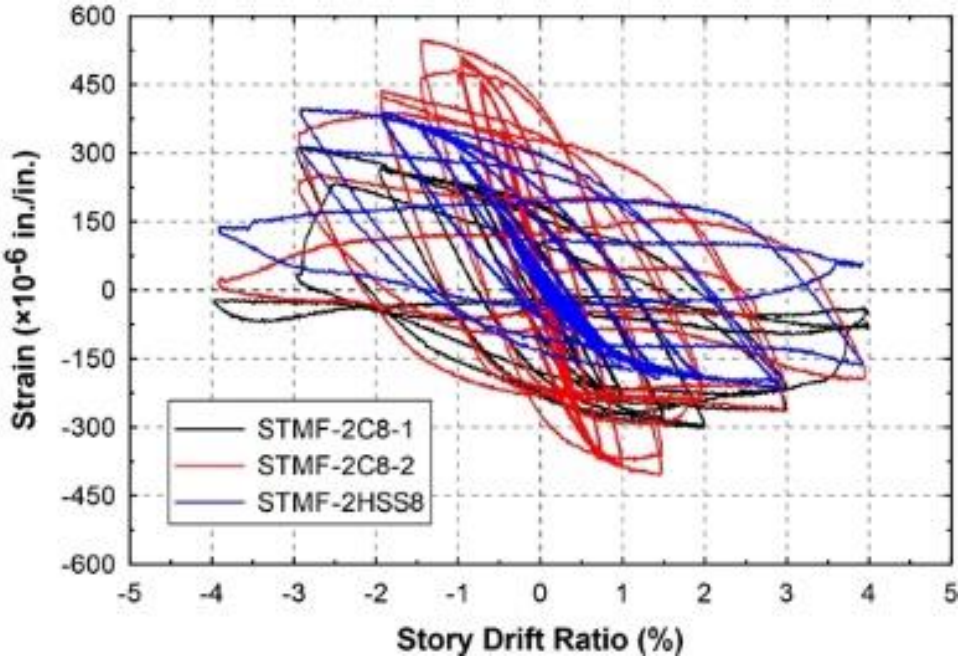

M9-RS-5-1

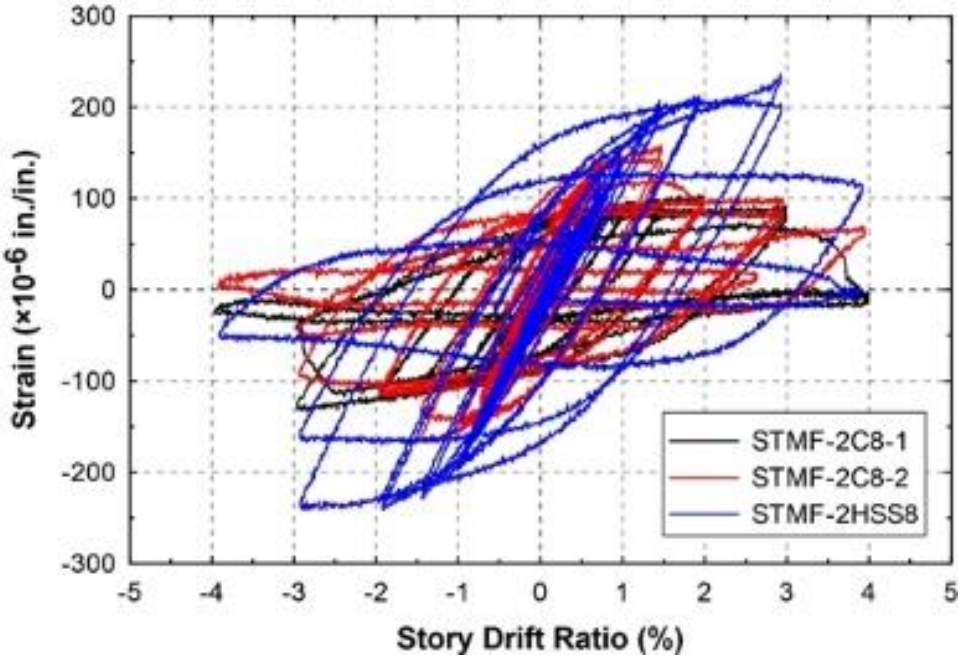

M9-RS-5-2

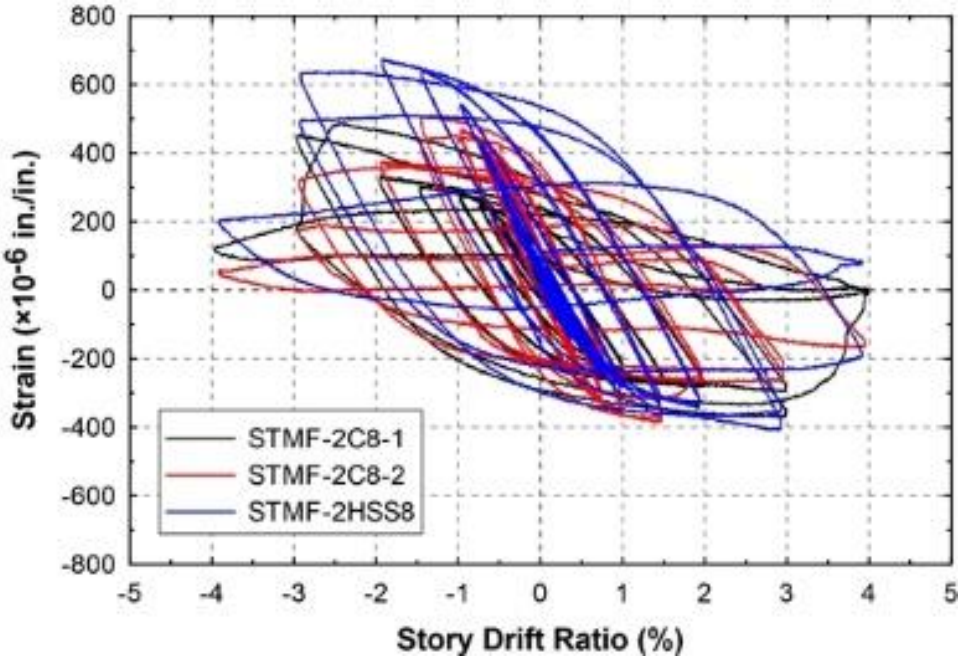

M9-RS-5-3

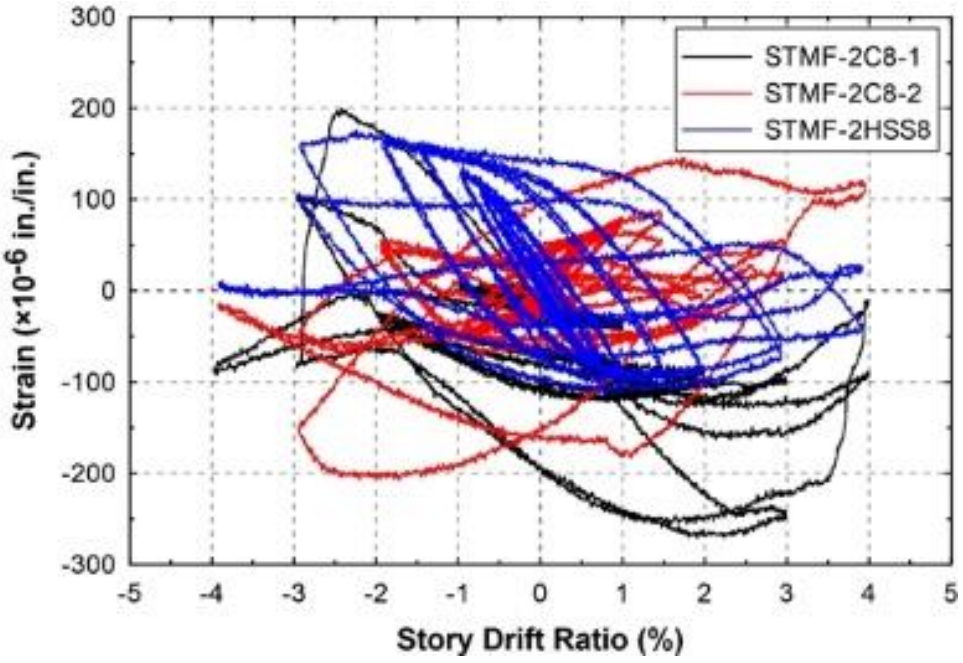

M9-RS-6-1

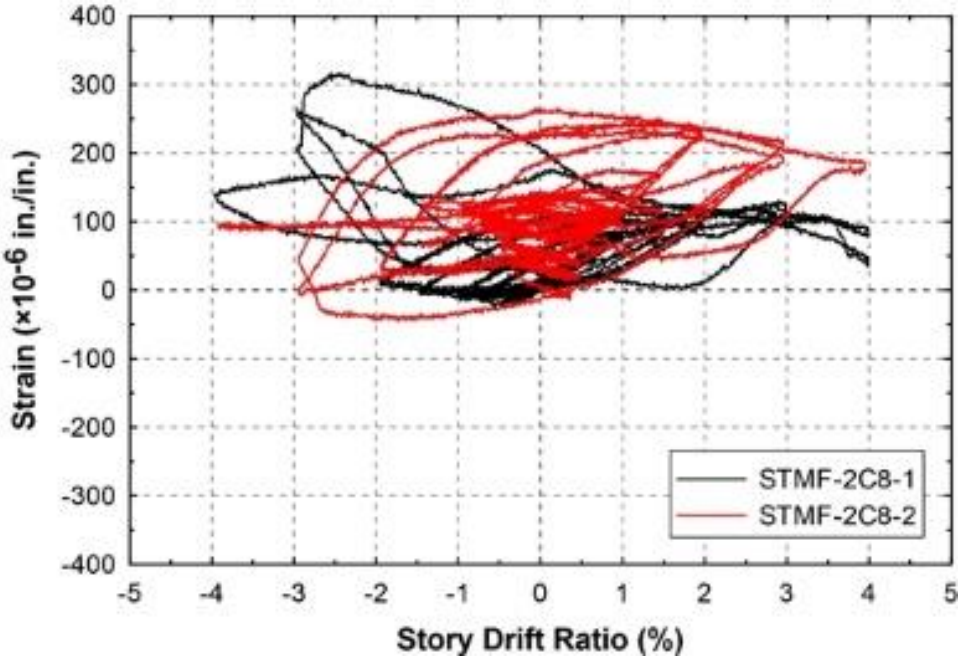

M9-RS-6-2

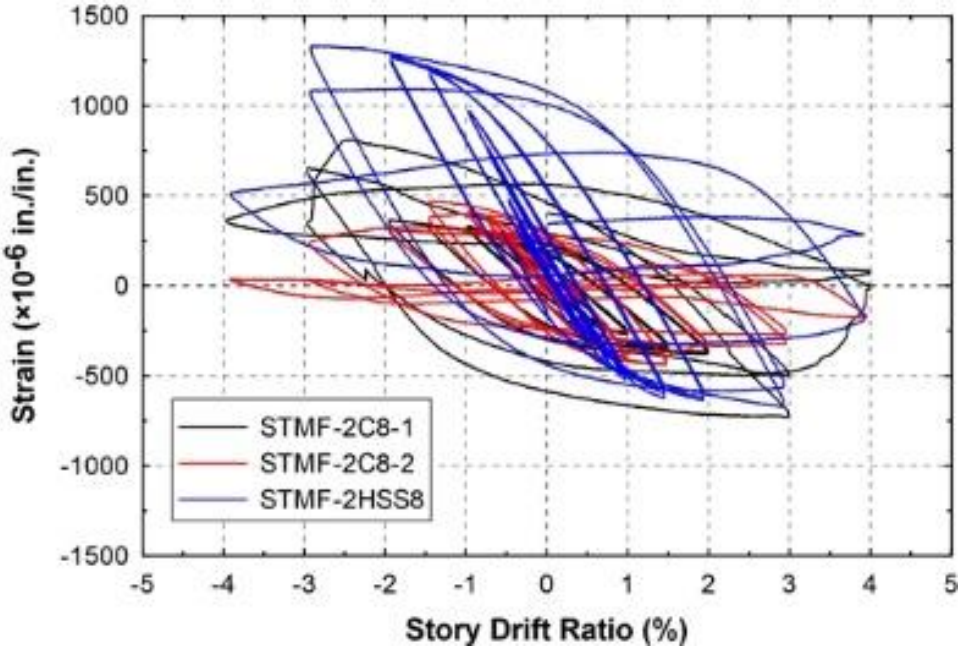

M9-RS-6-3

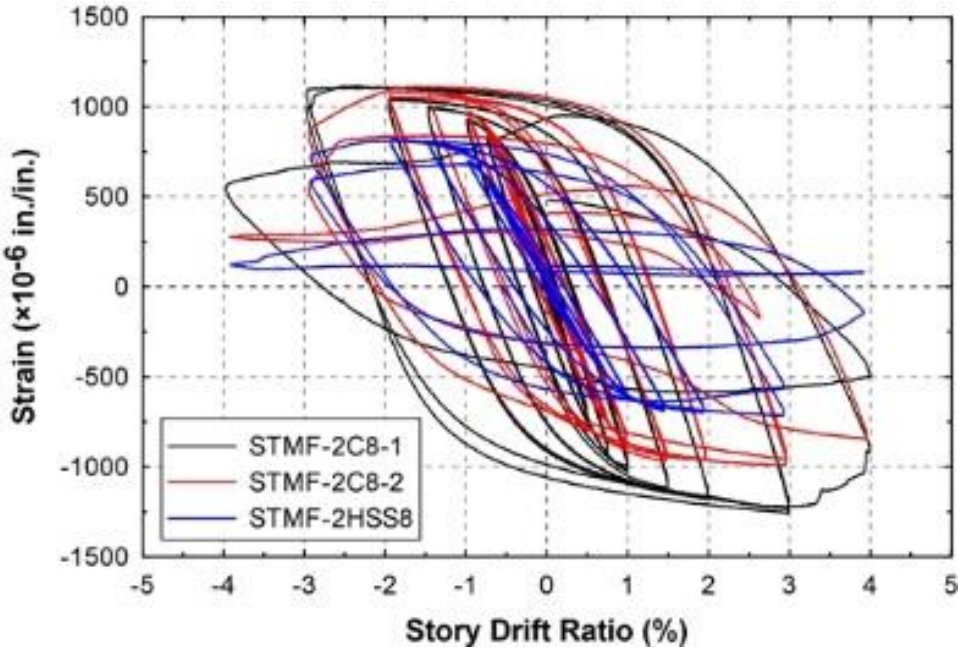
1500
1000
500
0
-500
-1000
-1500
-5
-4
-3
-2
-1
0
1
2
3
4
5
Strain (×10-6 in./in.)
Story Drift Ratio (%)
STMF-2C8-1
STMF-2C8-2
STMF-2HSS8

M10-1-1

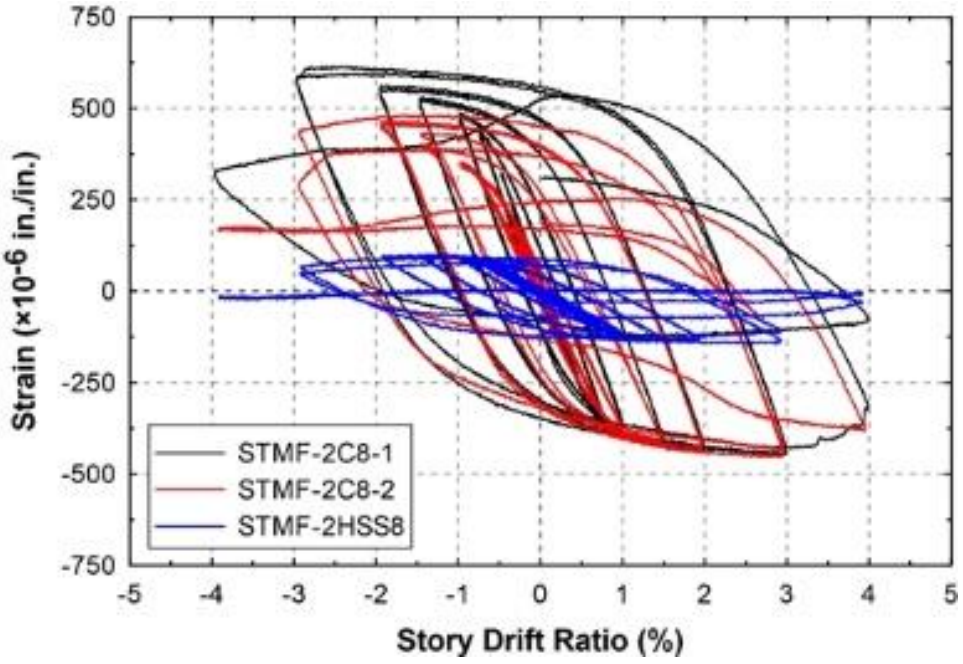
750
500
250
0
-250
-500
-750
-5
-4
-3
-2
-1
0
1
2
3
4
5
Strain (×10-6 in./in.)
Story Drift Ratio (%)
STMF-2C8-1
STMF-2C8-2
STMF-2HSS8

M10-1-2

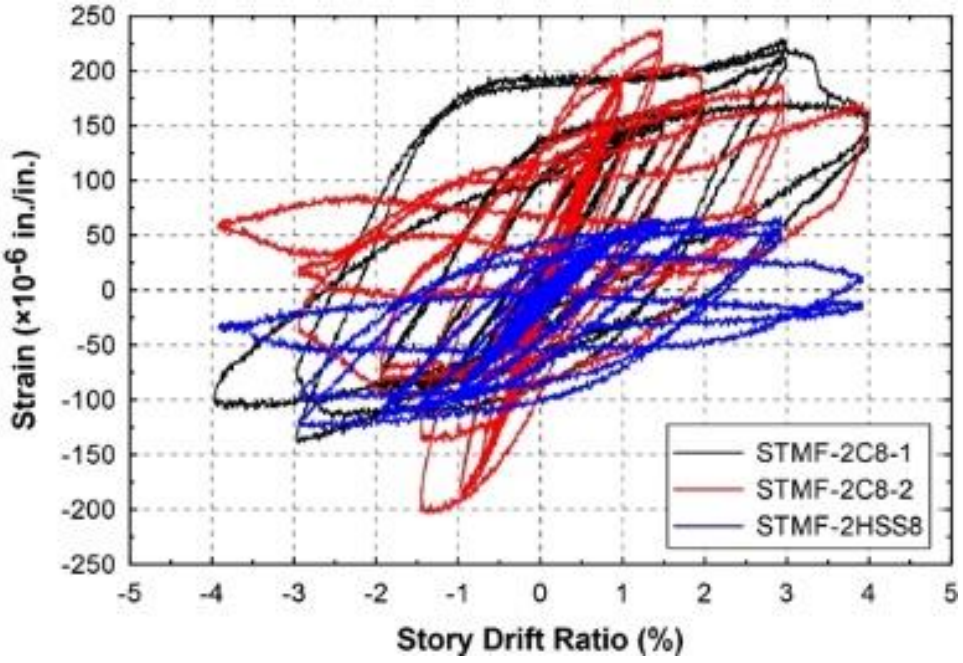
Strain (×10-6 in./in.)
Story Drift Ratio (%)
STMF-2C8-1
STMF-2C8-2
STMF-2HSS8

M10-1-3

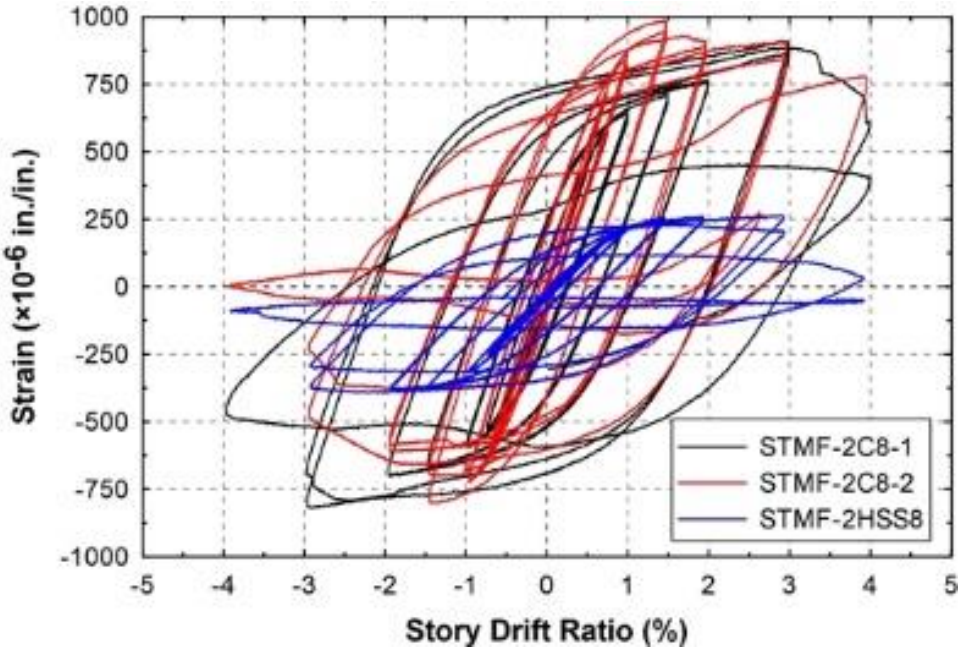
Strain (×10-6 in./in.)
Story Drift Ratio (%)
STMF-2C8-1
STMF-2C8-2
STMF-2HSS8

M10-1-4

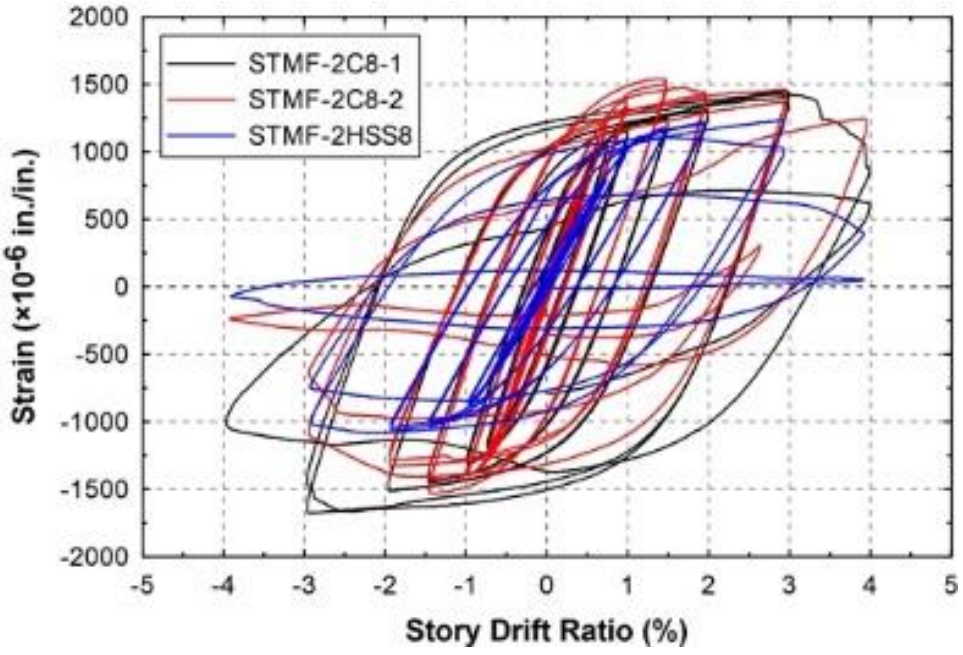
STMF-2C8-1
STMF-2C8-2
STMF-2HSS8
Strain (×10-6 in./in.)
Story Drift Ratio (%)
2000
1500
1000
500
0
-500
-1000
-1500
-2000
-5
-4
-3
-2
-1
0
1
2
3
4
5

M10-1-5

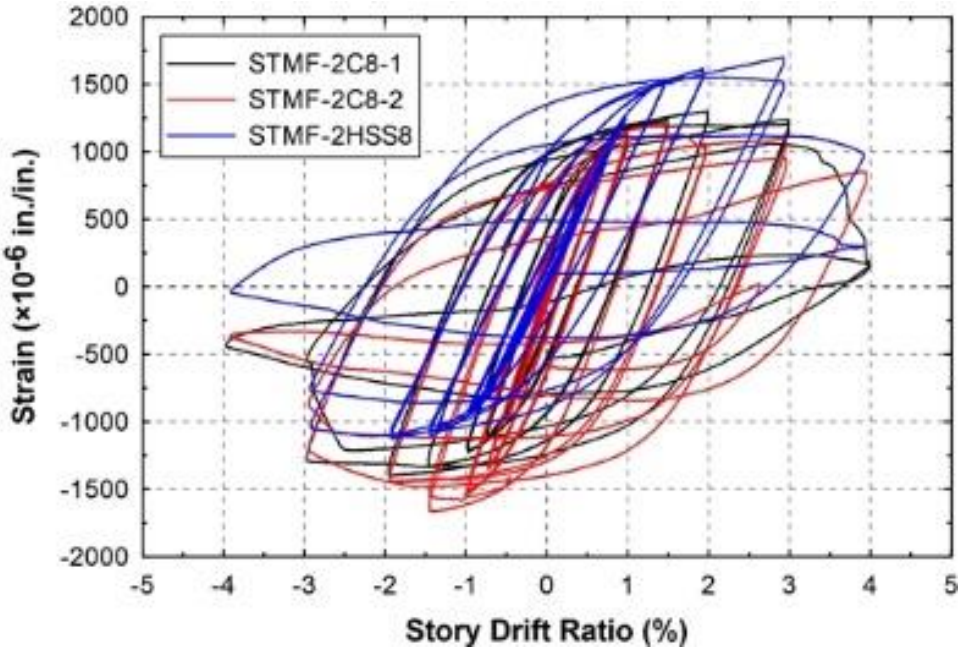
STMF-2C8-1
STMF-2C8-2
STMF-2HSS8
Strain (×10-6 in./in.)
Story Drift Ratio (%)
2000
1500
1000
500
0
-500
-1000
-1500
-2000
-5
-4
-3
-2
-1
0
1
2
3
4
5

M10-2-1

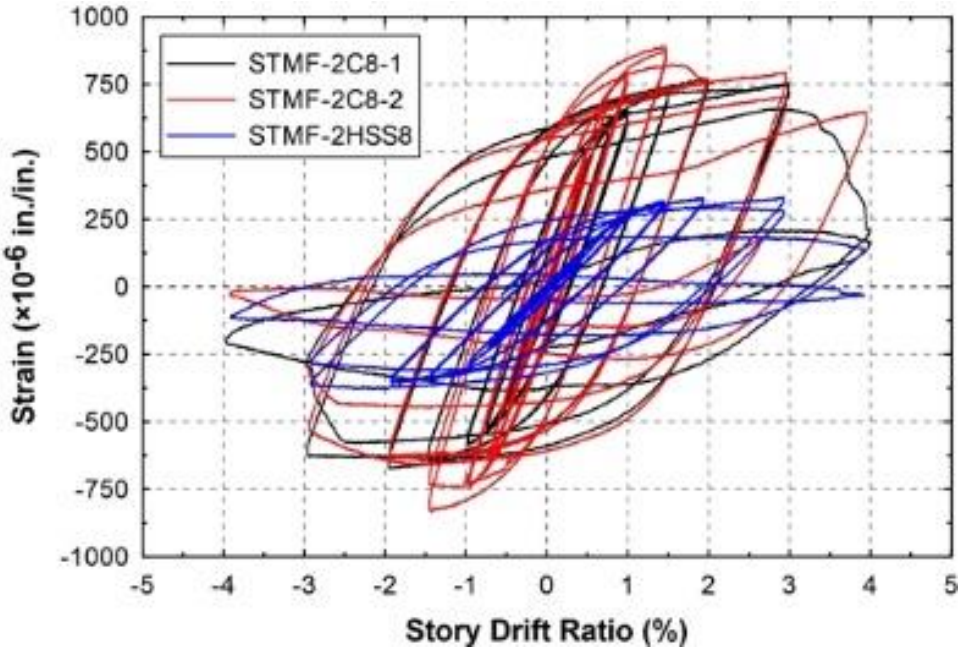
STMF-2C8-1
STMF-2C8-2
STMF-2HSS8
Strain (×10-6 in./in.)
Story Drift Ratio (%)
1000
750
500
250
0
-250
-500
-750
-1000
-5
-4
-3
-2
-1
0
1
2
3
4
5

M10-2-2

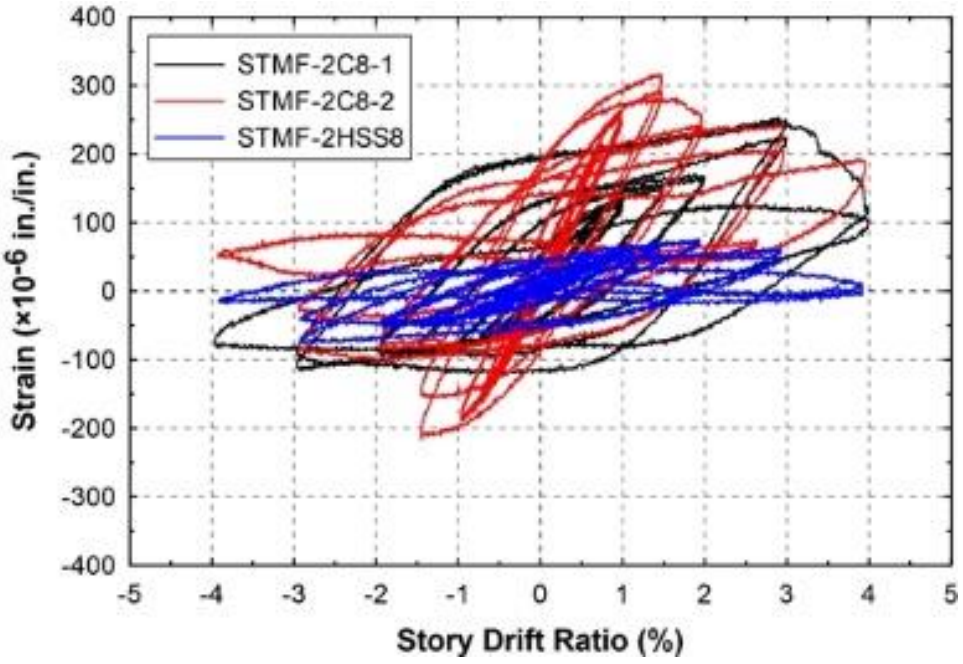
STMF-2C8-1
STMF-2C8-2
STMF-2HSS8
Strain (×10-6 in./in.)
Story Drift Ratio (%)
400
300
200
100
0
-100
-200
-300
-400
-5
-4
-3
-2
-1
0
1
2
3
4
5

M10-2-3

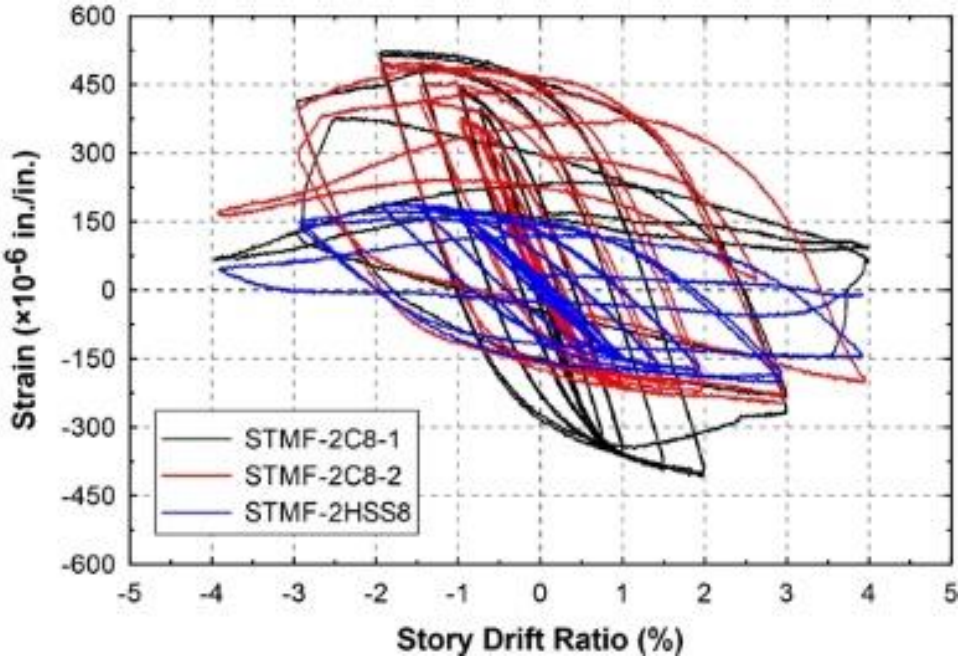
600
450
300
150
0
-150
-300
-450
-600
-5
-4
-3
-2
-1
0
1
2
3
4
5
Strain (×10-6 in./in.)
Story Drift Ratio (%)
STMF-2C8-1
STMF-2C8-2
STMF-2HSS8

M10-2-4

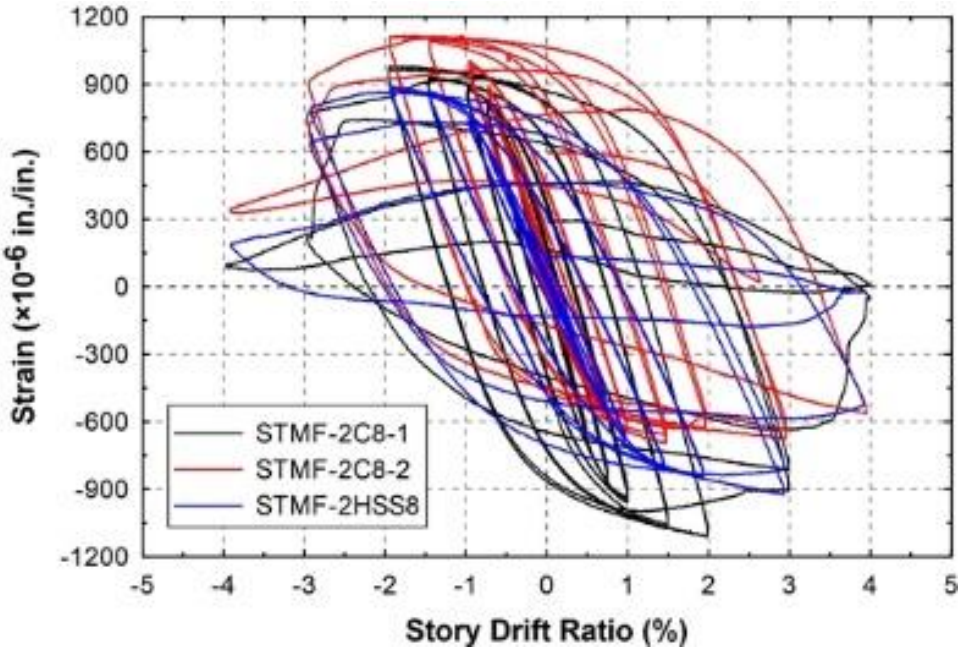
1200
900
600
300
0
-300
-600
-900
-1200
-5
-4
-3
-2
-1
0
1
2
3
4
5
Strain (×10-6 in./in.)
Story Drift Ratio (%)
STMF-2C8-1
STMF-2C8-2
STMF-2HSS8

M10-2-5

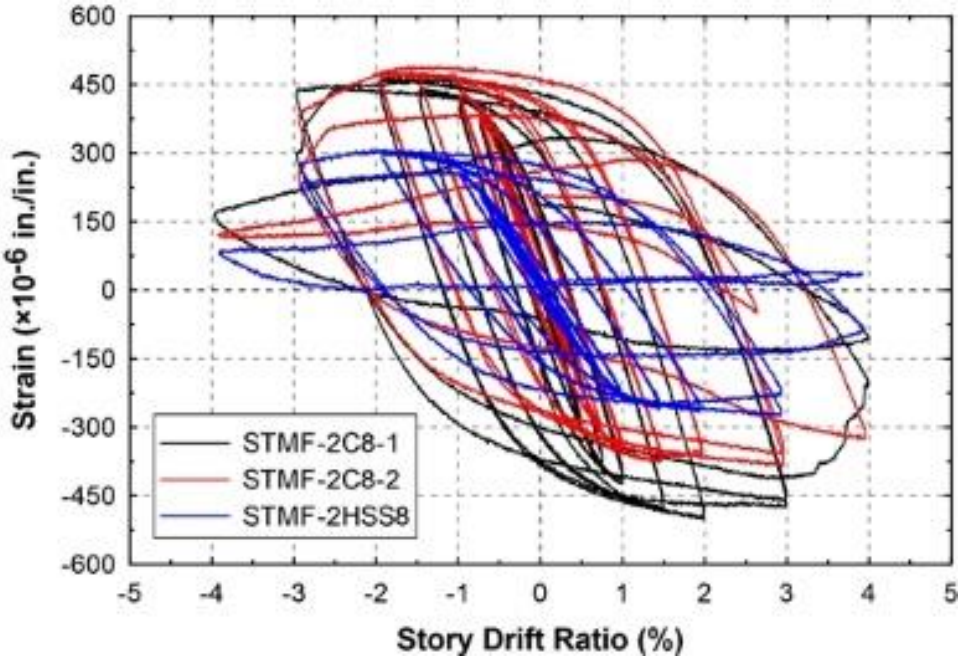

M10-RS-1

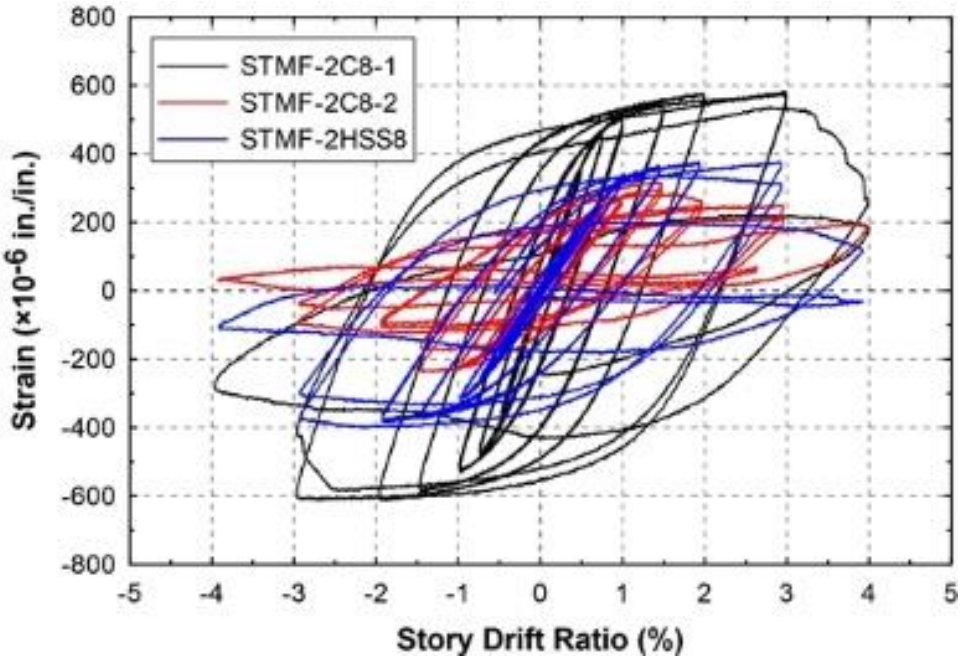

M10-RS-2

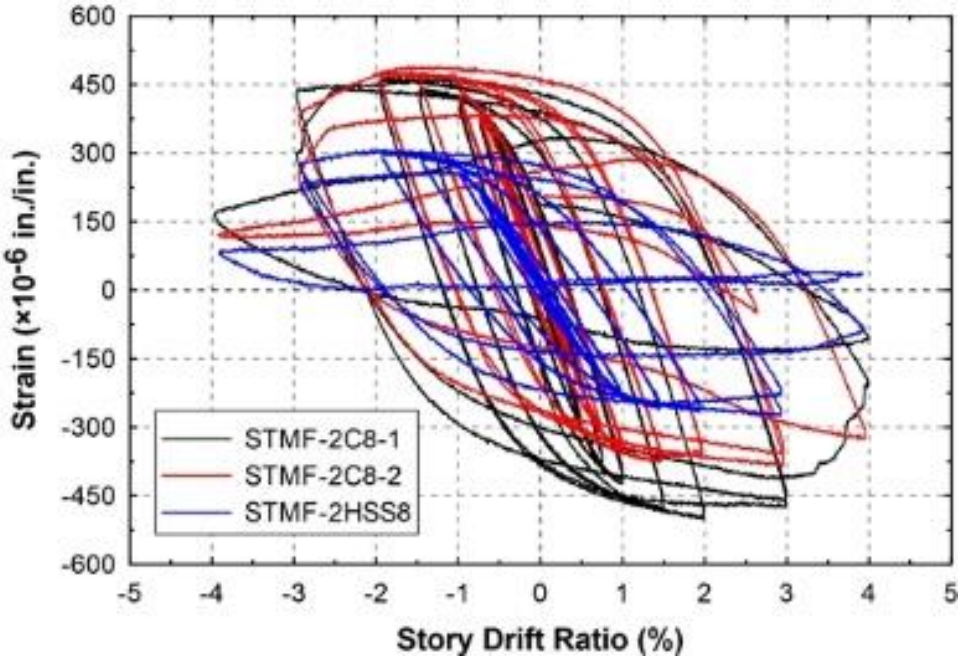

M10-RS-3

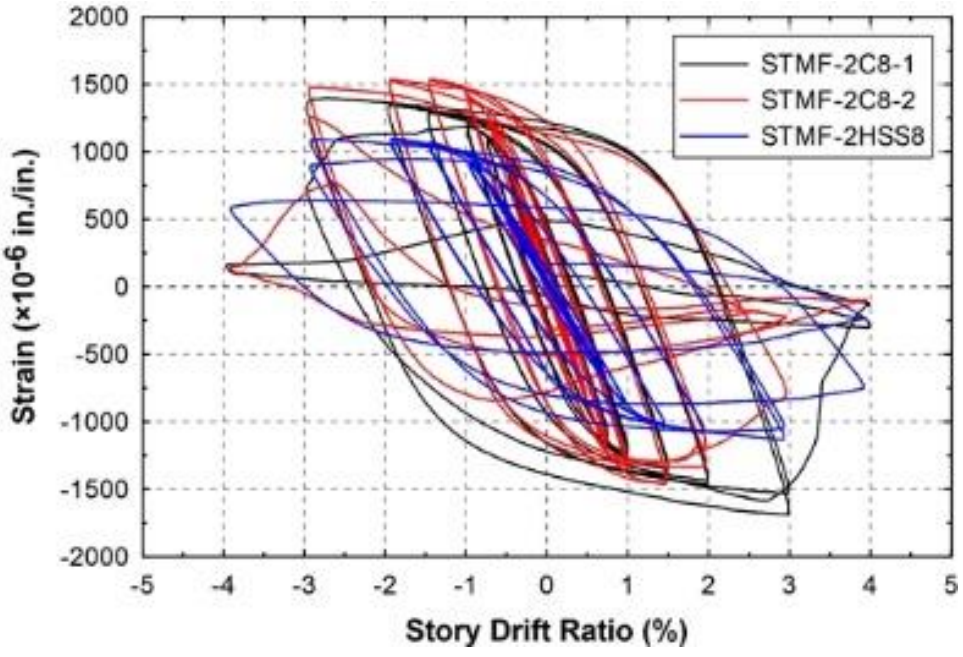

M10s-1-1

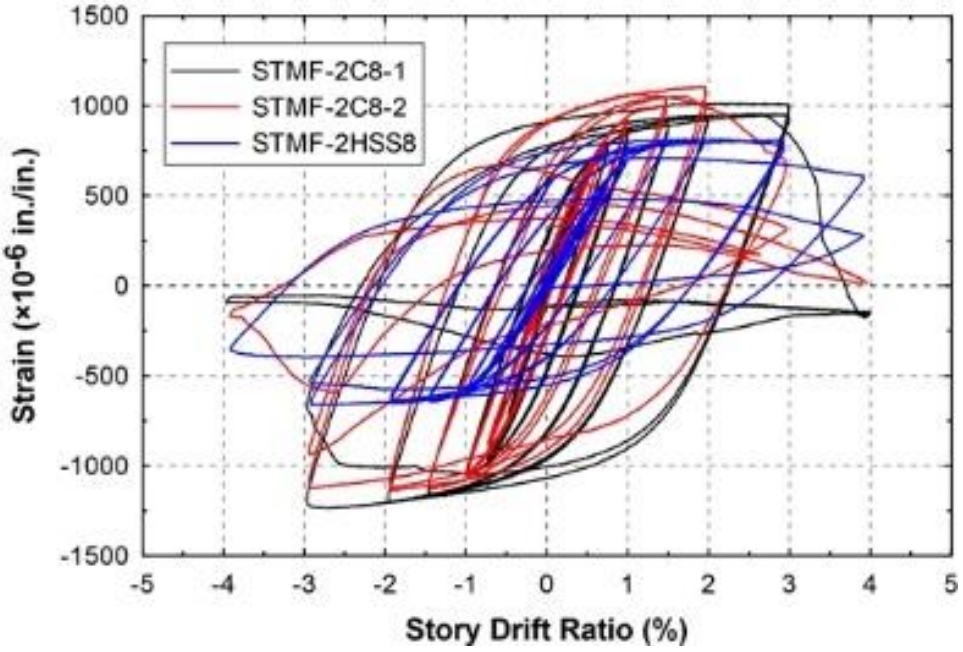

M10s-1-5

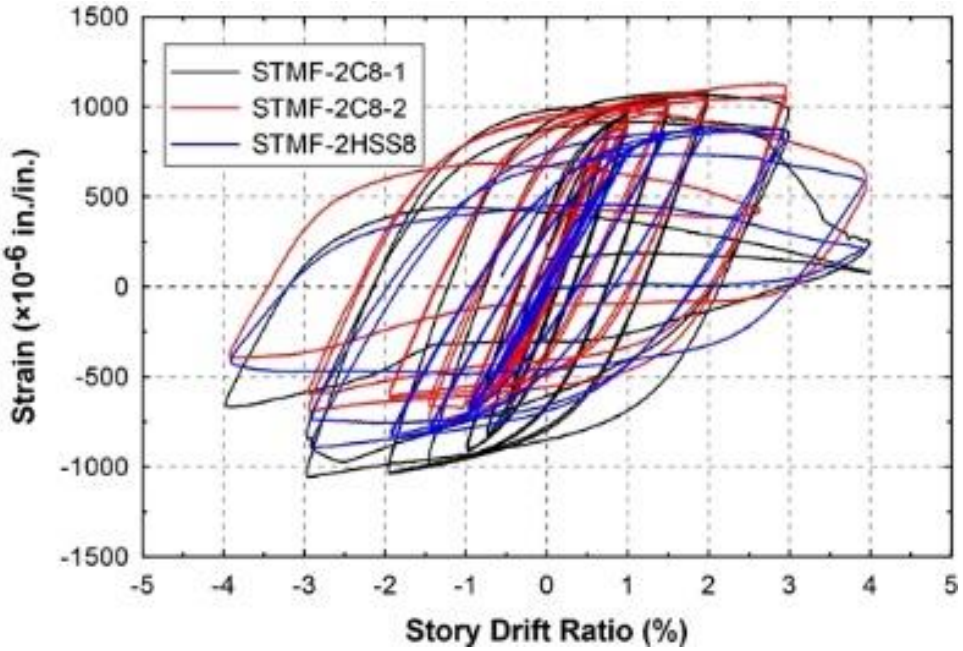

M10s-2-1

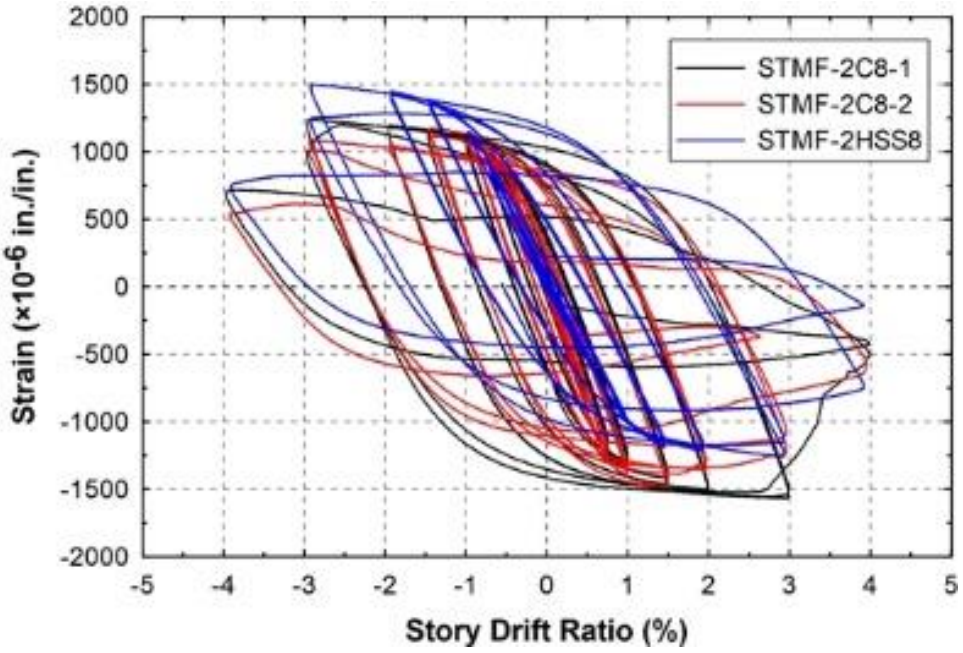

M10s-2-5

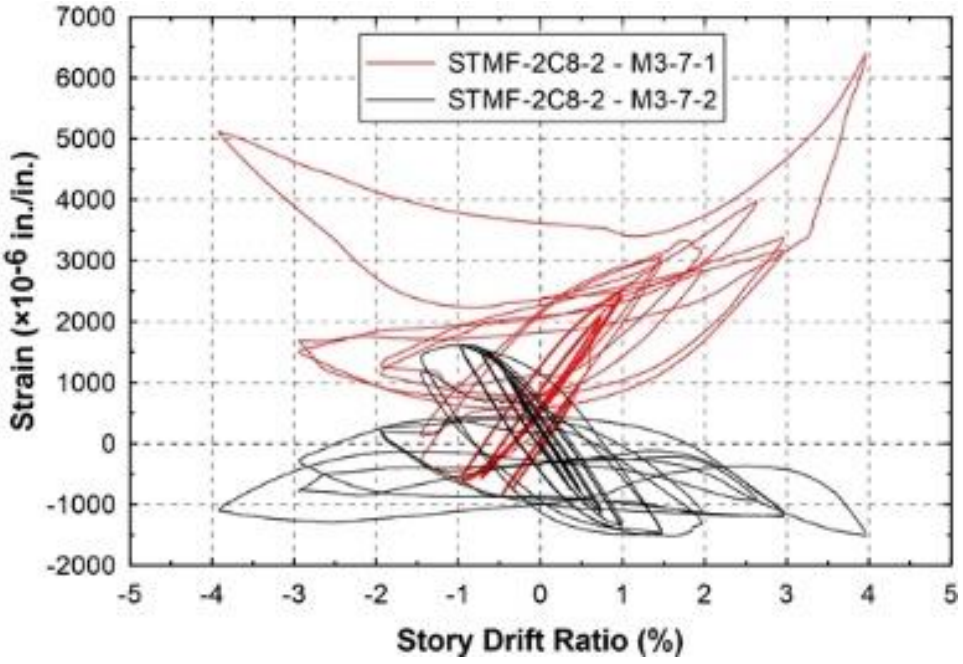

STMF-2C8-2 - M3-7

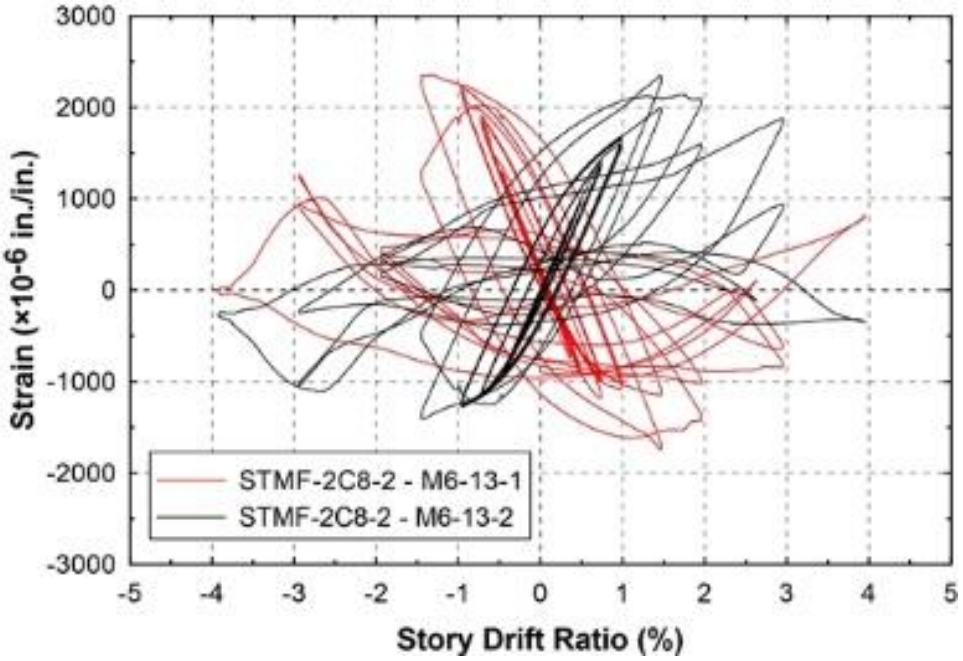

STMF-2C8-2 - M6-13

Appendix K

Acceptance Criteria Levels of Yielding Members of Prototype STF Buildings Subjected to 1% Target Roof Drift According to FEMA 356

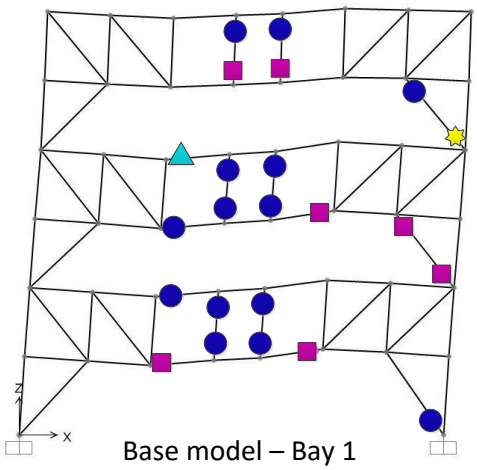

Base model – Bay 1

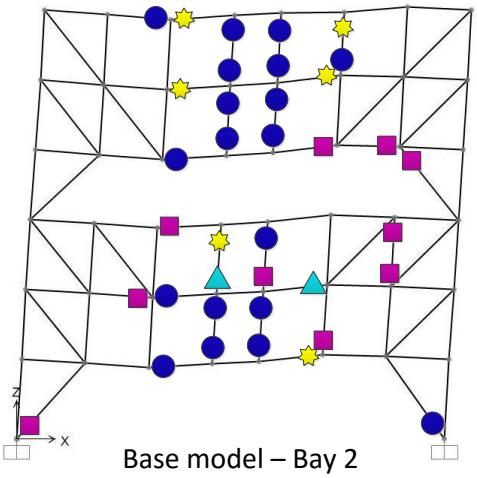

Base model – Bay 2

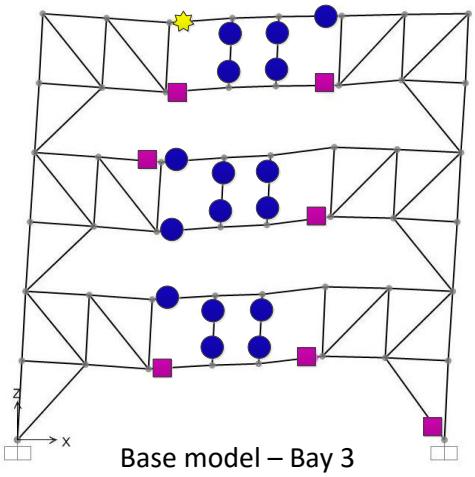

Base model – Bay 3

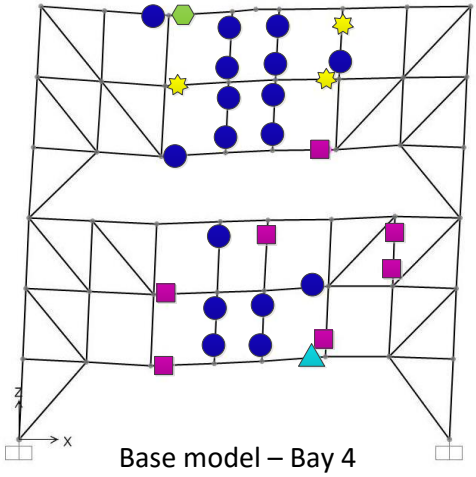

Base model – Bay 4

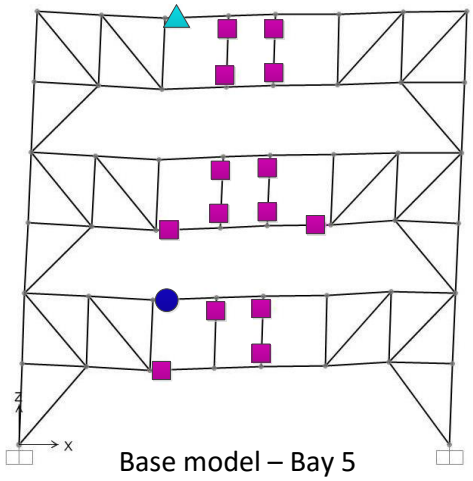

Base model – Bay 5

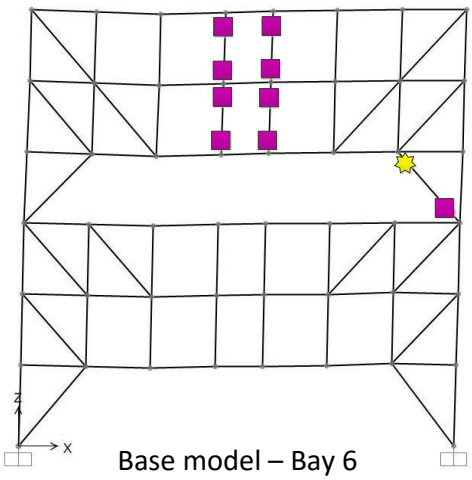

Base model – Bay 6

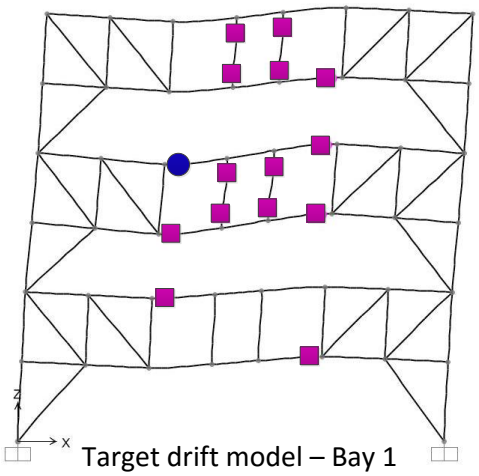

Target drift model – Bay 1

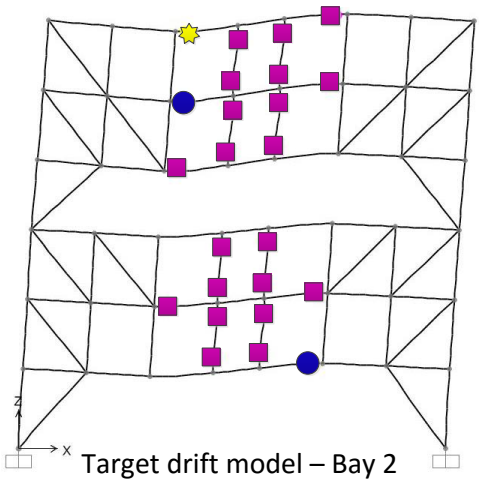

Target drift model – Bay 2

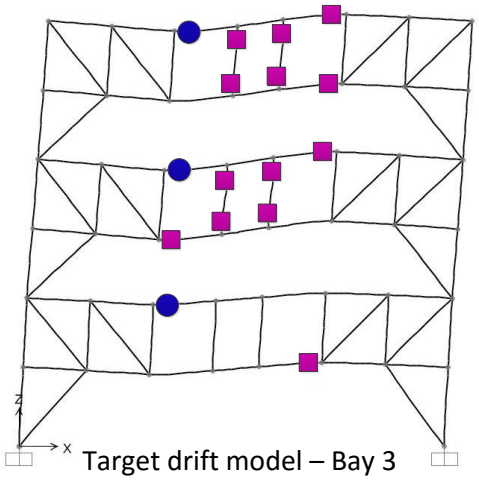

Target drift model – Bay 3

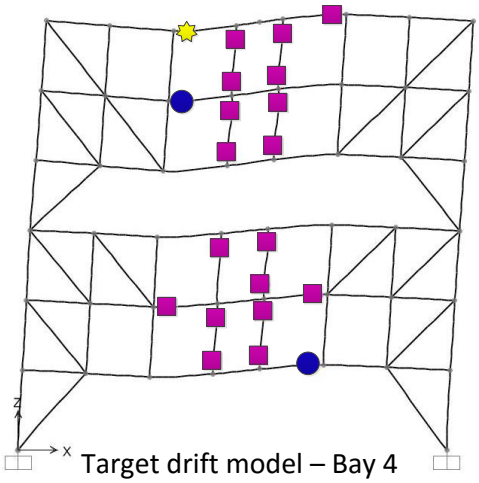

Target drift model – Bay 4

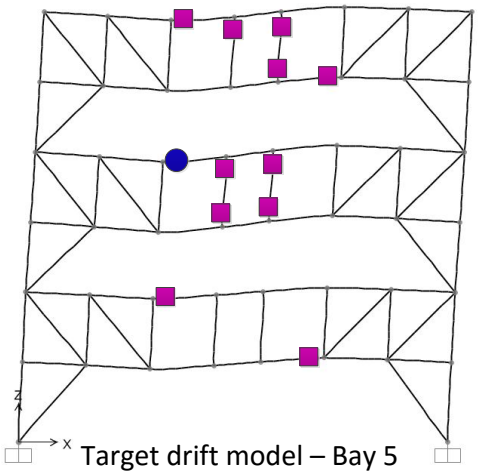

Target drift model – Bay 5

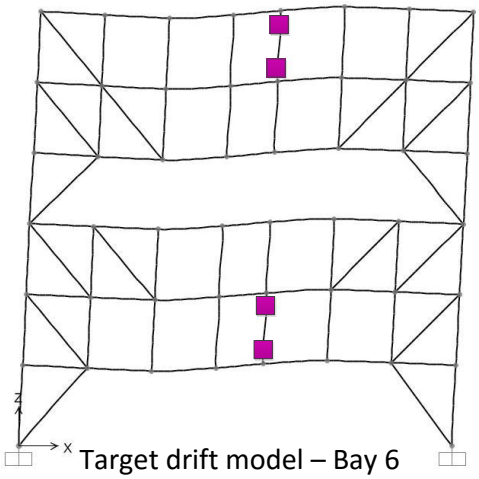

Target drift model – Bay 6

Appendix L

Deflected Shape of Prototype STF Buildings from Pushover Analysis

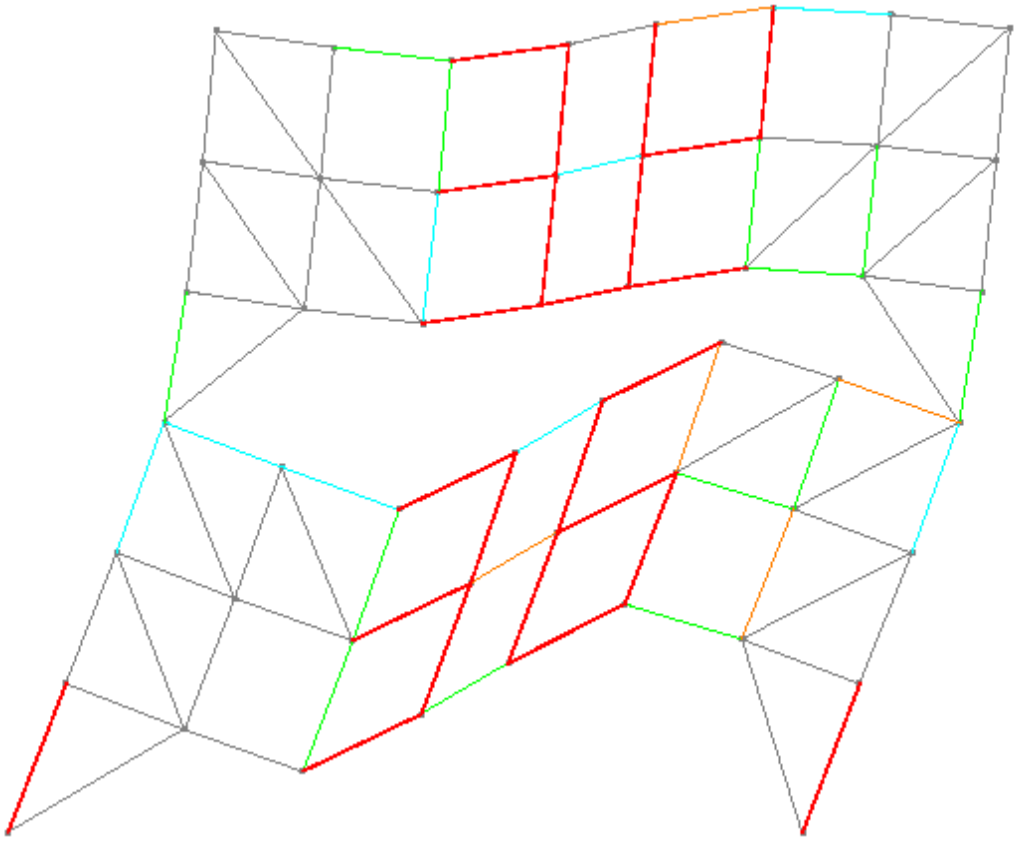

Bay 2 deflected shape of the Base Model at 2% roof drift

Note: The member colors indicate the minimum usage ratio (demand versus capacity of the member) as followed:

Color	Usage Ratio
Grey	0.0
Teal	0.4
Green	0.6
Orange	0.8
Red	1.0

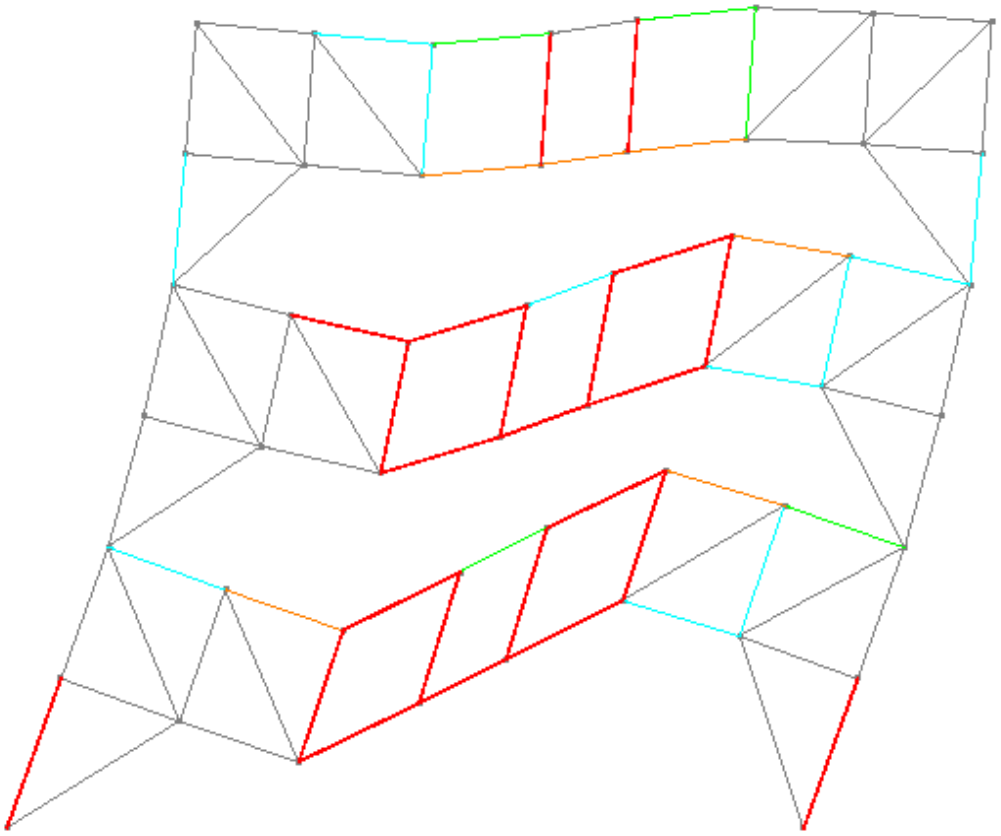

Bay 3 deflected shape of the Base Model at 2% roof drift

Note: The member colors indicate the minimum usage ratio (demand versus capacity of the member) as followed:

Color	Usage Ratio
Grey	0.0
Teal	0.4
Green	0.6
Orange	0.8
Red	1.0

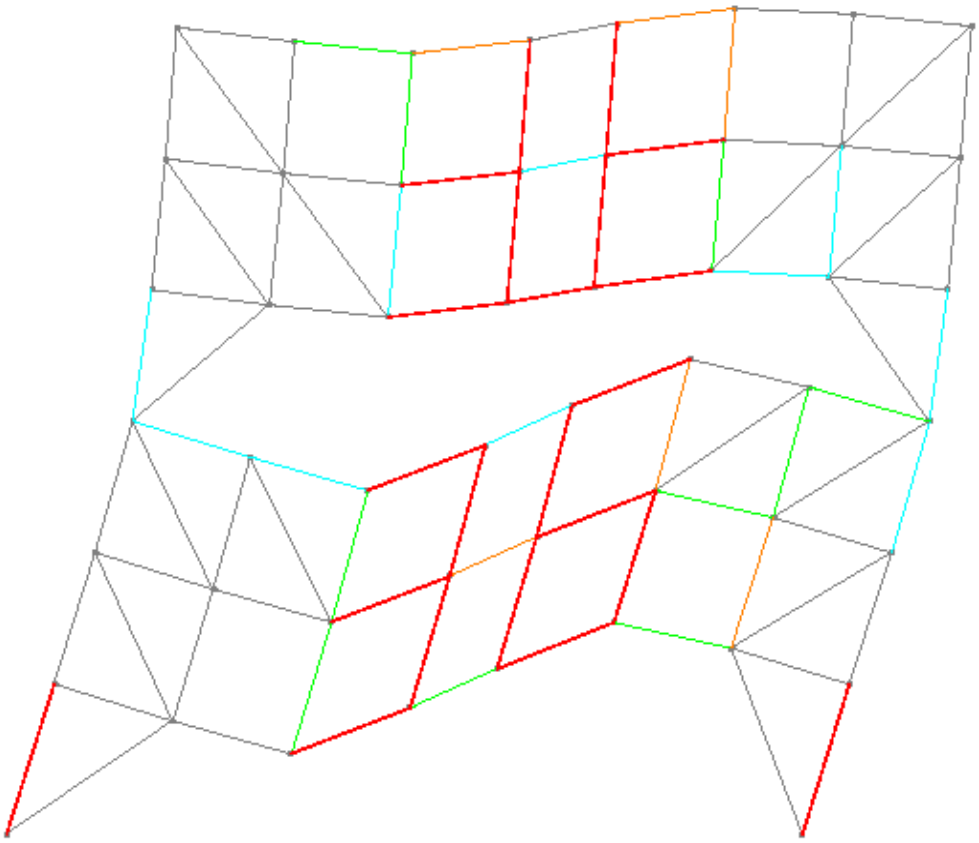

Bay 4 deflected shape of the Base Model at 2% roof drift

Note: The member colors indicate the minimum usage ratio (demand versus capacity of the member) as followed:

Color	Usage Ratio
Grey	0.0
Teal	0.4
Green	0.6
Orange	0.8
Red	1.0

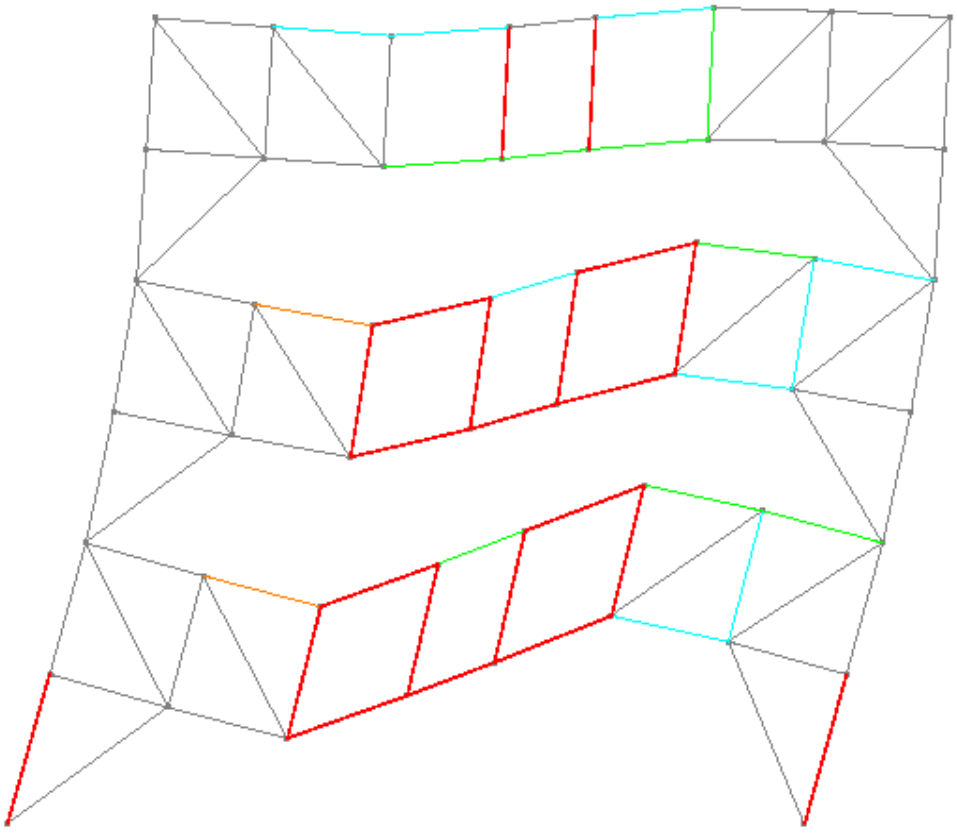

Bay 5 deflected shape of the Base Model at 2% roof drift

Note: The member colors indicate the minimum usage ratio as (demand versus capacity of the member) followed:

Color	Usage Ratio
Grey	0.0
Teal	0.4
Green	0.6
Orange	0.8
Red	1.0

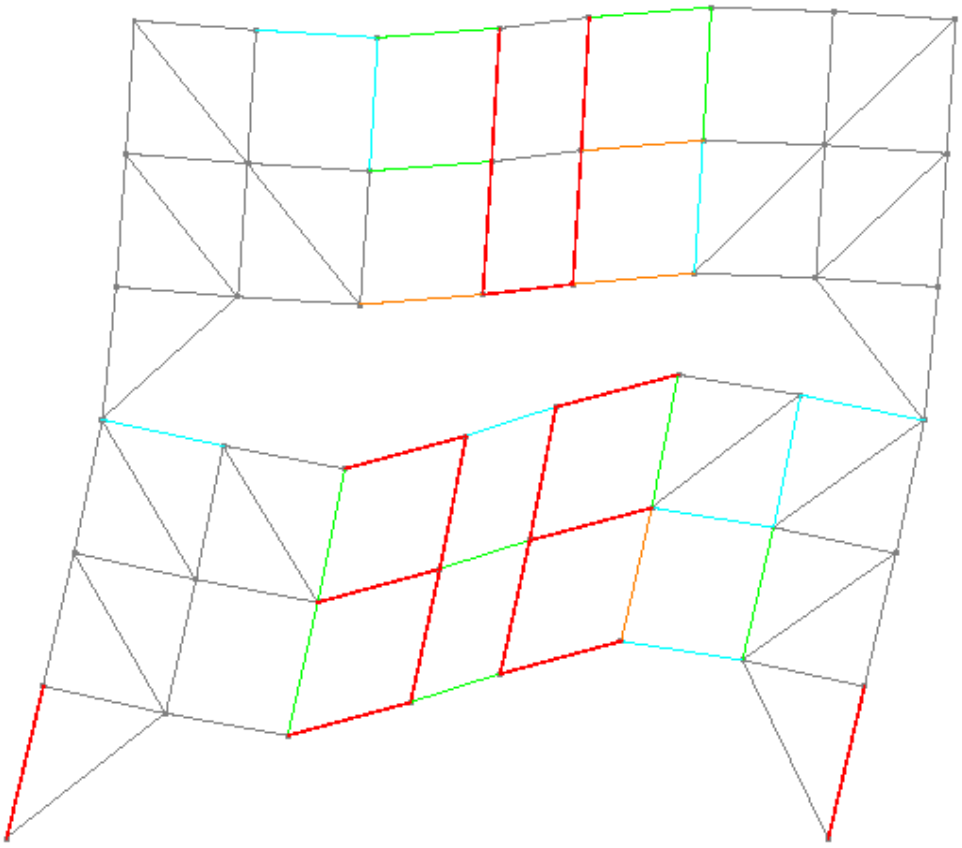

Bay 6 deflected shape of the Base Model at 2% roof drift

Note: The member colors indicate the minimum usage ratio (demand versus capacity of the member) as followed:

Color	Usage Ratio
Grey	0.0
Teal	0.4
Green	0.6
Orange	0.8
Red	1.0

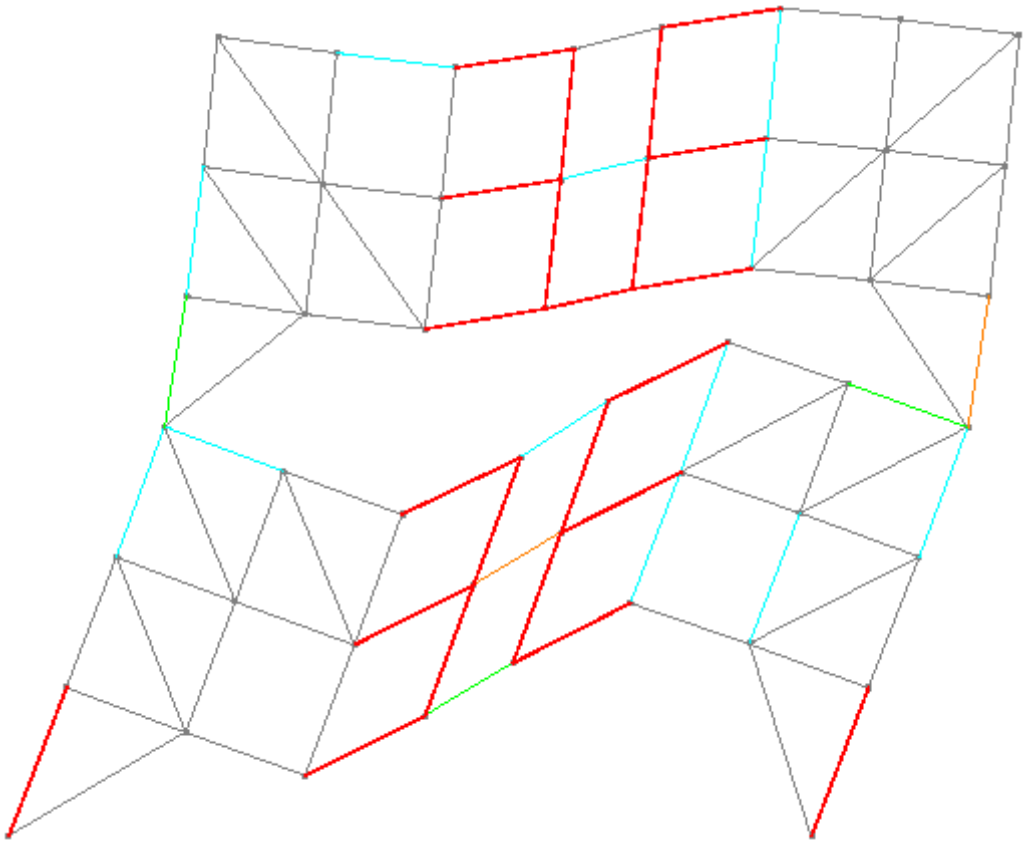

Bay 2 deflected shape of the Target Drift Model at 2% roof drift

Note: The member colors indicate the minimum usage ratio (demand versus capacity of the member) as followed:

Color	Usage Ratio
Grey	0.0
Teal	0.4
Green	0.6
Orange	0.8
Red	1.0

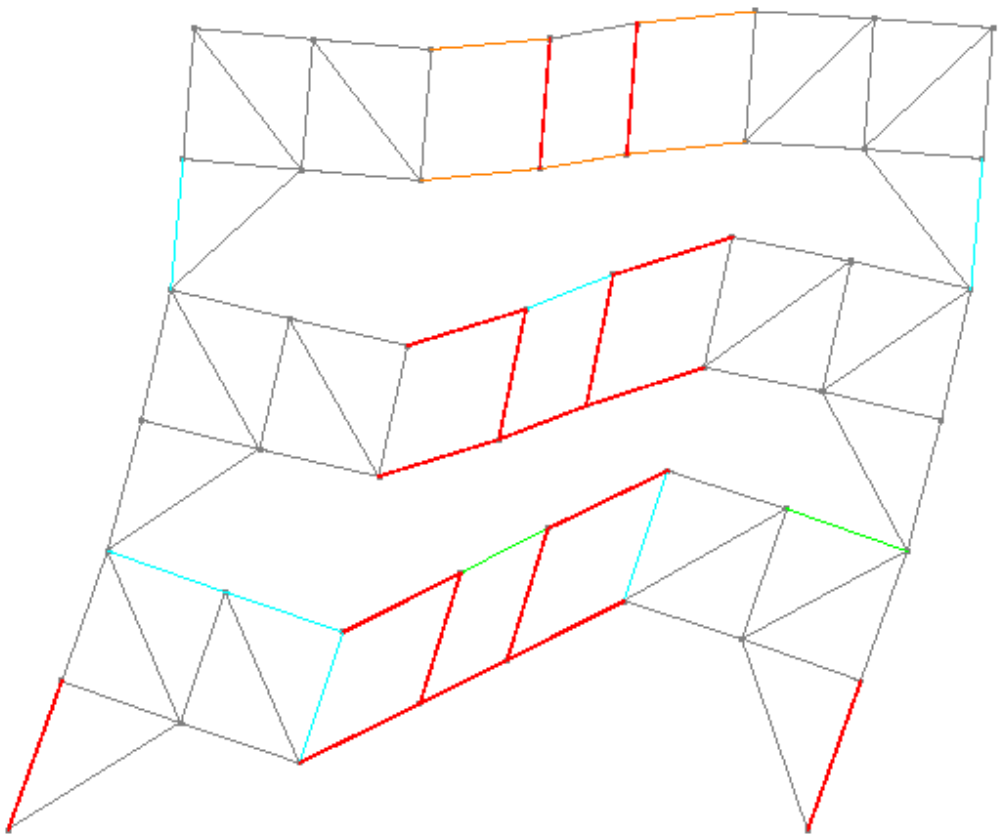

Bay 3 deflected shape of the Target Drift Model at 2% roof drift

Note: The member colors indicate the minimum usage ratio (demand versus capacity of the member) as followed:

Color	Usage Ratio
Grey	0.0
Teal	0.4
Green	0.6
Orange	0.8
Red	1.0

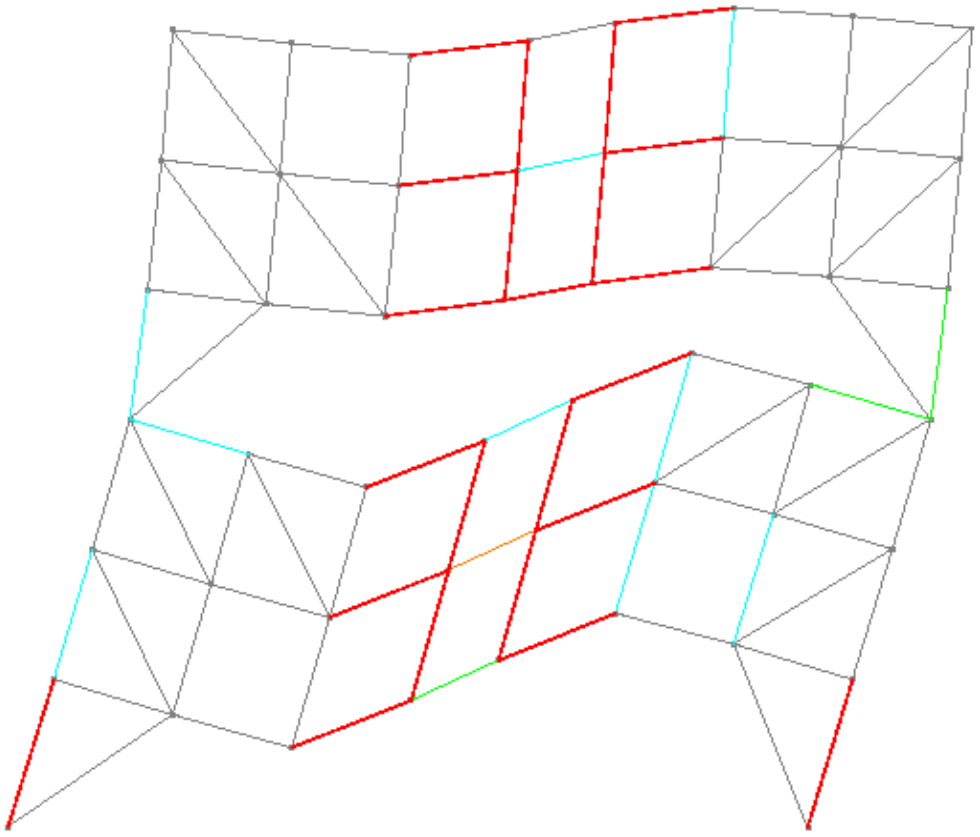

Bay 4 deflected shape of the Target Drift Model at 2% roof drift

Note: The member colors indicate the minimum usage ratio (demand versus capacity of the member) as followed:

Color	Usage Ratio
Grey	0.0
Teal	0.4
Green	0.6
Orange	0.8
Red	1.0

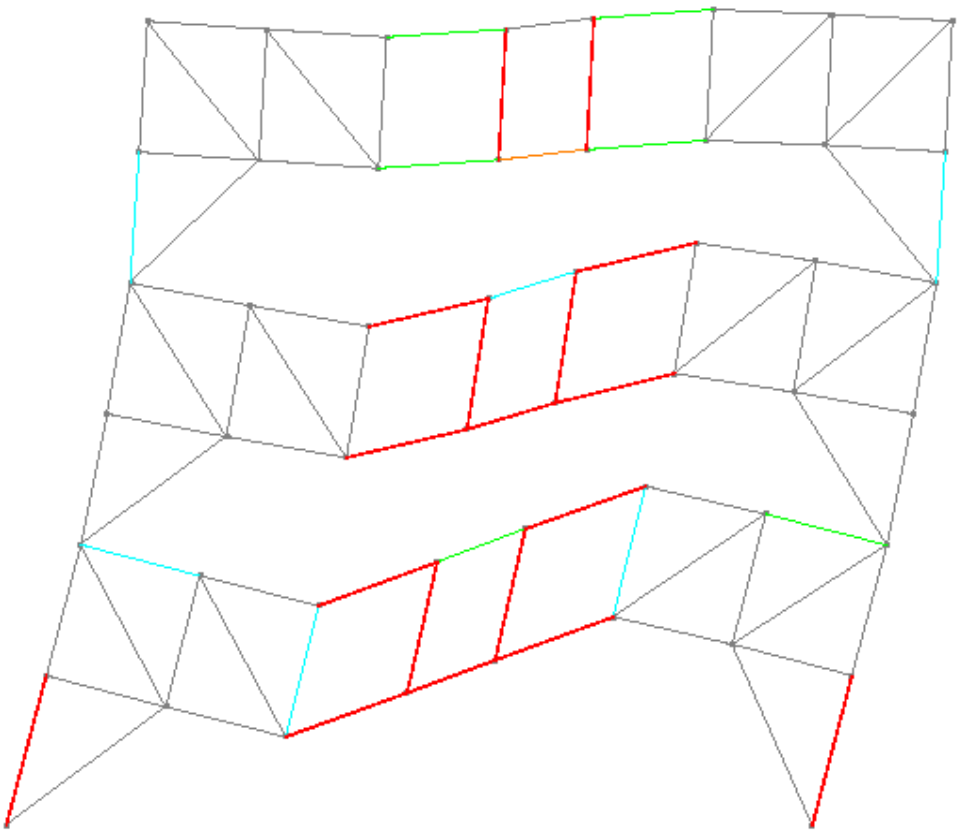

Bay 5 deflected shape of the Target Drift Model at 2% roof drift

Note: The member colors indicate the minimum usage ratio (demand versus capacity of the member) as followed:

Color	Usage Ratio
Grey	0.0
Teal	0.4
Green	0.6
Orange	0.8
Red	1.0

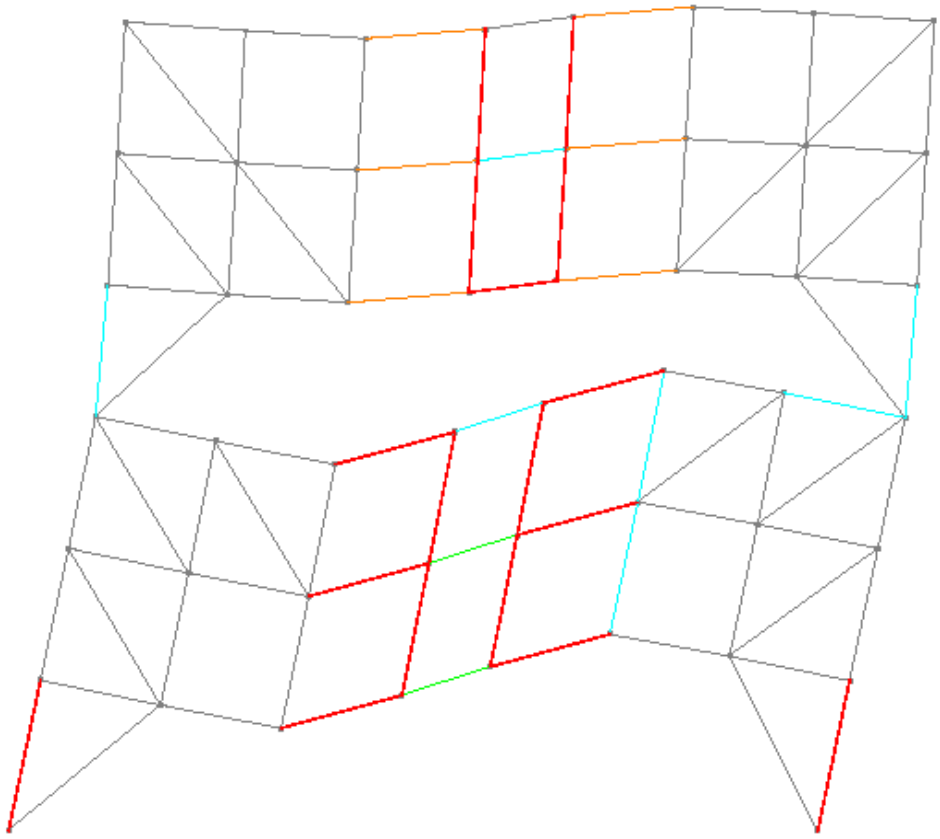

Bay 6 deflected shape of the Target Drift Model at 2% roof drift

Note: The member colors indicate the minimum usage ratio (demand versus capacity of the member) as followed:

Color	Usage Ratio
Grey	0.0
Teal	0.4
Green	0.6
Orange	0.8
Red	1.0

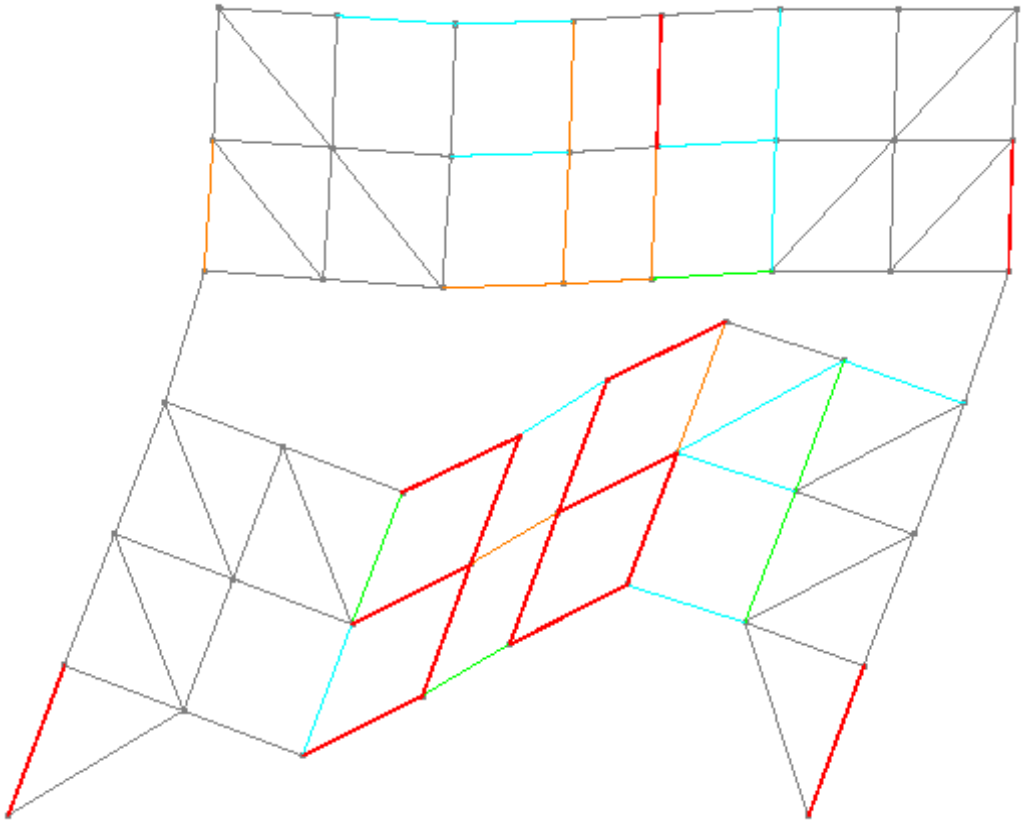

Bay 2 deflected shape of the No Kicker Model at 2% roof drift

Note: The member colors indicate the minimum usage ratio (demand versus capacity of the member) as followed:

Color	Usage Ratio
Grey	0.0
Teal	0.4
Green	0.6
Orange	0.8
Red	1.0

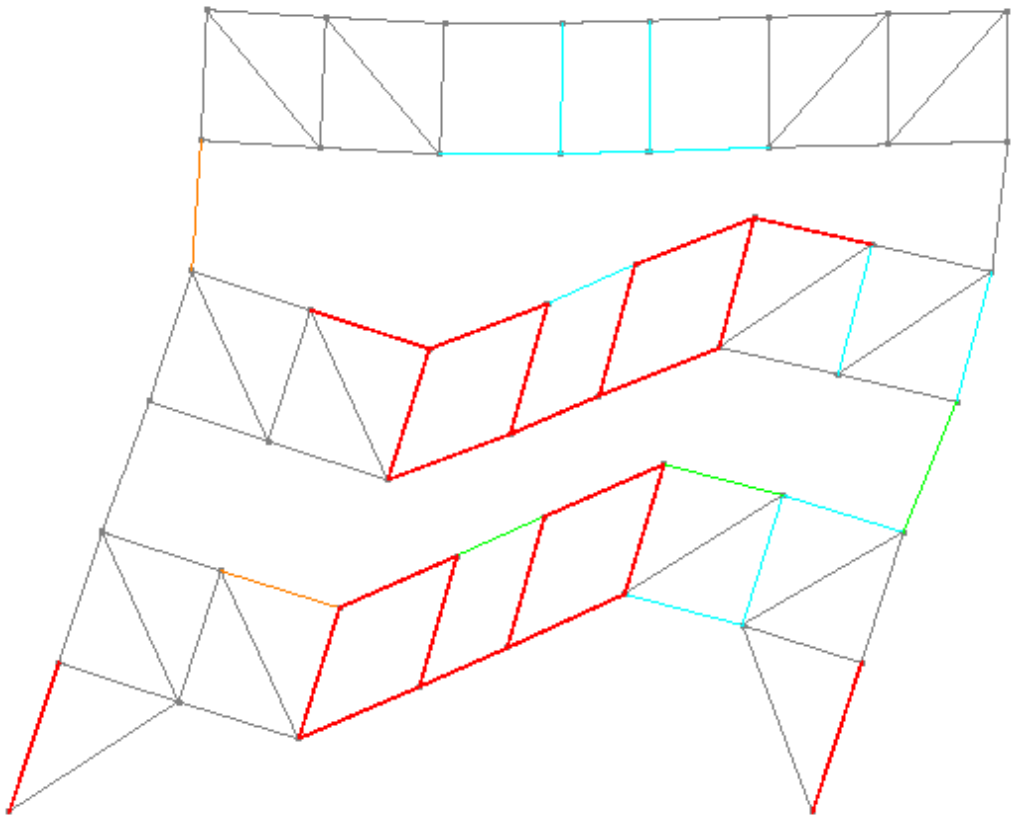

Bay 3 deflected shape of the No Kicker Model at 2% roof drift

Note: The member colors indicate the minimum usage ratio (demand versus capacity of the member) as followed:

Color	Usage Ratio
Grey	0.0
Teal	0.4
Green	0.6
Orange	0.8
Red	1.0

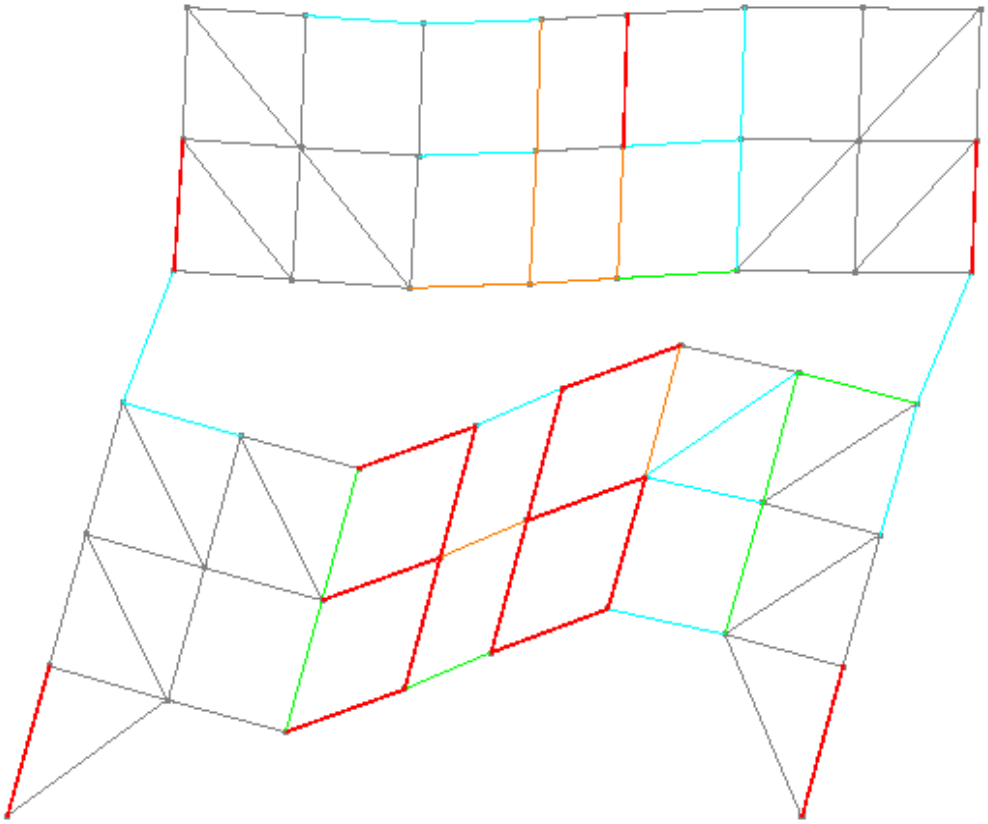

Bay 4 deflected shape of the No Kicker Model at 2% roof drift

Note: The member colors indicate the minimum usage ratio (demand versus capacity of the member) as followed:

Color	Usage Ratio
Grey	0.0
Teal	0.4
Green	0.6
Orange	0.8
Red	1.0

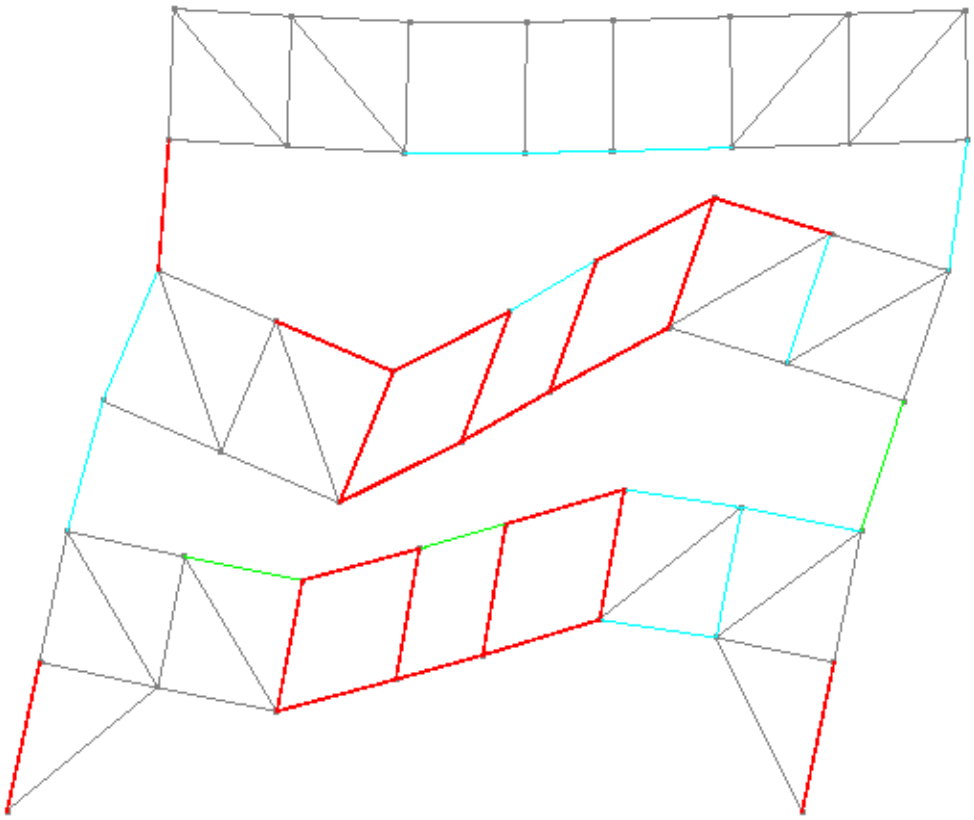

Bay 5 deflected shape of the No Kicker Model at 2% roof drift

Note: The member colors indicate the minimum usage ratio (demand versus capacity of the member) as followed:

Color	Usage Ratio
Grey	0.0
Teal	0.4
Green	0.6
Orange	0.8
Red	1.0

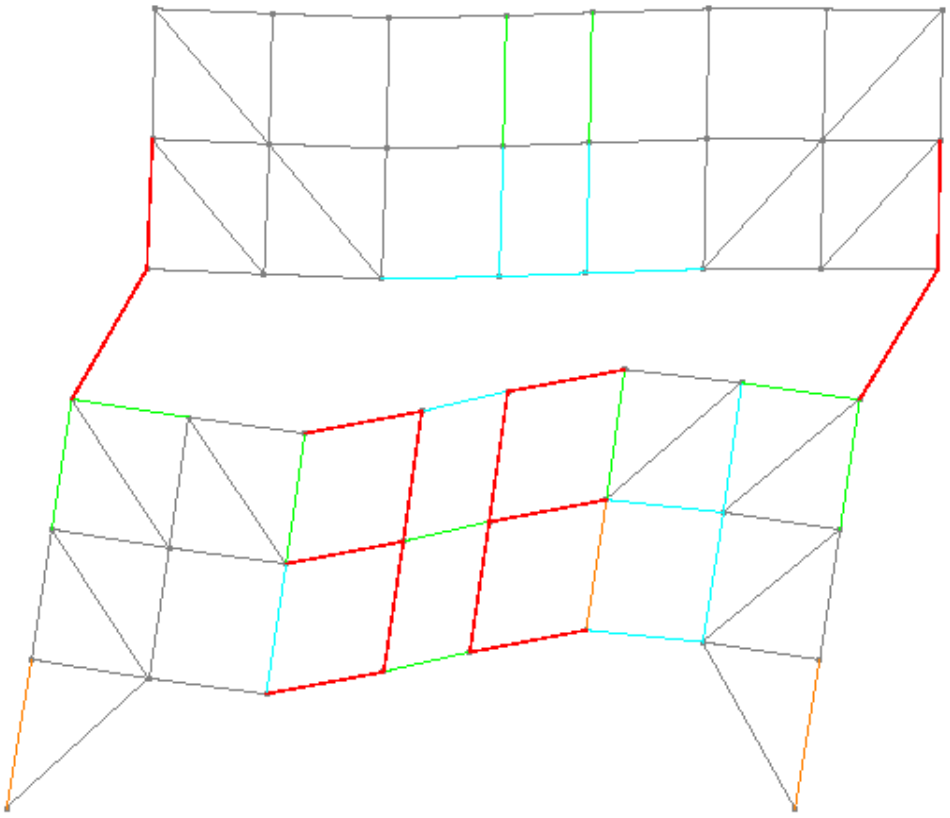

Bay 6 deflected shape of the No Kicker Model at 2% roof drift

Note: The member colors indicate the minimum usage ratio (demand versus capacity of the member) as followed:

Color	Usage Ratio
Grey	0.0
Teal	0.4
Green	0.6
Orange	0.8
Red	1.0

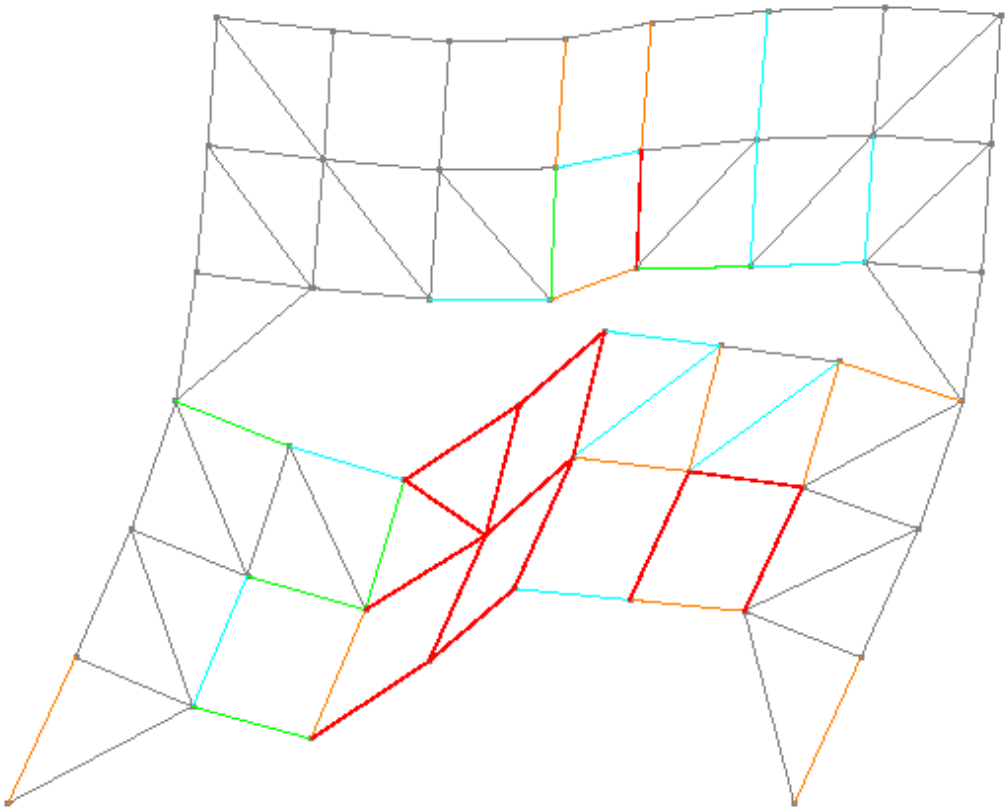

Bay 2 deflected shape of the SVP Model at 0.77%* roof drift

Note: *The pushover analysis failed to converge and was terminated at 0.77% roof drift due to excessive deformation of the yielded members.

The member colors indicate the minimum usage ratio (demand versus capacity of the member) as followed:

Color	Usage Ratio
Grey	0.0
Teal	0.4
Green	0.6
Orange	0.8
Red	1.0

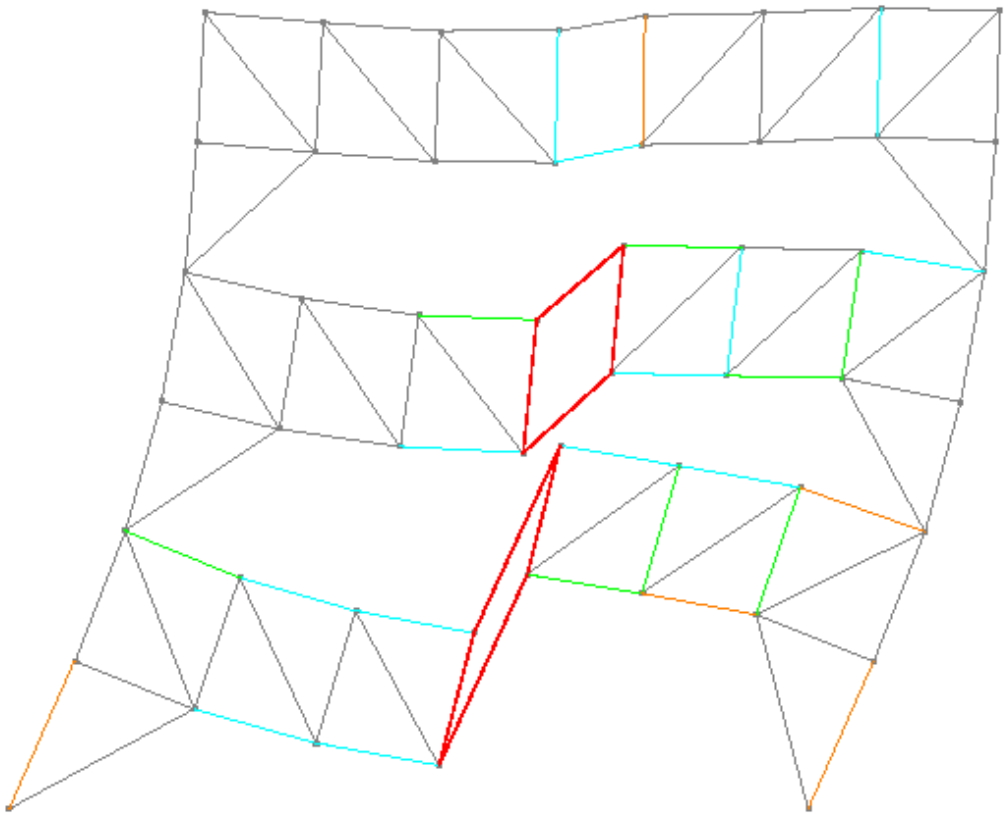

Bay 3 deflected shape of the SVP Model at 0.77%* roof drift

Note: *The pushover analysis failed to converge and was terminated at 0.77% roof drift due to excessive deformation of the yielded members.

The member colors indicate the minimum usage ratio (demand versus capacity of the member) as followed:

Color	Usage Ratio
Grey	0.0
Teal	0.4
Green	0.6
Orange	0.8
Red	1.0

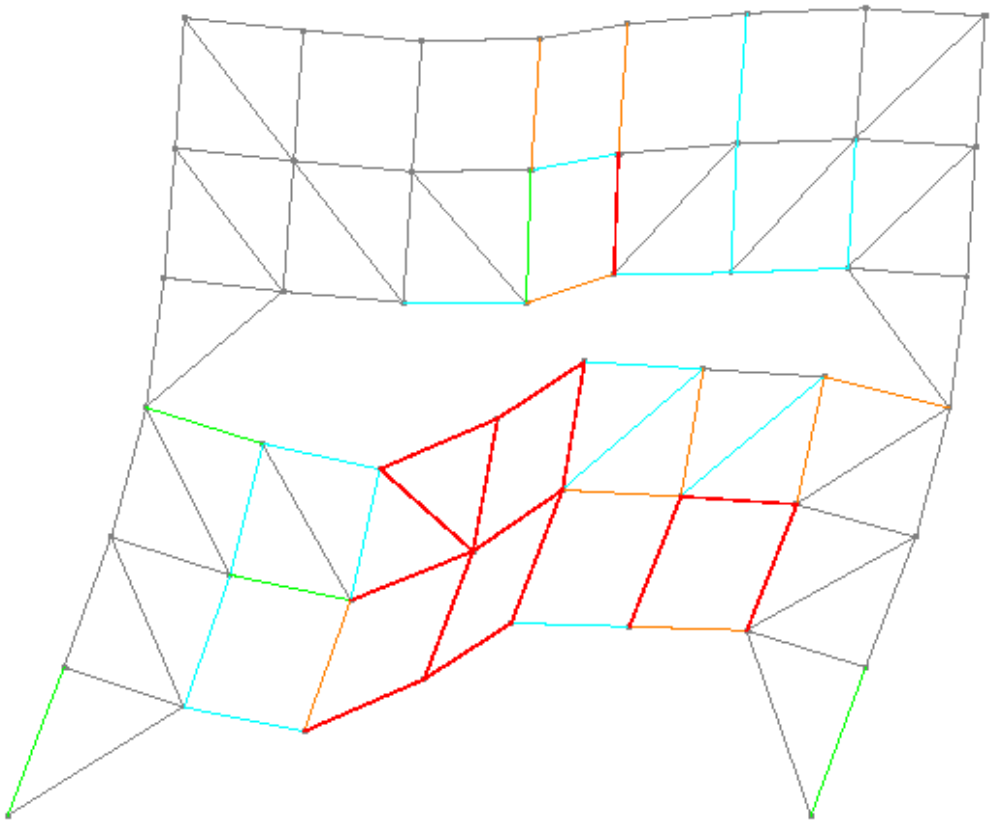

Bay 4 deflected shape of the SVP Model at 0.77%* roof drift

Note: *The pushover analysis failed to converge and was terminated at 0.77% roof drift due to excessive deformation of the yielded members.

The member colors indicate the minimum usage ratio (demand versus capacity of the member) as followed:

Color	Usage Ratio
Grey	0.0
Teal	0.4
Green	0.6
Orange	0.8
Red	1.0

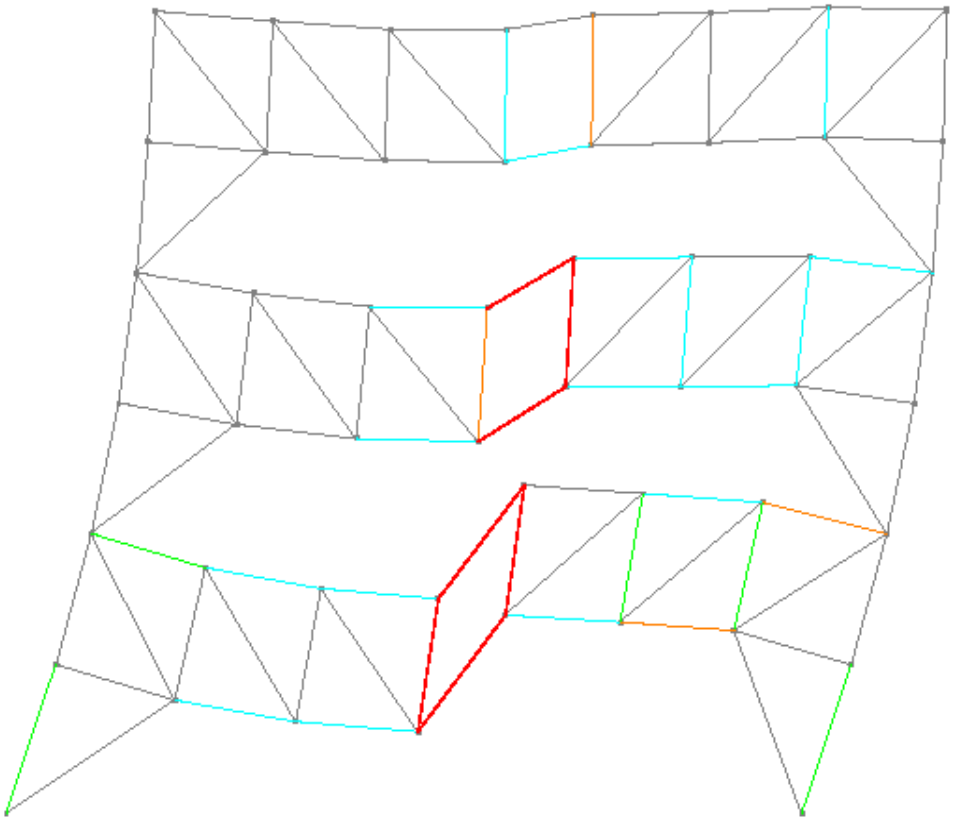

Bay 5 deflected shape of the SVP Model at 0.77%* roof drift

Note: *The pushover analysis failed to converge and was terminated at 0.77% roof drift due to excessive deformation of the yielded members.

The member colors indicate the minimum usage ratio (demand versus capacity of the member) as followed:

Color	Usage Ratio
Grey	0.0
Teal	0.4
Green	0.6
Orange	0.8
Red	1.0

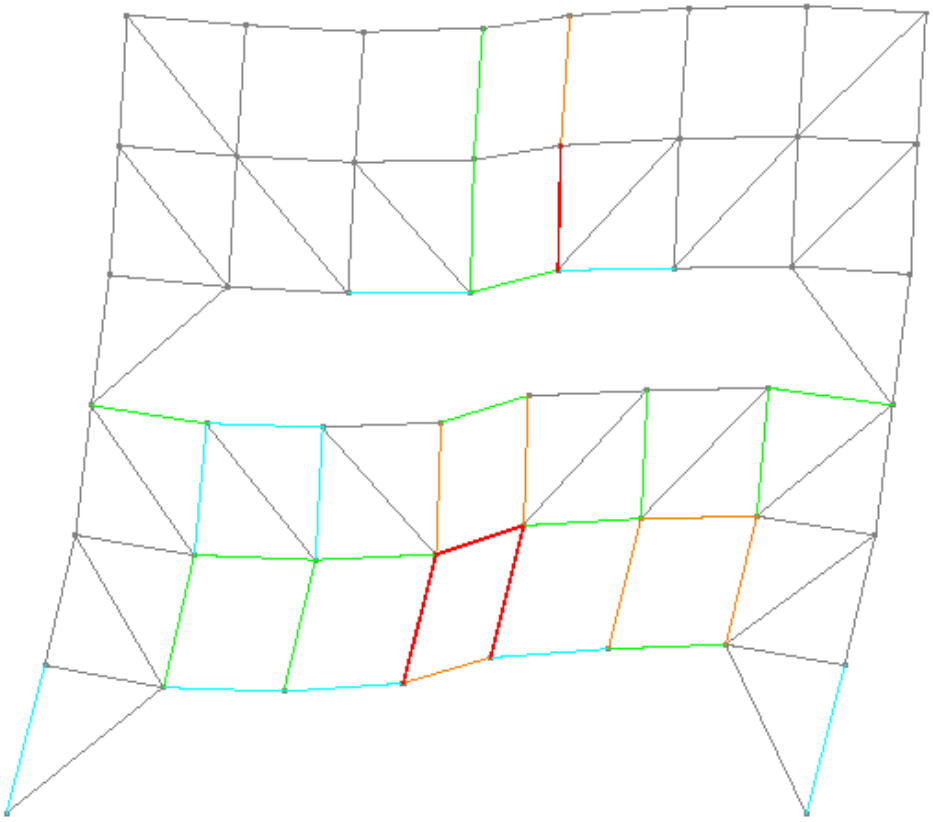

Bay 6 deflected shape of the SVP Model at 0.77%* roof drift

Note: *The pushover analysis failed to converge and was terminated at 0.77% roof drift due to excessive deformation of the yielded members.

The member colors indicate the minimum usage ratio (demand versus capacity of the member) as followed:

Color	Usage Ratio
Grey	0.0
Teal	0.4
Green	0.6
Orange	0.8
Red	1.0

References

AISC (1997), *Seismic Provisions for Structural Steel Buildings*, American Institute of Steel Construction, Chicago, IL.

AISC (2002), *Seismic Provisions for Structural Steel Buildings*, ANSI/AISC 341-02, American Institute of Steel Construction, Chicago, IL.

AISC (2005), *Seismic Provisions for Structural Steel Buildings*, ANSI/AISC 341-05, American Institute of Steel Construction, Chicago, IL.

AISC (2010a), *Seismic Provisions for Structural Steel Buildings*, ANSI/AISC 341-10, American Institute of Steel Construction, Chicago, IL.

AISC (2010b), *Specification for Structural Steel Buildings*, ANSI/AISC 360-10, American Institute of Steel Construction, Chicago, IL.

ASCE (2010), *Minimum Design Loads for Buildings and Other Structures*, ASCE 7-10, American Society of Civil Engineers, Reston, VA.

ASTM International (2015), *E8/E8M-15a Standard Test Methods for Tension Testing of Metallic Materials*, American Society of Testing Material, West Conshohocken, PA.

Basha, H.S., and Goel, S.C. (1994), "Seismic Resistance Truss Moment Frames with Ductile Vierendeel Segment," *Report No. UMCEE 94-29*, Department of Civil and Environmental Engineering, University of Michigan, Ann Arbor, MI.

Basha, H.S., and Goel, S.C. (1995), "Special Truss Moment Frames with Vierendeel Middle Panel," *Engineering Structures*, vol. 17, no. 5, pp. 352-358.

Basha, H.S., and Goel, S.C. (1996), "Seismic Resistant Truss Moment Frames with Ductile Vierendeel Segment," *Paper No. 487, 11th World Conference on Earthquake Engineering*, Acapulco, Mexico.

Brazil, A. (2000), “Staggered truss system proves economical for hotels,” *Modern Steel Construction*, vol. 50, no. 9.

CBSC (2001), *2001 California Building Code* (California Code of Regulations, Title 24), California Building Standards Commission, Sacramento, CA.

Chao, S.-H., and Goel, S.C. (2006), “Performance-Based Plastic Design of Seismic Resistant Special Truss Moment Frames,” *Report No. UMCEE 06-03*, Department of Civil and Environmental Engineering, University of Michigan, Ann Arbor, MI.

Chao, S.-H., and Goel, S.C. (2006), “Performance-Based Seismic Design of Special Truss Moment Frames,” *Proceedings of the 4th International Conference on Earthquake Engineering*, Taipei, Taiwan.

Chao, S.-H., and Goel, S.C. (2008a), “A Modified Equation for Expected Maximum Shear Strength of the Special Segment for Design of Special Truss Moment Frames,” *Engineering Journal*, American Institute of Steel Construction, vol. 45, no. 2, pp.117-125.

Chao, S.-H., and Goel, S.C. (2008b), “Performance-Based Plastic Design of Special Truss Moment Frames,” *Engineering Journal*, American Institute of Steel Construction, vol. 45, no. 2, pp.127-150.

Chopra, A.K. (2011), *Dynamics of structures – Theory and Applications to Earthquake Engineering, 4th Ed.*, Pearson Prentice Hall, Upper Saddle River, NJ.

Cohen, M.P. (1986), “Design Solutions Utilizing the Staggered-Steel Truss System”, *Engineering Journal*, American Institute of Steel Construction, vol. 23, no. 3, pp.97-106.

CSi (2011a), *Components and Elements for PERFORM-3D and PERFORM-COLLAPS*, Computers and Structures, Inc., Berkeley, CA.

CSi (2011b), *CSI analysis reference manual for SAP2000, ETABS, SAFE and CSiBridge*, Computers and Structures, Inc., Berkeley, CA.

Department of Architecture and Civil Engineering (1967), “High Rise Housing in Steel – The Staggered Truss System,” *Research report R67-7*, Massachusetts Institute of Technology, Cambridge, MA.

Dusicka, P., Itani, A.M., and Sahai, R. (2002), “Advances in the Seismic Design of Special Truss Moment Frames,” *Proceedings of the 71st Annual Convention of the Structural Engineers of California*, Santa Barbara, CA.

El-Tawil, S., and Deierlein, G.G. (2001a), “Nonlinear Analysis of Mixed Steel-Concrete Frames. I: Element Formulation,” *Journal of Structural Engineering*, American Society of Civil Engineers, vol. 127, no. 6, pp.647-655.

El-Tawil, S., and Deierlein, G.G. (2001b), “Nonlinear Analysis of Mixed Steel-Concrete Frames. II: Implementation and Verification,” *Journal of Structural Engineering*, American Society of Civil Engineers, vol. 127, no. 6, pp.656-665.

Fadden, M., and McCormick, J. (2012), “Cyclic quasi-static testing of hollow structural section beam members,” *Journal of Structural Engineering*, American Society of Civil Engineers, vol. 135, no. 5, pp.561-570.

FEMA (1997), *NEHRP Recommended Provisions for Seismic Regulations for New Buildings and Other Structures, Part 1: Provisions*, FEMA 450, Federal Emergency Management Agency, Washington, D.C.

FEMA (2000a), *Prestandard and Commentary for the Seismic Rehabilitation of Buildings*, FEMA 356, Federal Emergency Management Agency, Washington, D.C.

FEMA (2000b), *Recommended seismic design criteria for new steel moment- frame buildings*, FEMA-350, Federal Emergency Management Agency, Washington, D.C.

FEMA (2009), *Quantification of Building Seismic Performance Factors*, FEMA P695, Federal Emergency Management Agency, Washington, D.C.

Goel, S.C. (1998), "A Commentary on Seismic Provision for Special Concentrically Braced Frames (SCBF) and Special Truss Moment Frames," *Proceedings of the 1998 AISC Steel Conference*, New Orleans, LA.

Goel, S.C., and Chao, S.-H. (2008), *Performance-Based Plastic Design: Earthquake-Resistant Steel Structures*, ICC, County Club Hills, IL.

Goel, S.C., and Itani, A.M. (1991), "Seismic resistant special truss moment frames," *Journal of Structural Engineering*, American Society of Civil Engineers, vol. 120, no. 6, pp.1781-1797.

Goel, S.C., and Itani, A.M. (1994a), "Seismic Behavior of Open-Web Truss-Moment Frames," *Journal of Structural Engineering*, American Society of Civil Engineers, vol. 120, no. 6, pp.1763-1780.

Goel, S.C., and Itani, A.M. (1994b), "Seismic-Resistant Special Truss-Moment Frames," *Journal of Structural Engineering*, American Society of Civil Engineers, vol. 120, no. 6, pp.1781-1797.

Goel, S.C., Rai, D.C., and Basha, H.S. (1998), "Special Truss Moment Frames – Design Guide," *Report No. UMCEE 98-44*, Department of Civil and Environmental Engineering, University of Michigan, Ann Arbor, MI.

Goody, M.E., Hansen, R.J., LeMessurier, W.J., Pahl, P.J., Pelletier, R.J., Doyen, J.H., Opitz, C.F., Sarno, J.S., Schildknecht, R., Schwarz, K.W., and Kayser, F. (1967), *High Rise Housing in Steel: the Staggered Truss System : a research project*, Massachusetts Institute of Technology. Department of Civil Engineering, Cambridge, MA.

Gupta, R.P. (1974), “Seismic Behavior of Staggered Truss Framing Systems – 1. Analysis of Dynamic Response,” *Steel Research for Construction*, American Iron and Steel Institute, vol.26, pp.3-46.

Hanson, R.D., and Martin, H.W. (1987), “Performance of Steel Structures in the September 19 and 20, 1985 Mexico Earthquakes,” *Earthquake Spectra*, Earthquake Engineering Research Institute, vol. 3, no. 2, pp. 329-346.

ICBO (1988), *Uniform Building code*, International Conference of Building Officials, Whittier, CA.

ICBO (1997), *Uniform Building code*, International Conference of Building Officials, Whittier, CA.

Itani, A.M., and Goel, S.C. (1991), “Earthquake Resistance of Open Web Framing Systems,” *Report No. UMCE 91-21*, Department of Civil Engineering, University of Michigan, Ann Arbor, MI.

Kim, J., Lee, J.-H., and Kim, Y.-M. (2007), “Inelastic Behavior of Staggered Truss Systems,” *The Structural Design of Tall and Special Buildings*, vol. 16, pp.85-105.

Lee, S.-S., and Goel, S.C. (2001), “Performance-Based Design of Steel Moment Frames Using Target Drift and Yield Mechanism,” *Report No. UMCEE 01-17*, Department of Civil and Environmental Engineering, University of Michigan, Ann Arbor, MI.

LATBSDC (2008), *An Alternative Procedure for Seismic Analysis and Design of Tall Buildings Located in the Los Angeles Region – A Consensus Document*, Los Angeles Tall Buildings Structural Design Council, Los Angeles, CA.

Marstellar, B., and Faraone, T. (2002), “Anatomy of a Staggered Truss,” *Modern Steel Construction*, vol. 42, no. 9, pp. 35.

Moore, K.S. (2005), “Staggered Truss Framing System in Areas of Moderate-High Seismic Hazard,” *Proceedings of the 2005 North American Steel Construction Conference*, Montreal, Canada.

Newell, J.D., and Uang, C.-M. (2008), “Cyclic Behavior of Steel Wide-Flange Columns Subjected to Large Drift,” *Journal of Structural Engineering*, American Society of Civil Engineering, vol. 134, no. 8, pp.1334-1342.

Ölmez, H.D., and Topkaya, C. (2011), "A Numerical Study on Special Truss Moment Frames with Vierendeel Openings," *Journal of Constructional Steel Research*, vol. 67, no. 4, pp.667-677.

Palmer, T.L. (2010), “Mineta San Jose International Airport – Delivering Form and Function,” *STRUCTURE Magazine*, vol. 11, no. 6, pp.35-37.

Parra-Montesinos, G.J., Goel, S.C., and Kim, K.-Y. (2006), “Behavior of Steel Double Channel Built-Up Chords of Special Truss Moment Frames under Reversed Cyclic Bending,” *Journal of Structural Engineering*, vol. 132, no. 9, pp.1343-1351.

Pekcan, G., Linke, C., Itani, A.M. (2009), “Damage Avoidance Design of Special Truss Moment Frames with Energy Dissipating Devices,” *Journal of Constructional Steel Research*, vol. 65, no. 6, pp.1374-1384.

Pekcan, G., and Itani, A. (2007), “Seismic Response of Innovative Special Truss Moment Frames with Energy Dissipating Devices,” Department of Civil Engineering, University of Nevada, Reno, NV.

RISA Technology (2011), *RISA-3D User’s Guide*, Foothill Ranch, CA.

Sahoo, D.R., and Chao, S.-H. (2010), “Performance-Based Plastic Design Method for buckling-restrained braced frames,” *Engineering Structures*, vol. 32, no. 9, pp.2950-2958.

Scalzi, J. B. (1971), “The Staggered Truss System-Structural Considerations,” *Engineering Journal*, American Institute of Steel Construction, October, pp.138-143.

SEAOC Seismology Committee (2006), “Staggered Truss Frames,” *The SEAOC Blue Book: Seismic Design Recommendations*, Structural Engineers Association of California, Sacramento, CA.

SEAOC Seismology Committee (2008), “Special Truss Moment Frames with Vierendeel Segments,” *The SEAOC Blue Book: Seismic Design Recommendations*, Structural Engineers Association of California, Sacramento, CA.

Simasathien, S., Chao, S.-H., Moore, K., and Okazaki, T. (2014), “Modified Structural Layouts for Staggered Truss Framing Systems Used in Seismically Active Areas,” *Proceedings of the 10th National Conference in Earthquake Engineering*, Earthquake Engineering Research Institute, Anchorage, AK.

Simasathien, S., Jiansinlapadamrong, C., Okazaki, T., and Chao, S.-H. (2014), “Cyclic Loading Performance of Special Truss Moment Frame with Double-Channel Chord Members,” *Proceedings of the 10th National Conference in Earthquake Engineering*, Earthquake Engineering Research Institute, Anchorage, AK.

Somerville, P.G., Smith, N.F., Punyamurthula S., and Sun, J.I. (1997), Development of Ground Motion Time Histories for Phrase 2 of the FEMA/SAC Steel Project,” *Rep. No. SAC/BD-97/04*, SAC joint Venture, Sacramento, CA.

Valley, M., and Hooper, J. (2003), “Issues in the Design of a Seattle-Area Special Truss Moment Frame Building,” *Proceedings of the 2003 Structures Congress & Exposition*, Seattle, WA.

Wendt, G. (2011), “Takeoffs That Helped Land an Aviation Marvel,” *Modern Steel Construction*, vol. 51, no. 7, pp. 32-36.

Wexler, N., and Lin, F.-B. (2003), *Steel Design Guide Series No. 14 – Staggered Truss Framing Systems*, American Institute of Steel Construction, Chicago, IL.

Biographical Information

Sanputt Simasathien obtained a Bachelor of Science in Civil Engineering from Kasetsart University in Bangkok, Thailand in 1997. He came to the University of Texas at Arlington (UTA) and received Master of Engineer (Civil Engineering) degree in 2000. He also received Master of Science in Industrial Engineering from UTA in 2006.

Sanputt worked as a graduate structural engineers in the Dallas/Fort Worth metroplex after he received his Master of Engineering degree for a few years. He also worked as a project assistant at the Small Business Development Center in Fort Worth while he was pursuing his second Master's degree in Industrial Engineering. He decided to come back to UTA to pursue his PhD and received his PhD in Structural Engineering in 2016. During his PhD study, he was heavily involved with numerous research projects including two NSF funded projects "Full-Scale RC and HPFRC Frame Subassemblages Subjected to Collapse-Consistent Loading Protocols for Enhanced Collapse Simulation and Internal Damage Characterization" and "Steel Truss Systems with Enhanced Seismic Safety and Performance." His research interests include precast/prestressed concrete, steel fiber-reinforced concrete, structural stability, and seismic-resistant structures in both concrete and steel.

After receiving his PhD, Sanputt plans to work as a Structural Engineer and gain design experience working towards his PE license. He is a member of a number of professional organizations such as American Concrete Institute (ACI), American Institute of Steel Construction (AISC), American Society of Civil Engineers (ASCE), Precast/Prestressed Concrete Institute (PCI), and Earthquake Engineering Research Institute (EERI). He is also a member of the Industrial Engineering Honor Society (Alpha Pi Mu), the Civil Engineering Honor Society (Chi Epsilon), and the Engineering Honor Society (Tau Beta Pi).